

## **Distribution Agreement**

In presenting this thesis or dissertation as a partial fulfillment of the requirements for an advanced degree from Emory University, I hereby grant to Emory University and its agents the non-exclusive license to archive, make accessible, and display my thesis or dissertation in whole or in part in all forms of media, now or hereafter known, including display on the world wide web. I understand that I may select some access restrictions as part of the online submission of this thesis or dissertation. I retain all ownership rights to the copyright of the thesis or dissertation. I also retain the right to use in future works (such as articles or books) all or part of this thesis or dissertation.

Signature:

---

Zackery W. Dentmon

---

Date

Studies in Small Molecule Drug Discovery:  
Part I. Synthesis of Novel Nucleoside-Based Antivirals to Treat Hepatitis C  
Part II. Validation and Implementation of a Machine Learning Algorithm to Create a Safer  
Kinase Inhibitor as a Potential First-in-Class Antiparkinsonian Agent

By

Zackery W. Dentmon  
Doctor of Philosophy

Chemistry

---

Dennis C. Liotta, Ph.D.  
Advisor

---

Cora E. MacBeth, Ph.D.  
Committee Member

---

William M. Wuest, Ph.D.  
Committee Member

Accepted:

---

Kimberly Jacob Arriola, Ph.D, MPH  
Dean of the James T. Laney School of Graduate Studies

---

Date

Studies in Small Molecule Drug Discovery:  
Part I. Synthesis of Novel Nucleoside-Based Antivirals to Treat Hepatitis C  
Part II. Validation and Implementation of a Machine Learning Algorithm to Create a Safer  
Kinase Inhibitor as a Potential First-in-Class Antiparkinsonian Agent

By

Zackery W. Dentmon  
B.S., B.A., Mercer University, 2009

Advisor: Dennis C. Liotta, Ph.D.

An abstract of  
A dissertation submitted to the Faculty of the  
James T. Laney School of Graduate Studies of Emory University  
in partial fulfillment of the requirements for the degree of  
Doctor of Philosophy  
in Chemistry  
2022

## Abstract

Studies in Small Molecule Drug Discovery:  
Part I. Synthesis of Novel Nucleoside-Based Antivirals to Treat Hepatitis C  
Part II. Validation and Implementation of a Machine Learning Algorithm to Create a Safer  
Kinase Inhibitor as a Potential First-in-Class Antiparkinsonian Agent

By Zackery W. Dentmon

Xenobiotics have been used to alleviate human pathology for thousands of years, yet average life expectancy remained flat until the Enlightenment when it began to increase rapidly. Many factors contributed to this rise, but some of the most influential were revolutions in medical science and technology, particularly in the fields of vaccination and anti-infective drug discovery. The invention of new medicines, however, is no trivial task as most contemporary small molecule drugs spend nearly a decade or more in clinical development before a new safe and effective agent is approved. Clearly there is a need not only for new drugs, but also for a new way of discovering them.

Part I of this dissertation discusses a traditional approach to discover new nucleoside-based antivirals to treat hepatitis C virus (HCV). The first chapter provides some historical context for nucleosides in medicine and briefly previews the following two chapters. Chapter 2 details our work building and evaluating a small set of prodrugs of 4'-thionucleoside analogs for anti-HCV activity. Having determined them to be relatively ineffective, Chapter 3 then reports our investigation of a hypothesis to rationalize the poor activity we observed with our analogs from Chapter 2 compared to their parent scaffold. We used a computational model to suggest some novel modifications which could bias the conformational dynamics of the parent scaffold and support an observed correlation between conformation and potency. This effort produced analogs with even less antiviral efficacy against HCV and confirmed that conformational bias is only one potential consideration in antiviral drug design.

Part II of this dissertation showcases an alternative approach to drug discovery which makes use of artificial intelligence to redesign and improve upon extant drugs exemplified in the literature. Chapter 4 discusses the discovery of our machine learning algorithm and the foundational retrospective and prospective case studies across three diverse biological and chemical targets which validated the AI workflow. The final chapter then relays our efforts at utilizing this technology to redesign a class of antineoplastic kinase inhibitors to make them less cardiotoxic and therefore safer to use in an unmet chronic disease state like neurodegeneration.

Studies in Small Molecule Drug Discovery:  
Part I. Synthesis of Novel Nucleoside-Based Antivirals to Treat Hepatitis C  
Part II. Validation and Implementation of a Machine Learning Algorithm to Create a Safer  
Kinase Inhibitor as a Potential First-in-Class Antiparkinsonian Agent

By

Zackery W. Dentmon  
B.S., B.A., Mercer University, 2009

Advisor: Dennis C. Liotta, Ph.D.

A dissertation submitted to the Faculty of the  
James T. Laney School of Graduate Studies of Emory University  
in partial fulfillment of the requirements for the degree of  
Doctor of Philosophy  
in Chemistry  
2022

## Acknowledgments

In a poem entitled “The Man Watching” the early 20<sup>th</sup> century Austrian poet Rainer Maria Rilke wrote these words: “What we choose to fight is so tiny! / What fights with us is so great.” (*transl. by Robert Bly*). As I reflect on my time in graduate school, I am drawn to these words. Often what we as students and academics choose to pursue can feel ... well, academic. That is to say sometimes it feels small, of no great importance, insignificant. We may spend quite a bit of time trying to convince other people (usually those with limited, competitive funding to award to researchers) that it is, in fact, important and worthy of investment. In my own line of work, small molecule drug discovery, this is true in a very literal way, even in the name. Viruses are tiny, proteins smaller still, and molecules ... well you get the idea. But it can also feel true in the more metaphorical way, the way in which I imagine Rilke intended. We can and do get caught up in small things that may be of very little ultimate consequence.

But what of the great thing that fights with us? While I can't be sure what Rilke had in mind, in the context of graduate school, what fights with us is Knowledge, or perhaps more precisely the *lack* of Knowledge. Both, really. We spend a great deal of time attempting to master a foundation of Knowledge, learning what is already known or what has already been established. I suppose you could say this is round 1, and often it feels like Knowledge beats us. But really, this is just preparation, a warmup for the next round, in which we will be wrestling with the Unknown, or the Not-Yet-Known. We turn from students of Knowledge to discoverers and teachers of Knowledge. What a great responsibility! But, in the best of cases, this process is not transitional or linear, as if we somehow arrived at our destination and won the bout. Instead, we take turns being students then teachers and students again. Rather than Sisyphean, you might call the process helical. From one vantage point, it seems we go round and round, but if we are careful to learn along the way and to look from a different perspective, we also *make* progress, sometimes quite literally. And so the fight continues. What fights with us is indeed great, and there's still so much to learn and discover.

There are many people who deserve acknowledgement for this work; any part of it that is good is owed to them, any part of it which is not falls on me.

First and foremost are my parents, **Larry** and **Lawren Dentmon**, who were my first teachers and contributed an untold investment of their time and resources to instill in me a value for education and hard work, and to support me throughout my life. Repayment is not an appropriate concept in this relationship, but gratitude surely is. My older brother **Josh Dentmon** has also been my continual companion from before I can even remember. You guys were my earliest cheerleaders, and I'll never forget that. Thank you.

There were educators in my life who inspired me to do science, none of whom were more impactful than my undergraduate research mentor at Mercer University, **Dr. Kevin Bucholtz**. He set the foundation for my interest and ability in organic chemistry. Thank you.

When I graduated from college, I took my first job at a small pharmaceutical spinout from Emory called NeurOp, Inc. There were 2 men there who took a chance on me and to whom I owe a great deal for getting my scientific career started: **Vince La Terza** and **Dr. Scott Myers**. Both were valuable mentors to me during the time I spent at the company and allowed me the opportunity to see what being a full-time research scientist looked like. They convinced me I could do it, too. Scott especially played a hugely kind role in enabling me and my family to establish roots in Atlanta. Also, without my start at NeurOp, I likely never would have established a connection to Emory University and Dr. Liotta. Thank you.

**Prof. Dennis Liotta** also took a chance on me when the company downsized the technical staff. He invited me to work in his lab at Emory and then saw the potential in me to become an independent scientist. He has continued to invest in me and placed an incredible amount of trust in me over the near decade I've been working with him. He has limitlessly equipped and encouraged me to pursue our research in the way I deemed best without second guessing me at all. Thank you.

My other dissertation committee members, **Drs. Cora MacBeth** and **Bill Wuest**, were both early advocates of mine who played no small part in getting me started in the graduate program. They have continued to be strong supporters ushering me through to graduation. Thank you.

There are so many people in the Liotta lab with whom I've had the pleasure to work, attempting to name them all here creates some liabilities. I will offer a non-exhaustive list of members of the Liotta lab who have been dear friends and colleagues over my years and who have helped me accomplish this work (all Drs.): **Nicholas Akins, Pieter Burger, Madhuri Dasari, Matt Epplin, Russel Fritzmeier, Luke Hodson, Edgars Jecs, Michelle Kim, David Menaldino, Sonia Nijampatnam, Alex Orchard, Manohar Saindane, Valerie Truax, Alet van der Westhuyzen, Rob Wilson**. My immediate lab and office mates **Drs. Leon Jacobs, Eric Miller, Stephen Pelly, and Nicole Pribut** deserve special recognition. Their friendship and mentorship have made our lab a remarkably great place to work. Thank you.

There have been a few students with whom I've had the pleasure to work and mentor who contributed to my ability to accomplish this work: **Christopher Dalloul, Hannah Gold, and Dr. Amaan Kazerouni**. One of the most fun and rewarding parts about being in an academic environment for me is the ability to work with younger, bright individuals who affirmed my abilities as a teacher and communicator. They spent their time and energy listening to me and pursuing my projects and made me feel like I had something worth teaching. They, of course, in turn taught me to be a better, clearer thinker and communicator, and also contributed technically to the work reported herein. Thank you.

One individual that I worked with deserves special recognition here. **Dr. Tom Kaiser** was my first fully dedicated postdoctoral mentor and spent hours and hours sharing lab and office space from the time I arrived in 2013 until the time he left our lab in 2017. He was and continues to be a peculiar friend and mentor to me. By this, I do not mean that he is a peculiar person, although that is also true. What I mean is that his devotion to me as a friend and colleague are peculiar among my professional relationships. He left our lab and the US in 2017 to supplement his PhD with a MD from Oxford University (as one does), but his influence on me remained. In his spare time at medical school, he continued the research we were working on (which forms Part II of this dissertation), eventually co-founding a company with our colleague Dr. Pieter Burger to devote their early careers to developing the technology further. Now, in a continuation of his peculiar commitment to me, he convinced his company to be the next in line to take a chance on me. Thank you.

The final people who deserve acknowledgement for this work I have saved for last because, in my mind, this represents the place of highest honor. My wife **Erin Dentmon** and my daughters **Eleanor and Dorothy Dentmon** have inarguably sacrificed the most to let me accomplish this task. It would be egregious not to recognize them for their inspiration and influence in my life, but it would be equally ridiculous to think I could adequately describe it here. So I won't attempt to do that. I will just say that I love you beyond my ability to articulate, and I hope my work here and in the future makes you a fraction as proud of me as I am of you.

---

## **The Man Watching**

I can tell by the way the trees beat, after  
so many dull days, on my worried windowpanes  
that a storm is coming,  
and I hear the far-off fields say things  
I can't bear without a friend,  
I can't love without a sister.

The storm, the shifter of shapes, drives on  
across the woods and across time,  
and the world looks as if it had no age:  
the landscape, like a line in the psalm book,  
is seriousness and weight and eternity.

What we choose to fight is so tiny!  
What fights with us is so great.  
If only we would let ourselves be dominated  
as things do by some immense storm,  
we would become strong too, and not need names.

When we win it's with small things,  
and the triumph itself makes us small.  
What is extraordinary and eternal  
does not want to be bent by us.  
I mean the Angel who appeared  
to the wrestlers of the Old Testament:  
when the wrestlers' sinews  
grew long like metal strings,  
he felt them under his fingers  
like chords of deep music.

Whoever was beaten by this Angel  
(who often simply declined the fight)  
went away proud and strengthened  
and great from that harsh hand,  
that kneaded him as if to change his shape.  
Winning does not tempt that man.  
This is how he grows: by being defeated, decisively,  
by constantly greater beings.

-Rainer Maria Rilke (transl. by Robert Bly)

"No work is insignificant. All labor that uplifts humanity has dignity and importance and should be undertaken with painstaking excellence."

-Rev. Dr. Martin Luther King Jr.

# Table of Contents

## **Part I. Synthesis of Novel Nucleosides and their Monophosphate Prodrugs to Target the RNA-Dependent RNA Polymerase of the Hepatitis C Virus**

Chapter 1. Nucleoside & Nucleotide Antivirals: A Preface.....	1
<b>1.1 INTRODUCTION</b> .....	1
<b>1.2 A FORAY INTO NUCLEOSIDE-BASED INHIBITORS OF HEPATITIS C</b> .....	3
1.2.1 Thionucleoside Prodrugs – A Preview of Chapter 2.....	5
1.2.2 A Conformational Consideration – A Preview of Chapter 3.....	6
<b>1.3 REFERENCES AND NOTES</b> .....	11
Chapter 2. Synthesis and Antiviral Evaluation of a Series of 4'-Thio Congeners of 2'-C-Methyl-Substituted Ribonucleoside Prodrugs .....	14
<b>2.1 INTRODUCTION</b> .....	14
<b>2.2 RESULTS AND DISCUSSION</b> .....	17
2.2.1 Synthesis of the 4'-Thionucleosides & Phosphoramidate Prodrugs .....	17
2.2.2 Antiviral Evaluation of Monophosphate Prodrugs.....	23
<b>2.3 MATERIALS AND METHODS</b> .....	26
2.3.1 Synthetic Chemistry .....	26
2.3.2 Pharmacology .....	46
<b>2.4 REFERENCES AND NOTES</b> .....	60
Chapter 3. Synthesis and Antiviral Evaluation of 3'-C-Substituted Congeners of 2'-C-Methyluridine.....	65
<b>3.1 INTRODUCTION</b> .....	65
<b>3.2 RESULTS AND DISCUSSION</b> .....	71
3.2.1 Synthesis of the Key 3'-Ketonucleoside Intermediate for Diversification.....	71
3.2.2 Synthesis and Antiviral Evaluation of the Nucleoside Monophosphate Prodrugs .....	83
<b>3.3 MATERIALS AND METHODS</b> .....	90

3.3.1 Computational Methods .....	90
3.3.2 Synthetic Chemistry .....	90
3.3.3 Pharmacology .....	118
<b>3.4 REFERENCES AND NOTES .....</b>	<b>127</b>

## **Part II. Studies on the Machine Learning Algorithm-Enhanced Hit-to-Lead Optimization of Drug-Like Small Molecules**

<b>Chapter 4. The Discovery &amp; Development of FRESH: An Algorithm for Small Molecule Hit-to-Lead Optimization .....</b>	<b>135</b>
--	------------

<b>4.1 INTRODUCTION.....</b>	<b>135</b>
4.1.1 The Design of the FRESH Algorithm .....	136
<b>4.2 VALIDATION OF FRESH: RETROSPECTIVE CASE STUDIES .....</b>	<b>139</b>
4.2.1 Phosphatidylinositol 3-Kinase (PI3K) .....	140
4.2.2 Carbonic Anhydrase II (CA II) .....	142
4.2.3. Histone Deacetylase (HDAC) .....	145
<b>4.3 IMPLEMENTATION OF FRESH: PROSPECTIVE CASE STUDIES .....</b>	<b>146</b>
4.3.1 Predicting Potent, Novel Inhibitors of CA II .....	147
4.3.2 Predicting Potent, Novel Inhibitors of PI3K $\alpha$ .....	149
<b>4.4 REFERENCES AND NOTES .....</b>	<b>156</b>

<b>Chapter 5. The Machine Learning Algorithm-Enabled Design and Synthesis of Novel Abelson Non-Receptor Tyrosine Kinase Inhibitors as Safer Therapeutics for Parkinson's Disease.....</b>	<b>160</b>
---	------------

<b>5.1 INTRODUCTION.....</b>	<b>160</b>
<b>5.2 RESULTS AND DISCUSSION .....</b>	<b>163</b>
5.2.1 Core Scaffold and Single-NBN Compound Selection .....	164
5.2.2 Parallel Linear Synthetic Strategy to Access and Evaluate the Single-NBN Compounds .	168
5.2.3 Dual-NBN Compound Selection and a Divergent Synthetic Strategy.....	170
5.2.4 Divergent Synthesis to Access the Dual-NBN Compounds .....	173
5.2.5 <i>In vitro</i> Evaluation of the Dual-NBN Compounds .....	176
5.2.6 <i>In vivo</i> Pharmacokinetic Evaluation of 5.17a and 5.17b .....	181

<b>5.3 MATERIALS AND METHODS</b> .....	188
5.3.1 Synthetic Chemistry .....	188
5.3.2 <i>In vitro</i> Pharmacology .....	214
5.3.3 <i>In vivo</i> Pharmacology .....	222
<b>5.4 REFERENCES AND NOTES</b> .....	232
<b>Supplemental Appendix</b> .....	<b>238</b>
<b>SA.1 NMR Spectra of Compounds in Chapter 2</b> .....	239
SA.1.1 Construction of the Thiosugar Core (2.S1 – 2.9).....	239
SA.1.2 Thionucleosides and Monophosphate Prodrugs (2.11a-f; 2.13a-f) .....	255
<b>SA.2 NMR Spectra of Compounds in Chapter 3 (3.3 – 3.11)</b> .....	289
<b>SA.3 NMR Spectra of Compounds in Chapter 5</b> .....	305
SA.3.1 Single-NBN Compounds (5.1 – 5.9c).....	305
SA.3.2 Dual-NBN Compounds (5.10 – 5.17c) .....	342

# List of Illustrations

## FIGURES

<b>Figure 1.1</b> General annotated structure of a terminal ribonucleotide (top left) and an incoming NTP (bottom left) representing the polymerase chain elongation reaction .....	1
<b>Figure 1.2</b> Structures of (a) spongocytidine (Ara-C) and (b) azidothymidine (AZT), two of the earliest nucleoside analog drugs, as well as (c) ( $\pm$ )-FTC.....	2
<b>Figure 1.3</b> Structure of (a) 2'-C-methyladenosine and (b) sofosbuvir, a ProTide prodrug of the 2'- $\alpha$ -fluoro-2'- $\beta$ -methyluridine nucleoside analog .....	4
<b>Figure 1.4</b> Structure of our ProTide prodrug of 2'- $\beta$ -methyl-4'-thiouridine.....	6
<b>Figure 1.5</b> Equilibrium of the ribose ring conformational antipodes in uridine, with carbon atoms of the sugar ring numbered for clarity .....	7
<b>Figure 1.6</b> Rendering of the seven torsional parameters considered by the RNA force fields used in DFT .....	8
<b>Figure 1.7</b> (a) Scatter plot of NTP IC <sub>50</sub> ( $\mu$ M) vs $\Delta E_{\text{exo-endo}}$ ; (b) Comparison of the 3'-exo (blue) and endo (red) chain terminal conformations in the polymerase active site showing the maximal common alignment, and distances ( $\text{\AA}$ ) from the incoming phosphate; (c) The full molecule alignment shows the changes in angle of the 3' hydroxyl to the incoming phosphate .....	9
<b>Figure 1.8</b> A reaction coordinate diagram showing the proposed difference in transition state energies of the 3'-endo and exo antipodes in the active site.....	10
<b>Figure 1.9</b> Structures of the parent molecule 2'- $\beta$ -methyluridine ( <b>1.2</b> ) and the proposed 3'-modified analogs with associated model scores (in Hartree units) .....	11
<b>Figure 2.1</b> Examples of early modified nucleoside drugs ( <b>a-c</b> ) and the aryloxy phosphoramidate monophosphate prodrug sofosbuvir ( <b>d</b> ).....	14
<b>Figure 2.2</b> Representative examples of ( <b>a</b> ) essential antiviral nucleosides with non-natural sugar ring compositions, and ( <b>b</b> ) historical 4'-thionucleoside analogs having notable bioactivity.....	17
<b>Figure 2.3</b> Comparison of the structural features of the most potent nucleoside of this work ( <b>2.11a</b> ) to sofosbuvir ( <b>2.15</b> ), with the bridging structure of 2'- $\beta$ -methyluridine ( <b>2.14</b> ).....	24
<b>Figure 3.1</b> (A) Nucleotides considered by Fung et al.; (B) Positioning of the 3' terminal nucleotide (blue) and a UDP monomer (gray) in the NS5B pre-reaction complex (PDB ID:4WTA); (C) ROC curves associated with correlating antiviral activity of nucleotides in Table 1 with calculated DFT exo-endo $\Delta E$ or (D) Docking Scores. ....	67
<b>Figure 3.S1</b> Properties of nucleotides from Feng et al. compared to their measured IC <sub>50</sub> .....	68
<b>Figure 3.S2</b> (A) Activity of nucleotides in Table 3.1 plotted against Docking Scores and (B) calculated DFT exo-endo $\Delta E$ .....	69
<b>Figure 3.S3</b> Three-dimensional renderings of the minimized 3'-exo (left) and 3'-endo (right) antipodes of the two analogs chosen for this study.....	71

<b>Figure 3.2</b> Proposed (A) 6-membered transition state (green) and (B) 8-membered transition state (orange) for the delivery of the methyl group (red) to the top of the sugar ring, with the appropriate metal (blue) coordination. ....	86
<b>Figure 4.1</b> PI3K inhibitor scaffold <b>4.1</b> and analogue <b>4.2</b> .....	140
<b>Figure 4.2</b> ROC curve for the ECFP method in Case 1 (PI3K). ....	141
<b>Figure 4.3</b> ROC curve for the MM-GBSA score in Case 1 (PI3K) .....	141
<b>Figure 4.4</b> ROC curve for the Glide score method in Case 1 (PI3K) .....	142
<b>Figure 4.5.</b> Supuran’s CA II inhibitor scaffold <b>4.3</b> and analogue <b>4.4</b> .....	143
<b>Figure 4.6</b> ROC curve for the ECFP method in Case 2 (CA II) .....	144
<b>Figure 4.7</b> ROC curve for the Glide score in Case 2 (CA II) .....	144
<b>Figure 4.8</b> HDAC1 inhibitor scaffold <b>4.5</b> and the naphthalenyl analogue <b>4.6</b> .....	145
<b>Figure 4.9</b> ROC curve for the ECFP method in Case 3 (HDAC1) .....	146
<b>Figure 4.10</b> FDA-approved PI3K inhibitors .....	150
<b>Figure 4.11</b> Initial PI3K $\alpha$ hit scaffold ( <b>4.16</b> ) and proposed site-modified analogs ( <b>4.17</b> ) .....	151
<b>Figure 5.1</b> Approved first-, second- and third-generation inhibitors of BCR-ABL imatinib, nilotinib, and ponatinib .....	162
<b>Figure 5.2</b> Structure of ponatinib with the constituent pieces annotated .....	165
<b>Figure 5.3</b> Abl1 kinase dose-response curves in duplicate for experimental compounds <b>1 – 3</b> (left), <b>4 – 6</b> (middle) with nilotinib and ponatinib .....	215
<b>Figure 5.4</b> hERG channel dose-response curves in duplicate for experimental compounds <b>1 – 3</b> (left), <b>4 – 6</b> (middle) with nilotinib, ponatinib, and positive control E-4031 (right) .....	216
<b>Figure 5.5</b> Calculated CYP450 (3A4) inhibition data on compounds <b>1–3</b> (left), <b>4–6</b> (middle), nilotinib, and ponatinib (right). Ketoconazole was also run each time as a positive control .....	218
<b>Figure 5.6</b> Metabolic stability shown as the % remaining of compounds <b>4 – 6</b> , nilotinib, and ponatinib after every time point ( $t = 0, 5, 10, 15$ and $30$ min) from HLM and MLM .....	220
<b>Figure 5.7</b> Plasma concentrations-time profiles (mean $\pm$ SD) of ZD-3-392 ( <b>5.17a</b> ) in male C57BL/6 mice following a single intravenous and oral administration (Dose: 3 mg/kg, IV; 3, 10 and 30 mg/kg, PO) plotted on linear and semi-log scales .....	224
<b>Figure 5.8</b> Plasma concentrations-time profiles (mean $\pm$ SD) of ZD-3-372 ( <b>5.17b</b> ) in male C57BL/6 mice following a single intravenous and oral administration (Dose: 3 mg/kg, IV; 3, 10 and 30 mg/kg, PO) plotted on linear and semi-log scales .....	227
<b>Figure 5.9</b> Plasma concentrations-time profiles (mean $\pm$ SD) of ZD-3-188 (nilotinib) in male C57BL/6 mice following a single intravenous and oral administration (Dose: 3 mg/kg, IV; 3, 10 and 30 mg/kg, PO) .....	230

## SCHEMES

<b>Scheme 2.1</b> Multistep synthesis of the per-acetylated thiosugar core. ....	18
<b>Scheme 2.2</b> Two-step sequences used for glycosylation of nucleobases.....	20
<b>Scheme 2.3</b> Traditional base-activated reaction utilized to access the desired phosphoramidate monophosphate prodrugs <b>2.13a-e</b> . These conditions failed for <b>2.11f</b> where R = cytosine. ....	21
<b>Scheme 2.4</b> Alternative Lewis acid-activated phosphoramidation utilizing the transient 2',3'-phenylboronic ester protecting group strategy to access the cytidine analog.....	23
<b>Scheme 3.1</b> Synthesis of the parent nucleoside 2'-C-methyluridine from the commercially available per-benzoylated ribofuranoside and uracil. ....	72
<b>Scheme 3.S1</b> Complementary diastereofacial selective addition of TMS-acetylide as reported by Jung.....	73
<b>Scheme 3.S2</b> Proposed six step synthesis of 3'-modified nucleosides <b>3.9a</b> and <b>3.9b</b> from 2'-methyluridine .....	75
<b>Scheme 3.S3</b> Tertiary 2'-O-silylation and subsequent global deprotection .....	77
<b>Scheme 3.S4</b> Alternative eight step synthesis of 3'-modified nucleosides <b>3.9a</b> and <b>3.9b</b> from 2'-methyluridine .....	78
<b>Scheme 3.S5</b> Fate of the 5'-O-isobutryate protecting group .....	80
<b>Scheme 3.2</b> Four-step synthesis to the key $\beta$ -hydroxyketone intermediate (boxed) used for analog diversification. ....	82
<b>Scheme 3.3</b> Complementary 2-step routes from the 2'-OTBS-protected nucleoside analogs to the desired monophosphate prodrugs. ....	84
<b>Scheme 4.1</b> Retrosynthesis of compounds of type <b>4.17</b> .....	153
<b>Scheme 5.1</b> Parallel linear syntheses of single-NBN target compounds <b>5.9a-c</b> .....	168
<b>Scheme 5.2</b> Divergent synthesis of the dual-NBN compounds (Abl1 $\cap$ hERG) .....	173
<b>Scheme 5.3</b> Strategies to access the key intermediate for diversification .....	175
<b>Scheme 5.4</b> Complementary pathways used to access the target dual-NBN compounds <b>5.17a-c</b> .....	176

## TABLES

<b>Table 2.1</b> Antiviral dose-response data for 2'-C-methyl-4'-thionucleoside phosphoramidates..	24
<b>Table 2.2</b> Reference table for matching Compound No.'s used in this chapter with Notebook No.'s used by ImQuest BioSciences, Inc.....	47
<b>Table 3.1</b> Nucleotides considered in the conformer energy model .....	69
<b>Table 3.S1</b> Novel nucleotides considered for synthesis and corresponding DFT result.....	70
<b>Table 3.2</b> Broad-spectrum cellular antiviral screening.....	89-90

<b>Table 3.3</b> Reference table for matching Compound No.'s used in this chapter with Notebook No.'s used by ImQuest BioSciences, Inc. ....	118
<b>Table 4.1</b> Novel CA II inhibitors from Family 4.3 of Figure 4.5 .....	148
<b>Table 4.2</b> Enzymatic PI3K $\alpha$ and anti-proliferative potencies .....	154
<b>Table 5.1.</b> Structure, probability score, and rank of single-NBN (Abl1) compounds .....	166
<b>Table 5.2</b> Biochemical data of single-NBN target compounds compared to FDA-approved Inhibitors .....	169
<b>Table 5.3</b> Structure, probability scores, and ranks of dual-NBN (Abl1 $\cap$ hERG) compounds ....	172
<b>Table 5.4</b> Biochemical data of dual-NBN target compounds compared to FDA-approved inhibitors.....	177
<b>Table 5.5</b> ADMET redouts of successful dual-NBN compounds compared to FDA-approved inhibitors.....	178
<b>Table 5.6</b> Percent activity remaining [and IC <sub>50</sub> values] of dual-NBN compounds and FDA-approved inhibitors against selected screened kinases .....	179
<b>Table 5.7</b> Pharmacokinetic parameters calculated after a single bolus of the compounds of interest via i.v. (3 mg/kg) or oral (p.o.) administration .....	183
<b>Table 5.8</b> Additional DMPK properties for lead compounds and FDA-approved inhibitors .....	184
<b>Table 5.9</b> Compound codes used to assay final compounds .....	214
<b>Table 5.10</b> Scan parameters for the tested compounds and its transitions in multiple reaction monitoring mode .....	219
<b>Table 5.11</b> Pharmacokinetics data of ZD-3-392 ( <b>5.17a</b> ) in male C57BL/6 mice following a single intravenous and oral administration (Dose: 3 mg/kg; IV and 3, 10, 30 mg/kg; PO) .....	224
<b>Table 5.12</b> Individual plasma and brain concentrations and brain-Kp of ZD-3-392 ( <b>5.17a</b> ) in male C57BL/6 mice following a single oral administration (Dose: 3, 10 and 30 mg/kg) .....	225
<b>Table 5.13</b> Pharmacokinetics data of ZD-3-372 ( <b>5.17b</b> ) in male C57BL/6 mice following a single intravenous and oral administration (Dose: 3 mg/kg; IV and 3, 10, 30 mg/kg; PO) .....	227
<b>Table 5.14</b> Individual plasma and brain concentrations and brain-Kp of ZD-3-372 ( <b>5.17b</b> ) in male C57BL/6 mice following a single oral administration (Dose: 3, 10 and 30 mg/kg) .....	228
<b>Table 5.15</b> Pharmacokinetics data of ZD-3-188 (nilotinib) in male C57BL/6 mice following a single intravenous and oral administration (Dose: 3 mg/kg; IV and 3, 10, 30 mg/kg; PO) .....	230
<b>Table 5.16</b> Individual plasma and brain concentrations and brain-Kp of ZD-3-188 (nilotinib) in male C57BL/6 mice following a single oral administration (Dose: 3, 10 and 30 mg/kg) .....	231

Part I

Synthesis of Novel  
Nucleosides and their  
Monophosphate Prodrugs to  
Target the RNA-Dependent RNA  
Polymerase of the Hepatitis C Virus

---

## Chapter 1. Nucleoside & Nucleotide Antivirals: A Preface

### 1.1 INTRODUCTION

Nucleosides and nucleotides have long been recognized as a privileged scaffold in biology. As the monomers of nucleic acid polymers DNA and RNA, nature selected nucleotides as the biochemical entity responsible for carrying genetic information from cellular and organismal generation to generation with high fidelity, acting as the cellular blueprint. They are therefore of utmost importance in cellular as well as organismal reproduction and heredity. More specifically, nucleoside triphosphates (NTPs) are the endogenous substrates for nature's master architect enzymes, DNA and RNA polymerases. Polymerases build new strands of nucleic acid by catalyzing the reaction of the hydroxyl nucleophile at the C3'-position of the terminal nucleotide with the electrophilic  $\alpha$ -phosphate at the C5'-position of the incoming NTP. The reaction liberates pyrophosphate ( $PP_i$ ) and grows the polymeric strand by one nucleotide via a new 3'-to-5' bridging phosphodiester (Figure 1.1, with RNA shown). Nucleosides must therefore first be anabolized to nucleotides by being phosphorylated by three intracellular kinases.<sup>1</sup>

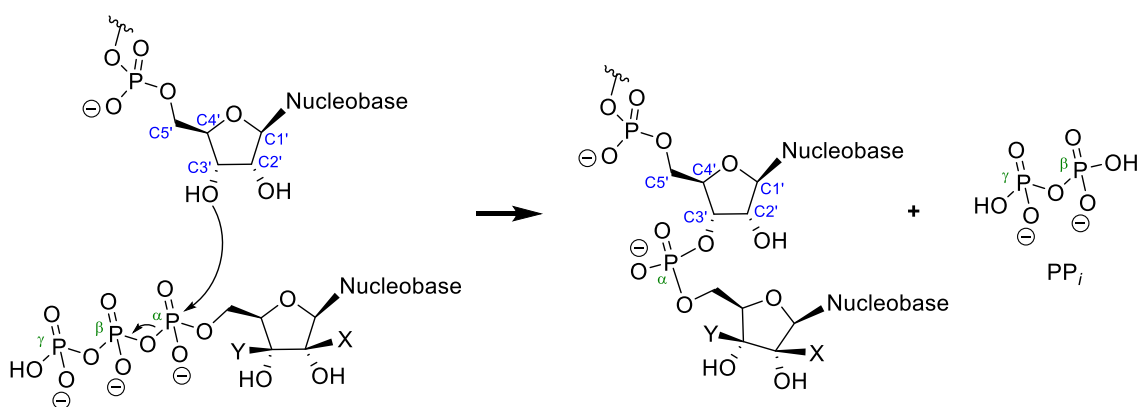


**Figure 1.1.** General annotated structure of a terminal ribonucleotide (top left) and an incoming NTP (bottom left) representing the polymerase chain elongation reaction to extend the nucleic acid polymer by one unit (right). In natural ribonucleosides, X and Y are H atoms.

Compounds that inhibit DNA polymerases lead to terminally ineffective cell replication, while inhibitors of RNA polymerases lead to ineffective transcription of DNA to RNA and eventual cell death

resulting from a lack of protein production.<sup>2</sup> For these reasons, nucleos(t)ides have been of interest to biomedical researchers hoping to eliminate entities engaged in undesired replication at all orders of speciation, including viruses, bacteria, parasites, fungi and human neoplasms.<sup>3</sup> Indeed, one of the first nucleoside-based therapeutics is the natural product spongocytidine (Ara-C), which is the arabinose epimer of the canonical ribonucleoside cytidine (Figure 1.2a). Approved in 1969, it has been considered by the World Health Organization (WHO) to be an essential medicine in the treatment of many cancers of the blood, including non-Hodgkin's Lymphoma, myeloid leukemia, acute lymphatic leukemia and chronic myelogenous leukemia.<sup>3</sup> Another WHO essential medicine which demonstrates the utility of nucleoside-based therapeutics is azidothymidine (AZT, Figure 1.2b), the first approved treatment against human immunodeficiency virus (HIV).<sup>4</sup>

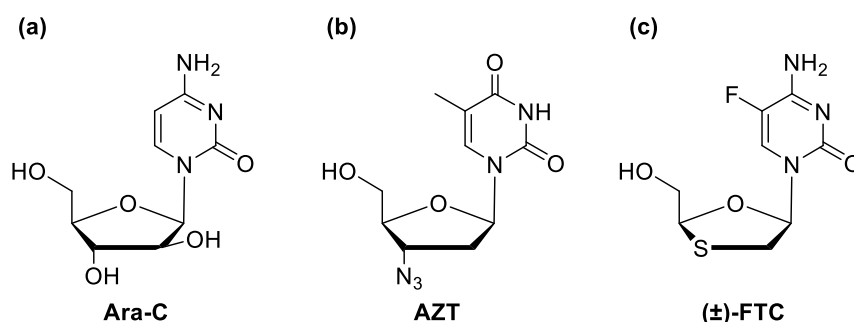


**Figure 1.2.** Structures of (a) spongocytidine (Ara-C) and (b) azidothymidine (AZT), two of the earliest nucleoside analog drugs, as well as (c) (±)-FTC. AZT and FTC are obligate chain terminators of HIV reverse transcriptase, while Ara-C is a non-obligate chain terminator of DNA and RNA polymerases used to treat hematological cancers.

While these two drugs serve to highlight the two most common medical uses of nucleoside analogs (*i.e.*, anticancer and antiviral agents), they also demonstrate structural features which discriminate between nucleoside analogs. Note Ara-C is a simple epimer at the 2' position of cytidine. To have activity, the compound must be a substrate for the necessary kinases, and its triphosphate should be recognized as a substrate by the target polymerase.<sup>5</sup> From where then does its anticancer activity stem? Once Ara-C is incorporated by a DNA (or RNA) polymerase into the growing strand, the polymerase is no longer able to continue efficiently building the elongating strand in spite of the availability of the 3'-OH nucleophile.<sup>2</sup> Such analogs which, like all endogenous nucleosides, contain

the 3'-hydroxyl nucleophile are termed "non-obligate chain terminators" as they terminate the polymerase chain elongation reaction by a non-obvious disturbance of the reaction. Contrast this to the "obligate chain terminators" such as AZT, where the 3'-hydroxyl moiety has been replaced by a non-nucleophilic group. These analogs force termination of the polymerization reaction because they lack the necessary nucleophile to continue building the nascent nucleic acid strand. A further example is emtricitabine ((-)FTC),<sup>6</sup> an obligate chain terminator originally discovered here at Emory and used extensively in the treatment and prophylaxis of HIV. FTC replaces the 3'-hydroxyl and associated carbon atom with a sulfide bridge (Figure 1.2c).

It is worth explicitly stating that compounds which inhibit polymerases can interfere with the endogenous functioning of these enzymes in normal, healthy cells. It is no surprise then that anticancer drugs like Ara-C carry the risk of associated cytotoxicity. But selectivity of target over host can be achieved if nucleosides can be made to inhibit pathogen-specific polymerases more potently than host polymerases. Such is the case with AZT and FTC which target the HIV-specific reverse transcriptase enzyme while leaving the host DNA polymerases largely unaffected at low therapeutic doses.<sup>7</sup> While the source of polymerase inhibition may be obvious and attractive for these obligate chain terminators, the compounds must still be good substrates for the polymerase and preceding kinases. As mentioned above, if they are good substrates for polymerases, they could participate in non-selective inhibition of host polymerases. For this reason, making obligate chain terminators selective for pathogen polymerases is a challenge — even AZT has associated toxicity at higher doses, necessitated by the emergence of viral resistance.<sup>3, 6</sup> The mechanistic basis for inhibition by non-obligate chain terminators is less clear, and it is here where the projects comprising Part I of this dissertation hope to contribute.

## 1.2 A FORAY INTO NUCLEOSIDE-BASED INHIBITORS OF HEPATITIS C

Our lab's interest in antiviral nucleosides naturally predates our success in the arena with emtricitabine. Since the early 1990s,<sup>8, 9</sup> our lab has been interested in antiviral nucleosides with

particular attention to HIV and hepatitis B virus. More recently, our lab has become interested in increasing our molecular understanding of what structural features confer antiviral activity onto some nucleosides but not others. In the field of competitive polymerase inhibitors, the rational design of nucleos(t)ide antivirals is hindered by a lack of mechanistic understanding of how molecular modifications affect inhibition of viral polymerases. Hit identification relies mostly on serendipitous findings, and large activity cliffs emerge upon structural diversification.<sup>10</sup> For example, Eldrup and coworkers<sup>11</sup> synthesized and evaluated sugar-modified purine nucleoside analogs for activity against hepatitis C virus (HCV) and reported that the most active substitution pattern observed in the cell-based replicon assay<sup>12, 13</sup> was 2'-*C*-methylribosides (Figure 1.3a); alternative stereo- and regioisomers of the adenine analog lost all activity. What might account for the specificity of these substituents? HCV is a single-stranded RNA virus whose genetic information codes for its own viral RNA-dependent RNA polymerase (RdRp), the NS5B protein. Therefore, a selective competitive inhibitor of this viral RdRp would need to mimic the polymerase's natural substrate, NTPs containing the ribose sugar scaffold. Thus, the authors rationalized the SAR cliff by the need for the natural 2'- and 3'-hydroxyl groups on the bottom (termed  $\alpha$ ) face as recognition elements combined with steric bulk at the 2' position which appeared necessary to interrupt chain elongation.<sup>11</sup>

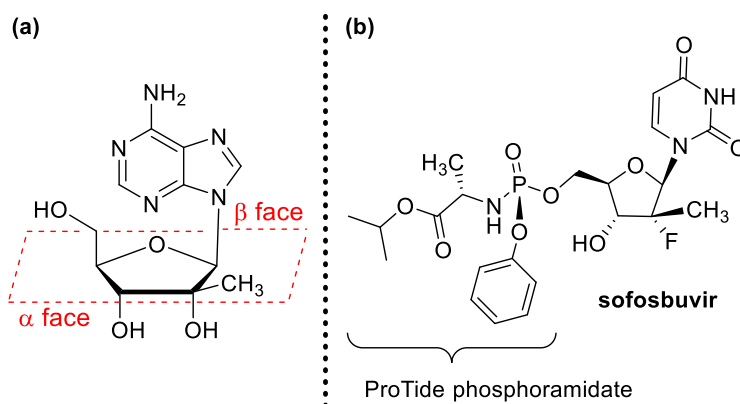


**Figure 1.3.** Structure of (a) 2'-*C*-methyladenosine prepared by Eldrup et al.<sup>10</sup> and (b) sofosbuvir, a ProTide prodrug of the 2'- $\alpha$ -fluoro-2'- $\beta$ -methyluridine nucleoside analog developed by Clark et al.<sup>13</sup> Substituents above the plane of the ribose ring (red dotted line) are termed  $\beta$  while those below are termed  $\alpha$ .

Clearly there is something at play in the substitution pattern of the ribose portion of the nucleoside that affects potency. Are the inactive molecules simply poor substrates for the kinases and never get converted to triphosphates? Do they get converted to their corresponding NTPs, but perhaps are poor substrates for the enzyme and therefore never get incorporated? Do they get incorporated, but simply do not disrupt the polymerase reaction, acting instead as competent mimics of endogenous nucleotides? Whatever the case, their study confirmed the need of the 2'- $\alpha$ -hydroxyl group for potency. Later, Clark and co-workers<sup>14</sup> would show that the 2'- $\alpha$ -hydroxyl group could be effectively replaced with the isosteric fluorine atom in the context of pyrimidine nucleosides while maintaining potency, but the 2'- $\beta$ -methyl group was necessary for selectivity of viral polymerase over host. Indeed, the sugar scaffold of the 2'- $\alpha$ -fluoro-2'- $\beta$ -methylcytidine nucleoside they disclosed would go on to be developed into the uracil-based prodrug sofosbuvir (Figure 1.3b), a current front-line therapy for HCV.

### 1.2.1 Thionucleoside Prodrugs – A Preview of Chapter 2

Another demonstration of subtle changes in the sugar scaffold drastically affecting anti-HCV potency was observed in our own lab and is the subject of Chapter 2 of this dissertation. Summarily, a small series of compounds containing the 2'- $\beta$ -methyl substitution along with a replacement of the ribose ring oxygen with sulfur were made in our lab and tested for antiviral potency in the HCV replicon assay (Figure 1.4). The cell-based replicon assay precludes the use of charged, highly polar NTPs as they fail to cross the cell membrane. The nucleoside itself could have been considered, but activity then relies on cell permeability as well as all three intracellular kinases to anabolize the nucleoside to the NTP. The kinase which installs the initial phosphate moiety is known to be particularly discriminating, leading to poor anabolism and low levels of NTP.<sup>5</sup> One effective solution to this problem is incorporation of a “ProTide” prodrug strategy—the use of an easily metabolized phosphoramidate as a monophosphate pronucleotide.<sup>15</sup> Perrone and co-workers<sup>16</sup> used ProTide technology to turn an inactive parent nucleoside into a sub-micromolar inhibitor of HCV replicons,

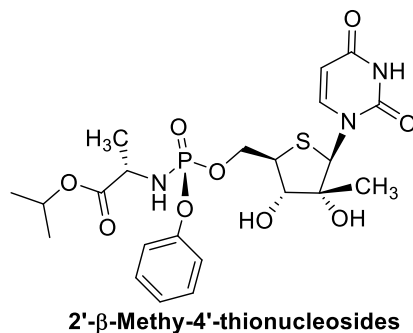


**Figure 1.4.** Structure of our ProTide prodrug of 2'-β-methyl-4'-thiouridine. The synthesis and antiviral evaluation of this and a series of nucleobase analogs is the topic of Chapter 2.

and Sofia and co-workers<sup>17</sup> would then apply this strategy to create sofosbuvir (Figure 1.3b). Each of our thionucleoside analogs was conjugated to this same ProTide phosphoramidate and sent out for testing in the cellular HCV replicon assay (additionally, the uridine and cytidine analogs were converted to their triphosphate and tested in an alternative enzymatic assay). Two things will be apparent from the data shown in Chapter 2: in this context there was a clear preference in the cell-based assay for the natural uracil nucleobase (though there was no significant difference in the cytidine and uridine analogs in the enzymatic assay), but more strikingly, the O-to-S change resulted in a surprising 28-fold loss in potency (2.10 μM compared to 0.03 μM for 2'-C-methyluridine).<sup>18</sup> We became interested in understanding what might account for this loss in potency, and suspected that the changes in bond length and angles associated with sulfur likely leads to a shift in the conformational preference of the compound, which has been shown to affect antiviral activity in other viruses.<sup>19, 20</sup>

### 1.2.2 A Conformational Consideration – A Preview of Chapter 3

In their seminal 1972 publication, Alton and Sundaralingam<sup>21</sup> describe the concept of carbohydrate pseudorotation ( $P$ ) to determine the conformation of the furanose ring in nucleosides. The value of  $P$  depends on the five endocyclic torsion angles of the furanose ring.<sup>20</sup> The authors describe the conformational extremes of the furanose ring in nucleic acids as either C(3')-endo (defined as  $P = 0^\circ$ ) or C(2')-endo ( $P = 180^\circ$ ), where the endo description designates the carbon atom which appears to be on the same face of the sugar as the C5' atom, conventionally the top face (Figure

1.5). Equivalently, where one carbon is labeled endo, the other carbon is labeled exo, and these “sugar puckerings” are generically referred to as North (3'-endo) and South (3'-exo).<sup>22</sup> For our purposes, we will use the endo/exo description at C3' to differentiate between these antipodal conformations. These conformational extremes give rise to structural changes in nucleic acid, as B-DNA crystallizes in the 3'-exo conformation while RNA crystallizes in 3'-endo;<sup>21</sup> however, in solution individual nucleosides are in a rapid equilibrium between the two extremes as the energy barrier for interconversion is low.<sup>20, 22</sup> Plavec and co-workers<sup>23</sup> later established that the main determinants of pseudorotational equilibrium of nucleosides in D<sub>2</sub>O were the stereoelectronic effects of the sugar substituents, in particular the gauche and anomeric effects of the three principal bonding networks: (a) N1-C1'-C2'-O2', (b) O4'-C1'-C2'-O2' and (c) O4'-C4'-C3'-O3'. Marquez and co-workers<sup>19, 20, 24</sup> would then go on to apply this analysis to conformationally locked bicyclic nucleosides and show discrepancies in antiviral activity between the antipodal conformations against herpes simplex virus (HSV) and HIV. Against these viruses, nucleosides locked in the 3'-endo conformation were more potent. Note that the inhibitors of these DNA replication assemblies (*i.e.*, DNA polymerase for HSV and reverse transcriptase for HIV) were more potent with a more RNA-like conformation (3'-endo). Might it be the case, then, that against an RNA polymerase like that of HCV, the opposite more DNA-like 3'-exo conformation would give rise to inhibitors? In support of this notion, the work of Martinez-

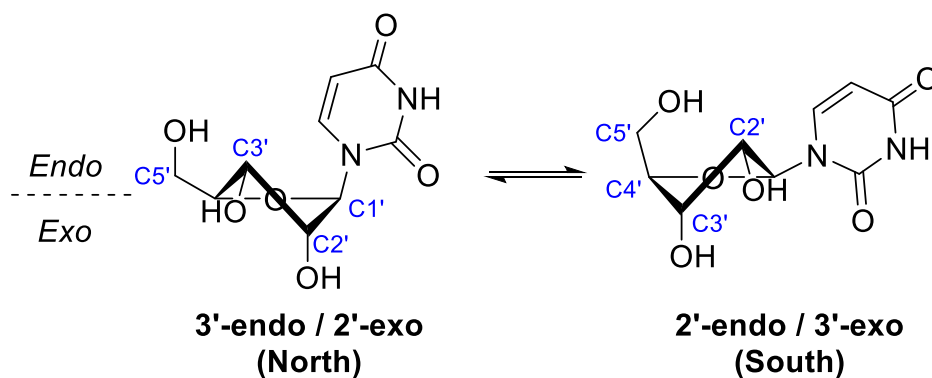


**Figure 1.5.** Equilibrium of the ribose ring conformational antipodes in uridine, with carbon atoms of the sugar ring numbered for clarity. The endo face is above the plane of the ring while the exo face is below.

Montero and co-workers<sup>25</sup> demonstrates that the triphosphate of the 3'-endo (RNA-like) conformationally locked 2',4'- $\alpha$ -difluorouridine indeed gets incorporated into a growing RNA strand by the NS5B polymerase of HCV. However, it does not appear to act as a chain terminator but instead functions to disrupt the initiation of RNA synthesis with only a modest  $IC_{50}$  of 54.7  $\mu$ M. Perhaps if the nucleoside could more readily access the 3'-exo conformation, more potent inhibition via chain termination could be realized.

To investigate the difference in conformational preference between our 4'-thionucleoside analog and its more potent oxo congener, our computational team (comprised of Dr. Christopher Butch and his student Kiraney Zhang) used density functional theory (DFT) calculations to assess the enthalpy associated with the compounds as they assume either the 3'-endo and 3'-exo conformational extremes (Figure 1.6). The difference in enthalpy between the two conformations ( $\Delta E_{\text{exo-endo}}$ ) represents a scoring function which should correspond to a thermodynamic conformational preference for the lower energy conformer. Larger, more positive scores correspond to a larger preference for the 3'-endo conformation while lower, more negative scores correspond to a preference for the 3'-exo conformation; a score close to 0 would indicate the two conformations were of similar energy and no particular preference would be expected. The DFT calculations for 2'- $\beta$ -methyluridine gave a  $\Delta E_{\text{exo-endo}}$  score of 0.0197 Hartree, whereas our 4'-thio congener has a score

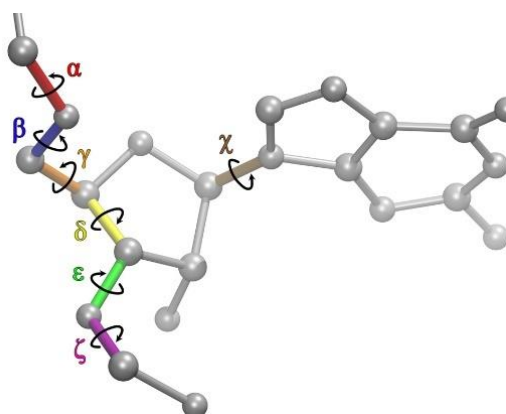


**Figure 1.6.** Rendering of the seven torsional parameters considered by the RNA force fields used in DFT. Image courtesy of Dr. C. Butch.

of 0.0238 Hartree. This 0.0041 Hartree difference corresponds to a roughly 2.6 kcal/mol difference in energy, on the order of an eclipsing vicinal CH<sub>3</sub>-H interaction. This indicates that the swap from oxygen to sulfur biases the conformational preference further towards the RNA-like 3'-endo conformation.

This led us to wonder if this conformational preference impacted anti-HCV potency. More precisely, we wondered whether a compound's energetic ease of access to the 3'-exo conformation corresponded with a compound's ability to disrupt the kinetics of incorporation of the subsequent nucleotide in the elongation reaction.<sup>26</sup> To investigate this proposal, the IC<sub>50</sub> data for these compounds as well as a dozen other in-house nucleotides were plotted against their conformational scores, and a correlation emerged (Figure 1.7a). Compounds with larger scores indicative of a stronger energetic bias towards the 3'-endo conformation tended to have poor potency. Alignments of the two conformers in the active site further demonstrated a catalytically compromised geometry for the 3'-exo conformer compared to the 3'-endo (Figure 1.7b and c). With these pieces of data, the following mechanistic rationale was proposed: in the active site, a Boltzmann distribution of conformers exists in a dynamic equilibrium between the 3'-endo and 3'-exo antipodes. The 3'-endo conformer appears more catalytically competent than the 3'-exo, so if a larger proportion of the Boltzmann population takes on the 3'-exo conformation, then that should correspond to an increase

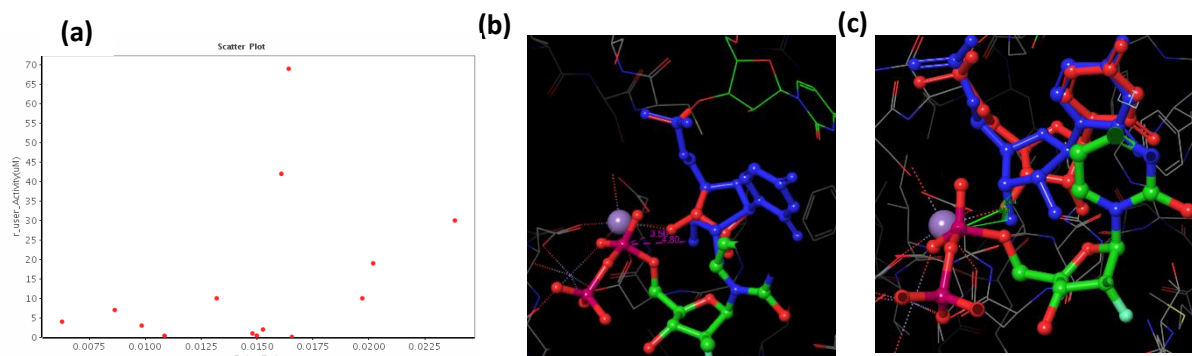


**Figure 1.7.** (a) Scatter plot of NTP IC<sub>50</sub> (μM) vs  $\Delta E_{\text{exo-endo}}$ . Compounds with lower scores (<0.02) tend to be more potent. (b) Comparison of the 3'-exo (blue) and 3'-endo (red) chain terminal conformations in the polymerase active site showing the maximal common alignment, and distances (Å) from the incoming phosphate. The catalytic Mg center (purple) and the incoming nucleotide (green) are also shown. (c) The full molecule alignment shows the changes in angle of the 3' hydroxyl to the incoming phosphate.

in the relative transition state energy for the overall elongation reaction. This effective increase in transition state energy slows the reaction down enough to disrupt the ternary complex of polymerase, template strand and growing strand and therefore inhibits the reaction (Figure 1.8). Hence, compounds that have a larger 3'-endo preference (like our 4'-thio analog) would be precluded from being good inhibitors because of the larger enthalpic penalty to access the 3'-exo conformation.

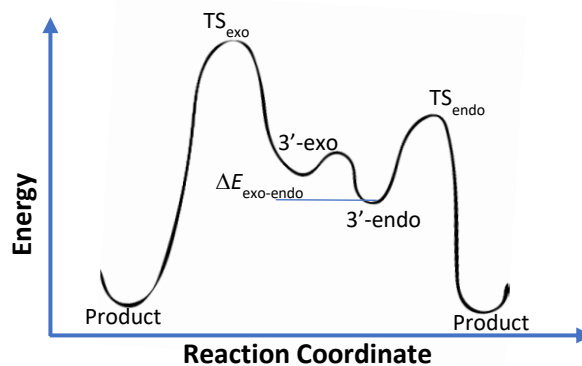


**Figure 1.8.** A reaction coordinate diagram showing the proposed difference in transition state energies of the 3'-endo and exo antipodes in the active site. Decreasing  $\Delta E_{exo-endo}$  should bias the conformational equilibrium towards the 3'-exo antipode. Consequently, if a larger proportion of the terminal nucleotide Boltzmann population is biased toward the 3'-exo conformer, this will slow the kinetics of elongation, lowering the catalytic efficiency enough to disrupt and inhibit the reaction. Conversely, a 3'-endo bias would yield a poorer inhibitor.

This should not be understood to suggest that compounds necessarily need to have a complete 3'-exo bias (*i.e.*, a negative score) to be good inhibitors. Indeed, the sofosbuvir nucleoside has a score of 0.0148 Hartree and the triphosphate has an  $IC_{50}$  of 1  $\mu$ M. Moreover, Marquez<sup>20</sup> has shown in the context of HSV that the viral kinase prefers the opposite antipode (3'-exo) from cellular DNA polymerase (3'-endo), so an ability to access both conformations seems beneficial if not necessary. The model also does not guarantee that compounds with a relatively low score will be good inhibitors. For example, unmodified canonical uridine has a score of 0.010 Hartree and is clearly not an inhibitor (though it is obviously a good substrate). Rather, the model simply suggests that a score function of less than 0.02 Hartree appears necessary but not sufficient for a nucleoside to be a good inhibitor of HCV. This score then could serve as a rational design parameter for the chemist to consider when proposing new nucleoside polymerase inhibitors.

Taken together, these studies led us to start a prospective investigation of the model with sugar-modified analogs of 2'-*C*-methyluridine, itself a reasonable inhibitor of HCV (NTP: 10  $\mu$ M, ProTide: 0.03  $\mu$ M), and this work is the subject of Chapter 3 of this dissertation. We proposed to modify the ribose ring at the C3' position to shift the conformational equilibrium in a computationally predicted direction. From the common synthetic intermediate of the 3'-ketone, we envisioned adding two different alkyl groups (acetylide or methyl) to produce novel 2',3'-dialkylated nucleosides, each of which is predicted to shift the equilibrium strongly but in opposing directions (Figure 1.9). The 2'- $\beta$ -methyl-3'- $\beta$ -ethynyluridine analog **1.1** has a score of 0.001 Hartree, the lowest positive score we've encountered in our small library, while the 2',3'- $\beta$ -dimethyluridine analog **1.3** would have the highest score at 0.089 Hartree. In this way, these two compounds test the extrema of the model. The model suggests that the methyl analog **1.3** would be highly biased towards the 3'-endo conformer and therefore be a poor inhibitor, while the ethynyl analog **1.1** would pay a significantly lower energetic penalty to access the purportedly active 3'-exo conformation. Since the 3'-exo conformation should be energetically more accessible to this analog, the model suggests it could have improved antiviral potency relative to the parent compound (**1.2**). The details and results of these studies will now be disclosed in the rest of Part I.

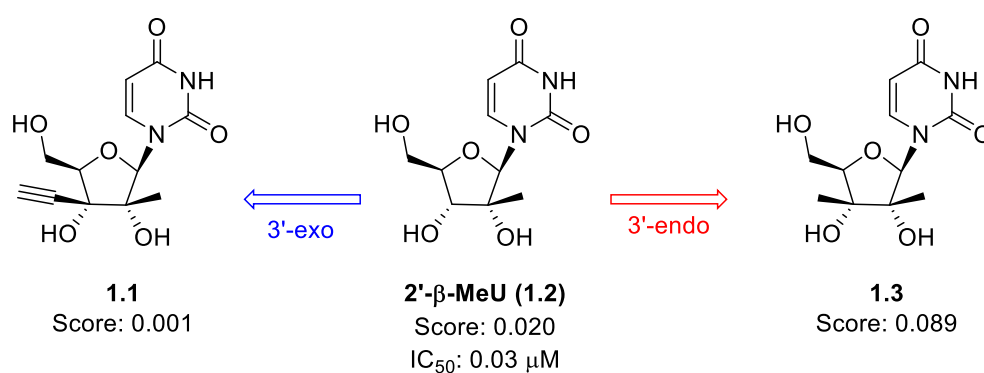


**Figure 1.9.** Structures of the parent molecule 2'- $\beta$ -methyluridine (**1.2**) and the proposed 3'-modified analogs with associated model scores (in Hartree units). The synthesis and antiviral evaluation of these novel disubstituted nucleoside analogs is the subject of Chapter 3.

### 1.3 REFERENCES AND NOTES

- De Clercq, E., Strategies in the design of antiviral drugs. *Nat. Rev. Drug Discov.* **2002**, *1* (1), 13-25.

2. Shelton, J.; Lu, X.; Hollenbaugh, J. A.; Cho, J. H.; Amblard, F.; Schinazi, R. F., Metabolism, Biochemical Actions, and Chemical Synthesis of Anticancer Nucleosides, Nucleotides, and Base Analogs. *Chem. Rev.* **2016**, *116* (23), 14379-14455.
3. Seley-Radtke, K. L.; Yates, M. K., The evolution of nucleoside analogue antivirals: A review for chemists and non-chemists. Part 1: Early structural modifications to the nucleoside scaffold. *Antiviral Res* **2018**, *154*, 66-86.
4. Broder, S., The development of antiretroviral therapy and its impact on the HIV-1/AIDS pandemic. *Antiviral Res.* **2010**, *85* (1), 1-18.
5. Murakami, E.; Bao, H. Y.; Ramesh, M.; McBrayer, T. R.; Whitaker, T.; Steuer, H. M. M.; Schinazi, R. F.; Stuyver, L. J.; Obikhod, A.; Otto, M. J.; Furman, P. A., Mechanism of activation of beta-D-2'-deoxy-2'-fluoro-2'-C-methylcytidine and inhibition of hepatitis C virus NS5B RNA polymerase. *Antimicrob. Agents Chemother.* **2007**, *51* (2), 503-509.
6. Liotta, D. C.; Painter, G. R., Discovery and Development of the Anti-Human Immunodeficiency Virus Drug, Emtricitabine (Emtriva, FTC). *Acc. Chem. Res.* **2016**, *49* (10), 2091-2098.
7. Mitsuya, H.; Weinhold, K. J.; Furman, P. A.; St Clair, M. H.; Lehrman, S. N.; Gallo, R. C.; Bolognesi, D.; Barry, D. W.; Broder, S., 3'-Azido-3'-deoxythymidine (BW A509U): an antiviral agent that inhibits the infectivity and cytopathic effect of human T-lymphotropic virus type III/lymphadenopathy-associated virus in vitro. *Proc. Natl. Acad. Sci. U.S.A.* **1985**, *82* (20), 7096-7100.
8. Wilson, L. J.; Liotta, D., A general method for controlling glycosylation stereochemistry in the synthesis of 2'-deoxyribose nucleosides. *Tetrahedron Lett.* **1990**, *31* (13), 1815-1818.
9. Doong, S. L.; Tsai, C. H.; Schinazi, R. F.; Liotta, D. C.; Cheng, Y. C., Inhibition of the replication of hepatitis B virus in vitro by 2',3'-dideoxy-3'-thiacytidine and related analogues. *Proc Natl Acad Sci U S A* **1991**, *88* (19), 8495-9.
10. De Clercq, E., Curious Discoveries in Antiviral Drug Development: The Role of Serendipity. *Med. Res. Rev.* **2015**, *35* (4), 698-719.
11. Eldrup, A. B.; Allerson, C. R.; Bennett, C. F.; Bera, S.; Bhat, B.; Bhat, N.; Bosserman, M. R.; Brooks, J.; Burlein, C.; Carroll, S. S.; Cook, P. D.; Getty, K. L.; MacCoss, M.; McMasters, D. R.; Olsen, D. B.; Prakash, T. P.; Prhavc, M.; Song, Q. L.; Tomassini, J. E.; Xia, J., Structure-activity relationship of purine ribonucleosides for inhibition of hepatitis C virus RNA-dependent RNA polymerase. *J. Med. Chem.* **2004**, *47* (9), 2283-2295.
12. Lohmann, V.; Korner, F.; Koch, J. O.; Herian, U.; Theilmann, L.; Bartenschlager, R., Replication of subgenomic hepatitis C virus RNAs in a hepatoma cell line. *Science* **1999**, *285* (5424), 110-113.
13. Krieger, N.; Lohmann, V.; Bartenschlager, R., Enhancement of hepatitis C virus RNA replication by cell culture-adaptive mutations. *J. Virol.* **2001**, *75* (10), 4614-4624.
14. Clark, J. L.; Hollecker, L.; Mason, J. C.; Stuyver, L. J.; Tharnish, P. M.; Lostia, S.; McBrayer, T. R.; Schinazi, R. F.; Watanabe, K. A.; Otto, M. J.; Furman, P. A.; Stec, W. J.; Patterson, S. E.; Pankiewicz, K. W., Design, synthesis, and antiviral activity of 2'-deoxy-2'-fluoro-2'-C-methylcytidine, a potent inhibitor of hepatitis C virus replication. *J. Med. Chem.* **2005**, *48* (17), 5504-5508.
15. Murakami, E.; Niu, C. R.; Bao, H. Y.; Steuer, H. M. M.; Whitaker, T.; Nachman, T.; Sofia, M. A.; Wang, P. Y.; Otto, M. J.; Furman, P. A., The mechanism of action of beta-D-2'-Deoxy-2'-fluoro-2'-C-methylcytidine involves a second metabolic pathway leading to beta-D-2'-deoxy-2'-fluoro-2'-C-methyluridine 5'-triphosphate,

a potent inhibitor of the hepatitis C virus RNA-dependent RNA polymerase. *Antimicrob. Agents Chemother.* **2008**, *52* (2), 458-464.

16. Perrone, P.; Daverio, F.; Valente, R.; Rajyaguru, S.; Martin, J. A.; Leveque, V.; Le Pogam, S.; Najera, I.; Klumpp, K.; Smith, D. B.; McGuigan, C., First example of phosphoramidate approach applied to a 4'-substituted purine nucleoside (4'-azidoadenosine): Conversion of an inactive nucleoside to a submicromolar compound versus hepatitis C virus. *J. Med. Chem.* **2007**, *50* (22), 5463-5470.

17. Sofia, M. J.; Bao, D.; Chang, W.; Du, J. F.; Nagarathnam, D.; Rachakonda, S.; Reddy, P. G.; Ross, B. S.; Wang, P. Y.; Zhang, H. R.; Bansal, S.; Espiritu, C.; Keilman, M.; Lam, A. M.; Steuer, H. M. M.; Niu, C. R.; Otto, M. J.; Furman, P. A., Discovery of a beta-D-2'-Deoxy-2'-alpha-fluoro-2'-beta-C-methyluridine Nucleotide Prodrug (PSI-7977) for the Treatment of Hepatitis C Virus. *J. Med. Chem.* **2010**, *53* (19), 7202-7218.

18. The difference in the enzymatic assay was consistent with this though less pronounced.

19. Marquez, V. E.; Ezzitouni, A.; Russ, P.; Siddiqui, M. A.; Ford, H.; Feldman, R. J.; Mitsuya, H.; George, C.; Barchi, J. J., HIV-1 Reverse Transcriptase Can Discriminate between Two Conformationally Locked Carbocyclic AZT Triphosphate Analogues. *J. Am. Chem. Soc.* **1998**, *120* (12), 2780-2789.

20. Marquez, V. E.; Ben-Kasus, T.; Barchi, J. J.; Green, K. M.; Nicklaus, M. C.; Agbaria, R., Experimental and Structural Evidence that Herpes 1 Kinase and Cellular DNA Polymerase(s) Discriminate on the Basis of Sugar Pucker. *J. Am. Chem. Soc.* **2004**, *126* (2), 543-549.

21. Altona, C.; Sundaralingam, M., Conformational analysis of the sugar ring in nucleosides and nucleotides. New description using the concept of pseudorotation. *J. Am. Chem. Soc.* **1972**, *94* (23), 8205-8212.

22. Saenger, W., *Principles of Nucleic Acid Structure*. Springer Science & Business Media: 2013.

23. Plavec, J.; Tong, W.; Chattopadhyaya, J., How do the gauche and anomeric effects drive the pseudorotational equilibrium of the pentofuranose moiety of nucleosides? *J. Am. Chem. Soc.* **1993**, *115* (21), 9734-9746.

24. Marquez, V. E.; Siddiqui, M. A.; Ezzitouni, A.; Russ, P.; Wang, J.; Wagner, R. W.; Matteucci, M. D., Nucleosides with a Twist. Can Fixed Forms of Sugar Ring Pucker Influence Biological Activity in Nucleosides and Oligonucleotides? *J. Med. Chem.* **1996**, *39* (19), 3739-3747.

25. Martínez-Montero, S.; Deleavey, G. F.; Kulkarni, A.; Martín-Pintado, N.; Lindovska, P.; Thomson, M.; González, C.; Götte, M.; Damha, M. J., Rigid 2',4'-Difluororibonucleosides: Synthesis, Conformational Analysis, and Incorporation into Nascent RNA by HCV Polymerase. *J. Org. Chem.* **2014**, *79* (12), 5627-5635.

26. Fung, A.; Jin, Z. N.; Dyatkina, N.; Wang, G. Y.; Beigelman, L.; Deval, J., Efficiency of Incorporation and Chain Termination Determines the Inhibition Potency of 2'-Modified Nucleotide Analogs against Hepatitis C Virus Polymerase. *Antimicrob. Agents Chemother.* **2014**, *58* (7), 3636-3645.

## Chapter 2. Synthesis and Antiviral Evaluation of a Series of 4'-Thio Congeners of 2'-C-Methyl-Substituted Ribonucleoside Prodrugs

Reproduced under the terms and conditions of the Creative Commons Attribution (CC BY) 4.0 license (<http://creativecommons.org/licenses/by/4.0/>) from (Zackery W. Dentmon, Thomas M. Kaiser and Dennis C. Liotta, Synthesis and Antiviral Activity of a Series of 2'-C-Methyl-4'-thionucleoside Monophosphate Prodrugs, *Molecules* **2020**, *25*, 5165.

<https://doi.org/10.3390/molecules25215165>)

Copyright © 2020 by the authors.

### 2.1 INTRODUCTION

Scientists have long been interested in the medicinal applications of non-canonical nucleosides and nucleotides due to their privileged bioactivity. Beginning in the late 1950s with idoxuridine (5-iodo-2'-deoxyuridine, see Figure 2.1a), modified nucleosides and nucleotides have found use predominantly as anti-neoplastics and antivirals for their ability to inhibit nucleic acid polymerization and replication by competing with nucleoside triphosphates (NTPs), the natural substrates of nucleic acid polymerases.<sup>1,2</sup> Cytarabine (arabinocytidine, Ara-C) was first approved by the FDA in 1969 and is still considered by the World Health Organization to be an essential medicine for cancers of the blood.<sup>3</sup> Likewise, 3'-azidothymidine (AZT), the first approved treatment against human immunodeficiency virus (HIV), also appears on this list along with a dozen other nucleos(t)ide analogs acting as antivirals alone.<sup>2-4</sup>

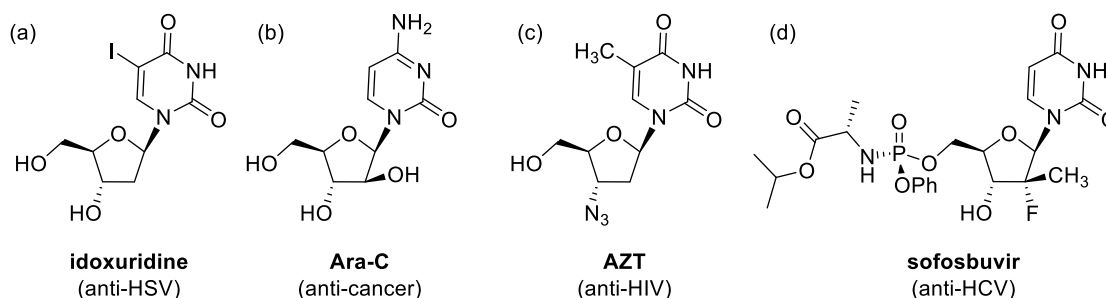


**Figure 2.1.** Examples of early modified nucleoside drugs (a–c) and the aryloxy phosphoramidate monophosphate prodrug sofosbuvir (d).

One such compound is sofosbuvir, a monophosphate prodrug of 2'- $\beta$ -methyl-2'- $\alpha$ -fluorouridine (Figure 2.1d). Approved in late 2013 for the treatment of chronic hepatitis C virus (HCV) infection, sofosbuvir has altered the landscape of HCV therapy.<sup>5, 6</sup> No fewer than 15 nucleos(t)ide analogs have gone into clinical trials for HCV since the early 2000s, and only sofosbuvir has been approved by both the US FDA and EU regulatory agencies. Furthermore, nearly all of the aforementioned analogs share the common 2'- $\beta$ -methyl sugar scaffold originally disclosed by Merck in 2003.<sup>7</sup> In addition to disrupting RNA chain elongation, subsequent studies showed the value of the 2'-methyl group in conferring selectivity of this class for the non-structural protein (NS5B) viral RNA-dependent RNA polymerase (RdRp) over host RNA polymerase.<sup>8-11</sup> Sofosbuvir also bears the hepatic-directing ProTide monophosphate prodrug moiety pioneered by Christopher McGuigan and co-workers at Cardiff University.<sup>12, 13</sup> Their lab has utilized ProTide technology to turn inactive parent nucleosides into sub-micromolar inhibitors of HCV replicons.<sup>14, 15</sup> Chemical incorporation of the first 5'-*O*-phosphoryl moiety with an easily metabolized phosphoramidate creates a monophosphate pronucleotide, bypassing the particularly discriminating first kinase in the phosphorylation cascade, which is known to be a culprit of poor anabolism and low levels of NTP.<sup>16-18</sup> It stands to reason then that these two structural features (2'- $\beta$ -methyl and 5'-phosphoramidate prodrug moieties) would be key design elements in the interrogation of next-generation NS5B inhibitors.

What structural feature(s) would set the next generation of nucleos(t)ide analogs apart from sofosbuvir? According to Michael Sofia, co-inventor of sofosbuvir, to compete with sofosbuvir a molecule would need to deliver an advantage in either its resistance profile or its pharmacokinetics (PK).<sup>6</sup> With regards to PK, the issues involve the interaction with intestinal *P*-glycoprotein and catabolism to the major metabolite – the corresponding dephosphorylated uridine nucleoside, which is cleared through renal secretion. These issues pose opportunities for a compound with alternative

metabolism leading to lower renal clearance, longer systemic half-life, and decreased treatment duration. Hence, alternative nucleobases and sugar modifications should be explored to this end.

Nucleosides with non-natural sugar ring composition have been successfully used to treat other viral diseases (Figure 2.2a). Acyclovir and tenofovir are acyclic nucleoside analogs while abacavir and entecavir are carbocyclic examples, all of which are essential antiviral medicines against herpes simplex virus (HSV), HIV, or HBV. In addition, lamivudine and emtricitabine are also on this list against HIV and they contain a 3'-thia substitution in the ring, the latter of which was discovered in our lab.<sup>3,19</sup> Replacement of the furanose 4'-oxygen with bioisosteric sulfur has also attracted some attention (Figure 2.2b).<sup>20, 21</sup> Bobek first synthesized 4'-thionucleosides in the early 1970s, which showed interesting antibiotic and anti-cancer activity.<sup>22,23</sup> In the 1990s, Dyson et al. showed antiviral activity of 2'-deoxy-4'-thiopyrimidines against HSV, Varicella Zoster virus (VZV), and cytomegalovirus (CMV),<sup>24</sup> while Secrist III showed anti-HIV activity with 2',3'-dideoxy-4'-thionucleosides.<sup>25</sup> Van Draanen and co-workers showed promising activity against HBV and CMV with 2'-deoxy-4'-thiopurine analogs.<sup>26</sup> Most of these authors make note of the differential metabolism of the sulfur analog compared to the 4'-oxo congener, in particular the resistance of the 4'-thio analogs to nucleoside phosphorylase. In one of the more provocative examples of the 4'-thio substitution in the literature, Yoshimura and colleagues showed that the swap from oxygen to sulfur in the sugar ring conferred low- to sub-micromolar antiviral activity onto previously inactive arabinopurines against HSV and CMV.<sup>27</sup> More recently in the context of HCV, a 2006 patent application by Merck disclosed 2'- $\beta$ -methyl-4'-thiopurines for use against NS5B.<sup>28</sup> In 2014 Idenix filed a patent claiming the triphosphates of 4'-thioguanosine, 4'-thiouridine, and 2'- $\beta$ -methyl-4'-thiouridine, as well as monophosphate prodrugs of the latter two, for the treatment of HCV;<sup>29</sup> they were acquired by Merck that same year, purportedly for their anti-HCV portfolio. It was out of this context that we became interested in supplementing the work of Idenix on this intriguing chemotype.

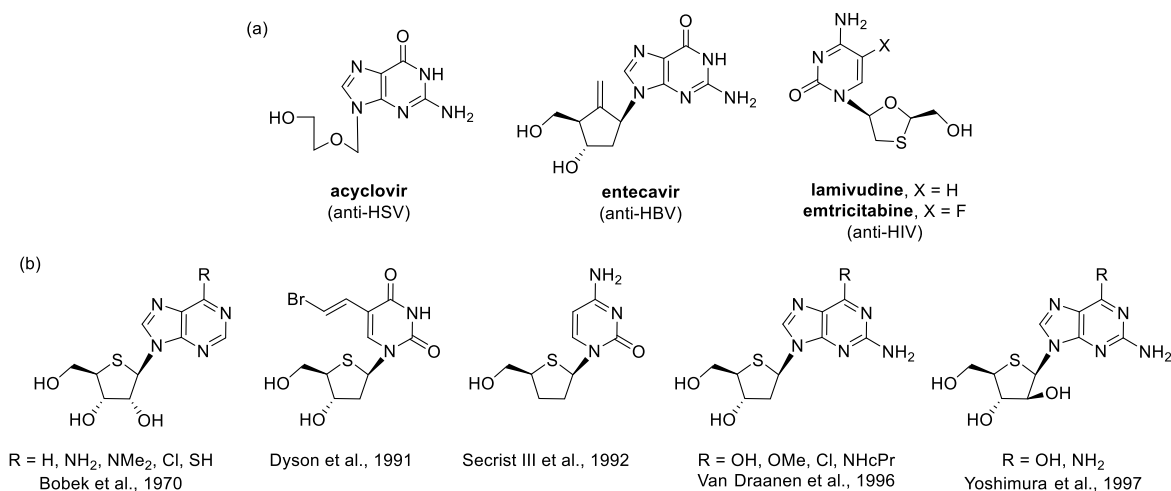


**Figure 2.2.** Representative examples of (a) essential antiviral nucleosides with non-natural sugar ring compositions, and (b) historical 4'-thionucleoside analogs having notable bioactivity.

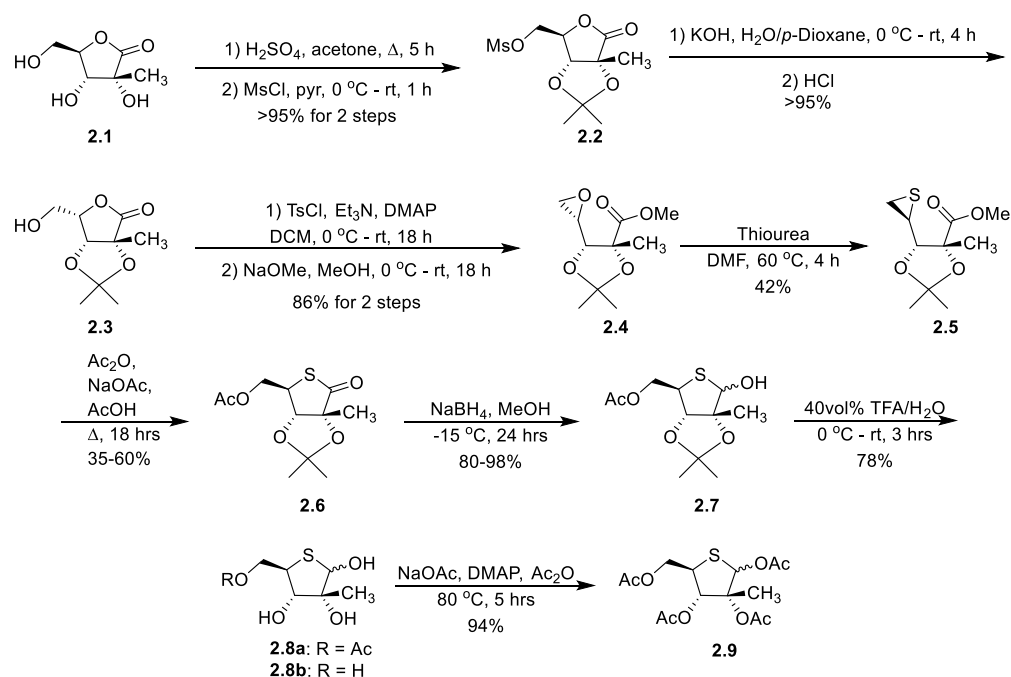
## 2.2 RESULTS AND DISCUSSION

### 2.2.1 Synthesis of the 4'-Thionucleosides & Phosphoramidate Prodrugs

#### 2.2.1.1 Synthesis of the Thiosugar Core

The synthesis of the target nucleosides began with the construction of the thiosugar core. Following the precedent disclosed by Dukhan and co-workers,<sup>30</sup> the synthesis started from the chiral building block 2-methyl-D-ribo-1,4-lactone (**2.1**, Scheme 2.1). After protecting the 2,3-diol system as an acetonide, the remaining primary alcohol at C5 was activated for displacement by conversion to the corresponding mesylate. Mesylate **2.2** presumably undergoes intramolecular attack by the 4-alkoxide liberated by selective saponification of the lactone with aqueous KOH. The resulting intermediate 4,5-epoxide is not isolated but protonated and hydrolyzed *in situ* upon treatment with aqueous HCl, resulting in subsequent acid-mediated lactonization and inversion of the stereocenter at C4. This inversion to the L-lyxonolactone **2.3** is necessary for overall retention of stereochemistry after an ensuing inversion to install the sulfur atom (*vide infra*). The addition of 1,4-dioxane as co-solvent for this reaction improved the yield from 55% as reported by Dukhan et al.<sup>30</sup> to essentially quantitative. Then, the primary alcohol was again activated and displaced upon transesterification of

the lactone with NaOMe to form the 4,5-epoxide. Treatment of epoxide **2.4** with thiourea incorporated the desired sulfur atom at C4 with inversion of stereochemistry, though the yield never improved beyond 50% despite substantial optimization efforts. Opening of the resulting thiirane **2.5** with acetate under refluxing acidic conditions was complicated by regioselectivity issues, producing a separable mixture of both the five- and six-membered thiolactones, accounting for another poorly yielding step even after extensive optimization. The desired five-membered thiolactone **2.6** was smoothly reduced to the corresponding thiolactol **2.7** (as a mixture of anomers) with NaBH<sub>4</sub> in methanol at reduced temperature. Finally, acid hydrolysis of the acetonide revealed the 2,3-diol (with partial hydrolysis of the 5-*O*-acetyl ester), and the per-acetylated thiosugar **2.9** was accessed upon treatment of the mixture of **2.8a** and **2.8b** with acetic anhydride and 4-(dimethylamino)pyridine (DMAP), which was a necessary acyl transfer catalyst to esterify the tertiary alcohol at C2 efficiently.



**Scheme 2.1.** Multistep synthesis of the per-acetylated thiosugar core.

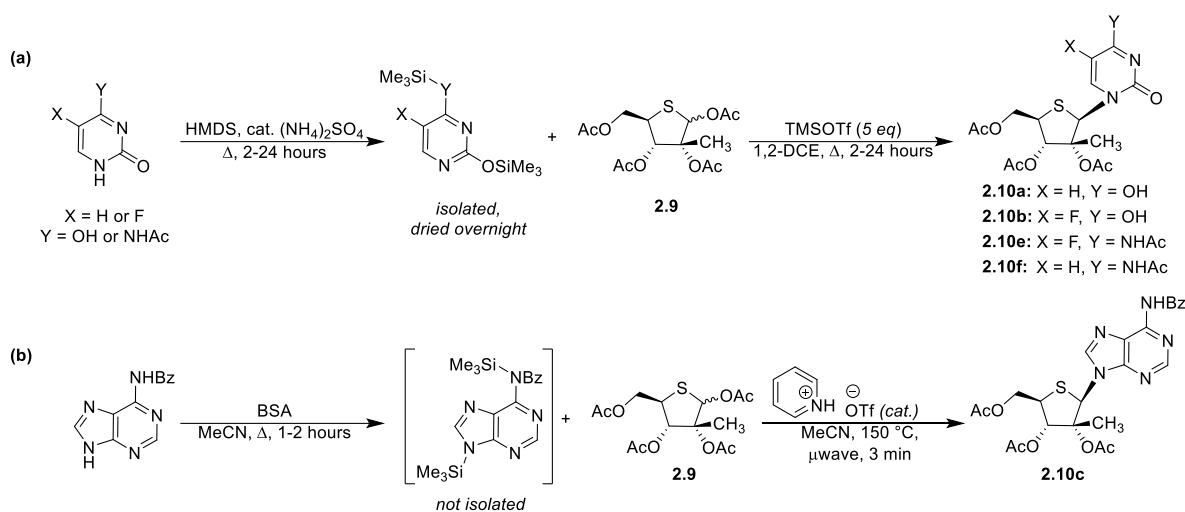
### 2.2.1.2 Thionucleoside Analog Synthesis

With the per-acetylated thiosugar core (**2.9**) in hand, nucleoside analogs could be made via the stereoselective Vorbrüggen glycosylation of the nucleobases of interest. Vorbrüggen's

methodology generally makes use of a per-silylated heterocyclic nucleobase as glycosyl acceptor and a potent Lewis acid to activate the glycosyl donor for coupling to the nucleobase.<sup>31</sup> In the presence of a Lewis acid (e.g., trimethylsilyl triflate or tin tetrachloride), the (thio)acetal at C1 of the glycosyl donor is thought to form an  $\alpha$ -chalcogen-stabilized carbenium ion, which is then intramolecularly trapped by the adjacent ester at C2 to delocalize the positive charge around a newly formed 1,3-dioxolane ring fused to the bottom of the sugar. This anchimeric assistance provides the basis for the stereoselective “top-side”  $\beta$ -addition of the silylated glycosyl acceptor nucleobase.<sup>32</sup> For its part, silylation of the nucleobase is reported to have two important effects—increased nucleophilicity and organic solubility of the nucleobase. The observation that trimethylsilyl (TMS) groups increase organic solubility is likely unsurprising given the lipophilicity of organosilicon compounds. However, the key benefit lies in the electron-releasing properties of silicon to impart increased nucleophilicity to the Lewis basic nitrogen atoms.<sup>33</sup>

Nucleobases were glycosylated using either one of two related yet distinct two-step protocols. The classical protocol (Scheme 2.2a) relies on pre-silylating the nucleobase by refluxing with neat hexamethyldisilazane (HMDS) in the presence of catalytic ammonium sulfate until the initially heterogeneous reaction mixture clarified.<sup>31</sup> This now persilylated nucleobase must be carefully concentrated to remove all traces of HMDS without exposure to moisture, as it easily hydrolyzes; failure to do so results in diminished yields of the glycosylated product. The concentrated crude persilylated nucleobase was then dissolved in 1,2-dichloroethane (DCE) and treated with **2.9** and TMS triflate (TMSOTf) under reflux conditions to afford the desired glycosylated product in good to excellent yields and diastereoselectivity. This protocol worked well for the natural and 5-fluorinated pyrimidine bases but struggled to produce the corresponding adenosine analog in an acceptable yield. Hence, an alternative procedure published by Sniady and co-workers<sup>34</sup> was employed, which utilizes *N,O*-bis(trimethylsilyl)acetamide (BSA) as silylating agent and pyridinium triflate instead as a Brønsted acid catalyst under microwave irradiation in acetonitrile solvent

(Scheme 2.2b). Following these conditions, *N*-benzoyl-protected adenine was first refluxed with BSA in acetonitrile solvent for an hour before this crude reaction mixture was used directly to treat a solution of **2.9** and catalytic pyridinium triflate in acetonitrile. Microwave irradiation of the reaction mixture to 150 °C for only 3 minutes afforded the desired adenosine analog **2.10c** in 84% yield. These same microwave-assisted reaction conditions additionally afforded the 6-azauridine analog **2.10d** in 89% yield but did not prove generally reproducible with other pyrimidine nucleobases (*e.g.*, uracil and cytosine).



**Scheme 2.2.** Two-step sequences used for glycosylation of nucleobases; (a) classical Vorbrüggen glycosylation sequence<sup>31</sup>; (b) modified microwave-assisted glycosylation using catalytic Brønsted acid<sup>34</sup>.

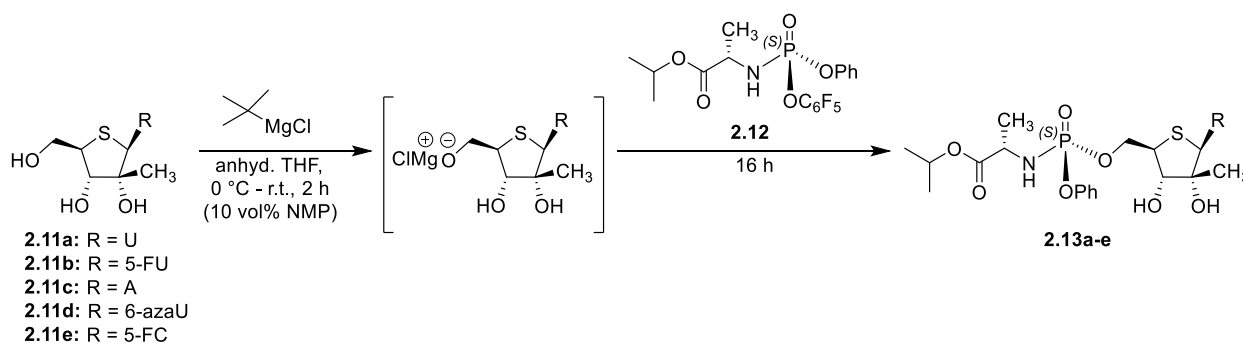
Interestingly, the two procedures could be successfully hybridized to a sequential one-pot reaction, using BSA as silylating agent in DCE solvent, followed by direct treatment with the glycosyl donor (**2.9**) and TMSOTf and heating to reflux. The use of BSA as silylating agent represents an improvement in efficiency over HMDS as the presence of excess BSA and silylation byproducts do not appear to impact the glycosylation reaction. Indeed, following an even more streamlined procedure published by Haluszczak et al.,<sup>35</sup> uracil could be combined with BSA and per-acetylated thiosugar **2.9** in 1,2-DCE and refluxed with TMSOTf to afford the glycosylated product in a single step with >90% yield, though diastereoselectivity was somewhat diminished (ca. 10:1 instead of 20:1). Once the glycosylated products were accessed, the free nucleoside analogs **2.11a-f** were prepared upon

ammonolysis of the acetyl esters by heating with ammonia in methanol in a sealed tube. Notably, while guanine may have completed a structure–activity relationship (SAR) study of the natural nucleobases, it was considered strategically undesirable due to synthetic and toxicological concerns.

### 2.2.1.3 Synthesis of the Phosphoramidate Monophosphate Prodrugs

Evaluation of the compounds in the cell-based replicon assay precludes the use of charged, highly polar NTPs as they fail to cross the cell membrane. The nucleoside itself could be considered, but antiviral activity then relies on cell permeability as well as all three intracellular kinases to anabolize the nucleoside to the NTP. Hence, the aryloxy phosphoramidate monophosphate prodrug utilized for sofosbuvir seemed like an obvious choice for testing the compounds (*vide supra*).

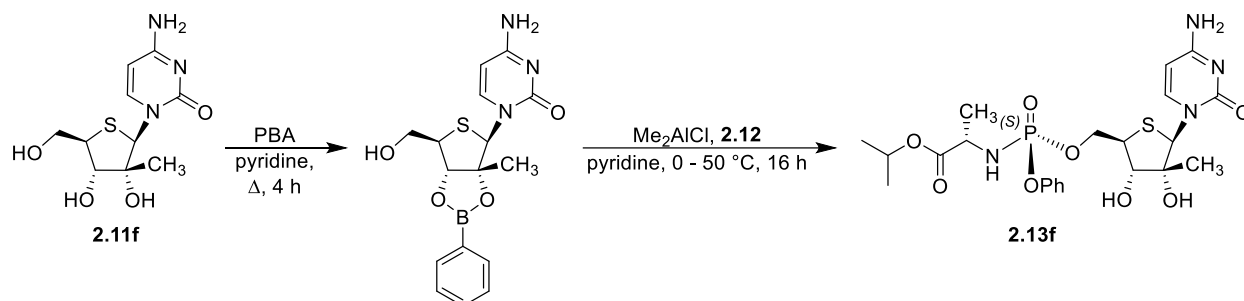
From the free nucleoside, the 5'-hydroxyl group needs to react selectively in the presence of the secondary and tertiary alcohols at C3' and C2', respectively. Additionally, nucleosides with an exocyclic amine (*i.e.*, cytidine and adenosine analogs) present an additional selectivity challenge. The use of the strong base *tert*-butylmagnesium chloride is one common approach to achieve this goal as the steric bulk of the *tert*-butyl group allows for a kinetic preference for the primary alcohol, while the oxophilicity of magnesium offers a thermodynamic bias over the amine moiety.<sup>36-38</sup> Accordingly, nucleoside phosphoramidates **2.13a-e** were prepared as shown in Scheme 2.3. Briefly, the nucleoside was dissolved in THF (with or without *N*-methylpyrrolidone co-solvent) and treated with the Grignard base to pre-form the magnesium alkoxide, followed by the addition of the chiral phosphorylating electrophile **2.12** which was synthesized following the method of Ross et al.<sup>39</sup>



**Scheme 2.3.** Traditional base-activated reaction utilized to access the desired phosphoramidate monophosphate prodrugs **2.13a-e**. These conditions failed for **2.11f** where R = cytosine.

This procedure allowed access to nucleoside phosphoramidates **2.13a-e** in serviceable yields. However, in the case where the nucleobase R was cytosine, the nucleoside (**2.11f**) appeared unreactive under these conditions. Cytidine analogs have been recognized before as problematic in prodrug synthesis, but Mayes and co-workers have made use of phenylboronic acid (PBA) to install a transient cyclic 2',3'-boronate ester to assist in solubility and regioselectivity.<sup>40, 41</sup> Encouragingly, performing the phosphoramidation reaction on 2',3'-PBA-protected natural cytidine as a model substrate afforded the desired cytidine phosphoramidate in 35% yield. While these conditions did not prove completely transferable to our 2'- $\beta$ -methyl-4'-thiocytidine analog **2.11f**, we saw approximately 26% crude conversion of the nucleoside to the desired phosphoramidate **2.13f**.

While this sequence was being explored, we became aware of an alternative solution to the ProTide synthesis problem offered by Simmons and co-workers wherein the authors report inverting the activation of the reagents to improve regioselectivity.<sup>42</sup> Rather than pre-activating the 5'-hydroxy nucleophile with a strong base, Simmons et al. report the use of sub-stoichiometric amounts of Lewis acid to lower the LUMO of the phosphoryl electrophile, allowing the reaction to proceed under general base-mediated conditions. Their optimized conditions utilize 0.5 equivalents of dimethylaluminum chloride with pyridine as base and solvent; in the cases of cytidine analogs, the authors report adding 5 equivalence of *N,N*-dimethylpropyleneurea (DMPU) as co-solvent. Again using natural cytidine as a model substrate, these reaction conditions were trialed without success. However, when these reaction conditions were applied to 2',3'-PBA-protected cytidine, the desired phosphoramidate was isolated in nearly 40% yield, which was increased to over 60% with gentle heating. With the combination of Mayes's PBA transient protecting group and Simmons's aluminum activation of the electrophile providing the highest yield on the cytidine model substrate, this same combination of conditions was applied to the 4'-thiocytidine analog and gratifyingly afforded the desired phosphoramidate **2.13f** in a 37% yield (Scheme 2.4).



**Scheme 2.4.** Alternative Lewis acid-activated phosphoramidation utilizing the transient 2',3'-phenylboronic ester protecting group strategy to access the cytidine analog.<sup>41,42</sup>

## 2.2.2 Antiviral Evaluation of Monophosphate Prodrugs

All synthesized phosphoramidates **2.13a–f** were evaluated for their anti-HCV activity in cultured Huh7 cells containing the HCV genotype 1b replicon as described elsewhere,<sup>43–45</sup> and the data are shown in Table 2.1 compared to approved anti-HCV drug sofosbuvir as the positive control. The incorporation of non-natural pyrimidines (entries 2, 4, and 5) appeared deleterious to potency, while the natural pyrimidines were superior to the purine adenine, inhibiting replication at single-digit micromolar potencies with uracil proving the most potent (entry 1). None of the compounds showed marked cytotoxicity ( $\text{TC}_{50}$ ) up to the maximum dose tested (200  $\mu\text{M}$ ). Additionally, a single-dose screen of the compounds at 5  $\mu\text{M}$  showed between 0–12% reduction in cytopathic effect (CPE) against Huh7 cells infected with the Dengue virus DENV2<sub>New Guinea</sub> and up to 20% against Zika<sub>PRVABC59</sub>, whereas sofosbuvir performed well against both (100% CPE reduction at 5  $\mu\text{M}$  against DENV2 and an antiviral potency ( $\text{EC}_{50}$ ) of 1.63  $\mu\text{M}$  against Zika).

**Table 2.1.** Antiviral dose-response data for 2'-C-methyl-4'-thionucleoside phosphoramidates.<sup>a</sup>

Entry	Compound No.	Nucleobase (R)	EC <sub>50</sub> (μM)	TC <sub>50</sub> (μM)	TI <sup>b</sup>
1	<b>2.13a</b>	uracil	2.10	>200	>95.2
2	<b>2.13b</b>	5-fluorouracil	113	>200	>1.77
3	<b>2.13c</b>	adenine	36.2	>200	>5.52
4	<b>2.13d</b>	6-azauracil	>200	>200	ND
5	<b>2.13e</b>	5-fluorocytosine	124	>200	>1.61
6	<b>2.13f</b>	cytosine	9.82	>200	>20.4
7	sofosbuvir	uracil	0.05	>2	>42.5

<sup>a</sup> Values reported are calculated from triplicate dose-response data from a single experiment; <sup>b</sup> therapeutic index (TI) = antiviral potency (EC<sub>50</sub>)/cytotoxicity (TC<sub>50</sub>)

Noting that sofosbuvir utilizes the same monophosphate prodrug moiety as our analogs, a comparison of the conjugated nucleosides can reasonably be made. Even the most potent analog (Table 2.1, entry 1) suffered a 42-fold drop in potency compared to sofosbuvir (entry 7) which could only be accounted for by the changes in the nucleoside (Figure 2.3). Two important structural features should be considered when comparing the nucleoside of our most potent compound (i.e., 2'-β-methyl-4'-thiouridine, **2.11a**) to the 2'-deoxy-2'-α-fluoro-2'-β-methyluridine nucleoside of sofosbuvir (**2.15**): the exchange of the 4'-chalcogen (red), as well as the 2'-α-hydroxy versus fluorine moiety (blue). Since the nucleobase and 5'-O-phosphoramidate are the same, is the observed loss of potency related to the 2'-substituent or the sugar ring heteroatom (or some combination of the two)?

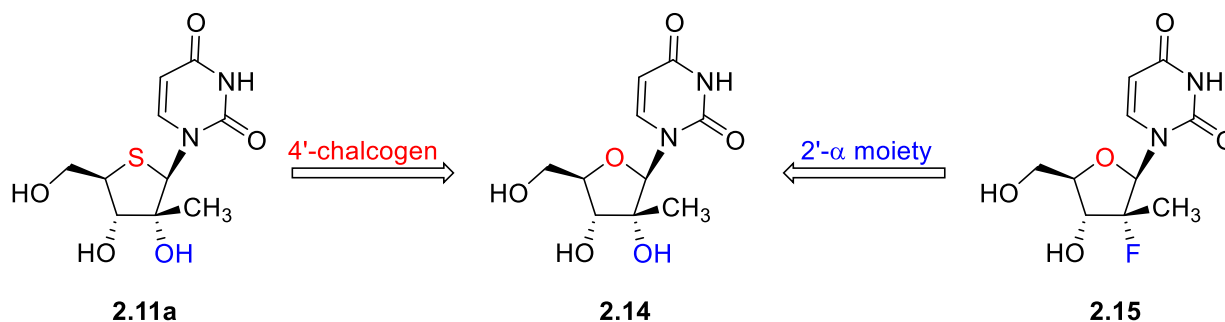


**Figure 2.3.** Comparison of the structural features of the most potent nucleoside of this work (**2.11a**) to sofosbuvir (**2.15**), with the bridging structure of 2'-β-methyluridine (**2.14**).

The molecule that could bridge the gap would therefore be the same aryloxy phosphoramidate prodrug of 2'- $\beta$ -methyluridine (**2.14**), bearing a 2'- $\alpha$ -hydroxy group and the natural tetrahydrofuran sugar ring. Butora and colleagues reported an EC<sub>50</sub> of 0.03  $\mu$ M for this prodrug in the same HCV genotype 1b replicon assay, in agreement with what we have observed for the *P*-racemate of pro-**2.14**.<sup>46, 47</sup> These data indicate a 70-fold drop in HCV potency when the natural tetrahydrofuran ring is replaced with tetrahydrothiophene. Moreover, Bernatchez and co-workers recently published an EC<sub>50</sub> of 1  $\mu$ M for the same aryloxy phosphoramidate prodrug of **2.14** against Zika, >5-fold more potent than our 4'-thio congener; however, their results were in neural stem cells, and anti-Zika potency has been suggested to be cell line-dependent.<sup>48</sup> For example, in that same study Bernatchez et al. recorded an EC<sub>50</sub> of 35  $\mu$ M for sofosbuvir in neural stem cells, whereas we observed a 1.63  $\mu$ M EC<sub>50</sub> in Huh7 cells. It is likely that this discrepancy can be attributed to differential metabolism of the prodrug in different cell lines.

It is not immediately obvious why this subtle structural change in the nucleoside would lead to such a pronounced drop in potency. The incorporation of sulfur is sure to have stereoelectronic effects resulting from the differences in polarizability of C-S bonds compared to C-O bonds. Relatedly, carbocyclic nucleosides that eliminate such polarizability are not well demonstrated in the literature, but a few examples exist with similarly poor results. Liu and co-workers synthesized and tested the A and C carbocyclic analogs of 2'-fluoro-2'-*C*-methyl nucleosides showing inferior anti-HCV activity compared to the 4'-oxo congener (>50 and 18.2  $\mu$ M versus 3.7  $\mu$ M).<sup>49</sup> Several groups have investigated base-modified analogs of the carbocyclic nucleoside natural product neplanocin A, with the only notable potency coming from the 7-deaza analog (ca. 1.7  $\mu$ M).<sup>50-52</sup> Note that, in all of these cases, the free nucleoside was tested in the cellular assay, leaving one to wonder how a corresponding monophosphate prodrug might perform.

In addition to electronic effects, differences in bond lengths and angles in the sugar ring can be expected to result from the O-to-S substitution, likely affecting the conformational dynamics of the

system. Additional studies were envisaged to better understand how these conformational changes might affect anti-HCV activity, noting the pioneering work of Victor Marquez's lab on other viruses<sup>53</sup>,<sup>54</sup> and Martínez-Montero and colleagues on HCV in particular.<sup>55</sup> Our hope was that a clearer picture of the effect of conformation on antiviral potency would become a general consideration for the design of nucleoside antivirals, leading to more potent molecules to combat diseases caused by other RNA viruses such as Dengue and Zika which currently have no antiviral therapy. Consequently, the principle of probing the effect of conformation on antiviral potency is the motivation of the investigation disclosed in the following chapter.

## **2.3 MATERIALS AND METHODS**

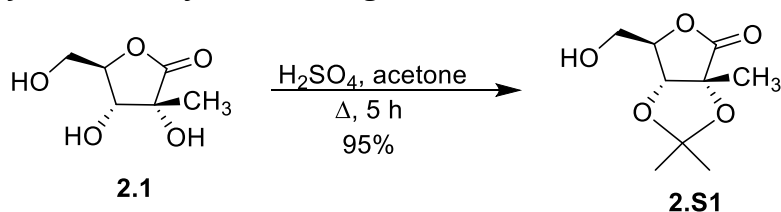
### **2.3.1 Synthetic Chemistry**

#### ***2.3.1.1 General Considerations***

All commercially available starting materials were purchased and used as provided unless otherwise specified. When anhydrous conditions are indicated, anhydrous solvents were used from commercial suppliers. Automated flash column chromatography was performed using a Teledyne ISCO (Lincoln, NE, USA) CombiFlash NextGen system with silica gel-packed columns (RediSep® R<sub>f</sub>). Analytical thin-layer chromatography (TLC, commercially available from VWR (Radnor, PA, USA)) was carried out on Merck aluminum-supported silica gel plates (thickness: 200 μm) with fluorescent indicator (F-254). Visualization of compounds on TLC plates was accomplished with UV light (254 nm) and/or with phosphomolybdic acid, ninhydrin, ceric ammonium molybdate, or potassium permanganate staining (Sigma-Aldrich, St. Louis, MO, USA). NMR spectra (<sup>1</sup>H, <sup>13</sup>C, <sup>19</sup>F and <sup>31</sup>P) were obtained in the Emory University NMR Research Center, directed by Dr. Shaoxiong Wu and Dr. Bing Wang, using either a Bruker INFINITY II 600 MHz spectrometer with cryogenic probe (funded by National Science Foundation grant CHE-1531620), a Varian INOVA 500 MHz spectrometer, a Varian INOVA 400 MHz spectrometer, or a Varian VNMR 400 MHz spectrometer. NMR samples were prepared and processed in deuterated chloroform (CDCl<sub>3</sub>), deuterated MeOH (CD<sub>3</sub>OD), deuterated

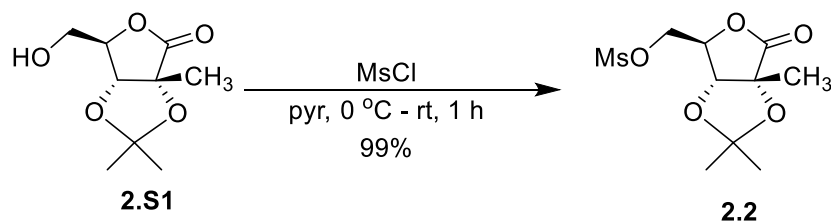
dimethyl sulfoxide ( $d_6$ -DMSO), or deuterated acetone ( $d_6$ -acetone) using the residual solvent peak (CDCl<sub>3</sub>: <sup>1</sup>H = 7.26 ppm, <sup>13</sup>C = 77.16 ppm; CD<sub>3</sub>OD: <sup>1</sup>H = 3.31 ppm, <sup>13</sup>C = 49.00 ppm;  $d_6$ -DMSO: <sup>1</sup>H = 2.50 ppm, <sup>13</sup>C = 39.52 ppm;  $d_6$ -acetone: <sup>1</sup>H = 2.05 ppm, <sup>13</sup>C = 29.84 ppm) as an internal reference. NMR data are reported to include chemical shifts ( $\delta$ ) reported in ppm, multiplicities indicated as s (singlet), d (doublet), dd (doubled doublet), t (triplet), td (tripled doublet), q (quartet), ddd (doubled doubled doublet), m (multiplet), or br s (broad singlet), coupling constants ( $J$ ) reported in Hz, and integration normalized to 1 atom. High-resolution mass spectrometry (HRMS) was performed by the Emory University Mass Spectrometry Center, directed by Dr. Fred Strobel. Liquid chromatography–mass spectrometry (LC–MS) was performed on an Agilent 1200 HPLC equipped with a 6120 Quadrupole mass spectrometer (ESI–API) eluting at a rate of 1.00 mL/min with mixtures of HPLC grade MeOH and water or acetonitrile and water (all spiked with 0.1% formic acid) through an analytical, reverse-phase Agilent C18 XDB eclipse column (50 mm  $\times$  4.6 mm, 3.5  $\mu$ M). LC–MS samples were prepared in a solution of 75:25 MeOH/water or 50:50 acetonitrile/water (spiked with 0.1% formic acid), and ultraviolet activity was monitored at 254 nm. Final compound purity was assessed to be  $\geq$ 95% pure using <sup>1</sup>H NMR and LC–MS.

### 2.3.1.2 Synthesis of the Per-Acetylated Thiosugar Core



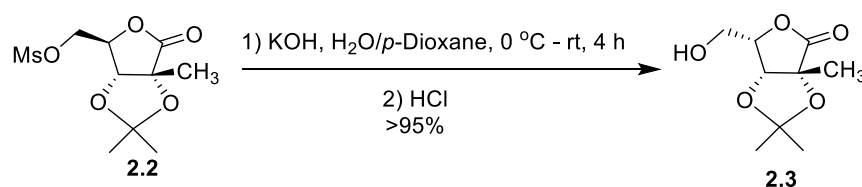
**(3aR,6R,6aR)-6-(hydroxymethyl)-2,2,3a-trimethyldihydrofuro [3,4-d][1,3]dioxol-4(3aH)-one (2.S1):** A 500-mL round-bottomed flask equipped with reflux condenser and magnetic stir bar was charged with (3R,4R,5R)-3,4-dihydroxy-5-(hydroxymethyl)-3-methyldihydrofuran-2(3H)-one (5 g, 30.8 mmol) and acetone (100 mL, 1363 mmol) to give a tan solution. Sulfuric acid (0.25 mL, 4.69 mmol) was added dropwise, and the solution was heated to reflux with stirring. After 4 h, the reaction was cooled with an ice bath and carefully neutralized with solid NaHCO<sub>3</sub> before the reaction mixture

was filtered through Celite®. The crude filtrate was concentrated to afford an off-white solid (5.94 g, 95% yield); NMR spectra were consistent with that previously reported.<sup>56</sup>



**[(3*a**R*,4*r*,6*a**R*)-2,2,6*a*-trimethyl-6-oxotetrahydrofuro[3,4-*d*][1,3]dioxol-4-yl)methyl**

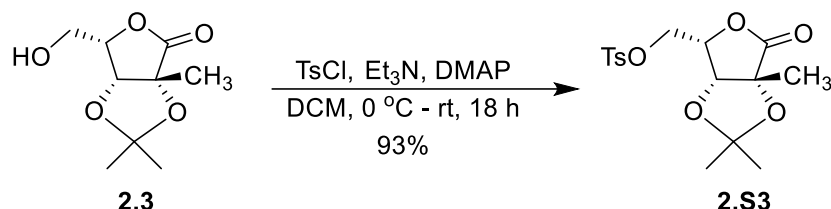
**methanesulfonate (2.2):** A 50-mL round-bottomed flask with magnetic stir bar was charged with acetonide **2.S1** (5.74 g, 28.4 mmol) and anhydrous pyridine (4.7 mL) under argon to give a colorless solution. The solution was cooled to 0 °C with an ice bath before methanesulfonyl chloride (3.3 mL, 42.6 mmol) was slowly added dropwise with stirring. The reaction was left to stir at 0 °C for approximately 30 min before the ice bath was removed, and the reaction warmed to ambient temperature for another 30 min. Approximately 15 mL of deionized H<sub>2</sub>O was added, and the product was extracted with dichloromethane (DCM). The organic layer was washed with 1M HCl followed by saturated NaHCO<sub>3</sub> solution. The organic phase was dried over Na<sub>2</sub>SO<sub>4</sub>, filtered and concentrated to afford a white solid (7.88 g, 99% yield); NMR spectra were consistent with that previously reported.<sup>56</sup>



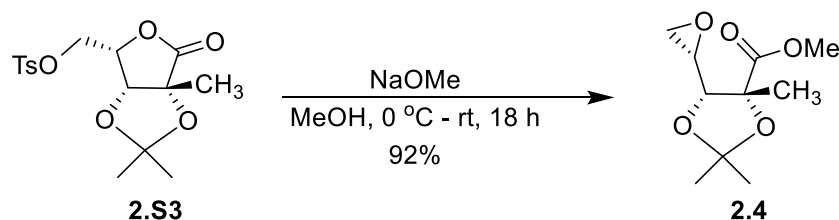
**(3*a**R*,6*S*,6*a**R*)-6-(hydroxymethyl)-2,2,3*a*-trimethyldihydrofuro[3,4-*d*][1,3]dioxol-4(3*a**H*)-one**

**(2.3):** A 500-mL round-bottomed flask with magnetic stir bar was charged with mesylate **2.2** (3.2 g, 11.42 mmol) and 1,4-dioxane (70.5 mL) to give a tan solution. In a separate beaker, solid KOH (1.92 g, 34.2 mmol) was dissolved in deionized water (55.0 mL), and after the heat of dissolution had dissipated the resulting solution was added to the reaction flask with stirring, noting an exotherm. The reaction was allowed to stir at ambient temperature for approximately 4 h. The reaction was

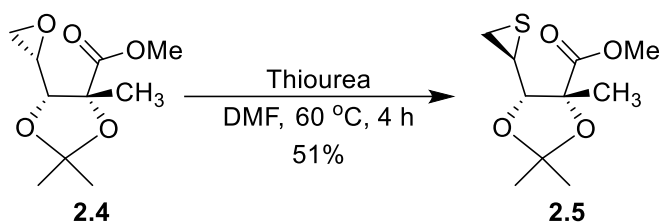
acidified with 3 N HCl to pH 1 with stirring, and the crude product was concentrated to dryness. The remaining white solid was triturated with ethyl acetate, and the insoluble material was filtered and further washed with ethyl acetate. The filtrate was concentrated to afford a tan oil (2.29 g, 99% yield); NMR spectra were consistent with those previously reported.<sup>56</sup>



**((3*aR*,4*S*,6*aR*)-2,2,6*a*-trimethyl-6-oxotetrahydrofuro[3,4-*d*][1,3]dioxol-4-yl)methyl 4-methylbenzenesulfonate (2.S3):** A flame-dried 250-mL round-bottom flask with stir bar was charged with argon, lactone **2.3** (2 g, 9.89 mmol) and DCM (30 mL) to give a colorless solution. The solution was chilled to 0 °C before *N,N*-dimethylpyridin-4-amine (0.06 g, 0.495 mmol) and *N*-ethyl-*N*-isopropylpropan-2-amine (3.5 mL, 19.78 mmol) were added with stirring to give a slightly yellow solution. Lastly, 4-methylbenzene-1-sulfonyl chloride (2.07 g, 10.88 mmol) was slowly added with stirring. The reaction was stirred for 30 min before the ice bath was removed and was then left to stir overnight while warming to ambient temperature. The next morning, TLC (3:2 hexanes:ethyl acetate) indicated the conversion of the starting material to a new UV-active spot, so the reaction was quenched by the addition of cold 1 N HCl. The product was twice extracted with DCM, and the organic extracts were combined and washed with saturated NaHCO<sub>3</sub> solution before being dried over sodium sulfate, filtered and concentrated to afford a brown oil (3.4 g, 93% yield); NMR spectra were consistent with that previously reported.<sup>57</sup>

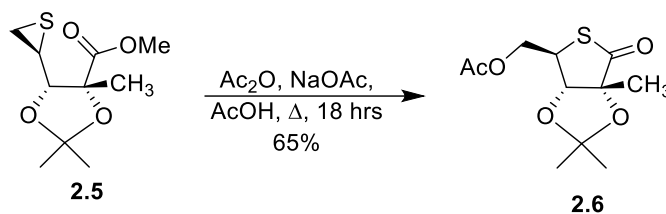


**(4*R*,5*R*)-methyl 2,2,4-trimethyl-5-((*S*)-oxiran-2-yl)-1,3-dioxolane-4-carboxylate (2.4):** An oven-dried 50-mL round-bottom flask with magnetic stir bar was charged with argon and tosylate **2.S3** (3.04 g, 8.53 mmol). The apparatus was chilled with an ice bath before NaOMe (18.8 mL, 9.38 mmol) was added as a solution in methanol dropwise with stirring to give a colorless solution. The reaction was stirred at 0 °C for 1 h before the ice bath was removed, allowing the reaction to warm to ambient temperature while stirring overnight. The reaction was quenched with 10 mL of saturated NH<sub>4</sub>Cl solution and diluted with 50 mL of deionized water before the product was extracted with ethyl acetate. The organic layers were combined, dried over Na<sub>2</sub>SO<sub>4</sub>, filtered and concentrated to afford the crude product, a pale yellow semisolid (1.70 g, 92% yield); <sup>1</sup>H NMR (400 MHz, CDCl<sub>3</sub>) δ 3.76 (s, 3H), 3.58 (d, *J* = 6.0 Hz, 1H), 3.00 (ddd, *J* = 6.0, 4.2, 2.7 Hz, 1H), 2.85 (dd, *J* = 4.8, 4.2 Hz, 1H), 2.71 (dd, *J* = 4.9, 2.7 Hz, 1H), 1.58 (s, 3H), 1.55 (s, 3H), 1.40 (s, 3H) ppm; <sup>13</sup>C NMR (101 MHz, CDCl<sub>3</sub>) δ 172.7, 111.1, 85.5, 82.3, 52.5, 49.7, 43.5, 26.6, 23.4 ppm.



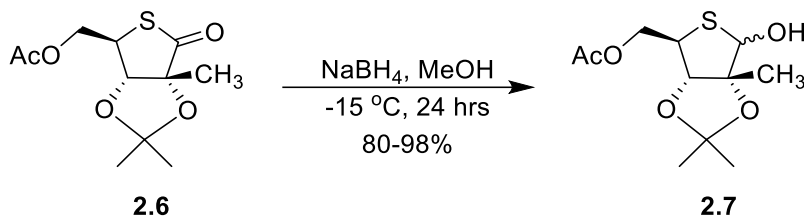
**(4*R*,5*S*)-methyl 2,2,4-Trimethyl-5-((*S*)-thiiran-2-yl)-1,3-dioxolane-4-carboxylate (2.5):** A 25-mL round-bottom flask with magnetic stir bar was charged with epoxide **2.4** (0.75 g, 3.47 mmol) and anhydrous DMF (1.88 mL), and the colorless solution was heated to 60 °C. Freshly recrystallized thiourea (0.46 g, 6.00 mmol) was added, and the reaction stirred for 2 h before another half equivalent of thiourea (0.132 g, 1.734 mmol) was added. Monitoring by TLC indicated complete conversion of starting material in 4.5 h. The reaction was quenched by the addition of water and diluted with 25 mL of brine solution before the product was extracted with ethyl acetate. The organic extracts were combined, dried over Na<sub>2</sub>SO<sub>4</sub>, filtered and concentrated to afford 1.06 g of crude product. The product mixture was brought up in DCM and filtered over a plug of silica gel, eluting

with a 25% ethyl acetate solution in hexanes. The filtrate fractions of interest were concentrated to afford the desired product as a white powder (0.41 g, 51% yield);  $^1\text{H}$  NMR (400 MHz,  $\text{CDCl}_3$ )  $\delta$  3.78 (s, 3H), 3.35 (d,  $J = 8.4$  Hz, 1H), 2.77 (ddd,  $J = 8.2, 5.9, 4.9$  Hz, 1H), 2.53 (dd,  $J = 6.0, 1.5$  Hz, 1H), 2.26 (dd,  $J = 5.0, 1.4$  Hz, 1H), 1.61 (s, 3H), 1.57 (s, 4H), 1.39 (s, 3H) ppm;  $^{13}\text{C}$  NMR (101 MHz,  $\text{CDCl}_3$ )  $\delta$  172.8, 110.7, 88.9, 84.2, 52.5, 30.2, 26.9, 26.8, 23.8, 22.9 ppm; HRMS (NSI)  $m/z$ :  $[\text{M} + \text{H}]^+$  Calcd for  $\text{C}_{10}\text{H}_{17}\text{O}_4\text{S}$  233.0842; Found 233.0844.



**[(3*aS*,4*R*,6*aR*)-2,2,6*a*-trimethyl-6-oxotetrahydrothieno[3,4-*d*][1,3]dioxol-4-yl)methyl acetate**

**(2.6):** An oven-dried 250-mL round-bottom flask equipped with stir bar and reflux condenser was charged with thiirane **2.5** (0.32 g, 1.378 mmol) and sodium acetate (11.75 g, 143 mmol) under argon. Acetic acid (23 mL) was added followed by acetic anhydride (1.3 mL, 13.78 mmol) to give a moist powder. The reaction was heated to reflux, dissolving the mixture, and allowed to stir for 21 h with monitoring by TLC. When the reaction was pulled from heat, the solution solidified. The solid was dissolved by the addition of DCM and careful addition of saturated  $\text{NaHCO}_3$  solution. The product was extracted with DCM, and the organic extracts were combined, dried over  $\text{Na}_2\text{SO}_4$ , filtered and concentrated to afford 0.3 g of a brown oil, which was purified via silica gel flash column chromatography (eluted with a 0–15% gradient of ethyl acetate in hexanes). The fractions of interest were combined to afford the desired five-membered product (0.23 g, 65% yield);  $^1\text{H}$  NMR (400 MHz,  $\text{CDCl}_3$ )  $\delta$  4.33 (d,  $J = 0.7$  Hz, 1H), 4.31 (d,  $J = 6.3$  Hz, 1H), 4.31 (d,  $J = 7.0$  Hz, 1H), 4.01 (ddd,  $J = 7.0, 6.3, 0.7$  Hz, 1H), 2.12 (s, 3H), 1.54 (s, 3H), 1.44 (d,  $J = 0.8$  Hz, 3H), 1.40 (d,  $J = 0.8$  Hz, 3H) ppm;  $^{13}\text{C}$  NMR (101 MHz,  $\text{CDCl}_3$ )  $\delta$  206.1, 170.4, 111.9, 89.9, 82.9, 64.7, 46.2, 27.5, 26.7, 20.9, 20.3 ppm; HRMS (NSI)  $m/z$ :  $[\text{M} + \text{Na}]^+$  Calcd for  $\text{C}_{11}\text{H}_{16}\text{O}_5\text{SNa}$  283.0611; Found 283.0615.



**[(3*aS*,4*R*,6*aR*)-6-hydroxy-2,2,6*a*-trimethyltetrahydrothieno[3,4-*d*][1,3]dioxol-4-yl)methyl**

**acetate (2.7):** A 250-mL round-bottom flask with magnetic stir bar was charged with thiolactone **2.6**

(0.606 g, 2.328 mmol) and methanol (36 mL) under argon to give a colorless solution. The solution

was chilled to  $-15\text{ }^{\circ}\text{C}$  before  $\text{NaBH}_4$  (0.176 g, 4.66 mmol) was added under argon with stirring. After

one hour, another portion of  $\text{NaBH}_4$  (0.176 g, 4.66 mmol) was added; two additional portions of the

reductant (0.176 g, 4.66 mmol each) were added on the hour for a total of 8 equivs, and the reaction

was allowed to stir at  $-15\text{ }^{\circ}\text{C}$  with monitoring by LC-MS. After the starting material was consumed,

the reaction was quenched at  $-15\text{ }^{\circ}\text{C}$  by the addition of 5 wt% aqueous citric acid solution. The

product mixture was then extracted with DCM, and the organic extracts were combined, dried over

$\text{Na}_2\text{SO}_4$ , filtered and concentrated to afford a lightly colored oil as the crude product, a 7:3 mixture of

anomers (0.56 g, 96% yield);  $^1\text{H NMR}$  (400 MHz,  $\text{CDCl}_3$ )  $\delta$  5.11 (d,  $J = 4.1\text{ Hz}$ , 0.7H, major), 5.10 (d,  $J =$

9.3 Hz, 0.3H, minor), 4.53 (s, 0.7H, major), 4.40 (d,  $J = 2.0\text{ Hz}$ , 0.3H, minor), 4.35 (d,  $J = 5.7\text{ Hz}$ , 0.3H,

minor), 4.33 (d,  $J = 5.7\text{ Hz}$ , 0.3H, minor), 4.20–4.13 (m, 1.4H), 3.55–3.51 (m, 0.3H, minor), 3.50–3.46

(m, 0.7H, major), 3.25 (d,  $J = 9.3\text{ Hz}$ , 0.3H, minor), 2.88 (d,  $J = 4.3\text{ Hz}$ , 0.7H, major), 2.09 (s, 2.1H, major),

2.08 (s, 0.9H, minor), 1.565 (s, 0.9H, minor), 1.560 (s, 2.1H, major), 1.54 (s, 0.9H, minor), 1.49 (s, 2.1H,

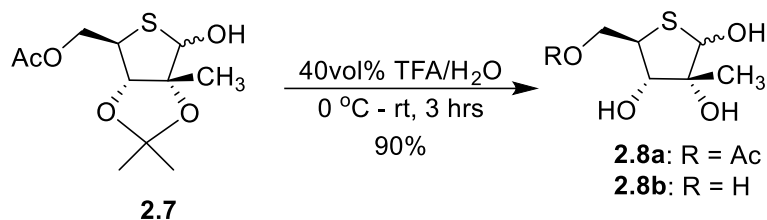
major), 1.44 (s, 0.9H, minor), 1.40 (s, 2.1H, major) ppm;  $^{13}\text{C NMR}$  (101 MHz,  $\text{CDCl}_3$ )  $\delta$  170.9 (major),

170.6 (minor), 113.1 (minor), 111.7 (major), 96.7 (major), 91.9 (major), 91.3 (minor), 90.3 (minor),

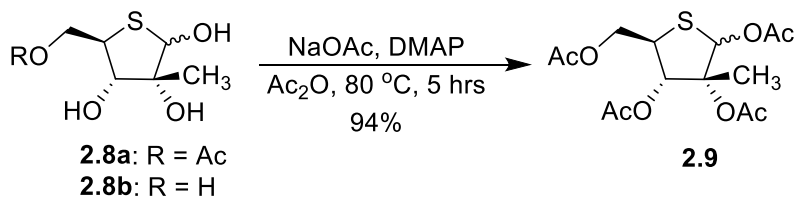
88.8 (major), 86.1 (minor), 66.5 (major), 65.7 (minor), 53.9 (major), 48.8 (minor), 28.1 (2C, major),

27.5 (minor), 27.1 (minor), 24.4 (minor), 22.4 (major), 21.1 (major), 21.0 (minor) ppm; HRMS (NSI)

$m/z$ :  $[\text{M} + \text{Na}]^+$  Calcd for  $\text{C}_{11}\text{H}_{18}\text{O}_5\text{SNa}$  285.0767; Found 285.0770.



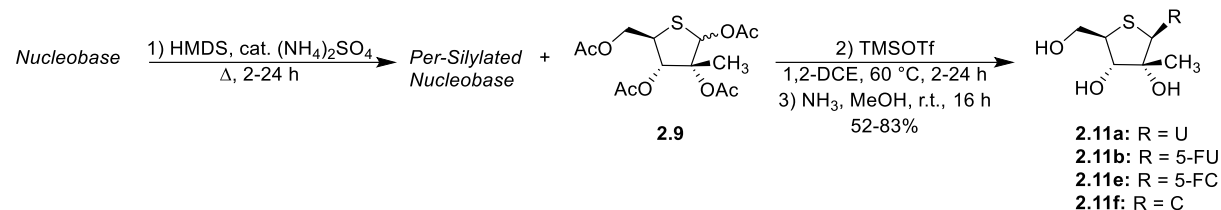
**((2*R*,3*S*,4*R*)-3,4,5-trihydroxy-4-methyltetrahydrothiophen-2-yl)methyl acetate (**2.8a**):** A 250-mL round-bottom flask with magnetic stir bar was charged with thiolactol **2.7** (0.68 g, 2.59 mmol) and 20 mL of an ice-cold 40 vol% aqueous solution of trifluoroacetic acid. The reaction was stirred at ambient temperature for 3 h when TLC (1:4 Hex:EA) showed conversion of starting material to two more polar products. The reaction mixture was concentrated via rotary evaporation followed by azeotropic removal of residual acid via co-evaporation with toluene followed by methanol then ethanol. The resulting oil was purified via silica gel flash column chromatography (eluted with a gradient of 0–15% methanol in ethyl acetate). The fractions of interest were combined for the desired 1,2,3-glycol ( $[M + Na]^+ = 245.0$ ) as a 3:2 mixture of anomers (later fractions were also collected for the 5-deacetylated product (**2.8b**,  $[M + Na]^+ = 203.0$ )) (0.52 g, 90% yield);  $^1\text{H NMR}$  (399 MHz,  $\text{CD}_3\text{OD}$ )  $\delta$  5.20 (s, 0.4H, minor), 4.82 (s, 0.6H, major), 4.61–4.47 (m, 1H, both), 4.12 (dd,  $J = 11.0, 8.2$  Hz, 0.6H, major), 4.02 (dd,  $J = 11.2, 7.9$  Hz, 0.4H, minor), 3.80–3.70 (m, 1H, both), 3.53–3.43 (m, 1H, both), 2.05 (s, 1.8H, major), 2.04 (s, 1.2H, minor), 1.33 (s, 1.8H, major), 1.28 (s, 1.2H, minor) ppm;  $^{13}\text{C NMR}$  (100 MHz,  $\text{CD}_3\text{OD}$ )  $\delta$  172.7 (major), 172.6 (minor), 85.6 (major), 85.3 (minor), 82.8 (major), 82.7 (minor), 79.5 (minor), 79.3 (major), 68.3 (major), 67.2 (minor), 49.8 (minor), 48.7 (major), 22.3 (both), 20.9 (major), 20.7 (minor) ppm; HRMS (NSI)  $m/z$ :  $[M + Na]^+$  Calcd for  $\text{C}_8\text{H}_{14}\text{O}_5\text{SNa}$  245.0454; Found 245.0455.



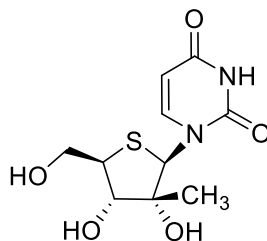
**(3*R*,4*S*,5*R*)-5-(acetoxymethyl)-3-methyltetrahydrothiophene-2,3,4-triyl triacetate (2.9):**

A 50-mL round-bottom flask with magnetic stir bar was charged with a mixture of thioribofuranose derivatives **2.8a** and **2.8b** (0.874 g, 3.93 mmol) which was dried *in vacuo* overnight. Solid anhydrous NaOAc (0.419 g, 5.11 mmol) was added under argon followed by acetic anhydride (3.7 mL, 39.3 mmol) to give a colorless slurry; finally *N,N*-dimethylpyridin-4-amine (48 mg, 0.393 mmol) was added. The reaction was heated to 80 °C and allowed to stir approximately 4 h with monitoring by TLC for consumption of starting material. The reaction was quenched by careful addition of saturated aqueous sodium bicarbonate solution. The product was extracted with DCM; the organic layers were combined, dried over Na<sub>2</sub>SO<sub>4</sub>, filtered and concentrated to a thin yellow-brown oil. The oil was brought up in DCM and purified via silica gel flash column chromatography (eluted with a 0–30% gradient of ethyl acetate in hexanes). The fractions of interest were combined and concentrated to afford the desired product as a 2:1 mixture of anomers (1.29 g, 94% yield); <sup>1</sup>H NMR (400 MHz, CDCl<sub>3</sub>) δ 6.44 (s, 0.7H, major), 6.28 (s, 0.3H, minor), 5.35 (d, *J* = 3.2 Hz, 0.3H, minor), 5.34 (d, *J* = 9.3 Hz, 0.7H, major), 4.36–4.38 (m, 1.4H), 4.17–4.09 (m, 1.4H), 3.80–3.72 (m, 1.4H), 2.18 (s, 2H, major), 2.11 (s, 2H, major), 2.10 (s, 3H, both), 2.083 (s, 1H, minor), 2.078 (s, 1H, minor), 2.04 (s, 2H, major), 2.03 (s, 1H, minor), 1.74 (s, 1H, minor), 1.58 (s, 2H, major) ppm; <sup>13</sup>C NMR (151 MHz, CDCl<sub>3</sub>) δ 170.5, 170.2, 169.8, 169.3, 88.0, 78.8, 78.0, 65.5, 44.8, 22.1, 21.3, 21.0, 20.8, 17.0 ppm; HRMS (ESI) *m/z*: [M + Na]<sup>+</sup> Calcd for C<sub>14</sub>H<sub>20</sub>O<sub>8</sub>SNa 371.0771; Found 371.0768.

### 2.3.1.3 Synthesis of the 4'-Thionucleosides

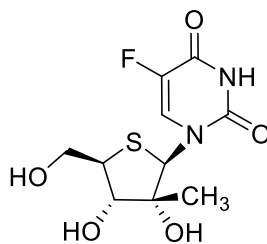


**General Procedure for Nucleoside Synthesis Using HMDS and TMSOTf:** The nucleobase of interest (5–6 eq) was suspended in anhydrous hexamethyldisilazane (HMDS, 0.5 M in nucleobase) with catalytic ammonium sulfate (7.5 mol% relative to nucleobase) and heated to reflux under argon until the reaction clarified (1–2 h). The reaction mixture was then carefully concentrated to dryness and placed under high vacuum overnight, after which time the silylated intermediate was brought up in 1,2-DCE (1 M in nucleobase) under argon and treated with (3*R*,4*S*,5*R*)-5-(acetoxymethyl)-3-methyltetrahydrothiophene-2,3,4-triyl triacetate **2.9** (1 eq) and TMSOTf, (5.5 eq). The reaction was heated to 60 °C and left to stir until starting material was consumed by TLC. The reaction was allowed to cool to ambient temperature before being quenched with a saturated aqueous solution of NaHCO<sub>3</sub>, and the product was extracted with DCM. The organic layer was dried over Na<sub>2</sub>SO<sub>4</sub>, filtered, concentrated and purified via silica gel flash column chromatography (eluted with 0–10% methanol gradient in DCM) to afford the glycosylated product, which was subsequently deprotected by stirring with a 7 N solution of ammonia in methanol overnight in a sealed vessel. The next day, the volatiles were removed, and the residue was purified via silica gel flash column chromatography (eluted with 0–15% methanol gradient in DCM) to afford the desired 4'-thionucleoside analog.



2.11a

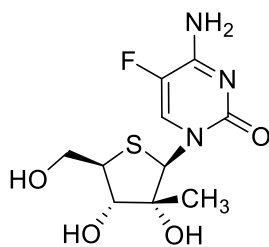
**1-((2R,3R,4S,5R)-3,4-dihydroxy-5-(hydroxymethyl)-3-methyltetrahydrothiophen-2-yl)pyrimidine-2,4(1H,3H)-dione (2.11a):** Following the general procedure, uracil (0.78 g, 6.95 mmol) was glycosylated with **2.9** (484 mg, 1.39 mmol) and subsequently deprotected to afford the desired product (245 mg, 64% yield over two steps);  $^1\text{H}$  NMR (399 MHz,  $\text{CD}_3\text{OD}$ )  $\delta$  8.36 (d,  $J = 8.2$  Hz, 1H), 5.95 (s, 1H), 5.75 (d,  $J = 8.1$  Hz, 1H), 3.99–3.90 (m, 2H), 3.73 (d,  $J = 9.5$  Hz, 1H), 3.48 (ddd,  $J = 9.4, 4.7, 2.9$  Hz, 1H), 1.17 (s, 3H) ppm;  $^{13}\text{C}$  NMR (100 MHz,  $\text{CD}_3\text{OD}$ )  $\delta$  165.4, 152.8, 143.8, 102.6, 83.2, 77.3, 68.0, 61.6, 53.6, 21.0 ppm; HRMS (NSI)  $m/z$ :  $[\text{M} + \text{Na}]^+$  Calcd for  $\text{C}_{10}\text{H}_{14}\text{O}_5\text{N}_2\text{SNa}$  297.0516; Found 297.0508.



2.11b

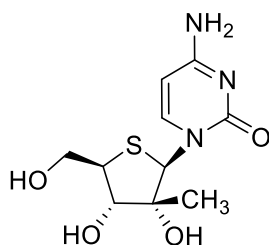
**1-((2R,3R,4S,5R)-3,4-dihydroxy-5-(hydroxymethyl)-3-methyltetrahydrothiophen-2-yl)-5-fluoropyrimidine-2,4(1H,3H)-dione (2.11b):** Following the general procedure, 5-fluorouracil (195 mg, 1.50 mmol) was glycosylated with **2.9** (80 mg, 0.23 mmol) and subsequently deprotected to afford the desired product (50 mg, 75% yield over two steps);  $^1\text{H}$  NMR (399 MHz,  $\text{CD}_3\text{OD}$ )  $\delta$  8.72 (d,  $^3J_{\text{H-F}} = 7.4$  Hz, 1H), 5.90 (d,  $^5J_{\text{H-F}} = 1.5$  Hz, 1H), 3.98 (dd,  $J = 11.9, 3.6$  Hz, 1H), 3.90 (dd,  $J = 11.8, 2.5$  Hz, 1H), 3.79 (d,  $J = 9.4$  Hz, 1H), 3.44 (ddd,  $J = 9.4, 3.5, 2.5$  Hz, 1H), 1.20 (s, 3H) ppm;  $^{13}\text{C}$  NMR (100 MHz,  $\text{CD}_3\text{OD}$ )  $\delta$  159.3 (d,  $^2J_{\text{C-F}} = 26.1$  Hz), 151.7, 141.2 (d,  $^1J_{\text{C-F}} = 233.6$  Hz), 127.8 (d,  $^2J_{\text{C-F}} = 35.8$  Hz),

83.4, 76.7, 68.9, 60.6, 53.4, 20.7 ppm;  $^{19}\text{F}$  NMR (376 MHz,  $\text{CD}_3\text{OD}$ )  $\delta$ -167.3 (d,  $^3J_{\text{F-H}} = 6.9$  Hz) ppm; HRMS (NSI)  $m/z$ :  $[\text{M} - \text{H}]^-$  Calcd for  $\text{C}_{10}\text{H}_{12}\text{O}_5\text{N}_2\text{FS}$  291.0456; Found 291.0458.



2.11e

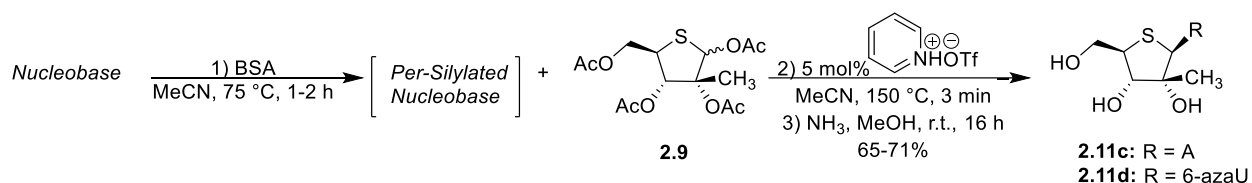
**4-amino-1-((2R,3R,4S,5R)-3,4-dihydroxy-5-(hydroxymethyl)-3-methyltetrahydrothiophen-2-yl)-5-fluoropyrimidin-2(1H)-one (2.11e):** Following the general procedure, *N*<sup>4</sup>-benzoyl-5-fluorocytosine (380 mg, 1.63 mmol) was glycosylated with **2.9** (97 mg, 0.28 mmol) and subsequently deprotected to afford the desired product (67 mg, 83% yield over two steps);  $^1\text{H}$  NMR (399 MHz,  $\text{CD}_3\text{OD}$ )  $\delta$  8.65 (d,  $^3J_{\text{H-F}} = 7.3$  Hz, 1H), 6.02 (d,  $^5J_{\text{H-F}} = 1.9$  Hz, 1H), 3.98 (dd,  $J = 11.9, 3.6$  Hz, 1H), 3.91 (dd,  $J = 11.9, 2.5$  Hz, 1H), 3.78 (d,  $J = 9.4$  Hz, 1H), 3.45 (ddd,  $J = 9.4, 3.6, 2.6$  Hz, 1H), 1.15 (s, 3H) ppm;  $^{13}\text{C}$  NMR (100 MHz,  $\text{CD}_3\text{OD}$ )  $\delta$  159.2 (d,  $^2J_{\text{C-F}} = 14.0$  Hz), 157.4, 137.9 (d,  $^1J_{\text{C-F}} = 243.7$  Hz), 128.4 (d,  $^2J_{\text{C-F}} = 33.1$  Hz), 83.4, 76.7, 69.3, 60.8, 53.3, 20.7 ppm;  $^{19}\text{F}$  NMR (376 MHz,  $\text{CD}_3\text{OD}$ )  $\delta$ -166.8 (d,  $^3J_{\text{F-H}} = 7.2$  Hz) ppm; HRMS (NSI)  $m/z$ :  $[\text{M} - \text{H}]^-$  Calcd for  $\text{C}_{10}\text{H}_{13}\text{O}_4\text{N}_3\text{FS}$  290.0616; Found 290.0619.



2.11f

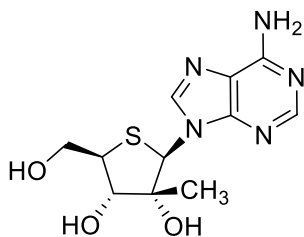
**4-amino-1-((2R,3R,4S,5R)-3,4-dihydroxy-5-(hydroxymethyl)-3-methyltetrahydrothiophen-2-yl)pyrimidin-2(1H)-one (2.11f):** Following the general procedure, *N*<sup>4</sup>-acetylcytosine (0.5 g, 3.27 mmol) was glycosylated with **2.9** (256 mg, 0.74 mmol) and subsequently deprotected to afford the desired product (104 mg, 52% yield over two steps);  $^1\text{H}$  NMR (400 MHz,  $\text{CD}_3\text{OD}$ )  $\delta$  8.36 (d,  $J = 7.6$  Hz,

1H), 6.11 (s, 1H), 5.93 (d,  $J = 7.5$  Hz, 1H), 3.97–3.92 (m, 2H), 3.72 (d,  $J = 9.5$  Hz, 1H), 3.47 (dt,  $J = 9.5$ , 3.6 Hz, 2H), 1.12 (s, 3H) ppm;  $^{13}\text{C}$  NMR (101 MHz,  $\text{CD}_3\text{OD}$ )  $\delta$  167.1, 159.0, 144.4, 96.2, 83.4, 77.2, 68.6, 61.5, 53.3, 20.7 ppm; HRMS (NSI)  $m/z$ :  $[\text{M} + \text{H}]^+$  Calcd for  $\text{C}_{10}\text{H}_{16}\text{O}_4\text{N}_3\text{S}$  274.0856; Found 274.0855.

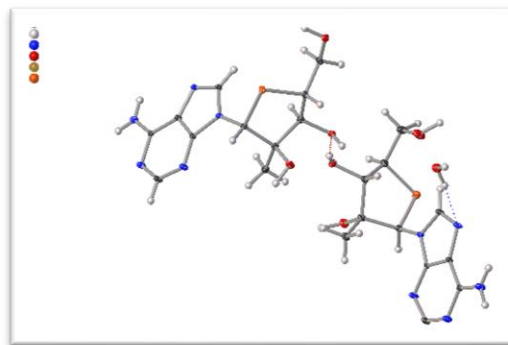


### General procedure for Nucleoside Synthesis via the Microwave-Assisted Glycosylation of

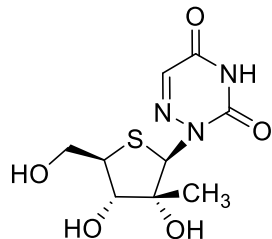
**Nucleobases with BSA and Pyridinium Triflate:** The nucleobase of interest (1.1 eq) was suspended in anhydrous acetonitrile (0.2 M in nucleobase) under argon and treated with *N,O*-bis(trimethylsilyl)acetamide (2.2 eq relative to nucleobase), and the reaction was heated to 75 °C for 1–2 h. Meanwhile, an oven-dried microwave vial was charged with argon, catalytic pyridinium triflate (5 mol% relative to glycosyl donor), and (3*R*,4*S*,5*R*)-5-(acetoxymethyl)-3-methyltetrahydrothiophene-2,3,4-triyl triacetate **2.9** (1 eq) as a 0.4 M solution in anhydrous acetonitrile. After cooling to ambient temperature, the crude silylated intermediate was delivered to the microwave vial under argon. The suspension stirred briefly before being irradiated to 150 °C until starting material was consumed by TLC. The reaction mixture was concentrated to dryness and purified via silica gel flash column chromatography (eluted with 0–10% methanol gradient in DCM) to afford the glycosylated product, which was subsequently deprotected by stirring with a 7 N solution of ammonia in methanol overnight in a sealed vessel. The next day, the volatiles were removed, and the residue was purified via silica gel flash column chromatography (eluted with 0–15% methanol in DCM) to afford the desired 4'-thionucleoside analog.



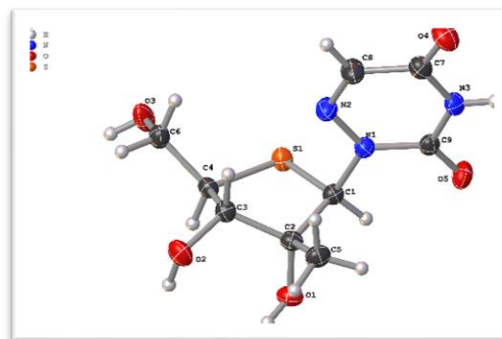
2.11c



**(2*R*,3*R*,4*S*,5*R*)-2-(6-amino-9*H*-purin-9-yl)-5-(hydroxymethyl)-3-methyltetrahydrothiophene-3,4-diol (2.11c):** Following the microwave-assisted general procedure, *N*<sup>6</sup>-benzoyladenine (52 mg, 0.22 mmol) was glycosylated with **2.9** (70 mg, 0.2 mmol) and subsequently deprotected to afford the desired product (42 mg, 71% yield over two steps); <sup>1</sup>H NMR (400 MHz, CD<sub>3</sub>OD) δ 8.68 (s, 1H), 8.22 (s, 1H), 5.83 (s, 1H), 4.10 (d, *J* = 9.4 Hz, 1H), 4.05–3.97 (m, 2H), 3.61 (ddd, *J* = 9.4, 4.2, 3.2 Hz, 1H), 0.92 (s, 3H) ppm; <sup>13</sup>C NMR (101 MHz, CD<sub>3</sub>OD) δ 157.4, 153.9, 151.1, 142.2, 83.4, 77.1, 66.4, 61.8, 53.5, 21.0 ppm; HRMS (NSI) *m/z*: [*M* + *H*]<sup>+</sup> Calcd for C<sub>11</sub>H<sub>16</sub>O<sub>3</sub>N<sub>5</sub>S 298.0968; Found 298.0969.

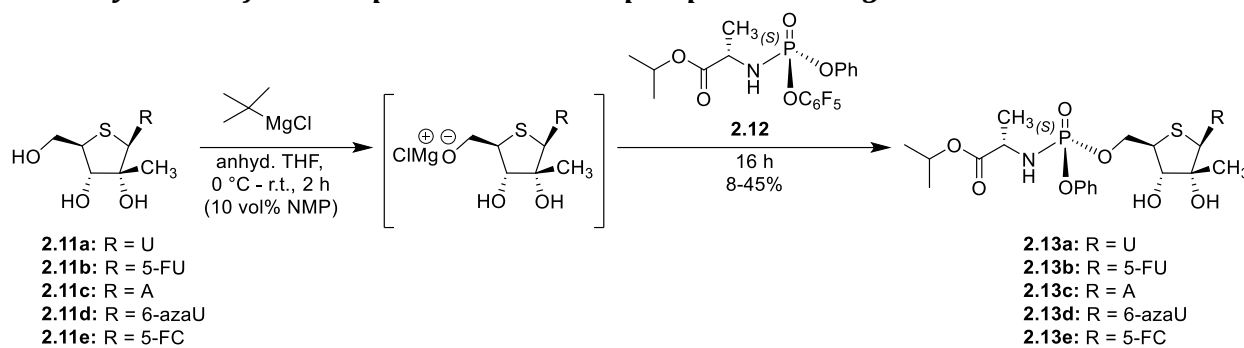


2.11d

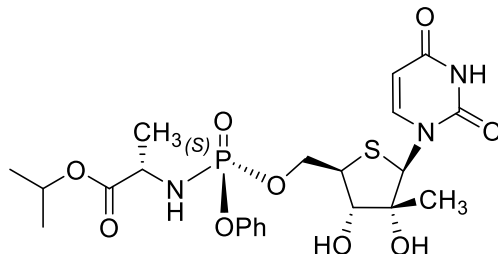


**2-((2*R*,3*R*,4*S*,5*R*)-3,4-dihydroxy-5-(hydroxymethyl)-3-methyltetrahydrothiophen-2-yl)-1,2,4-triazine-3,5(2*H*,4*H*)-dione (2.11d):** Following the microwave-assisted general procedure, 6-azauracil (18 mg, 0.158 mmol) was glycosylated with **2.9** (42 mg, 0.12 mmol) and subsequently deprotected to afford the desired product (20 mg, 65% yield over two steps); <sup>1</sup>H NMR (400 MHz, CD<sub>3</sub>OD) δ 7.52 (s, 1H), 6.01 (s, 1H), 4.07 (dd, *J* = 10.9, 3.7 Hz, 1H), 3.98 (d, *J* = 8.9 Hz, 1H), 3.74 (dd, *J* = 10.9, 8.6 Hz, 1H), 3.51 (td, *J* = 8.7, 3.7 Hz, 1H), 1.19 (s, 3H) ppm; <sup>13</sup>C NMR (126 MHz, CD<sub>3</sub>OD) δ 158.3, 150.3, 137.3, 83.4, 79.4, 69.8, 65.8, 53.9, 20.7 ppm; HRMS (NSI) *m/z*: [*M* - *H*]<sup>-</sup> Calcd for C<sub>9</sub>H<sub>12</sub>O<sub>5</sub>N<sub>3</sub>S 274.0492; Found 274.0505.

### 2.3.1.4 Synthesis of the Phosphoramidate Monophosphate Prodrugs



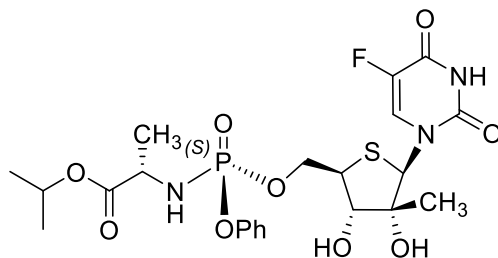
**General Procedure for the Phosphoramidate Coupling Reaction:** The 4'-thionucleoside of interest (1 eq) was dried *in vacuo* overnight and then dissolved in anhydrous THF (0.2 M) with or without 10 vol% *N*-methylpyrrolidone co-solvent, depending on solubility. The solution was cooled to 0 °C before being dropwise treated with tert-butylmagnesium chloride (1.2–2 eq) as a 1 M solution in THF under argon, resulting in a thick white slurry. The ice bath was removed, and the deprotonation proceeded while slowly warming to ambient temperature over 2–3 h. The intermediate magnesium alkoxide was then dropwise treated with (*S*)-isopropyl 2-(((*S*)-(perfluorophenoxy)(phenoxy)phosphoryl)amino)propanoate **2.12**<sup>39</sup> (1–2 eq) as a 0.4 M solution in anhydrous THF, and the resulting slurry stirred at ambient temperature overnight. The next day, the reaction was quenched by the addition of saturated aqueous NH<sub>4</sub>Cl solution, and the product was extracted with DCM. The organic layers were combined, dried over Na<sub>2</sub>SO<sub>4</sub>, filtered, concentrated and purified via silica gel flash column chromatography (eluting with 0–15% methanol in DCM) to afford the desired nucleoside phosphoramidate.



2.13a

**(2S)-isopropyl 2-((((((2R,3S,4R,5R)-5-(2,4-dioxo-3,4-dihydropyrimidin-1(2H)-yl)-3,4-dihydroxy-4-methyltetrahydrothiophen-2-**

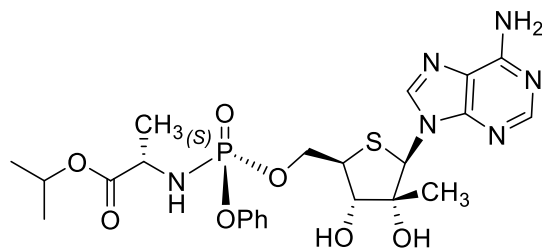
**yl)methoxy)(phenoxy)phosphoryl)amino)propanoate (2.13a):** Following the general phosphoramidation procedure, thionucleoside **2.11a** (51 mg, 0.19 mmol) was treated with **2.12** (84 mg, 0.19 mmol) to afford the desired product (45 mg, 45% yield);  $^1\text{H}$  NMR (600 MHz,  $\text{CD}_3\text{OD}$ )  $\delta$  8.08 (d,  $J = 8.2$  Hz, 1H), 7.37 (t,  $J = 7.9$  Hz, 2H), 7.29–7.26 (m, 2H), 7.23–7.17 (m, 1H), 5.99 (s, 1H), 5.68 (d,  $J = 8.1$  Hz, 1H), 4.97 (app hept,  $J = 6.3$  Hz, 1H), 4.56–4.53 (m, 1H), 4.49–4.46 (m, 1H), 3.93 (dq,  $J = 9.7$ , 7.1 Hz, 1H), 3.70 (d,  $J = 9.6$  Hz, 1H), 3.68–3.65 (m, 1H), 1.36 (d,  $J = 7.1$  Hz, 3H), 1.22 (d,  $J = 6.3$  Hz, 6H), 1.17 (s, 3H) ppm;  $^{13}\text{C}$  NMR (151 MHz,  $\text{CD}_3\text{OD}$ )  $\delta$  174.4 (d,  $^3J_{\text{C-P}} = 5.4$  Hz), 165.7, 152.9, 152.1 (d,  $^2J_{\text{C-P}} = 6.7$  Hz), 143.6, 130.9, 126.2, 121.3 (d,  $^3J_{\text{C-P}} = 4.9$  Hz), 102.9, 82.8, 77.6, 70.2, 68.2, 67.6 (d,  $^2J_{\text{C-P}} = 5.1$  Hz), 51.7, 51.1 (d,  $^2J_{\text{C-P}} = 8.4$  Hz), 22.0, 21.9, 20.7, 20.6 ppm;  $^{31}\text{P}$  NMR (121 MHz,  $\text{CD}_3\text{OD}$ )  $\delta$  3.6 ppm; HRMS (ESI)  $m/z$ :  $[\text{M} + \text{H}]^+$  Calcd for  $\text{C}_{22}\text{H}_{31}\text{N}_3\text{O}_9\text{PS}$  544.1513; Found 544.1511.



2.13b

**(S)-isopropyl 2-(((S)-(((2R,3S,4R,5R)-5-(5-fluoro-2,4-dioxo-3,4-dihydropyrimidin-1(2H)-yl)-3,4-dihydroxy-4-methyltetrahydrothiophen-2-**

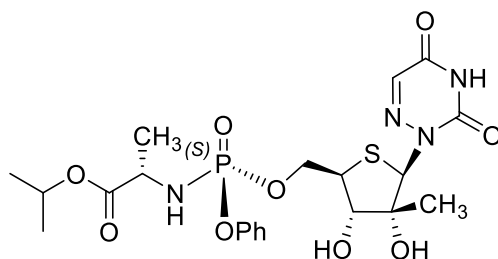
**yl)methoxy)(phenoxy)phosphoryl)amino)propanoate (2.13b):** Following the general phosphoramidation procedure, thionucleoside **2.11b** (38 mg, 0.13 mmol) was treated with **2.12** (59 mg, 0.13 mmol) to afford the desired product (16 mg, 22% yield);  $^1\text{H}$  NMR (500 MHz,  $\text{CD}_3\text{OD}$ )  $\delta$  8.21 (d,  $^3J_{\text{H-F}} = 6.8$  Hz, 1H), 7.37–7.324 (m, 2H), 7.27–7.25 (m, 2H), 7.20–7.17 (m, 1H), 5.96 (d,  $^5J_{\text{H-F}} = 1.7$  Hz, 1H), 4.97 (app hept,  $J = 6.2$  Hz, 1H), 4.55–4.52 (m, 1H), 4.50–4.46 (m, 1H), 3.92 (dq,  $J = 10.0, 7.1$  Hz, 1H), 3.71 (d,  $J = 9.6$  Hz, 1H), 3.67–3.63 (m, 1H), 1.35 (d,  $J = 7.1$  Hz, 3H), 1.22 (d,  $J = 6.3$  Hz, 6H), 1.20 (s, 3H) ppm;  $^{13}\text{C}$  NMR (151 MHz, MeOD)  $\delta$  174.3 (d,  $^3J_{\text{C-P}} = 5.4$  Hz), 159.0 (d,  $^2J_{\text{C-F}} = 26.4$  Hz), 152.0 (d,  $^2J_{\text{C-P}} = 6.5$  Hz), 151.5, 141.2 (d,  $^1J_{\text{C-F}} = 235.4$  Hz), 130.7, 127.1 (d,  $^2J_{\text{C-F}} = 35.0$  Hz), 126.1, 121.3 (d,  $^3J_{\text{C-P}} = 4.8$  Hz), 82.7, 77.4, 70.1, 68.6, 67.3 (d,  $^2J_{\text{C-P}} = 4.8$  Hz), 51.6, 51.0 (d,  $^2J_{\text{C-P}} = 8.6$  Hz), 22.0, 21.9, 20.62, 20.59 (d,  $^3J_{\text{C-P}} = 2.1$  Hz) ppm;  $^{19}\text{F}$  NMR (282 MHz,  $\text{CD}_3\text{OD}$ )  $\delta$  -165.6 (d,  $^3J_{\text{F-H}} = 6.3$  Hz);  $^{31}\text{P}$  NMR (121 MHz,  $\text{CD}_3\text{OD}$ )  $\delta$  3.7 ppm; HRMS (NSI)  $m/z$ :  $[\text{M} + \text{H}]^+$  Calcd for  $\text{C}_{22}\text{H}_{30}\text{N}_3\text{O}_9\text{FPS}$  562.1419; Found 562.1411.



2.13c

**(S)-isopropyl 2-(((S)-(((2R,3S,4R,5R)-5-(6-amino-9H-purin-9-yl)-3,4-dihydroxy-4-methyltetrahydrothiophen-2-yl)methoxy)(phenoxy)phosphoryl)amino)propanoate (2.13c):**

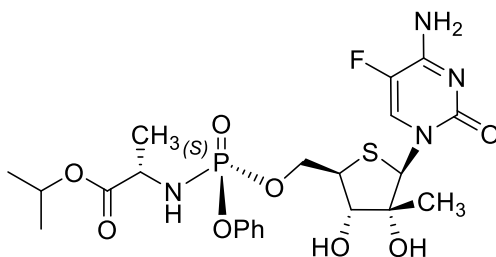
Following the general phosphoramidation procedure, thionucleoside **2.11c** (86 mg, 0.29 mmol) was treated with **2.12** (131 mg, 0.29 mmol) to afford the desired product after two rounds of purification (40 mg, 25% yield);  $^1\text{H}$  NMR (300 MHz,  $\text{CD}_3\text{OD}$ )  $\delta$  8.44 (s, 1H), 8.22 (s, 1H), 7.43–7.31 (m, 2H), 7.35–7.24 (m, 2H), 7.25–7.13 (m, 1H), 5.87 (s, 1H), 5.05–4.90 (m, 1H), 4.66–4.52 (m, 2H), 4.11 (d,  $J = 9.5$  Hz, 1H), 3.94 (dq,  $J = 9.9, 7.1$  Hz, 1H), 3.86–3.73 (m, 1H), 1.37 (dd,  $J = 7.1, 0.8$  Hz, 3H), 1.20 (d,  $J = 6.2$  Hz, 3H), 1.15 (d,  $J = 6.3$  Hz, 3H), 0.93 (s, 3H) ppm;  $^{13}\text{C}$  NMR (151 MHz,  $\text{CD}_3\text{OD}$ )  $\delta$  174.4 (d,  $^3J_{\text{C-P}} = 5.5$  Hz), 157.5, 154.0, 152.2 (d,  $^2J_{\text{C-P}} = 6.7$  Hz), 151.2, 141.9, 130.8, 126.2, 121.4 (d,  $^3J_{\text{C-P}} = 4.8$  Hz), 120.2, 83.0, 77.7, 70.1, 68.4 (d,  $^2J_{\text{C-P}} = 5.0$  Hz), 66.4, 51.7, 51.2 (d,  $^2J_{\text{C-P}} = 8.5$  Hz), 22.0, 21.9, 20.9, 20.7 (d,  $^3J_{\text{C-P}} = 6.3$  Hz) ppm;  $^{31}\text{P}$  NMR (121 MHz,  $\text{CD}_3\text{OD}$ )  $\delta$  3.7 ppm; HRMS (ESI)  $m/z$ :  $[\text{M} + \text{H}]^+$  Calcd for  $\text{C}_{23}\text{H}_{32}\text{N}_6\text{O}_7\text{PS}$  567.1785; Found 567.1778.



2.13d

**(2S)-isopropyl 2-((((2R,3S,4R,5R)-5-(3,5-dioxo-4,5-dihydro-1,2,4-triazin-2(3H)-yl)-3,4-dihydroxy-4-methyltetrahydrothiophen-2-yl)methoxy)(phenoxy)phosphoryl)amino)propanoate (2.13d):** Following the general

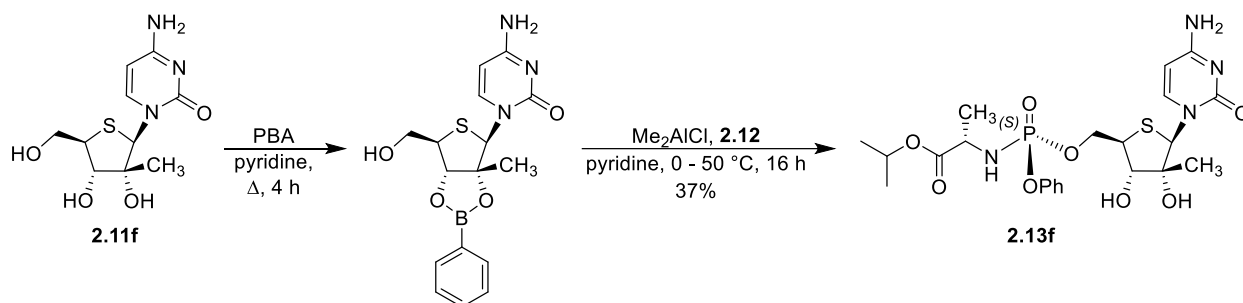
phosphoramidation procedure, thionucleoside **2.11d** (60 mg, 0.22 mmol) was treated with **2.12** (100 mg, 0.22 mmol) to afford the desired product (27 mg, 23% yield);  $^1\text{H}$  NMR (600 MHz,  $\text{CD}_3\text{OD}$ )  $\delta$  7.49 (s, 1H), 7.35 (t,  $J = 7.9$  Hz, 2H), 7.27–7.21 (m, 2H), 7.21–7.15 (m, 1H), 6.03 (s, 1H), 4.95 (dq,  $J = 12.5$ , 6.3 Hz, 1H), 4.59 (ddd,  $J = 10.0$ , 6.0, 3.9 Hz, 1H), 4.28–4.21 (m, 1H), 4.04 (d,  $J = 8.7$  Hz, 1H), 3.90 (dq,  $J = 9.7$ , 7.1 Hz, 1H), 3.64 (td,  $J = 8.9$ , 3.9 Hz, 1H), 1.34 (d,  $J = 7.1$  Hz, 3H), 1.22 (d,  $J = 6.3$  Hz, 6H), 1.20 (s, 3H) ppm;  $^{13}\text{C}$  NMR (151 MHz,  $\text{CD}_3\text{OD}$ )  $\delta$  174.4 (d,  $^3J_{\text{C-P}} = 5.9$  Hz), 158.3, 152.2 (d,  $^2J_{\text{C-P}} = 6.9$  Hz), 150.2, 137.5, 130.7, 126.1, 121.4 (d,  $^3J_{\text{C-P}} = 4.8$  Hz), 83.3, 79.3, 70.9 (d,  $^2J_{\text{C-P}} = 5.3$  Hz), 70.1, 51.6, 51.5 (d,  $^2J_{\text{C-P}} = 8.0$  Hz), 22.0, 21.9, 20.7, 20.6 (d,  $^3J_{\text{C-P}} = 6.1$  Hz) ppm;  $^{31}\text{P}$  NMR (121 MHz,  $\text{CD}_3\text{OD}$ )  $\delta$  3.3 ppm; HRMS (ESI-)  $m/z$ :  $[\text{M} + \text{Cl}]^-$  Calcd for  $\text{C}_{21}\text{H}_{29}\text{N}_4\text{O}_9\text{ClPS}$  579.1087; Found 579.1090.

**2.13e**

**Isopropyl (2S)-2-[[[(2R,3S,4R,5R)-5-(4-amino-5-fluoro-2-oxo-pyrimidin-1-yl)-3,4-dihydroxy-4-methyl-tetrahydrothiophen-2-yl]methoxy-phenoxy-phosphoryl]amino]propanoate**

**(2.13e):** Following the general phosphoramidation procedure, thionucleoside **2.11e** (72 mg, 0.25 mmol) was treated with **2.12** (224 mg, 0.5 mmol) to afford the desired product after three rounds of purification (12 mg, 8% yield);  $^1\text{H}$  NMR (600 MHz, MeOD)  $\delta$  8.19 (d,  $^3J_{\text{H-F}} = 6.8$  Hz, 1H), 7.39–7.33 (m, 2H), 7.29–7.26 (m, 2H), 7.20–7.18 (m, 1H), 6.09 (d,  $^5J_{\text{H-F}} = 1.8$  Hz, 1H), 4.97 (app hept,  $J = 6.3$  Hz, 1H), 4.57–4.52 (m, 1H), 4.50–4.46 (m, 1H), 3.93 (dq,  $J = 10.1$ , 7.1 Hz, 1H), 3.69 (d,  $J = 9.7$  Hz, 1H), 3.67–3.63 (m, 1H), 1.35 (d,  $J = 7.1$  Hz, 3H), 1.22 (d,  $J = 6.2$  Hz, 3H), 1.21 (d,  $J = 6.3$  Hz, 3H), 1.15 (s, 3H) ppm;  $^{13}\text{C}$  NMR (151 MHz,  $\text{CD}_3\text{OD}$ )  $\delta$  174.4 (d,  $^3J_{\text{C-P}} = 5.4$  Hz), 159.3 (d,  $^2J_{\text{C-F}} = 14.0$  Hz), 157.4, 152.2 (d,  $^2J_{\text{C-P}} = 6.6$  Hz), 138.0 (d,  $^1J_{\text{C-F}} = 244.9$  Hz), 130.8, 127.9 (d,  $^2J_{\text{C-F}} = 32.8$  Hz), 126.1, 121.4 (d,  $^3J_{\text{C-P}} = 4.9$  Hz), 82.9, 77.4, 70.2, 69.3, 67.6 (d,  $^2J_{\text{C-P}} = 4.8$  Hz), 51.7, 51.0 (d,  $^2J_{\text{C-P}} = 8.6$  Hz), 22.0, 21.9, 20.63, 20.59 ppm;  $^{19}\text{F}$

NMR (282 MHz, CD<sub>3</sub>OD)  $\delta$ -165.7 (d,  $^3J_{F-H} = 5.6$  Hz) ppm;  $^{31}\text{P}$  NMR (121 MHz, CD<sub>3</sub>OD)  $\delta$  3.7 ppm; HRMS (NSI)  $m/z$ :  $[\text{M} + \text{H}]^+$  Calcd for C<sub>22</sub>H<sub>31</sub>N<sub>4</sub>O<sub>8</sub>FPS 561.1579; Found 561.1578.



**Isopropyl (2S)-2-[[[(2R,3S,4R,5R)-5-(4-amino-2-oxo-pyrimidin-1-yl)-3,4-dihydroxy-4-methyl-tetrahydrothiophen-2-yl]methoxy-phenoxy-phosphoryl]amino]propanoate (2.13f):**

An oven-dried 50-mL round-bottom flask with stir bar and reflux condenser was charged with thionucleoside **2.11f** (80.5 mg, 0.29 mmol), and the apparatus and solid were dried overnight *in vacuo*. The flask was then charged with argon, phenylboronic acid (38 mg, 0.31 mmol), and anhydrous pyridine (0.75 mL) to give a yellow solution. The reaction was heated to 100 °C for approximately 4 h before the volatiles were removed. The crude yellow semi-solid was dried briefly *in vacuo* before the flask was again charged with argon followed by **2.12** (160 mg, 0.35 mmol) and anhydrous pyridine (1 mL) to give a yellow solution. The solution was chilled to 0 °C before Me<sub>2</sub>AlCl (0.15 mL, 0.15 mmol) was dropwise added as a 1 M solution in hexanes, and the reaction was warmed to 50 °C with stirring overnight. The next morning, the reaction was cooled to ambient temperature before being quenched with 0.4 mL of 30 wt% aqueous L-tartaric acid solution. The reaction mixture was then diluted with ethyl acetate and aqueous brine solution before being extracted with ethyl acetate. The organic extracts were combined, dried over Na<sub>2</sub>SO<sub>4</sub>, filtered, concentrated and purified via two rounds of silica gel flash column chromatography (eluted with a gradient of 0–15% methanol in DCM) to afford the desired product (59 mg, 37% yield);  $^1\text{H}$  NMR (600 MHz, CD<sub>3</sub>OD)  $\delta$  8.09 (d,  $J = 7.5$  Hz, 1H), 7.41–7.35 (m, 2H), 7.31–7.26 (m, 2H), 7.23–7.17 (m, 1H), 6.16 (s, 1H), 5.90 (d,  $J = 7.4$  Hz, 1H), 4.97 (app hept,  $J = 6.3$  Hz, 1H), 4.57–4.51 (m, 1H), 4.50–4.43 (m, 1H), 3.93 (dq,  $J = 9.9, 7.1$  Hz,

1H), 3.67 (br, 1H), 1.36 (d,  $J = 7.1$  Hz, 3H), 1.22 (d,  $J = 6.2$  Hz, 3H), 1.21 (d,  $J = 6.3$  Hz, 3H), 1.12 (s, 3H) ppm;  $^{13}\text{C}$  NMR (151 MHz,  $\text{CD}_3\text{OD}$ )  $\delta$  174.4 (d,  $^3J_{\text{C-P}} = 5.4$  Hz), 167.1, 159.0, 152.2 (d,  $^2J_{\text{C-P}} = 6.7$  Hz), 144.1, 130.9, 126.2, 121.3 (d,  $^3J_{\text{C-P}} = 4.8$  Hz), 96.5, 82.9, 77.5, 70.2, 68.7, 67.7 (d,  $^2J_{\text{C-P}} = 5.0$  Hz), 51.7, 50.9 (d,  $^2J_{\text{C-P}} = 8.6$  Hz), 22.0, 21.9, 20.7, 20.6 ppm;  $^{31}\text{P}$  NMR (121 MHz,  $\text{CD}_3\text{OD}$ )  $\delta$  3.5 ppm; HRMS (NSI)  $m/z$ :  $[\text{M} + \text{H}]^+$  Calcd for  $\text{C}_{22}\text{H}_{32}\text{N}_4\text{O}_8\text{PS}$  543.1673; Found 543.1676.

### 2.3.2 Pharmacology

**Anti-HCV and Cytotoxicity Evaluation:** For *in vitro* evaluation of the antiviral and cytotoxic effects, the compounds were submitted to ImQuest Biosciences, Inc. (Frederick, Maryland 21704) as a contracted fee-for-service body of work. According to their standard operating procedure, Huh-7 luc/neo ET cells bearing a dicistronic HCV genotype 1b luciferase reporter replicon were plated at  $7.5 \times 10^3$  cells/mL in duplicate 96-well plates for the parallel determination of antiviral efficacy ( $\text{EC}_{50}$ ) and cytotoxicity ( $\text{TC}_{50}$ ). These plates were cultured for 24 h prior to the addition of compounds. Six serial half-log dilutions of the test articles (high test of 1  $\mu\text{g}/\text{mL}$ ) and sofosbuvir (high test 1.0  $\mu\text{M}$ ) were prepared in cell culture medium and added to the cultured cells in triplicate wells for each dilution. Six wells in the test plates received medium alone as an untreated control. Following 72 h of culture in the presence of the compound, one of the plates was used for the determination of cytotoxicity by staining with XTT (2,3-bis-(2-methoxy-4-nitro-5-sulfophenyl)-2H-tetrazolium-5-carboxanilide) and the other for antiviral efficacy by determination of luciferase reporter activity. Cytotoxicity and efficacy data were collected and imported into a customized Microsoft Excel™ workbook for the determination of  $\text{TC}_{50}$  and  $\text{EC}_{50}$  values. The primary data appearing on the following pages are taken directly from the Final Report of SOW277-03-12 prepared by T. Hartman (PI) at ImQuest BioSciences, Inc. The compound IDs are cross-listed according to Table 2.2.

**Table 2.2.** Reference table for matching Compound No.'s used in this chapter with Notebook No.'s used by ImQuest BioSciences, Inc.

<b>Compound No.</b>	<b>Notebook No.</b>
<b>2.13a</b>	ZD-2-171
<b>2.13b</b>	ZD-2-176
<b>2.13c</b>	ZD-2-164
<b>2.13d</b>	ZD-2-166
<b>2.13e</b>	ZD-3-007
<b>2.13f</b>	ZD-3-022

**INHIBITION OF HCV REPLICATION BY ZD-2-171 IN Huh-luc/neo-ET**

Raw Data (ZD-2-171)

RLU (Relative Light Units)							
Conc (µM)	0	0.63	2	6.32	19.99	63.2	200
SAMPLE 1	103563.0	82440.0	50614.0	9908.0	664.0	614.0	684.0
SAMPLE 2	120130.0	93672.0	56302.0	10122.0	764.0	626.0	694.0
SAMPLE 3	124319.0	93432.0	73420.0	11022.0	1274.0	882.0	830.0

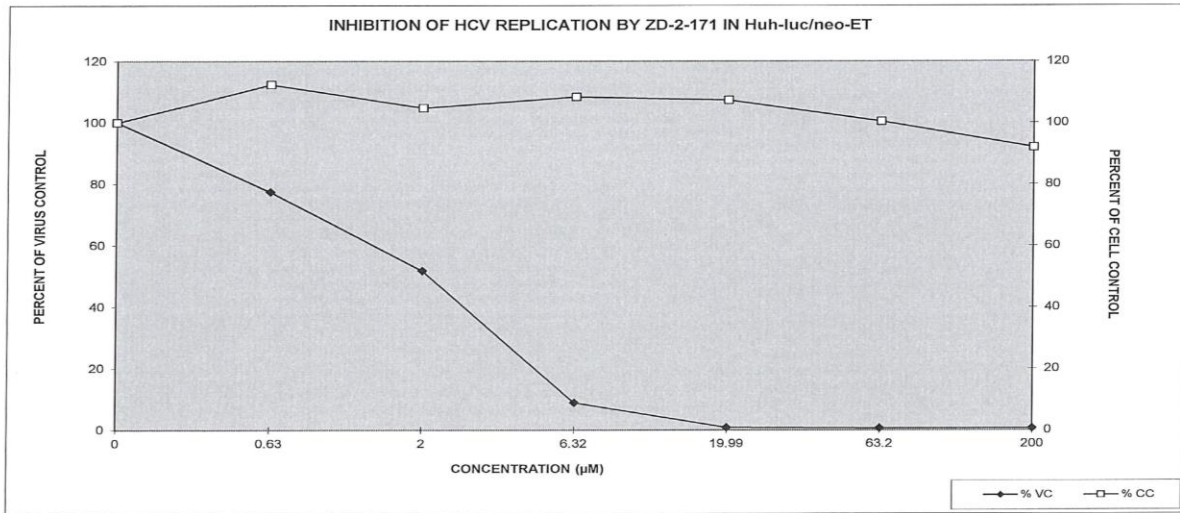
TOXICITY VALUES (XTT - O. D. @ 450/650 nm)							
Conc (µM)	0	0.63	2	6.32	19.99	63.2	200
SAMPLE 1	2.181	2.560	2.171	2.340	2.360	2.242	2.074
SAMPLE 2	2.158	2.439	2.338	2.376	2.281	2.163	2.016
SAMPLE 3	2.197	2.348	2.338	2.368	2.373	2.158	1.922

Cells: Huh-luc/neo-ET      Technician: C. Buchholz      Project #: 277-03-12  
 PI: T. Hartman  
 Client: Emory

**Antiviral Compound: ZD-2-171**

	25%	50%	95%
EC (µM)	0.704	2.10	11.0
TC (µM)	>200	>200	>200
Therapeutic Index (TI)	>284.09	>95.24	>18.18

Conc (µM)	Antiviral Test Values			Cytotoxicity Test Values		
	Mean RLU	St. Dev.	% Virus Control	Mean OD @ 450/650 nm	St. Dev.	% Cell Viability
0	116004.0	10975.919	100.00	2.179	0.01970573	100.00
0.63	89848.0	6416.6384	77.45	2.449	0.10670437	112.40
2	60112.0	11870.783	51.82	2.282	0.09633091	104.76
6.32	10350.7	591.15593	8.92	2.361	0.01895688	108.38
19.99	900.7	327.15949	0.78	2.338	0.04943747	107.31
63.2	707.3	151.38472	0.61	2.188	0.04696364	100.42
200	736.0	81.559794	0.63	2.004	0.07702015	91.99



### INHIBITION OF HCV REPLICATION BY ZD-2-176 IN Huh-luc/neo-ET

Raw Data (ZD-2-176)

RLU (Relative Light Units)							
Conc (µM)	0	0.63	2	6.32	19.99	63.2	200
SAMPLE 1	103563.0	129362.0	134312.0	112200.0	113138.0	74580.0	27618.0
SAMPLE 2	120130.0	111584.0	133446.0	158776.0	111246.0	90538.0	25626.0
SAMPLE 3	124319.0	142206.0	132886.0	128444.0	120022.0	103812.0	27378.0

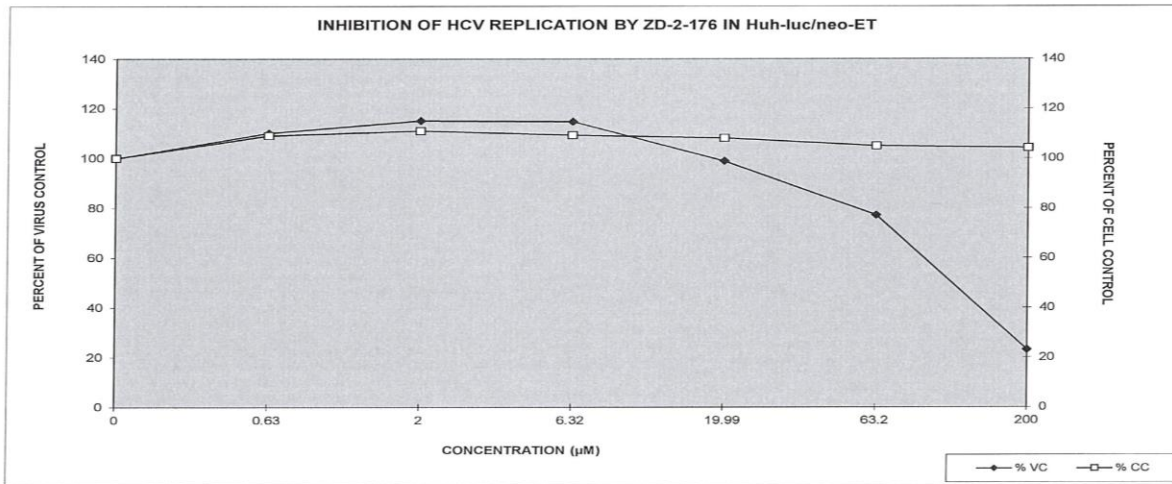
TOXICITY VALUES (XTT - O. D. @ 450/650 nm)							
SAMPLE	0	0.63	2	6.32	19.99	63.2	200
SAMPLE 1	2.181	2.378	2.410	2.368	2.418	2.303	2.353
SAMPLE 2	2.158	2.489	2.447	2.431	2.402	2.404	2.305
SAMPLE 3	2.197	2.264	2.398	2.346	2.251	2.154	2.151

Cells: Huh-luc/neo-ET      Technician: C. Buchholz      Project #: 277-03-12  
 PI: T. Hartman  
 Client: Emory

Antiviral Compound: ZD-2-176

	25%	50%	95%
EC (µM)	66.3	113	>200
TC (µM)	>200	>200	>200
Therapeutic Index (TI)	>3.02	>1.77	1

Conc (µM)	Antiviral Test Values			Cytotoxicity Test Values		
	Mean RLU	St. Dev.	% Virus Control	Mean OD @ 450/650 nm	St. Dev.	% Cell Viability
0	116004.0	10975.9187	100.00	2.179	0.019706	100.00
0.63	127717.3	15377.1069	110.10	2.377	0.112105	109.11
2	133548.0	718.451112	115.12	2.419	0.025741	111.01
6.32	133140.0	23640.4369	114.77	2.382	0.044454	109.31
19.99	114802.0	4618.57294	98.96	2.357	0.092129	108.18
63.2	89643.3	14636.522	77.28	2.287	0.125692	104.97
200	26874.0	1087.44103	23.17	2.269	0.105787	104.17



### INHIBITION OF HCV REPLICATION BY ZD-2-164 IN Huh-luc/neo-ET

Raw Data (ZD-2-164)

RLU (Relative Light Units)							
Conc (µM)	0	0.63	2	6.32	19.99	63.2	200
SAMPLE 1	113808.0	131868.0	138056.0	118938.0	101334.0	31610.0	8586.0
SAMPLE 2	148637.0	145856.0	148776.0	93626.0	77970.0	27510.0	7832.0
SAMPLE 3	135742.0	153380.0	135408.0	98086.0	111218.0	54300.0	14534.0

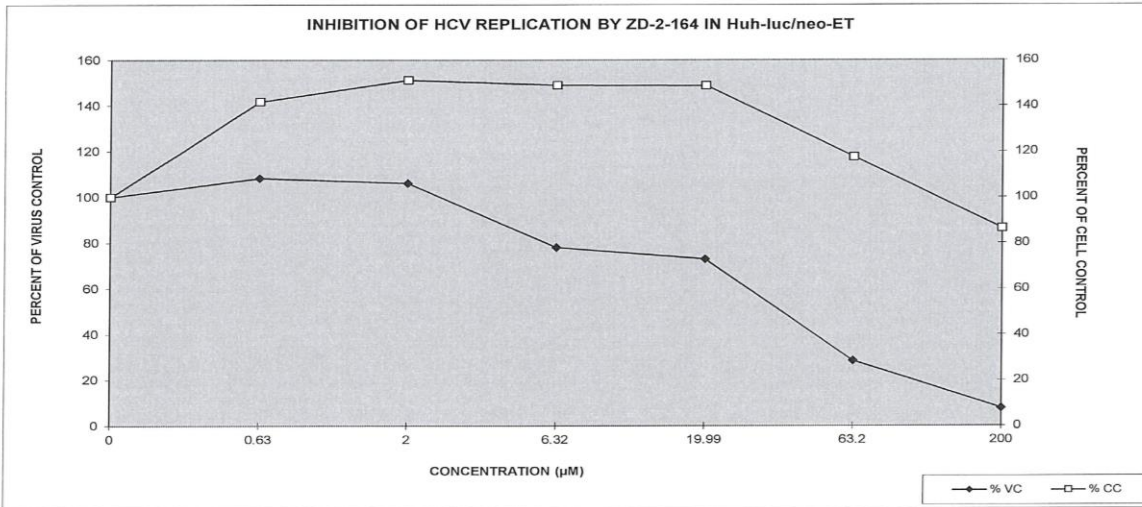
TOXICITY VALUES (XTT - O. D. @ 450/650 nm)							
SAMPLE 1	0	0.63	2	6.32	19.99	63.2	200
SAMPLE 1	1.845	2.542	2.611	2.580	2.629	2.301	1.724
SAMPLE 2	1.838	2.970	2.693	2.694	2.600	2.325	1.563
SAMPLE 3	1.619	1.999	2.711	2.623	2.659	1.609	1.294

Cells: Huh-luc/neo-ET      Technician: C. Buchholz      Project #: 277-03-12  
 PI: T. Hartman  
 Client: Emory

Antiviral Compound: ZD-2-164

	25%	50%	95%
EC (µM)	12.6	36.2	>200
TC (µM)	>200	>200	>200
Therapeutic Index (TI)	>15.87	>5.52	1

Conc (µM)	Antiviral Test Values			Cytotoxicity Test Values		
	Mean RLU	St. Dev.	% Virus Control	Mean OD @ 450/650 nm	St. Dev.	% Cell Viability
0	132729.0	17608.9022	100.00	1.767	0.128734	100.00
0.63	143701.3	10916.6605	108.27	2.504	0.486741	141.69
2	140746.7	7078.53243	106.04	2.672	0.053111	151.19
6.32	103550.0	13511.6915	78.02	2.632	0.057496	148.95
19.99	96840.7	17073.3684	72.96	2.629	0.029459	148.79
63.2	37806.7	14430.0046	28.48	2.079	0.406832	117.63
200	10317.3	3671.14932	7.77	1.527	0.217294	86.40



### INHIBITION OF HCV REPLICATION BY ZD-2-166 IN Huh-luc/neo-ET

Raw Data (ZD-2-166)

RLU (Relative Light Units)							
Conc (µM)	0	0.63	2	6.32	19.99	63.2	200
SAMPLE 1	113808.0	161860.0	131314.0	142210.0	218668.0	122556.0	130970.0
SAMPLE 2	148637.0	155106.0	175832.0	139452.0	140022.0	120702.0	97896.0
SAMPLE 3	135742.0	155362.0	133104.0	158222.0	162830.0	111404.0	100416.0

TOXICITY VALUES (XTT - O. D. @ 450/650 nm)

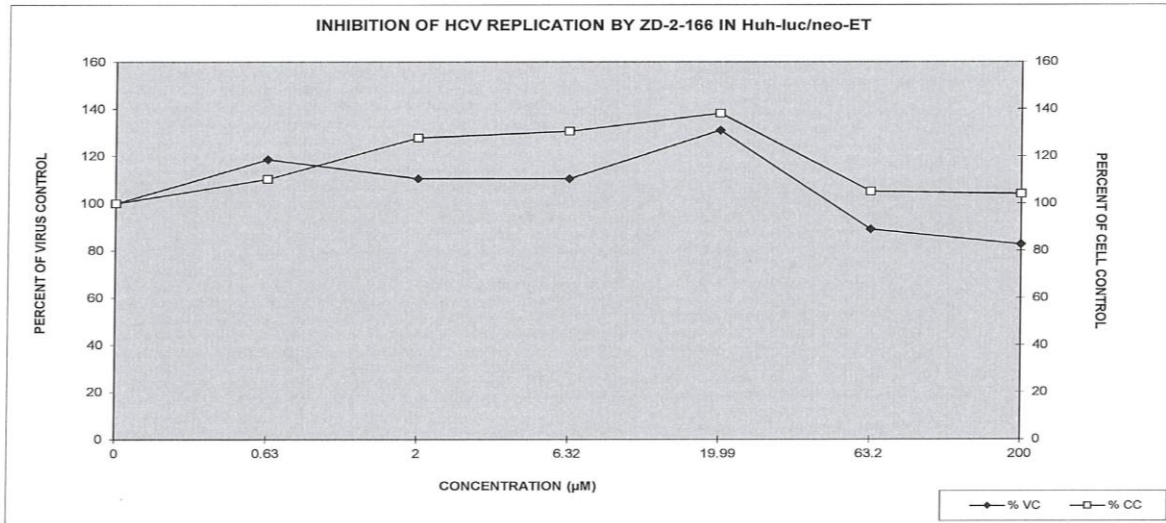
SAMPLE	0	0.63	2	6.32	19.99	63.2	200
SAMPLE 1	1.845	2.299	2.645	2.469	2.628	2.488	2.539
SAMPLE 2	1.838	1.755	2.381	2.503	2.392	1.583	1.668
SAMPLE 3	1.619	1.794	1.750	1.955	2.307	1.499	1.308

Cells: Huh-luc/neo-ET      Technician: C. Buchholz      Project #: 277-03-12  
 PI: T. Hartman  
 Client: Emory

Antiviral Compound: ZD-2-166

	25%	50%	95%
EC (µM)	>200	>200	>200
TC (µM)	>200	>200	>200
Therapeutic Index (TI)			

Conc (µM)	Antiviral Test Values			Cytotoxicity Test Values		
	Mean RLU	St. Dev.	% Virus Control	Mean OD @ 450/650 nm	St. Dev.	% Cell Viability
0	132729.0	17608.9022	100.00	1.767	0.128734	100.00
0.63	157442.7	3827.66369	118.62	1.949	0.303358	110.30
2	146750.0	25201.6481	110.56	2.259	0.459638	127.82
6.32	146628.0	10134.9528	110.47	2.309	0.307254	130.66
19.99	173840.0	40462.4938	130.97	2.442	0.166116	138.20
63.2	118220.7	5975.74576	89.07	1.857	0.548114	105.07
200	109760.7	18410.9876	82.70	1.838	0.633334	104.03



### INHIBITION OF HCV REPLICATION BY ZD-3-007 IN Huh-luc/neo-ET

Raw Data (ZD-3-007)

RLU (Relative Light Units)							
Conc (µM)	0	0.63	2	6.32	19.99	63.2	200
SAMPLE 1	103563.0	101570.0	132840.0	120154.0	108036.0	83906.0	60090.0
SAMPLE 2	120130.0	126358.0	110644.0	125892.0	95626.0	60914.0	49792.0
SAMPLE 3	124319.0	109070.0	103152.0	101628.0	111660.0	74844.0	32014.0

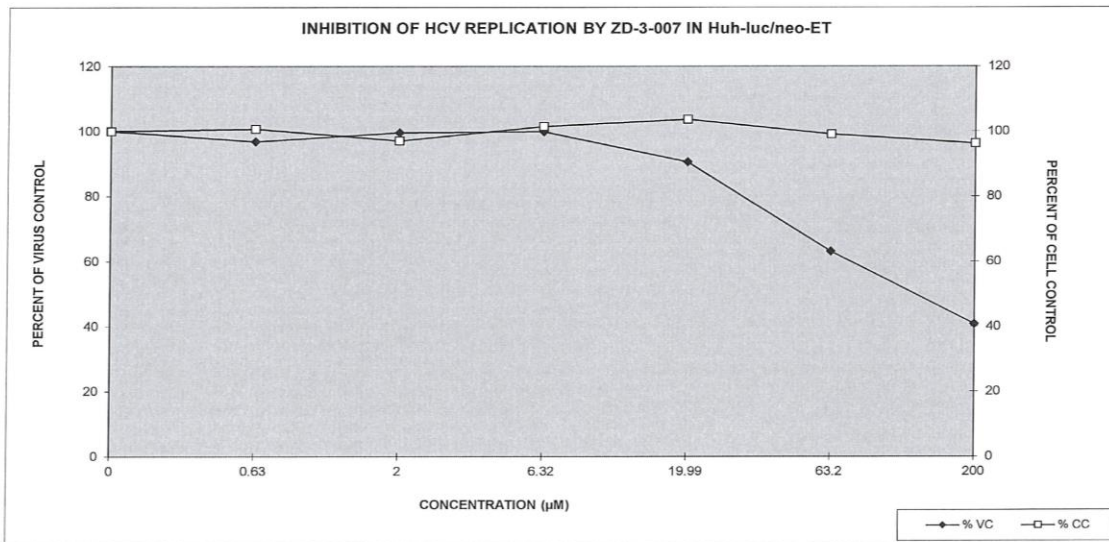
TOXICITY VALUES (XTT - O. D. @ 450/650 nm)							
SAMPLE	0	0.63	2	6.32	19.99	63.2	200
SAMPLE 1	2.181	2.311	2.345	2.247	2.356	2.242	2.074
SAMPLE 2	2.158	2.265	2.126	2.235	2.289	2.160	2.159
SAMPLE 3	2.197	2.005	1.872	2.150	2.131	2.075	2.059

Cells: Huh-luc/neo-ET      Technician: C. Buchholz      Project #: 277-03-12  
 PI: T. Hartman  
 Client: Emory

Antiviral Compound: ZD-3-007

	25%	50%	95%
EC (µM)	38.4	124	>200
TC (µM)	>200	>200	>200
Therapeutic Index (TI)	>5.21	>1.61	1

Conc (µM)	Antiviral Test Values			Cytotoxicity Test Values		
	Mean RLU	St. Dev.	% Virus Control	Mean OD @ 450/650 nm	St. Dev.	% Cell Viability
0	116004.0	10975.9187	100.00	2.179	0.019706	100.00
0.63	112332.7	12712.0015	96.84	2.194	0.164902	100.70
2	115545.3	15438.9649	99.60	2.114	0.236716	97.05
6.32	115891.3	12681.2132	99.90	2.211	0.05303	101.47
19.99	105107.3	8408.63279	90.61	2.258	0.115822	103.66
63.2	73221.3	11581.5716	63.12	2.159	0.083553	99.11
200	47298.7	14203.0975	40.77	2.098	0.054071	96.28



**INHIBITION OF HCV REPLICATION BY ZD-3-022 IN Huh-luc/neo-ET**

Raw Data (ZD-3-022)

RLU (Relative Light Units)							
Conc (µM)	0	0.63	2	6.32	19.99	63.2	200
SAMPLE 1	146640.0	149080.0	157040.0	113056.0	26128.0	2034.0	542.0
SAMPLE 2	153242.0	164168.0	128704.0	98152.0	19878.0	2064.0	878.0
SAMPLE 3	178054.0	167594.0	144704.0	127896.0	31192.0	3386.0	1326.0

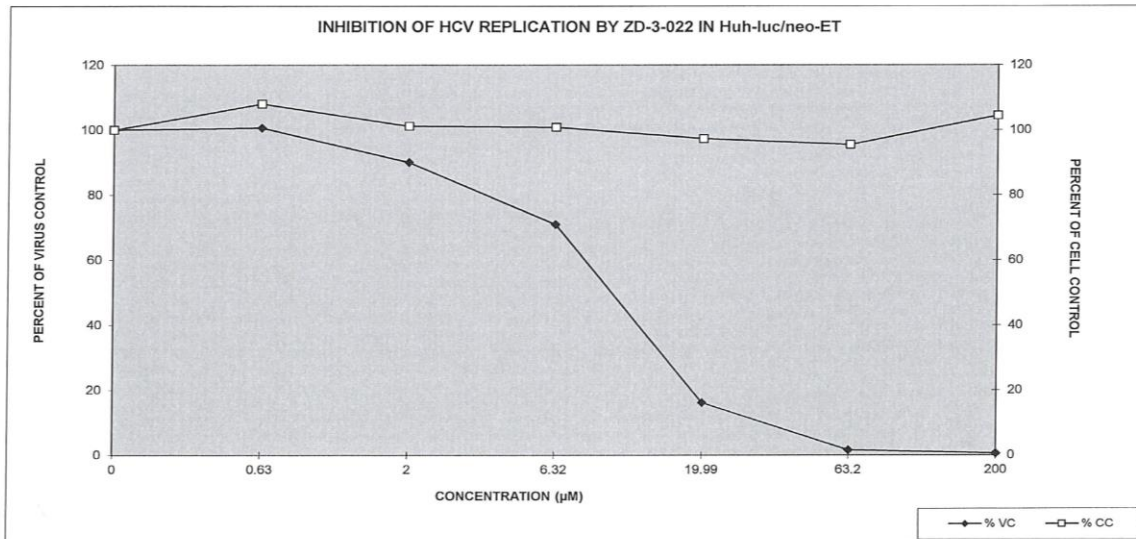
TOXICITY VALUES (XTT - O. D. @ 450/650 nm)							
Conc (µM)	0	0.63	2	6.32	19.99	63.2	200
SAMPLE 1	2.990	3.132	3.093	3.022	3.005	2.630	2.955
SAMPLE 2	2.781	2.933	2.660	2.687	2.518	2.795	2.764
SAMPLE 3	2.506	2.875	2.623	2.637	2.532	2.481	2.926

Cells: Huh-luc/neo-ET      Technician: C. Buchholz      Project #: 277-03-12  
 PI: T. Hartman  
 Client: Emory

Antiviral Compound: ZD-3-022

	25%	50%	95%
EC (µM)	4.95	9.82	48.2
TC (µM)	>200	>200	>200
Therapeutic Index (TI)	>40.40	>20.37	>4.15

Conc (µM)	Antiviral Test Values			Cytotoxicity Test Values		
	Mean RLU	St. Dev.	% Virus Control	Mean OD @ 450/650 nm	St. Dev.	% Cell Viability
0	159312.0	16563.319	100.00	2.759	0.24306384	100.00
0.63	160280.7	9850.1558	100.61	2.980	0.13466651	108.01
2	143482.7	14207.426	90.06	2.792	0.26146587	101.21
6.32	113034.7	14872.011	70.95	2.782	0.20919394	100.83
19.99	25732.7	5667.3508	16.15	2.685	0.27713378	97.32
63.2	2494.7	772.06304	1.57	2.635	0.15727479	95.51
200	915.3	393.33107	0.57	2.882	0.10303574	104.45



### INHIBITION OF HCV REPLICATION BY Sofosbuvir IN Huh-luc/neo-ET

Raw Data (Sofosbuvir)

RLU (Relative Light Units)							
Conc (µM)	0	0.006	0.02	0.063	0.199	0.63	2
SAMPLE 1	113808.0	162974.0	114896.0	48552.0	8146.0	708.0	482.0
SAMPLE 2	148637.0	147722.0	102136.0	54694.0	6956.0	666.0	434.0
SAMPLE 3	135742.0	146159.0	105534.0	53768.0	8538.0	1040.0	556.0

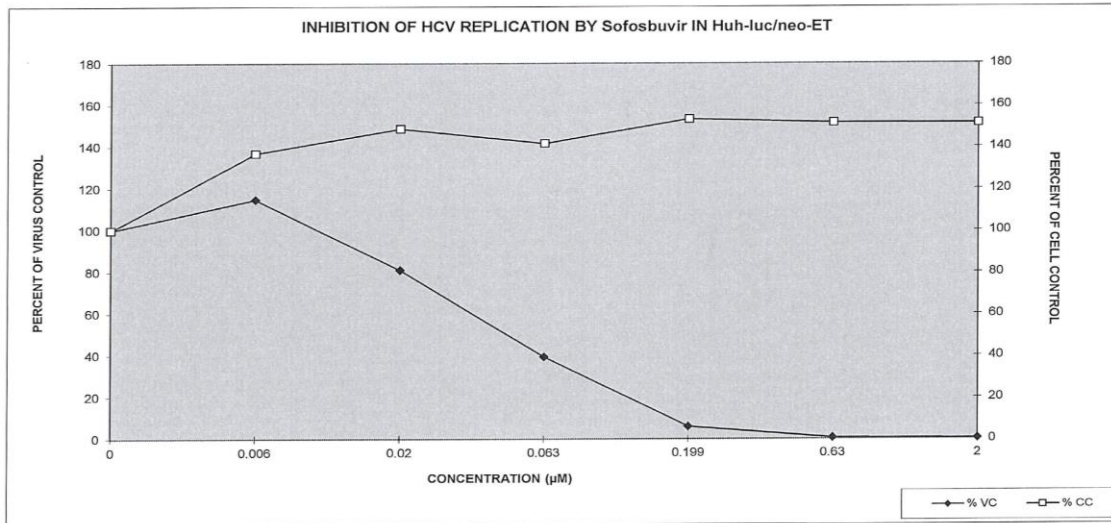
TOXICITY VALUES (XTT - O. D. @ 450/650 nm)							
Conc (µM)	0	0.006	0.02	0.063	0.199	0.63	2
SAMPLE 1	1.845	2.598	2.450	2.381	2.789	2.481	2.539
SAMPLE 2	1.838	2.599	2.668	2.628	2.720	2.759	2.867
SAMPLE 3	1.619	2.054	2.763	2.501	2.615	2.794	2.618

Cells: Huh-luc/neo-ET      Technician: C. Buchholz      Project #: 277-03-12  
 PI: T. Hartman  
 Client: Emory

Antiviral Compound: Sofosbuvir

	25%	50%	95%
EC (µM)	0.0236	0.0471	0.244
TC (µM)	>2.0	>2.0	>2.0
Therapeutic Index (TI)	>84.75	>42.46	>8.20

Conc (µM)	Antiviral Test Values			Cytotoxicity Test Values		
	Mean RLU	St. Dev.	% Virus Control	Mean OD @ 450/650 nm	St. Dev.	% Cell Viability
0	132729.0	17608.902	100.00	1.767	0.12873368	100.00
0.006	152284.7	9290.205	114.73	2.417	0.31430974	136.78
0.02	107522.0	6608.2152	81.01	2.627	0.16049431	148.67
0.063	52338.0	3311.3013	39.43	2.503	0.12351749	141.67
0.199	7880.0	823.86164	5.94	2.708	0.08761849	153.24
0.63	804.7	204.88371	0.61	2.678	0.17142115	151.56
2	490.7	61.460014	0.37	2.675	0.17076877	151.36



**Anti-Zika Evaluations:** The SOP and primary data appearing on the following pages are taken directly from the Final Report of SOW277-03-13 prepared by T. Hartman (PI) at ImQuest BioSciences, Inc.:

Cell Preparation – Huh7 cells (human hepatocarcinoma) were passaged in DMEM supplemented with 10% FBS, 2 mM L-glutamine, 100 U/mL penicillin, and 100 µg/mL streptomycin in T-75 flasks prior to use in the antiviral assay. On the day preceding the assay, the cells were split 1:2 to assure they were in an exponential growth phase at the time of infection. Total cell and viability quantification was performed using a hemocytometer and Trypan Blue dye exclusion. Cell viability was greater than 95% for the cells to be utilized in the assay. The cells were resuspended at  $5 \times 10^3$  cells per well in tissue culture medium and added to flat bottom microtiter plates in a volume of 100 µL. The plates were incubated at 37°C/5% CO<sub>2</sub> overnight to allow for cell adherence. Monolayers were observed to be approximately 70% confluent. Medium was removed and compound diluted to 2x the test concentration in assay medium (DMEM supplemented with 2% heat-inactivated FBS, 2 mM L-glutamine, 100 U/mL penicillin, and 100 µg/mL streptomycin) was added at 100 µL/well. Cells with added compound or assay medium incubated at room temperature for approximately 5 minutes while virus was thawed and diluted.

Virus Preparation – Zika<sup>PRVABC59</sup> virus obtained from BEI Resources (Manassas, VA) was grown in LLCMK2 cells and was titrated in Huh7 cells to define the appropriate inoculum for the performance of the antiviral assay. Virus was diluted into assay medium (DMEM supplemented with 2% heat-inactivated FBS, 2 mM L-glutamine, 100 U/mL penicillin, and 100 µg/mL streptomycin) such that the amount of virus added to each well in a volume of 100 µL was the amount determined to yield 85 to 95% cell killing at 4 days post-infection.

Plate Format – Each plate contains cell control wells (cells only), virus control wells (cells plus virus), a single drug toxicity well per compound (cells plus drug only), as well as duplicate experimental wells (drug plus cells plus virus).

Efficacy and Toxicity XTT - Following incubation at 37°C in a 5% CO<sub>2</sub> incubator, the test plates were stained with the tetrazolium dye XTT (2,3-bis(2-methoxy-4-nitro-5-sulfophenyl)-5-[(phenylamino)carbonyl]-2H-tetrazolium hydroxide). XTT-tetrazolium was metabolized by the mitochondrial enzymes of metabolically active cells to a soluble formazan product, allowing rapid quantitative analysis of the inhibition of virus-induced cell killing by antiviral test substances. XTT solution was prepared daily as a stock of 1 mg/mL in RPMI1640. Phenazine methosulfate (PMS) solution was prepared at 0.15 mg/mL in PBS and stored in the dark at –20°C. XTT/PMS stock was prepared immediately before use by adding 40 µL of PMS per ml of XTT solution. Fifty microliters of XTT/PMS was added to each well of the plate and the plate was reincubated for 4 hours at 37°C. Plates were sealed with adhesive plate sealers and shaken gently or inverted several times to mix the soluble formazan product and the plate was read spectrophotometrically at 450/650 nm with a Molecular Devices Vmax plate reader.

Data Analysis - The raw data was collected from Softmax Pro and imported into a Microsoft Excel 2010 spreadsheet for calculated percentage of reduction values for viral cytopathic effect (CPE) and cell viability.

### In Vitro Antiviral Results For sofosbuvir

Assay: Zika Cytoprotection (XTT)

Sponsor: Emory

Concentration sofosbuvir $\mu\text{M}$ 0.03 0.1 0.32 1 3.16 10	Media Control				Plastic Control			
	Toxicity Drug 1	Cell Control	Low	Toxicity Drug 1	Toxicity Drug 2	Low	Cell Control	Toxicity Drug 2
		Virus Control	Drug 1			Drug 2		
			High			High		
Color Control Drug 1 (High to Low)				Color Control Drug 2 (High to Low)				

Raw Data sofosbuvir ( $\mu\text{M}$ )

0.240	0.231	0.229	0.221	0.223	0.237	0.122	0.104	0.097	0.097	0.093	0.098
	1.970					1.781	0.490	0.272	0.226	1.508	1.545
	2.014					1.682	0.306	0.203	0.248	1.556	1.405
	2.030					1.690	0.250	0.355	0.388	1.439	1.501
	0.338					1.680	0.745	0.473	0.741	0.441	1.504
	0.328					1.775	1.641	1.528	1.415	0.204	1.441
	0.308					1.899	1.735	1.729	1.655	0.284	1.483
						0.230	0.221	0.220	0.223	0.227	0.247

Virus: Zika  
Strain: PRVABC59  
Cells: HUH7

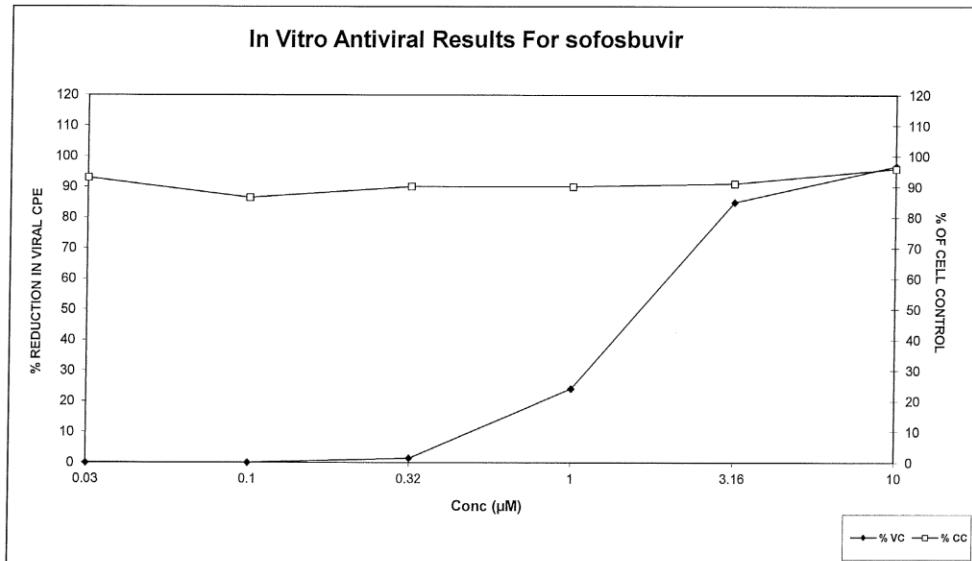
Project #: 0.000  
Sponsor: 0.000

Operator: C. Buchholz

Reagent: 0.230  
Virus Control: 0.087  
Cell Control: 1.523  
Differential: 1.436

sofosbuvir	25%	50%	95%
TC ( $\mu\text{M}$ )	> 10	> 10	> 10
EC ( $\mu\text{M}$ )	1.02	1.63	8.44
Therapeutic Index (TI)	> 9.8	> 6.13	> 1.18

sofosbuvir Conc ( $\mu\text{M}$ )	Antiviral Test Values		Cytotoxicity Test Values		Colorimetric Control
	Mean OD 450/650	% Red. In Viral CPE	Mean OD 450/650	% Cell Viability	
0.03	-0.004	0.00	1.416	93	0.018
0.1	-0.061	0.00	1.317	86	-0.004
0.32	0.021	1.43	1.372	90	-0.007
1	0.346	24.07	1.372	90	-0.010
3.16	1.220	84.96	1.387	91	-0.009
10	1.389	96.74	1.461	96	0.000



Emory University 277-03-13  
**Anti-Zika PRVABC59 Screen in HUH7**

	Compound	well 1	well 2	Mean	Reduction in Viral CPE	XTT	% CC
1	ZD-2-164	0.1055	0.2814	0.19345	7.91%	1.4598	92.53%
2	ZD-2-166	0.111	0.0468	0.0789	0.29%	1.57	99.51%
3	ZD-2-171	0.4768	0.2753	0.37605	20.06%	1.6385	103.85%
4	ZD-2-176	0.1318	0.0797	0.10575	2.08%	1.5844	100.42%
5	ZD-3-007	0.1273	0.269	0.19815	8.22%	1.5359	97.35%
6	ZD-3-022	0.1063	0.0943	0.1003	1.71%	1.5153	96.04%
7							

**Anti-DENV2<sub>New Guinea</sub> Evaluations:** The SOP and primary data appearing on the following pages are taken directly from the Final Report of SOW277-03-14 prepared by T. Hartman (PI) at ImQuest BioSciences, Inc.:

Cell Preparation – Huh7 cells (human hepatocarcinoma) were passaged in DMEM supplemented with 10% FBS, 2 mM L-glutamine, 100 U/mL penicillin, and 100 µg/mL streptomycin in T-75 flasks prior to use in the antiviral assay. On the day preceding the assay, the cells were split 1:2 to assure they were in an exponential growth phase at the time of infection. Total cell and viability quantification was performed using a hemocytometer and Trypan Blue dye exclusion. Cell viability was greater than 95% for the cells to be utilized in the assay. The cells were resuspended at  $5 \times 10^3$  cells per well in tissue culture medium and added to flat bottom microtiter plates in a volume of 100 µL. The plates were incubated at 37°C/5% CO<sub>2</sub> overnight to allow for cell adherence. Monolayers were observed to be approximately 70% confluent. Medium was removed and compound diluted to 2x the test concentration in assay medium

(DMEM supplemented with 2% heat-inactivated FBS, 2 mM L-glutamine, 100 U/mL penicillin, and 100 µg/mL streptomycin) was added at 100 µL/well. Cells with added compound or assay medium incubated at room temperature for approximately 5 minutes while virus was thawed and diluted.

Virus Preparation – DENV2<sup>New Guinea</sup> virus obtained from ATCC (Manassas, VA) was grown in LLCMK2 cells and was titrated in Huh7 cells to define the appropriate inoculum for the performance of the antiviral assay. Virus was diluted into assay medium (DMEM supplemented with 2% heat-inactivated FBS, 2 mM L-glutamine, 100 U/mL penicillin, and 100 µg/mL streptomycin) such that the amount of virus added to each well in a volume of 100 µL was the amount determined to yield 85 to 95% cell killing at 5 days post-infection.

Plate Format – Each plate contains cell control wells (cells only), virus control wells (cells plus virus), a single drug toxicity well per compound (cells plus drug only), as well as duplicate experimental wells (drug plus cells plus virus).

Efficacy and Toxicity XTT - Following incubation at 37°C in a 5% CO<sub>2</sub> incubator, the test plates were stained with the tetrazolium dye XTT (2,3-bis(2-methoxy-4-nitro-5-sulfophenyl)-5-[(phenylamino)carbonyl]-2H-tetrazolium hydroxide). XTT-tetrazolium was metabolized by the mitochondrial enzymes of metabolically active cells to a soluble formazan product, allowing rapid quantitative analysis of the inhibition of virus-induced cell killing by antiviral test substances. XTT solution was prepared daily as a stock of 1 mg/mL in RPMI1640. Phenazine methosulfate (PMS) solution was prepared at 0.15 mg/mL in PBS and stored in the dark at –20°C. XTT/PMS stock was prepared immediately before use by adding 40 µL of PMS per ml of XTT solution. Fifty microliters of XTT/PMS was added to each well of the plate and the plate was reincubated for 4 hours at 37°C. Plates were sealed with adhesive plate sealers and shaken gently or inverted several times to mix the soluble formazan product and the plate was read spectrophotometrically at 450/650 nm with a Molecular Devices Vmax plate reader.

Data Analysis - The raw data was collected from Softmax Pro and imported into a Microsoft Excel 2010 spreadsheet for calculated percentage of reduction values for viral cytopathic effect (CPE) and cell viability.

Emory University 277-03-14  
Anti-DENV2<sub>New Guinea</sub> Screen in HUH7

	Compound	well 1	well 2	Mean	Reduction in Viral CPE	XTT	% CC
1	ZD-2-164	0.268	0.259	0.264	3.077%	1.193	103.8%
2	ZD-2-166	0.221	0.197	0.209	-2.885%	1.162	101.1%
3	ZD-2-171	0.292	0.331	0.312	8.328%	1.108	96.39%
4	ZD-2-176	0.392	0.172	0.282	5.101%	1.145	99.61%
5	ZD-3-007	0.355	0.327	0.341	11.55%	1.133	98.56%
6	ZD-3-022	0.318	0.274	0.296	6.632%	1.285	111.8%
7	Sofosbuvir	1.374	1.278	1.326	119.3%	1.289	112.1%

## 2.4 REFERENCES AND NOTES

1. de Clercq, E., Milestones in the discovery of antiviral agents: nucleosides and nucleotides. *Acta Pharm. Sin. B* **2012**, *2* (6), 535-548.
2. Seley-Radtke, K. L.; Yates, M. K., The evolution of nucleoside analogue antivirals: A review for chemists and non-chemists. Part 1: Early structural modifications to the nucleoside scaffold. *Antiviral Res.* **2018**, *154*, 66-86.
3. World Health Organization Model List of Essential Medicines, 21st List, 2019 2019.
4. Broder, S., The development of antiretroviral therapy and its impact on the HIV-1/AIDS pandemic. *Antiviral Res.* **2010**, *85* (1), 1-18.
5. Sofia, M. J.; Bao, D.; Chang, W.; Du, J. F.; Nagarathnam, D.; Rachakonda, S.; Reddy, P. G.; Ross, B. S.; Wang, P. Y.; Zhang, H. R.; Bansal, S.; Espiritu, C.; Keilman, M.; Lam, A. M.; Steuer, H. M. M.; Niu, C. R.; Otto, M. J.; Furman, P. A., Discovery of a beta-D-2'-Deoxy-2'-alpha-fluoro-2'-beta-C-methyluridine Nucleotide Prodrug (PSI-7977) for the Treatment of Hepatitis C Virus. *J. Med. Chem.* **2010**, *53* (19), 7202-7218.

6. Sofia, M. J., Beyond sofosbuvir: What opportunity exists for a better nucleoside/nucleotide to treat hepatitis C? *Antiviral Res.* **2014**, *107*, 119-124.
7. Carroll, S. S.; Tomassini, J. E.; Bosserman, M.; Getty, K.; Stahlhut, M. W.; Eldrup, A. B.; Bhat, B.; Hall, D.; Simcoe, A. L.; LaFemina, R.; Rutkowski, C. A.; Wolanski, B.; Yang, Z.; Migliaccio, G.; De Francesco, R.; Kuo, L. C.; MacCoss, M.; Olsen, D. B., Inhibition of hepatitis C virus RNA replication by 2'-modified nucleoside analogs. *J. Biol. Chem.* **2003**, *278* (14), 11979-84.
8. Eldrup, A. B.; Allerson, C. R.; Bennett, C. F.; Bera, S.; Bhat, B.; Bhat, N.; Bosserman, M. R.; Brooks, J.; Burlein, C.; Carroll, S. S.; Cook, P. D.; Getty, K. L.; MacCoss, M.; McMasters, D. R.; Olsen, D. B.; Prakash, T. P.; Prhavc, M.; Song, Q. L.; Tomassini, J. E.; Xia, J., Structure-activity relationship of purine ribonucleosides for inhibition of hepatitis C virus RNA-dependent RNA polymerase. *J. Med. Chem.* **2004**, *47* (9), 2283-2295.
9. Eldrup, A. B.; Prhavc, M.; Brooks, J.; Bhat, B.; Prakash, T. P.; Song, Q.; Bera, S.; Bhat, N.; Dande, P.; Cook, P. D.; Bennett, C. F.; Carroll, S. S.; Ball, R. G.; Bosserman, M.; Burlein, C.; Colwell, L. F.; Fay, J. F.; Flores, O. A.; Getty, K.; LaFemina, R. L.; Leone, J.; MacCoss, M.; McMasters, D. R.; Tomassini, J. E.; Von Langen, D.; Wolanski, B.; Olsen, D. B., Structure-activity relationship of heterobase-modified 2'-C-methyl ribonucleosides as inhibitors of hepatitis C virus RNA replication. *J. Med. Chem.* **2004**, *47* (21), 5284-97.
10. De Clercq, E., The design of drugs for HIV and HCV. *Nat. Rev. Drug Discov.* **2007**, *6* (12), 1001-18.
11. Clark, J. L.; Hollecker, L.; Mason, J. C.; Stuyver, L. J.; Tharnish, P. M.; Lostia, S.; McBrayer, T. R.; Schinazi, R. F.; Watanabe, K. A.; Otto, M. J.; Furman, P. A.; Stec, W. J.; Patterson, S. E.; Pankiewicz, K. W., Design, synthesis, and antiviral activity of 2'-deoxy-2'-fluoro-2'-C-methylcytidine, a potent inhibitor of hepatitis C virus replication. *J. Med. Chem.* **2005**, *48* (17), 5504-5508.
12. Cahard, D.; McGuigan, C.; Balzarini, J., Aryloxy Phosphoramidate Triesters as Pro-Tides. *Mini-Rev. Med. Chem.* **2004**, *4* (4), 371-381.
13. Mehellou, Y.; Balzarini, J.; McGuigan, C., Aryloxy Phosphoramidate Triesters: a Technology for Delivering Monophosphorylated Nucleosides and Sugars into Cells. *ChemMedChem* **2009**, *4* (11), 1779-1791.
14. Perrone, P.; Daverio, F.; Valente, R.; Rajyaguru, S.; Martin, J. A.; Leveque, V.; Le Pogam, S.; Najera, I.; Klumpp, K.; Smith, D. B.; McGuigan, C., First example of phosphoramidate approach applied to a 4'-substituted purine nucleoside (4'-azidoadenosine): Conversion of an inactive nucleoside to a submicromolar compound versus hepatitis C virus. *J. Med. Chem.* **2007**, *50* (22), 5463-5470.
15. Perrone, P.; Luoni, G. M.; Kelleher, M. R.; Daverio, F.; Angell, A.; Mulready, S.; Congiatu, C.; Rajyaguru, S.; Martin, J. A.; Levêque, V.; Le Pogam, S.; Najera, I.; Klumpp, K.; Smith, D. B.; McGuigan, C., Application of the Phosphoramidate ProTide Approach to 4'-Azidouridine Confers Sub-micromolar Potency versus Hepatitis C Virus on an Inactive Nucleoside. *J. Med. Chem.* **2007**, *50* (8), 1840-1849.
16. Murakami, E.; Niu, C. R.; Bao, H. Y.; Steuer, H. M. M.; Whitaker, T.; Nachman, T.; Sofia, M. A.; Wang, P. Y.; Otto, M. J.; Furman, P. A., The mechanism of action of beta-D-2'-Deoxy-2'-fluoro-2'-C-methylcytidine involves a second metabolic pathway leading to beta-D-2'-deoxy-2'-fluoro-2'-C-

methyluridine 5'-triphosphate, a potent inhibitor of the hepatitis C virus RNA-dependent RNA polymerase. *Antimicrob. Agents Chemother.* **2008**, *52* (2), 458-464.

17. Murakami, E.; Bao, H. Y.; Ramesh, M.; McBrayer, T. R.; Whitaker, T.; Steuer, H. M. M.; Schinazi, R. F.; Stuyver, L. J.; Obikhod, A.; Otto, M. J.; Furman, P. A., Mechanism of activation of beta-D-2'-deoxy-2'-fluoro-2'-C-methylcytidine and inhibition of hepatitis C virus NS5B RNA polymerase. *Antimicrob. Agents Chemother.* **2007**, *51* (2), 503-509.

18. Furman, P. A.; Murakami, E.; Bao, H.; Symons, J.; Otto, M. J., Inhibition of HCV replication by PSI-6130: Mechanism of biochemical activation and inhibition. *J. Hepatol.* **2007**, *46*, S224-S224.

19. Liotta, D. C.; Painter, G. R., Discovery and Development of the Anti-Human Immunodeficiency Virus Drug, Emtricitabine (Emtriva, FTC). *Acc. Chem. Res.* **2016**, *49* (10), 2091-2098.

20. Piperno, A.; Cordaro, M.; Scala, A.; Iannazzo, D., Recent Highlights in the Synthesis of Anti-HCV Ribonucleosides. *Curr. Med. Chem.* **2014**, *21* (16), 1843-1860.

21. Yokoyama, M., Synthesis and biological activity of thionucleosides. *Synthesis-Stuttgart* **2000**, (12), 1637-1655.

22. Bobek, M.; Whistler, R. L.; Bloch, A., Preparation and activity of the 4'-thio-derivatives of some 6-substituted purines nucleosides. *J. Med. Chem.* **1970**, *13* (3), 411-413.

23. Bobek, M.; Bloch, A.; Parthasarathy, R.; Whistler, R. L., Synthesis and biological activity of 5-fluoro-4'-thiouridine and some related nucleosides. *J. Med. Chem.* **1975**, *18* (8), 784-787.

24. Dyson, M. R.; Coe, P. L.; Walker, R. T., The synthesis and antiviral activity of some 4'-thio-2'-deoxy nucleoside analogs. *J. Med. Chem.* **1991**, *34* (9), 2782-2786.

25. Secrist, J. A.; Riggs, R. M.; Tiwari, K. N.; Montgomery, J. A., Synthesis and anti-HIV activity of 4'-thio-2',3'-dideoxynucleosides. *J. Med. Chem.* **1992**, *35* (3), 533-538.

26. Van Draanen, N. A.; Freeman, G. A.; Short, S. A.; Harvey, R.; Jansen, R.; Szczech, G.; Koszalka, G. W., Synthesis and Antiviral Activity of 2'-Deoxy-4'-thio Purine Nucleosides. *J. Med. Chem.* **1996**, *39* (2), 538-542.

27. Yoshimura, Y.; Watanabe, M.; Satoh, H.; Ashida, N.; Ijichi, K.; Sakata, S.; Machida, H.; Matsuda, A., A Facile, Alternative Synthesis of 4'-Thioarabinonucleosides and Their Biological Activities. *J. Med. Chem.* **1997**, *40* (14), 2177-2183.

28. Olsen, D. B.; Bhat, B.; Cook, P. D. Thionucleoside Derivatives as Inhibitors of RNA-Dependent RNA Viral Polymerase. US 2006/0122154 A1, June 8, 2006, 2006.

29. Dukhan, D.; Gosselin, G.; Dousson, C. B. 1',4'-Thio Nucleosides for the Treatment of HCV. WO 2014/197578 A1, Dec. 11, 2014, 2014.

30. Dukhan, D.; Bosc, E.; Peyronnet, J.; Storer, R.; Gosselin, G., Synthesis of 2'-C-methyl-4'-thio ribonucleosides. *Nucleosides, Nucleotides Nucleic Acids* **2005**, *24* (5-7), 577-80.

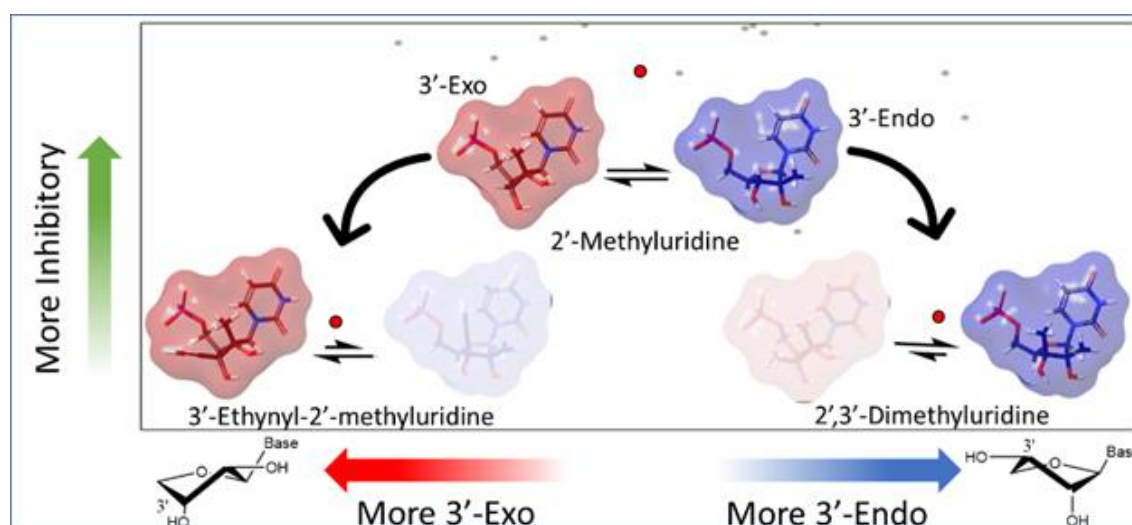
31. Vorbrüggen, H.; Lagoja, I. M.; Herdewijn, P., Synthesis of Ribonucleosides by Condensation Using Trimethylsilyl Triflate. *Curr. Protoc. Nucleic Acid Chem.* **2006**, 27 (1), 1.13.1-1.13.16.
32. Vorbrüggen, H.; Höfle, G., Nucleoside Syntheses, XXIII(1) On the Mechanism of Nucleoside Synthesis. *Chem. Ber.* **1981**, 114 (4), 1256-1268.
33. Vorbrüggen, H.; Ruh-Pohlentz, C., Synthesis Of Nucleosides. In *Organic Reactions*, Wiley Online Library: 2004; pp 1-630.
34. Sniady, A.; Bedore, M. W.; Jamison, T. F., One-flow, multistep synthesis of nucleosides by Bronsted acid-catalyzed glycosylation. *Angew. Chem., Int. Ed. Engl.* **2011**, 50 (9), 2155-8.
35. Haluszczak, J.; Macdonald, S. J.; Migaud, M. E., A one pot three-step process for the synthesis of an array of arylated benzimidazoribosyl nucleosides. *Org. Biomol. Chem.* **2011**, 9 (8), 2821-31.
36. Bordoni, C.; Cima, C. M.; Azzali, E.; Costantino, G.; Brancale, A., Microwave-assisted organic synthesis of nucleoside ProTide analogues. *RSC Adv.* **2019**, 9 (35), 20113-20117.
37. Uchiyama, M.; Aso, Y.; Noyori, R.; Hayakawa, Y., O-selective phosphorylation of nucleosides without N-protection. *J. Org. Chem.* **1993**, 58 (2), 373-379.
38. Serpi, M.; Madela, K.; Pertusati, F.; Slusarczyk, M., Synthesis of Phosphoramidate Prodrugs: ProTide Approach. *Curr. Protoc. Nucleic Acid Chem.* **2013**, 53 (1), 15.5.1-15.5.15.
39. Ross, B. S.; Reddy, P. G.; Zhang, H. R.; Rachakonda, S.; Sofia, M. J., Synthesis of diastereomerically pure nucleotide phosphoramidates. *J. Org. Chem.* **2011**, 76 (20), 8311-8319.
40. Meppen, M.; Pacini, B.; Bazzo, R.; Koch, U.; Leone, J. F.; Koeplinger, K. A.; Rowley, M.; Altamura, S.; Di Marco, A.; Fiore, F.; Giuliano, C.; Gonzalez-Paz, O.; Laufer, R.; Pucci, V.; Narjes, F.; Gardelli, C., Cyclic phosphoramidates as prodrugs of 2'-C-methylcytidine. *Eur. J. Med. Chem.* **2009**, 44 (9), 3765-70.
41. Mayes, B. A.; Arumugasamy, J.; Baloglu, E.; Bauer, D.; Becker, A.; Chaudhuri, N.; Latham, G. M.; Li, J.; Mathieu, S.; McGarry, F. P., Synthesis of a nucleoside phosphoramidate prodrug inhibitor of HCV NS5B polymerase: phenylboronate as a transient protecting group. *Org. Proc. Res. Dev.* **2014**, 18 (6), 717-724.
42. Simmons, B.; Liu, Z.; Klapars, A.; Bellomo, A.; Silverman, S. M., Mechanism-Based Solution to the ProTide Synthesis Problem: Selective Access to Sofosbuvir, Acelarin, and INX-08189. *Org. Lett.* **2017**, 19 (9), 2218-2221.
43. Lohmann, V.; Korner, F.; Koch, J. O.; Herian, U.; Theilmann, L.; Bartenschlager, R., Replication of subgenomic hepatitis C virus RNAs in a hepatoma cell line. *Science* **1999**, 285 (5424), 110-113.
44. Krieger, N.; Lohmann, V.; Bartenschlager, R., Enhancement of hepatitis C virus RNA replication by cell culture-adaptive mutations. *J. Virol.* **2001**, 75 (10), 4614-4624.
45. Bartenschlager, R., Hepatitis C virus molecular clones: from cDNA to infectious virus particles in cell culture. *Curr. Opin. Microbiol.* **2006**, 9 (4), 416-22.

46. Butora, G.; Qi, N.; Fu, W.; Nguyen, T.; Huang, H.-C.; Davies, I. W., Cyclic-Disulfide-Based Prodrugs for Cytosol-Specific Drug Delivery. *Angew. Chem., Int. Ed.* **2014**, *53* (51), 14046-14050.
47. Liotta, D. C.; Painter, G. R.; Bluemling, G. R.; de la Rosa, A. Nucleotide and Nucleoside Therapeutic Compositions and Uses Related Thereto. WO 2016/145142 A1, Sept 15, 2016.
48. Bernatchez, J. A.; Coste, M.; Beck, S.; Wells, G. A.; Luna, L. A.; Clark, A. E.; Zhu, Z.; Hecht, D.; Rich, J. N.; Sohl, C. D.; Purse, B. W.; Siqueira-Neto, J. L., Activity of Selected Nucleoside Analogue ProTides against Zika Virus in Human Neural Stem Cells. *Viruses* **2019**, *11* (4), 365.
49. Liu, L.-J.; Kim, S.-W.; Lee, W.-J.; Hong, J.-H., Selective Ring-opening Fluorination of Epoxide: An Efficient Synthesis of 2'-C-Fluoro-2'-C-methyl Carbocyclic Nucleosides. *B. Kor. Chem. Soc.* **2009**, *30* (12), 2989-2992.
50. Kim, H.-J.; Sharon, A.; Bal, C.; Wang, J.; Allu, M.; Huang, Z.; Murray, M. G.; Bassit, L.; Schinazi, R. F.; Korba, B.; Chu, C. K., Synthesis and Anti-Hepatitis B Virus and Anti-Hepatitis C Virus Activities of 7-Deazaneplanocin A Analogues in Vitro. *J. Med. Chem.* **2009**, *52* (1), 206-213.
51. Thiyagarajan, A.; Salim, M. T. A.; Balaraju, T.; Bal, C.; Baba, M.; Sharon, A., Structure based medicinal chemistry approach to develop 4-methyl-7-deazaadenine carbocyclic nucleosides as anti-HCV agent. *Bioorg. Med. Chem. Lett.* **2012**, *22* (24), 7742-7747.
52. Kasula, M.; Balaraju, T.; Toyama, M.; Thiyagarajan, A.; Bal, C.; Baba, M.; Sharon, A., A Conformational Mimetic Approach for the Synthesis of Carbocyclic Nucleosides as Anti-HCV Leads. *ChemMedChem* **2013**, *8* (10), 1673-1680.
53. Marquez, V. E.; Ezzitouni, A.; Russ, P.; Siddiqui, M. A.; Ford, H.; Feldman, R. J.; Mitsuya, H.; George, C.; Barchi, J. J., HIV-1 Reverse Transcriptase Can Discriminate between Two Conformationally Locked Carbocyclic AZT Triphosphate Analogues. *J. Am. Chem. Soc.* **1998**, *120* (12), 2780-2789.
54. Marquez, V. E.; Ben-Kasus, T.; Barchi, J. J.; Green, K. M.; Nicklaus, M. C.; Agbaria, R., Experimental and Structural Evidence that Herpes 1 Kinase and Cellular DNA Polymerase(s) Discriminate on the Basis of Sugar Pucker. *J. Am. Chem. Soc.* **2004**, *126* (2), 543-549.
55. Martínez-Montero, S.; Deleavey, G. F.; Kulkarni, A.; Martín-Pintado, N.; Lindovska, P.; Thomson, M.; González, C.; Götte, M.; Damha, M. J., Rigid 2',4'-Difluororibonucleosides: Synthesis, Conformational Analysis, and Incorporation into Nascent RNA by HCV Polymerase. *J. Org. Chem.* **2014**, *79* (12), 5627-5635.
56. Hotchkiss, D. J.; Kato, A.; Odell, B.; Claridge, T. D. W.; Fleet, G. W. J., Homochiral carbon branched piperidines from carbon branched sugar lactones: 4-C-methyl-deoxyfuconojirimycin (DFJ) and its enantiomer—removal of glycosidase inhibition. *Tetrahedron: Asymmetry* **2007**, *18* (4), 500-512.
57. Ayers, B. J.; Fleet, G. W. J., One-Pot Tandem Strecker Reaction and Iminocyclisations: Syntheses of Trihydroxypiperidine  $\alpha$ -Iminonitriles. *Eur. J. Org. Chem.* **2014**, *2014* (10), 2053-2069.

## Chapter 3. Synthesis and Antiviral Evaluation of 3'-C-Substituted Congeners of 2'-C-Methyluridine

Portions of this chapter are reproduced with permission from (Zackery Dentmon, Christopher Butch, Hannah B Gold, and Dennis Liotta, Synthesis and Antiviral Evaluation of 2',3'- $\beta$ -C-Disubstituted Nucleoside Analog ProTides to Test a Conformational Model of Potency Against Hepatitis C, *Synlett*, **2022**). This is an Accepted Manuscript of an article published by Thieme Publishing Group in *Synlett* on 19 July 2022, available online at <https://www.thieme-connect.de/products/ejournals/abstract/10.1055/a-1904-0249>.

Copyright © 2022 by Georg Thieme Verlag KG

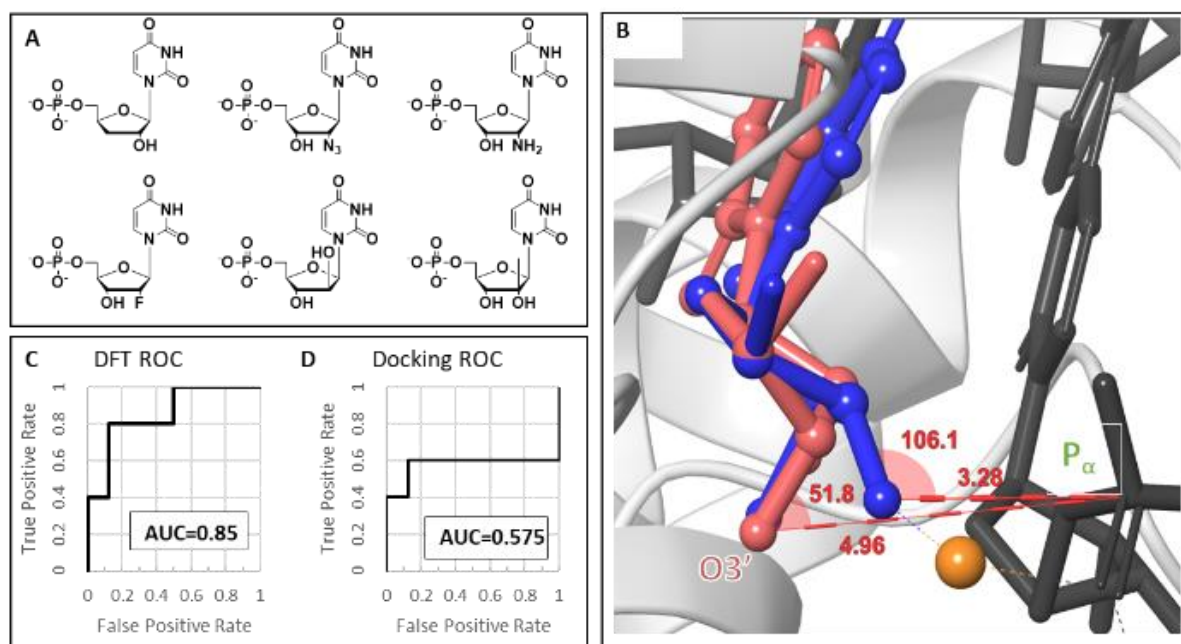


### 3.1 INTRODUCTION

As stated in the previous chapters, nucleosides and nucleotides have long been recognized as privileged chemical structures due to their integral role to life as the monomers of nucleic acids. For this reason, nucleoside and nucleotide analogs (NAs) that inhibit the enzymes responsible for the replication of pathogenic nucleic acids have been a cornerstone of anticancer and antiviral therapy since the mid-20<sup>th</sup> century.<sup>1-5</sup> Their role in inhibiting the replication of human immunodeficiency virus (HIV) marks a particularly compelling example of NAs changing the prognosis of an acutely fatal infection to a manageable chronic disease.<sup>6-8</sup> Indeed, the use of NA prodrugs remdesivir<sup>9-11</sup> and molnupiravir<sup>12-15</sup> during the ongoing SARS-CoV-2 pandemic once

again highlights the utility of NAs as key weapons in the human medical arsenal to fight viral infections.

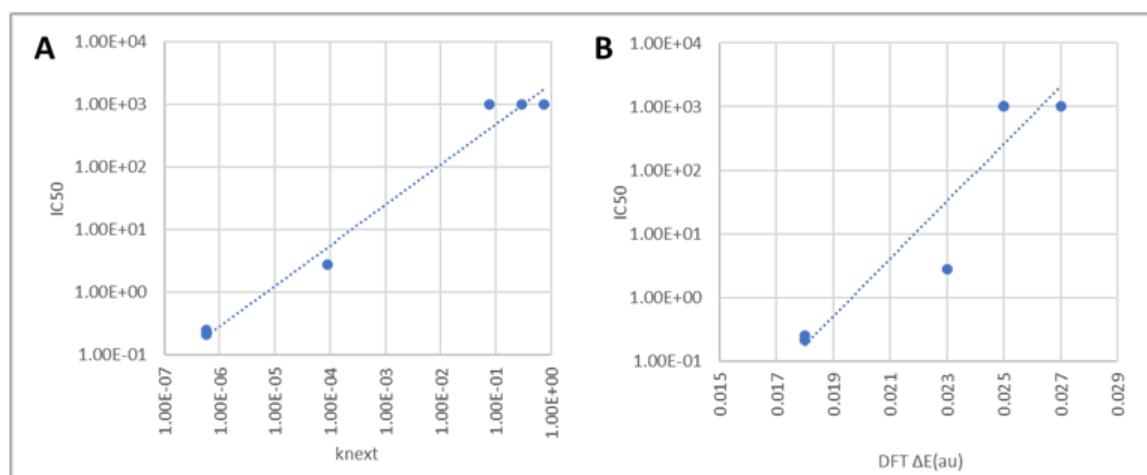
Another watershed in the use of antiviral NA prodrugs was the development of sofosbuvir to treat and in many cases cure HCV infection.<sup>8, 16, 17</sup> Despite these successes, however, the discovery of potent antiviral NAs is hindered by the lack of a clear mechanistic understanding of the dynamic and elaborate system in play to establish reliable structure-activity relationships (SARs). The system is comprised, at a minimum, of the interactions of the NA with the multiple kinases necessary to anabolize it to the active triphosphate as well as the replicase complex consisting of the target polymerase, protein co-factors, and template nucleic acid to which the NA must base pair. To gain a better understanding of this intricate system in the context of HCV, in 2014 Fung et al.<sup>18</sup> showed experimentally that for a selection of NAs (Figure 3.1A) the observed  $IC_{50}$  against the HCV polymerase (non-structural protein 5B, NS5B) was highly correlated not with the kinetics of incorporation of those nucleotides, nor with the substrate discrimination toward those nucleotides relative to the canonical UTP substrate, but rather the kinetics of further elongation after antiviral NA incorporation. Stated alternately, it is the reactivity of the 3'-hydroxyl group toward the subsequent incoming nucleoside 5'-*O*-triphosphate (NTP) which seems to determine the antiviral efficacy of these NAs. Separately, work in the Szostak group has shown that the kinetics of enzyme-free nucleotide polymerization are highly dependent on the energetics of sugar pucker transitions.<sup>19, 20</sup> Additionally, it has been long documented that substituent moieties<sup>21, 22</sup> can significantly alter the equilibrium conformational preference of the furanose ring, a phenomenon that has been incorporated to significant effect in enhancing the binding energy of siRNA molecules.<sup>23</sup> Indeed, we<sup>24</sup> as well as others<sup>25-29</sup> have reported modifications that alter the geometry of the furanose ring having pronounced effects on antiviral potency. Taken together, these facts collectively led us to the hypothesis that the efficacy of non-obligate chain-terminating nucleotides may in part be related to the geometry of the thermodynamically preferred conformation and the extent of that thermodynamic preference.



**Figure 3.1.** (A) Nucleotides considered by Fung et al. who showed that reactivity at the C3' position is the controlling factor in NTP inhibitory effect against NS5B. (B) Positioning of the 3' terminal nucleotide (blue) and a UDP monomer (gray) in the NS5B pre-reaction complex (PDB ID:4WTA). The canonical 3'-exo geometry of the 3' terminal nucleotide (pink) is also shown, with the C1', C4', and O4' positions aligned, showing the large effect this conformational shift can have on the O3'-P $\alpha$  distance (3.28Å  $\rightarrow$  4.96Å) and the C3'-O3'-P $\alpha$  angle (106.1°  $\rightarrow$  51.8°). (C) ROC curves associated with correlating antiviral activity of nucleotides in Table 1 with calculated DFT exo-endo  $\Delta E$  or (D) Docking Scores. An AUC closer to 1 is indicative of a more predictive model, while an AUC closer to 0.5 is indicative of a binary chance model.

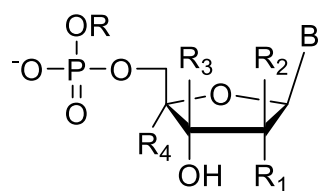
A 2.8 Å crystal structure of the HCV polymerase in complex with an RNA dimer and UDP is available on the Protein Data Bank (PDB ID 4WTA).<sup>30</sup> Inspection of the active site (Figure 3.1B) shows the 3' terminus of the elongating RNA to exist in the 3'-endo form (A Form, blue) and comparison to the 3'-exo antipode (B Form, red) illustrates how a bias away from the A form would retard elongation. To test whether the nucleotide conformational preference had any relation to antiviral activity, we first conducted density functional theory (DFT) modeling of the energy and geometry of the nucleotides considered by Fung et. al<sup>18</sup> to determine their conformational preference. This preference was calculated based on initial structures which reflect the canonical A (3'-endo) and B (3'-exo) forms of RNA, as the two most biologically relevant conformations. The models built from these forms were relaxed to their local minimum and the energy difference between the two antipodes was used as a proxy for the overall geometric preference. While this is not a complete picture of the overall conformational landscape, nucleotides tend to have minima in this general conformation, and the interconversion between

the geometries tends to be rapid and barrierless due to procession through the pseudorotational cycle, rather than a traditional ring inversion with planar intermediate.<sup>31, 32</sup> Through this approach, we observed a correlation between the reported kinetics and the calculated conformer energetic preference (Figure 3.S1).



**Figure 3.S1.** Properties of nucleotides from Feng et al<sup>7</sup> compared to their measured IC<sub>50</sub>. **(A)** Comparison of the rate of incorporation of subsequent nucleotides ( $k_{next}$ ) and IC<sub>50</sub>. **(B)** Comparison of the DFT energy difference ( $\Delta E$ ) and IC<sub>50</sub>.

While this result was heartening, the number of nucleotides considered was small, and the analysis relied on IC<sub>50</sub> values from the literature which can vary substantially based on the experimental method. To expand the analysis, we next considered a selection of 13 more nucleotides for which we had consistent IC<sub>50</sub> measurements for the triphosphate form against the HCV polymerase (Table 3.1). The calculated conformer energetic preference (DFT  $\Delta E$ ) also correlated with IC<sub>50</sub>, as nucleotides with a bias toward the 3'-endo conformation of >0.0125 au showed a far lower likelihood of having single-digit micromolar or better activity. However, more deviation from the linear correlation was observed within this set than for the Fung nucleotides. While the correlation is less robust, it is stronger than that generated by a plot of the nucleotide Docking scores in the 4WTA binding site (Figure 3.S2). Furthermore, when considered as a decision-making criterion, the nucleotides as ranked by the DFT energies are more enriched in active compounds (IC<sub>50</sub> < 10  $\mu$ M) than when the Docking score is used as the ranking metric by ROC analysis (Figure 1C and D).

**Table 3.1.** Nucleotides considered in the conformer energy model

Entry	B	R <sub>1</sub>	R <sub>2</sub>	R <sub>3</sub>	IC <sub>50</sub> ( $\mu\text{M}$ ) <sup>a</sup>	DFT $\Delta E$ (au) <sup>b</sup>	Docking Score <sup>b</sup>	Docking RMSD <sup>b</sup>
1	U	OH	H	N <sub>3</sub>	4	0.0062	-9.72	1.71
2	U	OH	H	FCH <sub>2</sub>	7	0.0086	-9.29	1.26
3	4-ThioU	OH	H	N <sub>3</sub>	3	0.0099	-9.73	1.60
4	2-ThioU	OH	H	N <sub>3</sub>	0.4	0.0108	-9.42	1.63
5	5-FlouroU	F	Me	H	>10	0.0132	-9.82	1.18
6	U	F	Me	H	1	0.0148	-9.47	1.18
7	5-FlouroC	F	Me	H	0.43	0.0150	-8.95	1.25
8	2-ThioU	OH	Me	H	2	0.0153	-9.14	1.19
9	2-ThioU	H	Me	H	42	0.0161	-8.37	0.96
10	4-ThioU	H	Me	H	69	0.0164	-8.55	1.12
11	C	F	Me	H	0.1	0.0166	-8.77	1.25
<b>12</b>	<b>U</b>	<b>OH</b>	<b>Me</b>	<b>H</b>	<b>&gt;10</b>	<b>0.0198</b>	<b>-9.75</b>	<b>0.99</b>
13	4-ThioU	OH	Me	H	19	0.0202	-8.83	1.43

<sup>a</sup> Data was generated with triphosphates ( $R = \text{P}_2\text{O}_6$ ). <sup>b</sup> Data were generated on the methyl ester of the monophosphate ( $R = \text{Me}$ ).

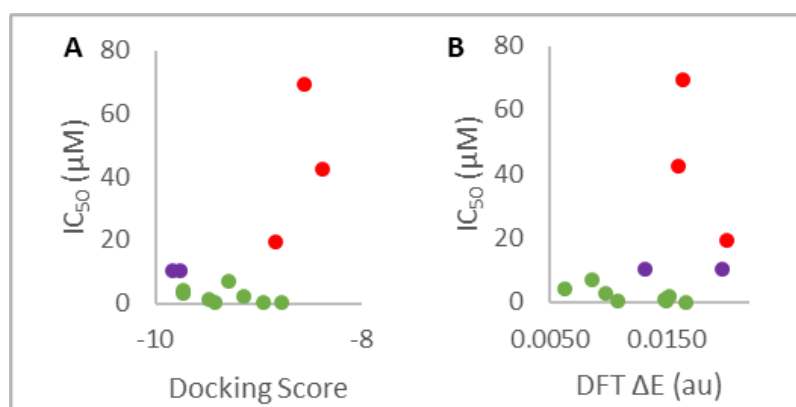
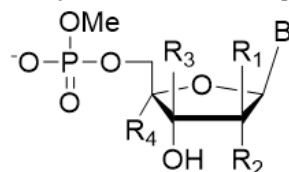


**Figure 3.S2.** (A) Activity of nucleotides in Table 3.1 plotted against Docking Scores and (B) calculated DFT exo-endo  $\Delta E$ . Compounds in green have IC<sub>50</sub> less than 10  $\mu\text{M}$ , red have IC<sub>50</sub> greater than 10  $\mu\text{M}$ , and purple have activity determined to be >10  $\mu\text{M}$  but for which the specific value is unknown.

Having observed this trend between the conformer energies and activity, we conducted these calculations on several novel nucleotides (Table 3.S1), and from these selected the 3'- $\beta$ -ethynyl and 3'- $\beta$ -methyl analogs of 2'-*C*-methyluridine (2'-MeU). We found these analogs to be especially attractive for two reasons: (1) the established success of the 2'-*C*- $\beta$ -methyl scaffold in conferring potency and selectivity for HCV;<sup>16, 33, 34</sup> and (2) the contrasting antipodal energetic differences of these analogs relative to their 3'-unsubstituted parent congener. According to our model, the 3'- $\beta$ -ethynyl analog should be less biased toward the A form than the parent NA 2'-MeU, while the 3'- $\beta$ -methyl analog would be more biased toward the A form. With these compounds, we could efficiently explore a large spread of calculated energy differences ( $\Delta E$  from 0.0012 au to 0.0888 au) using a divergent synthesis starting from a common parent nucleoside precursor whose exo-endo energetic bias lied in between the two new analogs (cf. Table 3.1, bolded entry 12 and Table 3.S1, bolded entries 4 and 8).

**Table 3.S1.** Novel nucleotides considered for synthesis and corresponding DFT result.



Entry	B	R <sub>1</sub>	R <sub>2</sub>	R <sub>3</sub>	R <sub>4</sub>	DFT $\Delta E$ (au)
1	U	Me	OH	H	CN	-0.0142
2	U	H	OH	H	CN	-0.0114
3	U	H	OH	CCH	H	-0.0031
<b>4</b>	<b>U</b>	<b>Me</b>	<b>OH</b>	<b>CCH</b>	<b>H</b>	<b>0.0012</b>
5	U	Me	OH	CN	H	0.0028
6	U	-CH <sub>2</sub> O-		H	H	0.0613
7	U	-CH <sub>2</sub> O-		Me	H	0.0816
<b>8</b>	<b>U</b>	<b>Me</b>	<b>OH</b>	<b>Me</b>	<b>H</b>	<b>0.0888</b>

Intrigued by the large difference in  $\Delta E$  of the two chosen analogs, a further examination of each of the conformers provided a rationale (Figure 3.S3). Two primary drivers exist for the energetic difference between the two nucleotides. First is the relief of steric congestion in the 3'-exo conformation by substituting the methyl (top left) with an ethynyl group (bottom left) which increases the interatomic distances from the 5'-O and 2'-methyl hydrogen (red numbers and

dotted lines) by 0.7 and 0.8 Å, respectively. The second is an unfavorable  $\pi$  overlap in the 3'-endo conformation of 3'-ethynyl-2'-methyluridine (bottom right) between the 3'-ethynyl group and the C-C double bond of the uracil nucleobase (purple). These effects cause the 3'-exo conformation of 3'-ethynyl-2'-methyluridine to be relatively lower, and the 3'-endo conformation energy to be relatively higher than 2',3'-dimethyluridine. It should be noted that neither conformation is a global minimum, nor is either likely to be the lowest energy conformation which could be labeled as 3'-endo or 3'-exo. Rather, each is the local minimum closest to the canonical A and B forms, which we suspect would be most likely to engage the enzyme.

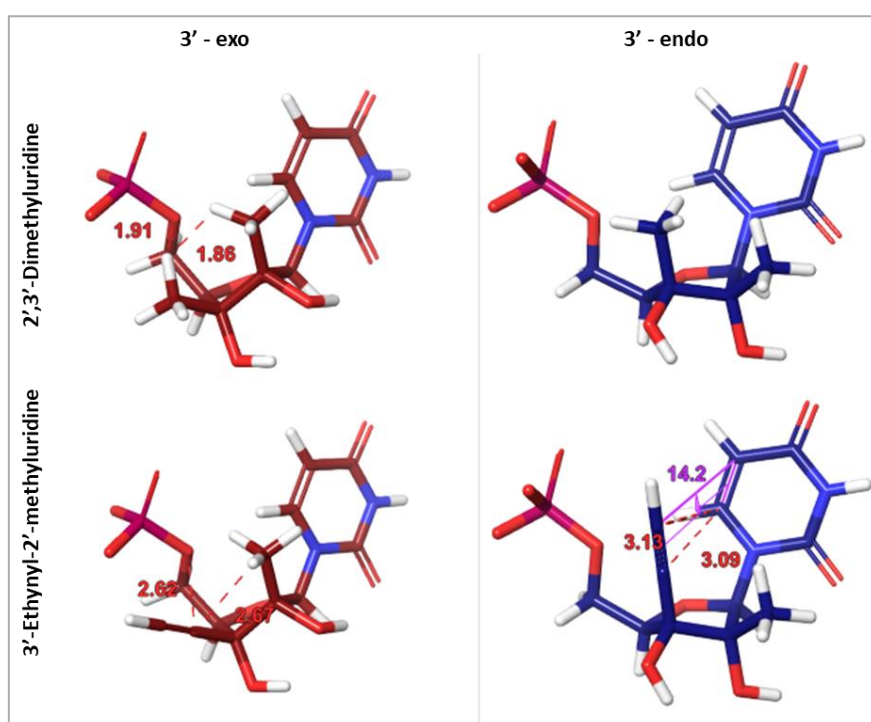


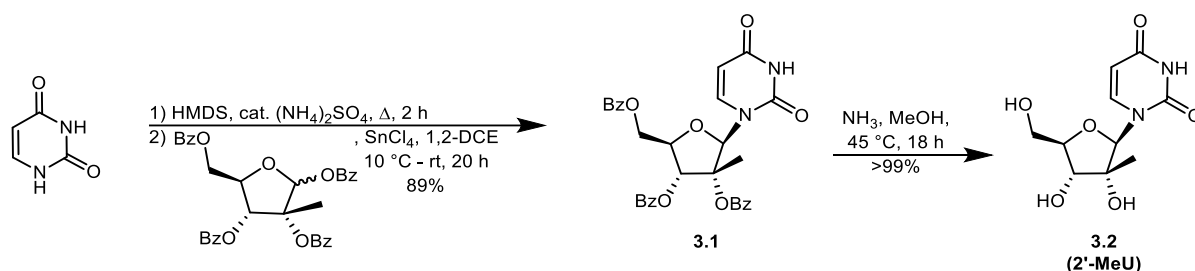
**Figure 3.S3.** Three-dimensional renderings of the minimized 3'-exo (left) and 3'-endo (right) antipodes of the two analogs chosen for this study. The relevant measured atomic distances (steric effects) are indicated by dotted red lines, while the relevant electronic effects are indicated by solid purple lines.

## 3.2 RESULTS AND DISCUSSION

### 3.2.1 Synthesis of the Key 3'-Ketonucleoside Intermediate for Diversification

Our synthetic campaign initially began with the commercially available NA 2'-MeU (**3.2**). However, in the course of our studies, it became apparent that larger quantities would be needed which could be efficiently provided via a 2-step sequence from the much more economical per-benzoylated 2-C-methyl- $\beta$ -D-ribofuranose and uracil (Scheme 3.1). Following Vorbrüggen's

methodology,<sup>35, 36</sup> the nucleobase was first per-silylated by refluxing in hexamethyldisilazane (HMDS) in the presence of catalytic  $(\text{NH}_4)_2\text{SO}_4$ , then, after removal of the volatiles, was subsequently glycosylated in excellent yield and stereoselectivity with the chiral pool sugar benzoate and  $\text{SnCl}_4$  as Lewis acid promoter. The high degree of stereoselectivity for the desired top-side (termed  $\beta$ ) addition of the nucleobase is proposed to stem from anchimeric assistance by the adjacent ester moiety at the C2 position of the glycosyl donor. The free nucleoside **3.2** was then provided upon removal of the benzoyl esters with methanolic ammonia in quantitative yield.

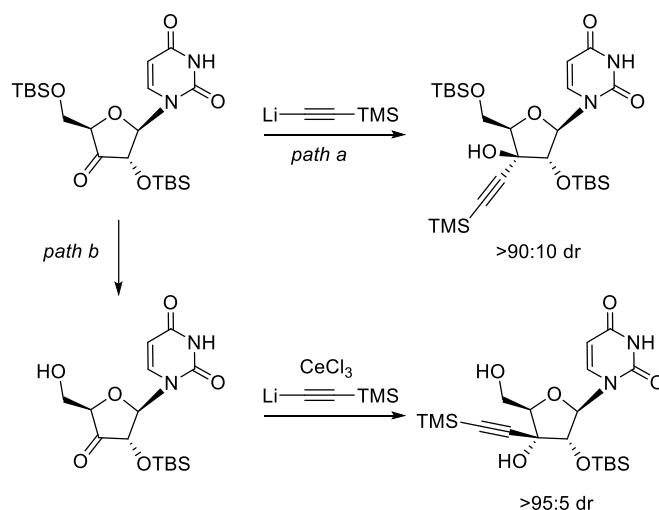


**Scheme 3.1.** Synthesis of the parent nucleoside 2'-C-methyluridine from the commercially available per-benzoylated ribofuranoside and uracil.

At this point, the independent work of Jung<sup>37, 38</sup> and Ludwig<sup>39</sup> on 3'-C-modified ribonucleosides offered a promising precedent for our desired  $\beta$  addition of nucleophiles of interest at the C3' position. Extending the work of Robins,<sup>40</sup> Jung et al. showed that diastereofacial control of an acetylide nucleophile addition to a 3'-ketonucleoside could be achieved by the appropriate manipulation of 2'-O- and 5'-O-protecting groups. If both hydroxyl groups were blocked as *tert*-butyldimethylsilyl (TBS) ethers, then bottom-side (termed  $\alpha$ ) addition was preferred, yielding the xylo diastereomer with high (95:5) selectivity. However, this diastereoselectivity could be inverted by removing the TBS group from the 5'-OH on the top face of the sugar, citing a combination of chelation, steric, and/or stereoelectronic effects as a rationale for the observed difference in facial preference.<sup>37</sup> Ludwig et al. employed this same strategy in their preparation of the anticancer drug 3'-C-ethynylcytidine.<sup>39</sup> Hence, the 3'-ketonucleoside appeared to be a tenable synthetic intermediate to access our desired 2',3'- $\beta$ -dialkylated nucleosides in a stereoselective manner, noting the potential complication arising from additional steric congestion conferred by the quaternary center at our C2' position.

### 3.2.1.1 Protecting Strategy #1: 5'-O-Triphenylmethyl (Trityl) Ether

With Jung and Ludwig's precedents in mind, the target molecules were envisioned to be accessed via the diastereofacialselective addition of the desired alkyl group to the 3'-ketone from the top face of the sugar ring. Working on canonical uridine, Jung and co-workers<sup>37, 38</sup> suggested that  $\beta$ -selective addition (in the case of an ethynyl nucleophile) could be realized by considering two important factors: (1) the use of a 5'-hydroxy-2'-O-protected ketonucleoside, and (2) the use of an organocerium reagent. The authors initially report the reaction of a 2',5'-bis(*tert*-butyldimethylsilyl)-protected ketonucleoside with lithium TMS-acetylide resulted in a modest 60:40 preferential  $\alpha$ -addition which was further improved by the use of an organocerium reagent (Scheme 3.S1, path a). The reagent was prepared by transmetalating the lithium acetylide with a half or one equivalence of cerium(III) chloride to form ethynylcerium dichloride or diethynylcerium chloride, respectively. Both served to increase the  $\alpha$  diastereoselectivity to greater than 90:10. This stereochemical preference could be completely reversed by removing the 5'-O-*tert*-butyldimethylsilyl (TBS) group prior to treatment with the carbon nucleophile (Scheme 3.S1, path b). With the TBS group still intact at the C2' position, the use of lithium TMS-acetylide gave a modest 70:30 preference for  $\beta$ -addition which was improved to >95:5 by the use of the organocerium reagent. The offered explanation for the increase in stereoselectivity stems from chelation effects wherein the cerium reagent first deprotonates the 5'-hydroxyl group to

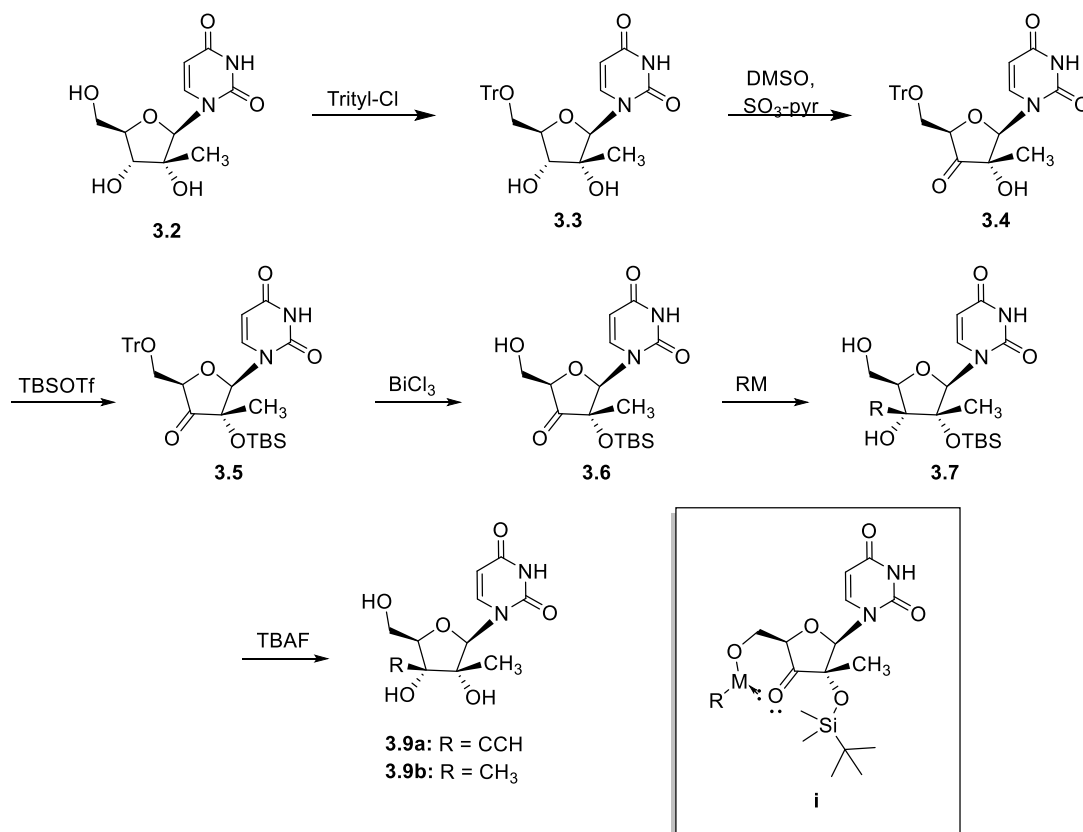


**Scheme 3.S1.** Complementary diastereofacial selective addition of TMS-acetylide as reported by Jung<sup>25,26</sup>

give presumably the 5'-cerium alkoxide which then delivers the nucleophile from the same (top) face. Notably, no data is offered on the corresponding divalent Grignard reagent.

The appropriately 2'-protected hydroxyketone would come from a protecting group strategy wherein the 5'-alcohol could be revealed while keeping the 2'-alcohol orthogonally blocked. The choice of protecting groups at these two positions is key then: the group on the 2'-OH needs to be inert to organometallic nucleophiles while also attenuating the Lewis basicity of the alcohol to avoid chelation of the organometallic nucleophile and directing undesired bottom-side addition. This precludes common ester and ethereal groups such as acetate, benzoate, MOM, BOM and benzyl groups. Bulky silanes<sup>41</sup> such as TBS would be the ideal protecting group and was in fact the protecting group employed by Jung and co-workers<sup>38</sup> for this transformation. They were able to selectively remove a primary 5'-*O*-TBS group while keeping the secondary TBS group at C2' intact, having arrived at the bis-protected keto precursor by a reasonably selective 2',5'-bis(silylation) prior to oxidation of the remaining secondary alcohol at C3'. The presence of the 2'-methyl group in our scaffold presents an interesting challenge in that the tertiary alcohol at C2' is sterically less reactive than the secondary alcohol at the C3' position. Consequently, it will need to be protected after oxidation of the C3'-alcohol to the corresponding  $\alpha$ -hydroxyketone. This acyloin could be accessed via chemoselective oxidation of the 5'-protected 2',3'-*tert,sec*-diol system with a judicious choice of oxidant which avoids oxidative cleavage of the C-C bond. Oxidative cleavage of glycols is a known feature of aggressive oxidants such as periodic acid or potassium permanganate, as well as with some milder, more routine reagents such as the Dess-Martin periodinane and the Ley-Griffith oxidation.<sup>42</sup> This notwithstanding, there were a host of oxidation conditions worth considering, the most obvious being the "activated DMSO" oxidations, such as the Swern or Pfitzner-Moffat oxidations, as well as those catalyzed by the *N*-oxoammonium species produced by an *N*-oxyl radical precatalyst and terminal co-oxidant, such as TEMPO and hypochlorite. Prior to this oxidation, the primary alcohol at the C5' position must be protected selectively in the presence of the secondary and tertiary alcohols at C3' and C2', respectively.

Our revised route thus began with selective protection of the primary 5'-alcohol of 2'-MeU as the triphenylmethyl (trityl) ether (Scheme 3.S2). The 5'-trityl group was smoothly installed in >80% yield by refluxing the nucleoside with excess trityl chloride in pyridine as solvent and base with DMAP as alkyl transfer catalyst. The 5'-*O*-trityl ether was sparingly soluble in the typical organic solvents which may contribute to the slightly diminished yield. For the next step, previous unpublished work in our lab showed that the Parikh-Doering oxidation conditions proved the most amenable to the resulting *sec,tert*-glycol system; a small amount of glycol **3.3** was reacted with SO<sub>3</sub>·pyridine complex and triethylamine (TEA) in a 1:1 solution of anhydrous DMSO and DCM to give the desired ketone **3.4** by LCMS. However, allowing the reaction to proceed at room temperature for 4 hours also yielded a substantial amount of the well-known methylthiomethyl ether side product resulting from a Pummerer rearrangement. The Parikh-Doering oxidation was repeated with more careful attention to time, allowing it to go for 1 hour at ambient temperature. However, a very similar result was observed, namely the Pummerer side product still accounted for some loss of conversion to desired product. It is also challenging to purify away from the

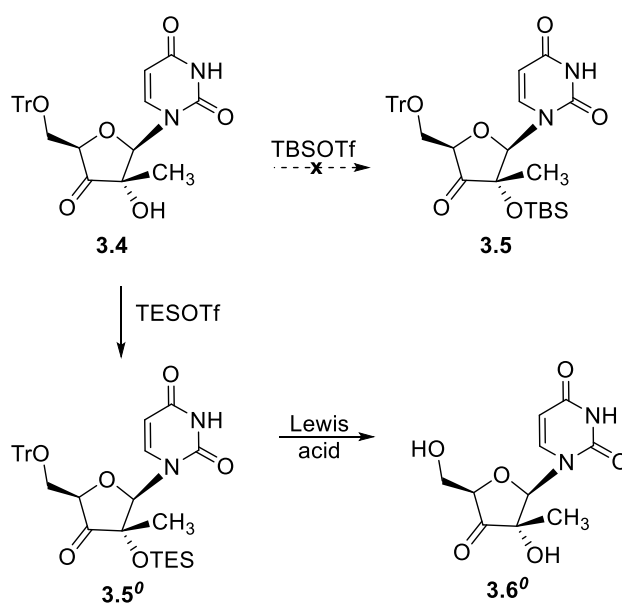


**Scheme 3.S2.** Proposed six step synthesis of 3'-modified nucleosides **3.9a** and **3.9b** from 2'-methyluridine

desired compound, and clean ketone was isolated in an average yield of only 7%. Hence, alternative oxidants were investigated, including catalytic TEMPO with sodium hypochlorite, IBX, and the Swern conditions, none of which gave satisfactory results. With the oxidation proving elusive, the Parikh-Doering conditions were again investigated, this time with more care towards reaction temperature. Keeping the reaction at reduced temperature (0 - 5 °C) seemed to diminish Pummerer side product formation but required longer reaction times. The best yield achieved was 68% on 0.3 grams of material; scale up to 1.5 grams of material saw a reduction in yield to 53%, still a dramatic improvement compared to previous efforts. The acyloin product **3.4** can be isolated by precipitation out of the crude mixture with methanol or by a combination of hexanes in MTBE, however a substantial amount remains in the filtrate and can be further purified via column chromatography. Clearly these results left room for further optimization but were deemed reasonable enough to move forward.

With acyloin **3.4** in hand, the installation of the TBS group onto the tertiary 2'-alcohol was attempted. Common conditions for the installation of a TBS group on a sterically hindered alcohol are TBS triflate in the presence of 2,6-lutidine, but this led to no reaction. Additional conditions investigated including TBSCl with either silver(I) nitrate or *N*-methylimidazole (NMI) and molecular iodine similarly failed. Treatment of the alcohol with the strong base sodium hydride followed by treatment with TBS triflate also failed, indicating that perhaps the tertiary alcohol is simply too sterically hindered for the bulky TBS group and that a smaller protecting group is necessary. Indeed, as a proof-of-concept reaction, the alcohol reacted with the smaller trimethylsilyl (TMS) triflate, but the resulting TMS ether is too labile for further manipulation. This led to the investigation of silyl protecting groups of intermediate steric bulk and stability, namely the triisopropylsilyl (TIPS) and triethylsilyl (TES) groups. Explored conditions included treatment of the tertiary alcohol with either TES triflate or TIPS triflate and either 2,6-lutidine or TEA base, or sodium hydride base followed by TIPSCl. Several observations are noteworthy: none of the reactions appeared to go to completion as residual starting material was observed in all cases; TES triflate appeared to work better than TIPS triflate with TEA base while 2,6-lutidine

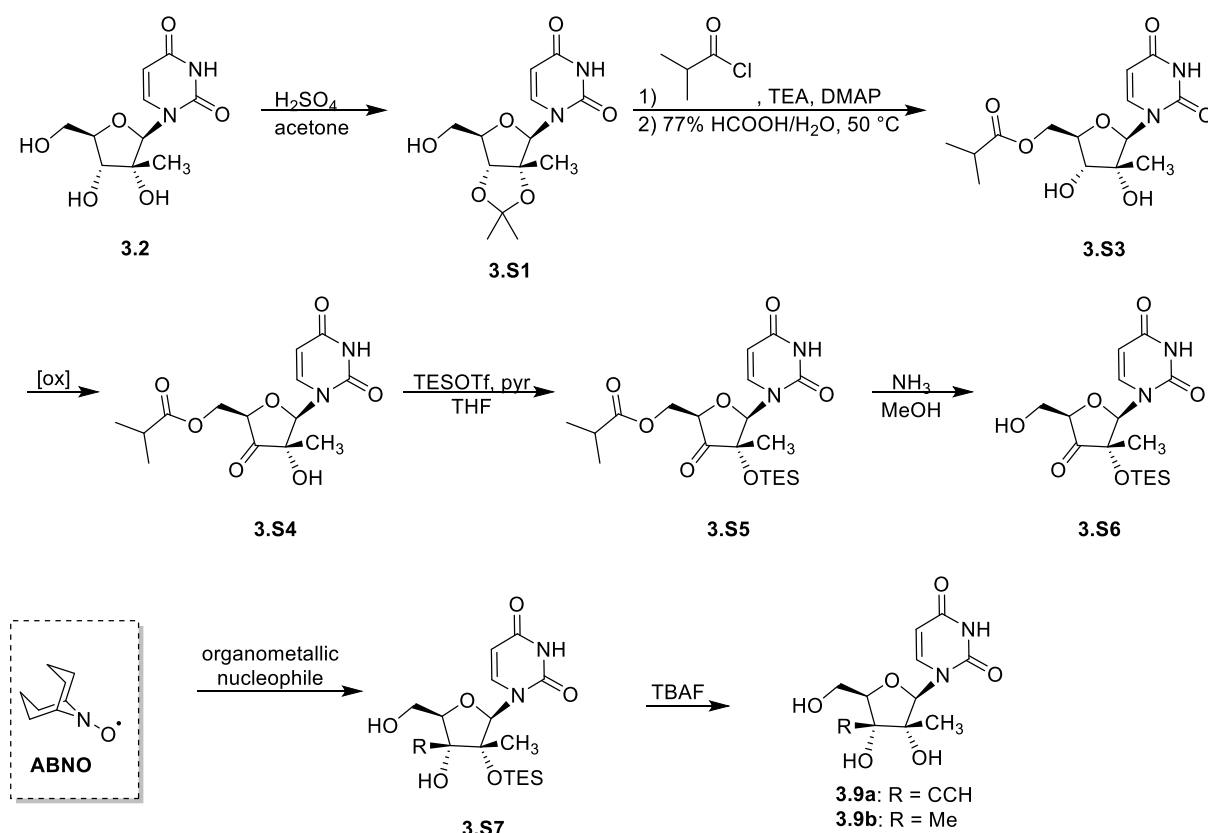
shut the reactions down; NaH/TIPS triflate appeared to work, but such an aggressive base has the potential for silyl enol ether formation at the C3' position. Follow-up studies with TES triflate showed that swapping the base to pyridine served to increase the yield of TES-protected product to 73% (**3.5<sup>o</sup>**, Scheme 3.S3). It should be noted that the combination of TBS triflate and pyridine did make product, but not in what was considered at the time to be synthetically useful yields (<30%). With the TES ether **3.5<sup>o</sup>** in hand, conditions were needed to selectively remove the 5'-trityl group while leaving the 2'-TES group intact. The most common ways to remove the trityl group include hydrolysis with aqueous acid, but the TES group is known to be labile under these conditions as well. Hence, a small battery of Lewis acids were investigated, including bismuth(III) triflate, Et<sub>2</sub>AlCl, BF<sub>3</sub>·etherate, SbCl<sub>3</sub> and BiCl<sub>3</sub>. Unfortunately, all conditions investigated removed both protecting groups to afford the free 3'-ketonucleoside **3.6<sup>o</sup>**.



**Scheme 3.S3.** Tertiary 2'-*O*-silylation and subsequent global deprotection

### 3.2.1.2 Protecting Strategy #2: 5'-O-Isobutyl Ester

Since (a) the trityl and TES groups appeared incompatible, and (b) bulkier, more stable silyl groups appeared to be poorly installed at the C2' tertiary site, an alternative 5'-O-protecting group was considered that may be orthogonal to the TES group. Esters such as acetate and benzoate have been used extensively in nucleoside protection and are easily removed in the presence of a mild organic base such as methanolic ammonia. A small campaign was therefore initiated to selectively install an acetate group at the primary 5'-hydroxyl group, but this ultimately proved unsuccessful. However, the isobutyrate ester had been shown by colleagues at the EIDD to be easily installed at the 5'-position through the intermediacy of the 2',3'-isopropylidene ketal. With this in mind, the starting nucleoside **3.2** was acetonide-protected in good yield using standard conditions and subsequently esterified with isobutyl chloride and TEA in the presence of catalytic DMAP to afford the diol **3.S3** in near quantitative yield after formic acid hydrolysis (Scheme 3.S4). Further optimization of conditions showed that acetonide **3.S1** could be telescoped directly into the isobutyryl ester formation with a simple filtration and

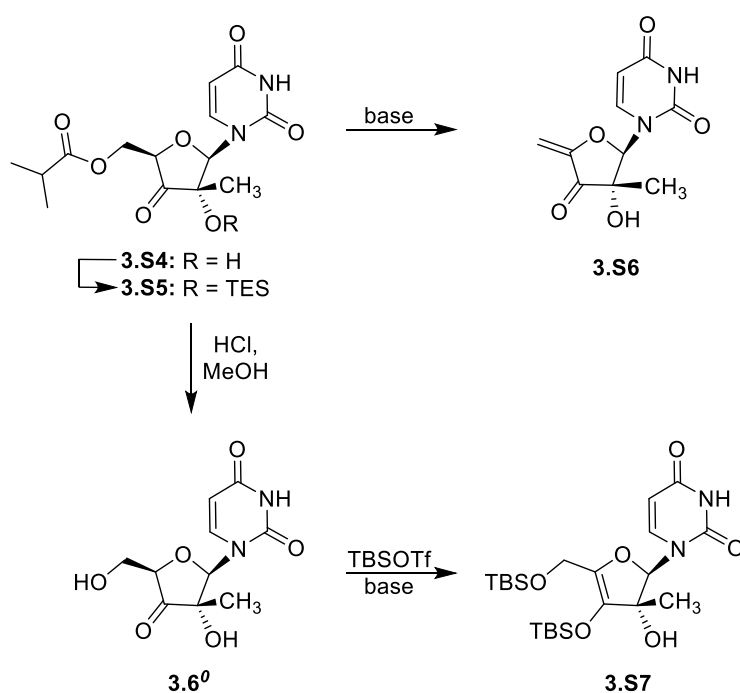


**Scheme 3.S4.** Alternative eight step synthesis of 3'-modified nucleosides **3.9a** and **3.9b** from 2'-methyluridine

solvent swap, and the crude organic extract of that reaction could be deprotected to afford the 5'-*O*-protected diol with only one isolation and purification.

With glycol **3.S3** in hand, oxidation to the 3'-ketone was pursued. Unfortunately, the Parikh-Doering oxidation conditions which had proven successful on the previous scaffold appeared unreactive to the new substrate, so additional oxidation conditions were investigated. Fifteen different oxidations were investigated before arriving at conditions which made use of the highly active 9-azabicyclo[3.3.1]nonane *N*-oxyl radical (ABNO) as a catalytic oxidant and an azo compound (*e.g.*, DIAD) as the stoichiometric terminal oxidant.<sup>43</sup> A less sterically hindered derivative of the common oxidant TEMPO, ABNO has found considerable use in the catalytic aerobic oxidation of alcohols and is the reagent of choice for hindered secondary alcohols.<sup>44, 45</sup> According to Hayashi and co-workers,<sup>43</sup> in the presence of acetic acid, the radical disproportionates to the hydroxylamine and oxoammonium acetate salt, the active oxidant which oxidizes the alcohol to ketone and is reduced to the hydroxylamine, which is then reoxidized back to the radical by the azo compound, completing the catalytic cycle. Reaction of glycol **3.S3** under these conditions in DCM solvent smoothly afforded the corresponding acyloin **3.S4** in excellent yield. There are a number of interesting observations to note concerning this reaction: a) the substrate is insoluble in DCM, so the oxidation proceeds as a heterogeneous mixture—changing the solvent to THF results in a homogenous solution but leads to lower conversion; b) both DEAD and DIAD serve well in the oxidation, but the corresponding crystalline *tert*-butyl analog (DBAD) shows no activity; c) importantly, the product is unstable to a basic quench of the acetic acid. Treatment of the product mixture (**3.S4**) with TEA followed by column purification led to a quantitative elimination of the isobutyrate group to give the conjugated enone **3.S6** (Scheme 3.S5). While this was an unanticipated and undesired result, this intermediate could be of some synthetic utility as the exocyclic olefin may allow access to modification at the C4' and/or C5' positions (*e.g.*, iodofluorination).

The base lability of the 5'-*O*-ester protecting group ultimately proved terminal for this route. Even though the TES group could be installed with the triflate and very mild pyridine base to yield silyl ether **3.S5**, subsequent treatment of this bis(protected) substrate with methanolic ammonia resulted in removal of the TES group followed by elimination of the ester again to the exocyclic enone **3.S6** (Scheme 3.S5). Alternative deprotection methods were investigated including treatment with hydrazine hydrochloride, magnesium metal, molecular sieves or iodine in methanol, and titanium(IV) isopropoxide in THF — all resulted in either no reaction, elimination of the ester, or concomitant hydrolysis of the TES protecting group rather than the selective deprotection of the ester to the desired  $\beta$ -hydroxyketone. Alternatively, treatment of mono-protected substrate **3.S4** with methanolic HCl yielded unprotected 3'-ketonucleoside **3.6<sup>o</sup>**, and it was thought this intermediate could potentially be silylated at the 2' and 5' positions, providing an intermediate very similar to that used by Jung et al.<sup>25,26</sup> who then selectively removed the primary 5'-OTBS group in the presence of a secondary TBS ether at the 2' position. Pursuing this, treatment of the 2',5'-diol **3.6<sup>o</sup>** with excess TBS triflate and pyridine base appeared to afford only the monosilylated product, presumably the primary 5'-*O*-silyl ether. The use of stronger base like TEA quickly installed two TBS groups by LCMS. Unfortunately, the acidity of

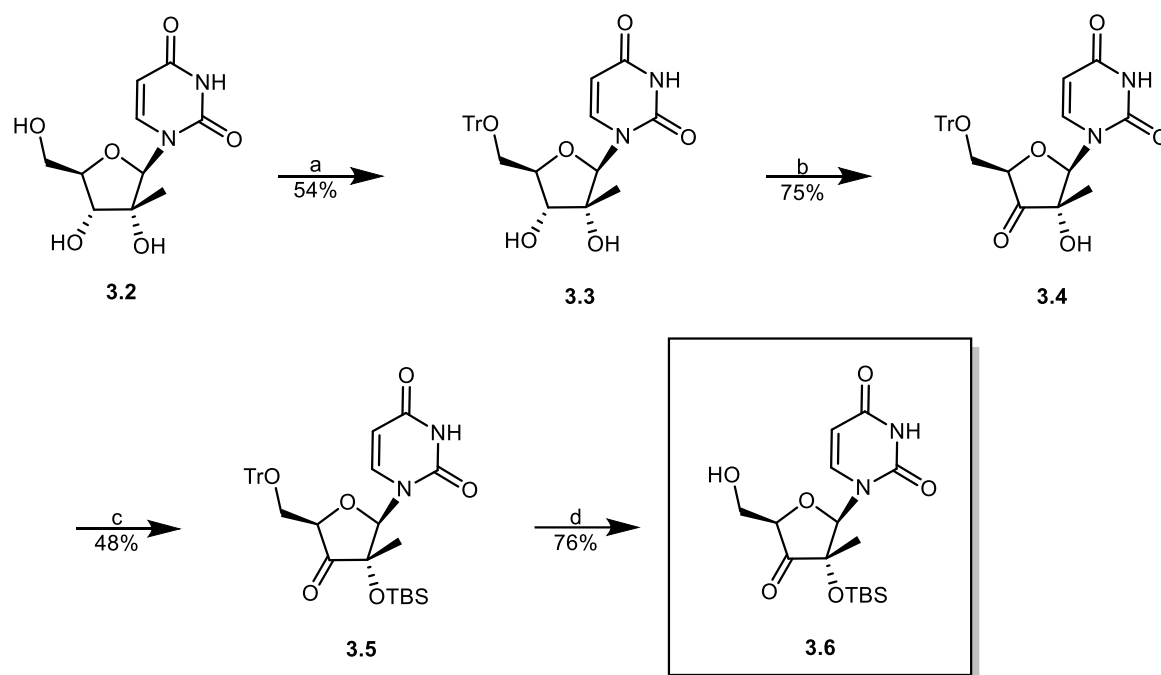


**Scheme 3.S5.** Fate of the 5'-*O*-isobutyrate protecting group

the 4'-H again proved a liability as the second TBS group was installed as the 3'-silyl enol ether (**3.S7**) instead of giving the desired 2',5'-bis(OTBS)-protected product. Clearly the use of an ester protecting group at C5' turned out to be to be unsatisfactory since it allowed for the elimination of a reasonable leaving group to form a conjugated system after the necessary oxidation to the ketone. Upon the realization that this was an intractable pathway, the 5'-*O*-trityl protection strategy was reevaluated for further optimization. In particular, two reactions had been run previously on intermediate acyloin **3.4** using TBS triflate and pyridine in THF solvent to afford the 5'-*O*-trityl-2'-OTBS-protected intermediate **3.5**, though not in a synthetically attractive yield (<30%, *vide supra*). Perhaps these conditions could be further explored to improve the yield.

### **3.2.1.3 Back to the Future: Revisiting the 5'-*O*-Trityl Ether Protecting Strategy**

Analogous to Ludwig's work, our synthesis of key intermediate **3.6** began by protecting the primary 5'-hydroxyl group of **3.2** with the primary-selective triphenylmethyl (trityl, Tr) group (Scheme 3.2). Transformation to trityl ether **3.3** could be achieved by heating the nucleoside with trityl chloride and 4-dimethylaminopyridine (DMAP);<sup>46, 47</sup> alternatively, we saw much quicker installation by using DABCO in DCM solvent.<sup>48</sup> Given the presence of the *sec,tert*-glycol system, the subsequent oxidation to acyloin **3.4** required a judicious choice of oxidant to provide the 3'-ketone without cleavage of the C-C bond. A host of oxidants were trialed and failed to deliver **3.4** reproducibly in synthetically useful yields until we explored the use of stabilized 9-azabicyclo[3.3.0]nonane *N*-oxyl radical (ABNO).<sup>49-51</sup> A sterically less-hindered analog of the more commonly encountered TEMPO radical, ABNO can be used in conjunction with an azodicarboxylate (DEAD or DIAD) as terminal oxidant to catalyze the oxidation of secondary alcohols to ketones<sup>43</sup> and afforded **3.4** in reproducibly high yield.



**Scheme 3.2.** Four-step synthesis to the key  $\beta$ -hydroxyketone intermediate (boxed) used for analog diversification. *Reagents and conditions:* (a) trityl chloride, cat. DMAP, pyridine, 80 °C, 16 h; (b) cat. ABNO, DIAD, AcOH, DCM, rt, 16 h; (c) TBSOTf, pyridine, PhMe, 0 °C – 35 °C, 16 h; (d) cat. BiCl<sub>3</sub>, 1-octanethiol, MeCN, rt, 2 h. Yields are reported as an average across  $\geq 4$  repeats.

Transformation of the resulting acyloin to the corresponding silyl ether **3.5** also proved non-trivial. We wished to convert the sterically encumbered tertiary alcohol at C2' to the bulky TBS ether per Jung and Ludwig's precedent.<sup>37, 39</sup> The presence of an enolizable ketone put us in the precarious position of driving a kinetically unfavorable silylation of the alcohol at C2' without forming the silyl enol ether at C3' and ablating the stereochemistry at the C4' position. Initially the TBS group appeared too bulky, as standard tertiary alcohol silylating conditions (i.e., TBS triflate and 2,6-lutidine)<sup>52</sup> led to no reaction. When the smaller triethylsilyl (TES) group was employed,<sup>53</sup> it unfortunately proved too labile to stay intact during the subsequent 5'-O-trityl group removal. Gratifyingly, the use of the potent silylating agent TBS triflate (TBSOTf) with pyridine as a mild and sterically less encumbered base afforded **5** in modest yield<sup>53, 54</sup> (*vide supra*). Interestingly, a solvent screen allowed for the observation of solvent effects for this transformation: ethereal solvents such as THF, 1,4-dioxane, and 1,2-dimethoxyethane led to clean but slow and incomplete conversion, while non-coordinating solvents like 1,2-dichloroethane and chlorobenzene led to much quicker but competing reaction pathways, as did acetonitrile

(MeCN). Luckily, toluene (PhMe) appeared to strike the right balance of improved reaction rate with minimal side product formation.

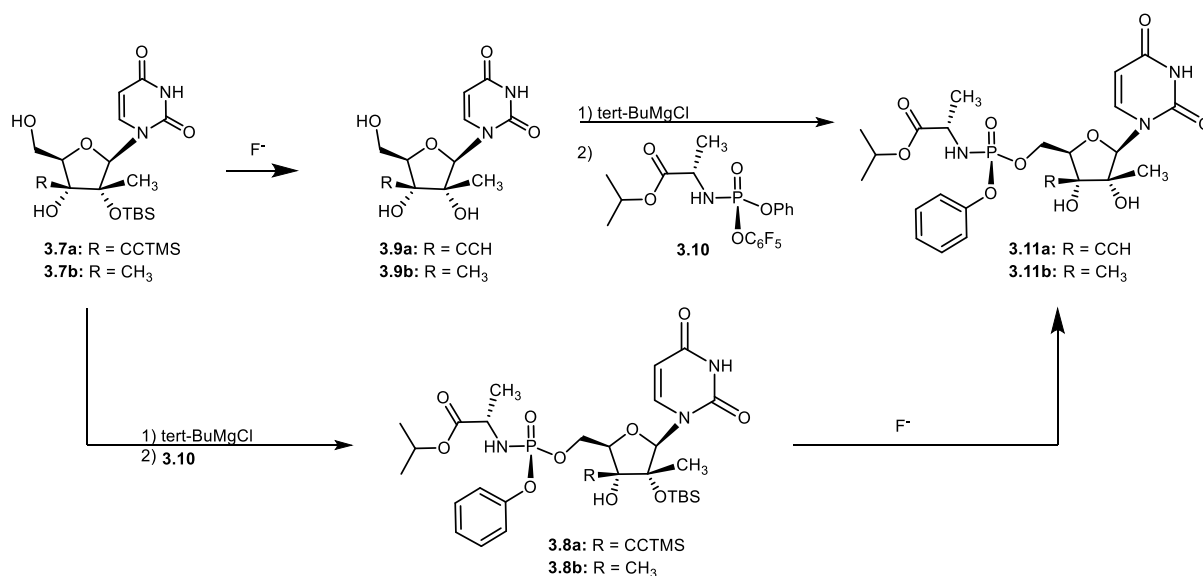
With the trityl-protected  $\alpha$ -silyloxyketone **3.5** in hand, orthogonal removal of the trityl group was accomplished using the mild Lewis acid BiCl<sub>3</sub> in MeCN solvent.<sup>55,56</sup> This reagent set has been shown to remove trityl ethers in the presence of TBS ethers using only catalytic amounts of bismuth salt,<sup>55</sup> but in our hands, stoichiometric amounts were needed on small scale. As the scale increased, we found that conversion to **3.6** diminished to roughly 50%, even with extended reaction times and the use of superstoichiometric amounts of bismuth. We hypothesized that the liberated bismuth alkoxide and trityl chloride were reacting in the reverse direction to set up an equilibrium which could be driven in the forward direction with a trityl scavenger. The scavenger would need to be more nucleophilic than the bismuth alkoxide, and the resulting tritylated adduct would need to be inert to the reaction conditions. A thiol was reasoned to suffice, and indeed, addition of a stoichiometric amount of the less noxious 1-octanethiol proved to increase conversion while reducing both reaction time and bismuth loading to substoichiometric amounts.

## 3.2.2 Synthesis and Antiviral Evaluation of the Nucleoside Monophosphate Prodrugs

### 3.2.2.1 Stereoselective Addition to C3' and the Synthesis of the Corresponding Phosphoramidates

Having accessed the key intermediate for diversification (**3.6**), we set about installing the acetylide moiety as precedented.<sup>37-39</sup> Lithium trimethylsilyl (TMS) acetylide was prepared *in situ* and subsequently treated with CeCl<sub>3</sub> pre-ligated with THF according to Imamoto's procedure.<sup>57-59</sup> The presumed cerium-transmetalated nucleophile was then treated with ketone **3.6**, providing the tertiary alcohol **3.7a** in high yield (based on ca. 25-35% recovered starting material) and diastereoselectivity (>10:1 dr); x-ray diffraction of a single crystal confirmed the desired ribo configuration at the new C3' stereocenter. At this point, two steps were needed to convert **3.7a** to the testable entity, the monophosphate prodrug: (1) removal of the silyl protecting groups, and (2) installation of McGuigan's 5'-*O*-phosphoramidate moiety.<sup>60,61</sup> The reason and order of these steps deserves some consideration. McGuigan's phosphoramidation reaction is commonly

carried out on free, unprotected NAs (Scheme 3.3, top) to accomplish two important tasks simultaneously: (1) it produces a more lipophilic, cell permeable prodrug, and (2) it circumvents reliance on intracellular conversion of the NA to the corresponding 5'-*O*-monophosphate, a key barrier to anabolism of the drug to its active metabolite, the NTP.<sup>24, 33, 34, 62, 63</sup> On this substrate, however, the  $pK_a$  values of the primary alcohol and terminal acetylene are quite comparable in organic solvent (ca. 30), so competing deprotonation by a strong base like that which is commonly employed in the reaction (*i.e.*, *tert*-BuMgCl) was a concern. Hence, the phosphoramidate was first installed on the silyl-protected substrate **3.7a** by reaction with the pentafluorophenoxy phosphoramidation reagent **3.10** under standard conditions with gentle heating.<sup>27, 64</sup> The silyl protecting groups were then smoothly removed by treatment of **3.8a** with TBAF trihydrate and acetic acid to afford the desired phosphoramidate prodrug **3.11a** in 82% yield over two steps (Scheme 3.3, bottom).



**Scheme 3.3.** Complementary 2-step routes from the 2'-OTBS-protected nucleoside analogs to the desired monophosphate prodrugs. The 3'-ethynyl analog **3.11a** was prepared via the bottom route, while the 3'-methyl analog **3.11b** was prepared via the top route.

While the success of acetylide addition to the 3'-ketonucleoside is consistent with previous reports, Jung and co-workers indicated they were unable to enjoy the same success with the corresponding methyl nucleophile.<sup>38</sup> Similarly, our methyl addition to **3.6** required extensive optimization. We initially explored reacting **3.6** with typical methyl carbanion nucleophiles,

including methylmagnesium reagents (MeMgX where X was chloride, bromide, and iodide<sup>65</sup>) as well as methyllithium with and without CeCl<sub>3</sub>. In each case, these reactions produced a mixture of diastereomers with incomplete (<60%) conversion even after extended reaction times at relatively high temperature, though the diastereomeric ratio was affected by reagent choice. For example, methyllithium (MeLi) produced one diastereomer in a slight (2.5:1 dr) preference to the other, while the use of cerium or methylmagnesium reagents inverted this facial preference. With these conventional conditions proving unsatisfactory, a further review of the literature provided more esoteric options to consider. In their total synthesis of calyciphylline B-type alkaloids, Sarpong and co-workers<sup>66</sup> refer to the work of Knochel who compared the effect of variously activated lanthanide additives on organometallic additions to ketones.<sup>67</sup> In contrast to Imamoto's method, Sarpong and Knochel reported greater success with the method of Dimitrov<sup>68,69</sup> wherein the ketone electrophile is pre-activated with the lanthanide salt (complexed with lithium chloride) prior to addition of the organometallic nucleophile. Encouraged by these results, we pre-treated **3.6** with a commercially available solution of LaCl<sub>3</sub>·2LiCl complex before addition of methylmagnesium chloride and found one of the tertiary alcohols was produced with much higher diastereoselectivity (>14:1 dr), though the stereochemical configuration was not yet identified and conversion was still mediocre (48-56%). Interestingly, when we used other methyl Grignard sources or MeLi, we saw little or no reaction. This suggests some sort of salt and/or solvent effect given that commercial solutions of MeMgCl are in THF while MeMgBr, MeMgI, and MeLi are in diethyl ether. Additional conditions trialed included transmetalating methyl carbanion sources with either titanium(IV) chloride as reported by Reetz<sup>70,71</sup> or zinc(II) chloride as reported by Ishihara<sup>72</sup> before treatment with ketone **3.6**. While both Lewis acids appeared to give a similar diastereofacial preference to the lanthanide salts, neither proved reproducibly superior.

Intrigued by the observation that these metal additives (Ce, La, Ti, Zn) all appeared to prefer the same major diastereomer to various degrees as judged by <sup>1</sup>H NMR of the crude reaction mixture, column chromatography allowed for enrichment of this major product for further

characterization. While experiments interrogating the nuclear Overhauser effect (NOE) proved inconclusive in assigning the configuration of the major diastereomer at C3', we were gratified to find that x-ray diffraction of the desilylated product **3.9b** confirmed the desired  $\beta$  addition of the methyl group. While the exact source of the observed diastereoselectivity is currently unknown, many factors are likely at play. The sterics and electronics of the proximal  $\alpha$ -silyloxy group on the bottom face of **3.6** in conjunction with the pendant  $\beta$ -alkoxide on the top face likely provide key interactions with the metal additives, as could the C2-oxo group of the nucleobase. Our leading hypothesis to rationalize the observed diastereoselectivity is related to a phenomenon our lab has previously observed called ligand-assisted nucleophilic addition.<sup>73, 74</sup> Should the organometallic counterion (blue) coordinate with the 5'-alkoxide, the methyl nucleophile (red) could be delivered from the  $\beta$ -face through a 6-membered transition state (Figure 3.2A). Alternatively, a similar result could be realized if the coordination occurs at the C2-oxo group after deprotonation of the imide proton at N3, resulting in an 8-membered transition state (Figure 3.2B), and we expect the lower energy transition state to provide the dominant kinetically controlled reaction pathway. These processes should be facilitated by increased metal size, multivalency, and/or oxophilicity, consistent with our observation that lithium alone appears to deliver the methyl nucleophile more readily to the bottom face (*vide supra*).

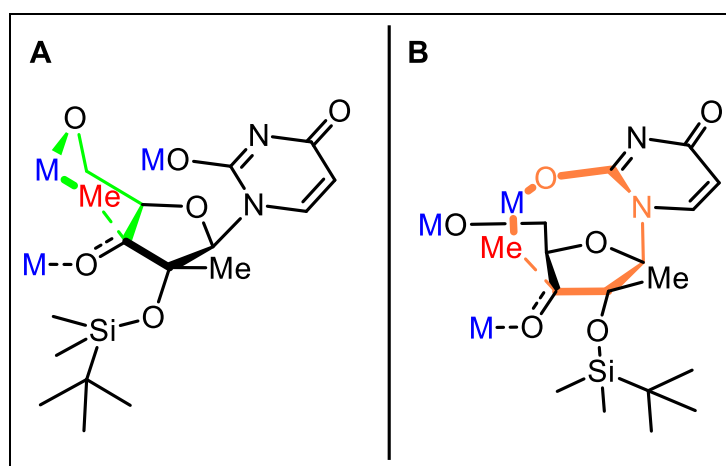


**Figure 3.2.** Proposed (A) 6-membered transition state (green) and (B) 8-membered transition state (orange) for the delivery of the methyl group (red) to the top of the sugar ring, with the appropriate metal (blue) coordination.

Having arrived at the 2'-*O*-silyl-protected NA **3.7b**, the same choice existed as to the order of the final two steps (see Scheme 3.3). Since the phosphoramidation reaction proceeded smoothly on the silylated intermediate in the previous case, the same sequence was repeated and indeed phosphoramidation again occurred in excellent yield.<sup>27</sup> However, the TBS group of **3.8b** was now surprisingly inert to the same TBAF-mediated deprotection conditions at room temperature and disappointingly decomposed when heated. The substrate smoothly reacted with triethylamine trihydrofluoride (TREAT-HF), but <sup>1</sup>H NMR revealed that the more polar product was missing the alaninate signals while retaining the characteristic TBS signals; a new <sup>19</sup>F signal was also observed. These data, as well as the *m/z*, were consistent with fluorodeamination at the phosphorus center. Since the phosphoramidate moiety appeared more reactive than the tertiary silyl ether of **3.8b**, inversion of the final two steps to remove the silyl group prior to phosphoramidation seemed reasonable. Unfortunately, substrate **3.7b** was also either unreactive or decomposed under a host of silyl removal conditions, including treatment with various fluoride sources (e.g., TBAF, HF-pyridine, CsF, KF, NH<sub>4</sub>F) or Lewis acids (e.g., BF<sub>3</sub>-etherate, Bi(OTf)<sub>3</sub>, Hf(OTf)<sub>4</sub>, NiCl<sub>2</sub>, CeCl<sub>3</sub> or BiCl<sub>3</sub> with NaI). Use of an aqueous Brønsted acid afforded a surprisingly less polar product with *m/z* consistent with installation of the conjugate base (formate) without desilylation. Ultimately, refluxing **3.7b** in concentrated (0.5 M) TBAF/THF solution afforded the free nucleoside **3.9b**, and phosphoramidation provided **3.11b**.<sup>27</sup>

### 3.2.2.2 Antiviral Evaluation

The two nucleoside phosphoramidate prodrugs **3.11a** and **3.11b** were then evaluated for their antiviral activity in Huh7 cells harboring the HCV genotype 1b replicon.<sup>75-77</sup> While the prodrugs showed negligible cytotoxicity up to the maximum tested dose of 200 μM, they were also shown to be completely ineffective at inhibiting viral replication compared to the positive control sofosbuvir. Interestingly, at doses > 10 μM, the 3'-β-methyl analog **3.11b** showed increased inhibition of viral replication relative to the 3'-β-ethynyl congener **3.11a**, which contradicted our expectation based on our computational model. The model suggested that a small exo-endo energy difference (ΔE) is necessary, but not sufficient, for potent anti-HCV

activity. However, the evaluated compounds did not appear to act in accordance with the model since the more active compound had the larger  $\Delta E$ . Clouding the picture further is the fact that the  $\Delta E$  of the parent NA 2'-MeU (**3.2**) lies in between the two disubstituted analogs ( $0.0012 < 0.0198 < 0.0888$ ), yet it demonstrates far superior antiviral potency ( $EC_{50} = 0.03 \mu\text{M}$ ).<sup>78</sup>

Before drawing too strong a conclusion, several variables which cannot be controlled should be considered. Since sofosbuvir uses the same prodrug strategy as our compounds, we can be assured that the cells are capable of appropriately metabolizing prodrugs of this class to the active inhibitor. However, it is unknown to what extent our 2',3'- $\beta$ -disubstituted analog prodrugs permeate the cells and are competent substrates for the host of enzymes necessary to see antiviral activity, including the target NS5B polymerase itself. The simplest explanation for the observed lack of antiviral activity is that the polymerase active site does not tolerate the added steric bulk at the C3' position of either novel NA. However, bearing in mind the work of Marquez,<sup>79,80</sup> it is conceivable that the diverging calculated conformational biases of the two NAs confer inactivity to them for different reasons. While per the DFT model, the low activity of **3.11b** was expected, the low activity of **3.11a** was less so. One possible explanation is the compound may be poorly phosphorylated to either the di- or triphosphate, and cursory inspection of the highest resolution UMP kinase crystal structure (PDB ID: 2J4K) shows all bound uridines to be in the 3'-endo conformation, a mode which may be disrupted by the stronger preference toward the 3'-exo conformation. Alternatively, either or both NAs could be perfectly reasonable substrates for the enzymes and get incorporated into the growing RNA strand with minimal impact on chain elongation, acting instead as competent UTP mimics. This level of mechanistic detail cannot be discerned with the available cellular reporter assay, so these rationalizations remain speculative at this time. Be that as it may, we believe the synthesis of these novel NAs to be instructive to the field as this 2',3'- $\beta$ -dialkylated nucleoside scaffold has not been demonstrated in the scientific literature to the best of our knowledge, and we hope this disclosure enables others to join us in exploring this intriguing chemotype for alternative biological activity.

In addition to evaluating the NA prodrugs **3.11a** and **3.11b** against HCV, they (or their corresponding nucleosides **3.9a** and **3.9b**) were also evaluated for cellular antiviral activity against a small panel of other representative RNA viruses, maintained by the National Institute of Allergy and Infectious Diseases (NIAID). Compounds were tested across a concentration range of 0.1-100  $\mu\text{M}$  for  $\text{EC}_{50}$  determination against viral-infected Vero, Huh7, RD, MDCK, BHK-21, or MA-104 cell lines, and the data are provided in Table 3.2. In some virus-cell line combinations, only nucleosides (**3.9a** and **3.9b**) were tested, while in other virus-cell line combinations, only phosphoramidate prodrugs (**3.11a** and **3.11b**) were tested, and the choice was motivated by which cell lines (*i.e.*, Huh7 and BHK-21) could appropriately metabolize the phosphoramidate prodrug. The compounds showed little-to-no antiviral effect against the viruses screened, indicating  $\text{EC}_{50}$  values of  $>100 \mu\text{M}$  with two exceptions. Firstly, prodrug **3.11a** showed a slightly more potent  $\text{EC}_{50}$  value of  $46 \mu\text{M}$  against the representative picornavirus Coxsackievirus B<sub>3</sub>. While the compound is somewhat more active here than against the other viruses tested, it is not very potent. For comparison, the positive control in the assay was enviroxime, a benzimidazole-based small molecule with published antiviral activity against rhinoviruses and enteroviruses,<sup>81</sup> which showed an  $\text{EC}_{50}$  of  $0.12 \mu\text{M}$ .

**Table 3.2.** Broad-spectrum cellular antiviral screening<sup>a</sup>

<b>Virus</b>	<b>Cell Line</b>	<b>3.9a</b>	<b>3.9b</b>	<b>3.11a</b>	<b>3.11b</b>
Chikungunya	Vero	>100	>100	NT <sup>e</sup>	NT
Coxsackie B <sub>3</sub>	Vero	NT	NT	46	>100
Dengue type-2	Huh7	>100	>100	>100	>100
Enterovirus-68	RD	NT	NT	>100	>100
Enterovirus-71	Vero	>100	>100	>100	>100
Influenza A H <sub>1</sub> N <sub>1</sub>	MDCK	>100	>100	NT	NT
JEV <sup>b</sup>	Vero	NT	NT	>100	>100
MERS CoV	Vero	>100	>100	NT	NT
Poliovirus-1	Vero	NT	NT	>100	>100
Powassan	BHK-21	NT	NT	>100	>100

RSV	MA-104	>100	>100	NT	NT
RVFV <sup>c</sup>	Vero	>100	>100	NT	NT
Tacaribe	Vero	>100	>100	NT	NT
Usutu	Vero	NT	NT	>100	>100
West Nile	Vero	NT	NT	>100	>100
Yellow Fever	Huh7	NT	NT	>100	>100
Zika	Vero	NT	NT	>100	>100

<sup>a</sup>Data reported as EC<sub>50</sub> values for cytopathic effect ( $\mu\text{M}$ ); <sup>b</sup>Japanese encephalitis virus; <sup>c</sup>Rift Valley fever virus; <sup>d</sup>0% inhibition at 19  $\mu\text{M}$ ; <sup>e</sup>NT = Not tested

### 3.3 MATERIALS AND METHODS

#### 3.3.1 Computational Methods

Density functional theory (DFT) calculations were conducted by Dr. C. Butch using the TeraChem<sup>82</sup> software package in mixed-precision mode. Calculations were conducted at the B3LYP/6-311G(d,p) level using COSMO implicit solvation<sup>83</sup> with a dielectric constant of 78 (corresponding to water at 298 K).<sup>84</sup> Calculations were conducted beginning from the canonical A and B forms of RNA as represented by the AMBER forcefield as implemented in the Nucleic Acid Builder software package.<sup>85, 86</sup> Initial geometries were constructed in Maestro by atom-by-atom substitution from the initial geometry, followed by minimization of the added atoms with the MMFF forcefield. This process resulted in initial scaffolds with little to no RMSD deviation of the common substructure (the phosphate moiety, C5', O3', N1, and the furan ring). This process was replicated for both the A and B geometries, after which the initial structures were minimized using the package default parameters.

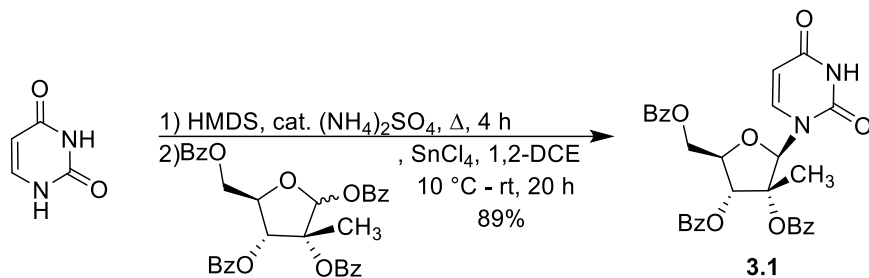
#### 3.3.2 Synthetic Chemistry

##### 3.3.2.1 General Considerations

All commercially available starting materials were purchased and used as provided unless otherwise specified. When anhydrous conditions are indicated, anhydrous solvents were used from commercial suppliers. Automated flash column chromatography was performed using

a Teledyne ISCO CombiFlash Companion system with silica gel-packed columns (RediSep® R<sub>f</sub>). Analytical thin-layer chromatography (TLC, commercially available from VWR) was carried out on Merck aluminum-supported silica gel plates (thickness: 200 μm) with fluorescent indicator (F-254). Visualization of compounds on TLC plates was accomplished with UV light (254 nm) and/or with phosphomolybdic acid, ninhydrin, ceric ammonium molybdate, or potassium permanganate staining. NMR spectra (<sup>1</sup>H, <sup>13</sup>C, <sup>19</sup>F and <sup>31</sup>P) were obtained in the Emory University NMR Research Center, directed by Dr. Shaoxiong Wu and Dr. Bing Wang, using either a Bruker INFINITY II 600 MHz spectrometer with cryogenic probe (funded by NSF grant CHE-1531620), a Varian INOVA 500 MHz spectrometer, or a Bruker AVANCE 400 MHz spectrometer. NMR samples were prepared and processed in deuterated chloroform (CDCl<sub>3</sub>), deuterated MeOH (CD<sub>3</sub>OD), deuterated DMSO (d<sub>6</sub>-DMSO), deuterated acetone (d<sub>6</sub>-acetone), deuterated water (D<sub>2</sub>O) using the residual solvent peak (CDCl<sub>3</sub>: <sup>1</sup>H = 7.26 ppm, <sup>13</sup>C = 77.16 ppm; CD<sub>3</sub>OD: <sup>1</sup>H = 3.31 ppm, <sup>13</sup>C = 49.00 ppm; d<sub>6</sub>-DMSO: <sup>1</sup>H = 2.50 ppm, <sup>13</sup>C = 39.52 ppm; d<sub>6</sub>-acetone: <sup>1</sup>H = 2.05 ppm, <sup>13</sup>C = 29.84 ppm; D<sub>2</sub>O: <sup>1</sup>H = 4.79 ppm) as an internal reference, and <sup>31</sup>P NMR were referenced using the absolute frequency of this peak. NMR data are reported to include chemical shifts (δ) reported in ppm, multiplicities indicated as s (singlet), d (doublet), dd (doubled doublet), t (triplet), td (tripled doublet), q (quartet), dq (doubled quartet), ddd (doubled doubled doublet), m (multiplet), or br s (broad singlet), coupling constants (*J*) reported in Hz, and integration normalized to 1 atom. High resolution mass spectrometry (HRMS) was performed by the Emory University Mass Spectrometry Center, directed by Dr. Fred Strobel. Liquid chromatography-mass spectrometry (LC-MS) was performed on an Agilent 1200 HPLC equipped with a 6120 Quadrupole mass spectrometer (ESI-API) eluting at a rate of 1.00 mL/min with mixtures of HPLC grade MeOH and water or acetonitrile and water (all spiked with 0.1% formic acid) through an analytical, reverse-phase, Agilent C18 XDB eclipse column (50 mm x 4.6 mm, 3.5 μM). LC/MS samples were prepared in acetonitrile, methanol, water, or mixtures thereof, and ultraviolet activity was monitored at 254 nm. Final compound purity was assessed to be ≥95% pure using <sup>1</sup>H NMR and LC/MS.

### 3.3.2.2 Synthesis of Starting Nucleoside 2'-C- $\beta$ -Methyluridine (3.2)

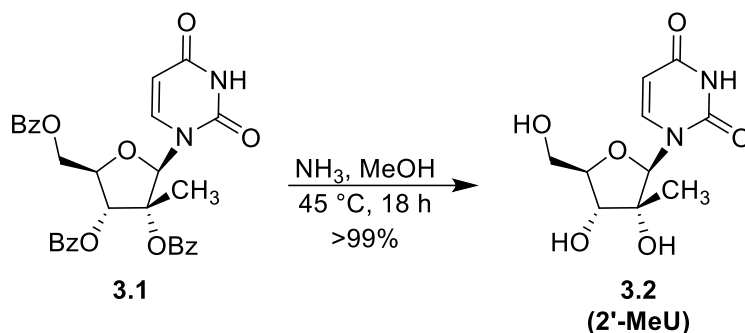


#### [(2R,3R,4R,5R)-3,4-dibenzoyloxy-5-(2,4-dioxypyrimidin-1-yl)-4-methyl-tetrahydrofuran-

#### 2-yl]methyl benzoate (3.1)

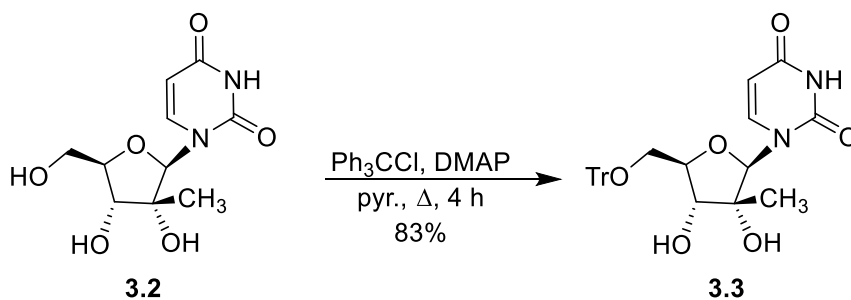
A 500-mL round-bottom flask was charged with uracil (21.43 g, 191.19 mmol), HMDS (100 mL, 477 mmol), and catalytic ammonium sulfate (56.9 mg, 0.43 mmol), and the atmosphere was exchanged with argon before the mixture was heated to 135 °C for approximately 4 hours, over which time the reaction clarified. The reaction was pulled from heat and allowed to stir overnight at ambient temperature. The next day, the volatiles were removed via rotary evaporation, and the resulting oil was heated to 50 °C and placed under high vacuum for 1 hour before being diluted with anhydrous 1,2-DCE (100 mL). Separately, a 2-liter 3-neck round-bottom flask equipped with overhead stirrer was charged with [(2R,3R,4R)-3,4,5-tribenzoyloxy-4-methyl-tetrahydrofuran-2-yl]methyl benzoate (50 g, 86.12 mmol) as a solution in anhydrous 1,2-DCE (200 mL), and the mixture was set to stir under argon. The solution of silylated nucleobase was then added via cannula under argon [the flask was rinsed with another portion of anhydrous DCE (100 mL)], and the resulting beige mixture was cooled with an ice bath. Lastly, tin(IV) chloride (22 mL, 187.74 mmol) was added over a period of 15 minutes, keeping the temperature below 10 °C. The ice bath was removed, and the resulting olive-green solution was left to stir while warming to ambient temperature overnight. After 20 hours, TLC showed complete conversion of the starting sugar to a more polar spot consistent with desired product, as well as a baseline spot. The reaction was quenched by the addition of 50 grams of Celite, 50 grams of solid sodium bicarbonate and 25 mL of water. The suspension stirred for 4 hours before being filtered over a bed of Celite. The solids were washed with DCM (100 mL), and the filtrate was extracted with DCM and washed with saturated aqueous sodium bicarbonate solution (100 mL). The organic layer was collected, dried over magnesium sulfate, filtered, and concentrated to

dryness. The resulting white solid was slurried into 300 mL of 35% v/v ethyl acetate in hexanes, chilled with an ice bath, filtered and washed with hexanes. The amorphous solid was transferred to a crystallizing dish, covered, and placed in the vacuum oven to dry at 40 °C (43.7 g, 89% yield);  $^1\text{H}$  NMR in  $\text{CDCl}_3$  conformed to that previously reported.<sup>87</sup>



**1-[(2R,3R,4R,5R)-3,4-dihydroxy-5-(hydroxymethyl)-3-methyl-tetrahydrofuran-2-yl]pyrimidine-2,4-dione (2'-C- $\beta$ -methyluridine, 2'-MeU, 3.2)** A 500-mL heavy wall pressure vessel was charged with a stir bar, [(2R,3R,4R,5R)-3,4-dibenzoyloxy-5-(2,4-dioxypyrimidin-1-yl)-4-methyl-tetrahydrofuran-2-yl]methyl benzoate (43.70 g, 76.59 mmol), methanol (50 mL), and lastly ammonia (300 mL, 2100 mmol) as a 7N solution in methanol (300 mL). The vessel was sealed, and the thick white suspension was heated to 45 °C for 18 hours, over which time the solid dissolved. The next day, the reaction was concentrated to dryness. The resulting mixture was triturated with MTBE, filtered, and further washed with MTBE. The resulting white amorphous solid was collected and dried in a vacuum oven at 45°C overnight to afford the desired product (19.7 g, >99% yield);  $^1\text{H}$  NMR in  $\text{D}_2\text{O}$  conformed to that previously reported.<sup>87</sup>

### 3.3.2.3 Protecting Strategy 1: 5'-O-Triphenylmethyl (Trityl) Ether



**1-[(2R,3R,4R,5R)-3,4-dihydroxy-3-methyl-5-((trityloxy)methyl)tetrahydrofuran-2-yl]pyrimidine-2,4(1H,3H)-dione (3.3)** In a flame-dried 100-mL 2-neck round-bottom flask

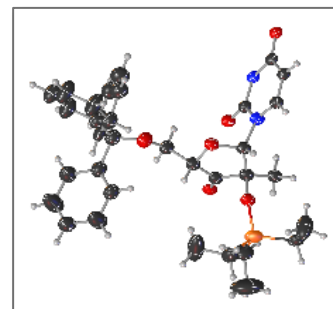
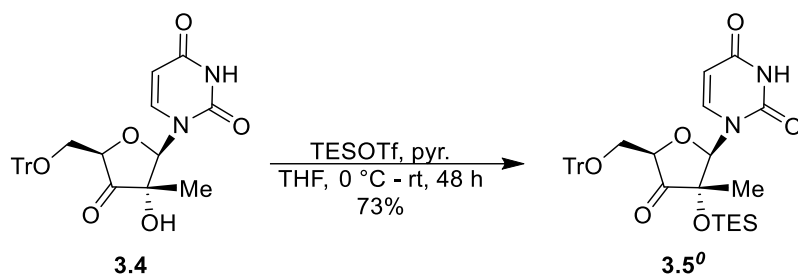
with stir bar were dissolved the solid reagents 1-[(2R,3R,4R,5R)-3,4-dihydroxy-5-(hydroxymethyl)-3-methyl-tetrahydrofuran-2-yl]pyrimidine-2,4-dione (1.3 g, 5.03 mmol) and trityl chloride (2.11 g, 7.55 mmol) in anhydrous pyridine (13 mL) to give a light yellow solution. The solution was heated to 140 °C and allowed to stir ~1 hour when TLC (1:3 Hex:EtOAc) showed partial conversion of the starting nucleoside to a less polar product; hence, the reaction was allowed to reflux another hour with no change by TLC. At this time, another 0.5 equivalence of trityl chloride (0.7 g, 2.52 mmol) was added along with a catalytic amount of DMAP (12.3 mg, 0.10 mmol), and the reaction was set to reflux for an additional ~2 hours, again with no change by TLC. Hence, another 0.5 equivalence of trityl chloride (0.7 g, 2.52 mmol) (for a total of 2.5 eq) was added, and the reaction was left to stir at ambient temperature overnight. The next day, starting material was mostly consumed, so the reaction was concentrated via rotary evaporation followed by iterative coevaporations with toluene, and the resulting solid was dried *in vacuo* overnight. LCMS of the crude solid was positive for desired product ( $m/z$ :  $[M + Na]^+ = 523.2$ ) and trityl byproducts (trityl cation at 243.0 and triphenylmethanol at 283.0). The solid was purified via silica gel flash column chromatography (0-15% methanol in DCM). Fractions of interest were pooled for the desired product, contaminated with what appears to be residual pyridine; concentration afforded the desired product as an off-white solid (2.08 g, 83% yield);  $^1\text{H}$  NMR (400 MHz,  $\text{CD}_3\text{OD}$ )  $\delta$  8.14 (d,  $J = 8.1$  Hz, 1H), 7.41 – 7.38 (m, 5H), 7.34 – 7.19 (m, 10H), 5.96 (s, 1H), 5.68 (d,  $J = 8.1$  Hz, 1H), 3.99 (dd,  $J = 12.5, 2.1$  Hz, 1H), 3.92 (dt,  $J = 9.2, 2.3$  Hz, 1H) 3.84 (d,  $J = 9.2$  Hz, 1H), 3.78 (dd,  $J = 12.6, 2.4$  Hz, 1H), 1.16 (s, 3H) ppm; pending  $^{13}\text{C}$  NMR; HRMS (APCI)  $m/z$ :  $[M + H]^+$  calcd for  $\text{C}_{29}\text{H}_{29}\text{N}_2\text{O}_6$  501.20201; found 501.20238.



**1-((2R,3S,5R)-3-hydroxy-3-methyl-4-oxo-5-((trityloxy)methyl)tetrahydrofuran-2-**

**yl)pyrimidine-2,4(1H,3H)-dione (3.4)**

In a 250-mL round-bottom flask was 1-[(2R,3R,4R,5R)-3,4-dihydroxy-3-methyl-5-(trityloxymethyl)tetrahydrofuran-2-yl]pyrimidine-2,4-dione (1.52 g, 3.04 mmol) which was dried briefly *in vacuo* before being dissolved in a 1:1 mixture of anhydrous DCM (8.5 mL) and anhydrous DMSO (8.5 mL) to give a deep yellow solution. The solution was chilled to 0 °C before triethylamine (2.96 mL, 21.26 mmol) was added followed by sulfur trioxide-pyridine complex (2.42 g, 15.18 mmol) in two equal portions over 10 minutes. The reaction was allowed to stir at reduced temperature with monitoring by LCMS. After 15 minutes, partial conversion of the starting material ( $m/z$   $[\text{M}+\text{Na}]^+ = 523.2$ ) to the ketone ( $m/z$   $[\text{M}+\text{Na}]^+ = 521.2$ ) was observed. After ~3 hours, the reaction was quenched with ~1 mL of isopropyl alcohol and diluted with ethyl acetate and water. The product was extracted with ethyl acetate and washed with brine and saturated ammonium chloride solution. The organic was dried over sodium sulfate, filtered and concentrated to ~2.5 grams of yellow oil. The product was precipitated out of isopropanol, and the resulting white solid was filtered and collected (0.8 g, 53% yield);  $^1\text{H}$  NMR (400 MHz,  $d_6$ -DMSO)  $\delta$  11.43 (s, 1H), 7.87 (d,  $J = 8.0$  Hz, 1H), 7.40 – 7.34 (m, 6H), 7.30 (app t,  $J = 7.5$  Hz, 6H), 7.26 – 7.23 (m, 3H), 6.45 (s, 1H), 5.70 (s, 1H), 5.65 (d,  $J = 7.9$  Hz, 1H), 4.64 (d,  $J = 9.5$  Hz, 1H), 3.54 (dd,  $J = 10.5, 7.8$  Hz, 1H), 3.13 (dd,  $J = 10.3, 1.5$  Hz, 1H), 1.11 (s, 3H) ppm;  $^{13}\text{C}$  NMR pending; HRMS (APCI)  $m/z$ :  $[\text{M} + \text{H}]^+$  calcd for  $\text{C}_{29}\text{H}_{27}\text{N}_2\text{O}_6$  499.1864; found 499.1861.



**1-[(2R,3S,5R)-3-methyl-4-oxo-3-(triethylsilyloxy)-5-(trityloxymethyl)tetrahydrofuran-2-**

**yl]pyrimidine-2,4-dione (3.5<sup>o</sup>)** In a 2-neck round-bottom flask with stir bar was dissolved 1-

[(2R,3S,5R)-3-hydroxy-3-methyl-4-oxo-5-(trityloxymethyl)tetrahydrofuran-2-yl]pyrimidine-

2,4-dione (177 mg, 0.36 mmol) in anhydrous THF (5 mL) under argon to give a colorless solution.

The solution was cooled to 0 °C before being treated with anhydrous pyridine (115  $\mu$ L, 1.42

mmol) followed by triethylsilyl trifluoromethanesulfonate (0.28 mL, 1.24 mmol) dropwise added

under argon. Almost immediately, a white precipitate crashed out of solution. The reaction was

allowed to stir ~48 hours while slowly warming to ambient temperature. TLC (3:1 DCM:EtOAc)

showed mostly complete conversion to the desired less polar spot. Reaction was chilled to 0 °C,

diluted with ethyl acetate and quenched with an aqueous solution of ammonium chloride. The

product was extracted with ethyl acetate and washed with ammonium chloride and water before

the organics were dried over sodium sulfate, filtered and concentrated to 0.28 g of white solid.

The sample was purified via flash column chromatography (0-90% ethyl acetate in DCM over 15

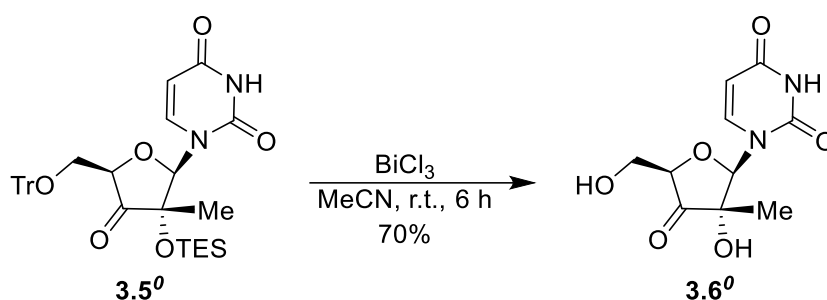
minutes) to afford the desired product as a white solid (0.158 g, 73% yield); <sup>1</sup>H NMR (400 MHz,

CDCl<sub>3</sub>)  $\delta$  8.43 (s, 1H), 7.64 (d,  $J$  = 8.2 Hz, 1H), 7.34 (t,  $J$  = 1.9 Hz, 2H), 7.33 – 7.31 (m, 3H), 7.28 –

7.18 (m, 9H), 6.01 (s, 1H), 5.23 (dd,  $J$  = 8.1, 2.3 Hz, 1H), 4.46 (dd,  $J$  = 4.0, 2.4 Hz, 1H), 3.71 (dd,  $J$  =

11.0, 4.0 Hz, 1H), 3.44 (dd,  $J$  = 11.0, 2.4 Hz, 1H), 1.25 (s, 3H), 0.90 (t,  $J$  = 7.9 Hz, 9H), 0.60 (q,  $J$  = 7.9

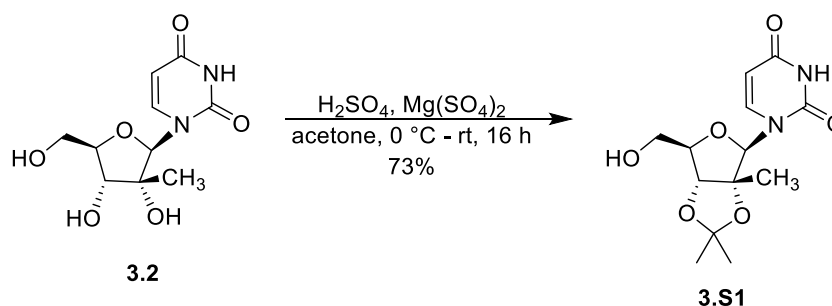
Hz, 6H) ppm; HRMS (APCI)  $m/z$ : [M – H]<sup>-</sup> Calcd for C<sub>16</sub>H<sub>25</sub>N<sub>2</sub>O<sub>6</sub>Si 369.1487; found 369.1487.



### 1-[(2R,3S,5R)-3-hydroxy-5-(hydroxymethyl)-3-methyl-4-oxo-tetrahydrofuran-2-

**yl]pyrimidine-2,4-dione (3.6<sup>o</sup>)** In a 1.5-dram vial with stir bar was dissolved 1-[(2R,3S,5R)-3-methyl-4-oxo-3-triethylsilyloxy-5-(trityloxymethyl)tetrahydrofuran-2-yl]pyrimidine-2,4-dione (32 mg, 0.05 mmol) in anhydrous MeCN (0.83 mL) to give a colorless solution. The solution was treated with catalytic bismuth(III) chloride (2 mg, 0.01 mmol), turning the solution a light yellow. The reaction stirred at ambient temperature for 15 minutes when monitoring by TLC (90:10 DCM:MeOH) showed partial conversion of the starting material to two more polar spots. The reaction progress was monitored by TLC over the course of 6 hours, ultimately resulting in the reaction proceeding overnight. The next day, TLC showed complete consumption of starting material. LCMS of the sample was indicative of mostly bis-deprotected ketonucleoside (~70%) with some desired detritylated product (~13%), as well as desilylated product alone (~9%), triphenylmethanol (~5%) and slight unreacted starting material (~3%).

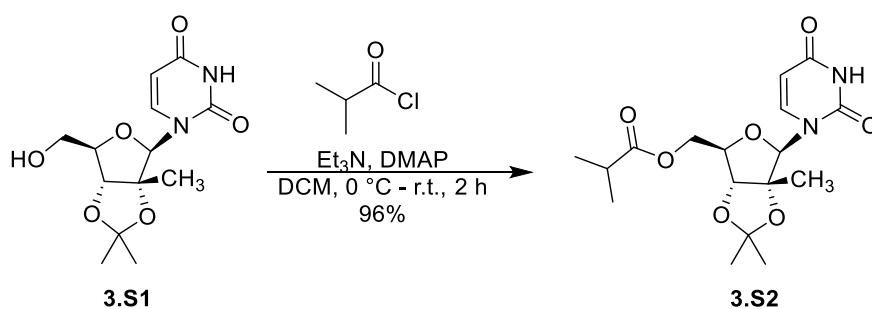
#### 3.3.2.4 Protecting Strategy 2: 5'-O-Isobutyl Ester



### 1-[(3aR,4R,6R,6aR)-6-(hydroxymethyl)-2,2,3a-trimethyl-6,6a-dihydro-4H-furo[3,4-

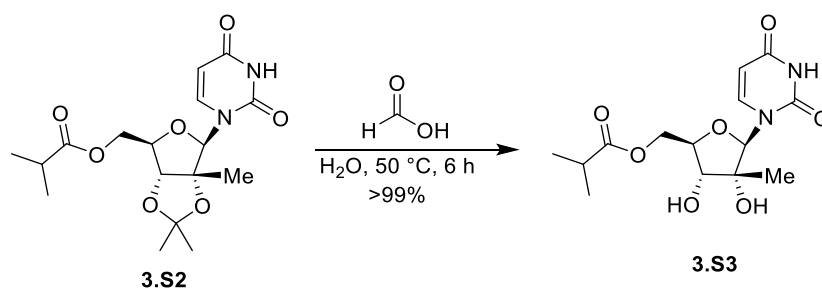
**d][1,3]dioxol-4-yl]pyrimidine-2,4-dione (3.S1)** In a flame-dried 50-mL 3-neck round-bottom flask with stir bar, a cooled suspension of 1-[(2R,3R,4R,5R)-3,4-dihydroxy-5-(hydroxymethyl)-3-methyl-tetrahydrofuran-2-yl]pyrimidine-2,4-dione (0.6 g, 2.32 mmol) and anhydrous magnesium sulfate (0.73 g, 6.04 mmol) in acetone (12 mL) (dried over activated molecular sieves)

was treated with concentrated sulfuric acid (0.1 mL, 1.86 mmol). The ice bath was removed, and the reaction mixture stirred while warming to ambient temperature with monitoring by TLC (90:10 DCM:MeOH). Note that reaction changes color from colorless to light yellow within 10 minutes. The reaction stirred under a balloon of argon overnight at ambient temperature. The next day, TLC showed mostly desired product, with some slight residual starting material; hence, another ca. half portion of magnesium sulfate (0.39g, 3.25mmol) was added (for a total of 4 eq), and the reaction stirred for a further ~2 hours with minimal change to TLC. The reaction was chilled with an ice bath before being neutralized by the addition of triethylamine (0.56 mL). The product mixture was filtered over a plug of Celite, and the solids were washed with acetone and DCM. The filtrate was concentrated to 0.96 g of off-white foam; the product was brought up in DCM and purified via silica gel flash column chromatography (0-10% methanol in DCM over 10 minutes, followed by a flush with 15% methanol in DCM). The fractions of interest were pooled and concentrated to yield the product as a fluffy white solid (0.505 g, 73% yield);  $^1\text{H}$  NMR (400 MHz,  $\text{CDCl}_3$ )  $\delta$  8.47 (s, 1H), 7.68 (d,  $J = 8.2$  Hz, 1H), 6.10 (s, 1H), 5.72 (d,  $J = 8.2$  Hz, 1H), 4.52 (d,  $J = 3.0$  Hz, 1H), 4.31 (q,  $J = 3.0$  Hz, 1H), 4.00 (dd,  $J = 11.7, 2.8$  Hz, 1H), 3.88 (dd,  $J = 11.7, 3.1$  Hz, 1H), 1.61 (s, 3H), 1.43 (s, 3H), 1.33 (s, 3H) ppm;  $^{13}\text{C}$  NMR (125 MHz,  $\text{CDCl}_3$ )  $\delta$  164.4, 150.6, 141.5, 114.3, 101.6, 93.5, 90.2, 85.9, 84.4, 62.0, 28.2, 27.2, 19.4 ppm; HRMS (APCI)  $m/z$ :  $[\text{M} + \text{H}]^+$  Calcd for  $\text{C}_{13}\text{H}_{19}\text{N}_2\text{O}_6$  299.1238, found 299.1239.



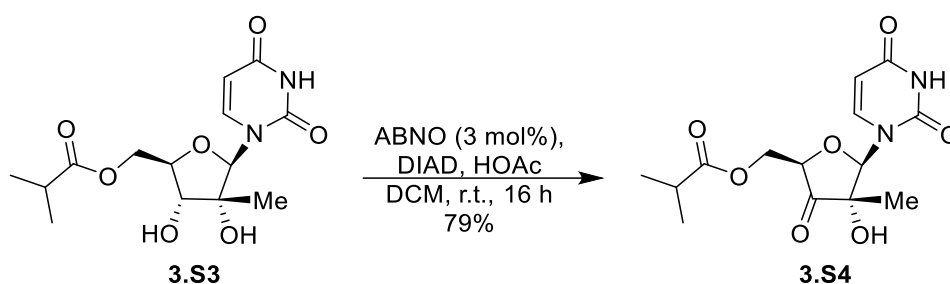
**[(3aR,4R,6R,6aR)-4-(2,4-dioxypyrimidin-1-yl)-2,2,3a-trimethyl-6,6a-dihydro-4H-furo[3,4-d][1,3]dioxol-6-yl]methyl 2-methylpropanoate (3.S2)** In a 20-mL vial with stir bar was dissolved 1-[(3aR,4R,6R,6aR)-6-(hydroxymethyl)-2,2,3a-trimethyl-6,6a-dihydro-4H-furo[3,4-d][1,3]dioxol-4-yl]pyrimidine-2,4-dione (110 mg, 0.37 mmol) in anhydrous DCM (1.5

mL) under argon. The solution was chilled with an ice bath before being treated with triethylamine (0.16 mL, 0.93 mmol), DMAP (2.3 mg, 0.02 mmol), and lastly 2-methylpropanoylchloride (47  $\mu$ L, 0.45 mmol). The ice bath was removed, and the reaction stirred while warming to ambient temperature for  $\sim$ 2 hours when monitoring by TLC (90:10 DCM:MeOH) showed spot-to-spot conversion of the starting material to a slightly less polar spot consistent with desired product. Hence, the reaction was chilled with an ice bath and diluted with ethyl acetate before being quenched by the addition of water. The product mixture was transferred to a separatory funnel, and the product was extracted with ethyl acetate. TLC indicated product still in the aqueous layer, so it was acidified with 0.2 N HCl solution and extracted a second time with ethyl acetate. The combined organic layer was washed with 0.2 N HCl solution, followed by saturated sodium bicarbonate (twice) and finally brine solution before being dried over sodium sulfate, filtered and concentrated to afford the product as an off-white oily semisolid (131 mg, 0.356 mmol, 96% yield);  $^1\text{H}$  NMR (500 MHz,  $\text{CDCl}_3$ )  $\delta$  9.34 (s, 1H), 7.43 (d,  $J = 8.2$  Hz, 1H), 6.06 (s, 1H), 5.72 (dd,  $J = 8.2, 1.8$  Hz, 1H), 4.42 – 4.36 (m, 2H), 4.32 (d,  $J = 3.0$  Hz, 1H), 4.30 (dd,  $J = 11.8, 3.1$  Hz, 1H), 2.63 – 2.54 (m, 1H), 1.61 (s, 3H), 1.41 (s, 3H), 1.31 (s, 3H), 1.20 (d,  $J = 1.3$  Hz, 3H), 1.18 (d,  $J = 1.3$  Hz, 3H) ppm;  $^{13}\text{C}$  NMR (126 MHz,  $\text{CDCl}_3$ )  $\delta$  176.7, 163.2, 150.1, 139.8, 115.1, 102.1, 92.8, 89.8, 85.9, 81.2, 63.7, 34.1, 28.4, 27.3, 19.5, 19.12, 19.09 ppm; HRMS (APCI)  $m/z$ :  $[\text{M} + \text{H}]^+$  Calcd for  $\text{C}_{17}\text{H}_{25}\text{N}_2\text{O}_7$  369.1656, found 369.1659.



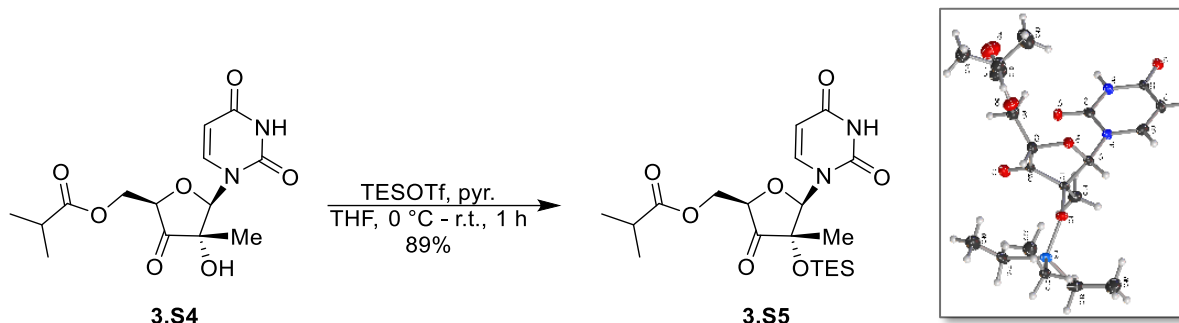
**[(2R,3R,4R,5R)-5-(2,4-dioxypyrimidin-1-yl)-3,4-dihydroxy-4-methyl-tetrahydrofuran-2-yl]methyl 2-methylpropanoate (3.S3)** In a 50-mL round-bottom flask with stir bar was suspended [(3aR,4R,6R,6aR)-4-(2,4-dioxypyrimidin-1-yl)-2,2,3a-trimethyl-6,6a-dihydro-4H-furo[3,4-d][1,3]dioxol-6-yl]methyl 2-methylpropanoate (98 mg, 0.27 mmol) in a 77% aqueous

solution of formic acid (0.6 mL), and the reaction was sealed and heated to 50 °C with monitoring by TLC (90:10 DCM:MeOH). After approximately 6 hours, TLC showed reaction was complete, so the reaction was concentrated via iterative co-evaporations with acetonitrile and dried *in vacuo* overnight, affording the product as a lightly purple solid (87 mg, >99% yield); <sup>1</sup>H NMR (600 MHz, CD<sub>3</sub>OD) δ 7.71 (d, *J* = 8.1 Hz, 1H), 5.96 (s, 1H), 5.72 (d, *J* = 8.1 Hz, 1H), 4.43 (dd, *J* = 12.6, 2.5 Hz, 1H), 4.39 (dd, *J* = 12.6, 4.4 Hz, 1H), 4.13 (ddd, *J* = 9.3, 4.4, 2.5 Hz, 1H), 3.74 (d, *J* = 9.3 Hz, 1H), 2.64 (app hept, *J* = 7.0 Hz, 1H), 1.20 (d, *J* = 2.8 Hz, 3H), 1.19 (d, *J* = 2.8 Hz, 3H), 1.17 (s, 3H) ppm; <sup>13</sup>C NMR (151 MHz, CD<sub>3</sub>OD) δ 178.3, 165.9, 152.4, 141.9, 102.8, 93.8, 81.0, 79.8, 74.8, 64.2, 35.3, 20.3, 19.50, 19.48 ppm; HRMS (APCI) *m/z*: [M + H]<sup>+</sup> Calcd for C<sub>14</sub>H<sub>21</sub>N<sub>2</sub>O<sub>2</sub> 329.1343, found 329.1339.



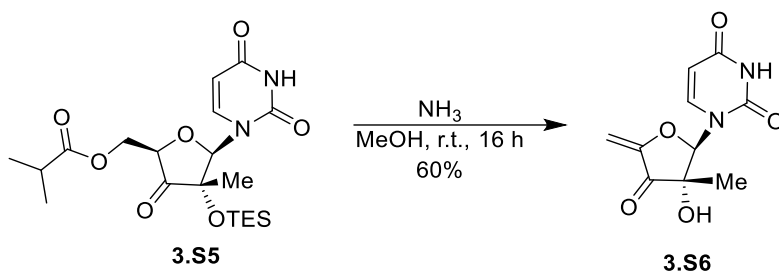
**[(2R,4S,5R)-5-(2,4-dioxypyrimidin-1-yl)-4-hydroxy-4-methyl-3-oxo-tetrahydrofuran-2-yl]methyl 2-methylpropanoate (3.S4)** A 50-mL round-bottom flask with stir bar was charged with [(2R,3R,4R,5R)-5-(2,4-dioxypyrimidin-1-yl)-3,4-dihydroxy-4-methyl-tetrahydrofuran-2-yl]methyl 2-methylpropanoate (320 mg, 0.97 mmol), anhydrous DCM (4.8 mL), and catalytic ABNO (4.8 mg, 0.03 mmol), followed by diisopropyl azodicarboxylate (0.38 mL, 1.95 mmol) and acetic acid (111  $\mu$ L, 1.95 mmol), and the yellow suspension stirred at ambient temperature overnight. The next day, TLC (90:10 DCM:MeOH) showed complete conversion to two spots, one slightly more and one slightly less polar than starting material. Hence, the reaction was quenched by the addition of 0.1 mL isopropanol, and the volatiles removed. The product mixture was brought up in DCM, adsorbed onto silica gel, and purified via silica gel flash column chromatography (10-100% ethyl acetate in hexanes). The fractions of interest were pooled and concentrated to afford the product as a white solid (252 mg, 79% yield); <sup>1</sup>H NMR (400 MHz, d<sub>6</sub>-DMSO) δ 11.58 (br s, 1H), 7.81 (d, *J* = 8.1 Hz, 1H), 6.49 (br s, 1H), 5.68 (d, *J* = 8.0 Hz, 1H), 5.65 (s, 1H), 4.62 (dd, *J* = 7.2, 2.1 Hz, 1H), 4.38 (dd, *J* = 12.3, 2.3 Hz, 1H), 4.17 (dd, *J* = 12.3, 7.2 Hz, 1H), 2.59

- 2.52 (m, 1H), 1.13 (s, 3H), 1.08 (d,  $J = 5.1$  Hz, 3H), 1.07 (d,  $J = 5.1$  Hz, 3H) ppm;  $^{13}\text{C}$  NMR (126 MHz,  $\text{d}_6\text{-DMSO}$ )  $\delta$  192.7, 177.8, 163.1, 153.2, 151.0, 144.9, 101.9, 96.1, 87.6, 72.4, 33.1, 18.9, 16.1 ppm; HRMS (APCI)  $m/z$ :  $[\text{M} - \text{H}]^-$  Calcd for  $\text{C}_{14}\text{H}_{17}\text{N}_2\text{O}_7$  325.1041, found 325.1040.



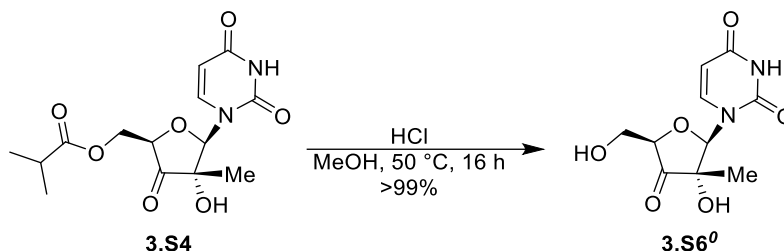
**[(2R,4S,5R)-5-(2,4-dioxypyrimidin-1-yl)-4-methyl-3-oxo-4-triethylsilyloxy-**

**tetrahydrofuran-2-yl]methyl 2-methylpropanoate (3.S5)** In a 20-mL scintillation vial with stir bar under a blanket of argon, a chilled solution of [(2R,4S,5R)-5-(2,4-dioxypyrimidin-1-yl)-4-hydroxy-4-methyl-3-oxo-tetrahydrofuran-2-yl]methyl 2-methylpropanoate (0.19 g, 0.58 mmol) in anhydrous THF (2.8 mL) was treated with anhydrous pyridine (0.20 mL, 2.48 mmol) and triethylsilyl triflate (0.40 mL, 1.77 mmol). The ice bath was removed, and the reaction was left to stir while warming to ambient temperature with monitoring by TLC (1:1 DCM:EtOAc). After ~1 hour, TLC showed complete conversion to a much less polar product; LCMS confirmed that the major product was consistent with installation of the TES group. Hence, the reaction was chilled and quenched by careful addition of saturated aqueous sodium bicarbonate solution. The product was extracted out of bicarbonate solution with ethyl acetate, and the organic layer was then washed with copper(II) sulfate solution, followed by water, and then twice washed with brine. The organic was dried over sodium sulfate, filtered and concentrated to afford the desired product as a white solid (227 mg, 89%);  $^1\text{H}$  NMR (399 MHz,  $\text{CDCl}_3$ )  $\delta$  8.58 (s, 1H), 7.33 (d,  $J = 8.1$  Hz, 1H), 5.75 (dd,  $J = 8.1, 1.4$  Hz, 1H), 5.69 (s, 1H), 4.61 (dd,  $J = 6.0, 2.5$  Hz, 1H), 4.50 (dd,  $J = 12.6, 2.5$  Hz, 1H), 4.39 (dd,  $J = 12.6, 6.1$  Hz, 1H), 2.56 (hept,  $J = 7.0$  Hz, 1H), 1.29 (s, 3H), 1.18 (d,  $J = 7.0$  Hz, 3H), 1.16 (d,  $J = 7.0$  Hz, 3H), 0.94 (t,  $J = 7.9$  Hz, 9H), 0.64 (q,  $J = 7.6$  Hz, 6H) ppm.



**1-((2R,3S)-3-hydroxy-3-methyl-5-methylene-4-oxotetrahydrofuran-2-yl)pyrimidine-**

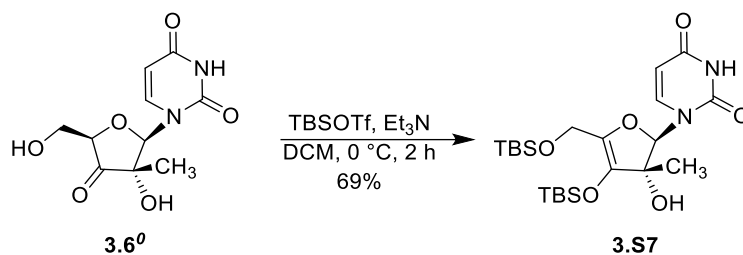
**2,4(1H,3H)-dione (3.S6)** In a 1.5-dram vial with stir bar, a suspension of [(2R,4S,5R)-5-(2,4-dioxypyrimidin-1-yl)-4-methyl-3-oxo-4-triethylsilyloxy-tetrahydrofuran-2-yl]methyl 2-methylpropanoate (28 mg, 0.06 mmol) in anhydrous methanol (0.43 mL) was treated with a 7N methanolic solution of ammonia (70  $\mu$ L, 0.49 mmol), immediately clarifying the reaction. The reaction was left to stir at ambient temperature overnight. The next day, a white precipitate had formed. LCMS of the sample showed a major (~60%) peak with a mass (261.0) consistent with concomitant desilylation and elimination of the ester, and a minor peak (28%) with a mass (327.0) consistent with desilylated starting material. This seems to indicate that the reaction proceeds by first removing the TES group, then eliminating the isobutyrate ester.



**1-[(2R,3S,5R)-3-hydroxy-5-(hydroxymethyl)-3-methyl-4-oxo-tetrahydrofuran-2-**

**yl]pyrimidine-2,4-dione (3.6<sup>0</sup>)** In a 20-mL microwave vial with stir bar, a solution of [(2R,4S,5R)-5-(2,4-dioxypyrimidin-1-yl)-4-hydroxy-4-methyl-3-oxo-tetrahydrofuran-2-yl]methyl 2-methylpropanoate (420 mg, 1.29 mmol) in anhydrous methanol (4.20 mL, 103.82 mmol) was treated with a substoichiometric amount of hydrogen chloride (0.20 mL, 0.6 mmol) as a 3M solution in methanol. The reaction was sealed and heated to 50  $^\circ$ C and left to stir overnight. The next morning, the slightly red reaction was concentrated to 0.37 g of lightly-colored powder (0.37 g, >99%);  $^1\text{H NMR}$  (399 MHz,  $d_6$ -acetone)  $\delta$  7.95 (d,  $J$  = 8.1 Hz, 1H), 6.07 (s, 1H), 5.67 (d,  $J$  = 8.2 Hz, 1H), 4.45 (m, 1H), 3.95 (dd,  $J$  = 12.4, 2.7 Hz, 1H), 3.89 (dd,  $J$  = 12.4, 3.5 Hz, 1H), 3.30 (s, 1H),

1.21 (s, 3H) ppm; HRMS (APCI)  $m/z$ :  $[M - H]^-$  calcd for  $C_{10}H_{11}N_2O_6$  255.0623, found 255.0619.

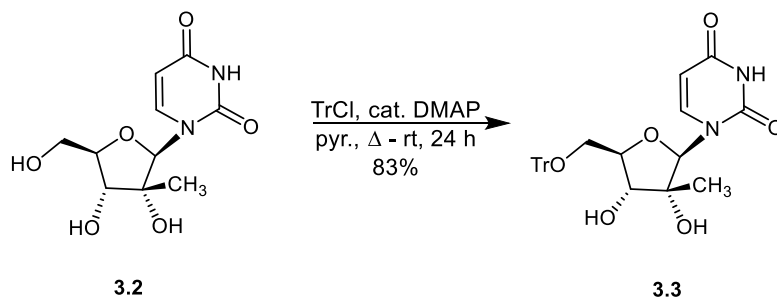
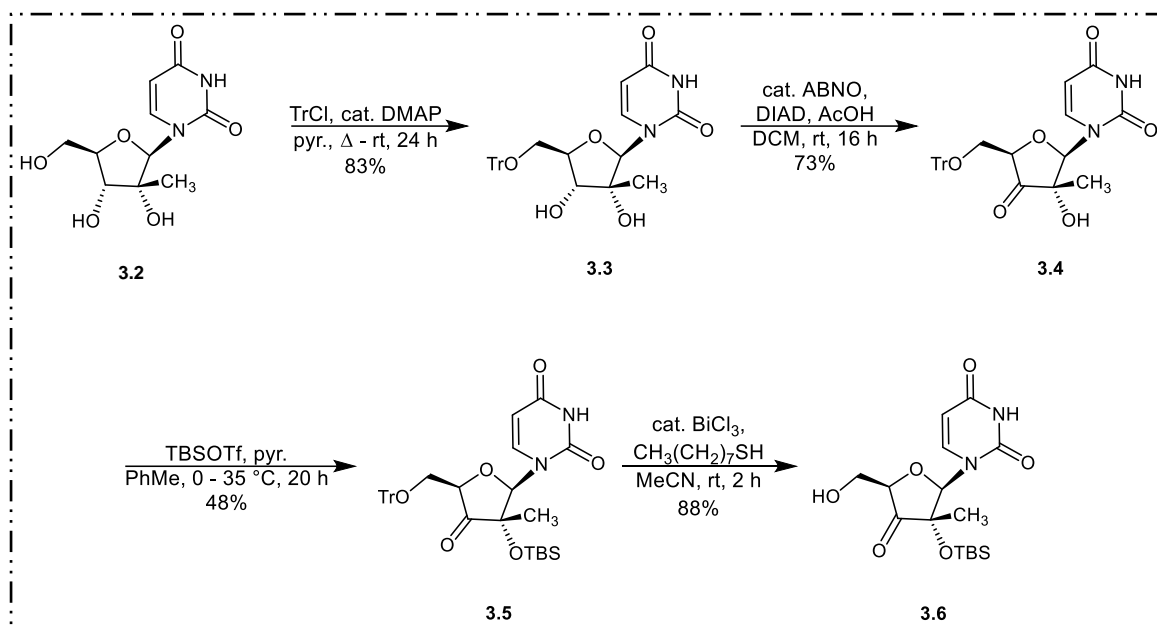


**1-[(2R,3R)-4-[(tert-butyl(dimethyl)silyl]oxymethyl]-3-**

**hydroxy-3-methyl-2H-furan-2-yl]pyrimidine-2,4-dione (3.S7)**

In a 100-mL round-bottom flask with stir bar, 1-[(2R,3S,5R)-3-hydroxy-5-(hydroxymethyl)-3-methyl-4-oxo-tetrahydrofuran-2-yl]pyrimidine-2,4-dione (369 mg, 1.44 mmol) was suspended in anhydrous DCM (14 mL) and treated with triethylamine (2.50 mL, 14.35 mmol), solubilizing the mixture. The yellow solution was chilled to 0 °C with an ice bath, and TBDMS triflate (1.70 mL, 7.4 mmol) was dropwise added, immediately changing color to dark red. After ~2 hours, TLC showed spot-to-spot conversion to a much less polar spot, so the reaction was quenched at reduced temperature with ice cold saturated aqueous sodium bicarbonate solution. The product mixture was diluted with ethyl acetate and washed with bicarbonate solution, followed by ice cold 0.15 N HCl solution (twice) and brine solution. The organic layer was dried over sodium sulfated, filtered and concentrated to 0.86 g of orange glassy semisolid which was brought up in DCM and purified via silica gel flash column chromatography (0-100% ethyl acetate in hexanes). The fractions of interest were combined and concentrated to afford the product as a glassy semisolid (0.478 g, 69%);  $^1\text{H NMR}$  (399 MHz,  $\text{CDCl}_3$ )  $\delta$  10.50 (s, 1H), 7.50 (d,  $J = 8.1$  Hz, 1H), 6.19 (s, 1H), 5.73 (d,  $J = 8.1$  Hz, 1H), 4.37 (d,  $J = 12.4$  Hz, 1H), 4.28 (s, 1H), 4.13 (d,  $J = 12.4$  Hz, 1H), 1.27 (s, 3H), 0.96 (s, 9H), 0.90 (s, 9H), 0.24 (s, 3H), 0.12 (s, 3H), 0.091 (s, 3H), 0.086 (s, 3H) ppm;  $^{13}\text{C NMR}$  (100 MHz,  $\text{CDCl}_3$ )  $\delta$  163.7, 151.5, 139.7, 135.6, 102.9, 92.3, 81.7, 54.8, 25.9, 25.8, 19.4, 18.4, 18.3, -3.7, -5.1, -5.2, -5.3 ppm.

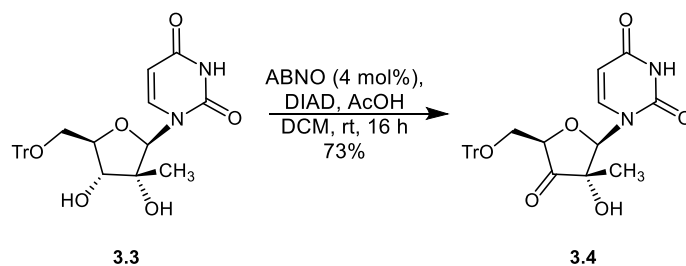
### 3.3.2.5 Final Protecting Strategy: 5'-O-Trityl Ether (Revisited)



#### 1-[(2R,3R,4R,5R)-3,4-dihydroxy-3-methyl-5-(trityloxymethyl)tetrahydrofuran-2-

yl]pyrimidine-2,4-dione (3.3) In a flame-dried 100-mL 2-neck round-bottom flask with stir bar were dissolved the solid reagents 2'-C-methyluridine (1.30 g, 5.03 mmol) and trityl chloride (2.11 g, 7.55 mmol) in anhydrous pyridine (13 mL) to give a light yellow solution. The solution was heated to 140 °C and allowed to stir approximately 2 hours. At this time, another 0.5 equivalence of trityl chloride (0.70 g, 2.52 mmol) was added along with a catalytic amount of DMAP (12.30 mg, 0.1 mmol), and the reaction was set to reflux for an additional 2 hours. Then, another 0.5 equivalence of trityl chloride (0.70 g, 2.52 mmol) (for a total of 2.5 eq) was added, and the reaction was left to stir at ambient temperature overnight. The next day, starting material was mostly consumed as judged by TLC, so the reaction was concentrated via rotary evaporation followed by iterative co-evaporations with toluene, and the resulting solid was dried *in vacuo*

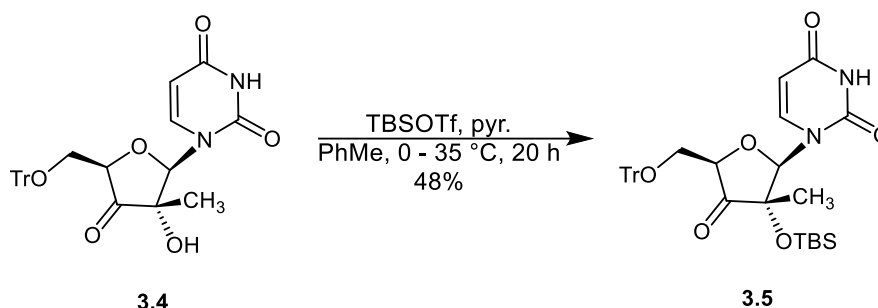
overnight. LC-MS of the crude solid was positive for desired product ( $m/z$ :  $[M + Na]^+ = 523.2$ ) and trityl byproducts. The solid was brought up in DCM/MeOH and adsorbed onto silica gel to dry load a flash silica gel column for purification (0-15% methanol in DCM). The fractions of interest were pooled for the desired product, contaminated with what appeared to be residual pyridine; concentration afforded an off-white amorphous solid (2.08 g, 83% yield);  $^1\text{H}$  NMR (400 MHz,  $d_6$ -DMSO)  $\delta$  11.40 (d,  $J = 2.2$  Hz, 1H), 7.89 (d,  $J = 8.1$  Hz, 1H), 7.45 – 7.23 (m, 15H), 5.82 (s, 1H), 5.30 (s, 1H), 5.23 (s, 1H), 5.05 (dd,  $J = 8.0, 2.2$  Hz, 1H), 4.02 – 3.88 (m, 2H), 3.44 (dd,  $J = 10.9, 3.5$  Hz, 1H), 3.28 (dd,  $J = 10.9, 1.5$  Hz, 1H), 1.05 (s, 3H) ppm;  $^{13}\text{C}$  NMR (101 MHz,  $d_6$ -DMSO)  $\delta$  162.8, 150.5, 143.4, 140.2, 128.4, 128.0, 127.2, 101.2, 91.3, 86.5, 80.4, 78.0, 72.5, 61.9, 19.8 ppm; HRMS (APCI)  $m/z$ :  $[M + H]^+$  calcd for  $\text{C}_{29}\text{H}_{29}\text{N}_2\text{O}_6$  501.2020, found 501.2024.



**1-[(2R,3S,5R)-3-hydroxy-3-methyl-4-oxo-5-(trityloxymethyl)tetrahydrofuran-2-**

**yl]pyrimidine-2,4-dione (3.4)** A 125-mL round-bottom flask with stir bar was charged with 1-[(2R,3R,4R,5R)-3,4-dihydroxy-3-methyl-5-(trityloxymethyl)tetrahydrofuran-2-yl]pyrimidine-2,4-dione (5.02 g, 10.0 mmol), DCM (31 mL), and catalytic 9-azabicyclo[3.3.0]nonane *N*-oxyl radical (56.9 mg, 0.41 mmol), followed by diisopropyl azodicarboxylate (3.95 mL, 20.1 mmol) and acetic acid (1.15 mL, 20.1 mmol), and the resulting yellow suspension stirred sealed at ambient temperature overnight. The next day, TLC showed mostly complete conversion of starting material to 2 less polar spots, so the reaction was diluted with DCM and diethyl ether. The resulting paste-like solid was filtered, washed with diethyl ether, collected and dried in a vacuum oven (4.12 g, 73% yield);  $^1\text{H}$  NMR (600 MHz,  $d_6$ -DMSO)  $\delta$  11.42 (s, 1H), 7.86 (d,  $J = 8.0$  Hz, 1H), 7.37 (dd,  $J = 8.3, 1.3$  Hz, 6H), 7.30 (dd,  $J = 8.3, 6.9$  Hz, 6H), 7.28 – 7.22 (m, 3H), 6.43 (s, 1H), 5.70 (s, 1H), 5.64 (dd,  $J = 8.0, 1.9$  Hz, 1H), 4.64 (dd,  $J = 7.7, 2.2$  Hz, 1H), 3.54 (dd,  $J = 10.6, 7.7$  Hz, 1H), 3.15

(dd,  $J = 10.7, 2.2$  Hz, 1H), 1.11 (s, 3H) ppm;  $^{13}\text{C}$  NMR (151 MHz,  $\text{d}_6\text{-DMSO}$ )<sup>1</sup>  $\delta$  163.1, 150.9, 144.3, 143.5, 128.2, 127.9, 127.1, 101.6, 86.2, 78.6, 74.2, 64.0, 15.9 ppm; HRMS (APCI)  $m/z$ :  $[\text{M} + \text{H}]^+$  calcd for  $\text{C}_{29}\text{H}_{27}\text{N}_2\text{O}_6$  499.1864, found 499.1861.

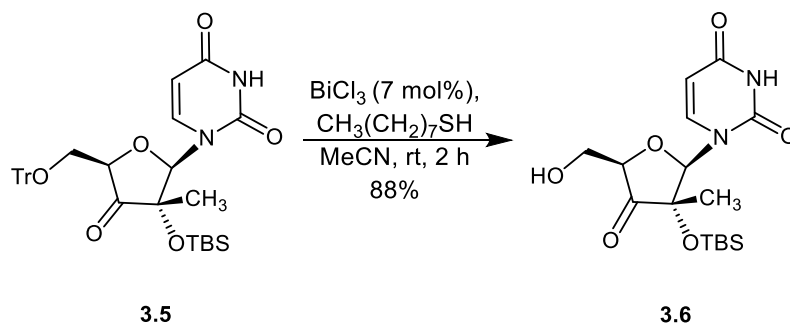


**1-[(2R,3S,5R)-3-[(tert-butyl(dimethyl)silyl]oxy-3-methyl-4-oxo-5-**

**(trityloxymethyl)tetrahydrofuran-2-yl]pyrimidine-2,4-dione (3.5)** In a flame-dried 100-mL Schlenk flask with stir bar was suspended 1-[(2R,3S,5R)-3-hydroxy-3-methyl-4-oxo-5-(trityloxymethyl)tetrahydrofuran-2-yl]pyrimidine-2,4-dione (876 mg, 1.76 mmol) in anhydrous toluene (17 mL); anhydrous pyridine (0.97 mL, 12 mmol) was added, and the resulting mixture was chilled with an ice bath before TBDMS triflate (1.4 mL, 6.1 mmol) was dropwise added. The reaction was pulled from the ice bath and gently heated to 35 °C overnight. The next day, TLC showed near complete conversion of the starting material. Hence, the reaction was quenched by the addition of saturated aqueous brine solution and diluted with ethyl acetate. The product was extracted with ethyl acetate, twice washed with 0.1 M HCl aqueous solution and then twice with brine solution. The organic layer was dried over sodium sulfate, filtered, and concentrated to a white solid, which was brought up in DCM, adsorbed onto silica gel and purified via flash column chromatography (0-40% ethyl acetate in hexanes). The fractions of interest were pooled and concentrated to afford the desired product as an amorphous white solid (511 mg, 48% yield);  $^1\text{H}$  NMR (400 MHz,  $\text{CDCl}_3$ )  $\delta$  8.36 (s, 1H), 7.69 (d,  $J = 8.2$  Hz, 1H), 7.39 (t,  $J = 1.9$  Hz, 2H), 7.37 (q,  $J = 2.0$  Hz, 3H), 7.33 – 7.23 (m, 10H), 6.03 (s, 1H), 5.31 (dd,  $J = 8.1, 2.0$  Hz, 1H),

<sup>1</sup> The diagnostic ketone signal in the  $^{13}\text{C}$  NMR is inconsistently observed; however, one of the hydroxyl carbons from the precursor is absent. We believe this is due to either ketone hydration or strong “partial” bonding observed by x-ray diffraction from the C2-oxo group, leading to unusually high electron shielding and a correspondingly upfield chemical shift.

4.49 (dd,  $J = 4.2, 2.4$  Hz, 1H), 3.76 (dd,  $J = 11.0, 4.1$  Hz, 1H), 3.49 (dd,  $J = 11.0, 2.5$  Hz, 1H), 1.29 (s, 3H), 0.87 (s, 9H), 0.21 (s, 3H), 0.11 (s, 3H) ppm;  $^{13}\text{C}$  NMR (151 MHz,  $\text{CDCl}_3$ )  $\delta$  207.5, 162.7, 150.0, 143.1, 141.4, 128.8, 128.2, 127.5, 102.2, 92.6, 87.9, 79.6, 78.1, 62.3, 25.6, 18.2, 17.4, -2.4, -3.1 ppm; HRMS (NSI)  $m/z$ :  $[\text{M} + \text{Na}]^+$  calcd for  $\text{C}_{35}\text{H}_{40}\text{N}_2\text{O}_6\text{SiNa}$  635.2548, found 635.2539.

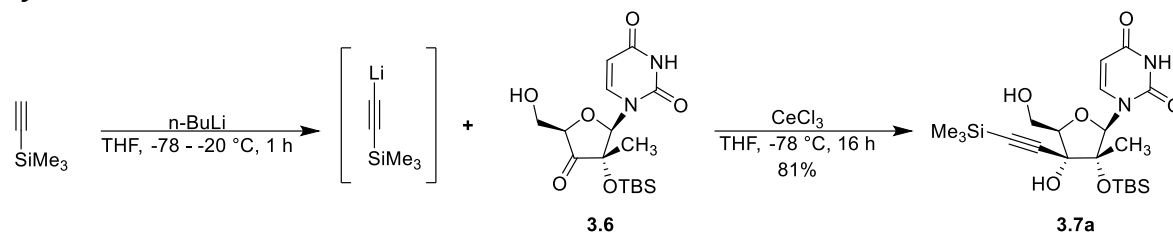


**1-[(2R,3S,5R)-3-[tert-butyl(dimethyl)silyl]oxy-5-(hydroxymethyl)-3-methyl-4-oxo-tetrahydrofuran-2-yl]pyrimidine-2,4-dione (3.6)**

A 250-mL round-bottom flask with stir bar was charged with 1-[rac-(2R,3S,5R)-3-[tert-butyl(dimethyl)silyl]oxy-3-methyl-4-oxo-5-(trityloxymethyl)tetrahydrofuran-2-yl]pyrimidine-2,4-dione (1.00 g, 1.63 mmol), anhydrous MeCN (15 mL) and 1-octanethiol (0.3 mL, 1.73 mmol), and the resulting mixture was treated with a catalytic amount of bismuth(III) chloride (35 mg, 0.11 mmol). Within minutes, the reaction had homogenized and took on a pale-yellow color. After 2 hours, a thick precipitate had formed, and monitoring by TLC showed complete conversion of the starting trityl ether to two spots: one at the solvent front and one much more polar consistent with desired product. Hence, the reaction was diluted with ethyl acetate, clarifying the mixture, and quenched by the addition of saturated aqueous sodium bicarbonate solution, causing a color change to bright yellow which partitioned with the organic layer. The product was extracted with ethyl acetate, and the organic layer was washed with bicarbonate solution followed by brine solution. The organic layer was dried over sodium sulfate, filtered, and concentrated to a heterogeneous mixture of white solid and yellow oil. The sample was triturated with diethyl ether and hexanes, and the resulting amorphous white solid was filtered, washed with hexanes and collected to afford the desired product (532 mg, 88.0% yield);  $^1\text{H}$  NMR (400 MHz,  $d_6$ -acetone)  $\delta$  10.18 (s, 1H), 7.93 (d,  $J = 8.2$  Hz, 1H), 6.09 (s, 1H), 5.65 (d,  $J = 8.1$  Hz, 1H), 4.49 (t,  $J = 3.1$  Hz, 1H), 4.44 (app t,  $J =$

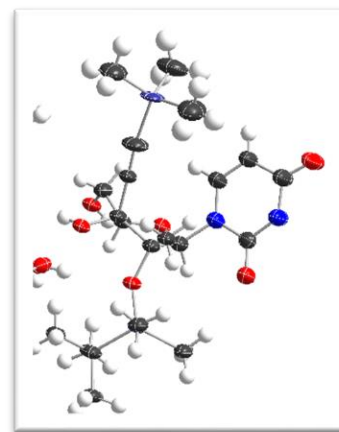
5.4 Hz, 1H), 4.00 – 3.95 (m, 1H), 3.94 – 3.88, (m, 1H), 1.28 (s, 3H), 0.88 (s, 9H), 0.21 (s, 3H), 0.12 (s, 3H) ppm;  $^{13}\text{C}$  NMR (151 MHz,  $d_6$ -acetone)  $\delta$  209.5, 163.3, 150.9, 142.2, 101.9, 92.3, 82.1, 79.0, 61.2, 25.7, 18.4, 17.2, -2.5, -3.1 ppm; HRMS (APCI)  $m/z$ :  $[\text{M} + \text{H}]^+$  calcd for  $\text{C}_{16}\text{H}_{27}\text{N}_2\text{O}_6\text{Si}$  371.1633, found 371.1628.

### 3.3.2.6 Stereoselective C3'-Ketone Additions and Corresponding Phosphoramidate Prodrug Syntheses

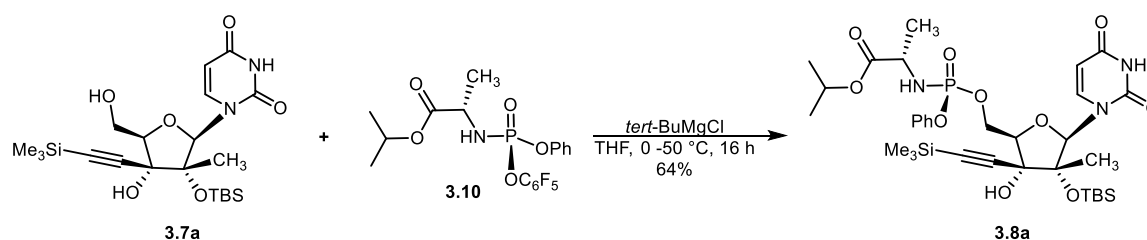


#### 1-[(2R,3R,4R,5R)-3-[tert-butyl(dimethyl)silyl]oxy-4-hydroxy-5-(hydroxymethyl)-3-methyl-4-(2-trimethylsilylethynyl)tetrahydrofuran-2-yl]pyrimidine-2,4-dione (3.7a)

A flame-dried 100-mL 2-neck round-bottom flask with stir bar was charged with argon and anhydrous cerium(III) chloride (770 mg, 3.13 mmol), which was dried briefly by heating *in vacuo*. The powder was then suspended in anhydrous THF (5 mL) and left to stir under argon overnight. A separate oven-dried 50-mL 2-neck round-bottom flask with stir bar was charged with anhydrous THF (5 mL) and trimethylsilylacetylene (453  $\mu\text{L}$ , 3.23 mmol), and the colorless solution was chilled to  $-78\text{ }^\circ\text{C}$  before being dropwise treated with *n*-butyllithium (1.37 mL, 3.28 mmol) as a ca. 2.4 M solution in hexanes. The reaction took on a light color; the deprotonation was allowed to warm to  $-20\text{ }^\circ\text{C}$  and stirred for 1 hour before being again cryogenically cooled and cannulated to the cerium suspension cooled to the same temperature. The heterogenous transmetalation took on a dark yellow color and stirred for 1 hour at reduced temperature before ketone **3.6** (193 mg, 0.52 mmol) was cannulated as a solution in anhydrous THF (5 mL). The still heterogenous reaction stirred at reduced temperature overnight. The next day, TLC showed partial conversion of the starting ketone to a less polar spot. The reaction was quenched with acetic acid (0.3 mL) and allowed to warm to ambient



temperature before being poured into a pH 7 aqueous potassium phosphate solution. The product was extracted with ethyl acetate and washed with brine solution. The organic layer was collected, dried over sodium sulfate, filtered, and concentrated to a glass-like solid, which was brought up in DCM and purified via silica gel flash column chromatography (0-80% ethyl acetate in hexanes). The fractions of interest were pooled and concentrated to afford the desired product as a glass-like semisolid (128 mg, 80.5% yield BRSM; 67 mg, 35% starting material recovered);  $^1\text{H}$  NMR (400 MHz,  $\text{CDCl}_3$ )  $\delta$  8.86 (s, 1H), 7.83 (d,  $J = 8.3$  Hz, 1H), 6.06 (s, 1H), 5.68 (dd,  $J = 8.2, 2.3$  Hz, 1H), 4.09 – 4.03 (m, 2H), 3.98 (dd,  $J = 6.1, 4.4$  Hz, 1H), 3.25 (s, 1H), 2.07 (br s, 1H), 1.40 (s, 3H), 0.93 (s, 9H), 0.36 (s, 3H), 0.25 (s, 3H), 0.19 (s, 9H) ppm;  $^{13}\text{C}$  NMR (151 MHz,  $d_6$ -acetone)  $\delta$  163.5, 151.7, 141.4, 103.8, 101.3, 96.1, 93.7, 86.3, 85.3, 77.3, 63.0, 26.3, 19.1, 18.5, 0.1, -0.4, -2.1, -2.3 ppm; HRMS (ACPI)  $m/z$ :  $[\text{M} + \text{H}]^+$  calcd for  $\text{C}_{21}\text{H}_{37}\text{N}_2\text{O}_6\text{Si}_2$  469.2185, found 469.2177.



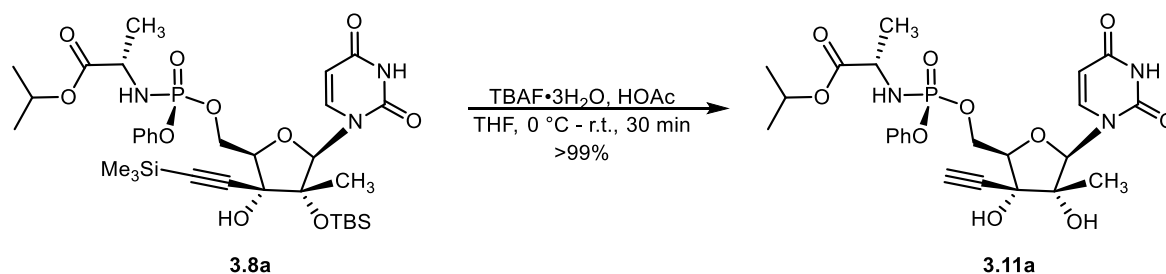
isopropyl

(2S)-2-[[[(2R,3R,4R,5R)-4-[tert-butyl(dimethyl)silyl]oxy-5-(2,4-

dioxypyrimidin-1-yl)-3-hydroxy-4-methyl-3-(2-trimethylsilylethynyl)tetrahydrofuran-2-yl]methoxy-phenoxy-phosphoryl]amino]propanoate (3.8a)

A 20-mL scintillation vial with stir bar was charged with argon, 1-[(2R,3R,4R,5R)-3-[tert-butyl(dimethyl)silyl]oxy-4-hydroxy-5-(hydroxymethyl)-3-methyl-4-(2-trimethylsilylethynyl)tetrahydrofuran-2-yl]pyrimidine-2,4-dione (84 mg, 0.18 mmol), phosphoramidate **3.10**<sup>64</sup> (146 mg, 0.32 mmol), and anhydrous THF (1.7 mL) to give a colorless solution which was chilled with an ice bath before being dropwise treated with *tert*-butylmagnesium chloride (0.27 mL, 0.27 mmol) as a 1 M solution in THF. The reaction was then heated to 50 °C and left to stir under a balloon of argon overnight. The next morning, TLC showed near complete conversion of the starting material to a slightly less polar spot. Hence, the reaction was quenched with saturated aqueous ammonium chloride solution and extracted with ethyl acetate. The organic extract was washed with saturated ammonium chloride

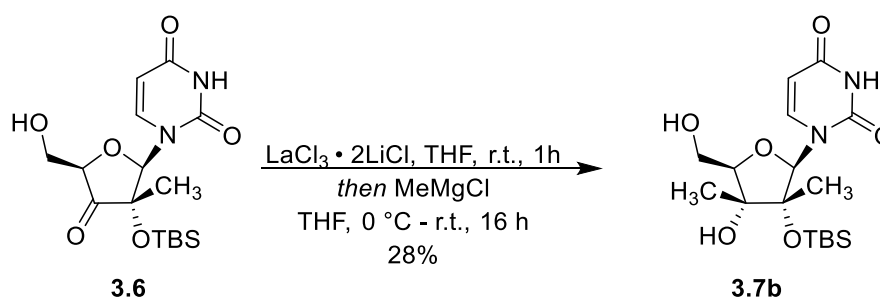
solution and brine solution before being collected, dried over sodium sulfate, filtered and concentrated to a colorless oil. The sample was brought up in ether, adsorbed onto silica gel and purified via silica gel flash column chromatography (0-5% methanol in DCM). The fractions of enriched product were combined and concentrated to afford the product, deemed pure enough for the next step (103 mg, 63.9% yield);  $^1\text{H}$  NMR (400 MHz,  $\text{CDCl}_3$ )  $\delta$  9.30 (s, 1H), 7.77 (d,  $J = 8.2$  Hz, 1H), 7.35 – 7.28 (m, 2H), 7.25 – 7.20 (m, 2H), 7.18 – 7.12 (m, 1H), 6.04 (s, 1H), 5.66 (d,  $J = 8.3$  Hz, 1H), 4.98 (hept,  $J = 6.3$  Hz, 1H), 4.61 – 4.53 (m, 1H), 4.48 – 4.38 (m, 1H), 4.11 (dd,  $J = 8.2, 2.7$  Hz, 1H), 4.04 – 3.92 (m, 1H), 3.77 (dd,  $J = 11.2, 9.2$  Hz, 1H), 1.37 (d,  $J = 7.2$  Hz, 6H), 1.22 (d,  $J = 2.0$  Hz, 3H), 1.20 (d,  $J = 2.0$  Hz, 3H), 0.91 (s, 8H), 0.34 (s, 3H), 0.23 (s, 3H), 0.18 (s, 9H) ppm;  $^{13}\text{C}$  NMR (151 MHz,  $\text{CDCl}_3$ )  $\delta$  172.9 (d,  $^3J_{\text{C-P}} = 7.9$  Hz), 162.8, 150.8 (d,  $^2J_{\text{C-P}} = 6.3$  Hz), 150.5, 140.8, 129.8, 125.1, 120.3 (d,  $^3J_{\text{C-P}} = 4.9$  Hz), 101.5, 100.1, 97.4, 92.1, 85.3, 82.7 (d,  $^2J_{\text{C-P}} = 6.9$  Hz), 76.8, 69.4, 66.6 (d,  $^3J_{\text{C-P}} = 4.9$  Hz), 50.4, 34.8, 31.7, 25.9, 22.8, 21.9, 21.8, 21.2 (d,  $^3J_{\text{C-P}} = 4.6$  Hz), 18.5, 18.0, 14.3, -0.3, -2.2, -2.8 ppm;  $^{31}\text{P}$  NMR (162 MHz,  $\text{CDCl}_3$ )  $\delta$  2.90 ppm; HRMS (NSI)  $m/z$ :  $[\text{M} + \text{H}]^+$  calcd for  $\text{C}_{33}\text{H}_{53}\text{N}_3\text{O}_{10}\text{PSi}_2$  738.3002, found 738.3007.



**isopropyl (2S)-2-[[[(2R,3R,4R,5R)-5-(2,4-dioxypyrimidin-1-yl)-3-ethynyl-3,4-dihydroxy-4-methyl-tetrahydrofuran-2-yl]methoxy-phenoxy-phosphoryl]amino]propanoate (3.11a)**

An ice-cold solution of isopropyl (2S)-2-[[[(2R,3R,4R,5R)-4-[tert-butyl(dimethyl)silyl]oxy-5-(2,4-dioxypyrimidin-1-yl)-3-hydroxy-4-methyl-3-(2-trimethylsilylethynyl)tetrahydrofuran-2-yl]methoxy-phenoxy-phosphoryl]amino]propanoate (125 mg, 0.14 mmol) in anhydrous THF (1 mL) was treated with a freshly prepared solution of tetrabutylammonium fluoride trihydrate (263 mg, 0.83 mmol) and acetic acid (48  $\mu\text{L}$ , 0.83 mmol) in anhydrous THF (1 mL), and the reaction was left to stir while warming to ambient temperature with monitoring by TLC. After 30

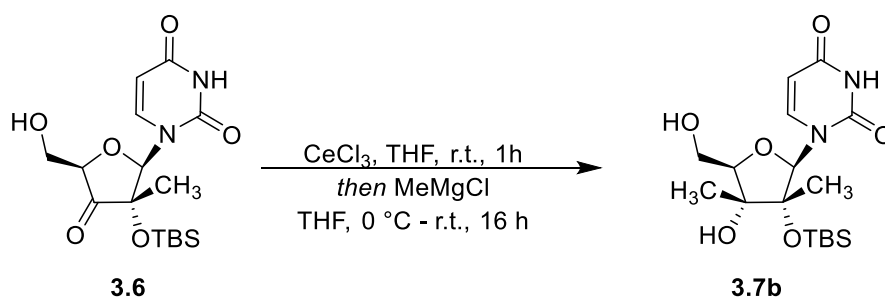
minutes, TLC showed spot-to-spot conversion of the starting material to a more polar product; LC-MS of the sample was consistent with desired product ( $m/z$ :  $[M+H]^+$  552.7). Hence, the reaction was diluted with ethyl acetate and quenched by careful addition of saturated aqueous sodium bicarbonate solution. The product was extracted with ethyl acetate and washed with bicarbonate solution then brine solution. The organic layer was collected, dried over sodium sulfate, filtered, and concentrated to a white residue which was brought up in DCM, adsorbed onto silica gel and purified via silica gel flash column chromatography (0-15% methanol in DCM). The fractions of interest were pooled and concentrated to afford the desired product as an amorphous white solid (77 mg, >99% yield);  $^1\text{H}$  NMR (600 MHz,  $\text{CD}_3\text{OD}$ )  $\delta$  7.89 (d,  $J = 8.2$  Hz, 1H), 7.36 (t,  $J = 8.0$  Hz, 2H), 7.25 (d,  $J = 8.0$  Hz, 2H), 7.19 (t,  $J = 7.4$  Hz, 1H), 5.99 (s, 1H), 5.69 (d,  $J = 8.2$  Hz, 1H), 4.95 (hept,  $J = 6.3$  Hz, 1H), 4.54 – 4.47 (m, 2H), 4.25 (dd,  $J = 7.8, 2.8$  Hz, 1H), 3.91 (dq,  $J = 9.8, 7.1$  Hz, 1H), 3.35 (s, 1H), 1.34 (d,  $J = 7.1$  Hz, 3H), 1.29 (s, 3H), 1.21 (d,  $J = 6.3$  Hz, 6H) ppm;  $^{13}\text{C}$  NMR (151 MHz,  $\text{CD}_3\text{OD}$ )  $\delta$  174.4 (d,  $^3J_{\text{C-P}} = 5.5$  Hz), 165.9, 152.3, 152.2 (d,  $^2J_{\text{C-P}} = 6.8$  Hz), 142.5, 130.8, 126.1, 121.4 (d,  $^3J_{\text{C-P}} = 4.8$  Hz), 101.6, 93.5, 82.9 (d,  $^2J_{\text{C-P}} = 7.7$  Hz), 82.5, 81.5, 81.2, 76.2, 70.1, 68.0 (d,  $^3J_{\text{C-P}} = 5.0$  Hz), 51.6, 22.0, 21.9, 20.5 (d,  $^3J_{\text{C-P}} = 6.5$  Hz), 18.4 ppm;  $^{31}\text{P}$  NMR (162 MHz,  $\text{CD}_3\text{OD}$ )  $\delta$  3.12 (s) ppm; HRMS (APCI)  $m/z$ :  $[M + H]^+$  Calcd for  $\text{C}_{24}\text{H}_{31}\text{N}_3\text{O}_{10}\text{P}$  552.1742; Found 552.1747.



**1-[(2R,3R,4R,5R)-3-[tert-butyl(dimethyl)silyl]oxy-4-hydroxy-5-(hydroxymethyl)-3,4-dimethyl-tetrahydrofuran-2-yl]pyrimidine-2,4-dione (3.7b)**

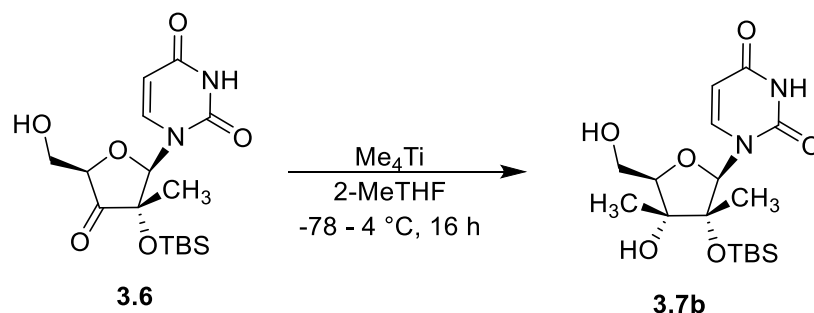
**Method A ( $\text{LaCl}_3 \cdot 2\text{LiCl}$ ):** In a flame-dried 100-mL Schlenk flask with stir bar, a ca. 0.45 M solution of trichlorolanthanum bis(lithium chloride) complex (1.1 mL, 0.66 mmol) in THF was treated with ketone **6** (200 mg, 0.54 mmol) and diluted with an equivolume amount of anhydrous THF (1.1 mL). The colorless solution stirred at ambient temperature for approximately 1 hour before being

chilled to 0 °C with an ice bath and treated with MeMgCl (0.6 mL, 1.8 mmol) as a ca. 3 M solution in THF; bubbles were observed, and the reaction turned yellow. The reaction was then left to stir under argon overnight. The next day, TLC of the now orange reaction showed what appears to be ca. 50% conversion of the starting material to a single more polar product. Hence, the reaction was chilled and another half-portion of MeMgCl (0.3 mL, 0.9 mmol) was added dropwise. The reaction proceeded for an additional hour before being quenched by addition of saturated aqueous ammonium chloride solution. The product mixture was diluted and extracted with ethyl acetate and washed with dilute HCl solution followed by brine solution. The organic was dried over magnesium sulfate, filtered, and concentrated to a yellow residue. Crude <sup>1</sup>H NMR in d<sub>6</sub>-acetone confirmed an almost 1:4 mixture of starting material (doublet at 7.94 ppm) to the more polar product (doublet at 7.99 ppm). The crude mixture was adsorbed onto silica gel and purified via silica gel flash column chromatography (0-10% methanol in DCM). The relevant fractions of interest were combined and concentrated for either recovered starting material (19 mg, 9.5% recovered) or desired methylated product (58 mg, 27.8% yield).



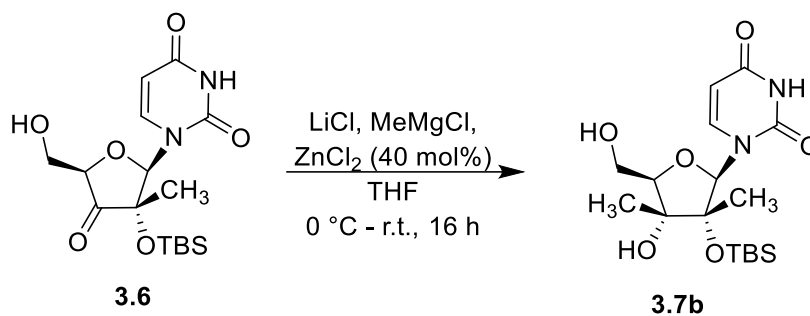
**Method B (CeCl<sub>3</sub>):** An oven-dried 25-mL Schlenk tube with stir bar was charged with argon, anhydrous cerium(III) chloride (13 mg, 0.05 mmol), and anhydrous THF (0.7 mL), and the suspension was heated to 50 °C for approximately 1 hour to ligate, over which time the suspension turned from white to yellow and back to white. The suspension was pulled from heat before 1-[(2R,3S,5R)-3-[tert-butyl(dimethyl)silyl]oxy-5-(hydroxymethyl)-3-methyl-4-oxotetrahydrofuran-2-yl]pyrimidine-2,4-dione (20 mg, 0.05 mmol) was added. The mixture stirred at ambient temperature for approximately 1 hour until a yellow gel-like consistency was observed whereupon it was chilled with an ice bath and treated dropwise with MeMgCl (0.10 mL,

0.20 mmol) as a ca. 2 M solution in THF. The reaction was observed to exotherm and bubble while forming a precipitate and was then left to stir for an hour before another portion of MeMgCl (0.10 mL, 0.20 mmol) was added. The reaction stirred while warming to ambient temperature overnight. The next day, TLC of the now orange reaction showed what appeared to be complete conversion of the starting ketone to two more polar spots, the less polar of which was consistent with the desired product. Hence, the reaction was chilled with an ice bath and quenched by the addition of an aqueous pH 7 potassium phosphate buffer solution. The product mixture was diluted with ethyl acetate and transferred to a separatory funnel, and the product was twice extracted with ethyl acetate, noting an emulsion. Addition of 5% (v/v) aqueous HCl solution clarified the emulsion. The organic layer was collected, dried over sodium sulfate, filtered, and concentrated to a yellow residue;  $^1\text{H}$  NMR in  $d_6$ -acetone showed a ca. 3:1 mixture of product to starting material.



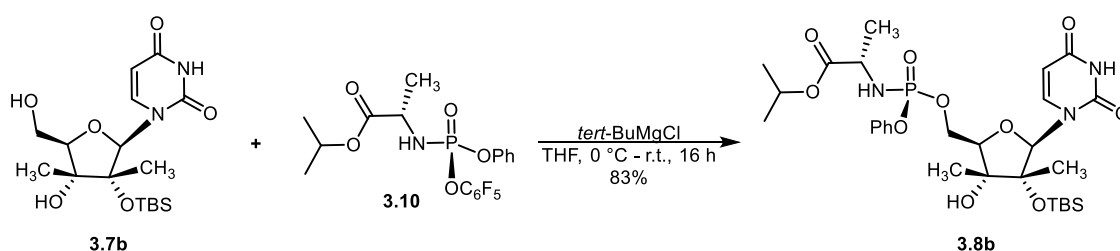
**Method C ( $\text{TiCl}_4$ ):** In a flame-dried 25-mL Schlenk tube with stir bar charged with argon, neat titanium tetrachloride (40  $\mu\text{L}$ , 0.36 mmol) was added to cryogenically cooled anhydrous 2-MeTHF (3.4 mL) to give a yellow solution, which was treated with MeMgCl (0.65 mL, 1.3 mmol) as a ca. 2 M solution in THF, whereupon the reaction turned dark green. The solution stirred while warming to -30 °C before being treated with 1-[(2R,3S,5R)-3-[tert-butyl(dimethyl)silyl]oxy-5-(hydroxymethyl)-3-methyl-4-oxo-tetrahydrofuran-2-yl]pyrimidine-2,4-dione (75 mg, 0.2 mmol). After multiple hours at reduced temperature, the reaction was moved into the cold room to stir at 4 °C overnight. TLC the next morning showed partial conversion to the desired product along with a more polar side product. The cooled reaction was quenched by addition of water.

The product mixture was diluted with ethyl acetate and water and extracted with ethyl acetate, noting an emulsion. A 5% (v/v) aqueous HCl solution was added, clarifying the emulsion, and the organic layer was collected, dried over sodium sulfate, filtered and concentrated;  $^1\text{H}$  NMR in  $d_6$ -acetone showed a ca. 1.5:1 mixture of product to starting material.



**Method D ( $\text{ZnCl}_2$ ):** A 10-mL Schlenk tube with stir bar was charged with lithium chloride (56 mg, 1.32 mmol) which was flame-dried under vacuum. The apparatus cooled *in vacuo* and was charged with argon, methylmagnesium chloride (0.66 mL, 1.31 mmol) as a ca. 2 M solution in THF (0.66 mL), and catalytic zinc(II) chloride (50  $\mu\text{L}$ , 0.1 mmol) as a ca. 1.9 M solution in 2-MeTHF. The reaction stirred at ambient temperature for approximately 1 hour before being chilled with an ice bath and treated with 1-[(2R,3S,5R)-3-[tert-butyl(dimethyl)silyl]oxy-5-(hydroxymethyl)-3-methyl-4-oxo-tetrahydrofuran-2-yl]pyrimidine-2,4-dione (98 mg, 0.26 mmol) as a solution in anhydrous THF (2 mL), whereupon the reaction went from a thick grey solution to a pale green solution. The reaction was allowed to stir overnight while slowly warming to ambient temperature. The next day, TLC of the now orange reaction showed the expected pattern of partial conversion to the more polar spot consistent with desired product, as well as the even more polar side product. Hence, the reaction was chilled with an ice bath and quenched by addition of saturated aqueous ammonium chloride solution. The product was diluted and extracted with ethyl acetate and washed with brine solution. The organic layer was dried over sodium sulfate, filtered and concentrated to 50 mg of yellow residue. Proton NMR of the crude product in  $d_6$ -acetone showed ca. 75% conversion, and as 1.2:1 mixture of desired product to a new undesired side product.

Regardless of method, the crude residue was adsorbed onto silica gel and purified via silica gel flash column chromatography (0-10% methanol in DCM). The fractions of interest were pooled and concentrated, cleanly affording the desired product (>20:1 dr);  $^1\text{H}$  NMR (500 MHz, acetone)  $\delta$  10.04 (s, 1H), 7.99 (d,  $J$  = 8.3 Hz, 1H), 5.96 (s, 1H), 5.51 (dd,  $J$  = 8.3, 2.0 Hz, 1H), 4.73 (s, 1H), 4.28 (dd,  $J$  = 6.0, 4.9 Hz, 1H), 4.12 (dd,  $J$  = 5.1, 3.9 Hz, 1H), 4.09 – 3.96 (m, 2H), 1.32 (s, 3H), 1.25 (s, 3H), 0.91 (s, 9H), 0.32 (s, 3H), 0.20 (s, 3H) ppm;  $^{13}\text{C}$  NMR (151 MHz,  $d_6$ -acetone)  $\delta$  163.7, 152.1, 142.8, 100.6, 93.7, 88.0, 86.7, 80.9, 61.4, 26.2, 18.8, 18.5, 15.6, -2.0, -2.5 ppm; HRMS (ESI)  $m/z$ :  $[\text{M}+\text{Na}]^+$  Calcd for  $\text{C}_{17}\text{H}_{30}\text{N}_2\text{O}_6\text{SiNa}$  409.1765; Found 409.1767.



isopropyl

(2S)-2-[[[(2R,3R,4R,5R)-4-[tert-butyl(dimethyl)silyloxy]-5-(2,4-

dioxypyrimidin-1-yl)-3-hydroxy-3,4-dimethyl-tetrahydrofuran-2-yl]methoxy-phenoxy-

phosphoryl]amino]propanoate (3.8b) A 20-mL scintillation vial with stir bar was charged

with argon, 1-[(2R,3R,4R,5R)-3-[tert-butyl(dimethyl)silyloxy]-4-hydroxy-5-(hydroxymethyl)-

3,4-dimethyl-tetrahydrofuran-2-yl]pyrimidine-2,4-dione (64 mg, 0.17 mmol), a stir bar, and

phosphoramidate **3.10**<sup>64</sup> (128 mg, 0.28 mmol) as a solution in anhydrous THF (1.5 mL). The

resulting yellow solution was chilled with an ice bath before being dropwise treated with *tert*-

butylmagnesium chloride (0.25 mL, 0.25 mmol) as a 1 M solution in THF; the absence of a white

precipitate was noted. The reaction was pulled from the ice bath and allowed to stir while

warming to ambient temperature. After 1.5 hours, TLC showed partial conversion of the starting

nucleoside to a slightly less polar spot; LC-MS was positive for a mass consistent with desired

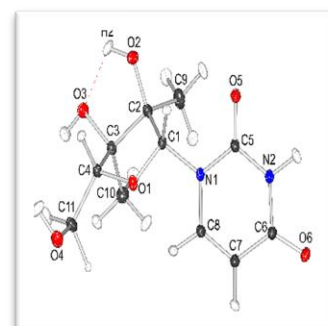
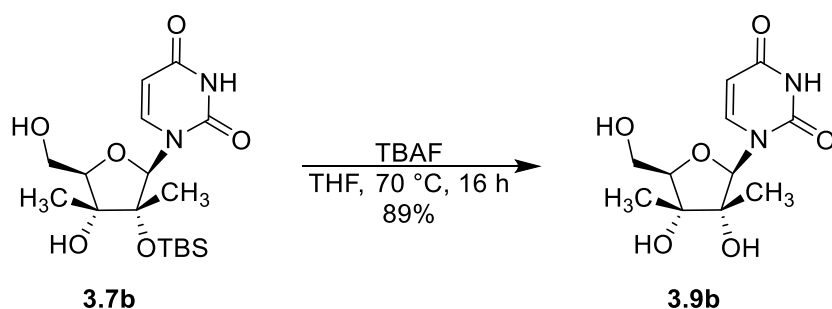
product ( $[\text{M}+\text{H}] = 656$ ). Hence, the reaction was left to stir at ambient temperature under a

balloon of argon overnight. The next morning, TLC indicated near complete conversion of the

starting material to a slightly less polar spot. Hence, the reaction was quenched with a small

volume of saturated aqueous ammonium chloride solution and concentrated to dryness. The

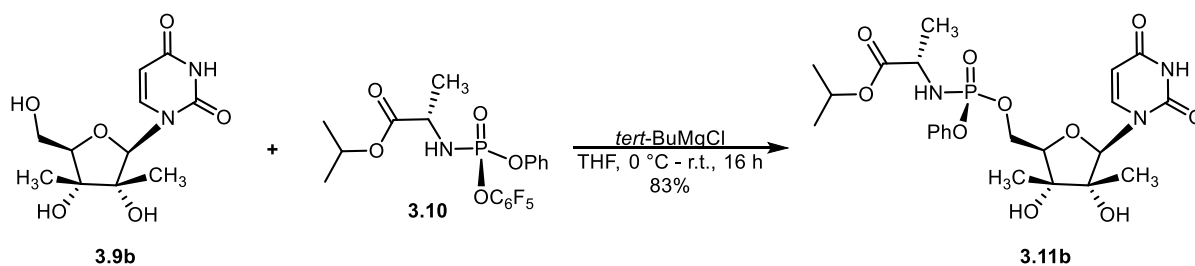
sample was brought up in DCM (MeOH to solubilize), adsorbed onto silica gel and purified via silica gel flash column chromatography (0-10% methanol in DCM). The fractions of interest were combined to afford the desired product, deemed pure enough for the next step (89.6 mg, 82.5% yield);  $^1\text{H}$  NMR (600 MHz,  $\text{CDCl}_3$ )  $\delta$  8.41 (s, 1H), 7.84 (d,  $J = 8.3$  Hz, 1H), 7.33 (t,  $J = 7.9$  Hz, 2H), 7.23 – 7.17 (m, 3H), 5.97 (s, 1H), 5.64 (dd,  $J = 8.3, 2.2$  Hz, 1H), 5.01 (ap p,  $J = 6.3$  Hz, 1H), 4.45 (ddd,  $J = 11.3, 9.4, 6.6$  Hz, 1H), 4.29 (ddd,  $J = 11.3, 8.0, 5.1$  Hz, 1H), 4.22 (dd,  $J = 6.6, 5.1$  Hz, 1H), 3.97 – 3.82 (m, 2H), 3.65 (s, 1H), 1.35 (d,  $J = 6.9$  Hz, 3H), 1.24 (dd,  $J = 6.3, 4.6$  Hz, 6H), 1.19 (s, 3H), 1.17 (s, 3H), 0.88 (s, 9H), 0.29 (s, 3H), 0.15 (s, 3H) ppm;  $^{13}\text{C}$  NMR (151 MHz,  $\text{CDCl}_3$ )  $\delta$  173.0 (d,  $^3J_{\text{C-P}} = 6.9$  Hz), 163.3, 151.0, 150.5 (d,  $^2J_{\text{C-P}} = 6.6$  Hz), 142.4, 129.9, 125.5, 120.5 (d,  $^3J_{\text{C-P}} = 4.5$  Hz), 100.8, 93.4, 87.0, 83.5 (d,  $^2J_{\text{C-P}} = 6.6$  Hz), 79.9, 69.7, 64.0 (d,  $^2J_{\text{C-P}} = 4.3$  Hz), 50.4, 25.9, 21.9, 21.8, 21.0 (d,  $^3J_{\text{C-P}} = 5.1$  Hz), 18.4, 18.3, 15.2, -2.1, -2.8 ppm;  $^{31}\text{P}$  NMR (243 MHz,  $\text{CDCl}_3$ )  $\delta$  4.28 ppm; HRMS (ESI)  $m/z$ :  $[\text{M}+\text{Na}]^+$  Calcd for  $\text{C}_{29}\text{H}_{46}\text{O}_{10}\text{N}_3\text{PSiNa}$  678.2582; Found 678.2587.



**1-[(2R,3R,4R,5R)-3,4-dihydroxy-5-(hydroxymethyl)-3,4-dimethyl-tetrahydrofuran-2-yl]pyrimidine-2,4-dione (3.9b)**

A 100-mL pear-shaped flask was charged with 1-[(2R,3R,4R,5R)-3-[tert-butyl(dimethyl)silyloxy]-4-hydroxy-5-(hydroxymethyl)-3,4-dimethyl-tetrahydrofuran-2-yl]pyrimidine-2,4-dione (120 mg, 0.31 mmol), a stir bar and argon before the substrate was dissolved in anhydrous THF (3.8 mL) and treated with an equivolume amount of TBAF (1M in THF) (3.80 mL, 3.8 mmol). The reaction was sealed and left to stir at 70 °C overnight. The next day, TLC of the now purple reaction showed nearly spot-to-spot conversion to a more polar spot consistent with desired product. Hence, the reaction was pulled from heat and treated with 2.0 mL of 10% (v/v) acetic acid in THF (4 mmol), and the volatiles were removed. The

residue was brought up in DCM, adsorbed onto silica gel and purified via silica gel flash column chromatography (0-10% methanol in DCM). The fractions of interest were pooled and concentrated to an off-white solid. Proton NMR in d<sub>4</sub>-methanol was positive for desired product contaminated with tetrabutylammonium acetate. Hence, the sample was brought up in DCM, adsorbed onto Celite and purified via reverse phase C18 column chromatography (10-100% methanol in water). The fractions of interest were pooled and concentrated to afford the desired product as a white residue (75 mg, 88.7% yield); <sup>1</sup>H NMR (500 MHz, CD<sub>3</sub>OD) δ 8.06 (d, *J* = 8.2 Hz, 1H), 5.93 (s, 1H), 5.63 (d, *J* = 8.2 Hz, 1H), 4.08 (dd, *J* = 5.7, 4.3 Hz, 1H), 3.92-3.91 (m, 2H), 1.25 (s, 3H), 1.12 (s, 3H) ppm; <sup>13</sup>C NMR (101 MHz, CD<sub>3</sub>OD) δ 166.4, 152.9, 144.3, 100.9, 94.8, 87.5, 84.7, 80.2, 61.9, 17.6, 15.9 ppm; HRMS (APCI) *m/z*: [M + H]<sup>+</sup> Calcd for C<sub>11</sub>H<sub>17</sub>O<sub>6</sub>N<sub>2</sub> 273.1081; Found 273.1080.



**isopropyl (2S)-2-[[[(2R,3R,4R,5R)-5-(2,4-dioxypyrimidin-1-yl)-3,4-dihydroxy-3,4-dimethyl-tetrahydrofuran-2-yl]methoxy-phenoxy-phosphoryl]amino]propanoate (3.11b)**

A 20-mL scintillation vial was charged with 1-[(2R,3R,4R,5R)-3,4-dihydroxy-5-(hydroxymethyl)-3,4-dimethyl-tetrahydrofuran-2-yl]pyrimidine-2,4-dione (75 mg, 0.28 mmol), a stir bar, and phosphoramidate **3.10**<sup>64</sup> (212 mg, 0.47 mmol) as a solution in anhydrous THF (1.6 mL) under argon. The resulting thin white suspension was chilled with an ice bath before being dropwise treated with *tert*-butylmagnesium chloride (0.40 mL, 0.4 mmol) as a 1 M solution in THF; the presence of a thick white precipitate was noted. The reaction was pulled from the ice bath and allowed to stir while warming to ambient temperature under a balloon of argon overnight. The next day, the reaction had homogenized; TLC showed complete conversion of the starting nucleoside to a less polar spot. Hence, the reaction was quenched with a small volume of saturated aqueous ammonium chloride solution and diluted with ethyl acetate. The product mixture was

extracted with ethyl acetate and washed with brine solution. The organic layer was collected, dried over sodium sulfate, filtered, and adsorbed onto silica gel and purified via two rounds of silica gel flash column chromatography (0-10% methanol in DCM). The fractions of interest were combined and concentrated to afford the product as a white residue (94 mg, 60.0% yield);  $^1\text{H}$  NMR (400 MHz,  $\text{CD}_3\text{OD}$ )  $\delta$  8.01 (d,  $J = 8.2$  Hz, 1H), 7.38 – 7.34 (m, 2H), 7.26 – 7.17 (m, 3H), 5.95 (s, 1H), 5.62 (d,  $J = 8.2$  Hz, 1H), 4.95 (p,  $J = 6.3$  Hz, 1H), 4.40 – 4.37 (m, 2H), 4.22 (dd,  $J = 5.7, 4.9$  Hz, 1H), 3.91 (dq,  $J = 9.8, 7.1$  Hz, 1H), 1.34 (dd,  $J = 7.1, 1.0$  Hz, 3H), 1.23 (s, 6H), 1.21 (d,  $J = 1.4$  Hz, 3H), 1.11 (s, 3H) ppm;  $^{13}\text{C}$  NMR (101 MHz,  $\text{CD}_3\text{OD}$ )  $\delta$  174.4 (d,  $^3J_{\text{C-P}} = 5.6$  Hz), 166.2, 152.8, 152.2 (d,  $^2J_{\text{C-P}} = 7.0$  Hz), 144.3, 130.8, 126.1, 121.5 (d,  $^3J_{\text{C-P}} = 4.8$  Hz), 101.1, 95.1, 86.1 (d,  $^2J_{\text{C-P}} = 8.1$  Hz), 84.5, 80.0, 70.1, 67.2 (d,  $^2J_{\text{C-P}} = 4.9$  Hz), 51.6, 22.0, 21.9, 20.5 (d,  $^3J_{\text{C-P}} = 6.3$  Hz), 17.4, 15.9 ppm;  $^{31}\text{P}$  NMR (162 MHz,  $\text{CD}_3\text{OD}$ )  $\delta$  3.28 ppm; HRMS (ESI+)  $m/z$ :  $[\text{M} + \text{Na}]^+$  Calcd for  $\text{C}_{23}\text{H}_{32}\text{O}_{10}\text{N}_3\text{PNa}$  564.1718; Found 564.1723.

### 3.3.3 Pharmacology

**Anti-HCV, Anti-Dengue Virus, Anti-Zika Virus, and Cytotoxicity Evaluation:** For *in vitro* evaluation of the antiviral and cytotoxic effects, the compounds were submitted to ImQuest Biosciences, Inc. (Frederick, Maryland 21704) as a contracted fee-for-service body of work. The SOPs and primary data appearing on the following pages are taken directly from the Final Report of SOW277-03-18 prepared by T. Hartman (PI) at ImQuest BioSciences, Inc. The compound IDs are cross-listed according to Table 3.3.

**Table 3.3.** Reference table for matching Compound No.'s used in this chapter with Notebook No.'s used by ImQuest BioSciences, Inc.

Compound No.	Notebook No.
3.11a	ZD-3-391
3.11b	ZD-3-466

**Anti-Hepatitis C Virus Assay:**

**Cell Culture** - The reporter cell line Huh-luc/neo-ET was obtained from Dr. Ralf Bartenschlager (Department of Molecular Virology, Hygiene Institute, University of Heidelberg, Germany) by ImQuest BioSciences through a specific licensing agreement. This cell line harbors the persistently replicating I<sub>399</sub>luc-ubi-neo/NS3-3'/ET replicon containing the firefly luciferase gene-ubiquitin-neomycin phosphotransferase fusion protein and EMCV IRES driven NS3-5B HCV coding sequences containing the ET tissue culture adaptive mutations (E1202G, T1208I, and K1846T). A stock culture of the Huh-luc/neo-ET was expanded by culture in DMEM supplemented with 10% FCS, 2 mM glutamine, penicillin (100 IU/mL)/streptomycin (100 µg/mL) and 1 X nonessential amino acids plus 1 mg/mL G418. The cells were split 1:4 and cultured for two passages in the same media plus 250 µg/mL G418. The cells were treated with trypsin and enumerated by staining with trypan blue and seeded into 96-well tissue culture plates at a cell culture density  $7.5 \times 10^3$  cells per well and incubated at 37°C 5% CO<sub>2</sub> for 24 hours. Following the 24 hour incubation, media was removed and replaced with the same media minus the G418 plus the test compounds in triplicate. Six wells in each plate received media alone as a no-treatment control. The cells were incubated an additional 72 hours at 37°C 5% CO<sub>2</sub> then anti-HCV activity was measured by luciferase endpoint. Duplicate plates were treated and incubated in parallel for assessment of cellular toxicity by XTT staining.

**Cellular Viability** - Following incubation at 37°C in a 5% CO<sub>2</sub> incubator, the test plates were stained with the tetrazolium dye XTT (2,3-bis(2-methoxy-4-nitro-5-sulfophenyl)-5-[(phenylamino)carbonyl]-2H-tetrazolium hydroxide). XTT-tetrazolium was metabolized by the mitochondrial enzymes of metabolically active cells to a soluble formazan product by live cells. XTT solution was prepared daily as a stock of 1 mg/mL in RPMI1640. Phenazine methosulfate (PMS) solution was prepared at 0.15 mg/mL in PBS and stored in the dark at -20°C. XTT/PMS stock was prepared immediately before use by adding 40 µL of PMS per ml of XTT solution. Fifty microliters of XTT/PMS was added to each well of the plate and the plate was reincubated for 4 hours at 37°C. Plates were sealed with adhesive plate sealers and shaken gently or inverted several times to mix the soluble formazan product and the plate was read spectrophotometrically at 450/650 nm with a Molecular Devices Vmax plate reader.

**Measurement of Virus Replication-** HCV replication from the replicon assay system was measured by luciferase activity using the britelite plus luminescence reporter gene kit according to the manufacturer's instructions (Perkin Elmer, Shelton, CT). Briefly, one vial of britelite plus lyophilized substrate was solubilized in 10 mL of britelite reconstitution buffer and mixed gently by inversion. After a 5 minute incubation at room temperature, the britelite plus reagent was added to the 96 well plates at 100  $\mu$ L per well. The plates were sealed with adhesive film and incubated at room temperature for approximately 10 minutes to lyse the cells. The well contents were transferred to a white 96-well plate and luminescence was measured within 15 minutes using the Wallac 1450 Microbeta Trilux liquid scintillation counter. The data were imported into a customized Microsoft Excel 2010 spreadsheet for determination of the 50% virus inhibition concentration ( $EC_{50}$ ) for single concentration evaluations.

#### **Anti-Dengue Virus Cytoprotection Assay:**

**Cell Preparation** – Huh7 cells (human hepatocarcinoma, licensed from Ralf Bartenschlager at ReBLikon GmbH) were passaged in DMEM supplemented with 10% FBS, 2 mM L-glutamine, 100 U/mL penicillin, and 100  $\mu$ g/mL streptomycin in T-75 flasks prior to use in the antiviral assay. Total cell and viability quantification was performed using a hemocytometer and Trypan Blue dye exclusion. Cell viability was greater than 95% for the cells to be utilized in the assay. The cells were resuspended at  $2.5 \times 10^3$  cells per well in tissue culture medium and added to flat bottom microtiter plates in a volume of 100  $\mu$ L. The plates were incubated at 37°C/5% CO<sub>2</sub> overnight to allow for cell adherence.

**Plate Format** – Each plate contains cell control wells (cells only), virus control wells (cells plus virus), drug toxicity wells (cells plus drug only), drug colorimetric control wells (drug only) as well as experimental wells (drug plus cells plus virus). Compound was added to the cell monolayers at 100  $\mu$ L per well immediately prior to infection. Ribavirin was evaluated as a positive control compound.

**Virus Preparation** – DENV2 New Guinea strain was obtained from ATCC (VR-1584) and was grown in LLC-MK2 (Rhesus monkey kidney cells, CCL-7.1) cells for the production of stock virus pools. An aliquot of virus was removed from the freezer (-80°C) and allowed to thaw slowly to room temperature in a biological safety cabinet. Virus was diluted into assay medium (DMEM supplemented with 2% heat-inactivated FBS, 2 mM L-glutamine, 100 U/mL penicillin, and 100 µg/mL streptomycin) such that the amount of virus added to each well in a volume of 100 µL was the amount determined to yield 85 to 95% cell killing at 6 days post-infection.

**Efficacy and Toxicity XTT** - Plates were stained with XTT as previously described following six days' incubation and data was collected by Softmax 4.6 software and imported into an Excel spreadsheet for calculation of percent reduction in viral CPE as compared to the untreated virus controls and percent cytotoxicity as compared to the untreated cell controls.

#### **Anti-Zika Virus Cytoprotection Assay:**

**Cell Preparation** – Huh7 cells were passaged in DMEM supplemented with 10% FBS, 2 mM L-glutamine, 100 U/mL penicillin, and 100 µg/mL streptomycin in T-75 flasks prior to use in the antiviral assay. Total cell and viability quantification was performed using a hemocytometer and Trypan Blue dye exclusion. Cell viability was greater than 95% for the cells to be utilized in the assay. The cells were resuspended at  $2.5 \times 10^3$  cells per well in tissue culture medium and added to flat bottom microtiter plates in a volume of 100 µL. The plates were incubated at 37°C/5% CO<sub>2</sub> overnight to allow for cell adherence.

**Plate Format** – Each plate contains cell control wells (cells only), virus control wells (cells plus virus), drug toxicity wells (cells plus drug only), drug colorimetric control wells (drug only) as well as experimental wells (drug plus cells plus virus). Compound was added to the cell monolayers at 100 µL per well immediately prior to infection. Sofosbuvir was evaluated as a positive control compound.

Virus Preparation – The PRVABC59 strain of Zika virus was obtained from ATCC (VR-1843) and was grown in LLC-MK2 cells for the production of stock virus pools. An aliquot of virus was removed from the freezer (-80°C) and allowed to thaw slowly to room temperature in a biological safety cabinet. Virus was diluted into assay medium (DMEM supplemented with 2% heat-inactivated FBS, 2 mM L-glutamine, 100 U/mL penicillin, and 100 µg/mL streptomycin) such that the amount of virus added to each well in a volume of 100 µL was the amount determined to yield 85 to 95% cell killing at 5 days post-infection.

Efficacy and Toxicity XTT - Plates were stained with XTT as previously described following six days' incubation and data was collected by Softmax 4.6 software and imported into an Excel spreadsheet for calculation of percent reduction in viral CPE as compared to the untreated virus controls and percent cytotoxicity as compared to the untreated cell controls.

### INHIBITION OF HCV REPLICATION BY ZD-3-391 IN Huh-luc/neo-ET

Raw Data (ZD-3-391)

RLU (Relative Light Units)							
Conc (µM)	0	0.63	2	6.32	19.99	63.2	200
SAMPLE 1	212711.7	318769.1	312560.4	318162.6	356683.3	330274.3	415785.1
SAMPLE 2	277932.9	292732.8	295095.9	316190.9	345168.0	369817.7	386276.5
SAMPLE 3	239676.8	299185.5	303440.8	359992.1	357601.7	325711.2	366028.8

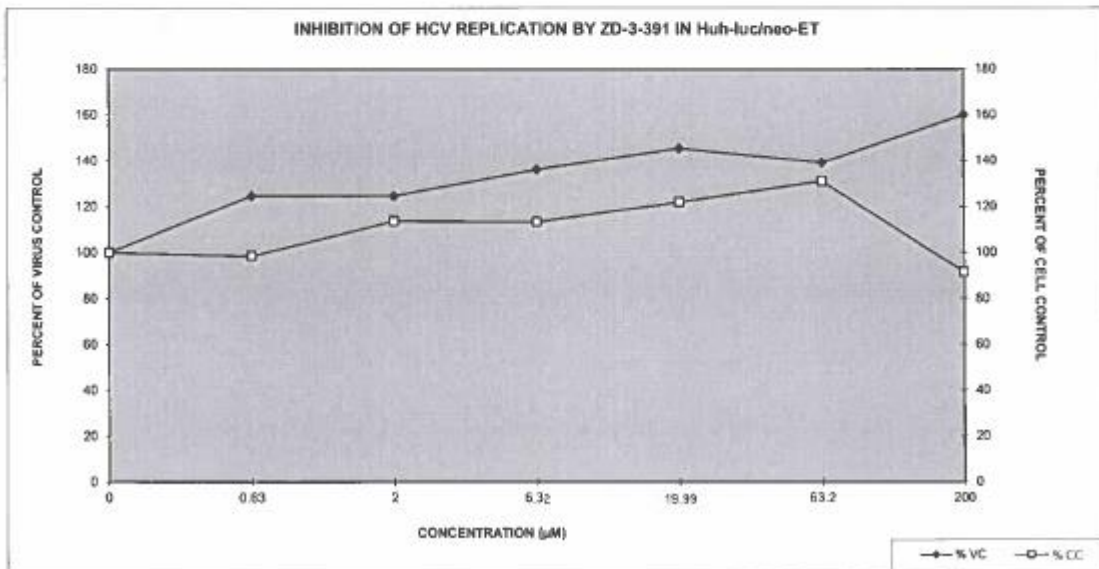
TOXICITY VALUES (XTT - O. D. @ 450/650 nm)							
SAMPLE	0	0.63	2	6.32	19.99	63.2	200
SAMPLE 1	1.402	1.483	1.751	1.703	1.797	1.992	1.374
SAMPLE 2	1.533	1.507	1.751	1.759	1.919	1.952	1.311
SAMPLE 3	1.666	1.545	1.727	1.755	1.894	2.090	1.525

Cells: Huh-luc/neo-ET      Technician: C. Buchholz    Project #: 277-03-18  
 Setup Date: 12/7/2021      PI: T. Hartman  
 Read Date: 12/10/2021      Client: Emory University

Antiviral Compound: ZD-3-391

	25%	50%	95%
EC (µM)	>200	>200	>200
TC (µM)	>200	>200	>200
Therapeutic Index (TI)	1	1	1

Conc (µM)	Antiviral Test Values			Cytotoxicity Test Values		
	Mean RLU	St. Dev.	% Virus Control	Mean OD @ 450/650 nm	St. Dev.	% Cell Viability
0	243507.1	32761.7793	100.00	1.533	0.132101	100.00
0.63	303569.1	13550.7988	124.67	1.512	0.031438	98.57
2	303709.0	8750.33396	124.72	1.743	0.013943	113.65
6.32	331748.3	24491.0055	136.24	1.739	0.031235	113.38
19.99	354151.0	7848.82038	145.44	1.870	0.064633	121.95
63.2	338934.4	19088.3363	139.19	2.011	0.071501	131.15
200	389357.5	25010.6959	159.90	1.403	0.109895	91.51



### INHIBITION OF HCV REPLICATION BY ZD-3-466 IN Huh-luc/neo-ET

Raw Data (ZD-3-466)

RLU (Relative Light Units)							
Conc (µM)	0	0.63	2	6.32	19.99	63.2	200
SAMPLE 1	212711.7	231887.7	284053.6	294360.9	291965.3	206645.7	176299.1
SAMPLE 2	277932.9	273096.8	315139.2	318991.5	255336.5	210256.4	189578.1
SAMPLE 3	239876.8	252651.2	301626.7	330756.9	283975.7	211591.3	169525.3

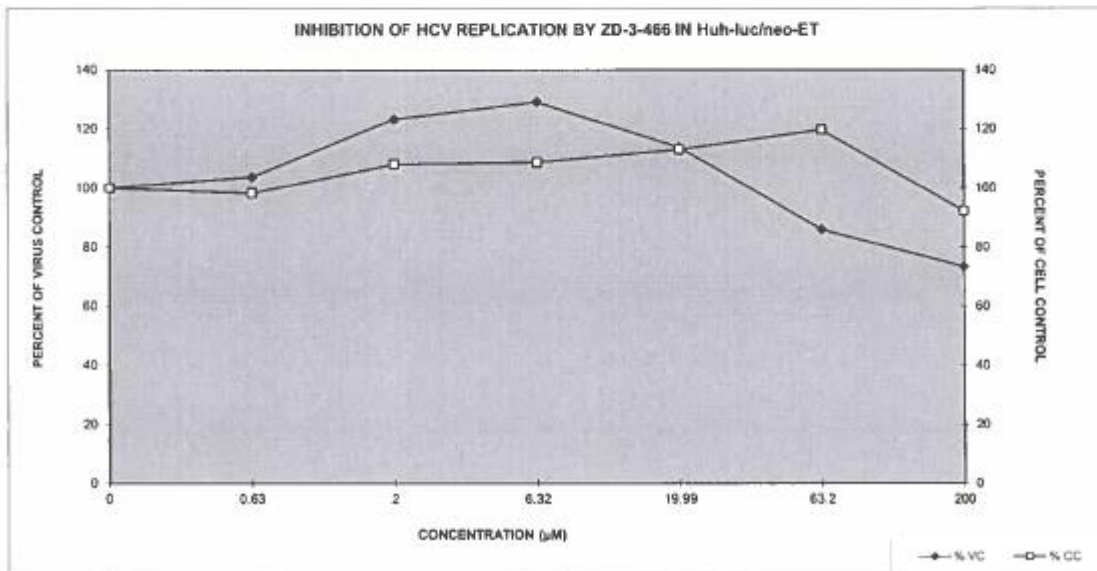
TOXICITY VALUES (XTT - O. D. @ 450/650 nm)							
SAMPLE 1	0	0.63	2	6.32	19.99	63.2	200
SAMPLE 1	1.402	1.495	1.705	1.638	1.669	1.829	1.315
SAMPLE 2	1.533	1.527	1.645	1.648	1.709	1.761	1.525
SAMPLE 3	1.666	1.499	1.620	1.719	1.822	1.896	1.401

Cells: Huh-luc/neo-ET      Technician: C. Buchholz    Project #: 277-03-18  
 Setup Date: 12/7/2021      PI: T. Hartman  
 Read Date: 12/10/2021      Client: Emory University

Antiviral Compound: ZD-3-466

	25%	50%	95%
EC (µM)	171	>200	>200
TC (µM)	>200	>200	>200
Therapeutic Index (TI)	>1.17	1	1

Conc (µM)	Antiviral Test Values			Cytotoxicity Test Values		
	Mean RLU	St. Dev.	% Virus Control	Mean OD @ 450/650 nm	St. Dev.	% Cell Viability
0	243507.1	32761.7793	100.00	1.533	0.132101	100.00
0.63	252545.2	20604.7544	103.71	1.507	0.017184	98.28
2	300276.5	15581.7364	123.31	1.657	0.044279	108.06
6.32	314693.1	18569.6428	129.23	1.668	0.044175	108.80
19.99	277092.5	19260.0903	113.79	1.733	0.079421	113.02
63.2	209297.8	2894.40932	85.95	1.836	0.057872	119.70
200	178500.2	10155.8912	73.30	1.414	0.105349	92.20



### INHIBITION OF HCV REPLICATION BY Sofosbuvir IN Huh-luc/neo-ET

Raw Data (Sofosbuvir)

RLU (Relative Light Units)							
Conc (µM)	0	0.00001	0.0001	0.001	0.01	0.1	1
SAMPLE 1	212711.7	292796.9	343726.4	344555.1	278632.7	134609.9	4172.9
SAMPLE 2	277932.9	343857.9	365770.4	325207.9	265037.7	167861.7	4753.9
SAMPLE 3	239876.8	304884.3	358962.9	362063.7	314775.9	170579.3	5965.9

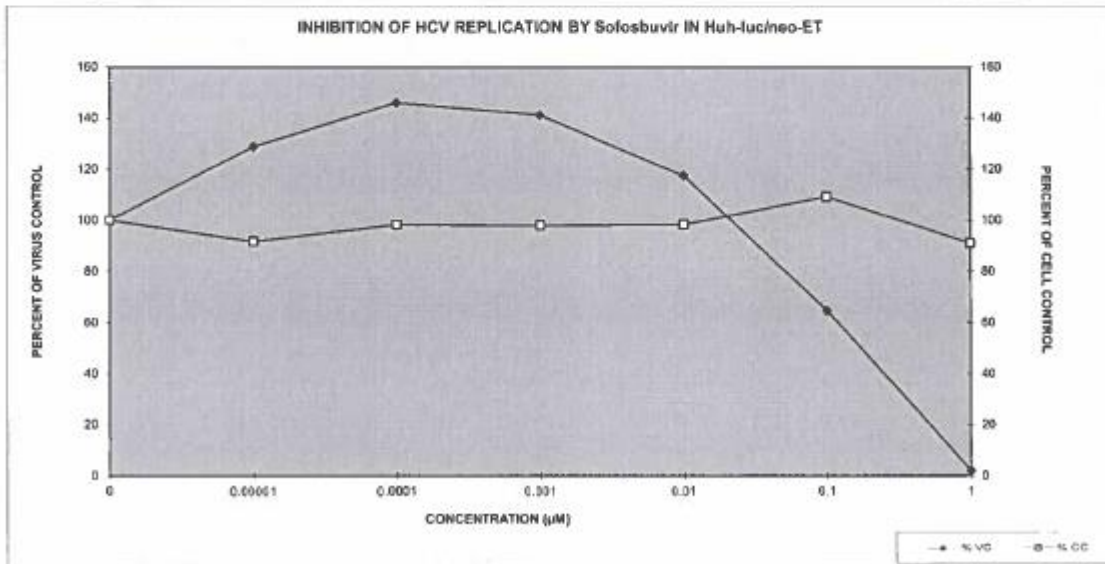
TOXICITY VALUES (XTT - O. D. @ 450/650 nm)							
Conc (µM)	0	0.00001	0.0001	0.001	0.01	0.1	1
SAMPLE 1	1.402	1.356	1.424	1.417	1.377	1.660	1.315
SAMPLE 2	1.533	1.381	1.561	1.551	1.562	1.838	1.418
SAMPLE 3	1.666	1.503	1.598	1.540	1.581	1.729	1.452

Cells: Huh-luc/neo-ET      Technician: C. Buchholz      Project #: 277-03-18  
 Setup Date: 12/7/2021      PI: T. Hartman  
 Read Date: 12/10/2021      Client: Emory University

Antiviral Compound: Sofosbuvir

	25%	50%	95%
EC (µM)	0.0639	0.172	0.897
TC (µM)	>1.0	>1.0	>1.0
Therapeutic Index (TI)	>15.65	>5.81	>1.11

Conc (µM)	Antiviral Test Values			Cytotoxicity Test Values		
	Mean RLU	St. Dev.	% Virus Control	Mean OD @ 450/650 nm	St. Dev.	% Cell Viability
0	243507.1	32761.779	100.00	1.533	0.13210102	100.00
0.00001	313779.7	26571.722	128.86	1.407	0.08351383	91.74
0.0001	355916.6	11173.831	146.16	1.508	0.08682893	98.32
0.001	343860.2	18432	141.21	1.503	0.07419874	98.01
0.01	286155.4	25698.609	117.51	1.507	0.11289399	98.25
0.1	157683.6	20028.585	64.76	1.676	0.04713003	109.26
1	4964.2	914.8182	2.04	1.395	0.07127358	90.98



### In Vitro Antiviral Results For Sofosbuvir

Assay: Zika Cytoprotection (XTT)

Sponsor: Emory University

Concentration  
Sofosbuvir (µM)  
0.0001  
0.001  
0.01  
0.1  
1  
10

Media Control				Plastic Control			
Toxicity Drug 1	Cell Control	Low		Toxicity Drug 2	Low		Toxicity Drug 2
	Virus Control	Drug 1			Drug 2		
High				High			
Color Control Drug 1 (High to Low)				Color Control Drug 2 (High to Low)			

Raw Data: Sofosbuvir (µM)

0.400	0.340	0.329	0.325	0.331	0.371	0.057	0.067	0.060	0.064	0.061	0.043
1.343	1.459	0.475	0.449	0.405	1.767					1.785	
1.706	1.387	0.360	0.335	0.567	1.704					1.604	
1.635	1.307	0.409	0.358	0.480	1.293					1.138	
1.653	0.494	0.533	0.334	0.421	1.771					0.364	
1.522	0.356	0.463	0.539	0.355	1.942					0.362	
1.632	0.356	1.514	1.416	1.507	1.580					0.450	
0.366	0.315	0.299	0.299	0.296	0.327						

Virus: Zika  
Strain: PRVABC59  
Cells: HUH7

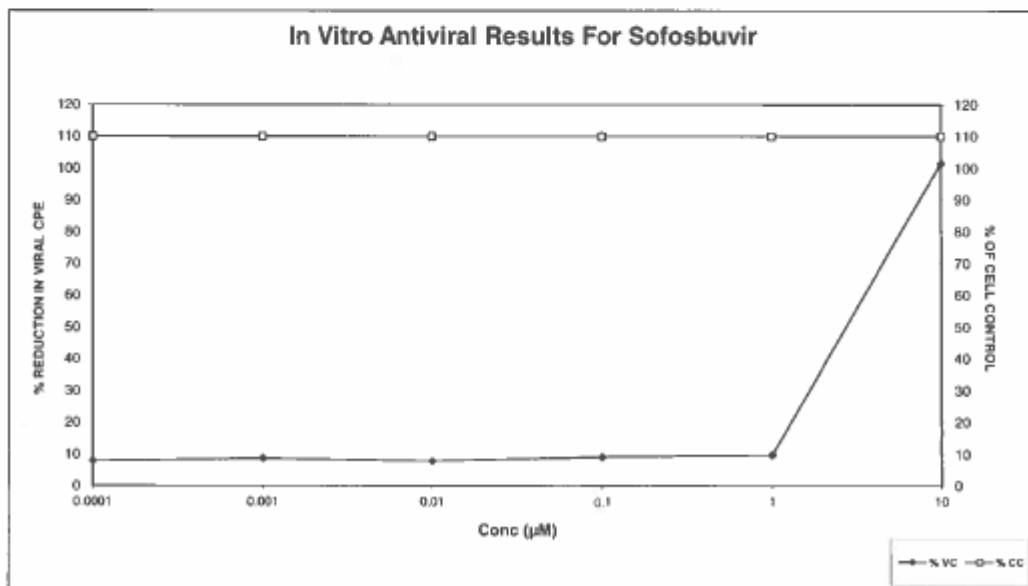
Test Date: 01/14/2022  
Date Read: 01/19/2022  
Operator: C. Buchholz

Sponsor: Emory University  
Principle Investigator: T. Hartman  
Project #: 277-03-18

Reagent: 0.349  
Virus Control: 0.033  
Cell Control: 1.097  
Differential: 1.065

Sofosbuvir	25%	50%	95%
TC (µM)	> 10	> 10	> 10
EC (µM)	1.46	2.74	8.49
Therapeutic Index (TI)	> 6.85	> 3.65	> 1.18

Sofosbuvir Conc (µM)	Antiviral Test Values		Cytotoxicity Test Values		Colorimetric Control
	Mean OD 450/650	% Red. In Viral CPE	Mean OD 450/650	% Cell Viability	
0.0001	0.084	7.85	1.228	110	-0.023
0.001	0.093	8.70	1.410	110	-0.054
0.01	0.084	7.85	1.216	110	-0.051
0.1	0.097	9.13	1.413	110	-0.050
1	0.104	9.80	1.416	110	-0.034
10	1.061	101.52	1.240	110	0.016



### ImQuest BioSciences: Anti-ZKV<sub>PRVABC59</sub> Cytoprotection Assay in HUH7 Cells

Compound	Efficacy 1	Efficacy 2	Efficacy 3	Mean	Reduction in Viral CPE	Tox 1	Tox 2	% CC
ZD-3-391	0.047	0.128	0.183	0.119333	6.14%	1.566	1.777	100.00%
ZD-3-466	0.05	0.091	0.096	0.079	2.34%	1.292	1.293	100.00%

### ImQuest BioSciences: Anti-DENV2<sub>New Guinea</sub> Cytoprotection Assay in Huh7 Cells

Compound	efficacy 1	efficacy 2	efficacy 3	Mean	% Reduction in Viral CPE	Mean Cytotoxicity	% CC
ZD-3-391	0.318	0.326	0.446	0.363	-6.67%	1.398	100%
ZD-3-466	0.372	0.679	0.560	0.537	11.82%	1.034	67.1%

## 3.4 REFERENCES AND NOTES

- Roy, V.; Agrofoglio, L. A., Nucleosides and emerging viruses: A new story. *Drug Discovery Today* **2022**.
- Yates, M. K.; Seley-Radtke, K. L., The evolution of antiviral nucleoside analogues: A review for chemists and non-chemists. Part II: Complex modifications to the nucleoside scaffold. *Antiviral Res.* **2019**, *162*, 5-21.
- Seley-Radtke, K. L.; Yates, M. K., The evolution of nucleoside analogue antivirals: A review for chemists and non-chemists. Part 1: Early structural modifications to the nucleoside scaffold. *Antiviral Res.* **2018**, *154*, 66-86.
- De Clercq, E.; Li, G., Approved Antiviral Drugs over the Past 50 Years. *Clin. Microbiol. Rev.* **2016**, *29* (3), 695-747.
- de Clercq, E., Milestones in the discovery of antiviral agents: nucleosides and nucleotides. *Acta Pharm. Sin. B* **2012**, *2* (6), 535-548.
- Liotta, D. C.; Painter, G. R., Discovery and Development of the Anti-Human Immunodeficiency Virus Drug, Emtricitabine (Emtriva, FTC). *Acc. Chem. Res.* **2016**, *49* (10), 2091-2098.
- Broder, S., The development of antiretroviral therapy and its impact on the HIV-1/AIDS pandemic. *Antiviral Res.* **2010**, *85* (1), 1-18.
- De Clercq, E., The design of drugs for HIV and HCV. *Nat. Rev. Drug Discov.* **2007**, *6* (12), 1001-18.
- Beigel, J. H.; Tomashek, K. M.; Dodd, L. E.; Mehta, A. K.; Zingman, B. S.; Kalil, A. C.; Hohmann, E.; Chu, H. Y.; Luetkemeyer, A.; Kline, S., Remdesivir for the treatment of Covid-19. *N. Engl. J. Med.* **2020**, *383* (19), 1813-1826.

10. Eastman, R. T.; Roth, J. S.; Brimacombe, K. R.; Simeonov, A.; Shen, M.; Patnaik, S.; Hall, M. D., Remdesivir: a review of its discovery and development leading to emergency use authorization for treatment of COVID-19. *ACS Cent. Sci.* **2020**, *6* (5), 672-683.
11. Williamson, B. N.; Feldmann, F.; Schwarz, B.; Meade-White, K.; Porter, D. P.; Schulz, J.; Van Doremalen, N.; Leighton, I.; Yinda, C. K.; Pérez-Pérez, L., Clinical benefit of remdesivir in rhesus macaques infected with SARS-CoV-2. *Nature* **2020**, *585* (7824), 273-276.
12. Fischer, W. A.; Eron, J. J.; Holman, W.; Cohen, M. S.; Fang, L.; Szewczyk, L. J.; Sheahan, T. P.; Baric, R.; Mollan, K. R.; Wolfe, C. R.; Duke, E. R.; Azizad, M. M.; Borroto-Esoda, K.; Wohl, D. A.; Coombs, R. W.; Loftis, A. J.; Alabanza, P.; Lipansky, F.; Painter, W. P., A phase 2a clinical trial of molnupiravir in patients with COVID-19 shows accelerated SARS-CoV-2 RNA clearance and elimination of infectious virus. *Sci. Transl. Med.* **2022**, *14* (628), eabl7430.
13. Jayk Bernal, A.; Gomes da Silva, M. M.; Musungaie, D. B.; Kovalchuk, E.; Gonzalez, A.; Delos Reyes, V.; Martín-Quirós, A.; Caraco, Y.; Williams-Diaz, A.; Brown, M. L., Molnupiravir for oral treatment of Covid-19 in nonhospitalized patients. *N. Engl. J. Med.* **2022**, *386* (6), 509-520.
14. Whitley, R., Molnupiravir—a step toward orally bioavailable therapies for Covid-19. *N. Engl. J. Med.* **2022**, *386* (6), 592-593.
15. Painter, G. R.; Natchus, M. G.; Cohen, O.; Holman, W.; Painter, W. P., Developing a direct acting, orally available antiviral agent in a pandemic: the evolution of molnupiravir as a potential treatment for COVID-19. *Curr. Opin. Virol.* **2021**, *50*, 17-22.
16. Sofia, M. J.; Bao, D.; Chang, W.; Du, J. F.; Nagarathnam, D.; Rachakonda, S.; Reddy, P. G.; Ross, B. S.; Wang, P. Y.; Zhang, H. R.; Bansal, S.; Espiritu, C.; Keilman, M.; Lam, A. M.; Steuer, H. M. M.; Niu, C. R.; Otto, M. J.; Furman, P. A., Discovery of a beta-D-2'-Deoxy-2'-alpha-fluoro-2'-beta-C-methyluridine Nucleotide Prodrug (PSI-7977) for the Treatment of Hepatitis C Virus. *J. Med. Chem.* **2010**, *53* (19), 7202-7218.
17. Sofia, M. J., Beyond sofosbuvir: What opportunity exists for a better nucleoside/nucleotide to treat hepatitis C? *Antiviral Res.* **2014**, *107*, 119-124.
18. Fung, A.; Jin, Z. N.; Dyatkina, N.; Wang, G. Y.; Beigelman, L.; Deval, J., Efficiency of Incorporation and Chain Termination Determines the Inhibition Potency of 2'-Modified Nucleotide Analogs against Hepatitis C Virus Polymerase. *Antimicrob. Agents Chemother.* **2014**, *58* (7), 3636-3645.
19. Zhang, N.; Zhang, S.; Szostak, J. W., Activated ribonucleotides undergo a sugar pucker switch upon binding to a single-stranded RNA template. *J. Am. Chem. Soc.* **2012**, *134* (8), 3691-3694.
20. Kim, S. C.; Zhou, L.; Zhang, W.; O'Flaherty, D. K.; Rondo-Brovetto, V.; Szostak, J. W., A model for the emergence of RNA from a prebiotically plausible mixture of ribonucleotides, arabinonucleotides, and 2'-deoxynucleotides. *J. Am. Chem. Soc.* **2020**, *142* (5), 2317-2326.
21. Guschlbauer, W.; Jankowski, K., Nucleoside conformation is determined by the electronegativity of the sugar substituent. *Nucleic Acids Res.* **1980**, *8* (6), 1421-1433.
22. Plavec, J.; Tong, W.; Chattopadhyaya, J., How do the gauche and anomeric effects drive the pseudorotational equilibrium of the pentofuranose moiety of nucleosides? *J. Am. Chem. Soc.* **1993**, *115* (21), 9734-9746.

23. Prakash, T. P., An overview of sugar-modified oligonucleotides for antisense therapeutics. *Chem. Biodiversity* **2011**, *8* (9), 1616-1641.
24. Dentmon, Z. W.; Kaiser, T. M.; Liotta, D. C., Synthesis and Antiviral Activity of a Series of 2'-C-Methyl-4'-thionucleoside Monophosphate Prodrugs. *Molecules* **2020**, *25* (21), 5165.
25. Guinan, M.; Huang, N.; Smith, M.; Miller, G. J., Design, chemical synthesis and antiviral evaluation of 2'-deoxy-2'-fluoro-2'-C-methyl-4'-thionucleosides. *Bioorg. Med. Chem. Lett.* **2022**, *61*, 128605.
26. Manchoju, A.; Zelli, R.; Wang, G.; Eymard, C.; Oo, A.; Nemer, M.; Prévost, M.; Kim, B.; Guindon, Y., Nucleotide Analogues Bearing a C2' or C3'-Stereogenic All-Carbon Quaternary Center as SARS-CoV-2 RdRp Inhibitors. *Molecules* **2022**, *27* (2), 564.
27. Wang, G.; Dyatkina, N.; Prhavc, M.; Williams, C.; Serebryany, V.; Hu, Y.; Huang, Y.; Wu, X.; Chen, T.; Huang, W.; Rajwanshi, V. K.; Deval, J.; Fung, A.; Jin, Z.; Stoycheva, A.; Shaw, K.; Gupta, K.; Tam, Y.; Jekle, A.; Smith, D. B.; Beigelman, L., Synthesis and Anti-HCV Activity of Sugar-Modified Guanosine Analogues: Discovery of AL-611 as an HCV NS5B Polymerase Inhibitor for the Treatment of Chronic Hepatitis C. *J. Med. Chem.* **2020**, *63* (18), 10380-10395.
28. Martínez-Montero, S.; Deleavey, G. F.; Kulkarni, A.; Martín-Pintado, N.; Lindovska, P.; Thomson, M.; González, C.; Götte, M.; Damha, M. J., Rigid 2',4'-Difluororibonucleosides: Synthesis, Conformational Analysis, and Incorporation into Nascent RNA by HCV Polymerase. *J. Org. Chem.* **2014**, *79* (12), 5627-5635.
29. Marquez, V. E.; Siddiqui, M. A.; Ezzitouni, A.; Russ, P.; Wang, J.; Wagner, R. W.; Matteucci, M. D., Nucleosides with a Twist. Can Fixed Forms of Sugar Ring Pucker Influence Biological Activity in Nucleosides and Oligonucleotides? *J. Med. Chem.* **1996**, *39* (19), 3739-3747.
30. Appleby, T. C.; Perry, J. K.; Murakami, E.; Barauskas, O.; Feng, J.; Cho, A.; Fox III, D.; Wetmore, D. R.; McGrath, M. E.; Ray, A. S., Structural basis for RNA replication by the hepatitis C virus polymerase. *Science* **2015**, *347* (6223), 771-775.
31. Altona, C.; Sundaralingam, M., Conformational analysis of the sugar ring in nucleosides and nucleotides. New description using the concept of pseudorotation. *J. Am. Chem. Soc.* **1972**, *94* (23), 8205-8212.
32. Olson, W. K.; Sussman, J. L., How flexible is the furanose ring? 1. A comparison of experimental and theoretical studies. *J. Am. Chem. Soc.* **1982**, *104* (1), 270-278.
33. Murakami, E.; Bao, H. Y.; Ramesh, M.; McBrayer, T. R.; Whitaker, T.; Steuer, H. M. M.; Schinazi, R. F.; Stuyver, L. J.; Obikhod, A.; Otto, M. J.; Furman, P. A., Mechanism of activation of beta-D-2'-deoxy-2'-fluoro-2'-C-methylcytidine and inhibition of hepatitis C virus NS5B RNA polymerase. *Antimicrob. Agents Chemother.* **2007**, *51* (2), 503-509.
34. Murakami, E.; Niu, C. R.; Bao, H. Y.; Steuer, H. M. M.; Whitaker, T.; Nachman, T.; Sofia, M. A.; Wang, P. Y.; Otto, M. J.; Furman, P. A., The mechanism of action of beta-D-2'-Deoxy-2'-fluoro-2'-C-methylcytidine involves a second metabolic pathway leading to beta-D-2'-deoxy-2'-fluoro-2'-C-methyluridine 5'-triphosphate, a potent inhibitor of the hepatitis C virus RNA-dependent RNA polymerase. *Antimicrob. Agents Chemother.* **2008**, *52* (2), 458-464.
35. Vorbrüggen, H.; Höfle, G., Nucleoside Syntheses, XXIII(1) On the Mechanism of Nucleoside Synthesis. *Chem. Ber.* **1981**, *114* (4), 1256-1268.

36. Vorbrüggen, H.; Ruh-Pohlentz, C., Synthesis Of Nucleosides. In *Organic Reactions*, Wiley Online Library: 2004; pp 1-630.

37. Jung, P. M.; Burger, A.; Biellmann, J.-F., Rapid and efficient stereocontrolled synthesis of C-3'-ethynyl ribo and xylonucleosides by organocerium additions to 3'-ketonucleosides. *Tetrahedron Lett.* **1995**, *36* (7), 1031-1034.

38. Jung, P. M.; Burger, A.; Biellmann, J.-F., Diastereofacial Selective Addition of Ethynylcerium Reagent and Barton– McCombie Reaction as the Key Steps for the Synthesis of C-3 '-Ethynylribonucleosides and of C-3 '-Ethynyl-2 '-deoxyribonucleosides. *J. Org. Chem.* **1997**, *62* (24), 8309-8314.

39. Ludwig, P. S.; Schwendener, R. A.; Schott, H., A new laboratory scale synthesis for the anticancer drug 3'-C-ethynylcytidine. *Synthesis* **2002**, *2002* (16), 2387-2392.

40. Robins, M. J.; Samano, V.; Johnson, M. D., Nucleic acid-related compounds. 58. Periodinane oxidation, selective primary deprotection, and remarkably stereoselective reduction of tert-butyl dimethylsilyl-protected ribonucleosides. Synthesis of 9-(. beta.-D-xylofuranosyl) adenine or 3'-deuterioadenosine from adenosine. *J. Org. Chem.* **1990**, *55* (2), 410-412.

41. Wutz, P. G. M.; Greene, T. W., Protection for the Hydroxyl Group, Including 1,2- and 1,3-Diols. In *Greene's Protective Groups in Organic Synthesis*, John Wiley & Sons, Inc.: 2007; pp 16-366.

42. Arterburn, J., Selective Oxidation of Secondary Alcohols. *Tetrahedron Lett.* **2001**.

43. Hayashi, M.; Shibuya, M.; Iwabuchi, Y., Oxidation of alcohols to carbonyl compounds with diisopropyl azodicarboxylate catalyzed by nitroxyl radicals. *J. Org. Chem.* **2012**, *77* (6), 3005-3009.

44. Lauber, M. B.; Stahl, S. S., Efficient aerobic oxidation of secondary alcohols at ambient temperature with an ABNO/NO<sub>x</sub> catalyst system. *ACS Catal.* **2013**, *3* (11), 2612-2616.

45. Steves, J. E.; Stahl, S. S., Copper (I)/ABNO-catalyzed aerobic alcohol oxidation: alleviating steric and electronic constraints of Cu/TEMPO catalyst systems. *J. Am. Chem. Soc.* **2013**, *135* (42), 15742-15745.

46. Reese, C. B.; Pei-Zhuo, Z., Phosphotriester approach to the synthesis of oligonucleotides: a reappraisal. *J. Chem. Soc., Perkin Trans. 1* **1993**, (19), 2291-2301.

47. Kicsák, M.; Mándi, A.; Varga, S.; Herczeg, M.; Batta, G.; Bényei, A.; Borbás, A.; Herczegh, P., Tricyclanos: conformationally constrained nucleoside analogues with a new heterocycle obtained from ad-ribofuranose unit. *Org. Biomol. Chem.* **2018**, *16* (3), 393-401.

48. Gadakh, B. K.; Patil, P. R.; Malik, S.; Kartha, K. P. R., Novel selectivity in carbohydrate reactions, IV: DABCO-mediated regioselective primary hydroxyl protection of carbohydrates. *Synth. Commun.* **2009**, *39* (13), 2430-2438.

49. Mendenhall, G. D.; Ingold, K. U., Reactions of bicyclic nitroxides involving reduction of the nitrosyl group. *J. Am. Chem. Soc.* **1973**, *95* (19), 6395-6400.

50. Shibuya, M.; Tomizawa, M.; Sasano, Y.; Iwabuchi, Y., An Expedient Entry to 9-Azabicyclo[3.3.1]nonane N-Oxyl (ABNO): Another Highly Active Organocatalyst for Oxidation of Alcohols. *J. Org. Chem.* **2009**, *74* (12), 4619-4622.

51. Ryland, B. L.; Stahl, S. S., Practical Aerobic Oxidations of Alcohols and Amines with Homogeneous Copper/TEMPO and Related Catalyst Systems. *Angew. Chem., Int. Ed.* **2014**, *53* (34), 8824-8838.

52. Corey, E. J.; Cho, H.; Rücker, C.; Hua, D. H., Studies with trialkylsilyltriflates: new syntheses and applications. *Tetrahedron Lett.* **1981**, *22* (36), 3455-3458.

53. Heathcock, C. H.; Young, S. D.; Hagen, J. P.; Pilli, R.; Badertscher, U., Acyclic stereoselection. 25. Stereoselective synthesis of the C-1 to C-7 moiety of erythronolide A. *J. Org. Chem.* **1985**, *50* (12), 2095-2105.

54. Shimizu, M.; Miyamoto, Y.; Kobayashi, E.; Shimazaki, M.; Yamamoto, K.; Reischl, W.; Yamada, S., Synthesis and biological activities of new 1 $\alpha$ , 25-dihydroxy-19-norvitamin D3 analogs with modifications in both the A-ring and the side chain. *Bioorg. Med. Chem.* **2006**, *14* (12), 4277-4294.

55. Sabitha, G.; Reddy, E. V.; Swapna, R.; Reddy, N. M.; Yadav, J. S., Bismuth (III) chloride catalyzed efficient and selective cleavage of trityl ethers. *Synlett* **2004**, *2004* (07), 1276-1278.

56. Wu, B.; Zhang, W.; Li, Z.; Gu, L.; Wang, X.; Wang, P. G., Concise Synthesis of 5-Methoxy-6-hydroxy-2-methylchromone-7-O- and 5-Hydroxy-2-methylchromone-7-O-rutinosides. Investigation of Their Cytotoxic Activities against Several Human Tumor Cell Lines. *J. Org. Chem.* **2011**, *76* (7), 2265-2268.

57. Imamoto, T.; Kusumoto, T.; Tawarayama, Y.; Sugiura, Y.; Mita, T.; Hatanaka, Y.; Yokoyama, M., Carbon-carbon bond-forming reactions using cerium metal or organocerium (III) reagents. *J. Org. Chem.* **1984**, *49* (21), 3904-3912.

58. Imamoto, T.; Takiyama, N.; Nakamura, K., Cerium chloride-promoted nucleophilic addition of grignard reagents to ketones an efficient method for the synthesis of tertiary alcohols. *Tetrahedron Lett.* **1985**, *26* (39), 4763-4766.

59. Imamoto, T.; Takiyama, N.; Nakamura, K.; Hatajima, T.; Kamiya, Y., Reactions of carbonyl compounds with Grignard reagents in the presence of cerium chloride. *J. Am. Chem. Soc.* **1989**, *111* (12), 4392-4398.

60. Cahard, D.; McGuigan, C.; Balzarini, J., Aryloxy Phosphoramidate Triesters as Pro-Tides. *Mini-Rev. Med. Chem.* **2004**, *4* (4), 371-381.

61. Mehellou, Y.; Balzarini, J.; McGuigan, C., Aryloxy Phosphoramidate Triesters: a Technology for Delivering Monophosphorylated Nucleosides and Sugars into Cells. *ChemMedChem* **2009**, *4* (11), 1779-1791.

62. Golitsina, N. L.; Danehy, F. T.; Fellows, R.; Cretton-Scott, E.; Standring, D. N., Evaluation of the role of three candidate human kinases in the conversion of the hepatitis C virus inhibitor 2'-C-methyl-cytidine to its 5'-monophosphate metabolite. *Antiviral Res.* **2010**, *85* (3), 470-481.

63. Furman, P. A.; Murakami, E.; Bao, H.; Symons, J.; Otto, M. J., Inhibition of HCV replication by PSI-6130: Mechanism of biochemical activation and inhibition. *J. Hepatol.* **2007**, *46*, S224-S224.

64. Ross, B. S.; Reddy, P. G.; Zhang, H. R.; Rachakonda, S.; Sofia, M. J., Synthesis of diastereomerically pure nucleotide phosphoramidates. *J. Org. Chem.* **2011**, *76* (20), 8311-8319.

65. We note that since  $MgI_2$  is insoluble in THF, the active methylating agent is likely  $Me_2Mg$  as a result of the Schlenk equilibrium. See Parris and Ashby, *J. Am. Chem. Soc.* **1971**, *93*, 1206.
66. Hugelshofer, C. L.; Palani, V.; Sarpong, R., Calyciphylline B-Type Alkaloids: Total Syntheses of (-)-Daphlongamine H and (-)-Isodaphlongamine H. *J. Am. Chem. Soc.* **2019**, *141* (21), 8431-8435.
67. Krasovskiy, A.; Kopp, F.; Knochel, P., Soluble Lanthanide Salts ( $LnCl_3 \cdot 2 LiCl$ ) for the Improved Addition of Organomagnesium Reagents to Carbonyl Compounds. *Angew. Chem., Int. Ed.* **2006**, *45* (3), 497-500.
68. Dimitrov, V.; Bratovanov, S.; Simova, S.; Kostova, K., Cerium(III) chloride as catalytic and stoichiometric promoter of the quantitative addition of organometallic reagents to (+)-camphor and (-)-fenchone. *Tetrahedron Lett.* **1994**, *35* (36), 6713-6716.
69. Dimitrov, V.; Kostova, K.; Genov, M., Anhydrous cerium(III) chloride — Effect of the drying process on activity and efficiency. *Tetrahedron Lett.* **1996**, *37* (37), 6787-6790.
70. Reetz, M. T.; Westermann, J.; Steinbach, R.; Wenderoth, B.; Peter, R.; Ostarek, R.; Maus, S., Chemoselective Addition of Organotitanium Reagents to Carbonyl-Compounds. *Chem Ber-Recl* **1985**, *118* (4), 1421-1440.
71. Reetz, M. T.; Kyung, S. H.; Hullmann, M.,  $CH_3Li/TiCl_4$  - a Non-Basic and Highly Selective Grignard Analog. *Tetrahedron* **1986**, *42* (11), 2931-2935.
72. Hatano, M.; Suzuki, S.; Ishihara, K., Highly Efficient Alkylation to Ketones and Aldimines with Grignard Reagents Catalyzed by Zinc(II) Chloride. *J. Am. Chem. Soc.* **2006**, *128* (31), 9998-9999.
73. Solomon, M.; Jamison, W. C. L.; McCormick, M.; Liotta, D.; Cherry, D. A.; Mills, J. E.; Shah, R. D.; Rodgers, J. D.; Maryanoff, C. A., Ligand-assisted nucleophilic additions. Control of site and face attack of nucleophiles on 4-oxido enones. *J. Am. Chem. Soc.* **1988**, *110* (11), 3702-3704.
74. Swiss, K. A.; Liotta, D. C.; Maryanoff, C. A., Mechanistic aspects of the ligand-assisted nucleophilic addition reaction. *J. Am. Chem. Soc.* **1990**, *112* (25), 9393-9394.
75. Lohmann, V.; Korner, F.; Koch, J. O.; Herian, U.; Theilmann, L.; Bartenschlager, R., Replication of subgenomic hepatitis C virus RNAs in a hepatoma cell line. *Science* **1999**, *285* (5424), 110-113.
76. Krieger, N.; Lohmann, V.; Bartenschlager, R., Enhancement of hepatitis C virus RNA replication by cell culture-adaptive mutations. *J. Virol.* **2001**, *75* (10), 4614-4624.
77. Bartenschlager, R., Hepatitis C virus molecular clones: from cDNA to infectious virus particles in cell culture. *Curr. Opin. Microbiol.* **2006**, *9* (4), 416-22.
78. Dasari, M.; Ma, P.; Pelly, S. C.; Sharma, S. K.; Liotta, D. C., Synthesis and biological evaluation of 5'-C-methyl nucleotide prodrugs for treating HCV infections. *Bioorg. Med. Chem. Lett.* **2020**, *30* (23), 127539.
79. Marquez, V. E.; Ben-Kasus, T.; Barchi, J. J.; Green, K. M.; Nicklaus, M. C.; Agbaria, R., Experimental and Structural Evidence that Herpes 1 Kinase and Cellular DNA Polymerase(s) Discriminate on the Basis of Sugar Pucker. *J. Am. Chem. Soc.* **2004**, *126* (2), 543-549.

80. Marquez, V. E.; Ezzitouni, A.; Russ, P.; Siddiqui, M. A.; Ford, H.; Feldman, R. J.; Mitsuya, H.; George, C.; Barchi, J. J., HIV-1 Reverse Transcriptase Can Discriminate between Two Conformationally Locked Carbocyclic AZT Triphosphate Analogues. *J. Am. Chem. Soc.* **1998**, *120* (12), 2780-2789.

81. Heinz, B. A.; Vance, L. M., The antiviral compound enviroxime targets the 3A coding region of rhinovirus and poliovirus. *J Virol* **1995**, *69* (7), 4189-97.

82. Seritan, S.; Bannwarth, C.; Fales, B. S.; Hohenstein, E. G.; Isborn, C. M.; Kokkila-Schumacher, S. I. L.; Li, X.; Liu, F.; Luehr, N.; Snyder Jr, J. W.; Song, C.; Titov, A. V.; Ufimtsev, I. S.; Wang, L.-P.; Martínez, T. J., TeraChem: A graphical processing unit-accelerated electronic structure package for large-scale ab initio molecular dynamics. *WIREs Computational Molecular Science* **2021**, *11* (2), e1494.

83. Barone, V.; Cossi, M., Quantum calculation of molecular energies and energy gradients in solution by a conductor solvent model. *J Phys Chem A* **1998**, *102* (11), 1995-2001.

84. Malmberg, C. G.; Maryott, A. A. J. J. o. r. o. t. N. B. o. S., Dielectric constant of water from 0 to 100 C. **1956**, *56*, 1.

85. Brown, R. A.; Case, D. A., Second derivatives in generalized Born theory. *Journal of Computational Chemistry* **2006**, *27* (14), 1662-1675.

86. Macke, T.; Svrcek-Seiler, W.; Case, D. A., Nucleic Acid Builder Users' Manual. 2004.

87. Li, N.-S.; Piccirilli, J. A., Synthesis of the Phosphoramidite Derivative of 2'-Deoxy-2'-C- $\beta$ -methylcytidine. *J. Org. Chem.* **2003**, *68* (17), 6799-6802.

Part II

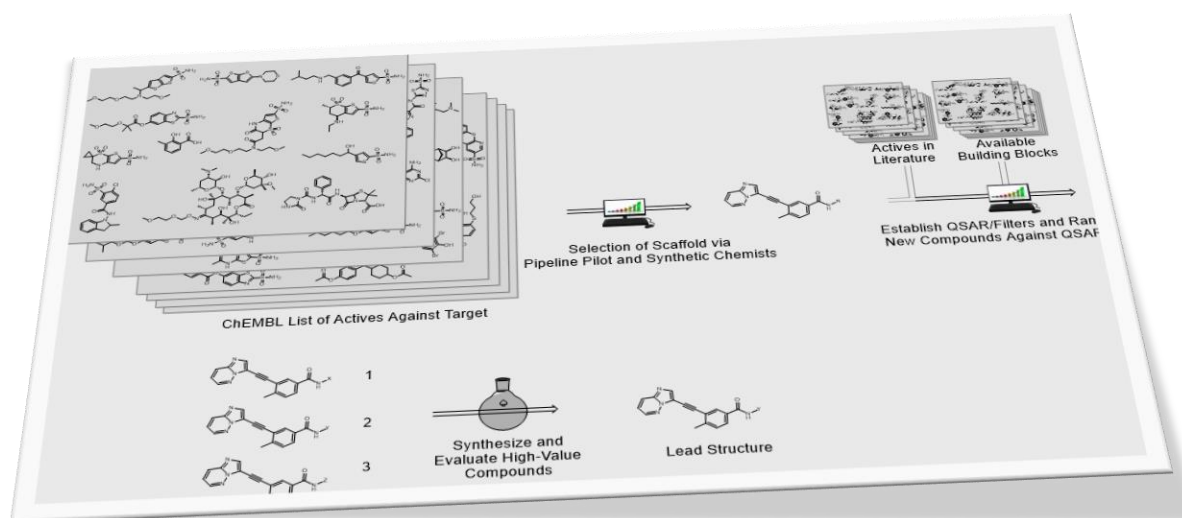
Studies on the  
Machine Learning Algorithm-Enhanced  
Hit-to-Lead Optimization of  
Drug-Like Small Molecules

---

## Chapter 4. The Discovery & Development of FRESH: An Algorithm for Small Molecule Hit-to-Lead Optimization

Portions of this chapter are reproduced or adapted with permission from (Qi Shi, Thomas M. Kaiser, Zackery W. Dentmon, Mariangela Ceruso, Daniela Vullo, Claudiu T. Supuran, and James P. Snyder, Design and Validation of FRESH, a Drug Discovery Paradigm Resting on Robust Chemical Synthesis, *ACS Med. Chem. Lett.*, **2015**, 6, 518-522. DOI: 10.1021/acsmedchemlett.5b00062). Copyright © 2015 American Chemical Society,

Or under the terms and conditions of the Creative Commons Attribution (CC BY) 4.0 license (<http://creativecommons.org/licenses/by/4.0/>) from (Thomas M. Kaiser, Zackery W. Dentmon, Pieter B. Burger, Qi Shi, James P. Snyder, Yuhong Du, Haian Fu, and Dennis C. Liotta, Prospective evaluation and success of a machine learning hit-to-lead drug development program against phosphatidylinositol 3-kinase  $\alpha$ , *ARKIVOC*, **2020**, 3, 25-43, <https://doi.org/10.24820/ark.5550190.p011.304>). Copyright © 2020 by the authors



### 4.1 INTRODUCTION

In Part I of this dissertation, the synthesis of novel nucleosides (and their monophosphate prodrugs) was disclosed, motivated by dual intentions. The primary motivation behind these chapters could certainly be considered basic science – to further a molecular understanding of the features which contribute to the mechanism of action of orthosteric, non-obligate chain terminating polymerase inhibitors. However, we deliberately selected target molecules which comprised novel

intellectual property (IP) and which had a therapeutically relevant disease target (in this case, hepatitis C). Hence, the secondary goal of the research was to contribute to the applied field of translational antiviral drug discovery. Were our efforts particularly successful, the technology could eventually find its way onto the prescribing pads of physicians and into the hands of sick patients.

However, the journey of a new chemical entity from benchtop to bedside is long, expensive, and arduous with a high rate of attrition. Ultimately, the synthesis of only 16 drug-like testable entities over the course of 7 years was described in Part I. This highlights one perhaps extreme example of the considerable cost of resources involved in creating new drug-like lead candidates,<sup>1</sup> and with such poor potency these compounds could not convincingly be described as “hit molecules,” much less lead candidates. Had these compounds been hits they would have moved on to the next step of a preclinical medicinal chemistry and drug discovery campaign anecdotally referred to as “hit-to-lead optimization.”<sup>2</sup> This process examines and enhances a host of other chemical characteristics beyond mere molecular target engagement and potency, such as properties related to undesired on- and off-target toxicity, favorable pharmacokinetics (*i.e.*, how a biological system acts on the drug, including absorption, distribution, metabolism, and elimination, or ADME), and the necessary *in vivo* pharmacodynamics (*i.e.*, how the drug acts on the biological system) to make a medicine that provides safe and efficacious clinical outcomes for patients.

#### 4.1.1 The Design of the FRESH Algorithm

A successful medicinal chemistry program, then, requires the balancing of target and pharmacological properties, IP issues, and synthetic considerations. As highlighted above, achieving this balance can consume considerable time and labor costs.<sup>1</sup> To help address this problem, researchers in our lab created a computational workflow termed “FRESH” (FRagment-based Exploitation of modular Synthesis by vHTS). FRESH was designed to prioritize potential synthetic targets during the drug lead-optimization stage with the aim of increasing efficiency in the hit-to-lead process. After a hit has been identified in a general drug discovery program, medicinal chemistry is

undertaken to develop a structure-activity relationship (SAR) around the hit structure. FRESH takes advantage of the often hundreds of compounds and their biological data obtained from that SAR to suggest new structures for further development.

FRESH was constructed primarily on the cheminformatics platform Pipeline Pilot (PLP, BIOVIA, Dassault).<sup>3</sup> PLP performs the task of enumerating an initial virtual compound library based on a core structure with user-marked attachment points for compound variability (R groups). Application of the FRESH workflow within PLP consists of four major steps. Since potency is frequently a primary selection criterion, the program is first complemented with one or more predictive quantitative structure-activity relationship (QSAR) expressions established from existing data. The QSAR input or training set is generally derived from published data deposited in external libraries such as ChEMBL<sup>4</sup> or BindingDB.<sup>5</sup> Furthermore, previously tested in-house compounds can also be added as additional data points. Various receptor or ligand-based methods, such as docking, MM-GBSA, and Extended Connectivity Fingerprints (ECFP)-Bayesian,<sup>6</sup> which estimate the interaction energies between small molecules and proteins may be used when available for evaluating binding affinity. The QSARs generated in this step are applied by FRESH for subsequent potency probability estimates for novel structures (see below). Since there is no universally applicable QSAR method, we have used at least two independent QSAR evaluations in order to increase the stringency and lessen the molecular case dependency of the QSAR filter.<sup>7</sup>

A virtual molecule library is constructed during the second step. As stated previously, this step is strictly based on established synthetic schemes and can be regarded as an *in silico* synthesis, mirroring a wet-lab synthesis. The variation of the R groups to be explored is derived from the various corresponding “building block” structures in a virtual compound library. The source for the building block may be a commercial electronic database, like Zinc, Maybridge, etc., or a laboratory’s proprietary inventory. Thus, the building block structures assembled at this step are considered to be readily available and reliably appended to the core structure. Fragments with potential liability,

stability and reactivity concerns are removed, as are building blocks violating the fragment rule of three.<sup>8</sup> This strategy of varying one site of the core structure works well because, in many cases, a large portion of the hit structure (*i.e.*, the pharmacophore) is conserved during hit-to-lead optimization.<sup>9</sup>

As stated previously, favorable physical/ADMET properties are crucial components of a successful drug discovery campaign, so in the third step the molecule library is filtered using widely accepted rules, such as Lipinski's Rule of Five<sup>10</sup> and Jorgensen's Rule of Three,<sup>11</sup> and ADME parameters from Schrödinger's QikProp package.<sup>12</sup> The previously established QSAR model is also applied in this step to prioritize molecules which are likely to have improved potency. Unlike many traditional QSAR studies, the cases presented below first use Bayesian statistics to construct a classification QSAR using a leave-one-out cross-validation in Pipeline Pilot v7.0.<sup>3</sup> Rather than giving a direct evaluation of the biological activity, as in the case with regression models which can be challenging and prone to failure, the Bayesian classifier method only gives a probability score corresponding to the likelihood of whether the compound in question meets a user-defined criterion (*e.g.*, on-target potency <100 nM).<sup>6,13</sup> Additionally, the Bayesian classifier has the additional property of being highly noise tolerant as compared to other machine learning methods.<sup>14</sup> Another advantage of using the Bayesian classifier applied in FRESH is that it uses two-dimensional (2D) ECFP rather than 3D methods, making it suitable for use on large data sets due to its rapid speed.<sup>15</sup> The Bayesian classifier is therefore applied ahead of more computationally expensive 3D methods like docking (Glide) and free energy of binding (Prime MM-GBSA) calculations in the task-stream of FRESH. Altogether, the Bayesian classifier is more applicable to FRESH early on in the program, as it fits exactly the purpose of prioritizing rather than precisely evaluating compounds in a timely fashion.

The fourth and final part of the FRESH protocol is the processing and merging of the calculated results. These aggregate results (docking, free energy of binding, and Bayesian classification) are then used to rank the compounds in descending order of probability to achieve the

user-defined criteria, such as on-target potency, before the final structures of interest are scrutinized by the medicinal chemistry team for synthetic tractability. Members of this final list of prioritized structures are regarded as highly attractive candidates for synthesis.

## 4.2 VALIDATION OF FRESH: RETROSPECTIVE CASE STUDIES

To validate the FRESH program, three retrospective case studies were performed by our computational team, with special acknowledgment to Dr. Qi Shi and his mentor and Ph.D. co-advisor the late Prof. James P. Snyder.<sup>16</sup> The purpose of these exercises was to demonstrate how FRESH can independently capture highly potent compounds from diverse projects reported in the literature. The three case study targets were chosen based on four main criteria: (1) the protein target should have validated therapeutic potential; (2) the biological target must have recent data generated within the past 15-20 years; (3) the core scaffold must have been modular and not a potent ligand itself ( $IC_{50} > 100$  nM); (4) the literature must have contained at least one highly potent molecule ( $IC_{50} < 10$  nM) that was not used in the QSAR model built by FRESH (*i.e.*, the training set). With these criteria, we expected the data to be sufficiently stringent for FRESH to work.

It is important to acknowledge that all QSAR methods, whether they are ligand-based or receptor-based, have limitations. A universal QSAR method that can accurately predict the potency of all the unknown compounds in a given project currently does not exist. Considering the shortcomings and limitations of QSAR methods, at least two independent QSAR evaluations are generally used in FRESH to select target compounds when data depth permits it (*vide supra*).

All three cases described below require the evaluation of potency. As described above, two receptor-based approaches, Glide docking and Prime MM-GBSA, were chosen as scoring functions for cases involving an explicit protein co-crystal structure. A third approach takes ECFP as the molecular portrait and Bayesian statistics (an estimate of probability based on the presence/absence of specific features from the binary data input) as the modeling method. One significant advantage of this 2D-based approach is the speed of calculation. The ECFP descriptor is particularly useful within FRESH

when probing a large chemical space. To maximize computational efficiency in the prioritization of candidate structures, QSAR selections based on ECFP are placed in the task-stream ahead of the more computationally expensive score generators like Glide or MM-GBSA.

#### 4.2.1 Phosphatidylinositol 3-Kinase (PI3K)

Phosphatidylinositol 3-kinase (PI3K) phosphorylates the 3-hydroxyl group of the inositol ring of phosphatidylinositol and converts phosphatidylinositol (3,4)-biphosphate (PIP<sub>2</sub>) to phosphatidylinositol (3,4,5)-triphosphate (PIP<sub>3</sub>). PI3K is a crucial component in a number of pathways, which regulates cell proliferation, survival, chemotaxis and differentiation.<sup>17-19</sup> Among all the isoforms, PI3K $\alpha$  is an interesting cancer therapeutic target. It has been recognized that up-regulation of the PI3K signaling pathway promotes angiogenesis and is associated with development of human cancers. In addition, the pathway has been implicated in conferring resistance to conventional therapies.<sup>20</sup> At the time of this study, there were no FDA approved anti-PI3K drugs available; in the time since, four have been approved with various isoform selectivity profiles — idelalisib (PI3K $\delta$ ), copanlisib (PI3K $\alpha/\delta$ ), duvelisib (PI3K $\gamma/\delta$ ), and alpelisib (PI3K $\alpha$ ).

The present PI3K-based case study originates from the 2011 report by Kim et al.<sup>21</sup> in which the R<sub>1</sub> extension of scaffold **4.1** in Figure 4.1 was examined. The initial hit compound (R<sub>1</sub> = H) is a 360 nM (IC<sub>50</sub>) agent that emerged from scaffold screening at a concentration of 10  $\mu$ M. Various aromatic substituents within the R<sub>1</sub> group modified by Suzuki coupling were tested.

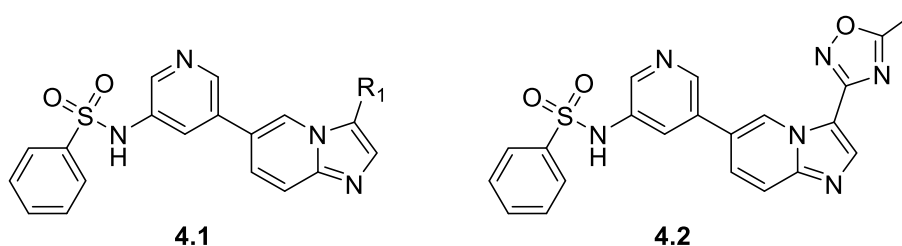


**Figure 4.1.** PI3K inhibitor scaffold **4.1** and analogue **4.2**.

The QSAR scoring functions for evaluating potency were established as described above in the description of FRESH. The performance of QSAR scores was evaluated by the area under the curve (AUC) of the receiver operating characteristic (ROC) curve, with an AUC close to 1 being good and an

AUC under 0.6 being unacceptable.<sup>22</sup> Among them, the Bayesian score has the highest AUC (0.93, Figure 4.2), followed by the MM-GBSA score (0.72, Figure 4.3) and the Glide score (0.64, Figure 4.4). Since all three QSAR scores performed acceptably, all three QSAR scores were implemented in FRESH for this case.

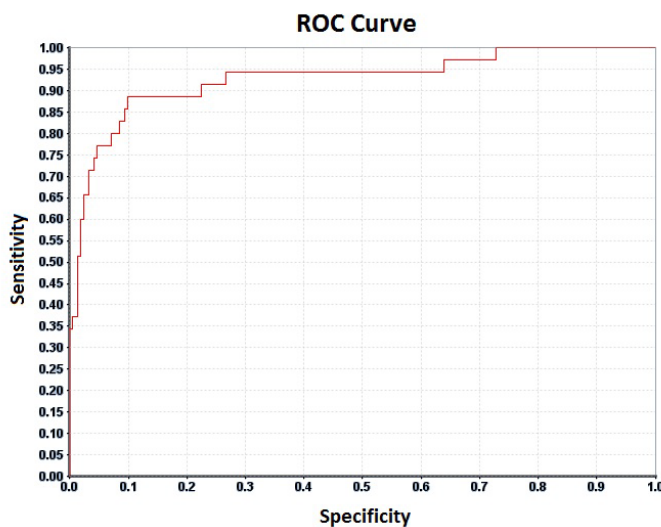


**Figure 4.2.** ROC curve for the ECFP method in Case 1 (PI3K). AUC = 0.93

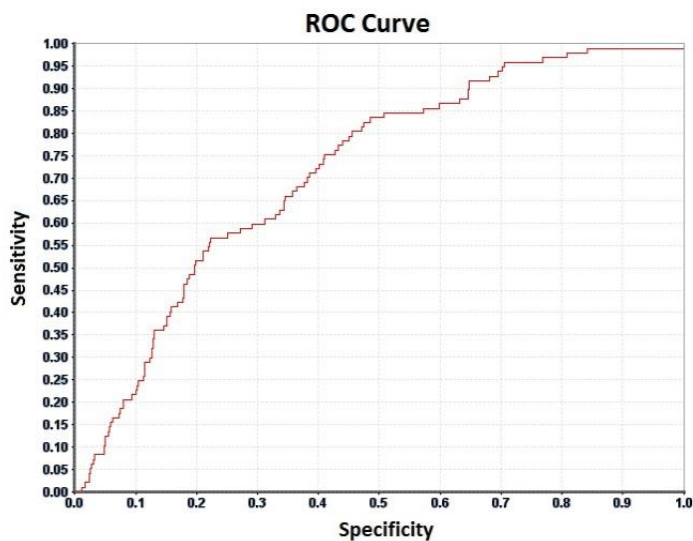


**Figure 4.3.** ROC curve for the MM-GBSA score in Case 1 (PI3K). AUC = 0.72

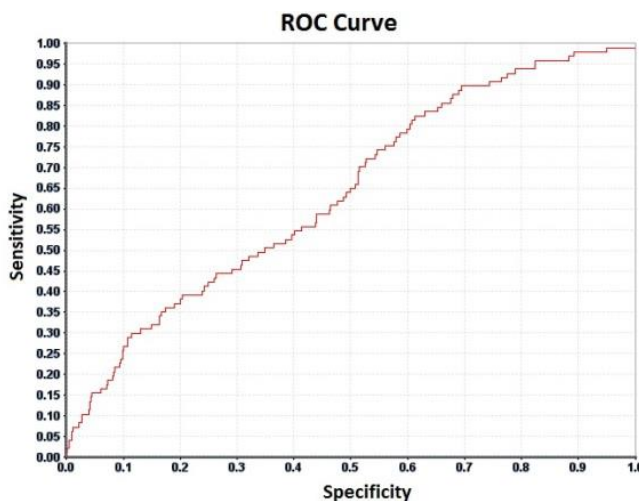


**Figure 4.4.** ROC curve for the Glide score method in Case 1 (PI3K). AUC = 0.64

According to the synthesis route, the aromatic  $R_1$  moiety is attached to the core structure by Suzuki coupling in which arylboronic acids (or bromides) are the building blocks. The corresponding fragments were obtained from the latter by querying the “Zinc bb now” database. The fragments were covalently linked to the core structure **4.1** in Figure 4.1 to generate structures of all possible PI3K $\alpha$  inhibitors in this subclass. Synthetic targets were then chosen as described above. Examination of the prioritized structure list revealed the third best structure with an  $R_1$  oxadiazole ring to be literature analogue **4.2** (Figure 4.1). With an  $IC_{50} = 2$  nM, the compound is a potent inhibitor for PI3K $\alpha$  and featured in the Table of Contents graphic of the original paper.<sup>21</sup> Thus, the method successfully captures a known potent molecule among the top five in the final FRESH list.

#### 4.2.2 Carbonic Anhydrase II (CA II)

Carbonic anhydrases (CAs) are ubiquitously expressed in all organisms. This family of enzymes catalyzes the reversible hydration of  $CO_2$  to bicarbonate and a proton. CAs are categorized as metalloenzymes since the catalytic center contains a functional zinc ion. Such proteins (including HDAC1 below) are generally regarded as difficult targets for virtual screening exercises. The enzymes are involved in many physiological processes, and their inhibitors have been explored clinically for various therapeutic purposes such as antiglaucoma, anticonvulsant, antiobesity, pain-relief and

antitumor activities. The physiologically dominant isoform, CA II, is one of the most extensively studied proteins among all known protein targets.<sup>23</sup>

The Supuran group at the University of Florence has reported CA inhibitors with the ureido-benzenesulfonamide scaffold **4.3** shown in Figure 4.5, an application of the popular sulfonamide moiety.<sup>24, 25</sup> The R<sub>2</sub> group contains at least one phenyl ring, and the corresponding synthetic building blocks for R<sub>2</sub> were isocyanates or acid chlorides.

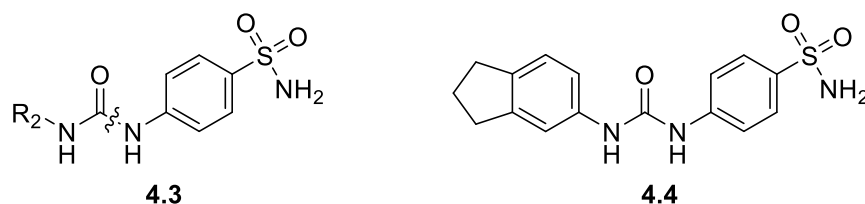


**Figure 4.5.** Supuran's CA II inhibitor scaffold **4.3** and analogue **4.4**.

Construction of a FRESH protocol is similar to the case study for PI3K $\alpha$  inhibitors. Since the CA II work involved two previous reports, the publication cutoff year for mining prospective inhibitor candidates in this case study was selected to be the earlier one (2010). The corresponding Bayesian model furnished an AUC of 0.88 for the ROC curve (Figure 4.6), indicating an excellent separation of actives and inactives. The AUC for Glide scores is 0.63 (Figure 4.7), which is acceptable. The MM-GBSA score failed to provide a separation of activity classes (AUC < 0.6, figure not shown) and was therefore excluded from the FRESH potency analysis.

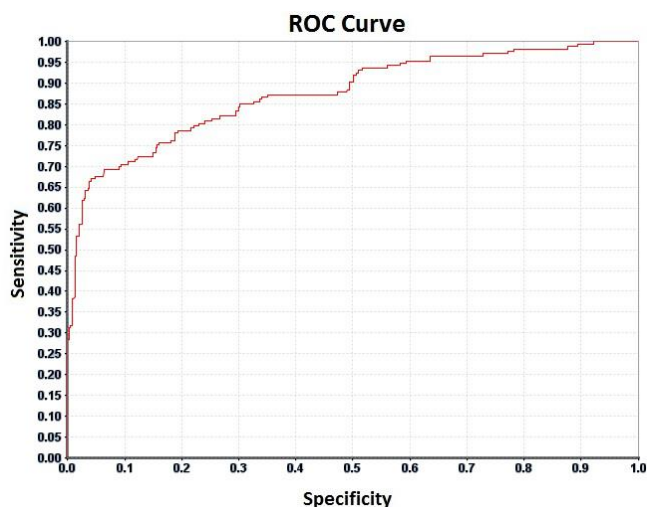


**Figure 4.6.** ROC curve for the ECFP method in Case 2 (CA II). AUC = 0.88

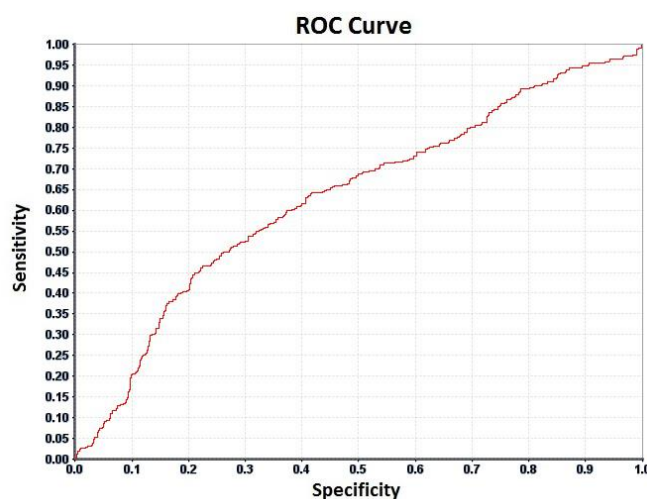


**Figure 4.7.** ROC curve for the Glide score in Case 2 (CA II). AUC = 0.63

The two CA II reported studies did not explicitly specify a starting compound suitable for use as a reference for FRESH QSAR scores. However, since the authors investigated mainly phenyl substitution effects on activity, the unsubstituted phenyl compound ( $R_2 = \text{Ph}$ ,  $K_i = 3.7 \mu\text{M}$ ) was selected as the reference standard. Application of the FRESH target selection scheme provided candidate targets with indane **4.4** ( $K_i = 8.9 \text{ nM}$ ,<sup>25</sup> Figure 4.5) ranked fourth in the final list. FRESH again successfully identified a potent CA II inhibitor along with several other previously unconsidered potential CA II blockers once the zinc dication was incorporated into the docking scheme (*vide infra*).

### 4.2.3. Histone Deacetylase (HDAC)

HDAC enzymes catalyze the removal of acetyl groups from acetylated lysine amino acids on histone proteins in the nucleosome. This allows histones to be more tightly wrapped around DNA and consequently regulates DNA expression. HDAC enzymes fall into four different classes. Among these, Class I and II isozymes have been associated with uncontrolled tumor growth.<sup>26</sup> An example knockdown study on HDACs performed by Glaser et al. suggested that HDAC1 is essential to the proliferation and survival of mammalian carcinoma cells.<sup>27</sup> In 2006, the FDA approved suberoylanilide hydroxamic acid (SAHA) for the treatment of cutaneous T-cell lymphoma which validated HDAC inhibitors as a strategy for cancer therapy.<sup>28</sup>

The present HDAC1 case study was based on a 2010 report by Wang et al.<sup>29</sup> wherein the authors explored the urea scaffold **4.5** shown in Figure 4.8. The right-hand part of the scaffold is a hydroxamic acid functionality designed to bind to the zinc dication within the catalytic pocket. The length of the aliphatic chain linker ( $n$ ) was varied, and the left-hand sector of the scaffold ( $R_3$ ) consisted of at least one aromatic ring. The corresponding building blocks for  $R_3$  were aryl acid chlorides.

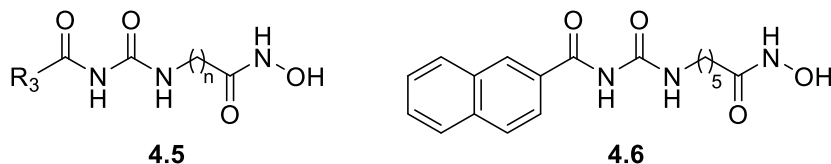


**Figure 4.8.** HDAC1 inhibitor scaffold **4.5** and the naphthalenyl analogue **4.6**

We elected to treat this case as a ligand-based example instead of an X-ray structure-based analysis to demonstrate the usefulness of FRESH under circumstances where only limited biostructural information is available.<sup>30</sup> In addition to manipulating  $R_3$  group information, the FRESH application was formulated to vary the linker length  $n$  from 1 to 7 simultaneously with variations in  $R_3$  to intentionally increase the complexity of potent inhibitor identification.

Construction of the FRESH protocol was similar to the previous two case studies on PI3K $\alpha$  and CA II. However, since only ligand-based methodology was allowed in this study, the Glide and MM-GBSA scores were not utilized. The Bayesian score with the ECFP descriptor<sup>6, 13, 15</sup> was the only SAR-type filter applied in this case, which provided an AUC of 0.87 (Figure 4.9). FRESH-searching delivered the naphthalene analogue **4.6** (Figure 4.8) among the top five hits. With an  $IC_{50} = 6$  nM, it was the most potent HDAC1 blocker yet reported at that time.<sup>29</sup> Consistent with its performance in the previous case studies, FRESH likewise pinpoints a highly potent inhibitor along with a novel set of potentially potent alternative structures.

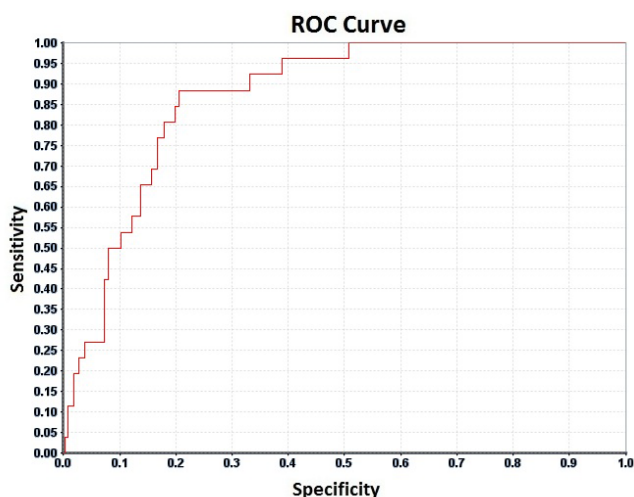


**Figure 4.9.** ROC curve for the ECFP method in Case 3 (HDAC1). AUC = 0.87

### 4.3 IMPLEMENTATION OF FRESH: PROSPECTIVE CASE STUDIES

In an effort to push beyond traditional limitations of virtual screening method evaluation,<sup>7</sup> we tested FRESH prospectively in cases that would mimic a lead optimization program. Our prospective studies were therefore designed to function in a “real world” setting where the most synthetically accessible compounds with the highest output ranking would be evaluated first. For each case study, we set a limit that each test set would have only five compounds synthesized from it; if synthetic difficulties were encountered with a given compound, we would move to the next attractive target on the list.

Our lab's effective implementation of FRESH across distinct biological targets and chemical space has resulted in several publications and patent applications. Summarily, our compelling campaigns against CA II and PI3K $\alpha$  are highlighted below to build on the foundation of this enabling technology described above. For a yet further prospective example, the reader is referred to our team's publication of a similarly successful story against the fusion protein of respiratory syncytial virus (RSV).<sup>31</sup> In this context, our algorithm correctly predicted 4-out-of-5 synthesized candidates to have <30 nM EC<sub>50</sub> values, on par with the clinical candidate from Bristol-Myers Squibb. Our best compound improved upon its potency by 3-fold while also increasing metabolic stability ( $t_{1/2}$ ) in human liver microsomes by more than 20-fold. Finally, the details of our efforts to design and synthesize inhibitors of the Abelson non-receptor tyrosine kinase (c-Abl) will be the focus of the remainder of Part II of this dissertation.

#### 4.3.1 Predicting Potent, Novel Inhibitors of CA II

To prove the utility of the FRESH methodology, we further explored the final list of predictions from the restospective CA II case study described above in §4.2.2. The purpose of the work was to determine if the FRESH algorithm was indeed capable of providing additional potent molecules that were not previously disclosed in the literature.

After verifying that chemical intermediates were commercially available, five compounds composed of inexpensive building blocks for R<sub>2</sub> were selected from the FRESH final list of approx. 40 structures and synthesized simply by reacting sulfanilamide with the requisite aryl isocyanate (R<sub>2</sub>-N=C=O, Figure 4.5) The compounds (>95% pure) were shipped to the Supuran group at the University of Florence and subjected to the same CA II potency assay they have previously described;<sup>23-25</sup> the data are shown in Table 4.1. The K<sub>i</sub> values for all five novel inhibitors (**4.7-4.11**) are less than 10 nM, with two entries less than 1 nM. The K<sub>i</sub> for the most potent **4.9** (0.3 nM) was the lowest among agents for this scaffold at the time of this study and seven times more potent than that previously reported (2.1 nM).<sup>24</sup> One additional point of interest is that sulfonamides are able to

establish a strong interaction by complexation with the metal cation. Nonetheless, as demonstrated herein, synthetic manipulation at eight to ten heavy atoms from the SO<sub>2</sub>N can lead to significant improvements in *K<sub>i</sub>*.

**Table 4.1.** Novel CA II inhibitors from Family 4.3 of Figure 4.5.

Compound ID	R <sub>2</sub> moiety	<i>K<sub>i</sub></i> (nM)
4.7		2.6
4.8		3.9
4.9		0.3
4.10		2.7
4.11		0.8

A point raised by a reviewer of our initial disclosure was that the SAR for the compounds reported in Table 4.1 is rather flat. The nanomolar *K<sub>i</sub>* values are necessarily flat since, in this FRESH validation, we have reported the synthesis and activities of only those compounds predicted to be most active. In a “real world” application of a hit-to-lead development tool like FRESH, there is little interest in expending resources to synthesize compounds which are predicted to be inactive. As verified by Table 4.1, the predictions were borne out. The CA II blockers selected correspond to those

with the best Bayesian QSAR scores and ADMET properties. The “flat SAR” actually indicates good performance of the QSAR selection scheme in FRESH for this case study. Importantly, these compounds were not present in the training sets used for QSAR establishment. Furthermore, the activity spread for the latter training set, hardly flat, runs from 0.2 nM to greater than 20  $\mu$ M, a range of more than 100,000-fold.

As demonstrated by all three retro-analyzed case studies, the FRESH workflow was able to independently provide a set of synthetic candidates containing at least one potent and previously reported compound. The ranks of each of these substances are among the top five candidates derived by FRESH. Further exploration of the CA II case revealed five additional potent CA II inhibitors from the treatment. Since both CA II and HDAC1 are metalloenzymes with a cationic catalytic center, one additional apparent asset of the method is the ability to handle such proteins so long as molecular manipulation is distal to metal binding. We concluded at this time that the FRESH methodology was indeed a useful algorithm for assisting drug lead optimization and set out to demonstrate its utility in other medicinal chemistry hit-to-lead projects of biologically and chemically distinct spaces. Further examples of its application, particularly as it pertains to subsequent iteration steps for individual cases, are described below.

### **4.3.2 Predicting Potent, Novel Inhibitors of PI3K $\alpha$**

#### ***4.3.2.1 Construction of the FRESH Algorithm***

As stated above, the PI3K family of enzymes are involved in a number of cell signaling pathways and serve as regulators of cell proliferation, survival, chemotaxis and differentiation.<sup>17</sup> Upregulation of PI3K $\alpha$  promotes angiogenesis and is associated with the development of solid tumors. Also, dysregulated PI3K $\alpha$  has been found in 30% of human solid tumors.<sup>20</sup> Additionally, since the pathway has been implicated in the development of resistance to conventional therapies, the use of PI3K inhibitors in combination with standard chemotherapies represents a potentially attractive strategy for treating a variety of intractable solid tumors. An excellent review of the progression of

PI3K inhibitors in clinical trials was written by Yang et al. in 2019.<sup>32</sup> As mentioned earlier, there are currently four anti-PI3K drugs which have received FDA approval (Figure 4.10).

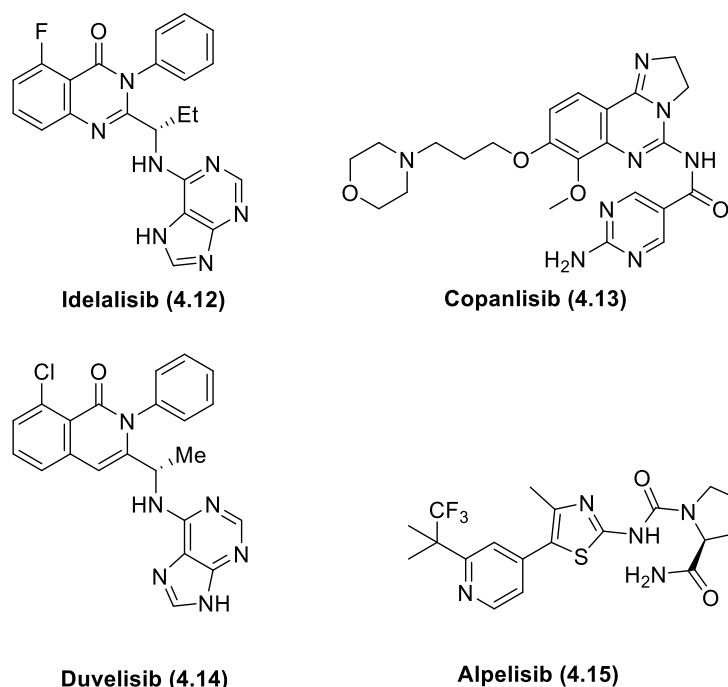


**Figure 4.10.** FDA-approved PI3K inhibitors.

As a continuation of our retrospective study highlighted in §4.2.1, the prospective PI3K-based case study originates from the work of Kim et al. in 2011.<sup>21</sup> The initial hit compound **4.16**, which emerged from a compound screen, exhibits an  $IC_{50}$  of 360 nM against PI3K $\alpha$  (Figure 4.11). Known PI3K $\alpha$  inhibitors present in the ChEMBL database were employed to construct the training and test sets for the QSAR in the FRESH program. This QSAR is one of the screens used to predict potencies of novel chemical structures. In order to accurately test the FRESH QSAR against PI3K $\alpha$  at the time of the Kim paper, all compounds with either the same structure as those in the Kim paper or those that appeared in the literature after 2010 were excluded.

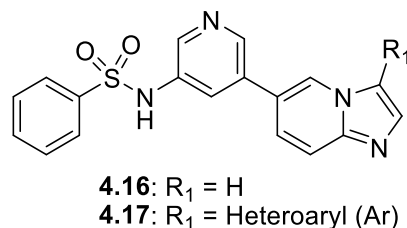


**Figure 4.11.** Initial PI3K $\alpha$  hit scaffold (**4.16**) and proposed site-modified analogs (**4.17**).

A 10 nM cutoff value was used to partition compounds between “active” and “inactive” analogs for constructing the ligand-based Bayesian model, and ECFP\_4 was used as the molecular descriptor. The selected ChEMBL database compounds were randomly divided into a 2:1 ratio using PLP<sup>3</sup> for training and test sets, respectively, to build the QSAR. The training set contained approximately 500 compounds with around 70 actives (14%) and the test set contained approximately 250 compounds with around 30 actives (12%). A Bayesian model was generated from the training set data using a leave-one-out cross-validation, and the performance of the Bayesian model was evaluated as described earlier (*vide supra*).<sup>22</sup> The test set was subjected to the above-generated Bayesian model and resulted in an AUC of 0.93 (see Figure 4.2). This high AUC demonstrates that the Bayesian model has a strong capacity for predicting activity. With this performance well validated, the Bayesian score with ECFP\_4 as the descriptor was used as one of the filters for evaluating activity of new chemical entities.

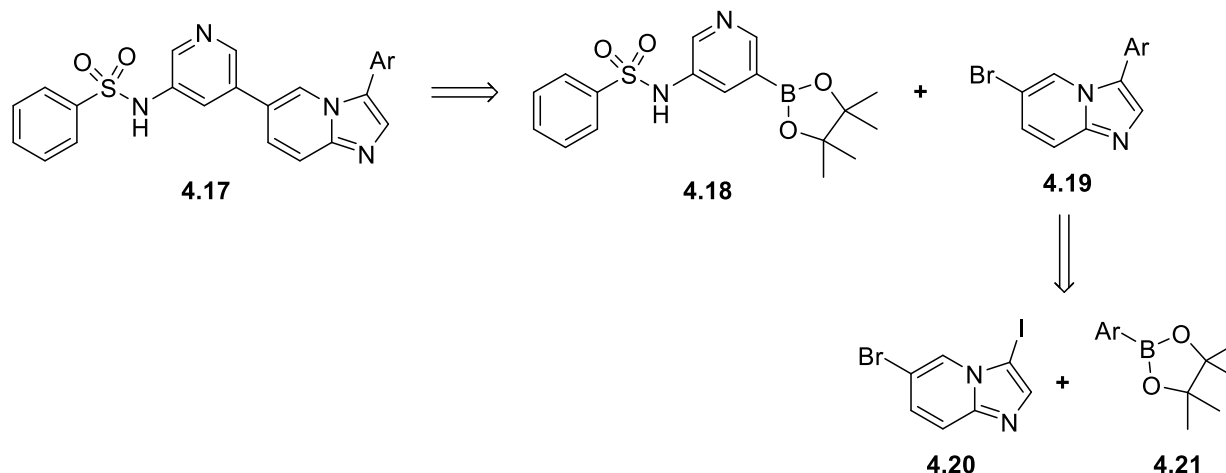
At the time of this project, there were no crystal structures of PI3K $\alpha$  available. However, Kim et al.<sup>21</sup> used a homology model based on PI3K $\gamma$  to model the interaction between small molecule ligands and the PI3K $\alpha$  kinase domain. A homology model using the same template (PDB code: 1E8Z) was constructed and used for receptor-based docking analysis.<sup>33</sup> The ChEMBL database compounds were prepared by LigPrep in the Maestro package and processed for both Glide and MM-GBSA scores.<sup>34, 35</sup> The AUC values of the corresponding ROC curves were 0.64 and 0.72 (acceptable, see Figures 4.3 and 4.4), so both the Glide and MM-GBSA scores were also used as criteria for potency evaluation.

According to the synthesis route from Kim et al.,<sup>21</sup> the -Ar group is attached to the core structure via Suzuki coupling (4.17, Figure 4.11). To obtain the fragment library for enumerating virtual structure libraries, the building blocks (aryl bromides and aryl boronic esters) were queried against the “Zinc bb now” commercial compound database. This resulted in approximately 44,000 fragments. The -Ar fragment was first filtered by fragment rule of three<sup>8</sup> and groups with potential liability and reactivity concerns were taken into account. The surviving fragments were then covalently connected to the core structure at the -Ar position of Figure 4.11 to generate structures of possible PI3K $\alpha$  inhibitors. Subsequently, a series of widely-accepted, drug-like filters (Lipinski Rule of Five,<sup>10</sup> Jorgensen Rule of Three,<sup>11</sup> etc.) was applied and structures with desirable drug-like properties were established for further processing. Finally, the Bayesian, Glide, and MM-GBSA scores were obtained for the filtered structures. Using the corresponding scores of the hit compound (4.16, 360 nM) as a reference, structures having all three scores better than the hit compound were included in the final list for this round. After all screens were applied, approximately 40 structures remained from this round of selection. Due to the ROC curve of the Bayesian score having the highest AUC, the ligand-based Bayesian model was used to rank and prioritize the remaining *ca.* 40 structures. The prioritized list obtained was further filtered for structures already extant in PubMed, thus removing the Kim et al. compounds.

#### 4.3.2.2 *Synthetic Considerations and Pharmacological Evaluation*

Similar to the CA II prospective analysis described in the previous section, we again pursued only those compounds that were quick to synthesize; those that had a high synthetic burden were discarded. General considerations for synthetic candidates could be summarized as follows: (1) the compound must be synthetically accessible from inexpensive building blocks; (2) the compound must have few to no stereocenters; (3) the compound must be outside the established IP; (4) the compound should be drug-like in appearance; (5) the compound should be made within two months or it is abandoned, and the next best-scoring compound should be attempted.

The compounds predicted by FRESH revolved around the synthesis employed by Kim et al.<sup>21</sup> with minor modifications (Scheme 4.1). The synthesis was highly modular in that final compounds of type **4.17** could be accessed by a Suzuki coupling between **4.18** and **4.19** with variation at the -Ar position of **4.19**. The fused heteroarenes of type **4.19** were expected to come from the known dihalo precursor **4.20** and an array of various aryl pinacolboronic esters of type **4.21**.



**Scheme 4.1.** Retrosynthesis of compounds of type **4.17**.

The molecules that were selected from FRESH for synthesis were chosen because they were anticipated to require the least time and synthetic effort to access and are shown below in Table 4.2. All chosen compounds were synthesized as described in our publication and found to have low (< 50) nanomolar potency against PI3K $\alpha$  using the ADP-Glo Lipid Kinase System (Table 4.2). Notably, of all the PI3K $\alpha$  inhibitors in the literature at the time of this study (2,149), only 44% (954) had an IC<sub>50</sub> less than or equal to 329 nM while only 23% (489) had an activity equal to or less than 43 nM. The compounds were further evaluated in an anti-proliferative assay against MCF-7 breast cancer cell lines housing either wild-type or E545K mutant PI3K $\alpha$ . This mutant kinase is one of the most clinically observed mutations in breast and gallbladder cancers and bears conflicting prognoses.<sup>36-39</sup> In each case, the compounds demonstrated increased potency to the mutant relative to wild-type, with single-digit to sub-micromolar potencies. We also calculated the Tanimoto score for each of our

compounds against the 30 most potent compounds against PI3K $\alpha$ . Again, the highest similarity coefficient for **4.17b-4.17e** was only 0.17822, which indicates that the new compounds proposed by FRESH are chemically distinct from the input training set.<sup>40</sup>

**Table 4.2.** Enzymatic PI3K $\alpha$  and anti-proliferative potencies<sup>a</sup>

Compound ID	Heteroaryl (Ar)	Enzymatic PI3K $\alpha$ IC <sub>50</sub> (nM) $\pm$ SD <sup>b</sup>	MCF-7 WT IC <sub>50</sub> ( $\mu$ M) $\pm$ SD	MCF-7 E545K IC <sub>50</sub> ( $\mu$ M) $\pm$ SD	Rank in FRESH
<b>4.17a</b>		6.10 $\pm$ 3.60	1.27 $\pm$ 0.28	0.46 $\pm$ 0.12	1
<b>4.17b</b>		23.9 $\pm$ 8.70	>10	0.94 $\pm$ 0.19	3
<b>4.17c</b>		11.5 $\pm$ 1.40	3.35 $\pm$ 0.80	0.78 $\pm$ 0.10	4
<b>4.17d</b>		47.4 $\pm$ 16.0	>10	4.08 $\pm$ 0.67	22
<b>4.17e</b>		7.40 $\pm$ 4.90	3.41 $\pm$ 0.55	0.81 $\pm$ 0.17	26

<sup>a</sup>Data were collected in triplicate and IC<sub>50</sub> values were calculated from n = 3 enzymatic and n = 2 cellular experiments; <sup>b</sup>SD: standard deviation

Several QSAR studies have been performed for PI3K $\alpha$ , HDAC1, and CA II. However, most were retrospective in that potency correlations were generated subsequent to biodata collection and not used to guide chemical synthesis.<sup>41-43</sup> Hage-Melim et al.<sup>44</sup> proposed PI3K synthesis candidates based on physicochemical and pharmacokinetic properties, while Tang et al.<sup>45</sup> and Zhao et al.<sup>46</sup> performed

prospective screening studies for HDAC. However, the screening pools in these studies were restricted to known compound databases such as Binding DB, PDB, ZINC, WDI, and PubMed, while novel chemical space attainable by a broadened synthesis campaign was not probed. By contrast, FRESH was fashioned to include not only a well-conceived QSAR and handpicked physical properties to select synthesis candidates from both available compound collections and synthetic reachable space, but also any number of user-defined ADMET factors in the final prediction of synthetic targets. Additionally, the CA II and PI3K $\alpha$  applications of FRESH described above were then further supported by synthesis and bioassay to demonstrate the practical and provocative utility of the methodology (Tables 4.1 and 4.2).

With this, we had evaluated the possibility of using FRESH as a lead development tool for reducing the intensity of synthetic preparation required in the optimization process. In both CA II and PI3K $\alpha$ , FRESH was capable of generating tens of thousands of synthesis candidates and reducing that pool to 10's of compounds predicted to be highly active and have good pharmacological parameters. In the case of PI3K $\alpha$ , all of our synthesized compounds were found to have low (< 50) nanomolar activity against the enzyme and low-to-submicromolar activity against the clinically relevant E545K mutant MCF-7 cell line. In the case of CA II, all synthesized compounds showed single digit-to-subnanomolar  $K_i$  values, two of which were the most potent on-target activities that had been demonstrated in this chemical class. The sites of variation were picked with the consult of synthetic chemists such that diversity and activity could both be accessed quickly through chemical synthesis. FRESH made use of structural information complemented with ligand-based methods, and also proved useful when only limited biostructural information was available. The possibility to create a list of proposed active compounds using only a machine learning/Bayesian model without the input of structural biology represents an exciting and successful feature of FRESH as well as an area for continued investigation.

Taken together, then, the prospective results of FRESH against both PI3K $\alpha$  and CA II strongly suggested that FRESH was capable of identifying compounds with a high likelihood of potent activity given a sufficient training set. One of the limitations inherent in the program is the requirement of a preexisting and broad activity profile for the training set to give predictive capability to the algorithm, and the lower limits of such a dataset which can still provide meaningfully predictive power continues to be investigated. Nevertheless, this limitation is absent in a sufficiently advanced lead development program, and FRESH can take advantage of substantial SAR to efficiently suggest a high-priority target list for further developmental investigation. This was again illustrated by our efforts against the RSV fusion protein, and the reader is once more referred to our publication for a full description.<sup>31</sup> These efforts set us up well to tackle our most ambitious and advanced preclinical project to date which is the topic of the following chapter — redesigning safer inhibitors of c-Abl kinase for the treatment of Parkinson's disease.

#### 4.4 REFERENCES AND NOTES

1. Jorgensen, W. L., Challenges for academic drug discovery. *Angew. Chem. Int. Ed.* **2012**, *51* (47), 11680-11684.
2. Blass, B. E., Chapter 1 - Drug discovery and development: An overview of modern methods and principles. In *Basic Principles of Drug Discovery and Development (Second Edition)*, Blass, B. E., Ed. Academic Press: 2021; pp 1-41.
3. BIOVIA <http://accelrys.com/products/collaborative-science/biovia-pipeline-pilot/>.
4. Gaulton, A.; Bellis, L. J.; Bento, A. P.; Chambers, J.; Davies, M.; Hersey, A.; Light, Y.; McGlinchey, S.; Michalovich, D.; Al-Lazikani, B.; Overington, J. P., ChEMBL: a large-scale bioactivity database for drug discovery. *Nuc. Acids Res.* **2012**, *40* (D1), D1100-D1107.
5. Liu, T.; Lin, Y.; Wen, X.; Jorissen, R. N.; Gilson, M. K., BindingDB: a web-accessible database of experimentally determined protein-ligand binding affinities. *Nuc. Acids Res.* **2007**, *35* (Database issue), D198-201.
6. Rogers, D.; Hahn, M., Extended-connectivity fingerprints. *J. Chem. Inf. Model.* **2010**, *50* (5), 742-54.
7. Stumpfe, D.; Bajorath, J., Critical Assessment of Virtual Screening for Hit Identification. In *Cheminformatics for Drug Discovery*, Bajorath, J., Ed. John Wiley & Sons, Inc.: 2013; pp 113-130.

8. Congreve, M.; Carr, R.; Murray, C.; Jhoti, H., A 'rule of three' for fragment-based lead discovery? *Drug Discovery Today* **2003**, *8* (19), 876-7.
9. Di, L.; Kerns, E. H.; Carter, G. T., Drug-like property concepts in pharmaceutical design. *Curr. Pharm. Des.* **2009**, *15* (19), 2184-94.
10. Lipinski, C. A.; Lombardo, F.; Dominy, B. W.; Feeney, P. J., Experimental and computational approaches to estimate solubility and permeability in drug discovery and development settings. *Adv Drug Deliv Rev* **2001**, *46* (1-3), 3-26.
11. Jorgensen, W. L., Efficient drug lead discovery and optimization. *Acc Chem Res* **2009**, *42* (6), 724-33.
12. Small-Molecule Drug Discovery Suite 2014-1. Glide, 6.2; Schrödinger, LLC: New York, NY,, 2014.
13. Mitchell, J. B. O., Machine learning methods in chemoinformatics. *Wiley Interdiscip. Rev.: Comput. Mol. Sci.* **2014**, *4*, 468-481.
14. Kaiser, T. M.; Burger, P. B., Error tolerance of machine learning algorithms across contemporary biological targets. *Molecules* **2019**, *24* (11), 2115.
15. Rogers, D.; Brown, R. D.; Hahn, M., Using Extended-Connectivity Fingerprints with Laplacian-Modified Bayesian Analysis in High-Throughput Screening Follow-Up. *J. Biomol. Screening* **2005**, *10*, 682-686.
16. Shi, Q., *Computer-Assisted Drug Discovery Part I: Design, Development, Validation and Application of FRESH, a Novel In-Silico High-throughput Screening Program Part II: Monocarbonyl Curcumin Analogues: Heterocyclic Pleiotropic Kinase Inhibitors that Mediate Anticancer Properties Part III: Development of 2nd Generation NAMFIS Software Program by Java*. Emory University: Atlanta, GA 2014.
17. Cain, R. J.; ARidley, A. J., Phosphoinositide 3-kinases in cell migration. *Biol. Cell* **2009**, *101*, 13-29.
18. Sawyer, C.; Sturge, J.; Bennett, D. C.; O'hare, M. J.; Allen, W. E.; Bain, J.; Jones, G. E.; Vanhaesebroeck, B., Regulation of breast cancer cell chemotaxis by the phosphoinositide 3-kinase p110delta. *Cancer Res.* **2003**, *63* (7), 1667-75.
19. Price, J. T.; Tiganis, T.; Agarwal, A.; Djakiew, D.; Thompson, E. W., Epidermal growth factor promotes MDA-MB-231 breast cancer cell migration through a phosphatidylinositol 3'-kinase and phospholipase C-dependent mechanism. *Cancer Res* **1999**, *59* (21), 5475-8.
20. Akinleye, A.; Avvaru, P.; Furqan, M.; Song, Y.; Liu, D., Phosphatidylinositol 3-kinase (PI3K) inhibitors as cancer therapeutics. *J. Hematol. Oncol.* **2013**, *6*, 88-104.
21. Kim, O.; Jeong, Y.; Lee, H.; Hong, S.-S.; Hong, S., Design and Synthesis of Imidazopyridine Analogues and Inhibitors of Phosphoinositide 3-Kinase Signaling and Angiogenesis. *J. Med. Chem.* **2011**, *54*, 2455-2466.
22. Swets, J. A., *Signal detection theory and ROC analysis in psychology and diagnostics: collected papers* Lawrence Erlbaum Associates: Mahwah, N.J., 1996.

23. Supuran, C. T., Carbonic anhydrases: novel therapeutic applications for inhibitors and activators. *Nat Rev Drug Discov* **2008**, *7* (2), 168-81.

24. Pacchiano, F.; Aggarwal, M.; Avvaru, B. S.; Robbins, A.; Scozzafava, A.; McKenna, R.; Supuran, C. T., Selective hydrophobic pocket binding observed within the carbonic anhydrase II active site accommodate different 4-substituted-ureido-benzenesulfonamides and correlate to inhibitor potency. *Chem. Commun. (Cambridge, U. K.)* **2010**, *46* (44), 8371-3.

25. Pacchiano, F.; Carta, F.; McDonald, P. C.; Lou, Y.; Vullo, D.; Scozzafava, A.; Dedhar, S.; Supuran, C. T., Ureido-substituted benzenesulfonamides potently inhibit carbonic anhydrase IX and show antimetastatic activity in a model of breast cancer metastasis. *J. Med. Chem.* **2011**, *54* (6), 1896-902.

26. de Ruijter, A. J.; van Gennip, A. H.; Caron, H. N.; Kemp, S.; van Kuilenburg, A. B., Histone deacetylases (HDACs): characterization of the classical HDAC family. *Biochem J* **2003**, *370* (Pt 3), 737-49.

27. Glaser, K. B.; Li, J.; Staver, M. J.; Wei, R. Q.; Albert, D. H.; Davidsen, S. K., Role of class I and class II histone deacetylases in carcinoma cells using siRNA. *Biochem Biophys Res Commun* **2003**, *310* (2), 529-36.

28. Richon, V. M., Cancer biology: mechanism of antitumour action of vorinostat (suberoylanilide hydroxamic acid), a novel histone deacetylase inhibitor. *Br. J. Cancer* **2006**, *95* (1), S2-S6.

29. Wang, H.; Lim, Z.-Y.; Zhou, Y.; Ng, M.; Lu, T.; Lee, K.; Sangthongpitag, K.; Goh, K. C.; Wang, X.; Wu, X.; Khng, H. H.; Goh, S. K.; Ong, W. C.; Bonday, Z.; Sun, E. T., Acylurea connected straight chain hydroxamates as novel histone deacetylase inhibitors: Synthesis, SAR, and in vivo antitumor activity. *Bioorg. Med. Chem. Lett.* **2010**, *20* (11), 3314-3321.

30. Wang, D., Computational studies on the histone deacetylases and the design of selective histone deacetylase inhibitors. *Curr Top Med Chem* **2009**, *9* (3), 241-56.

31. Pribut, N.; Kaiser, T. M.; Wilson, R. J.; Jecs, E.; Dentmon, Z. W.; Pelly, S. C.; Sharma, S.; Bartsch III, P. W.; Burger, P. B.; Hwang, S. S.; Le, T.; Sourimant, J.; Yoon, J. J.; Plemper, R. K.; Liotta, D. C., Accelerated Discovery of Potent Fusion Inhibitors for Respiratory Syncytial Virus. *ACS Infect. Dis.* **2020**, *6* (5), 922-929.

32. Yang, J.; Nie, J.; Ma, X.; Wei, Y.; Peng, Y.; Wei, X., Targeting PI3K in cancer: mechanisms and advances in clinical trials. *Mol. Cancer* **2019**, *18* (1), 26.

33. Walker, E. H.; Pacold, M. E.; Perisic, O.; Stephens, L.; Hawkins, P. T.; Wymann, M. P.; Williams, R. L., Structural Determinants of Phosphoinositide 3-Kinase Inhibition by Wortmannin, LY294002, Quercetin, Myricetin, and Staurosporine. *Mol. Cell* **2000**, *6*, 909-919.

34. *Small-Molecule Drug Discovery Suite 2014-1: Glide*, 6.2; Schrödinger, LLC: New York, NY, 2014.

35. *Schrödinger Release 2014-1: Prime*, 3.5; Schrödinger, LLC: New York, NY, 2014.

36. Janku, F.; Wheler, J. J.; Westin, S. N.; Moulder, S. L.; Naing, A.; Tsimberidou, A. M.; Fu, S.; Falchook, G. S.; Hong, D. S.; Garrido-Laguna, I.; Luthra, R.; Lee, J. J.; Lu, K. H.; Kurzrock, R.,

PI3K/AKT/mTOR Inhibitors in Patients With Breast and Gynecologic Malignancies Harboring PIK3CA Mutations. *J. Clin. Oncol.* **2012**, *30* (8), 777-782.

37. Janku, F.; Wheler, J. J.; Naing, A.; Falchook, G. S.; Hong, D. S.; Stepanek, V. M.; Fu, S.; Piha-Paul, S. A.; Lee, J. J.; Luthra, R.; Tsimberidou, A. M.; Kurzrock, R., PIK3CA Mutation H1047R Is Associated with Response to PI3K/AKT/mTOR Signaling Pathway Inhibitors in Early-Phase Clinical Trials. *Cancer Res.* **2013**, *73* (1), 276-284.

38. Zardavas, D.; Phillips, W. A.; Loi, S., PIK3CA mutations in breast cancer: reconciling findings from preclinical and clinical data. *Breast Cancer Res.* **2014**, *16* (1), 201.

39. Zhao, S.; Cao, Y.; Liu, S. B.; Wang, X. A.; Bao, R. F.; Shu, Y. J.; Hu, Y. P.; Zhang, Y. J.; Jiang, L.; Zhang, F.; Liang, H. B.; Li, H. F.; Ma, Q.; Xu, Y.; Wang, Z.; Zhang, Y. C.; Chen, L.; Zhou, J.; Liu, Y. B., The E545K mutation of PIK3CA promotes gallbladder carcinoma progression through enhanced binding to EGFR. *J. Exp. Clin. Cancer Res.* **2016**, *35* (1), 97.

40. Maggiora, G.; Vogt, M.; Stumpfe, D.; Bajorath, J., Molecular Similarity in Medicinal Chemistry. *J. Med. Chem.* **2014**, *57*, 3186-3244.

41. Ran, T.; Lu, T.; Yuan, H.; Liu, H.; Wang, J.; Zhang, W.; Leng, Y.; Lin, G.; Zhuang, S.; Chen, Y., A selectivity study on mTOR/PI3K $\alpha$  inhibitors by homology modeling and 3D-QSAR. *J. Mol. Model.* **2012**, *18* (1), 171-86.

42. Pacchiano, F.; Aggarwal, M.; Avvaru, B. S.; Robbins, A. H.; Scozzafava, A.; McKenna, R.; Supuran, C. T., Selective hydrophobic pocket binding observed within the carbonic anhydrase II active site accommodate different 4-substituted-ureido-benzenesulfonamides and correlate to inhibitor potency. *Chem. Commun. (Cambridge, U. K.)* **2010**, *46* (44), 8371-3.

43. Yang, J. S.; Chun, T.-G.; Nam, K.-Y.; Kim, H.; Han, G., Structure-Activity Relationship of Novel Lactam Based Histone Deacetylase Inhibitors as Potential Anticancer Drugs. *Bull. Korean Chem. Soc.* **2012**, *33*.

44. Hage-Melim, L. I. d. S.; Santos, C. B. R.; Poiani, J. G. C.; Vaidergom, M. d. M.; Manzolli, E. S.; da Silva, C. H. T. d. P., Computational Medicinal Chemistry to Design Novel Phosphoinositide 3- Kinase (PI3K) Alpha Inhibitors in View of Cancer. *Curr. Bioact. Compd.* **2014**, *10*, 147-157.

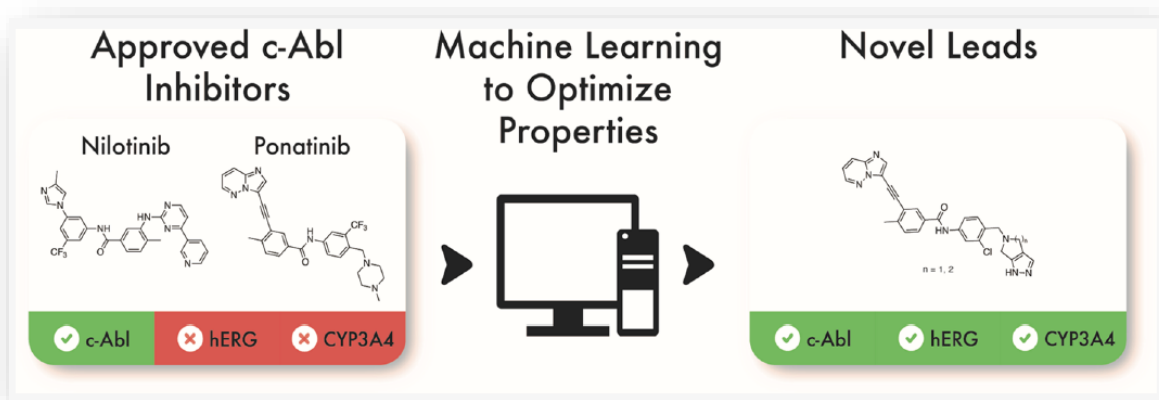
45. Tang, H.; Wang, X. S.; Huang, X.-P.; Roth, B. L.; Butler, K. V.; Kozikowski, A. P.; Jung, M.; Tropsha, A., Novel Inhibitors of Human Histone Deacetylase (HDAC) Identified by QSAR Modeling of Known Inhibitors, Virtual Screening, and Experimental Validation. *J. Chem. Inf. Model.* **2009**, *49* (2), 461-476.

46. Zhao, L.; Xiang, Y.; Song, J.; Zhang, Z., A novel two-step QSAR modeling work flow to predict selectivity and activity of HDAC inhibitors. *Bioorg Med Chem Lett* **2013**, *23* (4), 929-33.

## Chapter 5. The Machine Learning Algorithm-Enabled Design and Synthesis of Novel Abelson Non-Receptor Tyrosine Kinase Inhibitors as Safer Therapeutics for Parkinson's Disease

Portions of this chapter are reproduced or adapted with permission from (Thomas M. Kaiser, Zackery W. Dentmon, Christopher E. Dalloul, Savita K. Sharma, and Dennis C. Liotta, Accelerated Discovery of Novel Ponatinib Analogs with Improved Properties for the Treatment of Parkinson's Disease, *ACS Med. Chem. Lett.*, **2020**, *11*, 491-496. DOI: 10.1021/acsmchemlett.9b00612).

Copyright © 2020 American Chemical Society,



### 5.1 INTRODUCTION

Neurodegenerative disease, a category which includes Parkinson's disease (PD) and Alzheimer's disease among others, represents a significant healthcare burden worldwide that is expected to increase as lifespans are prolonged.<sup>1,2</sup> A 2015 United Nations report on world population aging anticipates a doubling of the number of people aged 60 years or older over the next 35 years, and this demographic is the most at risk for developing neurodegenerative disease.<sup>3</sup> PD is the second most common neurodegenerative disease, affecting 2-3% of those over 65 years of age.<sup>4</sup> The classic motor symptoms include bradykinesia, postural instability, resting tremor and muscle stiffness. Additionally, there is significant disability for the patient in that dementia, depression, dysphagia, insomnia and loss of smell frequently develop as PD progresses.<sup>5</sup> These non-motor symptoms are

key determinants of the quality of life in Parkinson's patients and are gaining recognition as important aspects to consider in therapeutic development.<sup>5,6</sup>

The underlying pathogenesis of PD is complex. A key component of the disease process is neurodegeneration due to selective and progressive loss of dopaminergic neurons in the *substantia nigra pars compacta*.<sup>7</sup> The intracellular accumulation of  $\alpha$ -synuclein and the subsequent formation of Lewy bodies in the brainstem and olfactory system is an additional histopathological feature of PD, but neither Lewy body formation nor dopaminergic neuron loss of the *substantia nigra* alone define Parkinson's.<sup>8</sup> Instead, it is the combination of these two histopathological features that results in the disease.<sup>8,9</sup>

Current therapy for PD is entirely focused on symptomatic relief and there are severe side effects associated with most of the first line agents in clinical use.<sup>10</sup> For example, dyskinesias, exacerbation of insomnia, movement freezing and dose failure are common consequences of L-DOPA/carbidopa therapy.<sup>11</sup> However, new insights into the pathological mechanisms have inspired a novel strategy for PD drug development. Work in both animal models of PD and in post-mortem analysis of human tissue affected by Parkinson's has revealed the role of oxidative stress in dopaminergic neurons as a potential pathogenic step in PD.<sup>2,12</sup> One of the key links between oxidative stress and neurodegeneration is the Abelson non-receptor tyrosine-protein kinase (c-Abl or Abl1), a kinase historically associated with the BCR-ABL fusion oncogene in certain leukemias.<sup>13</sup> Recent work has linked aberrations in c-Abl activity resulting from oxidative stress to neurodegeneration in both Alzheimer's and Parkinson's diseases.<sup>14-18</sup> For example, c-Abl activation and its subsequent phosphorylation of the E3 ubiquitin ligase parkin result in inhibition of the ubiquitin ligase activity of parkin, leading to the accumulation of toxic parkin substrates, including parkin interacting substrate (PARIS) and aminoacyl tRNA synthetase complex-interacting multifunctional protein 2 (AIMP2).<sup>19,20</sup> The findings that both PARIS and AIMP2 accumulate in familial PD caused by parkin mutations and in MPTP toxin mouse models of PD strongly implicates c-Abl in this pathogenic

pathway of the disease.<sup>19,20</sup> Furthermore,  $\alpha$ -synuclein has been established as a genuine substrate of c-Abl, phosphorylating at Tyr39, leading to enhanced aggregation into neurofibrillary tangles, a hallmark phenotype of post-mortem PD patient brain tissue.<sup>18, 21, 22</sup>

Based on these findings, several groups have explored the use of known BCR-Abl inhibitors that are used clinically for treating chronic myeloid leukemia to also treat PD. This class of drugs, which includes imatinib, nilotinib, and ponatinib among others (Figure 5.1), has exhibited activity against untranslocated c-Abl.<sup>23</sup> Provocatively, imatinib was found to restore parkin ubiquitin ligase activity and reduce PARIS and AIMP2 levels in the MPTP mouse model.<sup>16, 17</sup> Similarly, administration of nilotinib was found to improve autophagic degradation and clearance of aggregated  $\alpha$ -synuclein and protected against MPTP-induced dopaminergic deficits reversing the loss of dopamine neurons, a result known to improve motor behavior.<sup>22, 24</sup> Additionally, a 12-patient, non-randomized phase I trial conducted at Georgetown University demonstrated that nilotinib treatment improved motor and cognitive outcomes.<sup>25</sup> A follow-up study evaluating the pharmacokinetics and pharmacodynamics of nilotinib in PD patients found that a 200 mg single dose of nilotinib was capable of increasing cerebrospinal fluid concentrations of dopamine metabolites.<sup>26</sup> This led the group at Georgetown, as well as an independent group at Northwestern, to trial nilotinib in phase II, but the two studies yielded contradictory conclusions.<sup>27, 28</sup>

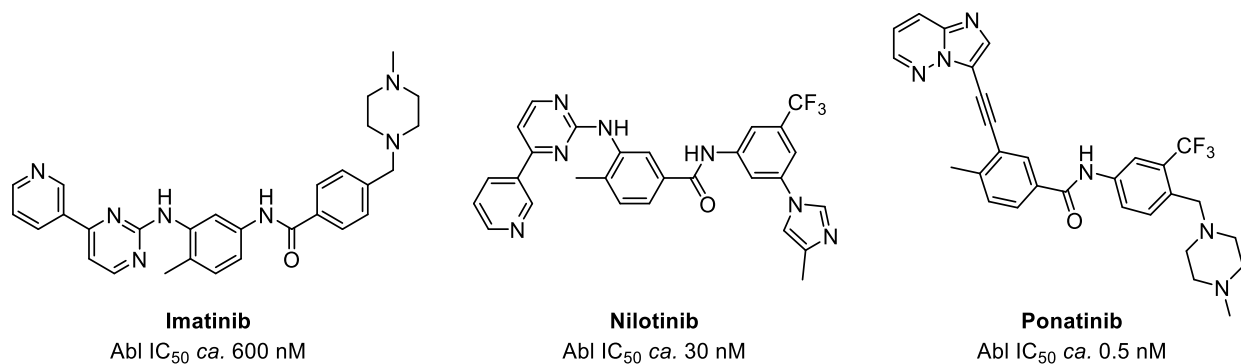


**Figure 5.1.** Approved first-, second- and third-generation inhibitors of BCR-ABL imatinib, nilotinib, and ponatinib

There are significant side effects associated with these drugs that may adversely impact their use in treating a chronic disease like PD. Nilotinib is known to be a potent submicromolar inhibitor of the human Ether-à-go-go-Related Gene (hERG), a potassium channel that generates the repolarization current in the cardiac action potential. Inhibition of this repolarization process leads to prolongation of the QT interval, which can progress to *torsades de points* and cardiac arrest. Nilotinib in fact carries a black box warning for QT prolongation and sudden death (2.1% of patients experience QT increases of >60ms, while <1% experience QT increases of >500ms; sudden deaths reported in 0.6% of patients).<sup>29, 30</sup> One potential rationalization of the conflicting Phase II results is sub-optimal brain penetrance,<sup>31, 32</sup> which could be addressed by increasing the dose; however, nilotinib's hERG liability presumably compromises its use as a chronic therapy, especially at higher doses which may be necessary for sufficient CNS target engagement. In addition, nilotinib is a potent inhibitor of the cytochrome P450 isozyme 3A4 (CYP3A4), which could preclude its use in a patient population which might be prone to adverse drug-drug interactions (DDIs), *i.e.*, patients taking other drugs which are also metabolized by this enzyme. Similarly, ponatinib has a black box warning for vascular occlusion, heart failure, and hepatotoxicity.<sup>33-35</sup>

We imagined that a new chemical entity which potently inhibited c-Abl with an improved safety margin relative to the off-targets hERG and CYP3A4 would have the potential to fill this intriguing gap and help to address this drastically unmet medical need. Given our accomplishments described in the previous chapter in using machine learning to optimize the properties of known drugs,<sup>34,35</sup> we sought to design novel c-Abl inhibitors with our algorithm which might include these hopeful features.

## 5.2 RESULTS AND DISCUSSION

As detailed in Chapter 4, we had achieved prior success with our machine learning algorithm by training the machine with a single Naïve Bayes Network (NBN) learner optimized for 'on-target' potency. Given those successful campaigns, we felt reasonably confident the algorithm could suggest

new chemical entities with a high probability of meeting a demanding criterion for on-target potency (e.g., <20 nM). This alone, however, would not suffice to address the problem; current inhibitors on the market are already exceedingly potent against Abl1. Success in this arena would require compounds optimized for on-target potency as well as avoiding off-target liabilities, especially hERG. Hence, our initial investigation began with the design of two machine learning workflows. The first employed a single NBN exclusively designed to calculate the probability of novel small molecules to have an  $IC_{50}$  of <20 nM against c-Abl. The second utilized two NBNs working in concert: one designed for potency against c-Abl, and the other to predict molecules with  $IC_{50}$  values greater than 1  $\mu$ M against hERG. Compounds ranked from the former workflow will be referred to as single-NBN compounds, while those ranked with the latter method will be referred to as dual-NBN compounds. We would therefore be most interested in the dual-NBN compounds as they lie, to borrow a term from mathematical logic, within the intersection of two sets: the set of compounds predicted to be potent on target (c-Abl), and the set which were predicted to be impotent off target (hERG).

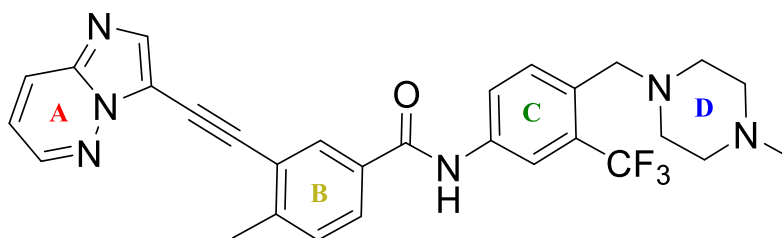
To this end, we acquired and curated Abl1 and hERG datasets from ChEMBL and enhanced them with additional information from the patent literature to train the desired NBNs.<sup>36-38</sup> We suspected that by incorporating the second learner, dual-NBN compounds emerging from this more stringent workflow may be less potent on target, but the degree to which this may be true was something we wished to test empirically. Hence, by prospectively testing both workflows individually, we could experimentally verify the quality of the on-target learner to suggest potent inhibitors of c-Abl and determine if there was indeed a potency reduction resulting from the additional filtering step in the dual-NBN workflow. A detailed overview of our machine learning approaches, as well as the general workflows employed, were discussed in the previous chapter.<sup>39, 40</sup>

### 5.2.1 Core Scaffold and Single-NBN Compound Selection

In selecting the core scaffolds that would be evaluated by our algorithms, we considered the medicinal chemistry profiles of nilotinib, since it had shown disease modification in animal studies

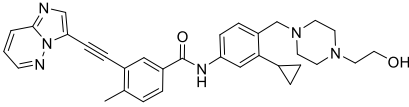
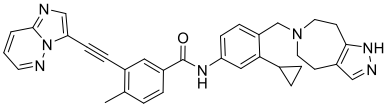
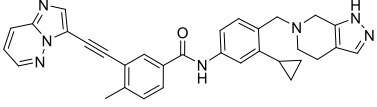
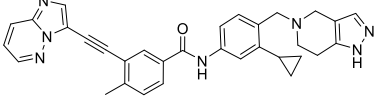
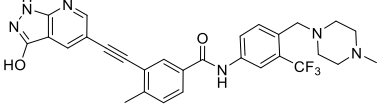
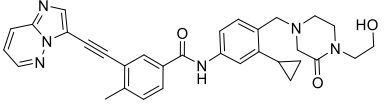
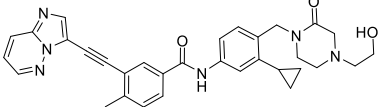
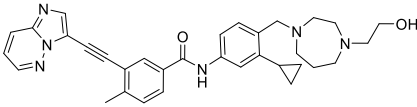
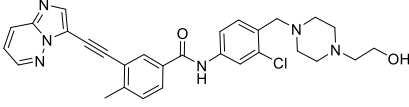
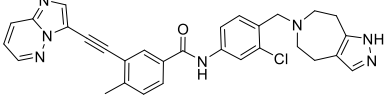
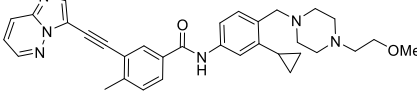
(*vide supra*), as well as ponatinib, which has not yet been evaluated in Parkinson's disease. From our perspective, analogs of ponatinib provided two key advantages over nilotinib analogs. Most apparently, as a third-generation TKI ponatinib offers a significantly more potent starting point for new analog creation. Consequently, losses in Abl1 potency that may result from the inclusion of the hERG NBN might still provide us with the opportunity to obtain low nanomolar inhibitors comparable to nilotinib. Secondly, while a direct comparison between the CNS penetration of nilotinib and ponatinib has not been made, there is evidence to suggest that ponatinib analogs may improve upon the moderate brain penetration displayed by nilotinib.<sup>24, 41-43</sup>

Workflows were constructed in Pipeline Pilot<sup>44</sup> and used to determine the chemical space most amenable to address the c-Abl / hERG selectivity problem. Using this approach, we were able to explore millions of synthetic candidates not previously reported in the scientific or patent literature. The rankings of the first dozen candidates produced by the single-NBN (Abl1 only) workflow are shown in Table 5.1, and several observations are notable. To aid in discussion, let's define the various pieces of the molecule according to Figure 5.2 such that the arenes connected via the alkyne linker are referred to as rings A and B, while the remaining arene is ring C. The last piece we'll refer to as ring D. Firstly, all but one (rank 5) share exactly the same diarylalkyne benzamide scaffold (*i.e.*, the left-hand half of the molecule) as ponatinib. It is logical the machine would be biased toward this pharmacophore given the remarkable potency of ponatinib against c-Abl relative to other scaffolds in the training set. Secondly, all but this same compound carry either a cyclopropyl (cPr) or chloro substituent on the C ring. The primary points of variability between the suggested structures



**Figure 5.2.** Structure of ponatinib with the constituent pieces annotated

**Table 5.1.** Structure, probability score, and rank of single-NBN (Abl1) compounds

Structure	Probability Score	NBN Rank
	0.7756	1
	0.7743	2
	0.7714	3i
	0.7714	3ii
	0.7690	5
	0.7689	6
	0.7682	7
	0.7646	8
	0.7624	9
	0.7611	10
	0.7588	11

are therefore this C ring substituent as well as ring D and its associated appendages, with all compounds carrying some nitrogen-containing heterocycle linked to the rest of the scaffold at the benzylic position of ring C. Upon inspection, one can easily appreciate both the similarity to ponatinib as well as the non-obvious suggested changes to the D ring.

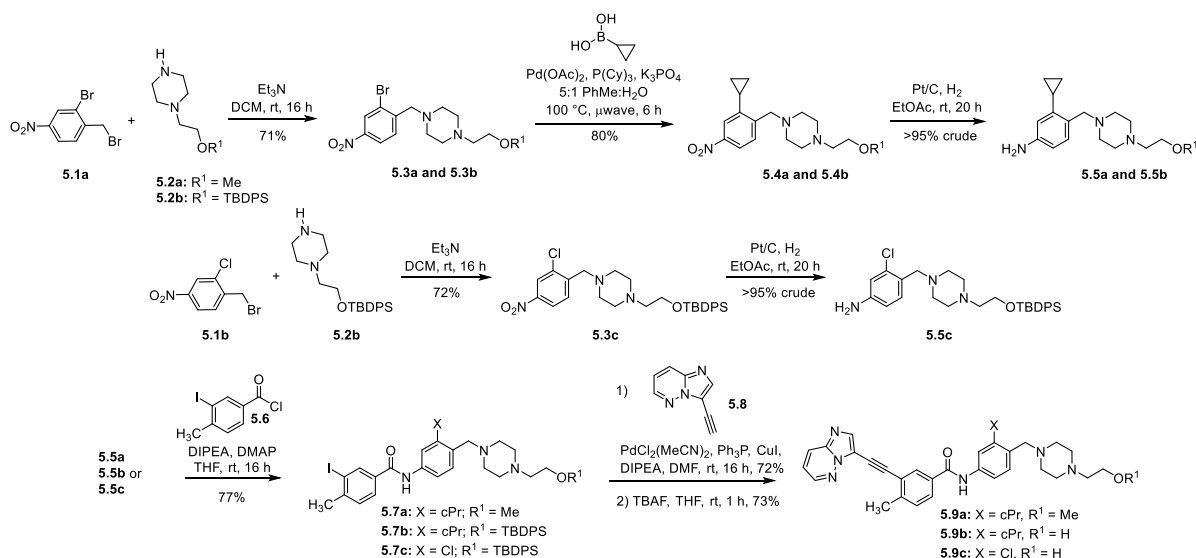
Lastly, the probability scores of these first dozen compounds are all within 1.75% of one another, meaning there is very little difference to the machine which D ring change is more likely to meet the on-target potency criterion of <20 nM. This allows for a high degree of discretion by the synthetic chemistry team as to which molecules to target for synthesis. The chemist is therefore free to choose structures that are most appealing, typically as a function of resource costs to access the molecule of interest, such that molecules perceived as having a high synthetic barrier (*e.g.*, unavailable building blocks, asymmetric centers, etc.) or are not drug-like in appearance can be omitted from consideration. The chemistry team is also free to target compounds which might address subtle SAR questions. For example, the highest ranked compound contains the cPr C ring substituent and *N*-(hydroxyethyl)piperazine D ring as its key structural determinants. Note then that the 9<sup>th</sup>-ranked compound holds this D ring constant while changing the C ring substituent from cPr to Cl. Conversely, the 11<sup>th</sup>-ranked compound holds the cPr substituent constant while making the subtle change of capping the D ring appendage with a methyl ether. Both of these structurally similar analogs of the top ranked compound were made to address the questions of which C ring substituent is better and what effect the terminal H-bond donor has on potency, while experiencing a less than 1.7% loss in probability of achieving the potency criterion. This struck our team as a very worthwhile tradeoff.

It is worth explicitly restating here that the probability score used to rank these novel analogs should not be interpreted as a quantitative prediction of on-target potency. Said differently, the top-ranked compound should not be assumed to be the most potent analog. Rather, the top-ranked compound contains structural features which according to the machine make it the most likely

candidate to achieve the user-defined criterion, in this case <20 nM potency on target. Therefore, the chemistry team should remain unbiased as to which of the prioritized target compounds would empirically be more potent. This is why the question of which C ring substituent is superior is still worth interrogating. Simply because the chloro compound is 1.32% less likely to meet criteria compared to the cPr congener in no way implies that it will be less potent. It is merely less likely to be reach the potency criterion according to the available data in the training set, and this semantic distinction is important to keep in mind when selecting and assessing target compounds. With these thoughts in mind, we initiated our synthetic campaign to access these three novel ponatinib analogs to validate our single-NBN learner.

## 5.2.2 Parallel Linear Synthetic Strategy to Access and Evaluate the Single-NBN Compounds

To access the three analogs of interest from the single-NBN learner, linear syntheses were employed in parallel (Scheme 5.1). We began with radical bromination of the *m*-bromo- and *m*-chloro-substituted *p*-nitrotoluene precursors with *N*-bromosuccinimide and benzoyl peroxide to afford benzylic bromides **5.1a** and **5.1b** in 63-72% yield. The *N*-ethylpiperazine building block was either purchased as the methyl ether (**5.2a**) or provided after TBDPS protection of the available



**Scheme 5.1.** Parallel linear syntheses of single-NBN target compounds **5.9a-c**

alcohol to give **5.2b**. Piperazines **5.2a** and **5.2b** were then reacted with the requisite 4-nitrobenzyl bromides and Et<sub>3</sub>N to afford the *N*-alkylated products **5.3a-c** in >70% yield. At this point, the cPr moiety was installed as needed via microwave-assisted Suzuki reaction of the boronic acid with aryl bromides **5.3a** and **5.3b**. Palladium(II) acetate with tricyclohexylphosphine (PCy<sub>3</sub>) appeared to be a competent ligand set for this transformation with tribasic K<sub>3</sub>PO<sub>4</sub> as oxo-base in a 5:1 water:toluene mixed solvent system. These nitroarene cross-coupled products along with **5.3c** were each reduced with H<sub>2</sub> over catalytic platinum to the corresponding anilines **5.5a-c** in excellent yield. Anilines **5.5a-c** were each allowed to react with acid chloride **5.6** (freshly prepared from the benzoic acid precursor and SOCl<sub>2</sub>) to afford iodoamides **5.7a-c** in 70-85% yield. Sonogashira coupling of aryl iodide **5.7a** with heteroarylalkyne **5.8** (itself prepared after Sonogashira coupling of the aryl bromide precursor with TMS-acetylene and silyl removal) afforded the target compound **5.9a** in 31% yield. The TBDPS-protected **5.7b** and **5.7c** were similarly coupled with alkyne **5.8** in 33% and 72% yield, respectively. Subsequent desilylation of these two penultimate compounds with TBAF furnished the target compounds **5.9b** and **5.9c** in 73% and 91%, respectively. With the single-NBN target compounds in hand, we delivered them, as well as positive control compounds nilotinib and ponatinib, to a third-party contract research organization (CRO, Reaction Biology Corp.) for biochemical evaluation against both Abl1 and hERG, and the data are shown in Table 5.2.

**Table 5.2.** Biochemical data of single-NBN target compounds compared to FDA-approved inhibitors

Compound ID	Probability Score	NBN Rank	Abl1 IC <sub>50</sub> (nM)	hERG IC <sub>50</sub> (nM)
<b>5.9a</b>	0.7588	11	0.65	81
<b>5.9b</b>	0.7756	1	0.39	103
<b>5.9c</b>	0.7624	9	0.30	345
Nilotinib	--	--	5.91	447
Ponatinib	--	--	0.34	768

We were quite pleased to see that our single-NBN target compounds kept the activity of their parent pharmacophore with exceptionally potent subnanomolar IC<sub>50</sub> values against Abl1 across the board. Like ponatinib, these compounds showed an order of magnitude improvement in on-target potency compared to nilotinib. Additionally, we found that empirically determined Abl1 potency of the compounds did not correlate directly with the NBN rank of their structures in this small series. The most potent compound **5.9c** was the ninth ranked structure, not the first, though the potency values of the two compounds are quite comparable. Considering the brief SAR, it appears that capping the hydroxyl group with a methyl ether diminishes potency somewhat (cf. **5.9a** and **b**), but more importantly, the aryl chloride substituent on ring C appears to be better suited for on-target potency as well as off-target non-potency as **5.9c** performed better than the cPr congener **5.9b**. Also like ponatinib, all three single-NBN compounds showed submicromolar IC<sub>50</sub> values against the off-target hERG channel. However, this is still an optimum outcome for our initial hypothesis—namely, our machine learning algorithm was indeed capable of suggesting novel compounds which met our on-target potency criterion of <20 nM (note that the somewhat arbitrarily selected analogs not only met but exceeded the criterion by over 46-fold).

### 5.2.3 Dual-NBN Compound Selection and a Divergent Synthetic Strategy

With our c-Abl learner having been prospectively well validated, we then turned our attention to incorporation of the second learner trained on hERG margin. Returning to our set theory paradigm, when one considers compounds in this second set (*i.e.*, the set of hERG non-inhibiting compounds), there may be quite a large chemical space which is completely orthogonal or unrelated to our on-target pharmacophore. Clearly compounds of this space would be less relevant to our current project. Hence, the hERG learner was placed downstream of the Abl1 learner in the workflow of the algorithm with the result that compounds which made it through the first “filter” were then subjected to a more stringent secondary filter. In this way, the compounds which make it through the second filter comprise a discrete subset of the compounds which made it through the first. Implicitly,

then, we might expect some of the highly ranked compounds from the first NBN not to make it through the second. Empirically, all three of the synthesized single-NBN compounds **5.9a-c** should fall into this category, and if our second learner is performing well, it will filter them out. As a necessary corollary, we will need to consider compounds further down the Abl1 NBN list, that is to say with a lower probability of meeting our on-target potency criterion. Tactically, we have good room to maneuver in this regard while still maintaining comparable Abl1 potency to nilotinib.

With the above points in mind, the ranked list of structures emerging from the dual NBN is shown in Table 5.3. The structures are again ponatinib-based since the starting set consisted of those which made it through the c-Abl learner. This set is more challenging to rank in an absolute sense because there are now two probability scores and corresponding ranks for each structure, one from each learner, which may “compete” for priority. The reader will notice that the top-ranked structure is more “Abl-probable” than “hERG-probable,” meaning that the absolute composite ranking is biased toward structures with a higher probability of meeting the Abl potency criterion than the hERG criterion. When comparing the probability scores of the top two highest composite ranked structures, it is obvious which one is more likely to meet both criteria and therefore should be ranked higher. However, when comparing the third ranked structure to either the first or second, it is less clear because the structure has a better hERG probability score than either of the higher composite ranked structures. From the first to the third structure, the reader will notice that the Abl probability score had to drop by 1.91% in order for the hERG probability score to increase only 0.97%. The machine therefore takes this differential “cost” into account when providing the composite rank. The sixth ranked structure is a curious case—it is the structure with the highest probability of meeting our hERG criterion of  $>1 \mu\text{M}$ , but the probability of meeting the primary Abl potency criterion is 2-5% lower than the higher composite ranked structures, and again the machine takes this into account.

Structurally speaking, the appended D rings in Table 5.3 are more diverse than those shown in Table 5.1. This indicates that a particular structural motif, namely a benzylic tertiary amine like

**Table 5.3.** Structure, probability scores, and ranks of dual-NBN (Abl1  $\cap$  hERG) compounds

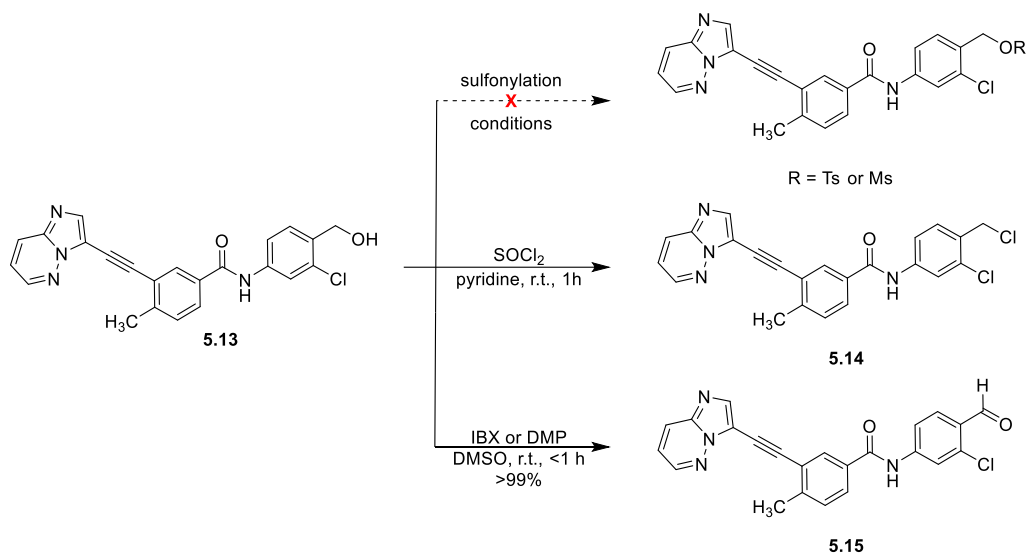
Structure	Abl Prob. Score	Abl NBN Rank	hERG Prob. Score	hERG NBN Rank	Composite Rank
	0.7581	12	0.7114	40	1
	0.7552	17	0.7091	48	2
	0.7390	38	0.7211	24	3
	0.7373	42	0.7075	55	4
	0.7327	58	0.7121	38	5
	0.7105	278	0.7543	1	6
	0.7304	74	0.7064	57	7
	0.7195	145	0.7252	22	8
	0.7264	100-102	0.7102	42-44	9-11
	0.7258	108	0.7089	50	12



acid precursor of **5.6**, but neither provided amide **5.12** in as high a yield as the acid chloride. The acid chloride **5.6** could be prepared effectively by either refluxing in neat  $\text{SOCl}_2$  for an hour or by use of the Vilsmeier salt catalyst prepared *in situ* by reacting oxalyl chloride with catalytic DMF in an ice bath.<sup>45</sup> Incidentally, one of the competing reaction pathways in this sequence turns out to be homocoupling of residual benzoate with the acid chloride to make the isolable symmetrical acid anhydride, proven by x-ray diffraction.

With iodoamide **5.12** in hand, Sonogashira coupling again with alkyne **5.8** afforded the diarylalkyne, and removal of the silyl protecting group then provided intermediate **5.13** in 51% yield over two steps. Upon removal of the bulky silane, the alcoholic product becomes sparingly soluble in organic or aqueous solvents, presumably due to favorable  $\pi$ - $\pi$  stacking between the heavily conjugated aromatic systems (note the compound becomes fluorescent under UV light once the alkyne is installed, and  $\pi$ -stacking was later corroborated by x-ray diffraction of a subsequent product). The low yield observed for this isolation could partially be attributed to poor solubility, but also the tetrabutylammonium cation from the TBAF reagent also appears to adhere well to this polar substrate and was challenging to purify away. Hence, other silyl removal conditions were trialed, including reaction with  $\text{NH}_4\text{F}$  and  $\text{HF} \cdot \text{pyridine}$ , but triethylamine  $\cdot$   $3\text{HF}$  (TREAT-HF) appeared to offer the optimum combination of reactivity and ease of operation and isolation.<sup>46, 47</sup>

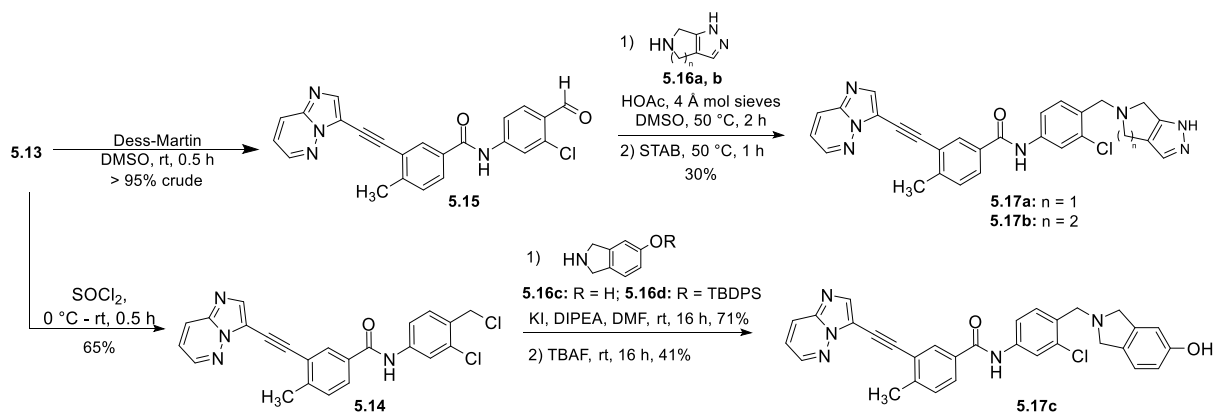
From alcohol **5.13**, our original strategy sought to alkylate our amines of interest after conversion of the benzylic alcohol to a sulfonate leaving group (Scheme 5.3, top). However, the alcohol appeared inert to a variety of tosylation or mesylation conditions in a range of solvents. Only polar, aprotic solvents like DMF, NMP, and DMSO provided homogenous reactions, and yet still no conversion to the desired sulfonate was observed. Noting that all the analogs we wished to prepare were tertiary amines, we considered reductive amination of the corresponding aldehyde as a potential pathway forward in parallel with an alternate alkylation strategy. Reaction of **5.13** with  $\text{SOCl}_2$  and  $\text{Et}_3\text{N}$  in benzene appeared to furnish the desired benzylic chloride **5.14**, but sluggishly,



**Scheme 5.3.** Strategies to access the key intermediate for diversification

while pyridine as base and solvent proved much quicker. We were also pleased to see that reaction of alcohol **5.13** with hypervalent iodine-based oxidants IBX or the Dess-Martin reagent in DMSO achieved the desired oxidation very quickly at ambient temperature with excellent yield where the Parikh-Doering conditions ( $\text{SO}_3 \cdot \text{pyridine}$  complex in DMSO) failed (Scheme 5.3).

Aldehyde derivative **5.15** was then subjected to one-pot reductive amination conditions with the commercially available cyclic amines **5.16a** and **5.16b** (Scheme 5.4). The aldehyde was again only soluble in DMSO solvent at elevated temperature ( $50^\circ\text{C}$ ), and sodium triacetoxyborohydride (STAB-H) was our reductant of choice. Notably, when the reaction was carried out at the elevated temperature used to solubilize the reaction mixture, the aldehyde was also competitively reduced back to the alcohol (**5.13**). Hence, the iminium ion was pre-formed by first heating the aldehyde and amine in the presence of substoichiometric acetic acid and activated molecular sieves to drive off the water and push the equilibrium towards the desired intermediate. Subsequent treatment with STAB-H at ambient temperature then furnished the target dual-NBN compounds **5.17a** and **5.17b** in *ca.* 30% yields, the poor yields again reflective of the limited solubility and challenging purification associated with these compounds.



**Scheme 5.4.** Complementary pathways used to access the target dual-NBN compounds **5.17a-c**

These conditions unfortunately proved untenable with amine **5.16c** (HBr salt), possibly due to the presence of the phenolic moiety. Hence, the *N*-(*tert*-butoxycarbonyl)-protected isoindoline was purchased, and the phenol was *O*-silyl-protected. The aryl OTBS silyl ether was smoothly installed but proved too base-labile as it was removed in the aqueous bicarbonate workup, but the bulkier OTBDPS silyl ether proved sufficiently stable. Removal of the BOC group with trifluoroacetic acid (TFA) in DCM provided **5.16d**; the reductive amination was reattempted but again failed, even in the presence of the Lewis acid activator titanium(IV) isopropoxide.<sup>48, 49</sup> With reductive amination proving evasive with this substrate, we turned back to benzylic chloride **5.14** in hopes of *N*-alkylating the isoindoline. Gratifyingly, heating **5.14** and amine **5.16d** in the presence of DIPEA and catalytic potassium iodide in DMF solvent afforded the desired *N*-alkylated product in >70 % yield.<sup>50, 51</sup> Fluoride-mediated silyl removal furnished the final target compound **5.17c**, again in poor yield.

### 5.2.5 *In vitro* Evaluation of the Dual-NBN Compounds

With these second-generation compounds in hand, they were shipped to the same CRO and evaluated for their biological activities against c-Abl and hERG to validate the dual-NBN workflow, and the data are shown in Table 5.4. With the two more highly ranked compounds, **5.17a** and **b**, the algorithm successfully met both on- and off-target criteria simultaneously, exceeding the Abl1 threshold of 20 nM by 3-to-3.5-fold and the hERG threshold of 1  $\mu$ M by 5-to-12-fold. Relative to our first-generation compounds (cf. Table 5.2), the successful dual-NBN compounds performed precisely

as anticipated, excepting the lowest ranked compound phenol **5.17c**. Our two best compounds exhibited very similar c-Abl IC<sub>50</sub> values to one another (and nilotinib), indeed forfeiting on-target potency on the order of *ca.* 13-fold relative to the single-NBN compounds. However, the concomitant *ca.* 49-fold drop in potency against the off-target hERG channel to >5  $\mu$ M more than makes up for this in our view. Collectively, these compounds improved the hERG safety margin over nilotinib by more than an order of magnitude as they have comparable on-target potency with substantially lower hERG liability, just as we had set out to accomplish.

**Table 5.4.** Biochemical data of dual-NBN target compounds compared to FDA-approved inhibitors

Compound ID	Composite Prob. Score	Composite NBN Rank	Abl1 IC <sub>50</sub> (nM)	hERG IC <sub>50</sub> (nM)
<b>5.17a</b>	0.5393	1	6.57	12100
<b>5.17b</b>	0.5329	3	5.60	5020
<b>5.17c</b>	0.5145	12	>30 <sup>a</sup>	783
Nilotinib	--	--	5.91	447
Ponatinib	--	--	0.34	768

<sup>a</sup> Observed 39% inhibition at the maximum tested dose of 30 nM

We were somewhat surprised to see that the outlying compound **5.17c** did not meet either criterion even though the calculated probability scores did not appear markedly lower than the higher ranked compounds **5.17a** and **b**. Currently we have no particularly compelling rationalization for this, and perhaps a more exhaustive evaluation of those compounds ranked between 1 and 12 would allow for a more substantive conclusion to be drawn in terms of how low a structure's probability score or rank can go and it still be reasonable to pursue. In effect, this compound had a 48.55% probability of failing to meet both criteria and did. We are left to wonder whether the structures ranked slightly better or worse than **5.17c** would have likewise failed to meet one or both criteria.

With the algorithm having provided two very intriguing compounds, we further profiled **5.17a** and **b** against other relevant preclinical drug discovery targets of interest, including ADME and toxicology readouts (*e.g.*, inhibition of CYP3A4, cellular cytotoxicity, stability in liver microsomes,) as

well as a screening panel for kinome selectivity. Representative data are shown in Tables 5.5 and 5.6, respectively. Our compounds compare favorably to nilotinib in each ADME category, with an order of magnitude improvement in CYP3A4 inhibition, negligible cytotoxicity against liver and kidney epithelial cells, and improved stability in mouse and human liver microsomes. The careful reader will note that ponatinib showed even better results in these ADME assays than our analogs. However, ponatinib still suffers from submicromolar potency against hERG, which the algorithm improved upon, and carries an even more pernicious cardiac liability with its black box warning for vascular occlusion, heart failure, and hepatotoxicity.<sup>33-35</sup> The molecular culprit of these issues is not fully identified, though some researchers have suggested activation of the Notch-1 signaling axis<sup>52</sup> as a potential cause while workers in the Lal lab point to inhibition of the cardiomyocyte pro-survival AKT/PKB and ERK signaling pathways.<sup>53</sup> In these and other studies, ponatinib was found to be the most cardiotoxic TKI studied among the 50+ approved drugs for CML.<sup>54</sup>

**Table 5.5.** ADMET redouts of successful dual-NBN compounds compared to FDA-approved inhibitors

Compound ID	CYP3A4 IC <sub>50</sub> ( $\mu\text{M}$ )	THLE-3 CC <sub>50</sub> ( $\mu\text{M}$ )	HEK293 CC <sub>50</sub> ( $\mu\text{M}$ )	Mouse LM <sup>a</sup> <i>t</i> <sub>1/2</sub> (min)	Human LM <sup>a</sup> <i>t</i> <sub>1/2</sub> (min)
<b>5.17a</b>	7.28	>50	>50	16.78	39.84
<b>5.17b</b>	5.58	17.0	14.5	10.95	26.87
Nilotinib	0.58	--	--	7.89	7.89
Ponatinib	11.4	--	--	31.94	182.4

<sup>a</sup>LM: liver microsome

This is not altogether surprising; because of the high structural homology of the ATP-binding pockets of kinases, all c-Abl inhibitors run the risk of inhibiting other kinases.<sup>55</sup> However, inhibition of multiple kinases may not necessarily be deleterious, as Fowler *et al.* have demonstrated that inhibition of the Discoidin Domain Receptors (DDR1/2), the platelet-derived growth factor receptor  $\alpha$  and  $\beta$  (PDGFRs) and the tyrosine kinase, Src, potentiate the effect of c-Abl inhibition.<sup>56</sup> To evaluate the kinase inhibition profiles of **5.17a** and **b**, we had them screened at 10  $\mu\text{M}$  concentrations alongside nilotinib and ponatinib against the panel of >300 kinases maintained by the University of

**Table 5.6.** Percent activity remaining [and IC<sub>50</sub> values] of dual-NBN compounds and FDA-approved inhibitors against selected screened kinases

KINASE	% Activity remaining <sup>a</sup>		% Activity remaining <sup>a</sup> [IC <sub>50</sub> (μM)]	
	Nilotinib	Ponatinib	5.17a	5.17b
ABL	2	1	8 [0.0031]	11 [0.0013]
DDR2	4	3	70 [>20]	14 [0.2862]
PDGFRα	56	25	10 [0.0021]	16 [0.0020]
SRC	74	11	23 [0.7097]	15 [0.4313]
EPHB2	25	2	2 [0.0932]	1 [0.0708]
EPHB3	52	1	6 [0.0505]	5 [0.0195]
ERK1	>100	>100	>100	99
ERK2	>100	>100	>100	>100
ERK5	70	41	43	48
ERK8	63	41	67	81
LCK	37	29	22 [0.0908]	17 [0.0261]
EPHA4	23	4	6 [0.1381]	2 [0.0846]
NEK6	97	52	45 [3.3060]	9 [5.3500]
PKBa	>100	49	80	91
PKBb	94	35	59	38
VEGFR	75	28	14 [0.0336]	13 [0.0448]
MAP4K3	107	2	62 [>20]	14 [0.2404]

<sup>a</sup> Screened at a single 10 μM dose to record % activity remaining

Dundee;<sup>57-59</sup> Table 5.6 shows the percent activity remaining of selected kinases, as well as the IC<sub>50</sub> values for our compounds. This screen revealed that at a 10 μM dose, nilotinib inhibited 9 kinases at >50%, ponatinib inhibited 73 kinases, while compounds **5.17a** and **b** were intermediate, inhibiting 42 and 31 kinases, respectively. Follow up dose-response curves showed compound **5.17a** was very potent against PDGFRα, modestly inhibited Src, but did not inhibit DDR2. Conversely, compound **5.17b** inhibited PDGFRα, Src and DDR2. In consideration of the Lal lab's work mentioned above, the table also highlights the data against ERK and PKB isoforms by these compounds. None show

inhibition of ERK1 or 2 at 10  $\mu$ M, but all show 19-59% inhibition of ERK5 and 8, with ponatinib being the most (and equally) efficacious against both. Similarly, ponatinib showed 51% and 65% inhibition against PKBa and PKBb, while nilotinib showed little to none. Our compounds showed between 9-20% inhibition of PKBa and 41-64% inhibition of PKBb. At the writing of this dissertation, our team is currently in talks with the Lal lab to have our lead compounds **5.17a** and **b** assessed by them for these same potential cardiotoxic liabilities associated with ponatinib. Incidentally, a group at Stanford very recently published hybrid molecules of ponatinib and nilotinib which they suggest show improved safety toward cardiomyocytes, also at a cost to on-target potency.<sup>60</sup>

Since our algorithm was not trained to predict CYP inhibition or kinase selectivity, we consider these features to be fortuitous. Moreover, since the structure of each compound encodes its intrinsic response in a given measurement, the structural similarities of our compounds to ponatinib undoubtedly bias them to have somewhat comparable on- and off-target profiles. These off-target profiles were not anticipated at the time of algorithm design and serve to highlight the important role serendipity often plays in drug development. However, given the success of the algorithm to provide lead-optimized compounds with desired on- and off-target profiles, key biological experiments were justified that would dictate the utility of our compounds. In particular, the BBB penetrance and cerebrospinal fluid concentration that can be achieved by **5.17a** and **b** would be integral to their efficacy in animal models of PD, and this is a key datapoint which we attempted to address in the *in vivo* PK studies described below (*vide infra*). Most importantly to the experiment at hand, by using our algorithm, not only were we again able to accelerate the hit-to-lead optimization of yet another chemically distinct set of inhibitors, we also simultaneously addressed multiple defects in the properties of one of the most advanced clinical agents, including especially attenuating cardiotoxic blockade of the off-target hERG channel. The work reported here boded well for the potential utility of the compounds designed in this study to treat Parkinson's disease, and our next step was to interrogate their *in vivo* pharmacokinetics.

### 5.2.6 *In vivo* Pharmacokinetic Evaluation of 5.17a and 5.17b

Given the promising *in vitro* profile described in the previous sections, our team was awarded a grant from the American Parkinson's Disease Association to evaluate the *in vivo* PK of these compounds in mice. At the time the grant was written, we were intending to recapitulate the efficacy studies in mouse models which had advanced nilotinib to clinical trials with whichever of our lead compounds had the superior PK profile.<sup>16, 17, 22, 24-26</sup> We therefore designed two *in vivo* studies—one sought to plot the concentration of compound in the plasma as a function of time and thereby establish standard pharmacokinetic parameters (*e.g.*, AUC,  $C_{\max}$ ,  $t_{\max}$ ,  $t_{1/2}$ , etc.); the other would inform a maximum tolerated dose (MTD) of orally administered drug. Both were carried out by a CRO.

The first, more complex study had two arms—one arm measured systemic exposure (AUC<sub>i.v.</sub>) by drawing plasma samples at specific timepoints post intravenous (i.v.) administration of either 5.17a, 5.17b, or nilotinib (3 mg/kg) and quantifying drug concentration at each time by tandem LC-MS/MS. The second arm would likewise analyze plasma draws at specified timepoints but after oral (p.o.) administration of each drug to establish oral exposure (AUC<sub>oral</sub>). Analyzing exposure after both oral and i.v. administration allows for a calculation of oral bioavailability (%F) according to Equation 5.1:<sup>43, 61, 62</sup>

$$\%F = \frac{AUC_{p.o.}}{AUC_{i.v.}} \times \frac{Dose_{i.v.}}{Dose_{p.o.}} \times 100 \quad (5.1)$$

Furthermore, each compound was investigated across three dose-escalating oral treatment groups (3, 10, and 30 mg/kg) to determine a dosing regimen for later *in vivo* efficacy studies. Additionally, brains were harvested at specified timepoints from a subset of animals in each oral treatment group to establish total brain-to-plasma concentration ratios (K<sub>p</sub>) as an indicator of BBB penetrance. The second study simply looked for clinical signs of acute distress or morbidity after oral doses of 75, 150, and 300 mg/kg of each compound, followed by a complete blood count (CBC) analysis.

Given nilotinib's clinical significance in our target indication, we decided to run both studies with our compounds in a head-to-head comparison with nilotinib. We were unable to examine

ponatinib concurrently due to cost restrictions. A full description of the experiments and all associated data are provided in supplemental appendices, but a summary of the PK parameters established from the i.v. and highest p.o. doses is shown in Table 5.7 (see also §5.3.3).

It is striking how much lower the exposure levels ( $C_0/C_{\max}$  and AUC) are for our test compounds compared to nilotinib at the same doses, resulting from substantially lower compound concentrations measured in the plasma at the same doses, regardless of route of administration. What could account for these lower plasma levels? It is possible that our compounds were significantly less soluble than nilotinib and simply precipitated once they were in an aqueous environment like the blood. With this hypothesis in mind, we measured the aqueous kinetic solubility of our compounds as well as nilotinib and ponatinib and found very similar limits of solubility with nephelometry (Table 5.8). In fact, at 19  $\mu\text{M}$  nilotinib was the least soluble compound in the series. Had plasma levels been low after only oral dosing, then we could point to poor gut absorption, but plasma levels are low even after i.v. dosing. In fact, comparing oral and i.v. exposure allowed for a %F calculation of >90% at the high dose. This indicates that the poor exposure is not a function of poor absorption and is instead related to distribution, metabolism, and/or excretion.

From the data on hand, it is difficult to make any legitimate claims about distribution. The parameter  $V_{\text{ss}}$  (volume of distribution) is a proportionality constant relating dose (mg) to plasma concentration (ng/mL),<sup>63</sup> and was calculated according to Equation 5.2:

$$V_{\text{ss}} \left( \frac{\text{L}}{\text{kg}} \right) = \text{MRT}(\text{min}) \times \text{Cl}_{\text{iv}} \left( \frac{\text{mL}}{\text{min} \cdot \text{kg}} \right) \quad (5.2)$$

where MRT is mean residence time and  $\text{Cl}_{\text{iv}}$  is *in vivo* clearance. It conceptually represents the affinity for a compound to partition into tissues of the body other than blood, thereby reducing the measurable concentration of compound in circulation. Our compounds give apparently large  $V_{\text{ss}}$  values which could rationalize the low measured concentration in the plasma. This rationalization, however, cannot be corroborated without quantifying the compound concentration in other tissues,

**Table 5.7.** Pharmacokinetic parameters calculated after a single bolus of the compounds of interest via i.v. (3 mg/kg) or oral (p.o.) administration.

Compound ID	Route	Dose (mg/kg)	T <sub>max</sub> (h)	<sup>a</sup> C <sub>0(max)</sub> (ng/mL)	AUC (h*ng/mL)	T <sub>1/2</sub> (h)	CL (mL/min/kg)	V <sub>ss</sub> (L/kg)	%F	MLM t <sub>1/2</sub> (min)	HLM t <sub>1/2</sub> (min)
Nilotinib	IV	3	0.08	16,200	12,300	2.78	4	0.59	-	7.89	10.1
	PO	30	8.00	9,800	149,000	2.82	-	-	>100		
5.17a	IV	3	-	319	119	0.15	NR (415)	6.40	-	11.0	28.7
	PO	30	8.00	224	1,680	-	-	-	>100		
5.17b	IV	3	-	1,420	446	0.80	111	3.66	-	16.8	39.8
	PO	30	2.00	765	4,090	-	-	-	92		

**Table 5.8.** Additional DMPK properties for lead compounds and FDA-approved inhibitors

Compound ID	Aq. Solubility ( $\mu\text{M}$ )	Plasma $t_{1/2}$ (min)	Brain Kp	Brain conc. <sup>a</sup> (ng/g)	Abl1 IC <sub>50</sub> (ng/mL)
5.17a	25	>240	0.09	14.1	3.34
5.17b	32	>240	0.14	63.7	2.92
Nilotinib	19	>240	0.04	353.8	3.13
Ponatinib	33	>240	--	--	0.18

<sup>a</sup> 4 hours post 30 mk/kg oral dose; BLQ at  $t = 24$  hours

which was beyond the scope of the current study. Note that  $V_{ss}$  is directly related to *in vivo* clearance ( $Cl_{iv}$ ) which was calculated to be incredibly high for our compounds according to Equation 5.3:

$$Cl_{iv} \left( \frac{\text{mL}}{\text{min} \cdot \text{kg}} \right) = \frac{\text{Dose (mg)}}{AUC(\text{h} \cdot \text{ng/mL})} \quad (5.3)$$

Clearly the high calculated  $Cl_{iv}$  results from the very low AUC. Considering Equations 5.2 and 5.3 together allows us to see that a high  $V_{ss}$  results from high clearance, itself a function of low AUC based on low measured plasma concentration levels. In other words, these parameters relatedly stem from the empirically low plasma concentration levels; they imply rather than explain the low exposure.

Conceptually, clearance is related to how quickly a compound is removed from circulation, which is not only a consequence of distribution into other tissues but also of chemical modification, or metabolism. Drug metabolism is generally divided into two phases, phase I and phase II. Phase I metabolism refers to those usually oxidative liver enzyme-catalyzed reactions that add nucleophilic handles onto the molecule (*e.g.*, hydroxyl groups) which are then used in subsequent phase II metabolism to conjugate the xenobiotic with large hydrophilic molecules (*e.g.*, glucuronic acid), increasing its polarity and aqueous solubility for eventual excretion through the kidneys. Our earlier *in vitro* profiling data examined the compounds' susceptibility to phase I metabolism with the liver microsome stability assay. As shown above in Table 5.5, both **5.17a** and **b** had greater stability than nilotinib as indicated by the longer half-lives in mouse liver microsomes (MLM). Additionally, we tested the compounds' susceptibility to cleavage by plasma esterases and peptidases by examining

stability in mouse plasma; all compounds showed little-to-no degradation over the 4-hour incubation (Table 5.8). This leaves phase II metabolism as the most likely culprit of depleting plasma concentration levels, likely through bioconjugation at one of the pyrazole nitrogen atoms. At the writing of this dissertation, our team is in the process of sending the compounds to be tested in whole mouse hepatocytes which, unlike microsomes, include the enzymes and co-factors necessary to see phase II metabolic degradation. Were we to see dramatically higher intrinsic clearance of our compounds in the mouse hepatocyte relative to nilotinib, this would rationalize well the lower systemic exposure we saw in mice and suggest a potential rescue strategy. If not, then the question would remain as to why there is so little compound detected in the plasma of mice, and exceedingly rapid renal elimination of the unmodified parent compounds would then be the leading hypothesis.

One encouraging piece of data which emerged from this study relates to the compounds' ability to cross the BBB and partition into the brain. In spite of the poor systemic exposure, the total brain concentration data show *ca.* 14 ng/mL and 64 ng/mL in the brain 4 hours post 30 mg/kg oral dosing of **5.17a** and **b**, respectively, which covers c-Abl IC<sub>50</sub> levels (see Table 5.8 above). It is also true that nilotinib showed >5-fold higher brain concentration than our best compound, clearly related to the much higher concentration in systemic circulation. When exposure is taken into account, however, our compounds have a slightly higher K<sub>p</sub> than nilotinib (Table 5.8). Additionally, no signs of morbidity were observed with any compound at the highest tested oral dose, indicating an MTD of >300 mg/kg.

Overall, the *in vivo* PK data on our lead compounds **5.17a** and **b** in mouse are relatively poor compared to nilotinib. This appears to be a liability associated with the ponatinib pharmacophore; though we have not established our own data in the same experiment, the literature shows the preclinical *in vivo* PK data on ponatinib is also poor compared to nilotinib.<sup>43, 61, 62</sup> Based on the above mouse PK experiment alone, it is not clear that our lead compounds would have a long enough residence time to show a positive outcome in an *in vivo* mouse model of Parkinson's disease.

However, mice are not the only species for which a valid PD efficacy study exists. Our collaborator at the Emory Medical School, Dr. Stella Papa, is an expert in the 6-hydroxydopamine (6-OHDA) neurotoxin lesion model of PD in rats and is interested in testing our lead compound for efficacy in this model.<sup>64</sup> Briefly, 6-OHDA is surgically injected into the nigrostriatal pathway leading to accumulation in dopaminergic neurons. There, it produces cytotoxic reactive oxygen species (ROS) that cause neuronal damage, degeneration, and death, ultimately leading to motor deficits analogous to those induced by PD.<sup>64</sup> Since c-Abl activity is abnormally increased in response to oxidative stress,<sup>65</sup> the 6-OHDA model is well-suited to test whether a c-Abl inhibitor like ours can play a therapeutically relevant role in functional and pathological outcomes vis-à-vis motor behavior and cell loss. It is her opinion that a positive outcome in this model would make a very compelling case to advance into the next stage of preclinical development, namely IND-enabling studies in a non-human primate. Therefore, we are currently in discussions with the same CRO who ran our mouse PK studies to establish the PK profile of **5.17a** and **b** in rats (along with both nilotinib and ponatinib).

In retrospect, it is worth contemplating whether or not it was strategically wise to limit our synthetic target list to only those structures exactly as they were provided by our machine learning algorithm. For example, reexamining Figure 5.2 and Table 5.3, one can imagine taking a “mix and match” approach to the C and D ring components such that the sixth or eighth ranked D ring structure is considered, but on the Cl instead of the cPr scaffold. While this seems like a reasonable way to easily expand the compound library, the point of the algorithm is that the machine considers these combinatorial options and assigns a probability score to them so that the chemist can streamline their list of high-priority synthetic targets to push to development. The answer is less straightforward when one considers modifying a suggested structure in a way that may be intuitive to a medicinal chemist but not necessarily to the machine. For example, could our lead structures **5.17a** and **b** not be modified to take away the H-bond donor of the pyrazole, perhaps by methylating or acylating it, or replacing the NH altogether with an alternate atom like carbon, oxygen, or sulfur? And could the

halogen on the C ring not be “walked” around the ring to find a more optimum position? Or perhaps multiple halogens would be better? Scientifically, the need to make structures modified by “chemist’s intuition” could be said to diminish the utility of the algorithm in accomplishing its task. However, it would be challenging to anticipate this need *a priori*. At the outset, we wished to determine how reliably the machine could suggest structures which met two user-defined criteria simultaneously. Here we needed to lean on the substantial QSARs utilized to train the NBNs to feel confident that the machine suggested the best compounds it was capable of suggesting. But the machine is limited. If no SAR exists about a particular substitution on which to train the machine, then the machine will have no way to predict it. This was the case in our RSV F protein inhibitor project where newly established SAR that was absent from the training set enjoyed substantial potency gains by adding an aryl bromide to a location the machine was not trained to consider.<sup>66,67</sup> It therefore bears keeping in mind that the machine is only as good as the training set it is given. Furthermore, if a building block is not available in a commercial database, the machine cannot suggest it.

Hence, there is certainly room for human ingenuity, but care must be taken to limit the “what if’s.” How does a chemistry team rank their intuitive hypotheses, and how many of those hypotheses is a lead optimization program willing to test? Herein lies the true value of the algorithm – it not only gives the team molecular inspiration but also a quantitative way to evaluate it. Knowing what we know now about the lead analogs suggested by the algorithm, perhaps now is the time to apply the medicinal chemist’s intuition to further optimize the PK properties of these molecules to push them forward through development.

## 5.3 MATERIALS AND METHODS

### 5.3.1 Synthetic Chemistry

#### 5.3.1.1 General Considerations

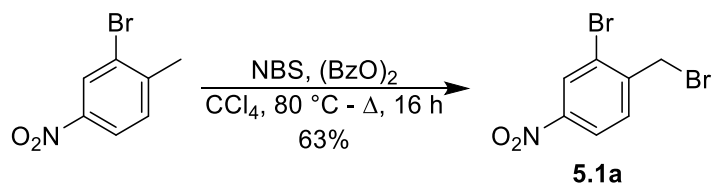
All reactions were performed by the synthesis team consisting of Dr. Thomas Kaiser, Zack Dentmon, or Christopher Dalloul (a student under the supervision of Zack Dentmon). All commercially available starting materials were purchased and used as provided unless otherwise specified. When anhydrous conditions are indicated, anhydrous solvents were used from commercial suppliers. Automated flash column chromatography was performed using a Teledyne ISCO CombiFlash Companion system with silica gel-packed columns (RediSep® R<sub>f</sub>). Analytical thin-layer chromatography (TLC, commercially available from VWR) was carried out on Merck aluminum-supported silica gel plates (thickness: 200 μm) with fluorescent indicator (F-254). Visualization of compounds on TLC plates was accomplished with UV light (254 nm) and/or with phosphomolybdic acid, ninhydrin, ceric ammonium molybdate, or potassium permanganate staining. NMR spectra (<sup>1</sup>H and <sup>13</sup>C) were obtained in the Emory University NMR Research Center, directed by Dr. Shaoxiong Wu and Dr. Bing Wang, using either a Bruker INFINITY II 600 MHz spectrometer with cryogenic probe (funded by NSF grant CHE-1531620), a Varian INOVA 500 MHz spectrometer, a Varian INOVA 400 MHz spectrometer, or a Varian VNMR 400 MHz spectrometer. NMR samples were prepared and processed in deuterated chloroform (CDCl<sub>3</sub>), deuterated MeOH (CD<sub>3</sub>OD), deuterated DMSO (*d*<sub>6</sub>-DMSO), or deuterated acetone (*d*<sub>6</sub>-acetone) using the residual solvent peak (CDCl<sub>3</sub>: <sup>1</sup>H = 7.26 ppm, <sup>13</sup>C = 77.16 ppm; CD<sub>3</sub>OD: <sup>1</sup>H = 3.31 ppm, <sup>13</sup>C = 49.00 ppm; *d*<sub>6</sub>-DMSO: <sup>1</sup>H = 2.50 ppm, <sup>13</sup>C = 39.52 ppm; *d*<sub>6</sub>-acetone: <sup>1</sup>H = 2.05 ppm, <sup>13</sup>C = 29.84 ppm) as an internal reference. NMR data are reported to include chemical shifts (δ) reported in ppm, multiplicities indicated as s (singlet), d (doublet), t (triplet), q (quartet), m (multiplet), or br s (broad singlet), coupling constants (*J*) reported in Hz, and integration normalized to 1 atom. High resolution mass spectrometry (HRMS) was performed by the Emory University Mass Spectrometry Center, directed by Dr. Fred Strobel. Liquid chromatography-mass

spectrometry (LC-MS) was performed on an Agilent 1200 HPLC equipped with a 6120 Quadrupole mass spectrometer (ESI-API) eluting at a rate of 1.00 mL/min with mixtures of HPLC grade MeOH and water or acetonitrile and water (all spiked with 0.1% formic acid) through an analytical, reverse-phase, Agilent C18 XDB eclipse column (50 mm x 4.6 mm, 3.5  $\mu$ M). LC-MS samples were prepared in a solution of 75:25 MeOH/water or 50:50 acetonitrile/water (spiked with 0.1% formic acid), and ultraviolet activity was monitored at 254 nm. Final compound purity was assessed to be  $\geq$ 95% pure using  $^1\text{H}$  NMR and LC-MS.

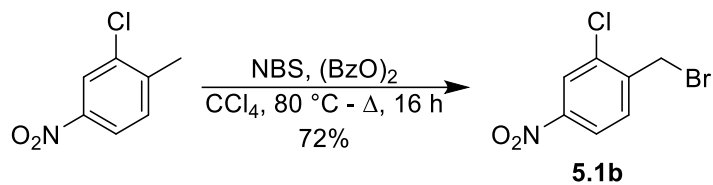
### 5.3.1.2 Synthetic Procedures

*Safety Statement:* No unexpected or unusually high safety hazards were encountered. Lab coats, goggles, gloves, and other PPE as appropriate were used at all times, and all synthetic experiments were performed in a fumehood.

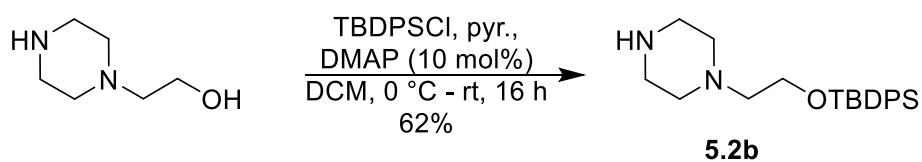
#### 5.3.1.2.1 Synthesis of Single-NBN Compounds (Scheme 5.1)



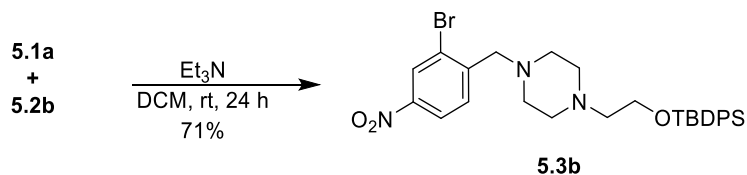
**2-bromo-1-(bromomethyl)-4-nitrobenzene (5.1a)** To a stirred, heated (80 °C) solution of 2-bromo-4-nitrotoluene (10.0 g, 46.3 mmol) and *N*-bromosuccinimide (8.24 g, 46.2 mmol) in anhydrous carbon tetrachloride (12 mL) was added, under argon, benzoyl peroxide (224 mg, 0.69 mmol, 75% pure), and the resulting mixture was heated to reflux overnight. After cooling to room temperature, the mixture was diluted with Et<sub>2</sub>O, water was added, and the phases were separated. The aqueous layer was extracted with Et<sub>2</sub>O, and the combined organic phases were dried with Na<sub>2</sub>SO<sub>4</sub>. After filtration and evaporation of the solvent, the residue was purified by column chromatography (0-40% EtOAc in hexanes) to give pure 2-bromo-4-nitrobenzyl bromide as a yellow solid (8.5 g, 63% yield).  $^1\text{H}$  NMR (400 MHz, CDCl<sub>3</sub>)  $\delta$  8.45 (d,  $J$  = 2.3 Hz, 1H), 8.16 (dd,  $J$  = 8.5, 2.3 Hz, 1H), 7.65 (d,  $J$  = 8.5 Hz, 1H), 4.62 (s, 2H) ppm.<sup>68</sup>



**1-(bromomethyl)-2-chloro-4-nitrobenzene (5.1b)** To a stirred, heated (80 °C) solution of 2-chloro-4-nitrotoluene (7.9424 g, 46.3 mmol) and *N*-bromosuccinimide (8.24 g, 46.2 mmol) in anhydrous carbon tetrachloride (12 mL) was added, under argon, benzoyl peroxide (224 mg, 0.69 mmol, 75% pure), and the resulting mixture was heated to reflux overnight. After cooling to room temperature, the mixture was diluted with Et<sub>2</sub>O, water was added, and the phases were separated. The aqueous layer was extracted with Et<sub>2</sub>O, and the combined organic phases were dried with Na<sub>2</sub>SO<sub>4</sub>. After filtration and evaporation of the solvent, the residue was purified by column chromatography (0-10% EtOAc in hexanes) to give pure 2-chloro-4-nitrobenzyl bromide as a yellow oil (8.3 g, 72% yield). <sup>1</sup>H NMR (400 MHz, CDCl<sub>3</sub>) δ 8.28 (d, *J* = 2.3 Hz, 1H), 8.12 (dd, *J* = 8.5, 2.3 Hz, 1H), 7.64 (d, *J* = 8.5 Hz, 1H), 4.60 (s, 2H) ppm.

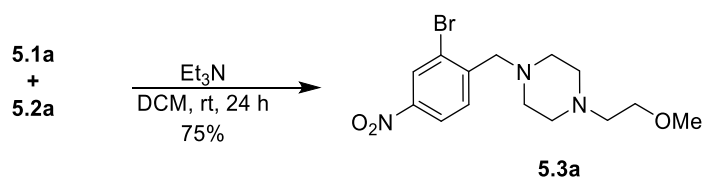


**tert-butyl-diphenyl-(2-piperazin-1-ylethoxy)silane (5.2b)** 2-(piperazin-1-yl)ethanol (15 g, 115.2 mmol) was dissolved in CH<sub>2</sub>Cl<sub>2</sub> (520 mL) under argon, and pyridine (14 mL, 172.8 mmol) followed by DMAP (1.41 g, 11.5 mmol) were added. The reaction was cooled to 0 °C and *tert*-butylchlorodiphenylsilane (36 mL, 138.3 mmol) was added to the solution. The reaction mixture was allowed to warm to ambient temperature and stirred overnight. The next day, the reaction mixture was concentrated under reduced pressure and the concentrate was purified by column chromatography (0-10% MeOH in CH<sub>2</sub>Cl<sub>2</sub>) to give the title product (26.4 g, 62% yield). <sup>1</sup>H NMR (400 MHz, CDCl<sub>3</sub>) δ 9.60 (br s, 2H), 7.65 (dd, *J* = 7.7, 1.3 Hz, 4H), 7.45-7.36 (m, 6H), 3.80 (s, 2H), 3.21 (s, 4H), 2.89 (s, 4H), 2.66 (s, 2H), 1.03 (s, 9H) ppm.



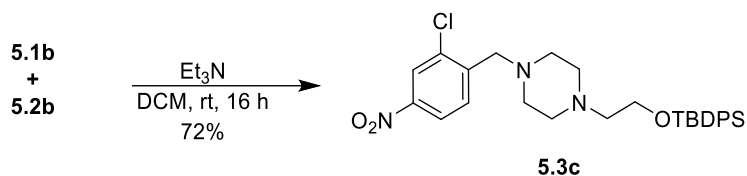
### 2-[4-[(2-bromo-4-nitro-phenyl)methyl]piperazin-1-yl]ethoxy-*tert*-butyl-diphenyl-silane

**(5.3b)** To a solution of 2-bromo-5-nitro-bromomethyl benzene (2.4 g, 8.14 mmol) in CH<sub>2</sub>Cl<sub>2</sub> (8.1 mL) was added NEt<sub>3</sub> (1.13 mL, 8.14 mmol) and *tert*-butyl-diphenyl-(2-piperazin-1-ylethoxy)silane (3 g, 8.14 mmol) under argon, and the reaction stirred at ambient temperature with monitoring by TLC. After approx. 24 hours, a saturated aqueous solution of NaHCO<sub>3</sub> was added and diluted with water, and the mixture was extracted with CH<sub>2</sub>Cl<sub>2</sub>. The combined organic layer was dried over Na<sub>2</sub>SO<sub>4</sub>, filtered, concentrated, and the resulting residue was purified by silica gel chromatography (0-20% EtOAc in hexanes) to provide the product as an orange oil (3.35 g, 71% yield). <sup>1</sup>H NMR (400 MHz, CDCl<sub>3</sub>) δ 8.41 (d, *J* = 2.2 Hz, 1H), 8.15 (dd, *J* = 8.5, 2.2 Hz, 1H), 7.71 (d, *J* = 8.5 Hz, 1H), 7.68 (dd, *J* = 7.7, 1.4 Hz, 4H), 7.45 – 7.35 (m, 6H), 3.82 (t, *J* = 5.9 Hz, 2H), 3.63 (s, 2H), 2.66 – 2.49 (m, 10H), 1.04 (s, 9H) ppm; <sup>13</sup>C NMR (101 MHz, CDCl<sub>3</sub>) δ 147.2, 145.7, 135.7, 133.7, 130.7, 129.8, 127.9, 127.8, 124.3, 122.3, 61.6, 60.3, 53.8, 53.3, 31.1, 27.0, 19.3 ppm; HRMS (APCI) *m/z* calcd for C<sub>29</sub>H<sub>36</sub>O<sub>3</sub>N<sub>3</sub>BrSi+H<sup>+</sup>: 582.1782 [M+H]<sup>+</sup>; found 582.1786.



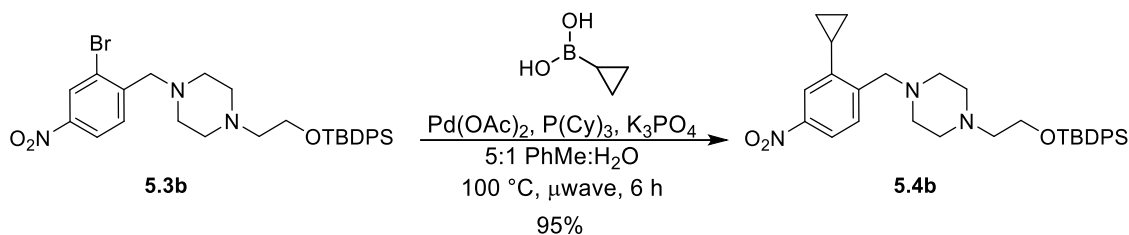
**1-[(2-bromo-4-nitro-phenyl)methyl]-4-(2-methoxyethyl)piperazine (5.3a)** To a solution of 2-bromo-5-nitro-bromomethyl benzene (2.4 g, 8.14 mmol) in CH<sub>2</sub>Cl<sub>2</sub> (8.1 mL) was added NEt<sub>3</sub> (1.13 mL, 8.14 mmol) and 1-(2-methoxyethyl)piperazine (1.17 g, 8.14 mmol) under argon. The reaction stirred at ambient temperature with monitoring by TLC. After approx. 24 hours, the reaction was quenched with saturated aqueous NaHCO<sub>3</sub> solution and diluted with water, and the mixture was extracted with CH<sub>2</sub>Cl<sub>2</sub>. The combined organic layer was dried over Na<sub>2</sub>SO<sub>4</sub>, filtered, concentrated, and

the resulting residue was purified by silica gel chromatography (0-30% MeOH in CH<sub>2</sub>Cl<sub>2</sub> with 1% NEt<sub>3</sub>) to afford the desired product as a yellow oil (2.19 g, 75% yield). <sup>1</sup>H NMR (400 MHz, CDCl<sub>3</sub>) δ 8.41 (d, *J* = 2.3 Hz, 1H), 8.14 (dd, *J* = 8.5, 2.3 Hz, 1H), 7.72 (d, *J* = 8.5 Hz, 1H), 3.64 (s, 2H), 3.52 (t, *J* = 5.6 Hz, 2H), 3.35 (s, 3H), 2.71 – 2.46 (m, 10H) ppm; <sup>13</sup>C NMR (101 MHz, CDCl<sub>3</sub>) δ 147.2, 145.7, 130.7, 127.9, 124.3, 122.2, 70.2, 61.5, 59.1, 58.0, 53.7, 53.2 ppm; HRMS (APCI) *m/z*: calcd for C<sub>14</sub>H<sub>20</sub>O<sub>3</sub>N<sub>3</sub>Br+H<sup>+</sup>; 358.0761 [M+H]<sup>+</sup>; found 358.0759.

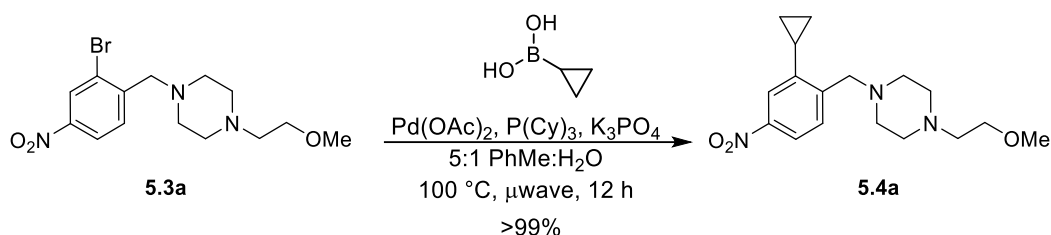


***tert*-butyl-[2-[4-[(2-chloro-4-nitro-phenyl)methyl]piperazin-1-yl]ethoxy]-diphenyl-silane**

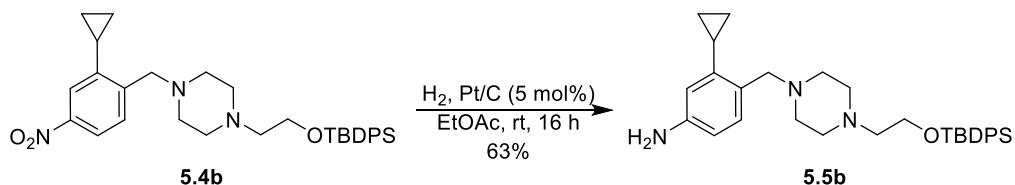
**(5.3c)** To a solution of 2-chloro-5-nitro-bromomethyl benzene (2.04 g, 8.14 mmol) in CH<sub>2</sub>Cl<sub>2</sub> (8.1 mL) was added NEt<sub>3</sub> (1.13 mL, 8.14 mmol) and *tert*-butyl-diphenyl-(2-piperazin-1-ylethoxy)silane (3 g, 8.14 mmol) under argon. The reaction was allowed to stir at ambient temperature overnight. After 16h, a saturated aqueous solution of NaHCO<sub>3</sub> was added and diluted with water, and the mixture was extracted with CH<sub>2</sub>Cl<sub>2</sub>. The combined organic layer was dried over Na<sub>2</sub>SO<sub>4</sub>, filtered, concentrated, and the resulting residue was purified by silica gel chromatography (0-20% EtOAc in hexanes) to afford the product as an orange oil (3.17 g, 72% yield). <sup>1</sup>H NMR (400 MHz, CDCl<sub>3</sub>) δ 8.23 (d, *J* = 2.3 Hz, 1H), 8.10 (dd, *J* = 8.5, 2.3 Hz, 1H), 7.73 (d, *J* = 8.5 Hz, 1H), 7.68 (dd, *J* = 7.8, 1.6 Hz, 4H), 7.45 – 7.35 (m, 6H), 3.81 (t, *J* = 6.1 Hz, 2H), 3.65 (s, 2H), 2.61 (t, *J* = 6.1 Hz, 2H), 2.54 (br s, 8H), 1.04 (s, 9H) ppm; <sup>13</sup>C NMR (101 MHz, CDCl<sub>3</sub>) δ 147.2, 144.1, 135.7, 134.8, 133.8, 130.7, 129.8, 127.8, 124.7, 121.7, 62.2, 60.3, 59.1, 53.9, 53.4, 27.0, 19.3 ppm; HRMS (APCI): *m/z* calcd for C<sub>29</sub>H<sub>37</sub>N<sub>3</sub>O<sub>3</sub>ClSi+H<sup>+</sup>: 538.2287 [M+H]<sup>+</sup>; found: 538.2289.



**tert-butyl-[2-[4-[(2-cyclopropyl-4-nitrophenyl)methyl]piperazin-1-yl]ethoxy]-diphenyl-silane (5.4b)** A solution of 2-[4-[(2-bromo-4-nitrophenyl)methyl]piperazin-1-yl]ethoxy-*tert*-butyl-diphenyl-silane (1.75 g, 3.0 mmol), cyclopropylboronic acid (0.773 g, 9.0 mmol), potassium phosphate tribasic (2.87 g, 13.5 mmol), palladium(II) acetate (67 mg, 0.3 mmol), and tricyclohexylphosphine (0.168 g, 0.6 mmol) in toluene (15 mL) and water (3 mL) was degassed with argon and then heated to 100 °C via microwave irradiation for approx. 6 hours. The reaction was quenched with saturated aqueous NaHCO<sub>3</sub> solution and extracted with CH<sub>2</sub>Cl<sub>2</sub>. The organics were dried over Na<sub>2</sub>SO<sub>4</sub>, filtered and concentrated. The material was purified via flash column chromatography (0-30% MeOH in CH<sub>2</sub>Cl<sub>2</sub>) to yield the product as an orange solid (1.55 g, 95% yield). <sup>1</sup>H NMR (400 MHz, CDCl<sub>3</sub>) δ 7.99 (dd, *J* = 8.4, 2.3 Hz, 1H), 7.83 (d, *J* = 2.3 Hz, 1H), 7.70 – 7.66 (m, 4H), 7.53 (d, *J* = 8.4 Hz, 1H), 7.45 – 7.35 (m, 6H), 3.81 (t, *J* = 6.2 Hz, 2H), 3.70 (s, 2H), 2.60 (t, *J* = 6.2 Hz, 2H), 2.50 (s, 8H), 2.15 (tt, *J* = 8.4, 5.4 Hz, 1H), 1.04 (s, 9H), 1.04 – 1.00 (m, 2H), 0.74 – 0.70 (m, 2H) ppm; <sup>13</sup>C NMR (101 MHz, CDCl<sub>3</sub>) δ 147.3, 145.8, 144.0, 135.7, 133.8, 129.9, 129.8, 127.8, 120.8, 120.7, 62.3, 60.3, 59.8, 54.0, 53.5, 27.0, 19.3, 12.9, 7.8 ppm; HRMS (APCI) *m/z* calcd for C<sub>32</sub>H<sub>43</sub>O<sub>3</sub>N<sub>3</sub>Si+H<sup>+</sup>: 544.2990 [M+H]<sup>+</sup>; found 544.2990.



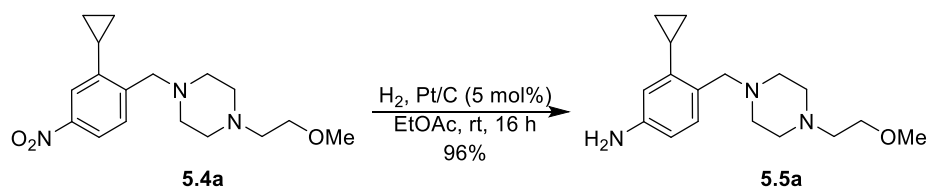
**1-[(2-cyclopropyl-4-nitro-phenyl)methyl]-4-(2-methoxyethyl)piperazine (5.4a)** In a 20 mL microwave vial, a yellow solution of 1-[(2-bromo-4-nitro-phenyl)methyl]-4-(2-methoxyethyl)piperazine (1.07 g, 3 mmol), cyclopropylboronic acid (0.77 g, 9 mmol), potassium phosphate (tribasic) (2.87 g, 13.5 mmol), palladium(II) acetate (0.07 g, 0.30 mmol), and tricyclohexylphosphine (0.17 g, 0.60 mmol) in toluene (15 mL) and water (3 mL) was degassed with argon for ~30 minutes before being heated at 100 °C overnight for 12 hours via microwave irradiation whereupon the reaction changed to a dark black-green color. The reaction was diluted with EtOAc and quenched with saturated sodium bicarbonate solution before the product was extracted with EtOAc then CH<sub>2</sub>Cl<sub>2</sub>. The organic extracts were combined and dried over Na<sub>2</sub>SO<sub>4</sub> before the solids were filtered over a pad of Celite; the yellow filtrate was concentrated to ~1.4 g of yellow oil which was purified via silica gel flash column chromatography (0-15% MeOH in CH<sub>2</sub>Cl<sub>2</sub>) to afford the desired product (0.992 g, >99% yield). <sup>1</sup>H NMR (400 MHz, CDCl<sub>3</sub>)  $\delta$  7.98 (dd,  $J$  = 8.4, 2.4 Hz, 1H), 7.83 (d,  $J$  = 2.4 Hz, 1H), 7.53 (d,  $J$  = 8.4 Hz, 1H), 3.71 (s, 2H), 3.51 (t,  $J$  = 5.6 Hz, 2H), 3.35 (s, 3H), 2.59 (t,  $J$  = 5.6 Hz, 2H), 2.55 (br s, 8H), 2.19 – 2.12 (m, 1H), 1.06 – 0.99 (m, 2H), 0.74 – 0.69 (m, 2H) ppm; <sup>13</sup>C NMR (100 MHz, CDCl<sub>3</sub>)  $\delta$  147.7, 145.8, 144.0, 129.9, 120.8, 120.7, 70.3, 59.7, 59.0, 58.0, 53.8, 53.4, 12.9, 7.8 ppm; HRMS (ESI)  $m/z$ : [M + H]<sup>+</sup> Calcd for C<sub>17</sub>H<sub>26</sub>N<sub>3</sub>O<sub>3</sub> 320.19687; found 320.19648.



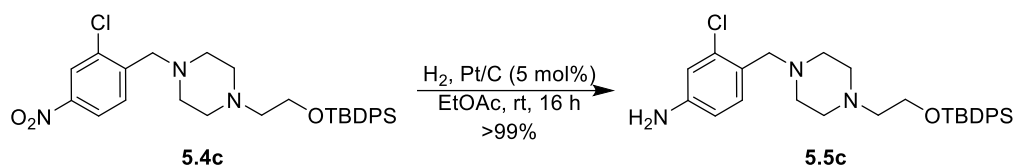
**4-[[4-[2-[*tert*-butyl(diphenyl)silyl]oxyethyl]piperazin-1-yl]methyl]-3-cyclopropyl-aniline**

**(5.5b)** A solution of *tert*-butyl-[2-[4-[(2-cyclopropyl-4-nitro-phenyl)methyl]piperazin-1-yl]ethoxy]-diphenyl-silane (1.55 g, 2.85 mmol) in EtOAc (61 ml) was catalytically hydrogenated over 5%

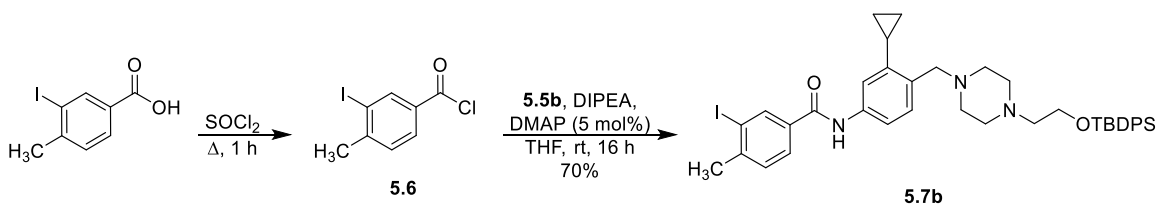
platinum on carbon (489 mg, 0.1254 mmol) under a balloon of H<sub>2</sub> gas at ambient temperature overnight. The reaction mixture was filtered through Celite, and the filtrate was concentrated to give the desired material as a green residue (0.93 g, 63% yield. <sup>1</sup>H NMR (400 MHz, CDCl<sub>3</sub>) δ 7.72 – 7.66 (m, 4H), 7.46 – 7.35 (m, 6H), 7.05 (d, *J* = 8.0 Hz, 1H), 6.47 (dd, *J* = 8.0, 2.2 Hz, 1H), 6.32 (d, *J* = 2.2 Hz, 1H), 3.82 (t, *J* = 6.4 Hz, 2H), 3.56 (br s, 2H), 3.54 (s, 2H), 2.60 (t, *J* = 6.4 Hz, 1H), 2.50 (br s, 8H), 2.16 (m, 1H), 1.06 (s, 9H), 0.91 – 0.87 (m, 1H), 0.65 – 0.58 (m, 1H) ppm; <sup>13</sup>C NMR (101 MHz, CDCl<sub>3</sub>) δ 145.5, 143.5, 135.7, 133.8, 131.1, 129.7, 127.8, 127.7, 112.2, 112.1, 62.3, 60.4, 60.0, 54.1, 53.3, 26.9, 19.3, 12.7, 7.4 ppm; HRMS (APCI) *m/z*: calcd for C<sub>32</sub>H<sub>43</sub>ON<sub>3</sub>Si+H<sup>+</sup>: 514.3248 [M+H]<sup>+</sup>; found 514.3252.



**3-cyclopropyl-4-[[4-(2-methoxyethyl)piperazin-1-yl]methyl]aniline (5.5a)** In a 200 mL round-bottom flask was 1-[(2-cyclopropyl-4-nitro-phenyl)methyl]-4-(2-methoxyethyl)piperazine (6.0 mL, 2.06 mmol). A stir bar and 3-way glass adapter were added, and the material was dried briefly before the flask was charged with argon, platinum on carbon (0.32 g, 0.08 mmol), and EtOAc (30 mL) to give a black suspension. The atmosphere was evacuated and restored with hydrogen gas, and the reaction stirred at ambient temperature overnight. The next day, the reaction mixture was filtered through Celite, and the filtrate was concentrated to give the desired material as a yellow oil (0.57 g, 96% yield). <sup>1</sup>H NMR (600 MHz, CDCl<sub>3</sub>) δ 7.02 (d, *J* = 8.0 Hz, 1H), 6.43 (dd, *J* = 8.0, 2.4 Hz, 1H), 6.28 (d, *J* = 2.4 Hz, 1H), 3.53 (s, 2H), 3.49 (t, *J* = 5.7 Hz, 2H), 3.32 (s, 3H), 2.55 (t, *J* = 5.7 Hz, 2H), 2.49 (br s, 8H), 2.14 – 2.09 (m, 1H), 0.87 – 0.84 (m, 2H), 0.59 – 0.56 (m, 2H) ppm; <sup>13</sup>C NMR (151 MHz, CDCl<sub>3</sub>) δ 145.5, 143.4, 131.0, 127.7, 112.2, 112.0, 70.1, 59.8, 58.9, 57.9, 53.8, 52.9, 12.6, 7.4 ppm; HRMS (APCI): *m/z* calcd for C<sub>17</sub>H<sub>27</sub>N<sub>3</sub>O+H<sup>+</sup>: 290.2227 [M+H]<sup>+</sup>; found 290.2224.

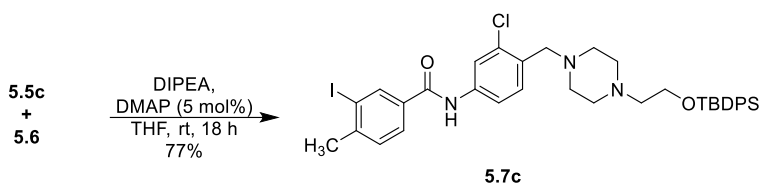


**4-[[4-[2-[*tert*-butyl(diphenyl)silyl]oxyethyl]piperazin-1-yl]methyl]-3-chloro-aniline (5.5c)** A solution of *tert*-butyl-[2-[4-[(2-chloro-4-nitro-phenyl)methyl]piperazin-1-yl]ethoxy]-diphenylsilane (3.17 g, 5.89 mmol) in EtOAc (125 ml) was catalytically hydrogenated over 5% platinum on carbon (1.011 g, 0.2592 mmol) under a balloon of H<sub>2</sub> gas at ambient temperature overnight. The reaction mixture was filtered through Celite, and the filtrate was concentrated to afford the desired product which was used as-is in the next step (quantitative crude yield). <sup>1</sup>H NMR (400 MHz, CDCl<sub>3</sub>) δ 7.71 – 7.67 (m, 4H), 7.45 – 7.35 (m, 6H), 7.17 (d, *J* = 8.2 Hz, 1H), 6.67 (d, *J* = 2.4 Hz, 1H), 6.53 (dd, *J* = 8.2, 2.4 Hz, 1H), 3.81 (t, *J* = 6.3 Hz, 2H), 3.68 (br s, 2H), 3.51 (s, 2H), 2.59 (t, *J* = 6.3 Hz, 2H), 2.51 (br s, 8H), 1.06 (s, 9H) ppm; HRMS (APCI): *m/z* calcd for C<sub>29</sub>H<sub>39</sub>N<sub>3</sub>OClSi+H<sup>+</sup>: 508.2545 [M+H]<sup>+</sup>; found: 508.2557.



***N*-[4-[[4-[2-[*tert*-butyl(diphenyl)silyl]oxyethyl]piperazin-1-yl]methyl]-3-cyclopropyl-phenyl]-3-iodo-4-methylbenzamide (5.7b)** 3-iodo-4-methylbenzoic acid (2.62 g, 10 mmol) was refluxed in thionyl chloride (10 mL) for 1 hr. The volatiles were removed, and the material was brought up in benzene (~10 mL). The solution was concentrated, and the material was placed on vacuum until solidification. The material was dissolved in 10 mL of THF. The resulting 3-iodo-4-methylbenzoyl chloride (1.8 mL, 1M in THF) was added to a solution of 4-[[4-[2-[*tert*-butyl(diphenyl)silyl]oxyethyl]piperazin-1-yl]methyl]-3-cyclopropyl-aniline (0.93 g, 1.81 mmol), DMAP (0.011 g, 0.091 mmol) and *N,N*-diisopropylethylamine (0.39 mL, 2.17 mmol) in THF (1.8 mL) under argon. The reaction stirred at ambient temperature overnight and was followed by TLC. The

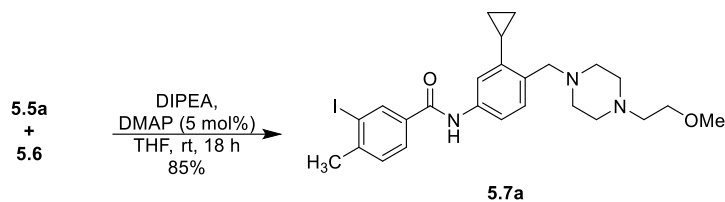
reaction was quenched with MeOH and concentrated. The material was purified by flash column chromatography (0-10% MeOH in CH<sub>2</sub>Cl<sub>2</sub>) to afford the product as a white solid (0.96 g, 70% yield). <sup>1</sup>H NMR (400 MHz, CDCl<sub>3</sub>) δ 8.27 (s, 1H), 7.91 (s, 1H), 7.71 (dd, *J* = 7.8, 1.6 Hz, 1H), 7.69 – 7.63 (m, 4H), 7.47 – 7.34 (m, 8H), 7.30 – 7.19 (m, 3H), 3.81 (t, *J* = 6.1 Hz, 2H), 3.61 (s, 2H), 2.60 (t, *J* = 6.1 Hz, 2H), 2.51 (br s, 8H), 2.46 (s, 3H), 2.18 (m, 1H), 1.03 (s, 9H), 0.91 (m, 2H), 0.64 (m, 2H) ppm; <sup>13</sup>C NMR (101 MHz, CDCl<sub>3</sub>) δ 164.0, 145.6, 143.4, 137.6, 136.9, 135.7, 134.2, 133.7, 130.4, 129.9, 129.7, 127.8, 127.0, 117.6, 117.4, 101.2, 62.1, 60.3, 59.9, 53.9, 53.1, 28.3, 26.9, 19.3, 12.9, 7.6 ppm; HRMS (APCI) *m/z*: calcd for C<sub>40</sub>H<sub>48</sub>IN<sub>3</sub>O<sub>2</sub>Si+H<sup>+</sup>: 758.2633 [M+H]<sup>+</sup>; found 758.2635.



***N*-[4-[[4-[2-[*tert*-butyl(diphenyl)silyl]oxyethyl]piperazin-1-yl]methyl]-3-chloro-phenyl]-3-iodo-4-methyl-benzamide (5.7c)** 3-iodo-4-methylbenzoic acid (2.62 g, 10 mmol) was refluxed in thionyl chloride (10 mL) for 1 hr. The volatiles were removed, and the material was brought up in benzene (~10 mL). The solution was concentrated, and the material was placed on vacuum until solidification. The material was dissolved in 10 mL of THF. The resulting 3-iodo-4-methylbenzoyl chloride (5.9 mL, 1M in THF) from the previous step was added to a solution of 4-[[4-[2-[*tert*-butyl(diphenyl)silyl]oxyethyl]piperazin-1-yl]methyl]-3-chloro-aniline (5.89 mmol), DMAP (0.036 g, 0.29 mmol) and *N,N*-diisopropylethylamine (1.27 mL, 7.1 mmol) in THF (5.9 mL) under argon. The reaction stirred at ambient temperature and followed by TLC. After approx. 18 hours, the reaction was quenched with MeOH and concentrated. The material was purified by flash column chromatography (0-10% MeOH in CH<sub>2</sub>Cl<sub>2</sub>) to afford the product as a white solid (3.40 g, 77% yield). <sup>1</sup>H NMR (400 MHz, CDCl<sub>3</sub>) δ 8.27 (d, *J* = 1.8 Hz, 1H), 7.78 – 7.72 (m, 3H), 7.67 (dd, *J* = 7.8, 1.5 Hz, 4H), 7.49 – 7.31 (m, 9H), 3.81 (t, *J* = 6.2 Hz, 2H), 3.58 (s, 2H), 2.60 (t, *J* = 6.2 Hz, 2H), 2.53 (br s, 8H), 2.49 (s, 3H), 1.04 (s, 9H) ppm; <sup>13</sup>C NMR (101 MHz, CDCl<sub>3</sub>) δ 164.0, 146.1, 137.6, 137.4, 135.7, 134.8, 133.8,

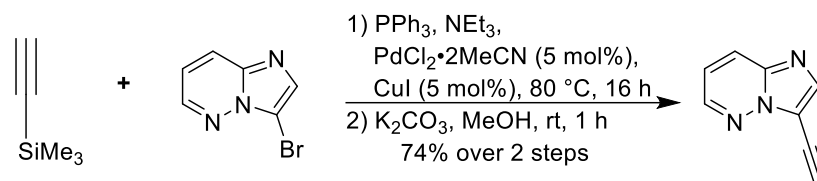
131.3, 130.0, 129.8, 127.8, 127.0, 121.1, 118.5, 101.3, 62.2, 60.3, 58.9, 53.9, 53.1, 28.4, 27.0, 19.3 ppm;

HRMS (APCI):  $m/z$  calcd for  $C_{37}H_{43}ClIN_3O_2Si+H^+$ : 752.1931  $[M+H]^+$ ; found 752.1912.

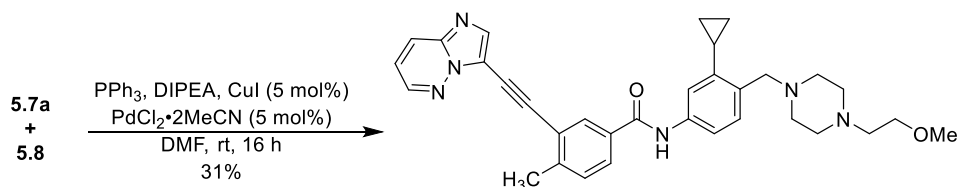


***N*-[3-cyclopropyl-4-[[4-(2-methoxyethyl)piperazin-1-yl]methyl]phenyl]-3-iodo-4-methyl-**

**benzamide (5.7a)** 3-iodo-4-methyl-benzoic acid (1.05 g, 4 mmol) was refluxed in thionyl chloride (6.1 mL, 84 mmol) for ~1 hour. The reaction was concentrated and the material was brought up in benzene (10 mL). The solution was concentrated, and the material was placed on vacuum until solidification. The material was dissolved in 4 mL of anhydrous THF to make a ~1 M solution be used directly in the next step. Under an argon atmosphere, the freshly prepared 3-iodo-4-methyl-benzoyl chloride (3.1 mL, 3.1 mmol) was added to a solution of 3-cyclopropyl-4-[[4-(2-methoxyethyl)piperazin-1-yl]methyl]aniline (0.9 g, 3.1 mmol), DMAP (0.02 g, 0.15 mmol) and *N,N*-diisopropylethylamine (0.67 mL, 3.72 mmol) in anhydrous THF (3.1 mL). The reaction was stirred at ambient temperature overnight; TLC (10% MeOH in EtOAc) the next morning showed complete conversion to a less polar product. The reaction was quenched with MeOH and concentrated before being purified via two rounds of silica gel flash column chromatography (0-20% MeOH in  $CH_2Cl_2$ ) to afford the desired product (1.4 g, 85% yield).  $^1H$  NMR (600 MHz,  $CDCl_3$ )  $\delta$  8.28 (s, 1H), 7.77 – 7.72 (m, 2H), 7.41 (dd,  $J$  = 8.1, 1.5 Hz, 1H), 7.32 (d,  $J$  = 7.9 Hz, 1H), 7.29 (d,  $J$  = 8.2 Hz, 1H), 7.23 (s, 1H), 3.66 (s, 2H), 3.54 (t,  $J$  = 5.4 Hz, 2H), 3.34 (s, 3H), 2.65 – 2.62 (m, 2H), 2.58 (br s, 8H), 2.49 (s, 3H), 2.19 – 2.14 (m, 1H), 0.96 – 0.91 (m, 2H), 0.68 – 0.65 (m, 2H) ppm;  $^{13}C$  NMR (151 MHz,  $CDCl_3$ )  $\delta$  164.0, 145.7, 143.5, 137.6, 136.9, 134.3, 130.5, 130.0, 127.0, 117.6, 117.4, 101.2, 70.0, 59.7, 59.0, 57.8, 53.7, 52.8, 28.3, 14.3, 12.9, 7.6 ppm; HRMS (APCI)  $m/z$ :  $[M + H]^+$  calcd for  $C_{25}H_{33}IN_3O_2$  534.1612, found 534.1616.

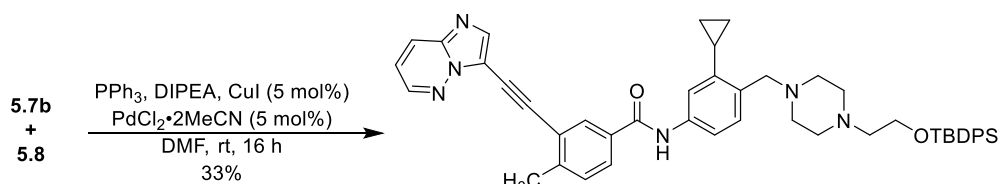
**5.8**

**3-ethynylimidazo[1,2-b]pyridazine (5.8)** To a 20 mL microwave reaction vial were added 3-bromoimidazo[1,2-b]pyridazine (1.5 g, 7.58 mmol), triphenylphosphine (0.199 g, 0.76 mmol), bis(acetonitrile)dichloropalladium (0.058 g, 0.38 mmol), copper(I) iodide (0.072 g, 0.38 mmol), NEt<sub>3</sub> (3.2 mL) and MeCN (7.5 mL). The reaction was sealed and sparged with argon for 30 min. To this solution was added trimethylsilylacetylene (3.15 mL, 22.7 mmol) and the reaction was microwave irradiated to 80 °C overnight. The next day, the reaction was transferred to a flask, the volatiles were removed and the residue was brought up in MeOH (7.5 mL). Potassium carbonate (2.1 g, 15.2 mmol) was added, and the mixture stirred for 1 hour. The solids were filtered over Celite, and the filtrate was concentrated and purified by flash column chromatography (0-50% EtOAc in hexanes) to afford the product as a brown solid (0.80 g, 74% yield over 2 steps). <sup>1</sup>H NMR (400 MHz, CDCl<sub>3</sub>) δ 8.49 (d, *J* = 4.2 Hz, 1H), 8.08 (br s, 1H), 8.02 (d, *J* = 9.2 Hz, 1H), 7.15 (dd, *J* = 9.2, 4.2 Hz, 1H), 3.81 (s, 1H) ppm.<sup>69</sup>

**5.9a**

***N*-[3-cyclopropyl-4-[[4-(2-methoxyethyl)piperazin-1-yl]methyl]phenyl]-3-(2-imidazo[1,2-b]pyridazin-3-ylethynyl)-4-methyl-benzamide (5.9a)** 3-ethynylimidazo[1,2-b]pyridazine (70 mg, 0.49 mmol), *N*-[3-cyclopropyl-4-[[4-(2-methoxyethyl)piperazin-1-yl]methyl]phenyl]-3-iodo-4-methyl-benzamide (200 mg, 0.37 mmol), triphenylphosphine (26 mg, 0.1 mmol), dichlorobis(acetonitrile)palladium(II) (6.32 mg, 0.02 mmol), and copper(I) iodide (6.96 mg, 0.0400 mmol) were combined in a flask and the atmosphere was cycled 3x with argon. *N,N*-diisopropylethylamine (0.13 mL, 0.56 mmol) and DMF (1.5 mL) were added and the reaction was stirred at room temperature overnight. The next day, TLC showed the reaction was complete and it

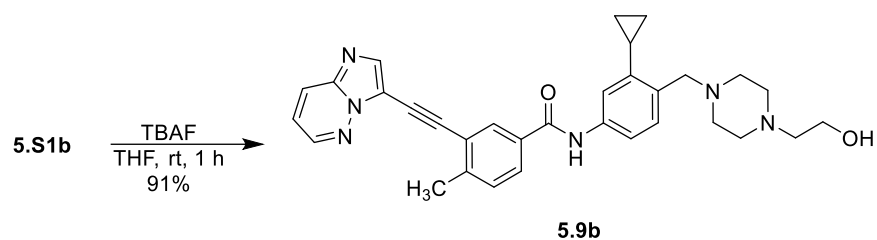
was quenched with water and extracted with EtOAc. Organic layers were combined and washed with brine solution. Organics were dried over Na<sub>2</sub>SO<sub>4</sub> and concentrated. The residue was purified via two rounds of silica gel flash chromatography (0-20% MeOH in CH<sub>2</sub>Cl<sub>2</sub>) and the collected fractions were again washed with saturated aqueous ammonium chloride. The organics were dried, filtered and concentrated to afford the product as a thin orange film (84 mg, 31% yield). <sup>1</sup>H NMR (600 MHz, CDCl<sub>3</sub>): δ = 8.49 – 8.46 (m, 1H), 8.21 (s, 1H), 8.07 (s, 1H), 8.04 (d, *J* = 1.7 Hz, 1H), 7.96 (d, *J* = 9.0 Hz, 1H), 7.82 (dd, *J* = 7.9, 1.8 Hz, 1H), 7.47 (dd, *J* = 8.1, 1.9 Hz, 1H), 7.36 (d, *J* = 8.0 Hz, 1H), 7.34 (s, 1H), 7.12 (dd, *J* = 9.1, 4.3 Hz, 1H), 3.77 (s, 2H), 3.70 (s, 2H), 3.34 (s, 3H), 2.95 – 2.74 (m, 10H), 2.61 (s, 3H), 2.15 – 2.07 (m, 1H), 0.94 (d, *J* = 8.2 Hz, 2H), 0.67 (d, *J* = 4.3 Hz, 2H) ppm; <sup>13</sup>C NMR (151 MHz, CDCl<sub>3</sub>) δ 165.0, 144.4, 144.3, 144.1, 143.6, 139.9, 138.5, 132.7, 130.8, 130.3, 130.2, 128.0, 126.2, 126.1, 122.9, 117.9, 117.8, 117.7, 113.2, 96.9, 80.8, 68.7, 59.0, 57.4, 53.1, 51.1, 29.8, 21.1, 13.0, 7.8 ppm; HRMS (APCI) *m/z*: [M + H]<sup>+</sup> Calcd for C<sub>33</sub>H<sub>37</sub>N<sub>6</sub>O<sub>2</sub>, 549.2973; Found 549.2992.



5.S1b

***N*-[4-[[4-[2-[*tert*-butyl(diphenyl)silyl]oxyethyl]piperazin-1-yl]methyl]-3-cyclopropyl-phenyl]-3-(2-imidazo[1,2-*b*]pyridazin-3-ylethynyl)-4-methyl-benzamide (5.S1b)** *N*-[4-[[4-[2-[*tert*-butyl(diphenyl)silyl]oxyethyl]piperazin-1-yl]methyl]-3-cyclopropyl-phenyl]-3-iodo-4-methyl-benzamide (0.76 g, 1.01 mmol), 3-ethynylimidazo[1,2-*b*]pyridazine (0.188 g, 1.32 mmol) bis(acetonitrile)dichloropalladium (17 mg, 0.066 mmol), copper(I) iodide (0.018 mg, 0.096 mmol) and triphenylphosphine (69 mg, 0.262 mmol) were combined in a flask under argon. DMF (7.6 mL) and *N,N*-diisopropylethylamine (0.26 mL) were added. The reaction was stirred at ambient temperature overnight and followed by TLC. The reaction was quenched by the addition of brine and extracted with CH<sub>2</sub>Cl<sub>2</sub>. The organics were dried over Na<sub>2</sub>SO<sub>4</sub>, filtered and concentrated. The material

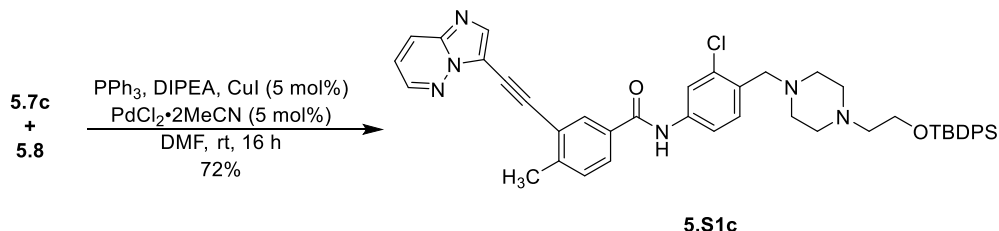
was purified by flash column chromatography (0-15% MeOH in CH<sub>2</sub>Cl<sub>2</sub>) to afford the product as a beige solid (0.256 g, 33% yield). <sup>1</sup>H NMR (400 MHz, CDCl<sub>3</sub>) δ 8.50 (dd, *J* = 4.4, 1.6 Hz, 1H), 8.08 (s, 1H), 8.05 (d, *J* = 1.9 Hz, 1H), 8.01 (dd, *J* = 9.2, 1.6 Hz, 1H), 7.89 (br s, 1H), 7.81 (dd, *J* = 7.9, 1.9 Hz, 1H), 7.64 (dd, *J* = 7.9, 1.5 Hz, 4H), 7.49 – 7.36 (m, 8H), 7.31 (br s, 2H), 7.15 (dd, *J* = 9.2, 4.4 Hz, 1H), 4.00 (br s, 2H), 3.76 (br s, 2H), 3.25 – 2.66 (m, 8H), 2.64 (s, 3H), 2.13 (m, 1H), 1.04 (s, 9H), 0.97 (m, 2H), 0.70 (m, 2H) ppm; <sup>13</sup>C NMR (151 MHz, CDCl<sub>3</sub>) δ 164.9, 144.5, 144.1, 139.9, 138.6, 135.7, 132.7, 130.4, 130.1, 128.0, 127.9, 126.2, 123.1, 117.9, 117.8, 117.6, 113.2, 96.9, 80.9, 59.5, 53.3, 29.9, 27.0, 21.1, 19.2, 13.0, 7.8 ppm; HRMS (APCI) *m/z*: calcd for C<sub>48</sub>H<sub>52</sub>N<sub>6</sub>O<sub>2</sub>Si+H<sup>+</sup>: 773.3994 [M+H]<sup>+</sup>; found 773.3980.



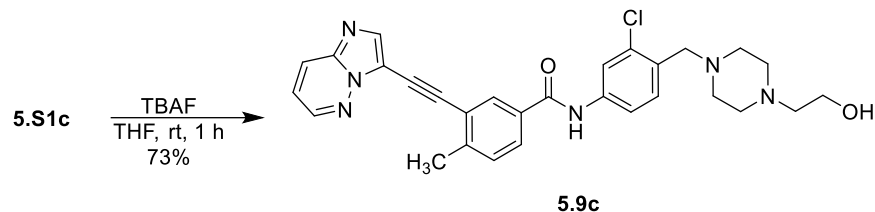
***N*-[3-cyclopropyl-4-[[4-(2-hydroxyethyl)piperazin-1-yl]methyl]phenyl]-3-(2-imidazo[1,2-b]pyridazin-3-ylethynyl)-4-methyl-benzamide** (**5.9b**)

*N*-[4-[[4-[2-*tert*-butyl(diphenyl)silyl]oxyethyl]piperazin-1-yl]methyl]-3-cyclopropyl-phenyl]-3-(2-imidazo[1,2-b]pyridazin-3-ylethynyl)-4-methyl-benzamide (251 mg, 0.325 mmol) was dissolved in THF (2.8 mL) under argon and TBAF (0.33 mL, 0.33 mmol, 1 M in THF) was added. The reaction was stirred at ambient temperature overnight. The next day, the reaction was concentrated and purified by silica gel flash chromatography (0-15% MeOH in CH<sub>2</sub>Cl<sub>2</sub>) to afford the title compound (157 mg, 91% yield). <sup>1</sup>H NMR (400 MHz, *d*<sub>6</sub>-DMSO) δ 10.30 (s, 1H), 8.84 (s, 1H), 8.41 – 8.32 (m, 2H), 8.29 (s, 1H), 8.03 (d, *J* = 7.6 Hz, 1H), 7.74 (d, *J* = 8.1 Hz, 1H), 7.63 (d, *J* = 7.9 Hz, 1H), 7.55 – 7.47 (m, 1H), 7.44 (s, 1H), 7.30 (d, *J* = 7.6 Hz, 1H), 4.50 (s, 1H), 3.65 (s, 2H), 3.58 (s, 2H), 3.46 (s, 4H), 2.70 (s, 3H), 2.61 (s, 2H), 2.58 – 2.41 (m, 6H), 2.34 – 2.27 (m, 1H), 1.04 (d, *J* = 7.9 Hz, 2H), 0.70 (t, *J* = 4.6 Hz, 2H) ppm; <sup>13</sup>C NMR (101 MHz, *d*<sub>6</sub>-DMSO) δ 164.1, 145.1, 143.1, 142.3, 138.2, 138.1, 132.7, 132.6, 130.1, 130.0, 129.7, 128.4,

126.1, 121.7, 119.1, 117.1, 116.8, 111.7, 109.6, 96.5, 81.0, 60.3, 59.4, 58.5, 53.3, 52.8, 20.4, 12.3, 7.6 ppm; HRMS (APCI)  $m/z$ :  $[M - H]^-$  Calcd for  $C_{32}H_{33}N_6O_2$  533.2670; Found 533.2679.

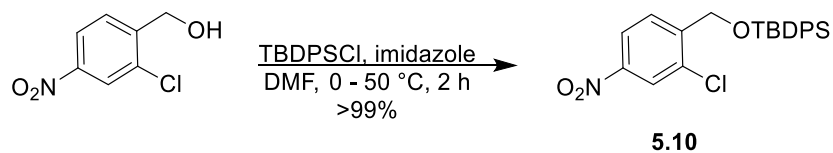


***N*-[4-[[4-[2-[*tert*-butyl(diphenyl)silyl]oxyethyl]piperazin-1-yl]methyl]-3-chloro-phenyl]-3-(2-imidazo[1,2-*b*]pyridazin-3-ylethynyl)-4-methyl-benzamide (5.S1c)** 3-ethynylimidazo[1,2-*b*]pyridazine (0.4 g, 2.79 mmol), *N*-[4-[[4-[2-[*tert*-butyl(diphenyl)silyl]oxyethyl]piperazin-1-yl]methyl]-3-chloro-phenyl]-3-iodo-4-methyl-benzamide (1.62 g, 2.15 mmol), triphenylphosphine (0.147 g, 0.56 mmol), bis(acetonitrile)dichloropalladium (0.0362 g, 0.14 mmol) and copper(I) iodide (0.039 g, 0.204 mmol) were combined in a flask and placed under argon. *N,N*-diisopropylethylamine (0.56 mL, 3.21 mmol) and DMF (16 mL) were added and the reaction was stirred overnight at ambient temperature. The reaction was quenched with water and extracted with EtOAc. The organics were washed with brine and dried over  $Na_2SO_4$ . The organics were filtered and concentrated, and the material was purified by flash column chromatography (0-10% MeOH in  $CH_2Cl_2$ ) to afford the product as a brown foam (1.54 g, 72% yield).  $^1H$  NMR (400 MHz,  $CDCl_3$ )  $\delta$  8.50 (d,  $J = 4.1$  Hz, 1H), 8.18-7.96 (m, 4H), 7.85-7.78 (m, 2H), 7.67 (dd,  $J = 7.7, 1.3$  Hz, 4H), 7.53-7.34 (m, 8H), 7.18-7.13 (m, 1H), 3.82 (br s, 2H), 3.61 (s, 2H), 2.64 (s, 3H), 2.56 (br s, 8H), 1.65 (br s, 2H), 1.04 (s, 9H) ppm;  $^{13}C$  NMR (151 MHz,  $CDCl_3$ )  $\delta$  164.9, 144.7, 144.1, 138.6, 137.8, 135.7, 134.9, 133.7, 132.4, 131.4, 130.4, 130.2, 129.8, 127.9, 127.8, 126.2, 123.1, 121.1, 118.5, 118.0, 96.8, 81.0, 62.0, 60.2, 58.8, 53.7, 52.9, 29.8, 27.0, 21.1, 19.3 ppm; HRMS (APCI):  $m/z$  calcd for  $C_{45}H_{46}ClN_6O_2Si-H$ : 765.3146  $[M-H]^-$ ; found 765.3145.



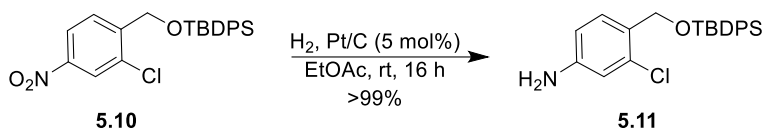
***N*-[3-chloro-4-[[4-(2-hydroxyethyl)piperazin-1-yl]methyl]phenyl]-3-(2-imidazo[1,2-b]pyridazin-3-ylethynyl)-4-methyl-benzamide (5.9c)** To a stirred solution of *N*-[4-[[4-[2-*tert*-butyl(diphenyl)silyl]oxyethyl]piperazin-1-yl]methyl]-3-chloro-phenyl]-3-(2-imidazo[1,2-b]pyridazin-3-ylethynyl)-4-methyl-benzamide (1.59 g, 2.07 mmol) in THF (17.6 mL) under argon was added TBAF (3.11 mL, 3.11 mmol, 1M in THF) and the reaction was followed by TLC. After approx. 1 hour, the reaction was concentrated and purified via two rounds of silica gel flash chromatography (0 to 20% MeOH in CH<sub>2</sub>Cl<sub>2</sub>) to yield the product as a light yellow solid (0.81 g, 73% yield). <sup>1</sup>H NMR (400 MHz, CDCl<sub>3</sub>) δ 8.60 (s, 1H), 8.47 (dd, *J* = 4.4, 1.6 Hz, 1H), 8.08 (s, 1H), 8.02 (d, *J* = 1.9 Hz, 1H), 7.92 (dd, *J* = 9.2, 1.6 Hz, 1H), 7.81 (dd, *J* = 9.1, 2.0 Hz, 2H), 7.56 (dd, *J* = 8.4, 2.2 Hz, 1H), 7.42 (d, *J* = 8.4 Hz, 1H), 7.34 (d, *J* = 8.1 Hz, 1H), 7.11 (dd, *J* = 9.2, 4.4 Hz, 1H), 3.63 – 3.59 (m, 4H), 3.48 – 3.47 (m, 4H), 2.59 (s, 3H), 2.55 (app t, *J* = 5.6 Hz, 7H) ppm; <sup>13</sup>C NMR (101 MHz, *d*<sub>6</sub>-DMSO) δ 164.5, 145.1, 143.4, 139.7, 139.0, 138.3, 133.1, 132.3, 130.9, 130.6, 130.2, 130.1, 128.5, 126.1, 121.8, 120.4, 119.1, 118.7, 111.7, 96.4, 81.1, 60.3, 58.5, 58.3, 53.2, 52.7, 20.4 ppm; HRMS (APCI) *m/z*: [M + H]<sup>+</sup> Calcd for C<sub>29</sub>H<sub>30</sub>ClN<sub>6</sub>O<sub>2</sub> 529.2113, Found 529.2107.

#### 5.3.1.2.2 Synthesis of Dual-NBN Compounds (Schemes 5.2 – 5.4)

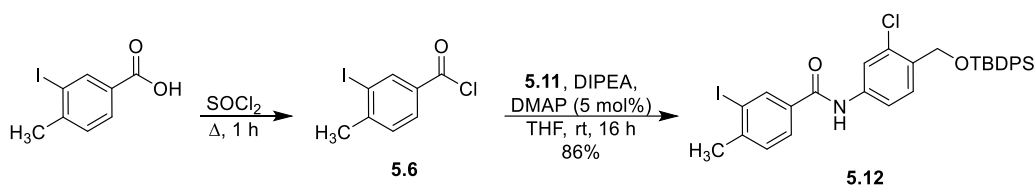


***tert*-butyl-[(2-chloro-4-nitrophenyl)methoxy]-diphenyl-silane (5.10)** In an oven-dried 250 mL round bottom flask with stir bar was dissolved 2-chloro-4-nitrophenyl (8.69 g, 46.35 mmol) in anhydrous DMF (16 mL) to give a light yellow solution. Imidazole (6.31 g, 92.69 mmol) was added, and the mixture was cooled to 0 °C before *tert*-butyldiphenylchlorosilane (14.29 mL, 55.61 mmol)

was added dropwise. The reaction was heated to 50 °C and followed by TLC. After ~2 hours, the reaction was cooled to 0 °C and quenched by addition of 1 M NaOH dropwise, whereupon the reaction bubbled vigorously and changed to a deep yellow color with complete dissolution of the white solid. After stirring for ~10 minutes, the THF was evaporated and the product was extracted with EtOAc and brine. The organic extract was dried over Na<sub>2</sub>SO<sub>4</sub>, filtered, and concentrated to yield *tert*-butyl-[(2-chloro-4-nitro-phenyl)methoxy]-diphenyl-silane as an orange solid (22.6 g, 53.1 mmol, >99% yield). <sup>1</sup>H NMR (400 MHz, CDCl<sub>3</sub>) δ 8.22 (dd, *J* = 8.5, 2.2 Hz, 1H), 8.19 (d, *J* = 2.2 Hz, 1H), 7.99 (d, *J* = 8.5 Hz, 1H), 7.70 (q, *J* = 1.6 Hz, 2H), 7.68 (q, *J* = 1.6 Hz, 2H), 7.47 – 7.39 (m, 6H), 4.88 (s, 2H), 1.16 (s, 9H) ppm; HRMS (APCI) *m/z*: calcd for C<sub>23</sub>H<sub>24</sub>ClNO<sub>3</sub>Si-H<sup>+</sup>: 424.1141 [M-H]<sup>-</sup>; found 424.1141.

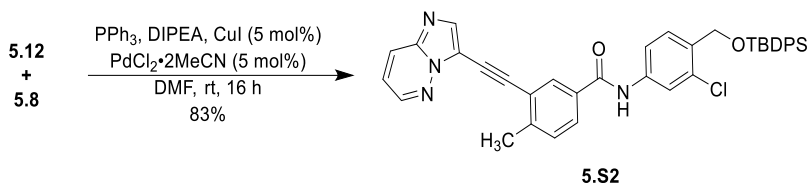


**4-[[*tert*-butyl(diphenyl)silyl]oxymethyl]-3-chloro-aniline (5.11)** A solution of *tert*-butyl-[(2-chloro-4-nitro-phenyl)methoxy]-diphenyl-silane (10.23 g, 24.02 mmol) in EtOAc (150 mL) was catalytically hydrogenated over Pt (4.12 g, 1.06 mmol) under H<sub>2</sub> gas overnight at ambient temperature. The next day, the reaction was filtered over Celite and concentrated to yield 4-[[*tert*-butyl(diphenyl)silyl]oxymethyl]-3-chloro-aniline as an orange oil (9.62 g, 24.3 mmol, >99% yield). <sup>1</sup>H NMR (400 MHz, CDCl<sub>3</sub>) δ 7.76 – 7.65 (m, 4H), 7.48 – 7.32 (m, 7H), 6.67 (d, *J* = 2.3 Hz, 1H), 6.62 (dd, *J* = 8.2, 2.3 Hz, 1H), 4.76 (s, 2H), 3.67 (br s, 2H), 1.11 (s, 9H) ppm; <sup>13</sup>C NMR (126 MHz, CDCl<sub>3</sub>) δ 146.4, 135.7, 134.9, 133.7, 132.6, 129.8, 129.0, 128.3, 127.8, 115.5, 113.7, 63.1, 27.0, 19.5 ppm; HRMS (NSI) *m/z*: calcd for C<sub>23</sub>H<sub>26</sub>ClNOSi+Na<sup>+</sup>: 418.1364 [M+Na]<sup>+</sup>; found 418.1362.



***N*-[4-[[*tert*-butyl(diphenyl)silyl]oxymethyl]-3-chloro-phenyl]-3-iodo-4-methyl-benzamide**

**(5.12)** 3-iodo-4-methylbenzoic acid (0.79 g, 3 mmol) was refluxed in thionyl chloride (4.55 mL) for 1 hr. The volatiles were removed, and the material was brought up in benzene (~10 mL). The solution was concentrated, and the material was placed on vacuum until solidification. The material was dissolved in 3 mL of THF. A portion of the 3-iodo-4-methylbenzoyl chloride (1.71 mL, 1M in THF) from the previous step was added to a solution of 4-[[*tert*-butyl(diphenyl)silyl]oxymethyl]-3-chloroaniline (0.68 g, 1.71 mmol), *N,N*-diisopropylethylamine (0.36 mL, 2.06 mmol), and DMAP (10.47 mg, 0.0900 mmol) in anhydrous THF (8 mL). Reaction was stirred under argon overnight. The next day, the reaction was quenched with MeOH. The product mixture was adsorbed onto Celite and purified via silica gel flash column chromatography (0-20% EtOAc in Hex) to yield *N*-[4-[[*tert*-butyl(diphenyl)silyl]oxymethyl]-3-chloro-phenyl]-3-iodo-4-methyl-benzamide as a white foam (946.7 mg, 1.48 mmol, 86.3% yield).  $^1\text{H}$  NMR (600 MHz,  $\text{CDCl}_3$ )  $\delta$  8.28 (d,  $J = 1.9$  Hz, 1H), 7.77 (br s, 1H), 7.74 (d,  $J = 2.1$  Hz, 1H), 7.73 (dd,  $J = 3.7, 1.7$  Hz, 1H), 7.71 – 7.69 (m, 5H), 7.50 (dd,  $J = 8.4, 2.2$  Hz, 1H), 7.46 – 7.42 (m, 2H), 7.42 – 7.36 (m, 4H), 7.34 (d,  $J = 8.0$  Hz, 1H), 4.82 (s, 2H), 2.50 (s, 3H), 1.12 (s, 9H) ppm;  $^{13}\text{C}$  NMR (151 MHz,  $\text{CDCl}_3$ )  $\delta$  164.1, 146.1, 137.6, 137.4, 135.6, 135.0, 134.9, 133.9, 133.3, 132.0, 130.02, 129.95, 129.8, 128.1, 128.0, 127.9, 127.0, 120.8, 118.6, 101.3, 63.0, 28.4, 27.0, 19.5 ppm; HRMS (APCI)  $m/z$ : calcd for  $\text{C}_{31}\text{H}_{31}\text{ClINO}_2\text{Si-H}^+$ : 638.0785 [M-H] $^-$ ; found 638.0787.



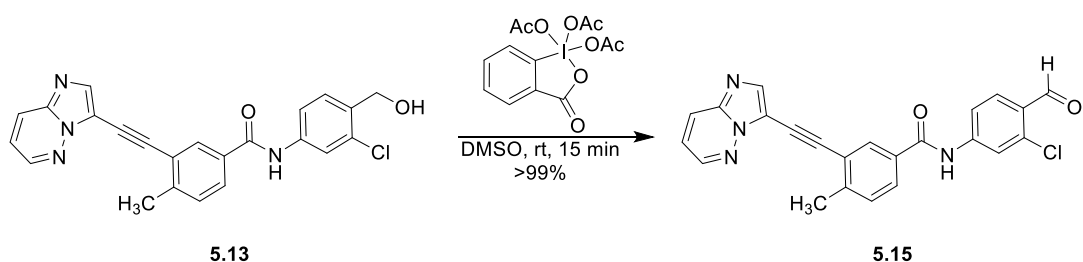
***N*-[4-[[*tert*-butyl(diphenyl)silyl]oxymethyl]-3-chloro-phenyl]-3-(2-imidazo[1,2-*b*]pyridazin-**

**3-ylethynyl)-4-methyl-benzamide (5.S2)** In a 2-neck round-bottom flask with stir bar were

combined *N*-[4-[[*tert*-butyl(diphenyl)silyl]oxymethyl]-3-chloro-phenyl]-3-iodo-4-methyl-benzamide (2.0 g, 3.12 mmol), 3-ethynylimidazo[1,2-*b*]pyridazine (0.6 g, 4.22 mmol) triphenylphosphine (204.9 mg, 0.7800 mmol), copper(I) iodide (59.51 mg, 0.3100 mmol), and dichlorobis(acetonitrile)palladium(II) (52.69 mg, 0.2000 mmol) under argon. The solids were dissolved in anhydrous DMF (10 mL) before *N,N*-diisopropylethylamine (0.82 mL, 4.69 mmol) was added with stirring, and the reaction stirred under argon at ambient temperature overnight. The next morning, TLC (1:1 CH<sub>2</sub>Cl<sub>2</sub>:EtOAc) showed conversion of the UV-active iodide and fluorescent alkyne starting materials to a new fluorescent spot of intermediate polarity. Hence, the reaction was diluted with EtOAc and quenched with water before the product was extracted with EtOAc and twice washed with brine solution. The organic layer was dried over Na<sub>2</sub>SO<sub>4</sub>, filtered and concentrated to a yellow oil. The sample was adsorbed onto silica gel purified via flash chromatography (0-50% EtOAc in CH<sub>2</sub>Cl<sub>2</sub>) to afford the desired compound as a white solid (1.7 g, 83% yield). <sup>1</sup>H NMR (500 MHz, CDCl<sub>3</sub>) δ 8.50 (d, *J* = 4.0 Hz, 1H), 8.31 (s, 1H), 8.14 (br s, 1H), 8.04 (d, *J* = 1.9 Hz, 1H), 8.02 (d, *J* = 9.2 Hz, 1H), 7.82 (dd, *J* = 8.1, 2.0 Hz, 2H), 7.72 – 7.68 (m, 5H), 7.57 (dd, *J* = 8.4, 2.1 Hz, 1H), 7.48 – 7.42 (m, 2H), 7.41 – 7.36 (m, 5H), 7.14 (dd, *J* = 9.1, 4.4 Hz, 1H), 4.82 (s, 2H), 2.62 (s, 3H), 1.12 (s, 9H) ppm; <sup>13</sup>C NMR (126 MHz, CDCl<sub>3</sub>) δ 165.1, 144.5, 144.1, 138.3, 137.8, 135.6, 134.7, 133.4, 132.5, 132.3, 132.2, 132.0, 130.3, 130.2, 129.9, 128.7, 128.6, 128.1, 128.0, 127.9, 126.0, 122.9, 120.9, 118.7, 118.0, 110.1, 96.9, 80.8, 63.0, 27.0, 21.1, 19.5 ppm; HRMS (APCI) *m/z*: calcd for C<sub>39</sub>H<sub>35</sub>ClN<sub>4</sub>O<sub>2</sub>Si-H<sup>+</sup>: 653.2145 [M-H]<sup>-</sup>; found 653.2150.

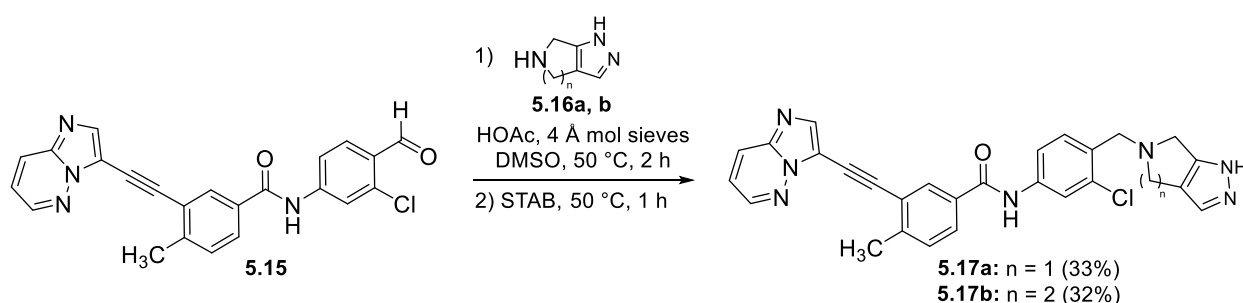


anhydrous NMP (1 mL) was added as co-solvent, somewhat solubilizing the mixture. To this mixture was added  $\text{NEt}_3$  (0.2 mL, 1.44 mmol) followed by dropwise addition of thionyl chloride (0.1 mL, 1.37 mmol), which released a vapor. The reaction stirred at ambient temperature for approx. 2 hours with monitoring by TLC (5% MeOH in  $\text{CH}_2\text{Cl}_2$ ). The reaction was chilled with an ice bath before being diluted with EtOAc and quenched with water. The product mixture was extracted with EtOAc and neutralized with saturated  $\text{NaHCO}_3$  solution before being washed with brine solution and 0.1 N HCl solution. The organic was dried over  $\text{Na}_2\text{SO}_4$ , filtered and concentrated to a crude brown solid which was purified via silica gel flash column chromatography using a 0-10% gradient of MeOH in  $\text{CH}_2\text{Cl}_2$  to afford the desired product (69 mg, 73% yield).  $^1\text{H}$  NMR (400 MHz,  $d_6$ -DMSO)  $\delta$  10.65 (s, 1H), 8.89 (d,  $J = 4.4$  Hz, 1H), 8.53 (br s, 1H), 8.40 (d,  $J = 9.0$  Hz, 1H), 8.21 (d,  $J = 1.8$  Hz, 1H), 8.08 (d,  $J = 2.1$  Hz, 1H), 7.99 (dd,  $J = 8.0, 1.9$  Hz, 1H), 7.79 (dd,  $J = 8.4, 2.1$  Hz, 1H), 7.65 – 7.52 (m, 3H), 4.81 (s, 2H), 2.61 (s, 3H) ppm; HRMS (APCI+)  $m/z$ :  $[\text{M} + \text{H}]^+$  calcd for  $\text{C}_{23}\text{H}_{17}\text{Cl}_2\text{N}_4\text{O}$  435.07739, found 435.07780.



***N*-(3-chloro-4-formyl-phenyl)-3-(2-imidazo[1,2-b]pyridazin-3-ylethynyl)-4-methylbenzamide (5.15)** In an oven-dried 25 mL Schlenk tube with stir bar was suspended *N*-[3-chloro-4-(hydroxymethyl)phenyl]-3-(2-imidazo[1,2-b]pyridazin-3-ylethynyl)-4-methylbenzamide (100 mg, 0.24 mmol) in anhydrous DMSO (1.4 mL) under argon; the suspension was heated briefly to give a yellow solution. 1,1,1-tris(acetyloxy)-1,1-dihydro-1,2-benzodioxol-3-(1H)-one (153 mg, 0.36 mmol) was then dropwise added as a solution in anhydrous DMSO (1 mL) with vigorous stirring. After 15 minutes, the reaction was quenched with *ca.* 20  $\mu\text{L}$  of isopropyl alcohol and diluted with EtOAc before being stirred with an aqueous solution of  $\text{NaHCO}_3$  and sodium thiosulfate. The mixture was transferred to a separatory funnel, the aqueous layer was removed, and the organic was washed

with brine solution. The solid and organic layer was collected, and the volatiles removed via rotary evaporation to afford the crude aldehyde product as a yellow solid (154 mg, >100% crude yield).  $^1\text{H}$  NMR (500 MHz,  $d_6$ -DMSO)  $\delta$  11.05 (s, 1H), 10.23 (s, 1H), 8.73 (d,  $J = 3.4$  Hz, 1H), 8.24 (m, 4H), 8.02 (m, 2H), 7.88 (d,  $J = 8.6$  Hz, 1H), 7.54 (d,  $J = 8.3$  Hz, 1H), 7.39 (dd,  $J = 9.2, 4.4$  Hz, 1H), 2.6 (s, 3H) ppm;  $^{13}\text{C}$  NMR (125 MHz,  $d_6$ -DMSO)  $\delta$  188.5, 165.2, 145.5, 145.1, 143.9, 139.7, 138.3, 136.9, 131.8, 130.6, 130.5, 130.0, 128.8, 127.2, 126.1, 121.8, 120.6, 119.1, 118.7, 111.7, 96.3, 81.2, 20.4 ppm; HRMS (APCI)  $m/z$ :  $[\text{M} + \text{H}]^+$  Calcd for  $\text{C}_{23}\text{H}_{16}\text{ClN}_4\text{O}_2$  415.09563, found 415.09534.



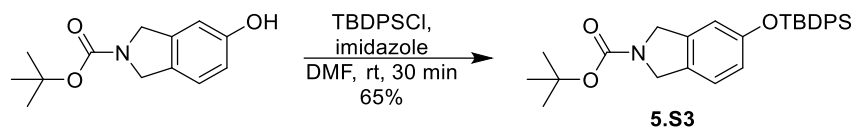
#### General procedure for the reductive amination of aldehyde **5.15** with amines **5.16a** or **b**:

To an oven-dried 25-mL Schlenk tube with stir bar was added powdered 4 Å molecular sieves which were then flame-activated under vacuum. After the apparatus was allowed to cool, *N*-(3-chloro-4-formyl-phenyl)-3-(2-imidazo[1,2-*b*]pyridazin-3-ylethynyl)-4-methyl-benzamide (**5.15**, 1 eq) and cyclic amine **5.16** (1.2 eq) were added under argon before being dissolved in anhydrous DMSO (0.25 M) to give a light yellow sludge. Lastly, acetic acid (0.5-0.6 eq) was added, and the reaction was heated to 50°C for 2-5 hours. The reaction was allowed to cool to ambient temperature before sodium triacetoxyborohydride (3 eq) was added in one portion. The reaction stirred for approx. 30 minutes before TLC showed spot-to-spot conversion of the initial intermediate to a more polar fluorescent spot. The reaction was then carefully added to a saturated sodium bicarbonate solution in a separatory funnel to quench. The heterogeneous product mixture was twice extracted with ethyl acetate, and the organic was washed with water and brine (4x), being sure to collect residual insoluble solids, before being dried over sodium sulfate, filtered and concentrated to a yellow solid.

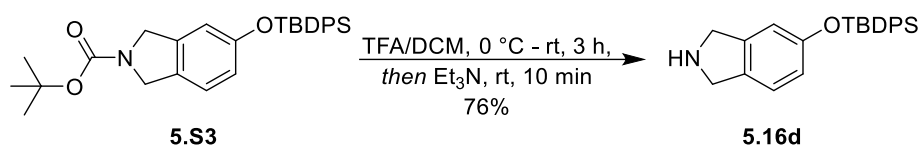
The product was adsorbed onto Celite and purified via silica gel flash column chromatography (0-30% methanol in DCM); the appropriate fractions were concentrated to afford a yellow solid. Purification was repeated as judged necessary by  $^1\text{H}$  NMR.

***N*-[3-chloro-4-(4,6-dihydro-1H-pyrrolo[3,4-c]pyrazol-5-ylmethyl)phenyl]-3-(2-imidazo[1,2-b]pyridazin-3-ylethynyl)-4-methyl-benzamide (5.17a)** Prepared according to the General Procedure to afford the product as a yellow solid (80 mg, 33% yield).  $^1\text{H}$  NMR (300 MHz,  $d_6$ -DMSO)  $\delta$  12.40 (br s, 1H), 10.46 (s, 1H), 8.73 (dd,  $J = 4.5, 1.6$  Hz, 1H), 8.23 (m, 3H), 8.01 (d,  $J = 2.0$  Hz, 1H), 7.94 (dd,  $J = 8.0, 1.9$  Hz, 1H), 7.75 (dd,  $J = 8.3, 2.1$  Hz, 1H), 7.54 (dd,  $J = 8.4, 3.3$  Hz, 2H), 7.39 (m, 2H), 3.99 (s, 2H), 3.72 (s, 4H), 2.61 (s, 3H) ppm;  $^{13}\text{C}$  NMR (101 MHz,  $d_6$ -DMSO)  $\delta$  164.5, 156.5, 145.1, 143.4, 139.7, 139.1, 138.3, 132.7, 132.4, 131.6, 130.7, 130.2, 130.1, 128.5, 126.1, 121.8, 120.8, 120.5, 120.0, 119.1, 118.8, 111.7, 96.5, 81.2, 56.1, 51.1, 50.9, 20.4 ppm; HRMS (APCI)  $m/z$ :  $[\text{M} - \text{H}]^-$  Calcd for  $\text{C}_{28}\text{H}_{21}\text{ClN}_7\text{O}$  506.15016, found 506.15061.

***N*-[3-chloro-4-(1,4,5,7-tetrahydropyrazolo[3,4-c]pyridin-6-ylmethyl)phenyl]-3-(2-imidazo[1,2-b]pyridazin-3-ylethynyl)-4-methyl-benzamide (5.17b)** Prepared according to the General Procedure to afford the product as a beige solid (115 mg, 32% yield);  $^1\text{H}$  NMR (400 MHz,  $\text{CDCl}_3$ )  $\delta$  9.06 (s, 1H), 8.42 (dd,  $J = 4.4, 1.6$  Hz, 1H), 8.03 (s, 1H), 7.99 (d,  $J = 1.7$  Hz, 1H), 7.88 (dd,  $J = 9.3, 1.5$  Hz, 1H), 7.83 (d,  $J = 2.0$  Hz, 1H), 7.76 (dd,  $J = 8.0, 1.8$  Hz, 1H), 7.50 (dd,  $J = 8.4, 2.0$  Hz, 1H), 7.42 (d,  $J = 8.42$  Hz, 1H), 7.24 (s, 1H), 7.07 (dd,  $J = 9.2, 4.4$  Hz, 1H), 3.77 (s, 2H), 3.62 (s, 2H), 2.78 (t,  $J = 5.3$  Hz, 2.64 (t,  $J = 5.11$ , 2H), 2.53 (s, 3H) ppm;  $^{13}\text{C}$  NMR (126 MHz,  $\text{CDCl}_3$ )  $\delta$  165.0, 144.6, 144.1, 139.9, 138.5, 137.9, 134.8, 132.4, 132.3, 131.2, 130.4, 130.2, 128.0, 126.1, 123.0, 121.2, 118.7, 118.0, 113.5, 113.2, 96.8, 80.9, 58.2, 51.1, 50.7, 21.1, 21.0 ppm; HRMS (NSI)  $m/z$   $[\text{M} + \text{H}]^+$  Calcd for  $\text{C}_{29}\text{H}_{25}\text{ClN}_7\text{O}$   $[\text{M} + \text{H}]^+$ , 522.18036; found, 522.18104.

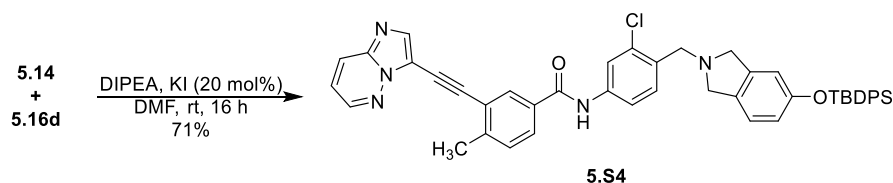


***tert*-butyl 5-[*tert*-butyl(diphenyl)silyl]oxyisindoline-2-carboxylate (5.S3)** In an oven-dried 250 mL round bottom flask with stirrer under argon, *tert*-butyl 5-hydroxyisindoline-2-carboxylate (825 mg, 3.51 mmol) was dissolved in DMF (3.3 mL) to give a light brown solution. *tert*-butyldiphenylchlorosilane (1.08 mL, 4.21 mmol) was added, immediately darkening the solution. Imidazole (597 mg, 8.77 mmol) was then added, lightening the solution color back to light brown. The reaction stirred for 30 minutes, after which time the mixture was diluted with water, extracted with EtOAc, and washed with brine 3 times. The organic layer was dried over Na<sub>2</sub>SO<sub>4</sub>, filtered, and concentrated, yielding an orange solid. The solid was purified using flash chromatography (0-50% EtOAc in hexanes). Fractions of interest were combined to yield *tert*-butyl 5-[*tert*-butyl(diphenyl)silyl]oxyisindoline-2-carboxylate as a white solid, slightly contaminated with TBDPS-containing byproduct (1080 mg, 65% yield). <sup>1</sup>H NMR (400 MHz, CDCl<sub>3</sub>) δ 7.75 - 7.72 (m, 4H), 7.44 - 7.37 (m, 6H), 6.93 (dd, *J* = 33.9, 8.3 Hz, 1H), 6.71 - 6.62 (m, 2H), 4.53 (d, *J* = 16.9 Hz, 2H), 4.48 (d, *J* = 18.6 Hz, 2H), 1.49 (d, *J* = 3.3 Hz, 9H), 1.12 (s, 9H) ppm; HRMS (NSI+) *m/z*: [M + H]<sup>+</sup> calcd for C<sub>29</sub>H<sub>36</sub>NO<sub>3</sub>Si 474.24590, found 474.24636.



***tert*-butyl-isoindolin-5-yloxy-diphenyl-silane (5.16d)** In a flame-dried 50 mL round-bottom flask with stir bar was dissolved *tert*-butyl 5-[*tert*-butyl(diphenyl)silyl]oxyisindoline-2-carboxylate (0.67 g, 1.41 mmol) in anhydrous CH<sub>2</sub>Cl<sub>2</sub> (6 mL) to give a colorless solution. The solution was chilled to 0 °C before being dropwise treated with trifluoroacetic acid (0.66 mL, 8.57 mmol); after approx. 2 hours, another half portion of trifluoroacetic acid (0.33 mL, 4.31 mmol) (for a total of 0.99 mL, 12.88 mmol) was added, and the reaction was allowed to stir an additional hour. The reaction was

quenched by dropwise addition of a slight excess of  $\text{NEt}_3$  (2.4 mL, 13.78 mmol). The reaction mixture was adsorbed onto silica gel and purified via flash chromatography (0-10% MeOH in  $\text{CH}_2\text{Cl}_2$ ). Fractions of interest were concentrated to yield a pink oil and then brought up in a mixture of EtOAc and diethyl ether and washed with water and brine before being dried over  $\text{Na}_2\text{SO}_4$ , filtered and concentrated to afford the product as a dark oil (0.415 g, 76% yield).  $^1\text{H}$  NMR (400 MHz,  $\text{CDCl}_3$ )  $\delta$  7.74 – 7.69 (m, 4H), 7.45 – 7.34 (m, 6H), 6.91 (d,  $J$  = 8.1 Hz, 1H), 6.66 (s, 1H), 6.64 – 6.61 (m, 1H), 5.13 (br s, 1H), 4.17 (s, 2H), 4.13 (s, 2H), 1.10 (s, 9H) ppm;  $^{13}\text{C}$  NMR (100 MHz,  $\text{CDCl}_3$ )  $\delta$  196.3, 156.5, 135.5, 135.2, 132.3, 130.3, 128.1, 126.0, 123.5, 120.7, 114.0, 50.4, 50.2, 26.5, 19.5 ppm; HRMS (NSI+)  $m/z$ :  $[\text{M} + \text{H}]^+$  calcd for  $\text{C}_{24}\text{H}_{28}\text{NOSi}$  374.19347, found 374.19399.

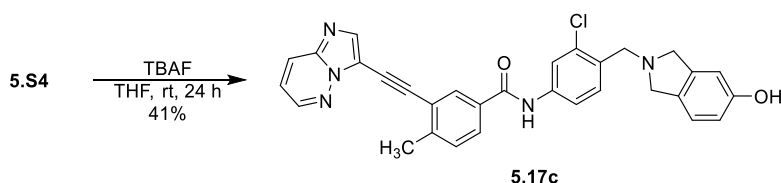


***N*-(4-((5-((*tert*-butyldiphenylsilyl)oxy)isoindolin-2-yl)methyl)-3-chlorophenyl)-3-**

**(imidazo[1,2-*b*]pyridazin-3-ylethynyl)-4-methyl benzamide (5.S4)**

A 25 mL round-bottom flask was charged with *tert*-butyl-isoindolin-5-yloxy-diphenyl-silane (378 mg, 1.01 mmol) followed by *N*-[3-chloro-4-(chloromethyl)phenyl]-3-(2-imidazo[1,2-*b*]pyridazin-3-ylethynyl)-4-methylbenzamide (220 mg, 0.51 mmol) and anhydrous DMF (4 mL) to give a dark brown solution. Lastly, *N,N*-diisopropylethylamine (0.2 mL, 1.16 mmol) and potassium iodide (16 mg, 0.1 mmol) were added, and the reaction stirred at ambient temperature overnight. The next morning, LC-MS showed conversion to the desired product ( $[\text{M} + 1]^+ = 772.2$ ) and a slight amount of the doubly alkylated side product. The reaction was quenched with water and extracted out of brine solution with EtOAc (3x). Organics were dried over  $\text{Na}_2\text{SO}_4$ , filtered, concentrated, and purified via silica gel flash column chromatography (0-20% MeOH in  $\text{CH}_2\text{Cl}_2$ ). Fractions of interest were collected and concentrated to yield the product as a brown solid (278 mg, 71% yield).  $^1\text{H}$  NMR (500 MHz,  $\text{CDCl}_3$ )  $\delta$  8.49 (dd,  $J$  = 4.4, 1.7 Hz, 1H), 8.09 (s, 1H), 8.04 (d,  $J$  = 2.0 Hz, 1H), 8.00 (dd,  $J$  = 9.2, 1.6 Hz, 1H), 7.96 (s, 1H), 7.83 (s, 1H),

7.81 (dd,  $J = 8.0, 1.9$  Hz, 1H), 7.72 – 7.70 (m, 4H), 7.50 (d,  $J = 1.1$  Hz, 2H), 7.43 – 7.34 (m, 8H), 7.14 (dd,  $J = 9.2, 4.5$  Hz, 1H), 6.88 (d,  $J = 8.2$  Hz, 1H), 6.62 (d,  $J = 2.3$  Hz, 1H), 6.58 (dd,  $J = 8.1, 2.4$  Hz, 1H), 3.96 (s, 2H), 3.88 (s, 2H), 3.84 (s, 2H), 2.65 (s, 3H), 1.08 (s, 9H) ppm;  $^{13}\text{C}$  NMR (100 MHz,  $\text{CDCl}_3$ )  $\delta$  164.9, 154.8, 144.7, 144.1, 141.4, 139.9, 138.5, 137.8, 135.6, 134.4, 133.1, 132.9, 132.5, 132.4, 131.1, 130.4, 130.1, 130.0, 127.9, 127.9, 126.1, 123.0, 122.8, 121.0, 118.6, 118.2, 118.0, 113.9, 113.2, 96.8, 80.9, 59.2, 58.6, 56.5, 26.6 (3C), 21.1, 19.6 ppm; HRMS (APCI-)  $m/z$ :  $[\text{M} - \text{H}]^-$  calcd for  $\text{C}_{47}\text{H}_{41}\text{ClN}_5\text{O}_2\text{Si}$  770.27235, found 770.27372.



***N*-(3-chloro-4-((5-hydroxyisindolin-2-yl)methyl)phenyl)-3-(imidazo [1,2-*b*]pyridazin-3-ylethynyl)-4-methylbenzamide (5.17c)** To a 5-dram vial under argon was added *N*-[4-[[5-[*tert*-butyl(diphenyl)silyl]oxyisindolin-2-yl]methyl]-3-chloro-phenyl]-3-(2-imidazo[1,2-*b*]pyridazin-3-ylethynyl)-4-methyl-benzamide (100 mg, 0.13 mmol). TBAF (0.4 mL, 0.4 mmol) was added as a ~1 M solution in THF, and the reaction stirred overnight. After 24 hours, LC-MS showed complete deprotection. The reaction was diluted with  $\text{CH}_2\text{Cl}_2$  and water and extracted with  $\text{CH}_2\text{Cl}_2$  (3x). The product was twice purified via silica gel flash column chromatography (0-15% MeOH in  $\text{CH}_2\text{Cl}_2$ ) to afford the product as a brown solid (28 mg; 41% yield).  $^1\text{H}$  NMR (600 MHz,  $d_6$ -acetone)  $\delta$  9.78 (s, 1H), 8.63 (dd,  $J = 4.4, 1.5$  Hz, 1H), 8.18 (d,  $J = 1.9$  Hz, 1H), 8.11 (td,  $J = 4.2, 1.6$  Hz, 3H), 7.96 (dd,  $J = 7.9, 1.9$  Hz, 1H), 7.77 (dd,  $J = 8.4, 2.2$  Hz, 1H), 7.56 (d,  $J = 8.4$  Hz, 1H), 7.48 (d,  $J = 8.0$  Hz, 1H), 7.35 (dd,  $J = 9.2, 4.4$  Hz, 1H), 7.01 (d,  $J = 8.1$  Hz, 1H), 6.71 (d,  $J = 1.9$  Hz, 1H), 6.67 (dd,  $J = 8.1, 2.3$  Hz, 1H), 3.97 (s, 2H), 3.87 (d,  $J = 14.5$  Hz, 4H), 2.63 (s, 3H) ppm;  $^{13}\text{C}$  NMR (150 MHz,  $d_6$ -acetone)  $\delta$  165.5, 157.5, 145.5, 144.7, 142.7, 140.9, 140.2, 139.1, 134.3, 133.8, 133.0, 131.9, 131.7, 131.1, 130.9, 129.0, 126.8, 123.6, 123.5, 121.5, 119.53, 119.47, 114.5, 113.5, 110.2, 97.3, 82.0, 59.8, 59.1, 57.0, 21.0 ppm; HRMS (APCI+)  $m/z$ :  $[\text{M} + \text{H}]^+$  calcd for  $\text{C}_{31}\text{H}_{25}\text{ClN}_5\text{O}_2$  534.16913, found 534.16941.

### 5.3.2 *In vitro* Pharmacology

The final single- and dual-NBN compounds, as well as the commercial inhibitors nilotinib and ponatinib, were assayed by colleagues at either Reaction Biology Corp. (Abl1; hERG; cellular cytotoxicity), the University of Dundee (kinome screening panel), or in-house (CYP3A4; aqueous solubility; microsome and plasma stability). Procedures and primary data are presented below with the compounds coded according to Table 5.9.

**Table 5.9.** Compound codes used to assay final compounds

Compound ID	Assay Compound Code
5.9a	1
5.9b	2
5.9c	3
5.17a	5
5.17b	4
5.17c	6

#### 5.3.2.1 *Abl1* Kinase Profiling (performed by Reaction Biology Corp.)

Compounds were tested in a 10-dose activity response assay in duplicate for IC<sub>50</sub> determination with 3-fold serial dilution starting at a highest dose of 30 nM. Control compound staurosporine was tested in 10-dose IC<sub>50</sub> mode with 4-fold serial dilution starting at 20 μM. Reactions were carried out at 10 μM ATP. Curve fits were performed where the enzyme activities at the highest concentration of compound tested were less than 65% and are shown as provided by Reaction Biology in Figure 5.3.

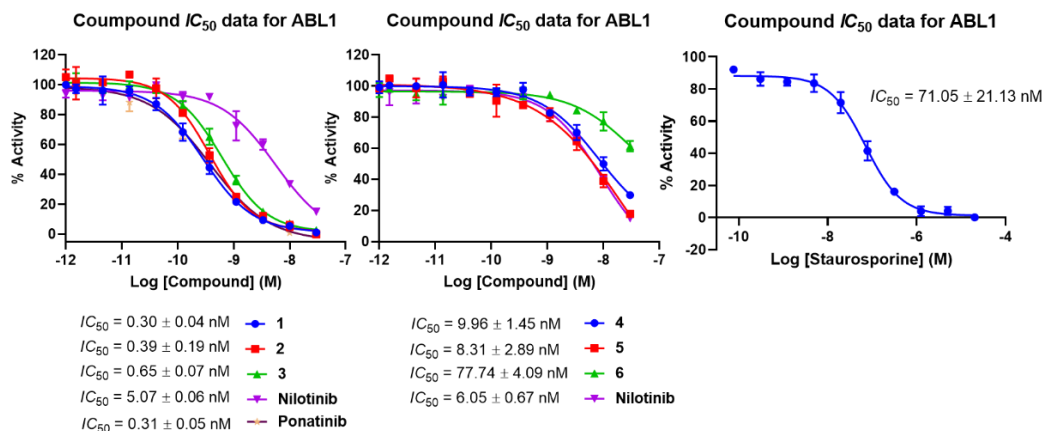


**Figure 5.3.** Abl1 kinase dose-response curves in duplicate for experimental compounds **1 – 3** (left), **4 – 6** (middle) with nilotinib and ponatinib, and associated positive control (staurosporine, right). Data analysis performed with GraphPad Prism software, version 8.3.0, for Windows using a dose-response 4-parameter logistic equation.

### 5.3.2.2 hERG Profiling (performed by Reaction Biology Corp.)

Compounds were prepared as 10mM DMSO stock and stored at  $-80^{\circ}\text{C}$ . Compounds were tested in a 10-dose  $IC_{50}$  duplicate mode with a 3-fold serial dilution starting at  $10\ \mu\text{M}$ . Control compounds, nilotinib and lapatinib, were tested in a 10-dose  $IC_{50}$  with 3-fold serial dilution starting at  $10\ \mu\text{M}$ . Control compound, E-4031, was tested in a 10-dose  $IC_{50}$  with 3-fold serial dilution starting at  $1\ \mu\text{M}$ .

**Assay Format:** The assay is based on the competition of fluorescently labeled Tracer binding to the membrane preparation containing hERG.

**Assay conditions:** 1 nM Predictor™ hERG Tracer Red; 1X Predictor™ hERG Membrane

**Assay Buffer:** 25 mM Hepes, pH 7.5, 15 mM KCl, 1 mM MgCl<sub>2</sub>, 0.05% PF-127, and 1% DMSO

**Assay Procedure:** Compounds in DMSO were added into the Membrane mixture by using Acoustic Technology. Tracer was added, and gently mixed in the dark. FP was measured after 4 hours incubation at room temperature and mP calculated.

**Measurement:** Ex = 531 nm FP, Em = 595 nm P and S

Curve fits were performed by GraphPad Prism software when the activities at the highest concentration of compounds were less than 65%, and the data are as shown in Figure 5.4. Background was established by the average FP signal in the presence of 30  $\mu\text{M}$  E-4031.

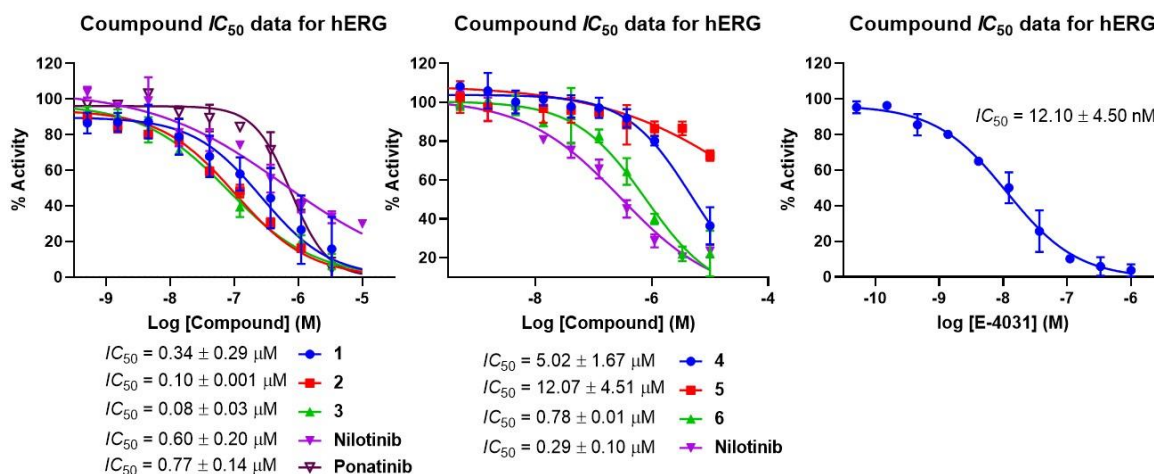


**Figure 5.4.** hERG channel dose-response curves in duplicate for experimental compounds 1 – 3 (left), 4 – 6 (middle) with nilotinib, ponatinib, and positive control E-4031 (right). Data analysis performed with GraphPad Prism software, version 8.3.0, for Windows using a dose-response 4-parameter logistic equation.

### 5.3.2.3 Fluorometric CYP450 Enzyme Inhibition Assays (performed by Dr. Savita Sharma)

The CYP450 inhibition assays utilize microsomes from insect cells expressing human recombinant individual cDNA-expressed CYP isoforms 3A4 enzyme, as well as the fluorogenic probe that produces fluorescent metabolite. Standard inhibitors were co-incubated with fluorogenic substrates, and their inhibitory potential ( $IC_{50}$ ) was determined. Assay conditions in terms of CYP450 protein concentration and time of incubation were standardized, enzyme kinetics parameters of each fluorescent probe substrate were estimated and  $IC_{50}$  values of inhibitors were determined and validated on different days to check reproducibility. This method is very robust, efficient and highly reproducible.

**Experimental Details:** Test compounds were prepared in 100 % DMSO and did not exceed a final concentration of <0.2% in the reaction. A 100 mM sodium phosphate buffer was prepared and adjusted to pH 7.4. In a separate Falcon tube, a 2X enzyme/substrate (E/S) solution was prepared in phosphate buffer. The final concentration of CYP3A4 (Corning) and BFC was 20 nM and 40  $\mu\text{M}$ ,

respectively. In a separate falcon tube, a 2X NADPH regenerating system (NRS) was prepared in phosphate buffer. The final concentration for each component in the assay was as follows: 2.45 mM NADPH, 24.7 mM glucose 6-phosphate, 1.25 U of glucose-6-phosphate dehydrogenase/mL

The enzymatic assays were conducted in a 96-well microtiter plate (Black, Corning Costar) with a final volume of 100  $\mu$ L. Preparation of the plate began with the addition of 74  $\mu$ L of the E/S in the first well, and 50  $\mu$ L to all subsequent wells (from 2-11). The test compounds (1  $\mu$ L) were dissolved in the first well to give the first row a final volume of 75  $\mu$ L. A 1:3 serial dilution of the test compound was conducted by removing 25  $\mu$ L from the first well and diluting it with the second and so forth until the tenth row. Final concentrations yielded a range from 200  $\mu$ M – 0.01  $\mu$ M. Well 11 contained no inhibitor, and well 12 contained no enzyme. Both were used as controls for background fluorescence. The plate was incubated for 30 min at 37 °C. After incubation, the reaction was initiated by the addition of 50  $\mu$ L of the 2X NRS to each well.

Immediately (within 1 min) the fluorescence was measured using a microplate reader (BioTek Synergy Neo 2). CYP3A4 was monitored at Ex/Em = 410/538 nm in kinetic mode that scanned every 5 min for 60 mins. Data was exported and analyzed using Graph Pad Prism 7®. Fluorescence readout was normalized to the fluorescence intensity of the reaction in the absence of the test substance (well 11, 0% inhibition) and the mixture of reaction components in the presence of “Inhibitor Cocktail” (well 12, 100% inhibition). The IC<sub>50</sub> value was derived after the data was fitted on a 10-point curve using a four-parameter logistic regression model, and the data are shown in Figure 5.5.

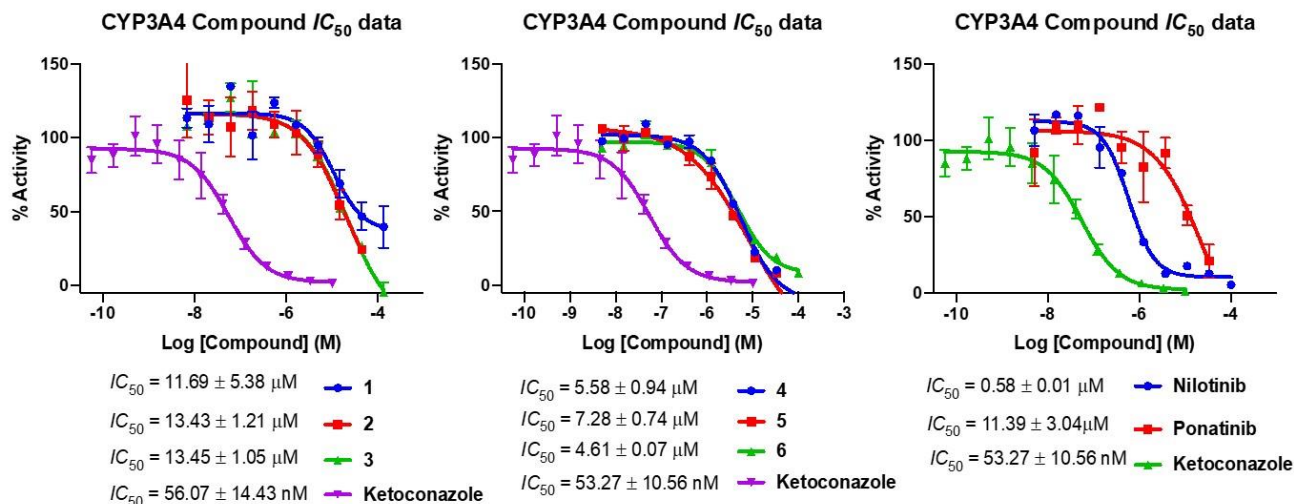


**Figure 5.5.** Calculated CYP450 (3A4) inhibition data on compounds 1–3 (left), 4–6 (middle), nilotinib, and ponatinib (right). Ketoconazole was also run each time as a positive control. Each point represents two data points. Data analysis performed with GraphPad Prism software, version 8.3.0, for Windows using a dose-response 4-parameter logistic equation.

#### 5.3.2.4 Metabolic Stability Assays (performed by Dr. Savita Sharma and Perry Bartsch, III)

Instrumentation and method development: The LC-MS/MS analysis was performed using Agilent 1260 Infinity II HPLC, coupled with an Agilent G6460 triple quadrupole mass spectrometer (Agilent Technologies, USA). All the data were acquired employing Agilent 6460 Quantitative Analysis data processing software. Reverse-phase HPLC separation for each compound (4, 5, 6, nilotinib, and ponatinib, verapamil and diphenhydramine) was achieved on an Agilent Eclipse plus – C18 column (2.1 X 100 mm, 3.5  $\mu\text{m}$ ), and Agilent Zorbax XDB C18 column (2.1 x 50 mm, 3.5 micron) with a mobile phase composed of MeOH-water-formic acid or acetonitrile-water-formic acid (0.1%) at a flow rate of 0.5 mL/min. The method has a chromatographic total run time of 10.10 min. Each method was developed in the presence of an internal standard (ISTD) *d*<sub>5</sub>-7-ethoxy coumarin. The column temperature was maintained at 40 °C. The detection was operated in the Agilent JetStream electrospray positive ionization using multiple reaction monitoring mode (MRM). The transitions of *m/z* 522.18 → 399.1/260.1 for the compound 4 (**5.17b**), and *m/z* 196.1 → 164.0 for the *d*<sub>5</sub>-7-Ethoxy Coumarin (internal standard) were monitored. Similarly, other compounds were also monitored in an MRM mode with an internal standard, and their transitions are: *m/z* 508.17 → 399.1/260.1 for 5

(5.17a); m/z 534.17 → 399.1/260.1 for 6 (5.17c); m/z 530.19 → 289.1/ 259.1/ 261.1 for Nilotinib; m/z 533.2 → 101.2/ 260.1 / 433.1 for Ponatinib; m/z 256.17 → 167.1 for diphenhydramine (positive control for the mouse liver microsomes); m/z 455.11 → 165.1/303.2 for Verapamil (positive control for the human liver microsomes), respectively.

Other MS conditions were as follows: dwell time 100 ms; gas flow 10 L/min; nebulizer pressure 45 psi; delta EMV 200 V; fragmentor voltage and collision energy for individual compounds are shown in the Table 5.10.

**Table 5.10.** Scan parameters for the tested compounds and its transitions in multiple reaction monitoring mode.

Cpd Name	Precursor Ion MS1	Product ion MS2	Dwell (ms)	Fragmentor voltage (V)	Collision Energy (V)	Cell Accelerator (v)	Polarity
4 (5.17b)	522.2	399.1 260.1	100	106	16 28	4	positive
5 (5.17a)	508.2	399.1 260.1	100	106	16 28	4	positive
6 (5.17c)	534.17	399.1 260.1	100	106	16 32	4	positive
Nilotinib	530.2	289.1	100	180	32	4	positive
		289.1	100		60		
		259.1			17		
Ponatinib	533.2	433.1	100	144	21	4	positive
		260.2			29		
		101.2			21		
Diphenhydramine	256.2	167.1	100	78	8	4	positive
Verapamil	455.1	165.1	100	126	28	4	positive
		303.2			24		
d5-7-Ethoxy coumarin (ISTD)	196.1	164	100	116	17	4	positive

**Experimental details:** Test compounds were dissolved in 100% DMSO to make 10 mM stock solutions. Verapamil (human liver microsomes, Sigma Aldrich) and diphenhydramine (Mouse liver microsomes, Sigma Aldrich) aided as positive controls and were dissolved in 100% DMSO to make 10 mM stock solutions. The 10 mM stock solution of test and control compounds were further diluted in potassium phosphate buffer (100 mM, pH 7.4) to 500 μM to ensure the organic solvent content was < 0.2%. Human and mouse liver microsomes were purchased from Xenotech at 20 mg/mL. NADPH (Sigma Aldrich) 10 mM stocks were prepared in deionized water.

The liver microsome (HLM or MLM) assay was prepared in a 1.5 mL Eppendorf tube with a final volume of 1100  $\mu\text{L}$  for duplicate runs. Each reaction contained phosphate buffer (928.4  $\mu\text{L}$ ), liver microsomes (55  $\mu\text{L}$ ), and test compound resulting in a final concentration of 3  $\mu\text{M}$  (6.6  $\mu\text{L}$  of 500  $\mu\text{M}$ ). The reaction was initiated with 110  $\mu\text{L}$  of 10 mM NADPH. Aliquots (100  $\mu\text{L}$ ) were removed in duplicate at 0, 5, 10, 15, 30 min time intervals and quenched in cold 100 mL of 100 % MeOH which contains internal standard (ISTD: *d*<sub>5</sub>-7-ethoxy coumarin 4 mM). The aliquots were centrifuged at 12,000 g for 5 min and the supernatant removed and placed in an LC-MS vial. Each time point was assessed on the LC-MS and the area, based on the MRM transition, was integrated w.r.t the ISTD. Positive controls were conducted at a final volume of 550  $\mu\text{L}$  to give each time point in a single run. A no-NADPH negative control with test and control compound was performed in a single (150  $\mu\text{L}$ ) at the longest time point. Controls were processed and analyzed like test compounds. Each time point was run in duplicates followed by in-between blank washes to avoid the carryover and to equilibrate the column. Data are shown in Figure 5.6.

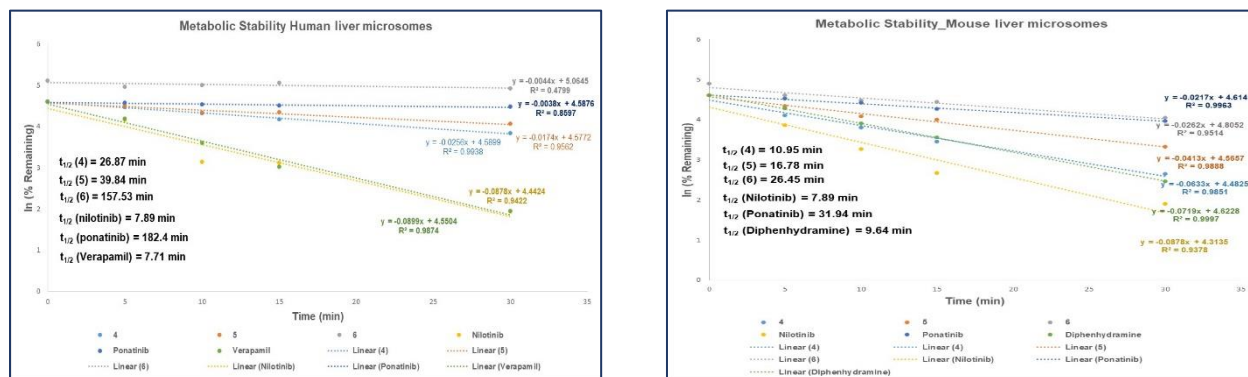


**Figure 5.6.** Metabolic stability shown as the % remaining of compounds 4 – 6, nilotinib, and ponatinib after every time point ( $t = 0, 5, 10, 15$  and 30 min) from HLM (left) and MLM (right). Each time point was taken in duplicate. Verapamil served as a positive control for HLM, and diphenhydramine is positive control for the MLM with each test compound. Data analysis was performed in Excel, using a linear regression equation on 5-time points to obtain the slope which was used to calculate half-life.

### 5.3.2.5 CellTiter-Glo Viability Assay Protocol (performed by Reaction Biology Corp.)

**Materials:** The reference compound staurosporine was purchased from Sigma-Aldrich (Saint Louis, MI). Cell Titer-Glo® 2.0 Luminescent cell viability assay reagent was purchased from Promega (Madison, WI). THLE-3 and HEK293 cell lines were purchased from American Type Culture

Collection (Manassas, VA). THLE-3 cells were cultured in BEGM purchased from Lonza/Clonetics Corporation (Walkersville, MD 21793; BEGM Bullet Kit; CC3170). The kit includes 500 mL basal medium and separate frozen additives from which we discard the Gentamycin/ Amphotericin (GA) and Epinephrine and to which we add extra 5 ng/mL EGF, 70 ng/mL Phosphoethanolamine. HEK293 cells were cultured in Dulbecco's Modified Eagle's Medium. All media were supplemented with 10% fetal bovine serum, 100 µg/ml of penicillin and 100 µg/ml of streptomycin. Cultures were maintained at 37°C in a humidified atmosphere of 5% CO<sub>2</sub> and 95% air.

#### Procedure:

1. Two test compounds (**4** and **5**) and reference compound staurosporine were diluted in DMSO solution with 10-dose and 3-fold dilution in a source plate starting at 50 mM (test compounds) and 10 mM (staurosporine).
2. 125 nl test compounds and 25 nl staurosporine were delivered from the source plate to each well of the 384-well cell culture plate by Echo 550.
3. 25 µl of culture media containing 2,000 THLE-3 or HEK293 cells was added to each of the wells of the cell culture plate in duplicate.
4. The cells were incubated with the compounds at 37°C, 5% CO<sub>2</sub> for 72 hours.
5. 25 µl of Cell Titer Glo 2.0 reagent was added to each well.
6. The contents were mixed on an orbital shaker for 2 min and incubated at room temperature for 15 min to stabilize luminescent signal.
7. Luminescence was recorded by Envision 2104 Multilabel Reader (PerkinElmer, Santa Clara, CA). The number of viable cells in culture was determined based on quantitation of the ATP present in each culture well.
8. The IC<sub>50</sub> curves were plotted and IC<sub>50</sub> values were calculated using the GraphPad Prism 4 program based on a sigmoidal dose-response equation.

#### **5.3.2.6 Kinase Selectivity Panel (performed by International Centre for Kinase Profiling, University of Dundee)**

General methodology:<sup>59</sup> All kinase assays are carried out using Multidrop 384's at room temperature in a total assay volume of 25.5 µL. To plates containing 0.5 µL of compounds, DMSO controls or acid blanks, 15 µL of an enzyme mix containing enzyme and peptide/protein substrate in buffer is added. Compounds are pre-incubated in the presence of the enzyme and peptide/protein

substrate for 5 minutes before initiation of the reaction by addition of 10  $\mu$ L of ATP (final concentration selected for each kinase at 5, 20 or 50  $\mu$ M). Assays are carried out for 30 minutes at room temperature before termination by the addition of 5  $\mu$ L orthophosphoric acid. The assay plates are then harvested onto P81 Unifilter Plates by a Perkinelmer Harvester and air dried. The dry Unifilter plates are then sealed on the addition of MicroScint O and are counted in Perkin-Elmer Topcount scintillation counters. The following exceptions to the general methodology are noted regarding the MKK1 and MKK2 assays:

MKK1 /MKK2 assays: This is a two-step assay where inactive MAPK (0.06 mg/ml) is activated by MKK1/MKK2 (diluted in 25 mM Tris, 0.1 mM EGTA, 0.1% b-mercaptoethanol, 0.01% Brij35, 1 mg/ml BSA) in 25.5  $\mu$ l containing 25 mM Tris, 0.1 mM EGTA, 0.01% Brij35, 10 mM magnesium acetate and 0.005 mM ATP. After incubating at room temperature for 30 min, 5  $\mu$ l from the first reaction is pipetted into 20  $\mu$ l of the second reaction mix containing (final concentration) 25 mM Tris pH 7.5, 0.1 mM EGTA, 0.1 mM Na<sub>3</sub>VO<sub>4</sub>, 0.66 mg/ml myelin basic protein (MBP), 10 mM magnesium acetate and 0.05 mM [33P-g-ATP] (500 -1000 cpm/pmole) and incubated for 30 min at room temperature. Assays are stopped by addition of 5  $\mu$ l of 0.5 M (3%) orthophosphoric acid and then harvested onto P81 Unifilter plates.

### 5.3.3 *In vivo* Pharmacology

The lead compounds **5.17a** and **b**, as well as the commercial inhibitor nilotinib, were evaluated for their *in vivo* pharmacokinetic profiles by colleagues at Sai Life Sciences, Ltd. (Pune, India). Complete procedures and primary data are given in the Final Reports as prepared by their staff which are appended to this dissertation as separate supplemental files. The Summary for each compound included on the following pages is taken directly from the Final Report for each compound with minor modifications for consistent numbering; credit is given to their staff.

#### 5.3.3.1 Pharmacokinetic Summary of 5.17a (ZD-3-392)

The objective of this study was to investigate the pharmacokinetics and brain distribution of ZD-3-392 (**5.17a**) in male C57BL/6 mice following a single intravenous and oral administration

(Dose: 3 mg/kg; IV and 3, 10, 30; PO). Study was conducted in two parts. Total thirty six male mice were included into the study and divided in to four groups as Group 1 to Group 4 with nine mice in each group.

**PK-21-06-568:** Animals in Group 1 (n=9) were administered intravenously with solution formulation of ZD-3-392 (**5.17a**) at 3 mg/kg dose. The formulation vehicle was 5% v/v NMP, 5% v/v Solutol HS-15 and 90% v/v normal saline.

**PK-21-06-565:** Animals in Group 2 (n=9), Group 3 (n=9) to Group 4 (n=9) were administered orally with solution formulation of ZD-3-392 (**5.17a**) at 3, 10 and 30 mg/kg dose, respectively. The formulation vehicle was % v/v NMP, 5% v/v Solutol HS-15 and 90% v/v normal saline.

Blood samples (approximately 60  $\mu$ L) were collected under light isoflurane anesthesia (Surgivet®) from retro orbital plexus from a set of three mice at 0.083, 0.25, 0.5, 1, 2, 4, 8, 12 and 24 h (IV) and 0.25, 0.5, 1, 2, 4, 8, 12 and 24 h (PO; Group 2 to Group 4). Immediately after blood collection, plasma was harvested by centrifugation at 4000 rpm, 10 min at 4°C and samples were stored at -70 $\pm$ 10°C until bioanalysis.

Following blood collection from Group 2 to Group 4, animals were sacrificed immediately followed by abdominal vena-cava was cut open and whole body was perfused from heart using 10 mL of normal saline. Brain samples were collected from set of three mice at 1, 4, and 24 h (PO) from respective mice. After isolation, brain samples were rinsed three times in ice cold normal saline (for 5-10 seconds/rinse using ~5-10 mL normal saline in disposable petri dish for each rinse) and dried on blotting paper. Brain samples were homogenized using ice-cold phosphate buffer saline (pH-7.4). Total homogenate volume was three times the brain weight. All homogenates were stored below -70 $\pm$ 10 °C until bioanalysis. All samples were processed for analysis of ZD-3-392 (**5.17a**) by protein precipitation method and analyzed with fit-for-purpose LC-MS/MS method (LLOQ = 2.03 ng/mL for plasma and brain). The pharmacokinetic parameters were estimated using non-compartmental analysis tool of Phoenix® WinNonlin software (Ver 8.0) and parameters are summarized below:

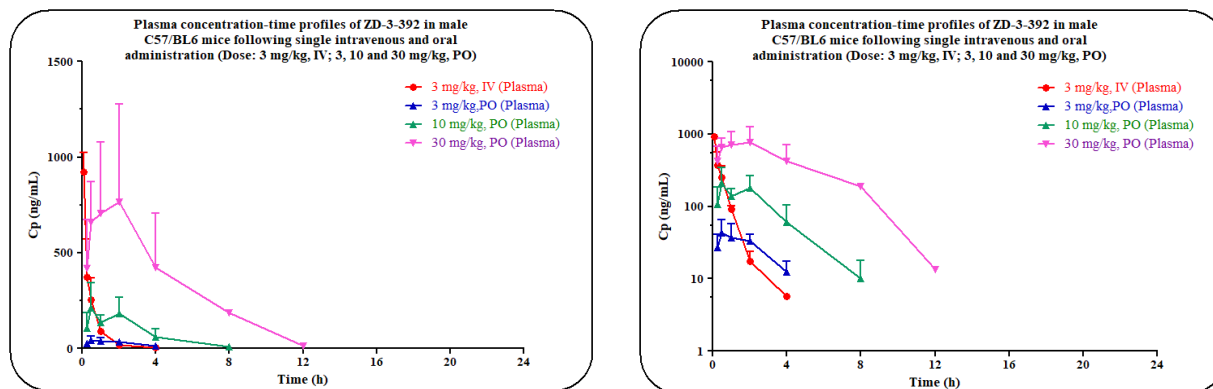


**Figure 5.7.** Plasma concentrations-time profiles (mean  $\pm$  SD) of ZD-3-392 (**5.17a**) in male C57BL/6 mice following a single intravenous and oral administration (Dose: 3 mg/kg, IV; 3, 10 and 30 mg/kg, PO) plotted on linear (left) and semi-log (right) scales.

**Table 5.11.** Pharmacokinetics data of ZD-3-392 (**5.17a**) in male C57BL/6 mice following a single intravenous and oral administration (Dose: 3 mg/kg; IV and 3, 10, 30 mg/kg; PO).

Matrix	Route	Dose (mg/kg)	T <sub>max</sub> (h)	<sup>a</sup> C <sub>0</sub> /C <sub>max</sub> (ng/mL)	AUC <sub>last</sub> (h*ng/mL)	T <sub>1/2</sub> (h)	CL (mL/min/kg)	V <sub>ss</sub> (L/kg)	%F
Plasma	IV	3	-	1419.98	445.91	0.80	110.73	3.66	-
	PO	3	0.50	43.10	113.59	-	-	-	25
		10	0.50	210.15	681.14	-	-	-	46
		30	2.00	764.53	4084.89	-	-	-	92

<sup>a</sup> – Back extrapolated concentration in IV group;

**Table 5.12.** Individual plasma and brain concentrations and brain-Kp of ZD-3-392 (**5.17a**) in male C57BL/6 mice following a single oral administration (Dose: 3, 10 and 30 mg/kg)

Dose (mg/kg)	Time (h)	Animal ID	Plasma Concentration (ng/mL)	Brain Concentration (ng/g)	Brain-Kp	Mean	
3 mg/kg	1	1	14.71	BLQ	NC	NC	
		2	43.24	BLQ	NC		
		3	53.78	BLQ	NC		
	4	4	10.98	BLQ	BLQ	NC	NC
		5	8.74	BLQ	BLQ	NC	
		6	17.86	BLQ	BLQ	NC	
	24	7	BLQ	BLQ	BLQ	NC	NC
		8	BLQ	BLQ	BLQ	NC	
		9	BLQ	BLQ	BLQ	NC	
10 mg/kg	1	10	111.86	27.81	0.25	0.15	
		11	123.04	16.35	0.13		
		12	178.44	13.62	0.08		
	4	13	110.35	11.31	0.10	0.15 <sup>d</sup>	
		14	41.36	8.34	0.20		
		15	29.54	BLQ	NC		
	24	16	BLQ	BLQ	BLQ	NC	NC
		17	BLQ	BLQ	BLQ	NC	
		18	BLQ	BLQ	BLQ	NC	
30 mg/kg	1	19	602.30	73.98	0.12	0.10	
		20	1120.71	116.88	0.10		
		21	398.39	34.59	0.09		
	4	22	311.54	59.01	0.19	0.16	
		23	217.81	37.38	0.17		
		24	745.44	94.77	0.13		
	24	25	BLQ	BLQ	BLQ	NC	NC
		26	BLQ	BLQ	BLQ	NC	
		27	BLQ	BLQ	BLQ	NC	

LLOQ: 2.03 ng/mL for plasma and brain; d - Average of two values reported; BLQ- Below limit of quantitation; NC- Not calculated

Following a single intravenous administration of ZD-3-392 (**5.17a**) in male C57BL/6 mice at 3 mg/kg dose, compound showed high plasma clearance (higher than the normal liver blood flow in mice: 90 mL/min/kg) and high V<sub>ss</sub> (~5-fold of total body water content: 0.7 L/kg) with terminal elimination plasma half-life of 0.80 h.

Following a single oral administration of ZD-3-392 (**5.17a**) in male C57BL/6 mice at 3, 10 and 30 mg/kg dose, peak plasma concentrations were observed in between 0.5 to 2 h, suggesting rapid to

prolonged absorption. Levels in brain were not quantifiable at 3 mg/kg dose while, quantifiable up to 4 h at 10 and 30 mg/kg dose. At 10 mg/kg dose, brain-Kp were 0.15 (1 and 4 h) and at 30 mg/kg dose, brain-Kp were 0.10 (1 h) and 0.16 (4 h).

Increase in plasma exposure from 3 mg/kg to 10 mg/kg and from 10 mg/kg to 30 mg/kg dose, was more than dose proportional.

In summary, ZD-3-392 (**5.17a**) exhibited high clearance, high Vss, short half-life and more than dose proportional increase in plasma exposure across the doses.

### **5.3.3.2 Pharmacokinetic Summary of 5.17b (ZD-3-372)**

The objective of this study was to investigate the pharmacokinetics and brain distribution of ZD-3-372 (**5.17b**) in male C57BL/6 mice following a single intravenous and oral administration (Dose: 3 mg/kg; IV and 3, 10, 30; PO). Study was conducted in two parts. Total thirty six male mice were included into the study and divided into four groups as Group 1 to Group 4 with nine mice in each group.

**PK-21-06-564:** Animals in Group 1 (n=9) were administered intravenously with solution formulation of ZD-3-372 (**5.17b**) at 3 mg/kg dose. The formulation vehicle was 5% v/v NMP, 5% v/v Solutol HS-15 and 90% v/v citric acid (10 mM).

**PK-21-06-567:** Animals in Group 2 (n=9), Group 3 (n=9) to Group 4 (n=9) were administered orally with solution formulation of ZD-3-372 (**5.17b**) at 3, 10 and 30 mg/kg dose, respectively. The formulation vehicle was 5% v/v NMP, 5% v/v Solutol HS-15 and 90% v/v citric acid (10 mM).

Blood samples (approximately 60  $\mu$ L) were collected under light isoflurane anesthesia (Surgivet®) from retro orbital plexus from a set of three mice at 0.083, 0.25, 0.5, 1, 2, 4, 8, 12 and 24 h (IV) and 0.25, 0.5, 1, 2, 4, 8, 12 and 24 h (PO; Group 2 to Group 4). Immediately after blood collection, plasma was harvested by centrifugation at 4000 rpm, 10 min at 4°C and samples were stored at -70 $\pm$ 10°C until bioanalysis.

Following blood collection from Group 2 to Group 4, animals were sacrificed immediately followed by abdominal vena-cava was cut open and whole body was perfused from heart using 10 mL of normal saline. Brain samples were collected from set of three mice at 1, 4, and 24 h (PO) from respective mice. After isolation, brain samples were rinsed three times in ice cold normal saline (for 5-10 seconds/rinse using ~5-10 mL normal saline in disposable petri dish for each rinse) and dried on blotting paper. Brain samples were homogenized using ice-cold phosphate buffer saline (pH-7.4). Total homogenate volume was three times the brain weight. All homogenates were stored below -70 $\pm$ 10 °C until bioanalysis. All samples were processed for analysis of ZD-3-372 (**5.17b**) by protein precipitation method and analyzed with fit-for-purpose LC-MS/MS method (LLOQ = 1.03 ng/mL for plasma and brain). The pharmacokinetic parameters were estimated using non-compartmental analysis tool of Phoenix® WinNonlin software (Ver 8.0) and parameters are summarized below:

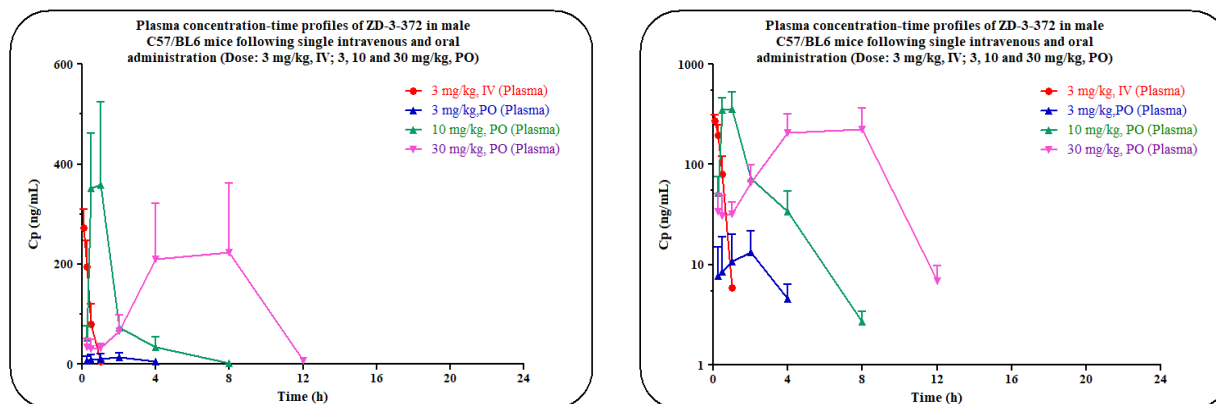


**Figure 5.8.** Plasma concentrations-time profiles (mean  $\pm$  SD) of ZD-3-372 (**5.17b**) in male C57BL/6 mice following a single intravenous and oral administration (Dose: 3 mg/kg, IV; 3, 10 and 30 mg/kg, PO) plotted on linear (left) and semi-log (right) scales.

**Table 5.13.** Pharmacokinetics data of ZD-3-372 (**5.17b**) in male C57BL/6 mice following a single intravenous and oral administration (Dose: 3 mg/kg; IV and 3, 10, 30 mg/kg; PO).

Matrix	Route	Dose (mg/kg)	T <sub>max</sub> (h)	<sup>a</sup> C <sub>0</sub> /C <sub>max</sub> (ng/mL)	AUC <sub>last</sub> (h*ng/mL)	T <sub>1/2</sub> (h)	CL (mL/min/kg)	V <sub>ss</sub> (L/kg)	%F
Plasma	IV	3	-	318.53	119.08	0.15	NR (415.32)	6.40	-
	PO	3	2.00	13.24	37.58	-	-	-	32
		10	1.00	358.25	629.28	-	-	-	>100
		30	8.00	223.82	1679.76	-	-	-	>100

<sup>a</sup> – Back extrapolated concentration in IV group; NR – Clearance is not reported since very high value

**Table 5.14.** Individual plasma and brain concentrations and brain-Kp of ZD-3-372 (**5.17b**) in male C57BL/6 mice following a single oral administration (Dose: 3, 10 and 30 mg/kg)

Dose (mg/kg)	Time (h)	Animal ID	Plasma Concentration (ng/mL)	Brain Concentration (ng/g)	Brain-Kp	Mean
3 mg/kg	1	1	11.12	BLQ	NC	NC
		2	1.30	BLQ	NC	
		3	19.67	BLQ	NC	
	4	4	3.64	BLQ	NC	NC
		5	3.30	BLQ	NC	
		6	6.70	BLQ	NC	
	24	7	BLQ	BLQ	NC	NC
		8	BLQ	BLQ	NC	
		9	BLQ	BLQ	NC	
10 mg/kg	1	10	427.00	4.95	0.01	0.02
		11	169.71	4.20	0.02	
		12	478.03	8.85	0.02	
	4	13	56.85	BLQ	NC	NC
		14	23.68	BLQ	NC	
		15	21.20	BLQ	NC	
	24	16	BLQ	BLQ	NC	NC
		17	BLQ	BLQ	NC	
		18	BLQ	BLQ	NC	
30 mg/kg	1	19	36.01	19.95	0.55	1.22
		20	20.84	28.35	1.36	
		21	39.00	67.80	1.74	
	4	22	181.03	10.08	0.06	0.09
		23	332.68	13.56	0.04	
		24	113.98	18.75	0.16	
	24	25	BLQ	BLQ	NC	NC
		26	BLQ	BLQ	NC	
		27	BLQ	BLQ	NC	

LLOQ: 1.03 ng/mL for plasma and brain; BLQ- Below limit of quantitation; NC- Not calculated; NA- Not applicable.

Following a single intravenous administration of ZD-3-372 (**5.17b**) in male C57BL/6 mice at 3 mg/kg dose, compound showed very high plasma clearance (higher than the normal liver blood flow in mice: 90 mL/min/kg) and high V<sub>ss</sub> (~9-fold of total body water content: 0.7 L/kg) with terminal elimination plasma half-life of 0.15 h.

Following a single oral administration of ZD-3-372 (**5.17b**) in male C57BL/6 mice at 3, 10 and 30 mg/kg dose, peak plasma concentrations were observed in between 1 to 8 h, suggesting rapid to

prolonged absorption. Levels in brain were not quantifiable at 3 mg/kg dose while, quantifiable up to 1 h and 4 h at 10 and 30 mg/kg dose, respectively. At 10 mg/kg dose, brain-K<sub>p</sub> were 0.02 (1 h) and at 30 mg/kg dose, brain-K<sub>p</sub> were 1.22 (1 h) and 0.09 (4 h).

Increase in plasma exposure from 3 mg/kg to 10 mg/kg was more than dose proportional while increase from 10 mg/kg to 30 mg/kg dose, was less than dose proportional.

In summary, ZD-3-372 (**5.17b**) exhibited high clearance, high V<sub>ss</sub>, short half-life and low to moderate plasma exposures across the doses.

### **5.3.3.3 Pharmacokinetic Summary of Nilotinib (ZD-3-188)**

The objective of this study was to investigate the pharmacokinetics and brain distribution of ZD-3-188 (nilotinib) in male C57BL/6 mice following a single intravenous and oral administration (Dose: 3 mg/kg; IV and 3, 10, 30; PO). Study was conducted in two parts. Total thirty six male mice were included into the study and divided into four groups as Group 1 to Group 4 with nine mice in each group.

**PK-21-06-563:** Animals in Group 1 (n=9) were administered intravenously with solution formulation of ZD-3-188 (nilotinib) at 3 mg/kg dose. The formulation vehicle was 5% v/v NMP, 5% v/v Solutol HS-15, 30% v/v PEG-300 and 60% v/v normal saline.

**PK-21-06-566:** Animals in Group 2 (n=9), Group 3 (n=9) to Group 4 (n=9) were administered orally with solution formulation of ZD-3-188 (nilotinib) at 3, 10 and 30 mg/kg dose, respectively. The formulation vehicle was 5% v/v NMP, 5% v/v Solutol HS-15, 30% v/v PEG-300 and 60% v/v normal saline.

Blood samples (approximately 60 µL) were collected under light isoflurane anesthesia (Surgivet®) from retro orbital plexus from a set of three mice at 0.083, 0.25, 0.5, 1, 2, 4, 8, 12 and 24 h (IV) and Pre-dose, 0.25, 0.5, 1, 2, 4, 8, 12 and 24 h (PO; Group 2 to Group 4). Immediately after blood collection, plasma was harvested by centrifugation at 4000 rpm, 10 min at 4°C and samples were stored at -70±10°C until bioanalysis.

Following blood collection from Group 2 to Group 4, animals were sacrificed immediately followed by abdominal vena-cava was cut open and whole body was perfused from heart using 10 mL of

normal saline. Brain samples were collected from set of three mice at 1, 4, and 24 h (PO) from respective mice. After isolation, brain samples were rinsed three times in ice cold normal saline (for 5-10 seconds/rinse using ~5-10 mL normal saline in disposable petri dish for each rinse) and dried on blotting paper. Brain samples were homogenized using ice-cold phosphate buffer saline (pH-7.4). Total homogenate volume was three times the brain weight. All homogenates were stored below  $-70 \pm 10$  °C until bioanalysis. All samples were processed for analysis of ZD-3-188 (nilotinib) by protein precipitation method and analyzed with fit-for-purpose LC-MS/MS method (LLOQ = 1.03 and 2.07 ng/mL for plasma and 1.03 ng/mL for brain). The pharmacokinetic parameters were estimated using non-compartmental analysis tool of Phoenix® WinNonlin software (Ver 8.0) and parameters are summarized below:

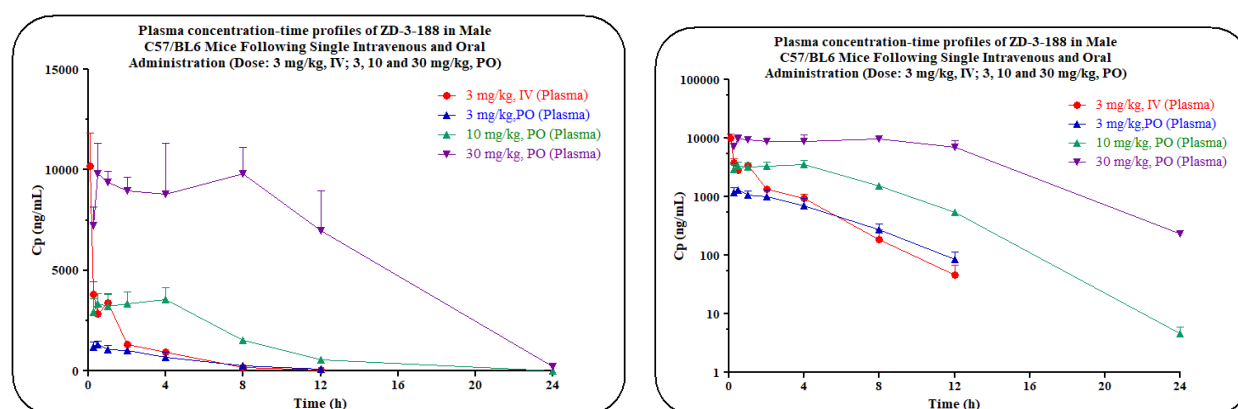


**Figure 5.9.** Plasma concentrations-time profiles (mean  $\pm$  SD) of ZD-3-188 (nilotinib) in male C57BL/6 mice following a single intravenous and oral administration (Dose: 3 mg/kg, IV; 3, 10 and 30 mg/kg, PO)

**Table 5.15.** Pharmacokinetics data of ZD-3-188 (nilotinib) in male C57BL/6 mice following a single intravenous and oral administration (Dose: 3 mg/kg; IV and 3, 10, 30 mg/kg; PO).

Matrix	Route	Dose (mg/kg)	T <sub>max</sub> (h)	<sup>a</sup> C <sub>0</sub> /C <sub>max</sub> (ng/mL)	AUC <sub>last</sub> (h*ng/mL)	T <sub>1/2</sub> (h)	CL (mL/min/kg)	V <sub>ss</sub> (L/kg)	%F
Plasma	IV	3	0.08	16152.1 0	12325.03	2.78	4.05	0.59	-
	PO	3	0.50	1300.80	6475.22	-	-	-	53
		10	4.00	3557.68	30597.59	-	-	-	74
		30	8.00	9799.59	148877.32	-	-	-	>100

<sup>a</sup> – Back extrapolated concentration in IV group;

**Table 5.16.** Individual plasma and brain concentrations and brain-K<sub>p</sub> of ZD-3-188 (nilotinib) in male C57BL/6 mice following a single oral administration (Dose: 3, 10 and 30 mg/kg)

Dose (mg/kg)	Time (h)	Animal ID	Plasma Concentration (ng/mL)	Brain Concentration (ng/g)	Brain-K <sub>p</sub>	Mean Brain-K <sub>p</sub>
3 mg/kg	1	1	1009.01	31.23	0.03	0.03
		2	924.85	35.31	0.04	
		3	1286.65	29.94	0.02	
	4	4	501.73	17.97	0.04	0.03
		5	643.78	25.65	0.04	
		6	951.49	14.82	0.02	
	24	7	BLQ	BLQ	NC	NA
		8	BLQ	BLQ	NC	
		9	BLQ	BLQ	NC	
10 mg/kg	1	10	2906.75	174.18	0.06	0.05
		11	3914.48	112.20	0.03	
		12	2807.23	128.07	0.05	
	4	13	3450.46	85.44	0.02	0.03
		14	4214.91	105.30	0.02	
		15	3007.67	123.06	0.04	
	24	16	5.64	BLQ	NC	NA
		17	BLQ	BLQ	NC	
		18	3.52	BLQ	NC	
30 mg/kg	1	19	9634.01	520.89	0.05	0.05
		20	9782.59	439.29	0.04	
		21	8741.04	427.77	0.05	
	4	22	11605.76	635.85	0.05	0.03
		23	8046.99	278.55	0.03	
		24	6695.47	146.94	0.02	
	24	25	421.90	BLQ	NC	NA
		26	1.93	BLQ	NC	
		27	42.77	BLQ	NC	

LLOQ: 1.03 ng/mL for plasma and brain; BLQ- Below limit of quantitation; NC- Not calculated.

Following a single intravenous administration of ZD-3-188 (nilotinib) min (*sic*) in male C57BL/6 mice at 3 mg/kg dose, compound showed low plasma clearance (~5% of the normal liver blood flow in mice: 90 mL/min/kg) and low V<sub>ss</sub> (less than the total body water content: 0.7 L/kg) with terminal elimination plasma half-life of 2.78 h.

Following a single oral administration of ZD-3-188 (nilotinib) in male C57BL/6 mice at 3, 10 and 30 mg/kg dose, peak plasma concentrations were observed in between 0.5 to 8 h, suggesting rapid to prolonged absorption.

The dose related (*sic*) increase in plasma exposure was observed from 3 to 10 mg/kg and 10 to 30 mg/kg.

In summary, ZD-3-188 (nilotinib) exhibited low clearance, low V<sub>ss</sub> and adequate elimination half-life, good oral bioavailability and dose related increase in plasma exposure at 3, 10 and 30 mg/kg in male C57BL/6 mice.

## 5.4 REFERENCES AND NOTES

1. Elbaz, A.; Carcaillon, L.; Kab, S.; Moisan, F., Epidemiology of Parkinson's disease. *Revue Neurologique* **2016**, *172*, 14-16.
2. Wyss-Coray, T., Ageing, neurodegeneration and brain rejuvenation. *Nature* **2016**, *539*, 180-186.
3. World Population Ageing 2015 (ST/ESA/SER.A/390). United Nations: New York, NY, 2015.
4. Poewe, W.; Seppi, K.; Tanner, C. M.; Halliday, G. M.; Brundin, P.; Volkmann, J.; Schrag, A.-E.; Lang, A. E., Parkinson disease. *Nature Reviews Disease Primers* **2017**, *3*, 17013.
5. Chaudhuri, K. R.; Schapira, A. H. V., Non-motor symptoms of Parkinson's disease: dopaminergic pathophysiology and treatment. *The Lancet Neurology* **2009**, *8*, 464-474.
6. *Parkinson's Disease: National Clinical Guideline for Diagnosis and Management in Primary and Secondary Care*. Royal College of Physicians: London, UK, 2006; Vol. 35.
7. Benarroch, E. E.; Cutsforth-Gregory, J. K.; Flemming, K. D., *Mayo Clinic Medical Neurosciences: Organized by Neurologic System and Level*. 6th ed.; Oxford University Press: New York, NY, 2018.
8. Dickson, D. W.; Braak, H.; Duda, J. E.; Duyckaerts, C.; Gasser, T.; Halliday, G. M.; Hardy, J.; Leverenz, J. B.; Tredici, K. D.; Wszolek, Z. K.; Litvan, I., Neuropathological assessment of Parkinson's disease: refining the diagnostic criteria. *The Lancet Neurology* **2009**, *8*, 1150-1157.
9. Braak, H.; Tredici, K. D.; Rübä, U.; Vos, R. A. I. d.; Steur, E. N. H. J.; Braak, E., Staging of brain pathology related to sporadic Parkinson's disease. *Neurobiology of Aging* **2003**, *24*, 197-211.
10. Poewe, W.; Mahlkecht, P.; Jankovic, J., Emerging therapies for Parkinson's disease. *Current Opinion in Neurology* **2012**, *25*, 448-459.

11. Jankovic, J.; Poewe, W., Therapies in Parkinson's disease. *Current Opinion in Neurology* **2012**, *25*, 433-447.
12. Zhang, Y.; Dawson, V. L.; Dawson, T. M., Oxidative Stress and Genetics in the Pathogenesis of Parkinson's Disease. *Neurobiology of Disease* **2000**, *7*, 240-250.
13. Druker, B. J.; Lydon, N. B., Lessons learned from the development of an Abl tyrosine kinase inhibitor for chronic myelogenous leukemia. *The Journal of Clinical Investigation* **2000**, *105*, 3-7.
14. Li, B., c-Abl in oxidative stress, aging and cancer. *Cell Cycle* **2005**, *4*, 201-203.
15. Schlatterer, S. D.; Acker, C. M.; Davies, P., c-Abl in Neurodegenerative Disease. *Journal of Molecular Neuroscience* **2011**, *45*, 445-452.
16. Imam, S. Z.; Zhou, Q.; Yamamoto, A.; Valente, A. J.; Ali, S. F.; Bains, M.; Roberts, J. L.; Kahle, P. J.; Clark, R. A.; Li, S., Novel Regulation of Parkin Function through c-Abl-Mediated Tyrosine Phosphorylation: Implications for Parkinson's Disease. *The Journal of Neuroscience* **2011**, *31*, 157-163.
17. Ko, H. S.; Lee, Y.; Shin, J.-H.; Karuppagounder, S. S.; Gadad, B. S.; Koleske, A. J.; Pletnikova, O.; Troncoso, J. C.; Dawson, V. L.; Dawson, T. M., Phosphorylation by the c-Abl protein tyrosine kinase inhibits parkin's ubiquitination and protective function. *Proceedings of the National Academy of Sciences* **2010**, *107*, 16691-16696.
18. Mahul-Mellier, A.-L.; Fauvet, B.; Gysbers, A.; Dikiy, I.; Oueslati, A.; Georgeon, S.; Lamontanara, A. J.; Bisquertt, A.; Eliezer, D.; Masliah, E.; Halliday, G.; Hantsche, O.; Lashuel, H. A., c-Abl phosphorylates  $\alpha$ -synuclein and regulates its degradation: implication for  $\alpha$ -synuclein clearance and contribution to the pathogenesis of Parkinson's disease. *Human Molecular Genetics* **2014**, *23*, 2858-2879.
19. Shin, J.-H.; Ko, H. S.; Kang, H.; Lee, Y.; Lee, Y.-I.; Pletinkova, O.; Troconso, J. C.; Dawson, V. L.; Dawson, T. M., PARIS (ZNF746) Repression of PGC-1 $\alpha$  Contributes to Neurodegeneration in Parkinson's Disease. *Cell* **2011**, *144*, 689-702.
20. Lee, Y.; Karuppagounder, S. S.; Shin, J.-H.; Lee, Y.-I.; Ko, H. S.; Swing, D.; Jiang, H.; Kang, S.-U.; Lee, B. D.; Kang, H. C.; Kim, D.; Tessarollo, L.; Dawson, V. L.; Dawson, T. M., Parthanatos mediates AIMP2-activated age-dependent dopaminergic neuronal loss. *Nature Neurosci.* **2013**, *16*, 1392-1400.
21. Brahmachari, S.; Ge, P.; Lee, S. H.; Kim, D.; Karuppagounder, S. S.; Kumar, M.; Mao, X.; Shin, J. H.; Lee, Y.; Pletnikova, O.; Troncoso, J. C.; Dawson, V. L.; Dawson, T. M.; Ko, H. S., Activation of tyrosine kinase c-Abl contributes to alpha-synuclein-induced neurodegeneration. *J Clin Invest* **2016**, *126* (8), 2970-88.
22. Hebron, M. L.; Lonskaya, I.; Moussa, C. E.-H., Nilotinib reverses loss of dopamine neurons and improves motor behavior via autophagic degradation of  $\alpha$ -synuclein in Parkinson's disease models. *Human Molecular Genetics* **2013**, *22*, 3315-3328.
23. Rossari, F.; Minutolo, F.; Orciuolo, E., Past, present, and future of Bcr-Abl inhibitors: from chemical development to clinical efficacy. *Journal of Hematology & Oncology* **2018**, *11*, 84.

24. Karuppagounder, S. S.; Brahmachari, S.; Lee, Y.; Dawson, V. L.; Dawson, T. M.; Ko, H. S., The c-Abl inhibitor, Nilotinib, protects dopaminergic neurons in a preclinical animal model of Parkinson's disease. *Sci. Rep.* **2014**, *4*, 4874.
25. Pagan, F.; Hebron, M.; Valadez, E. H.; Torres-Yaghi, Y.; Huang, X.; Mills, R. R.; Wilmarth, B. M.; Howard, H.; Dunn, C.; Carlson, A.; Lawler, A.; Rogers, S. L.; Falconer, R. A.; Ahn, J.; Li, Z.; Moussa, C., Nilotinib Effects in Parkinson's Disease and Dementia with Lewy Bodies. *Journal of Parkinson's Disease* **2016**, *6*, 503-517.
26. Pagan, F. L.; Hebron, M. L.; Wilmarth, B.; Torres-Yaghi, Y.; Lawler, A.; Mundel, E. E.; Yusuf, N.; Starr, N. J.; Arellano, J.; Howard, H. H.; Peyton, M.; Matar, S.; Liu, X.; Fowler, A. J.; Schwartz, S. L.; Ahn, J.; Moussa, C., Pharmacokinetics and pharmacodynamics of a single dose Nilotinib in individuals with Parkinson's disease. *Pharmacology Research & Perspectives* **2019**, e00470.
27. Pagan, F. L.; Hebron, M. L.; Wilmarth, B.; Torres-Yaghi, Y.; Lawler, A.; Mundel, E. E.; Yusuf, N.; Starr, N. J.; Anjum, M.; Arellano, J.; Howard, H. H.; Shi, W.; Mulki, S.; Kurd-Misto, T.; Matar, S.; Liu, X.; Ahn, J.; Moussa, C., Nilotinib Effects on Safety, Tolerability, and Potential Biomarkers in Parkinson Disease: A Phase 2 Randomized Clinical Trial. *JAMA Neurology* **2020**, *77* (3), 309-317.
28. Simuni, T.; Fiske, B.; Merchant, K.; Coffey, C. S.; Klingner, E.; Caspell-Garcia, C.; Lafontant, D. E.; Matthews, H.; Wyse, R. K.; Brundin, P.; Simon, D. K.; Schwarzschild, M.; Weiner, D.; Adams, J.; Venuto, C.; Dawson, T. M.; Baker, L.; Kostrzebski, M.; Ward, T.; Rafaloff, G., Efficacy of Nilotinib in Patients With Moderately Advanced Parkinson Disease: A Randomized Clinical Trial. *JAMA Neurol* **2021**, *78* (3), 312-320.
29. Doherty, K. R.; Wappel, R. L.; Talbert, D. R.; Trusk, P. B.; Moran, D. M.; Kramer, J. W.; Brown, A. M.; Shell, S. A.; Bacus, S., Multi-parameter in vitro toxicity testing of crizotinib, sunitinib, erlotinib, and nilotinib in human cardiomyocytes. *Toxicology and Applied Pharmacology* **2013**, *272*, 245-255.
30. Goldenberg, M. M., Pharmaceutical Approval Update. *Pharmacy and Therapeutics* **2008**, *33*, 54-57.
31. Lee, S.; Kim, S.; Park, Y. J.; Yun, S. P.; Kwon, S.-H.; Kim, D.; Kim, D. Y.; Shin, J. S.; Cho, D. J.; Lee, G. Y.; Ju, H. S.; Yun, H. J.; Park, J. H.; Kim, W. R.; Jung, E. A.; Lee, S.; Ko, H. S., The c-Abl inhibitor, Radotinib HCl, is neuroprotective in a preclinical Parkinson's disease mouse model. *Human Molecular Genetics* **2018**, *27* (13), 2344-2356.
32. Lopez-Cuina, M.; Guerin, P. A.; Canron, M.-H.; Delamarre, A.; Dehay, B.; Bezard, E.; Meissner, W. G.; Fernagut, P.-O., Nilotinib Fails to Prevent Synucleinopathy and Cell Loss in a Mouse Model of Multiple System Atrophy. *Movement Disorders* **2020**, *35* (7), 1163-1172.
33. Rivera, V. M.; Pritchard, J. R.; Gonzalez, F.; Baker, T.; Gozgit, J. M.; Hodgson, G., Comparative TKI Profiling Analyses to Explore Potential Mechanisms of Ponatinib-Associated Arterial Thrombotic Events. *Blood* **2014**, *124*, 1783.
34. Latifi, Y.; Moccetti, F.; Wu, M.; Xie, A.; Packwood, W.; Qi, Y.; Ozawa, K.; Shentu, W.; Brown, E.; Shirai, T.; McCarty, O. J.; Ruggeri, Z.; Moslehi, J.; Chen, J.; Druker, B. J.; López, J. A.; Lindner, J. R., Thrombotic microangiopathy as a cause for cardiovascular toxicity from the BCR-ABL1 tyrosine kinase inhibitor ponatinib. *Blood* **2019**, *133*, 1597-1606.

35. Hoy, S. M., Ponatinib: a review of its use in adults with chronic myeloid leukaemia or Philadelphia chromosome-positive acute lymphoblastic leukaemia. *Drugs* **2014**, *74*, 793-806.
36. P., B. A.; Gaulton, A.; Hersey, A.; Bellis, L. J.; Chambers, J.; Davies, M.; Kruger, F. A.; Light, Y.; Mak, L.; McGlinchey, S.; Nowotka, M.; Papadatos, G.; Santos, R.; Overington, J. P., The ChEMBL bioactivity database: an update. *Nuc. Acids Res.* **2014**, *42*, 1083-1090.
37. Papadatos, G.; Gaulton, A.; Hersey, A.; Overington, J. P., Activity, assay and target data curation and quality in the ChEMBL database. *Journal of Computer Aided Molecular Design* **2015**, *29*, 885-896.
38. Gaulton, A.; Bellis, L. J.; Bento, A. P.; Chambers, J.; Davies, M.; Hersey, A.; Light, Y.; McGlinchey, S.; Michalovich, D.; Al-Lazikani, B.; Overington, J. P., ChEMBL: a large-scale bioactivity database for drug discovery. *Nuc. Acids Res.* **2012**, *40* (D1), D1100-D1107.
39. Kaiser, T. M.; Burger, P. B.; Butch, C. J.; Pelly, S. C.; Liotta, D. C., A Machine Learning Approach for Predicting HIV Reverse Transcriptase Mutation Susceptibility of Biologically Active Compounds. *J. Chem. Inf. Model.* **2018**, *58*, 1544-1552.
40. Shi, Q.; Kaiser, T. M.; Dentmon, Z. W.; Ceruso, M.; Vullo, D.; Supuran, C. T.; Snyder, J. P., Design and Validation of FRESH, A drug Discovery Paradigm Resting on Robust Chemical Synthesis. *ACS Med. Chem. Lett.* **2015**, *6*, 518-522.
41. Porkka, K.; Koskenvesa, P.; Lundán, T.; Rimpiläinen, J.; Mustjoki, S.; Smykla, R.; Wild, R.; Luo, R.; Arnan, M.; Brethon, B.; Eccersley, L.; Hjorth-Hansen, H.; Höglund, M.; Klamova, H.; Knutsen, H.; Parikh, S.; Raffoux, E.; Gruber, F.; Brito-Babapulle, F.; Dombret, H.; Duarte, R. F.; Elonen, E.; Paquette, R.; Zwaan, C. M.; Lee, F. Y. F., Dasatinib crosses the blood-brain barrier and is an efficient therapy for central nervous system Philadelphia chromosome-positive leukemia. *Blood* **2008**, *112* (4), 1005-1012.
42. Soverini, S.; Martinelli, G.; Rosti, G.; Iacobucci, I.; Baccarani, M., Advances in treatment of chronic myeloid leukemia with tyrosine kinase inhibitors: the evolving role of Bcr-Abl mutations and mutational analysis. *Pharmacogenomics* **2012**, *13* (11), 1271-1284.
43. Ravi, K.; Franson, A.; Homan, M. J.; Roberts, H.; Pai, M. P.; Miklja, Z.; He, M.; Wen, B.; Benitez, L. L.; Perissinotti, A. J.; Bixby, D. L.; Koschmann, C.; Marini, B. L., Comparative pharmacokinetic analysis of the blood-brain barrier penetration of dasatinib and ponatinib in mice. *Leukemia & Lymphoma* **2021**, *62* (8), 1990-1994.
44. BIOVIA <http://accelrys.com/products/collaborative-science/biovia-pipeline-pilot/>.
45. Salmon, R., Oxalyl Chloride-Dimethylformamide. In *Encyclopedia of Reagents for Organic Synthesis*.
46. Pirrung, M. C.; Shuey, S. W.; Lever, D. C.; Fallon, L. J. B.; Letters, M. C., A convenient procedure for the deprotection of silylated nucleosides and nucleotides using triethylamine trihydrofluoride. **1994**, *4* (11), 1345-1346.
47. Nelson, T. D.; Crouch, R. D., Selective deprotection of silyl ethers. *Synthesis* **1996**, *1996* (09), 1031-1069.

48. Mattson, R. J.; Pham, K. M.; Leuck, D. J.; Cowen, K. A., An improved method for reductive alkylation of amines using titanium(IV) isopropoxide and sodium cyanoborohydride. *The Journal of Organic Chemistry* **1990**, *55* (8), 2552-2554.
49. Bhattacharyya, S., Titanium(IV) isopropoxide and sodium borohydride : A reagent of choice for reductive amination. *Tetrahedron Lett.* **1994**, *35* (15), 2401-2404.
50. O'Donnell, M. J.; Lugar, C. W.; Pottorf, R. S.; Zhou, C.; Scott, W. L.; Cwi, C. L., Solid-phase synthesis of unnatural amino acids using unactivated alkyl halides. *Tetrahedron Lett.* **1997**, *38* (41), 7163-7166.
51. Landini, D.; Albanese, D. C. M.; Mottadelli, S.; Penso, M., Finkelstein reaction with aqueous hydrogen halides efficiently catalysed by lipophilic quaternary onium salts. *J. Chem. Soc., Perkin Trans. 1 (1972-1999)* **1992**, 2309-2311.
52. Madonna, R.; Pieragostino, D.; Cufaro, M. C.; Doria, V.; Del Boccio, P.; Deidda, M.; Pierdomenico, S. D.; Dessalvi, C. C.; De Caterina, R.; Mercurio, G., Ponatinib Induces Vascular Toxicity through the Notch-1 Signaling Pathway. *Journal of clinical medicine* **2020**, *9* (3).
53. Singh, A. P.; Glennon, M. S.; Umbarkar, P.; Gupte, M.; Galindo, C. L.; Zhang, Q.; Force, T.; Becker, J. R.; Lal, H., Ponatinib-induced cardiotoxicity: delineating the signalling mechanisms and potential rescue strategies. *Cardiovascular research* **2019**, *115* (5), 966-977.
54. Singh, A. P.; Umbarkar, P.; Tousif, S.; Lal, H., Cardiotoxicity of the BCR-ABL1 tyrosine kinase inhibitors: Emphasis on ponatinib. *International journal of cardiology* **2020**, *316*, 214-221.
55. Robinson, D. D.; Sherman, W.; Farid, R., Understanding Kinase Selectivity Through Energetic Analysis of Binding Site Waters. *ChemMedChem* **2010**, *5*, 618-627.
56. Fowler, A. J.; Hebron, M.; Missner, A. A.; Wang, R.; Gao, X.; Kurd-Misto, B. T.; Liu, X.; Moussa, C. E. H., Multikinase Abl/DDR/Src Inhibition Produces Optimal Effects for Tyrosine Kinase Inhibition in Neurodegeneration. *Drugs in R&D* **2019**, *19*, 149-166.
57. Kitagawa, D.; Yokota, K.; Gouda, M.; Narumi, Y.; Ohmoto, H.; Nishiwaki, E.; Akita, K.; Kirii, Y., Activity-based kinase profiling of approved tyrosine kinase inhibitors. *Genes to Cells* **2013**, *18*, 110-122.
58. Hastie, C. J.; McLauchlan, H. J.; Cohen, P., Assay of protein kinases using radiolabeled ATP: a protocol. *Nat Protoc* **2006**, *1* (2), 968-71.
59. Bain, J.; Plater, L.; Elliott, M.; Shpiro, N.; Hastie, C. J.; McLauchlan, H.; Klevernic, I.; Arthur, J. S.; Alessi, D. R.; Cohen, P., The selectivity of protein kinase inhibitors: a further update. *Biochem J* **2007**, *408* (3), 297-315.
60. Pandrala, M.; Bruyneel, A. A. N.; Hnatiuk, A. P.; Mercola, M.; Malhotra, S. V., Designing Novel BCR-ABL Inhibitors for Chronic Myeloid Leukemia with Improved Cardiac Safety. *Journal of Medicinal Chemistry* **2022**.
61. Xia, B.; Heimbach, T.; He, H.; Lin, T.-h., Nilotinib preclinical pharmacokinetics and practical application toward clinical projections of oral absorption and systemic availability. *Biopharmaceutics & Drug Disposition* **2012**, *33* (9), 536-549.

62. Laramy, J. K.; Kim, M.; Parrish, K. E.; Sarkaria, J. N.; Elmquist, W. F., Pharmacokinetic Assessment of Cooperative Efflux of the Multitargeted Kinase Inhibitor Ponatinib Across the Blood-Brain Barrier. *Journal of Pharmacology and Experimental Therapeutics* **2018**, *365* (2), 249-261.
63. Greenblatt, D. J., Volume of distribution – Again. *Clinical Pharmacology in Drug Development* **2014**, *3* (6), 419-420.
64. Simola, N.; Morelli, M.; Carta, A. R., The 6-Hydroxydopamine model of parkinson's disease. *Neurotoxicity Research* **2007**, *11* (3), 151-167.
65. Brahmachari, S.; Karuppagounder, S. S.; Ge, P.; Lee, S.; Dawson, V. L.; Dawson, T. M.; Ko, H. S., c-Abl and Parkinson's Disease: Mechanisms and Therapeutic Potential. *J Parkinsons Dis* **2017**, *7* (4), 589-601.
66. Roymans, D.; Alnajjar, S. S.; Battles, M. B.; Sitthicharoenchai, P.; Furmanova-Hollenstein, P.; Rigaux, P.; Berg, J. V. d.; Kwanten, L.; Ginderen, M. V.; Verheyen, N.; Vranckx, L.; Jaensch, S.; Arnoult, E.; Voorzaat, R.; Gallup, J. M.; Larios-Mora, A.; Crabbe, M.; Huntjens, D.; Raboisson, P.; Langedijk, J. P.; Ackermann, M. R.; McLellan, J. S.; Vendeville, S.; Koul, A., Therapeutic efficacy of a respiratory syncytial virus fusion inhibitor. *Nature Communications* **2017**, *8* (1), 167.
67. Pribut, N.; Kaiser, T. M.; Wilson, R. J.; Jecs, E.; Dentmon, Z. W.; Pelly, S. C.; Sharma, S.; Bartsch III, P. W.; Burger, P. B.; Hwang, S. S.; Le, T.; Sourimant, J.; Yoon, J. J.; Plemper, R. K.; Liotta, D. C., Accelerated Discovery of Potent Fusion Inhibitors for Respiratory Syncytial Virus. *ACS Infectious Diseases* **2020**, *6* (5), 922-929.
68. Gabriele, B.; Veltri, L.; Maltese, V.; Spina, R.; Mancuso, R.; Salerno, G., Versatile Synthesis of Isoquinolines and Isochromenes by Pd-Catalyzed Oxidative Carbonylation of (2-Alkynyl)benzylideneamine Derivatives. *European Journal of Organic Chemistry* **2011**, *2011* (28), 5626-5635.
69. Li, Y.; Shen, M.; Zhang, Z.; Luo, J.; Pan, X.; Lu, X.; Long, H.; Wen, D.; Zhang, F.; Leng, F.; Li, Y.; Tu, Z.; Ren, X.; Ding, K., Design, Synthesis, and Biological Evaluation of 3-(1H-1,2,3-Triazol-1-yl)benzamide Derivatives as Potent Pan Bcr-Abl Inhibitors Including the Threonine315→Isoleucine315 Mutant. *Journal of Medicinal Chemistry* **2012**, *55* (22), 10033-10046.

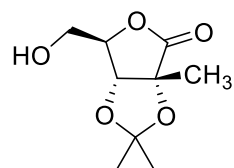
# Supplemental Appendix

---

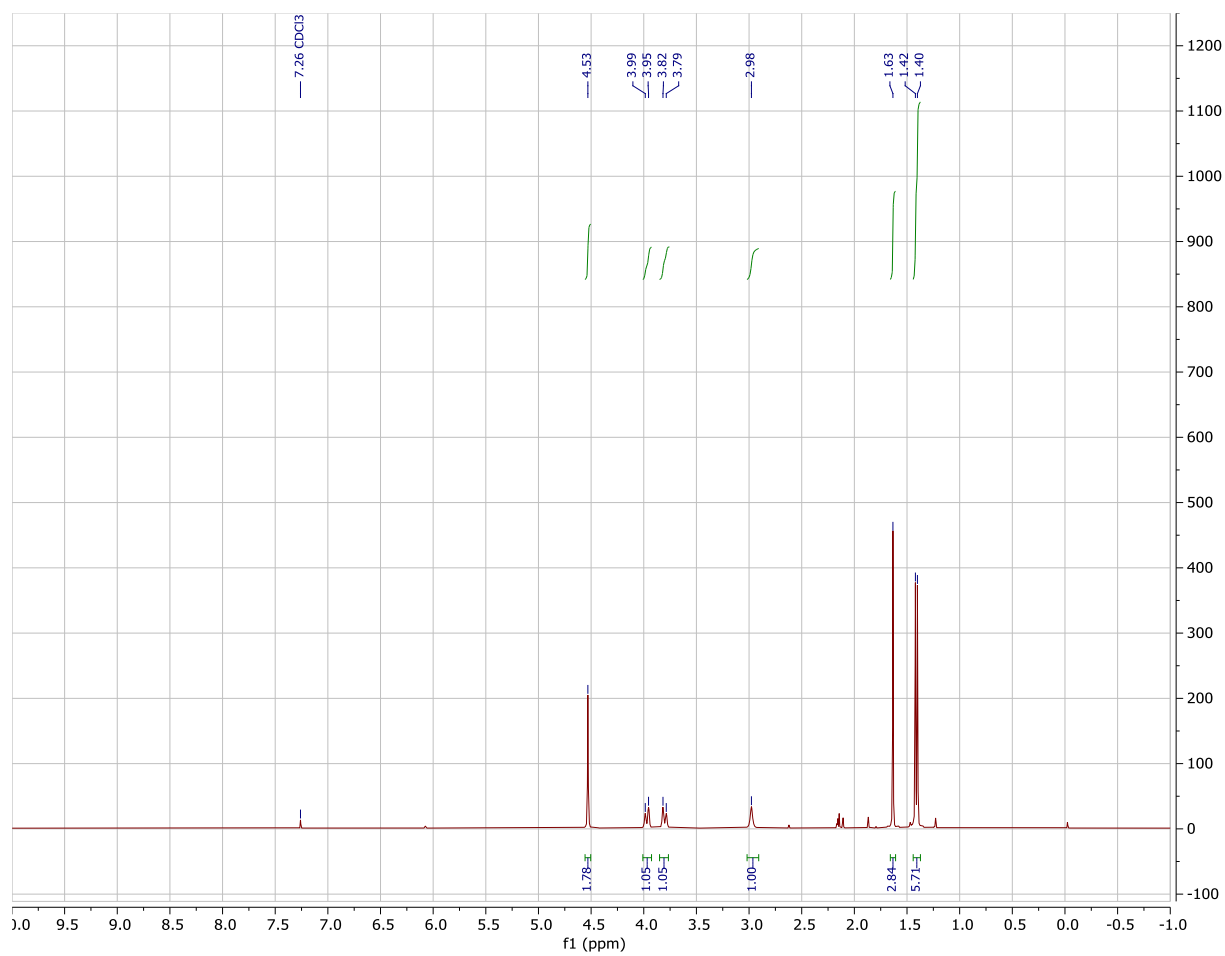
## Supplemental Appendix

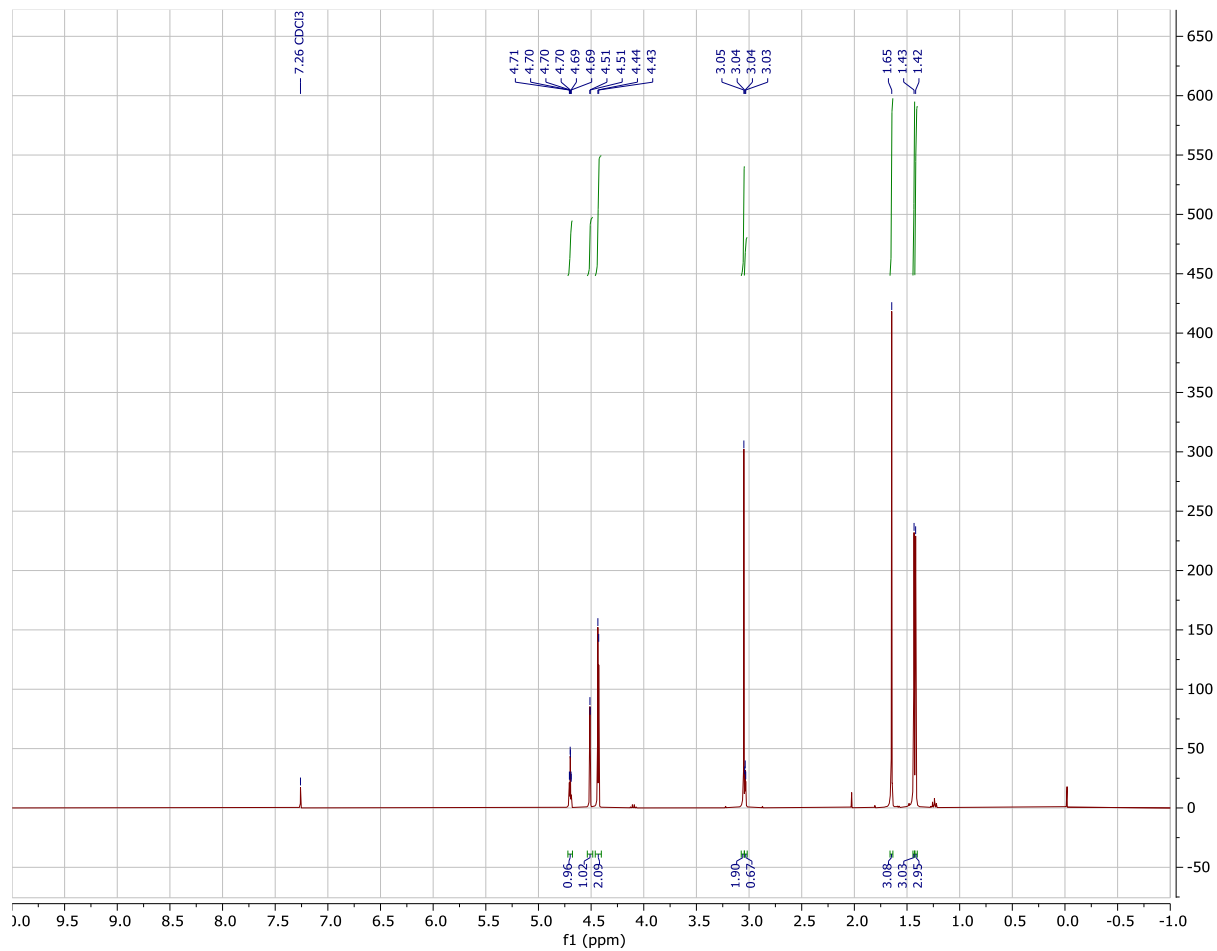
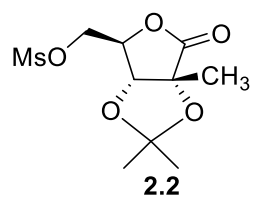
## SA.1 NMR Spectra of Compounds in Chapter 2

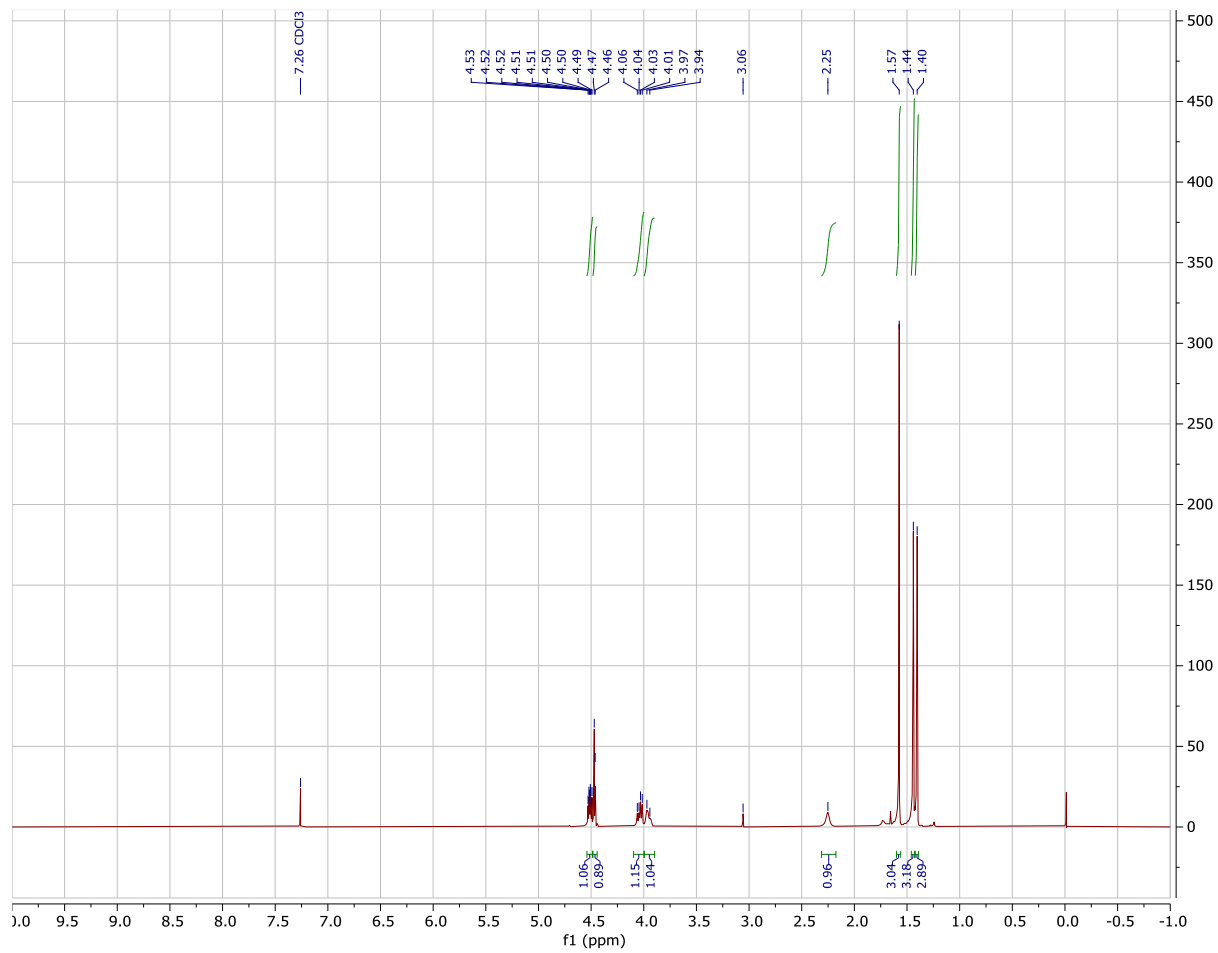
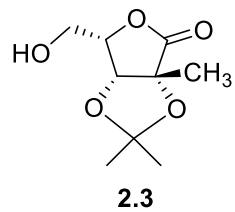
## SA.1.1 Construction of the Thiosugar Core (2.S1 - 2.9)

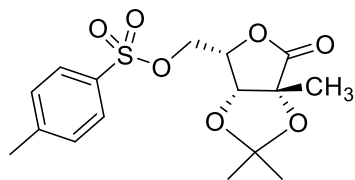


2.S1

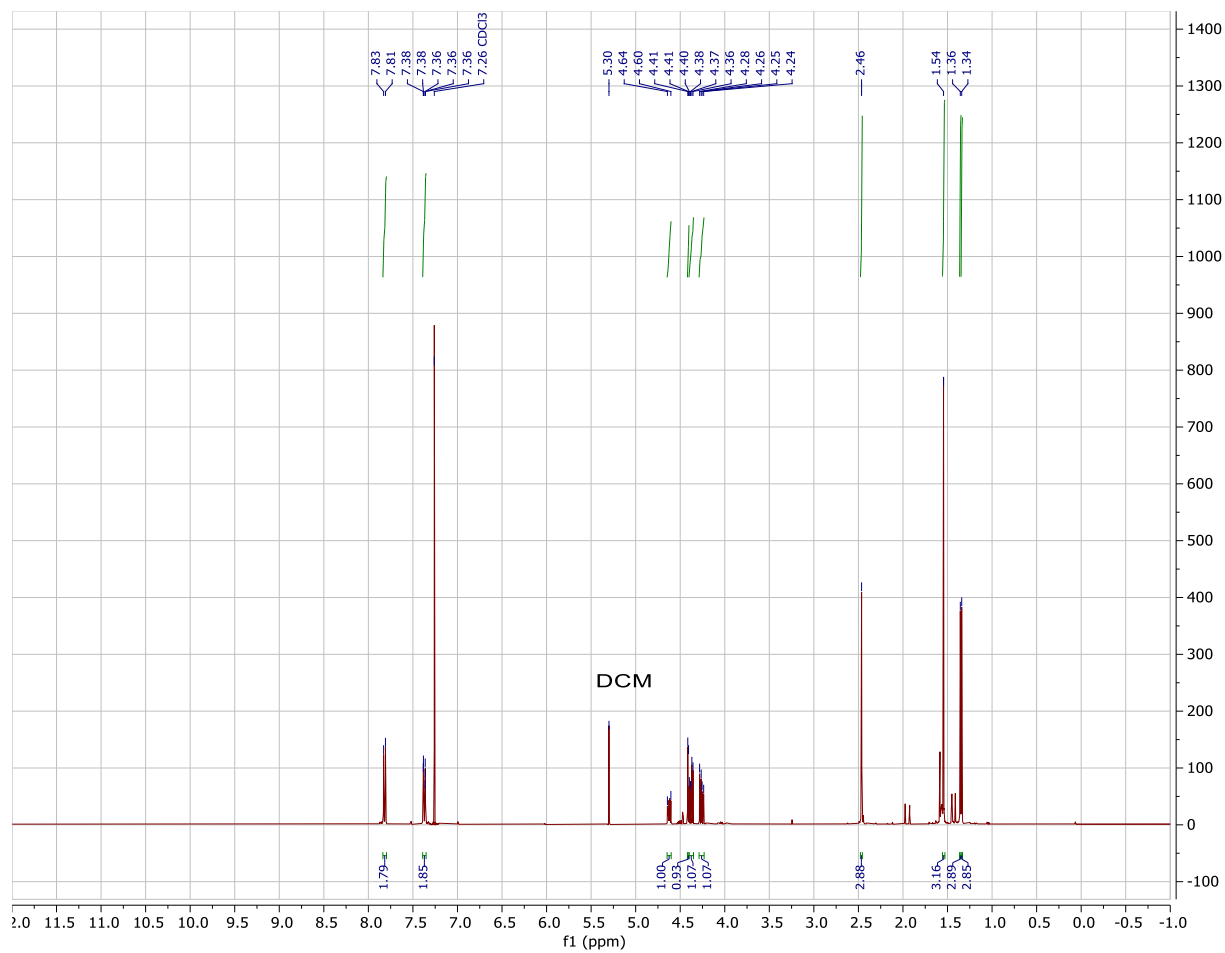


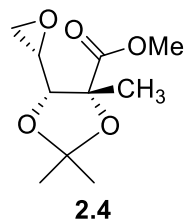




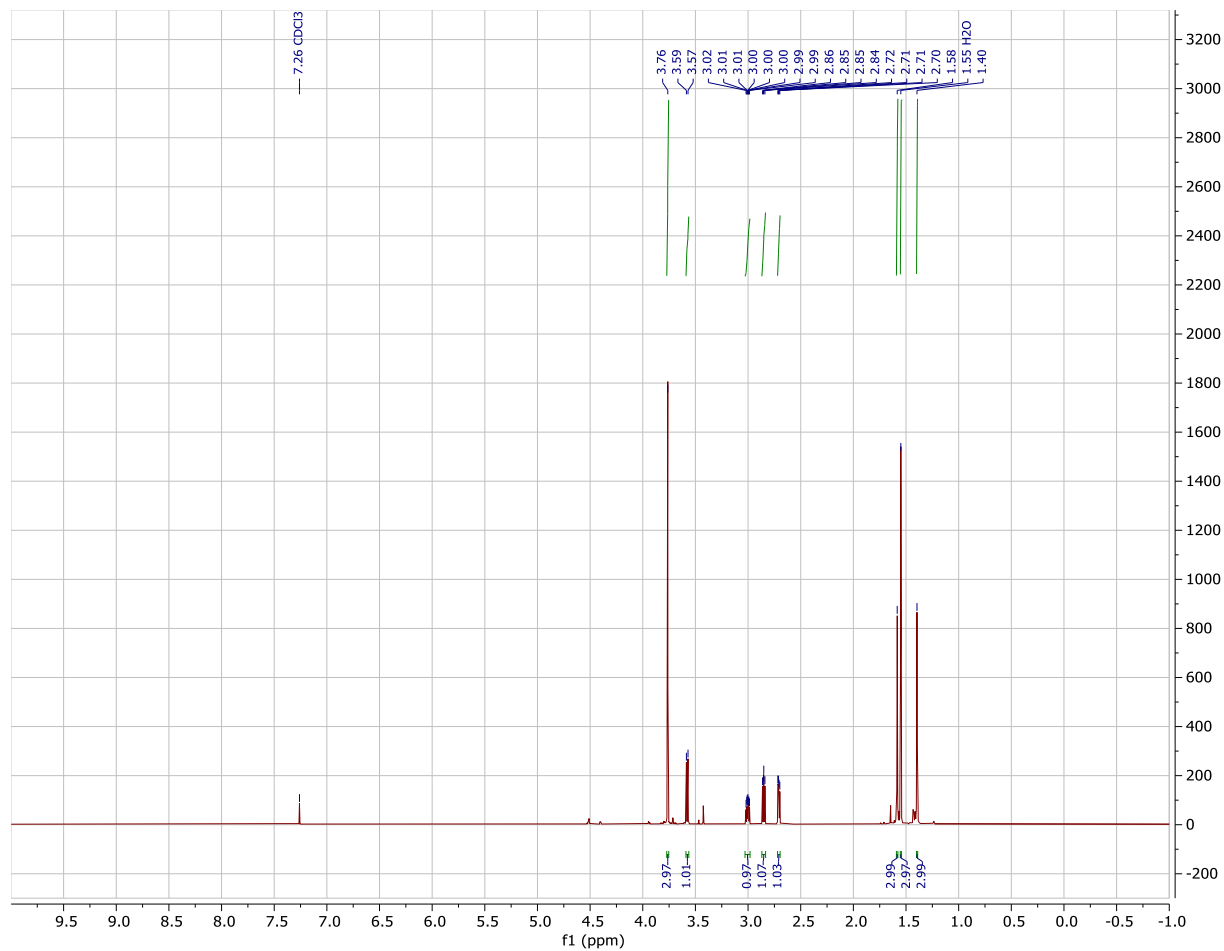


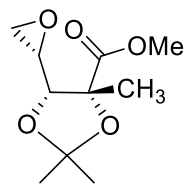
2.S3



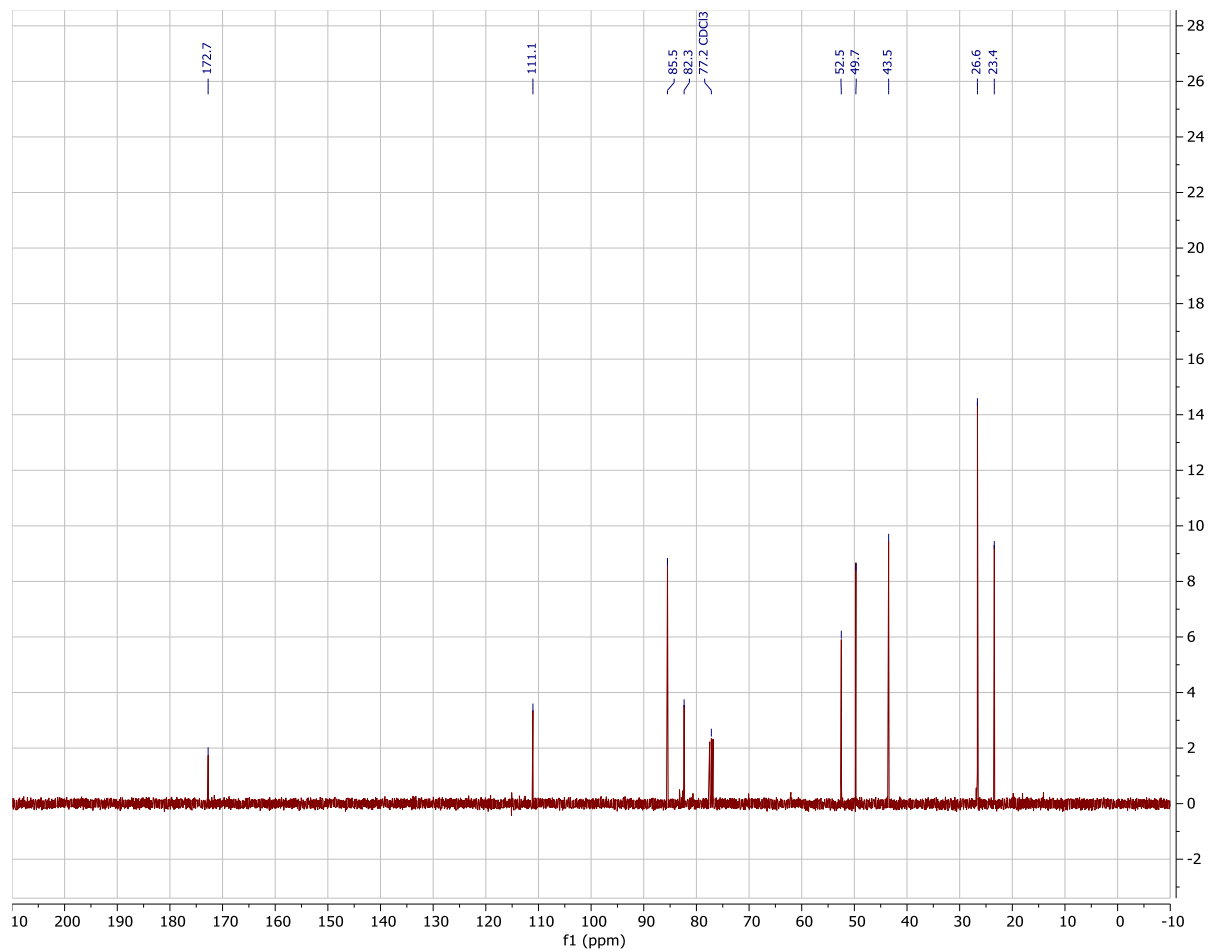


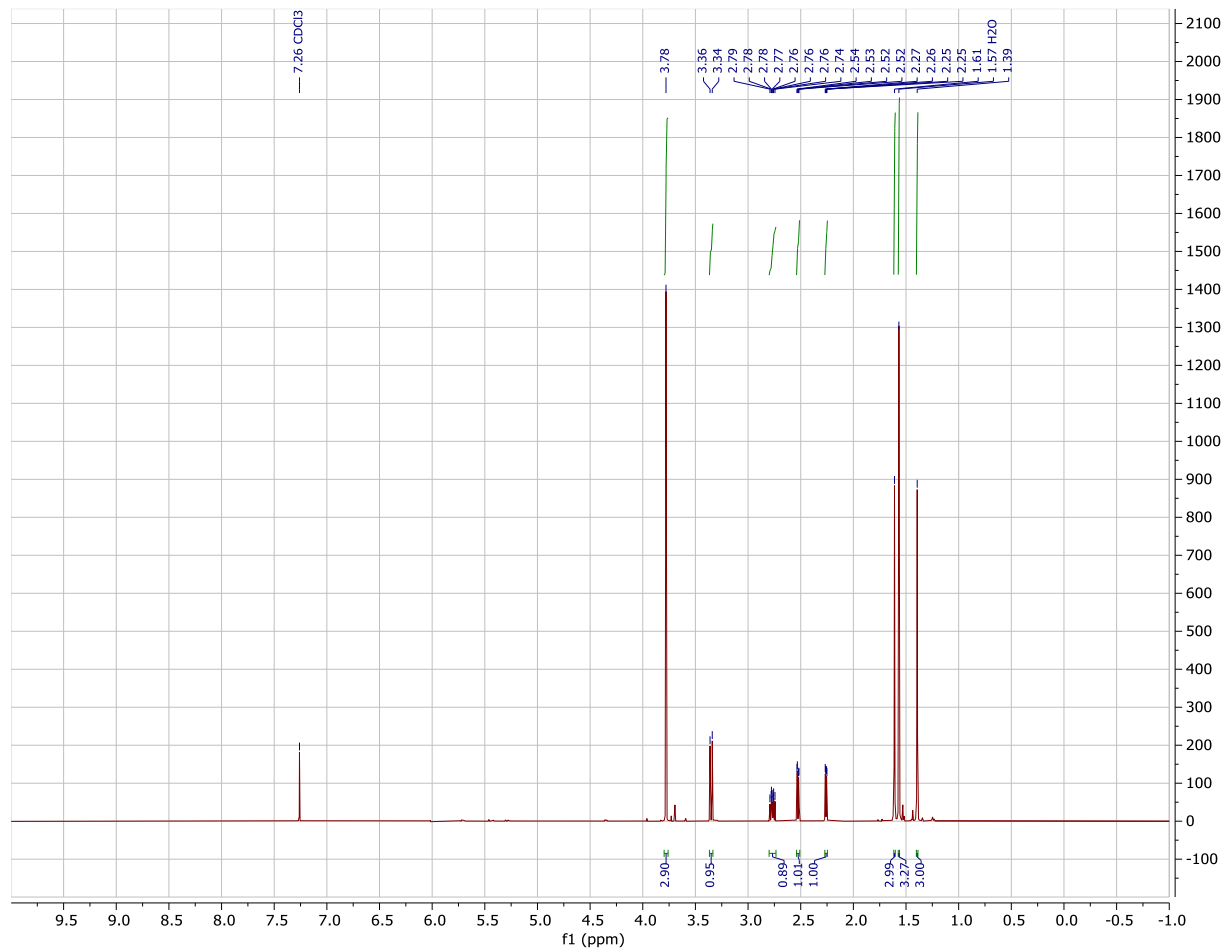
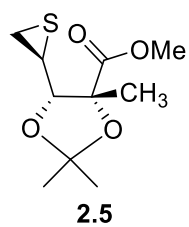
2.4

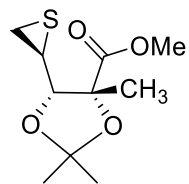




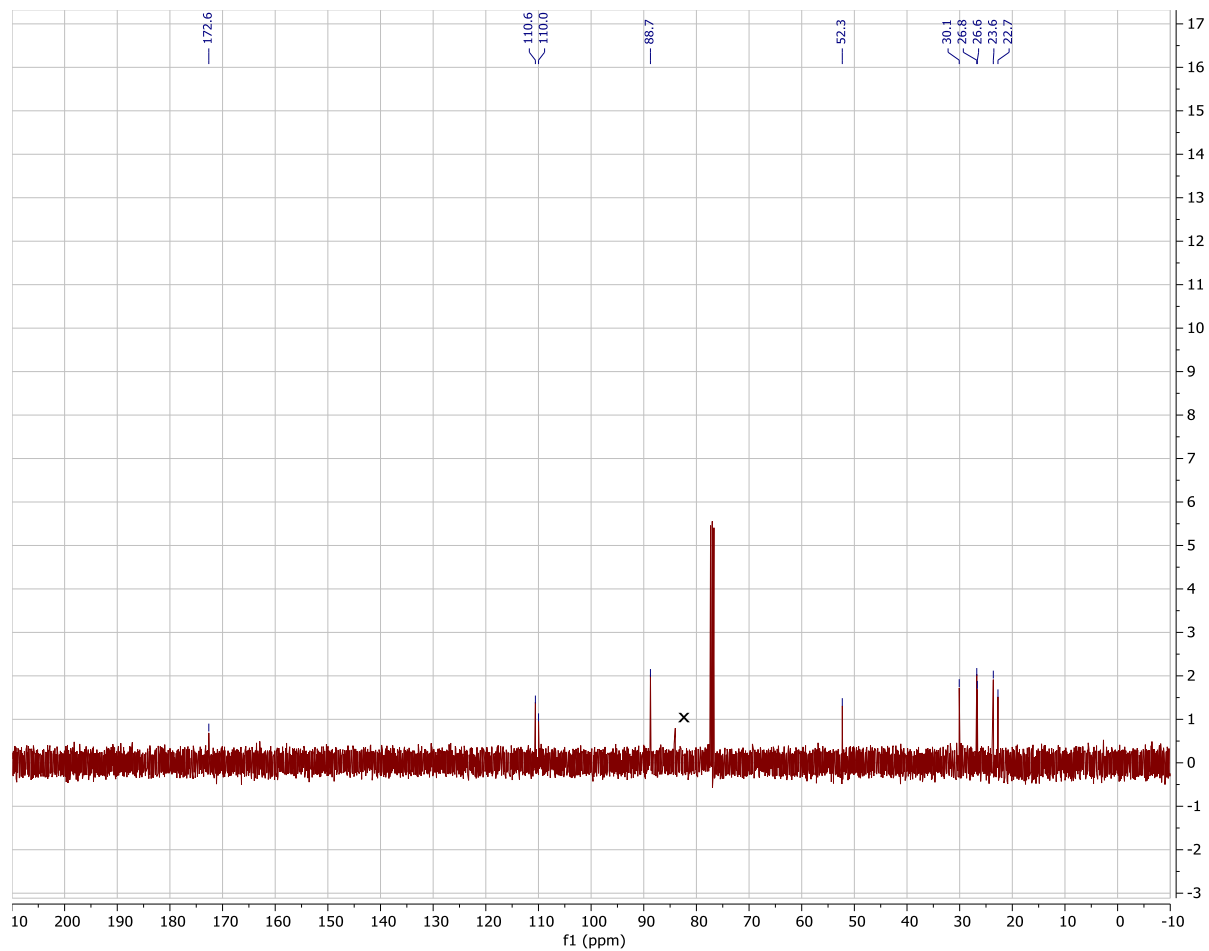
2.4

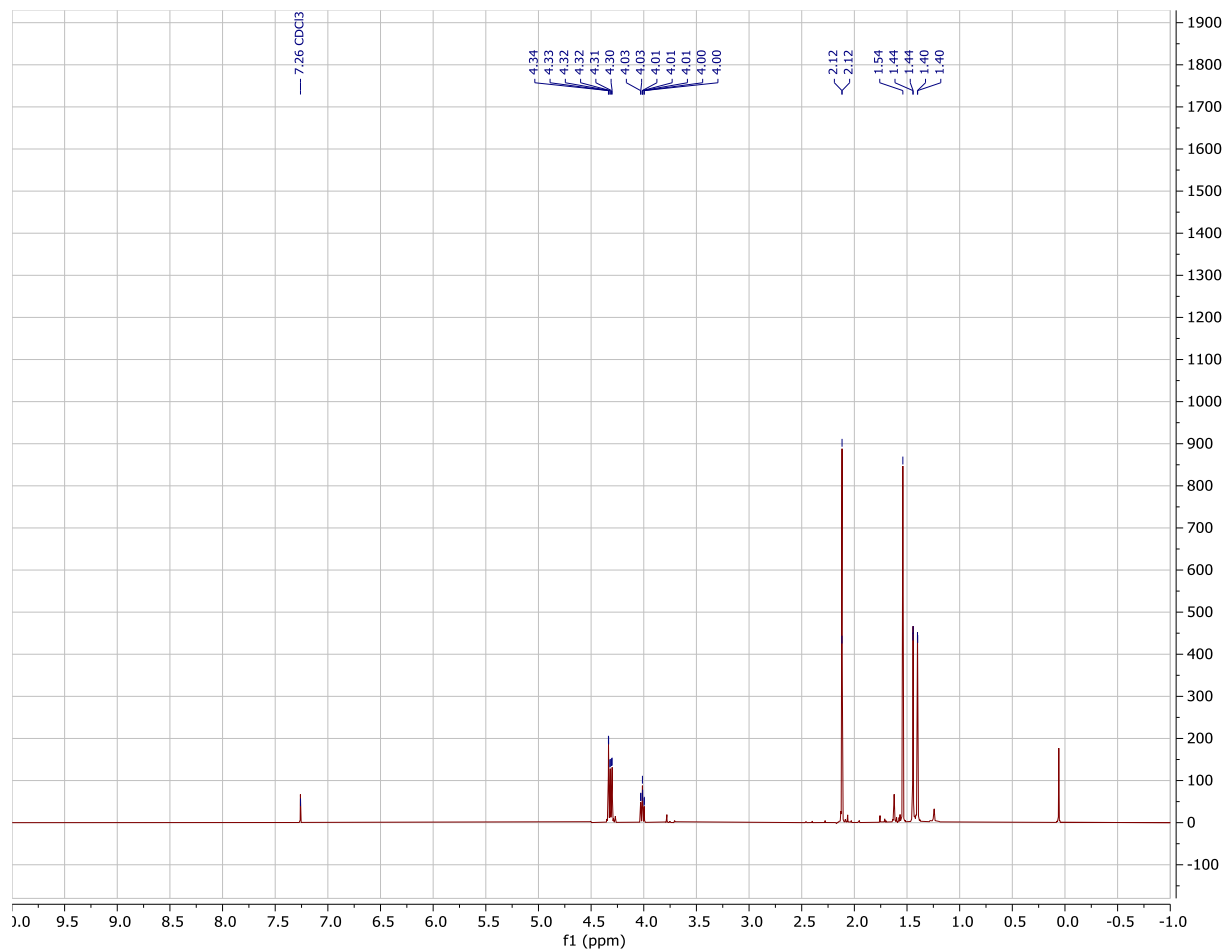
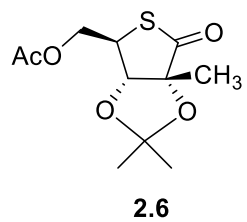


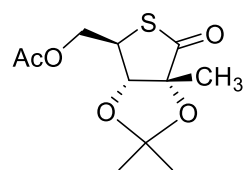
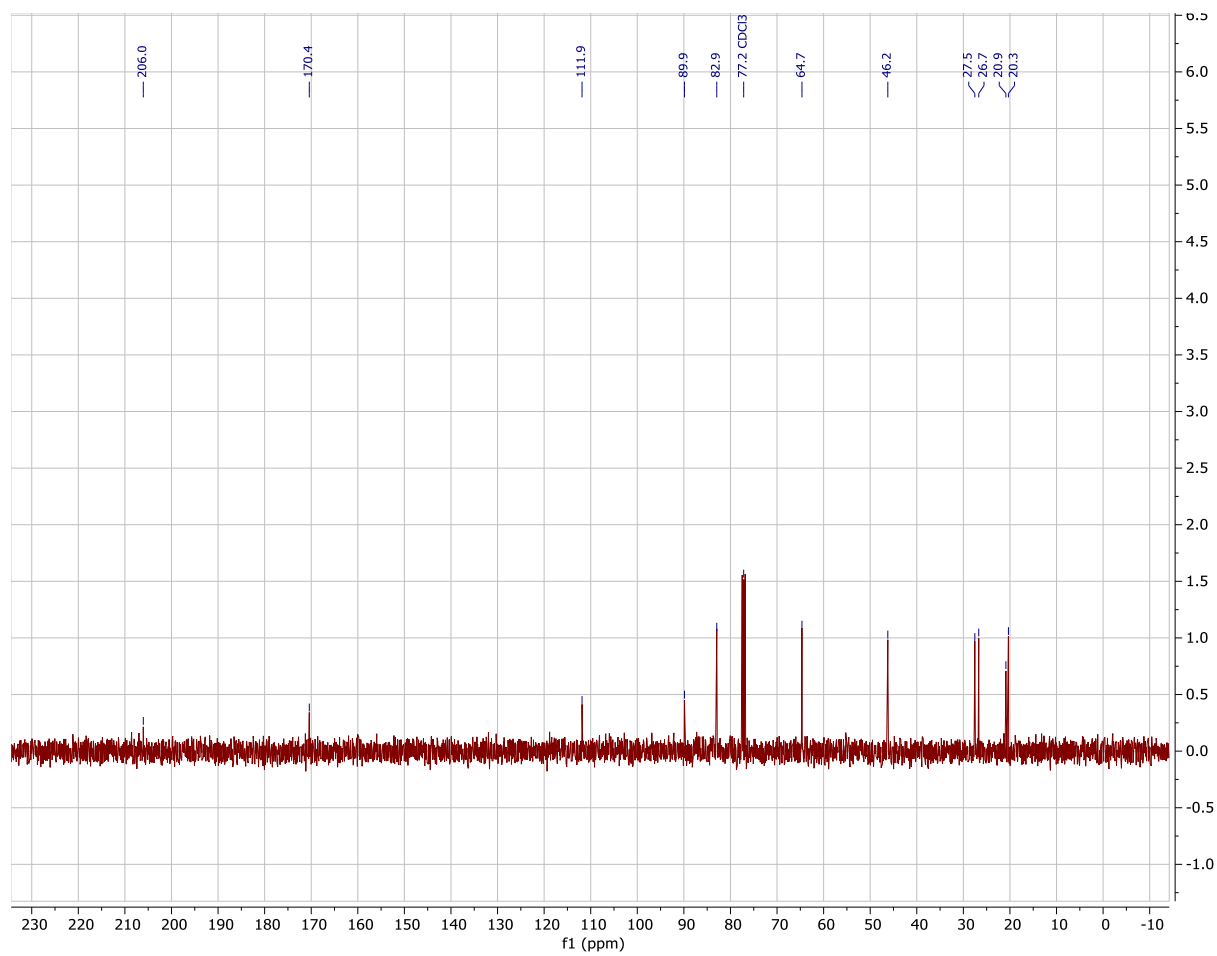


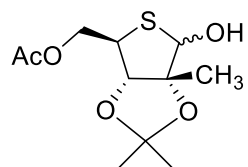


2.5

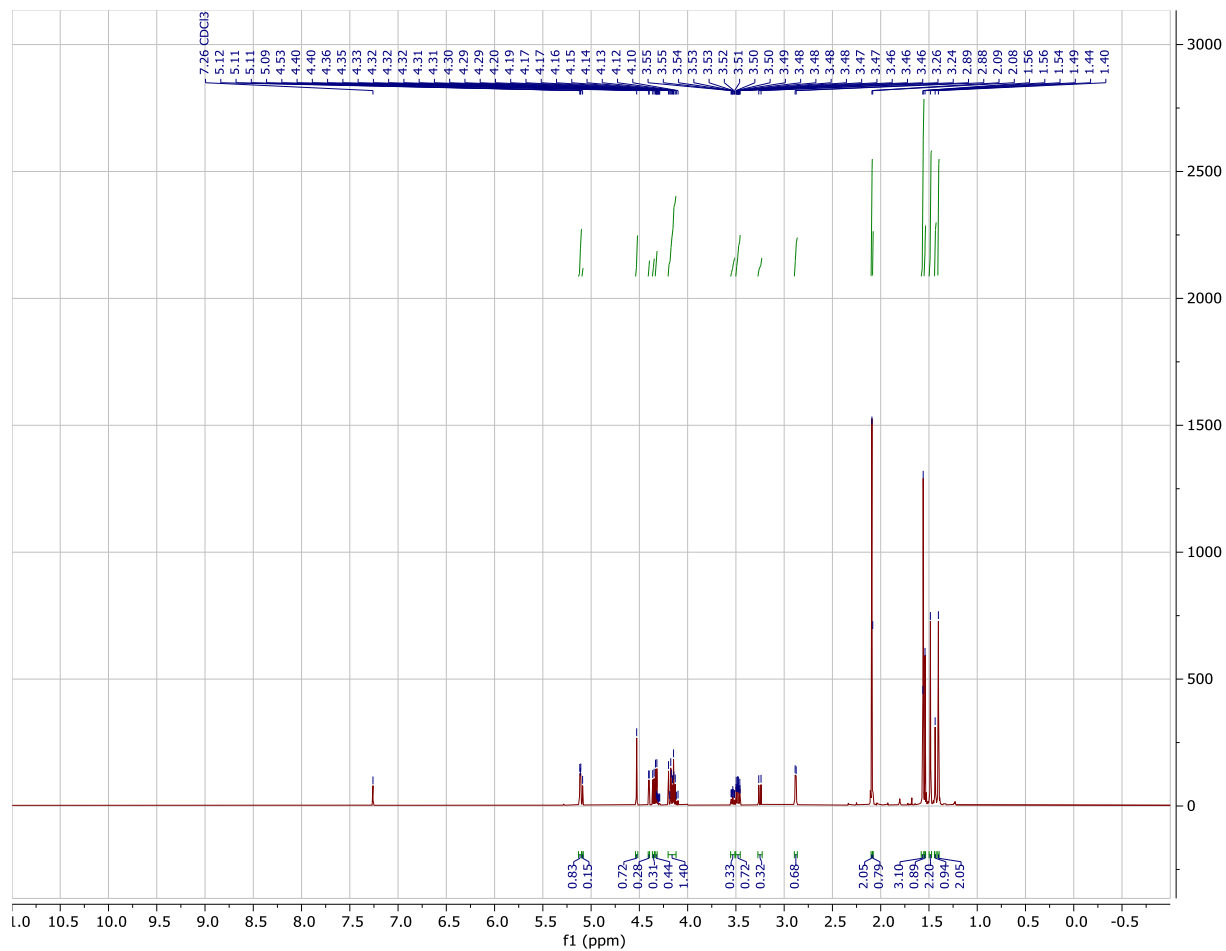


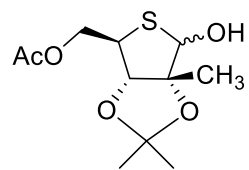


**2.6**

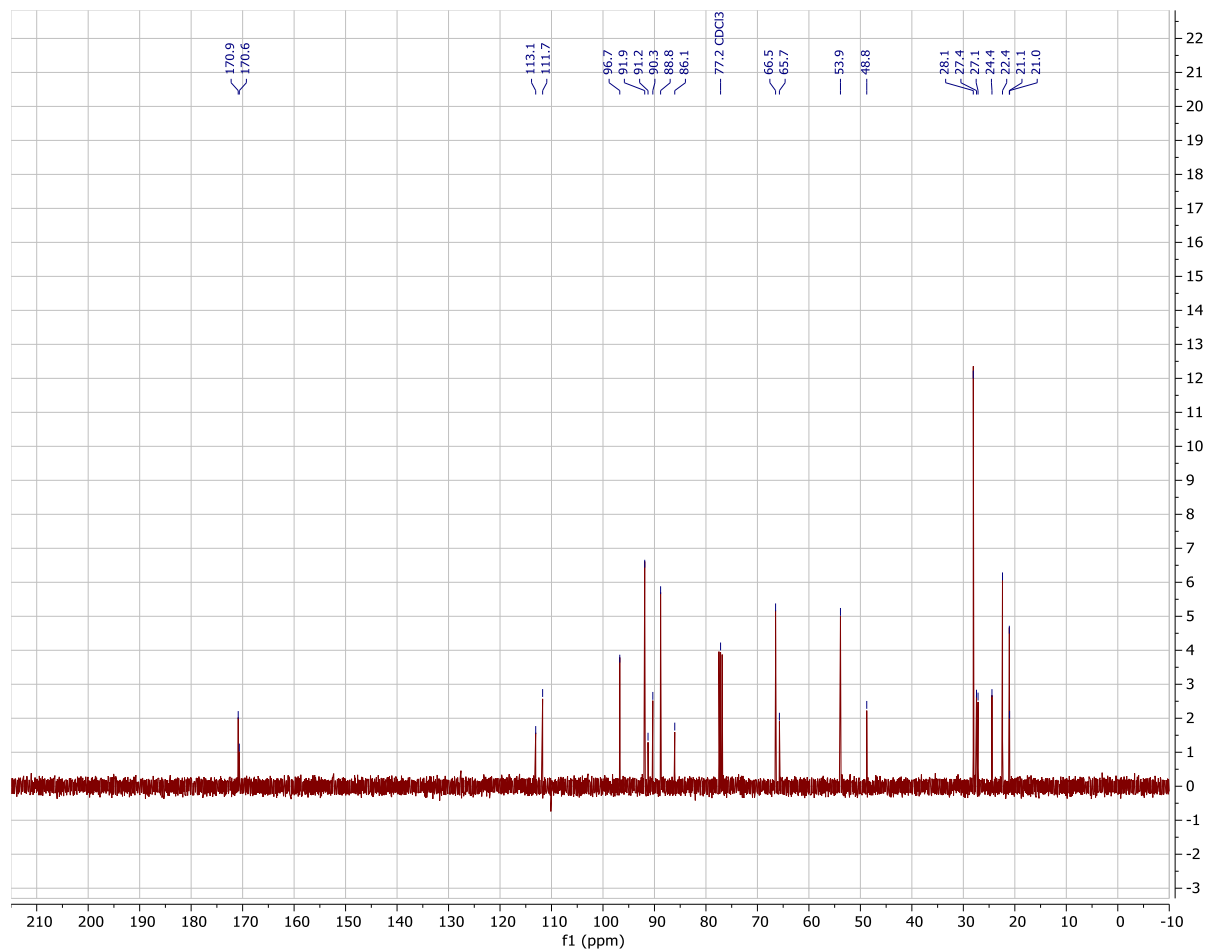


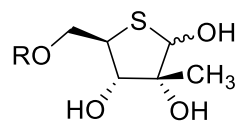
2.7





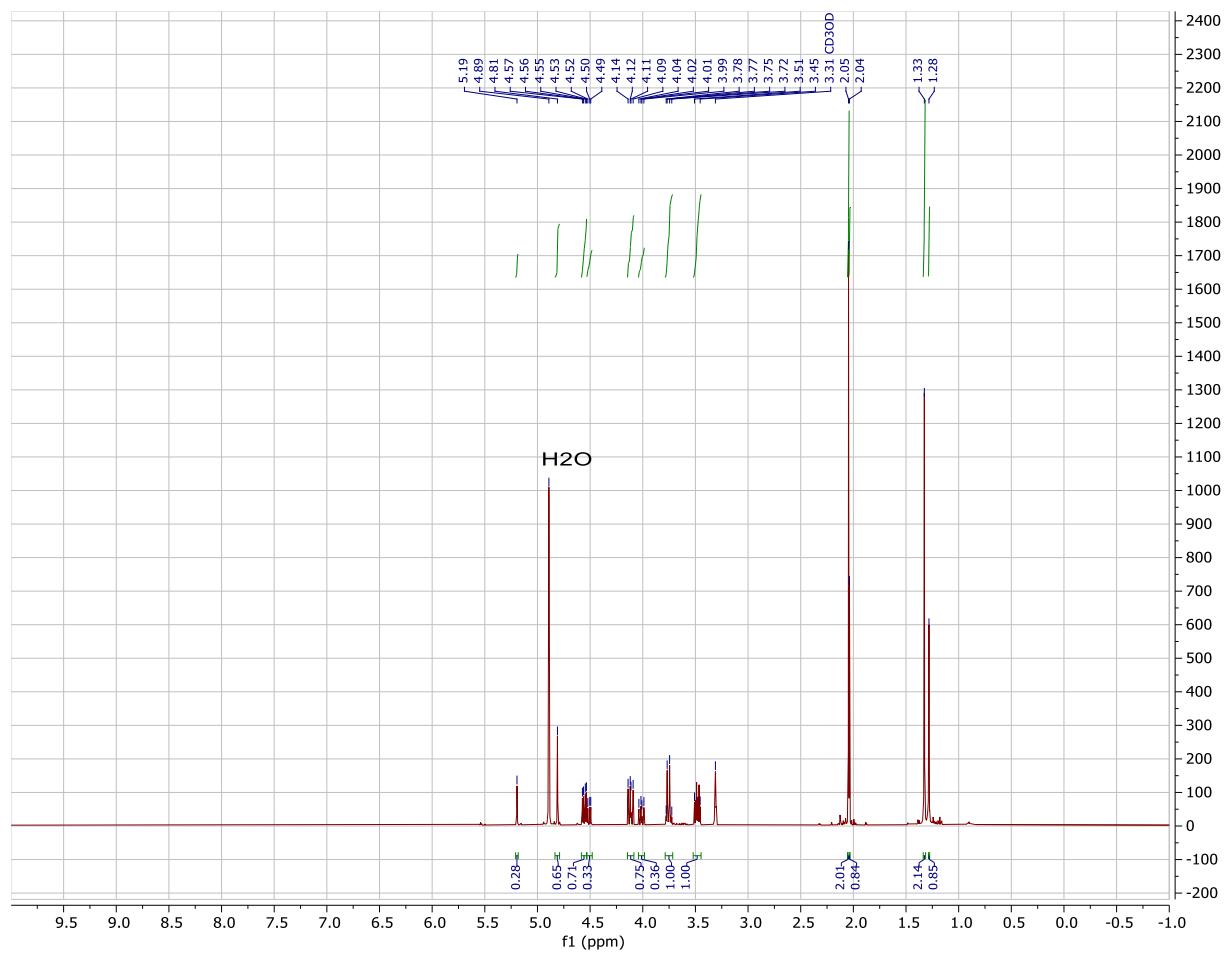
2.7

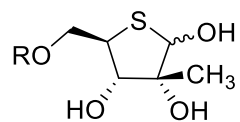




**2.8a:** R = Ac

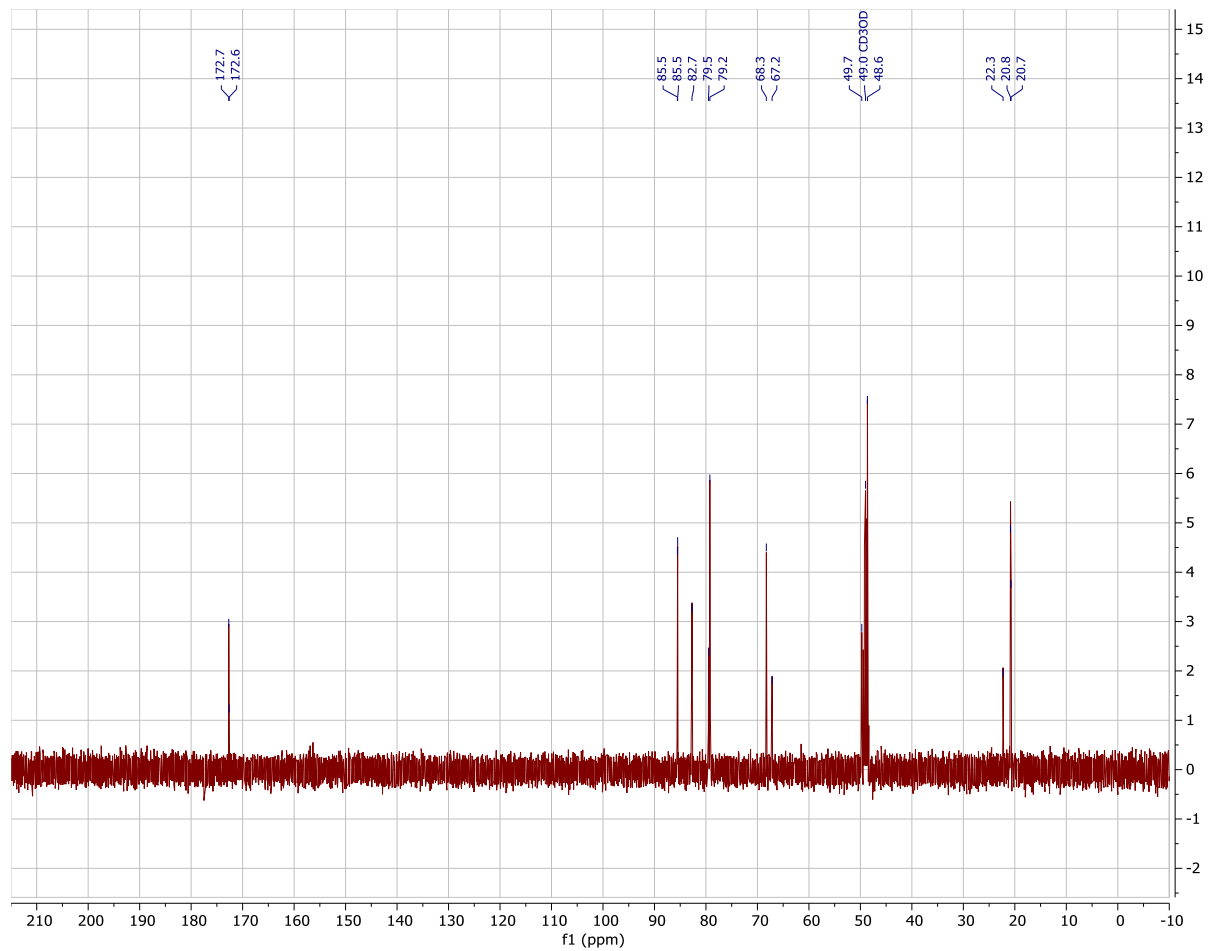
**2.8b:** R = H

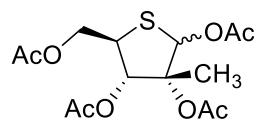




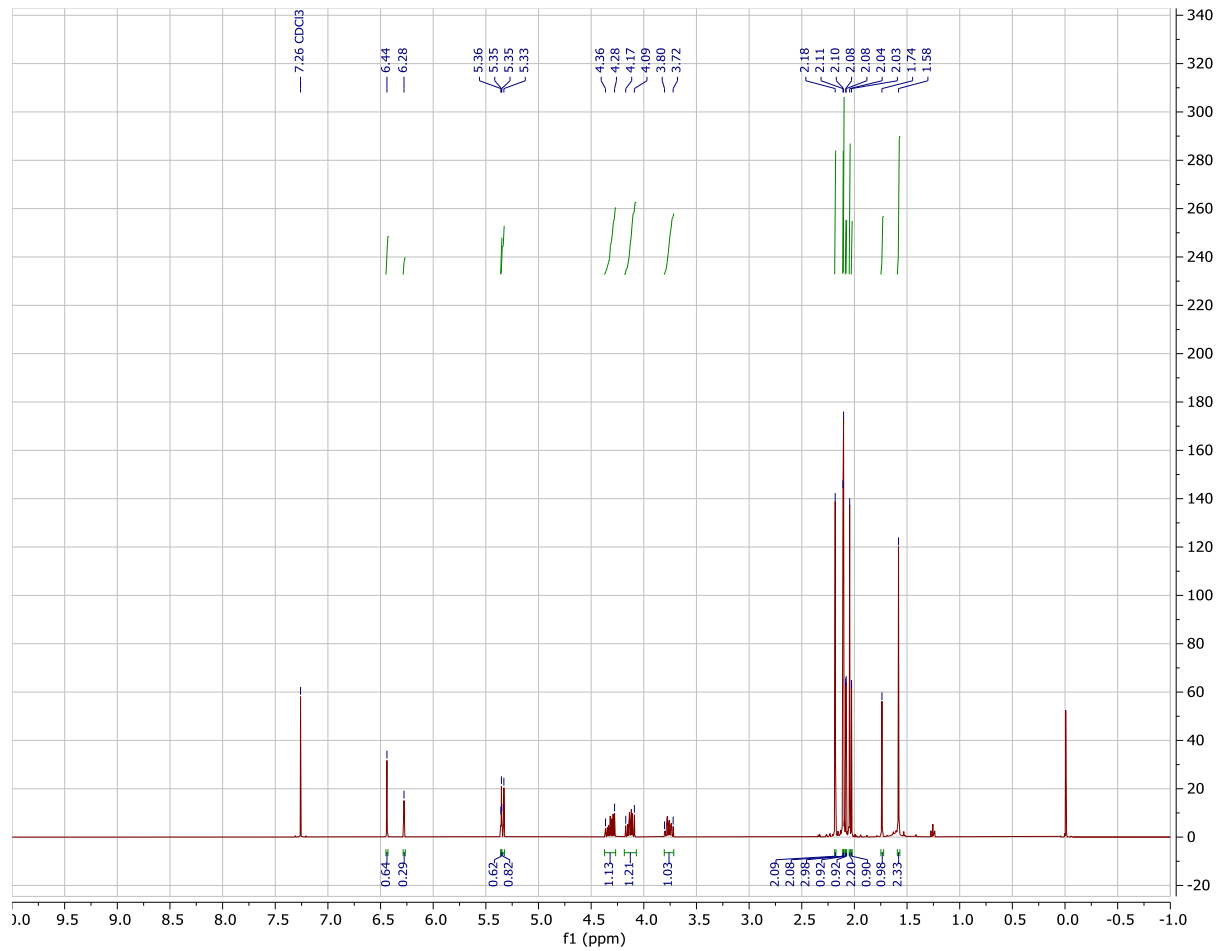
**2.8a:** R = Ac

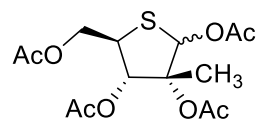
**2.8b:** R = H



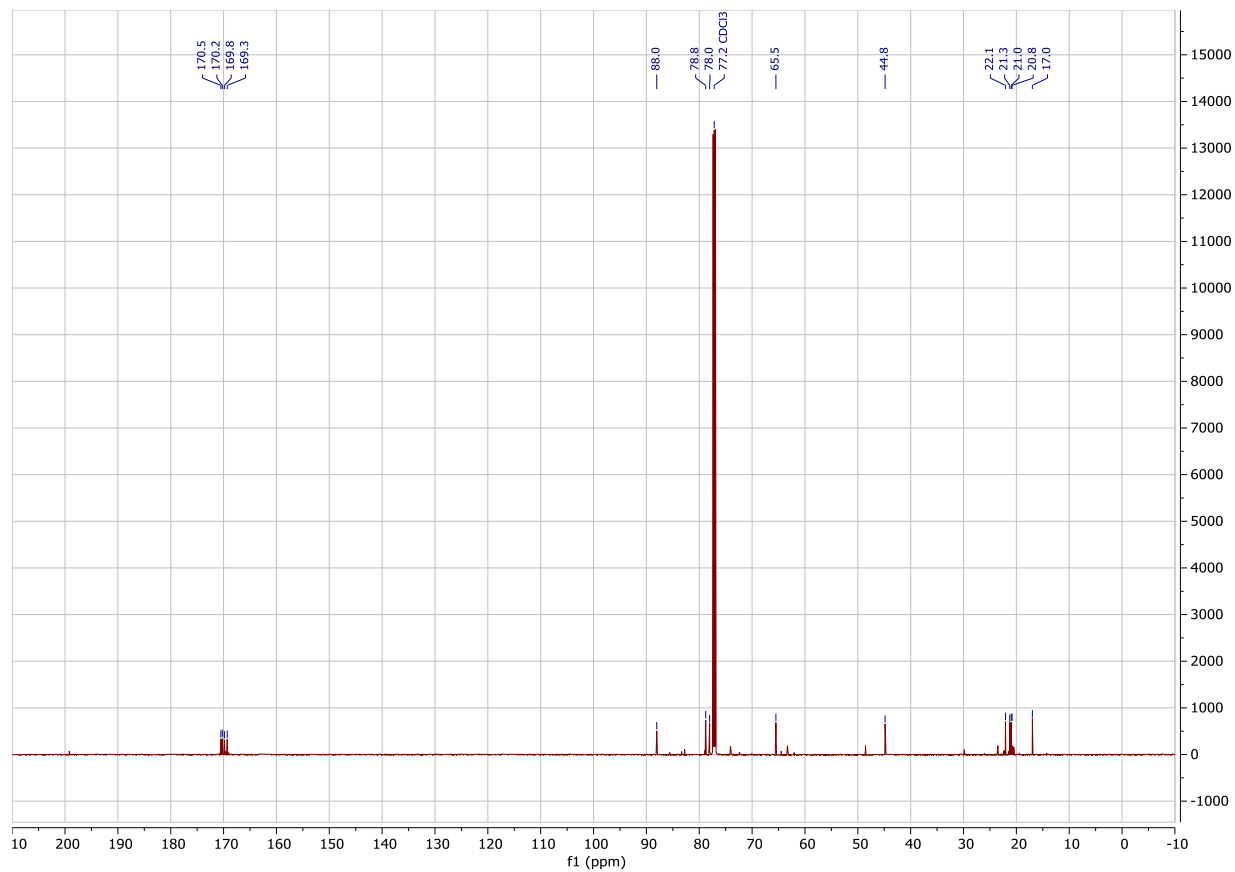


2.9

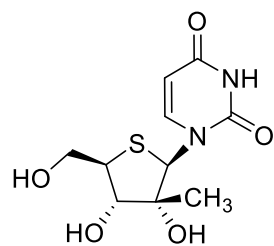




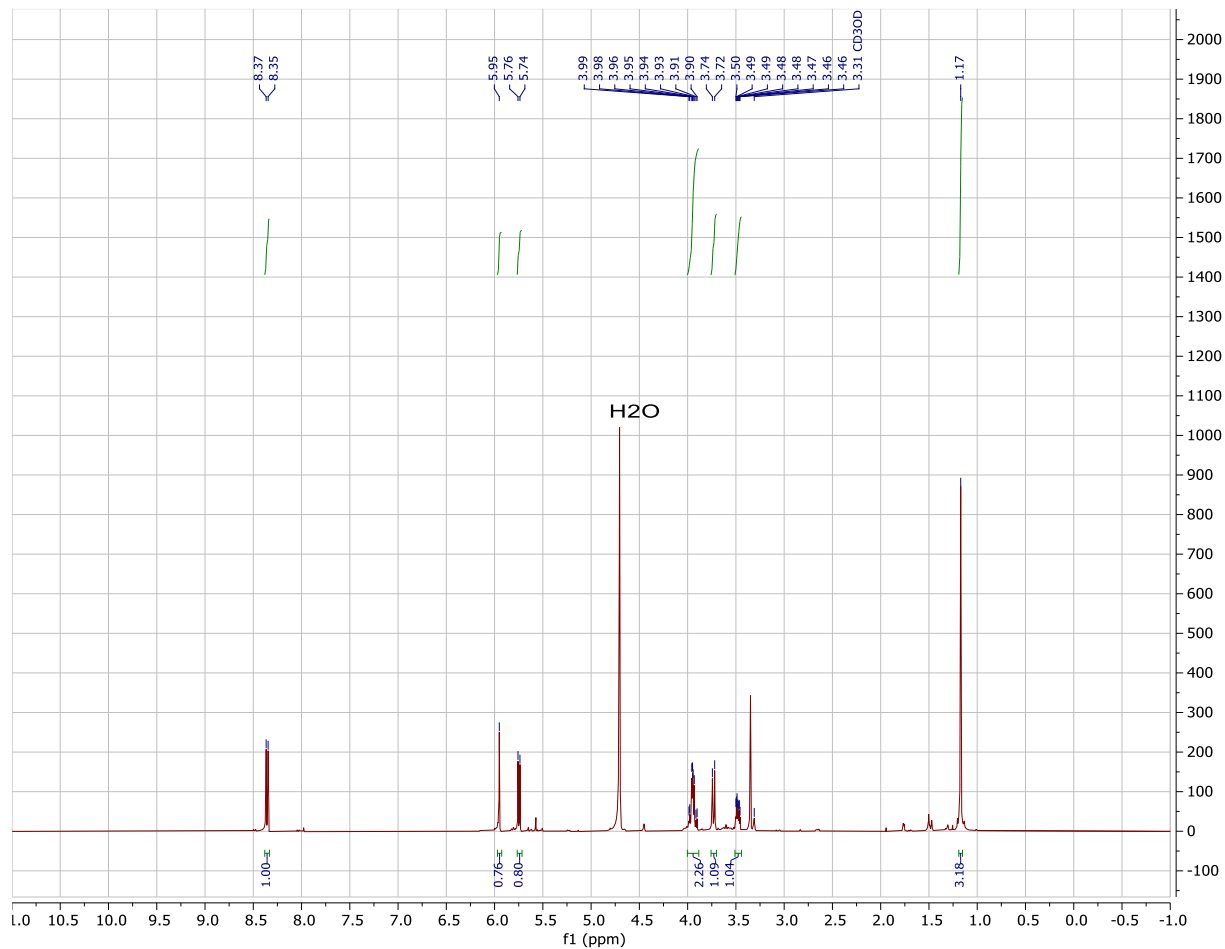
2.9

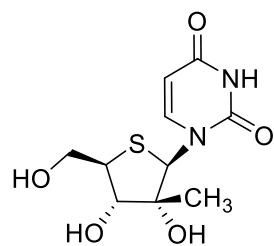


## SA.1.2 Thionucleosides and Monophosphate Prodrugs (2.11a-f; 2.13a-f)

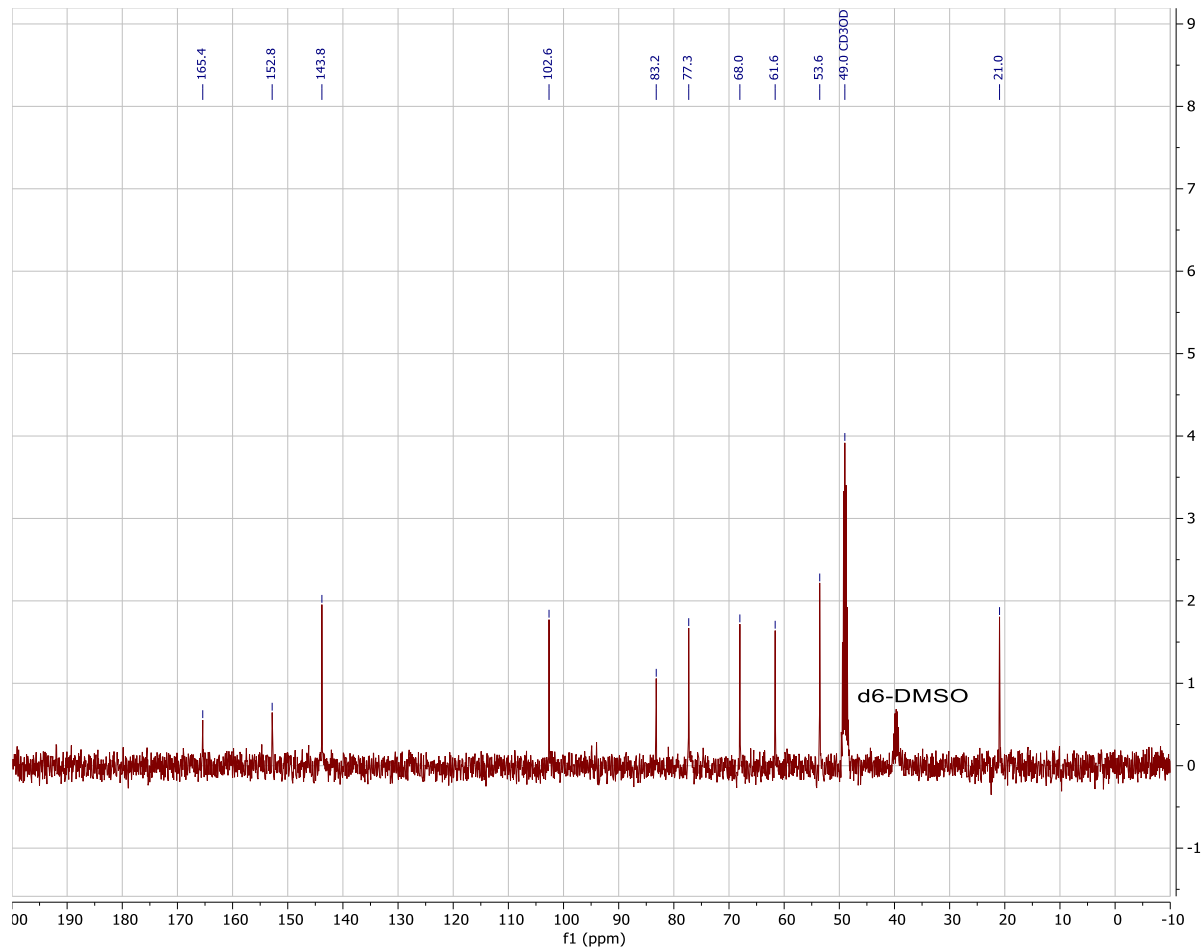


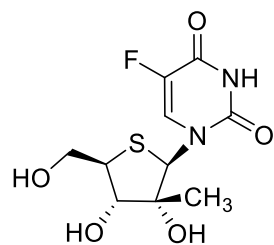
2.11a



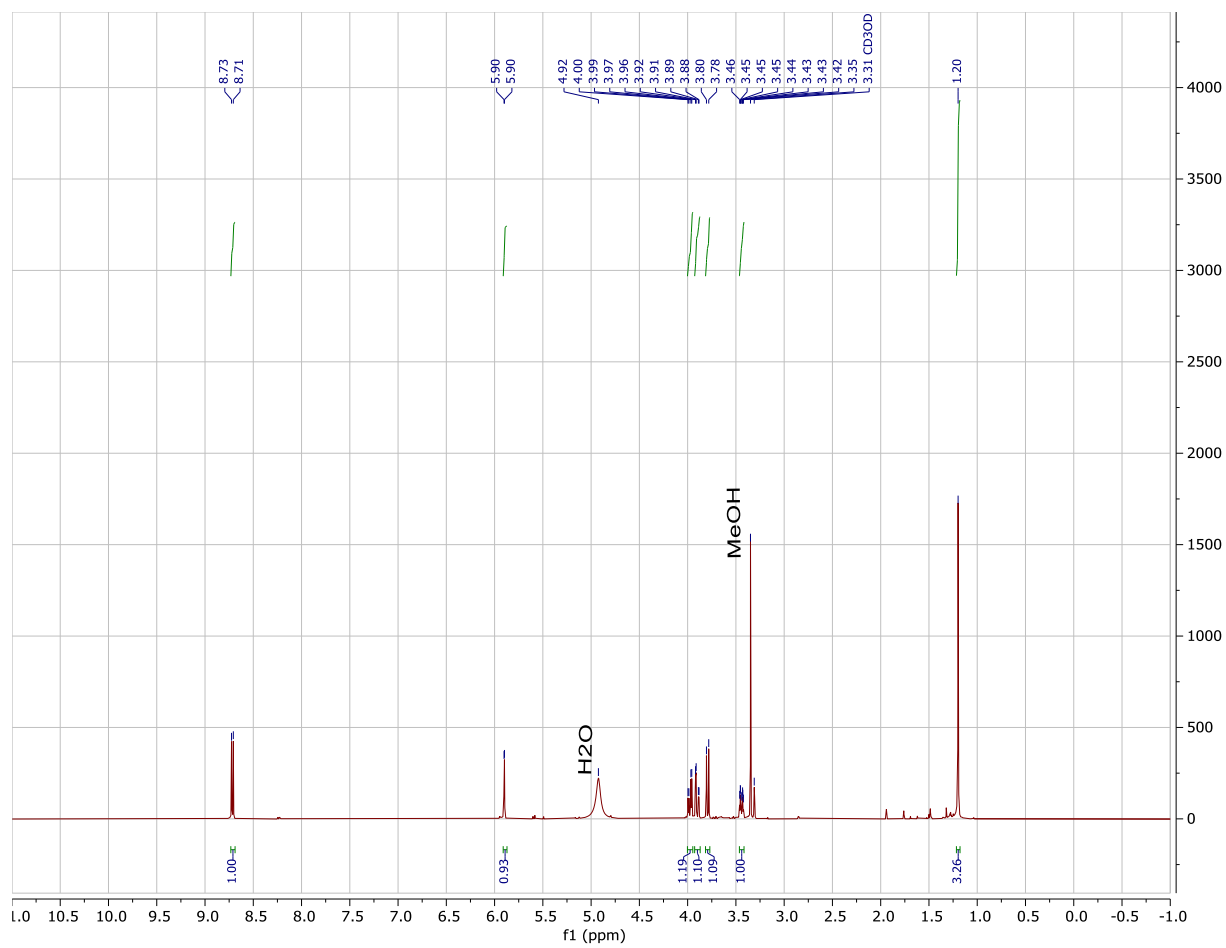


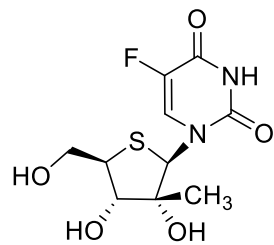
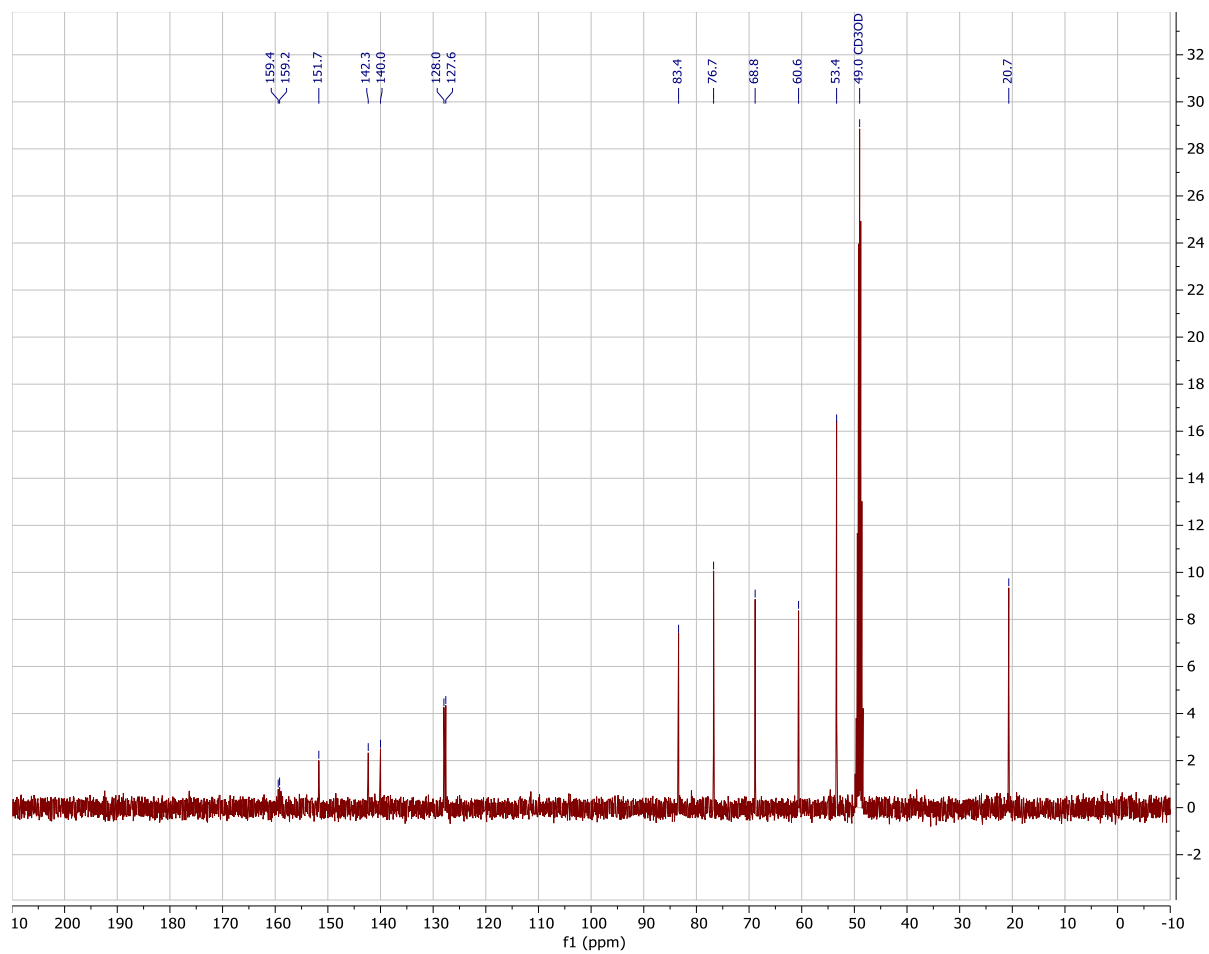
2.11a

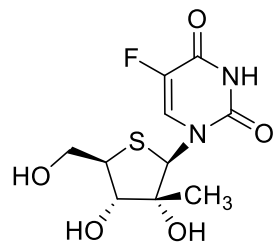
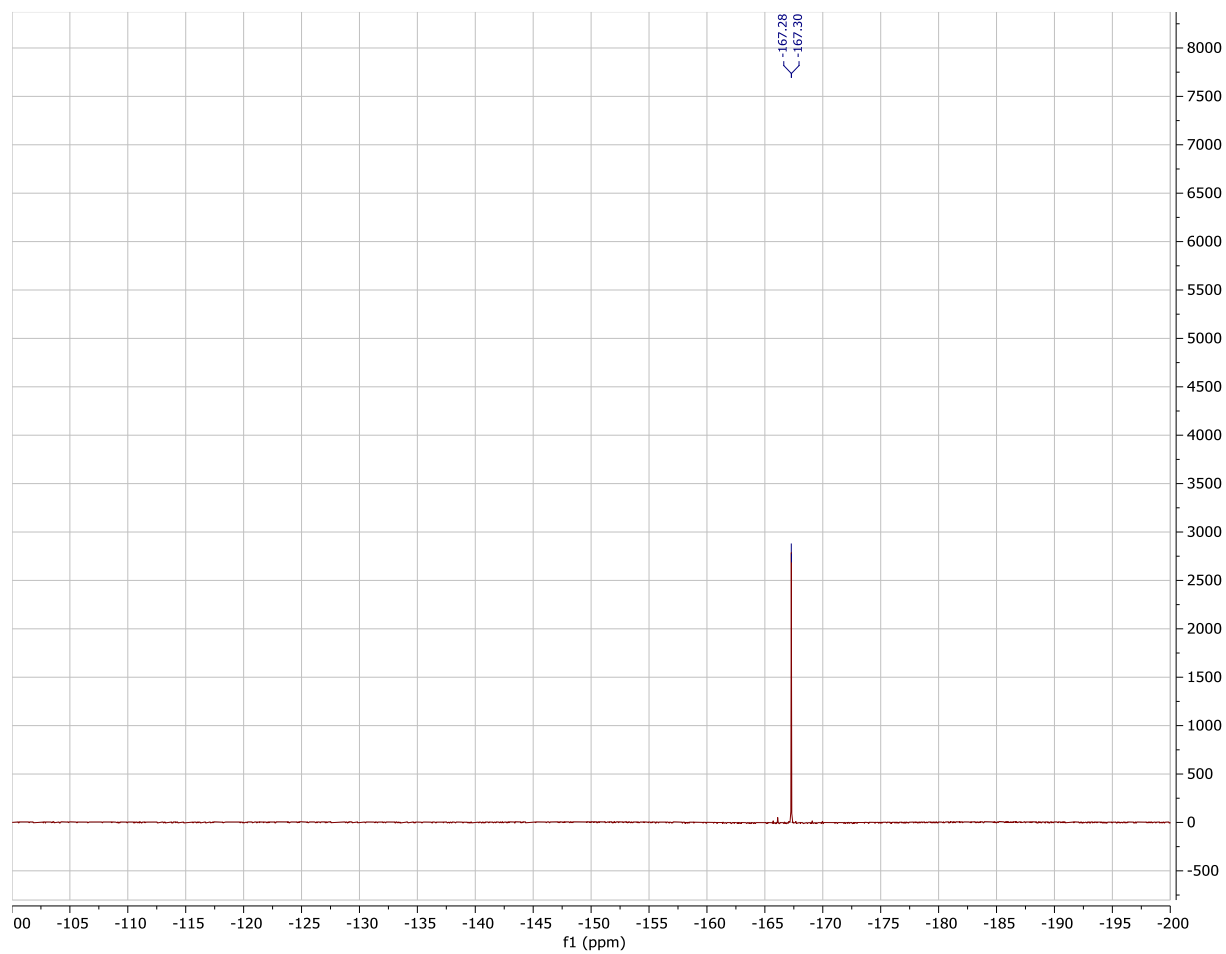


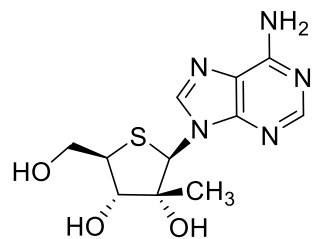


2.11b

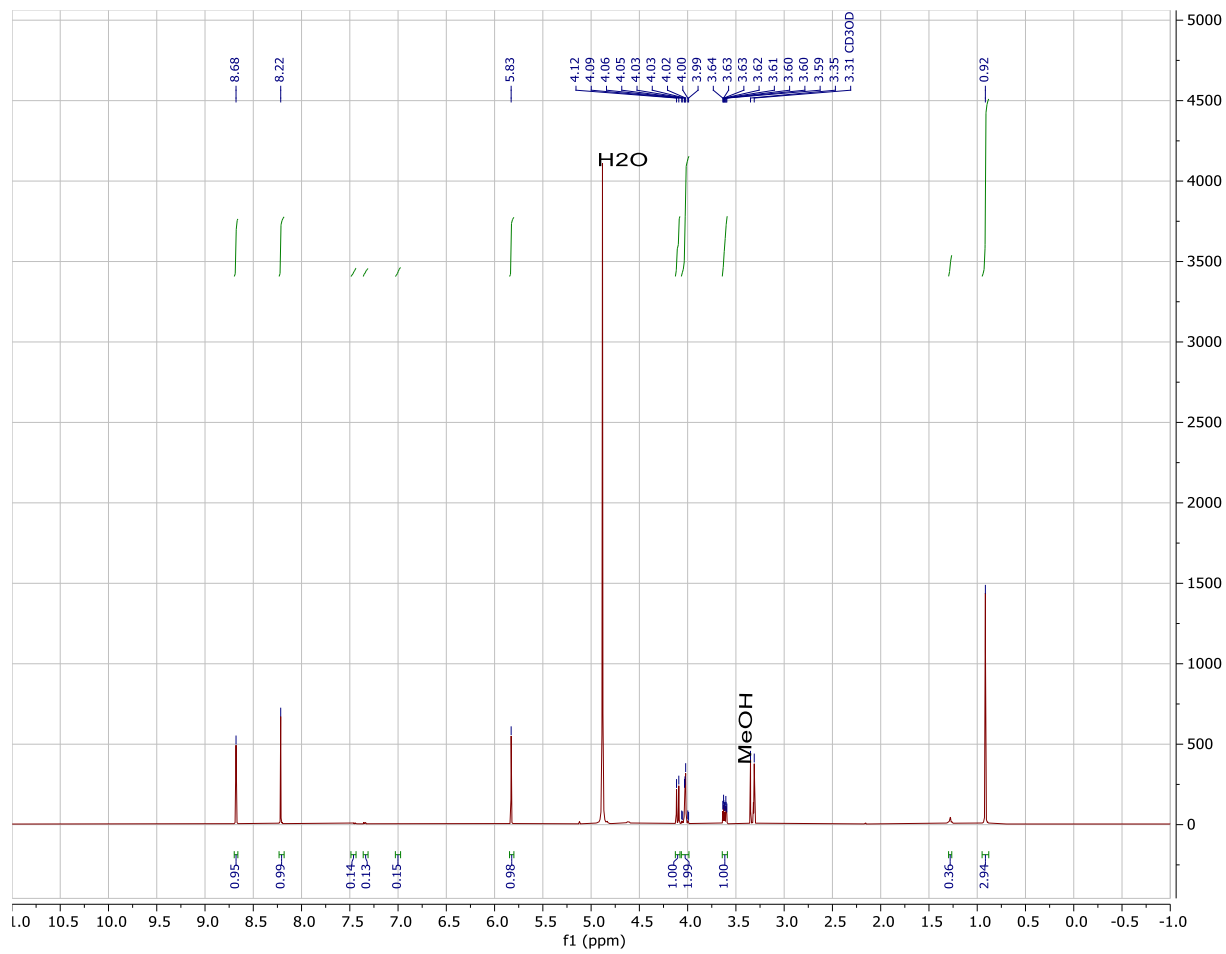


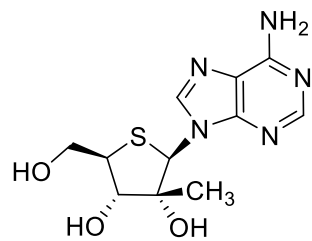
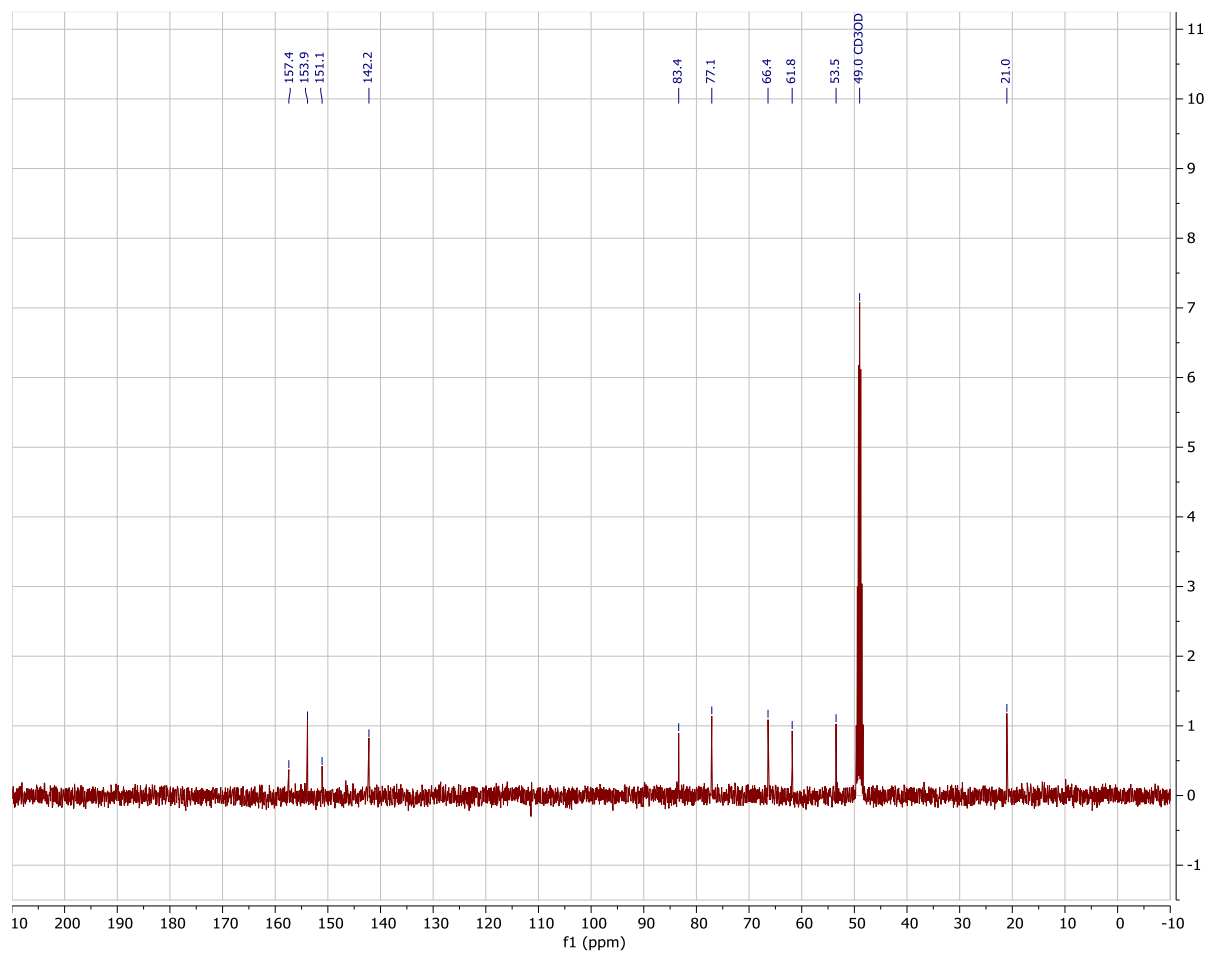
**2.11b**

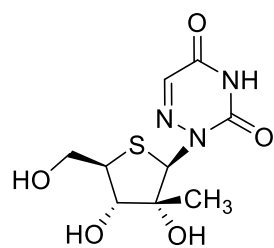
**2.11b**



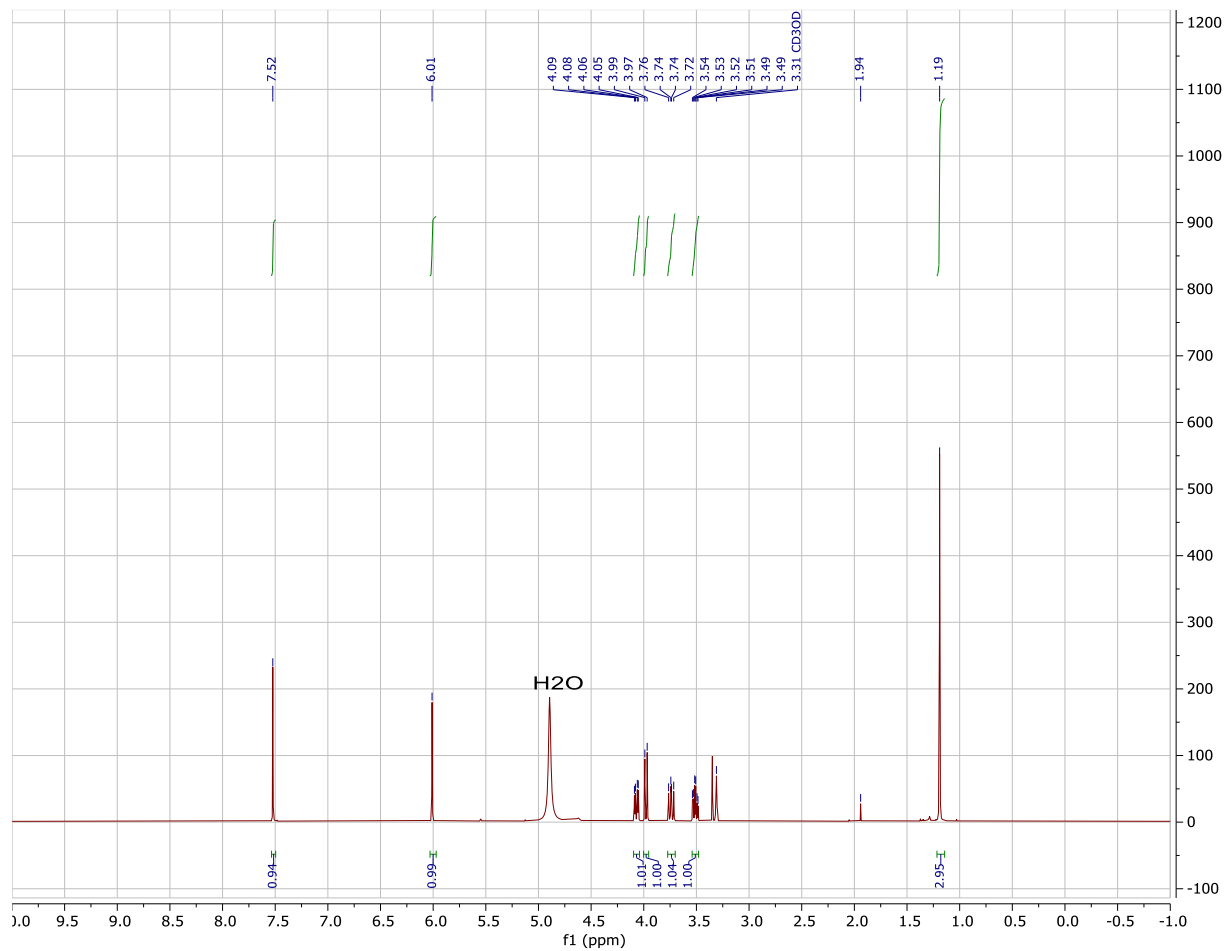
2.11c

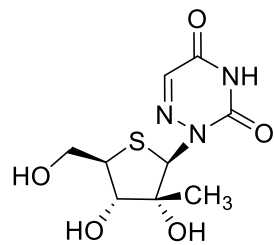
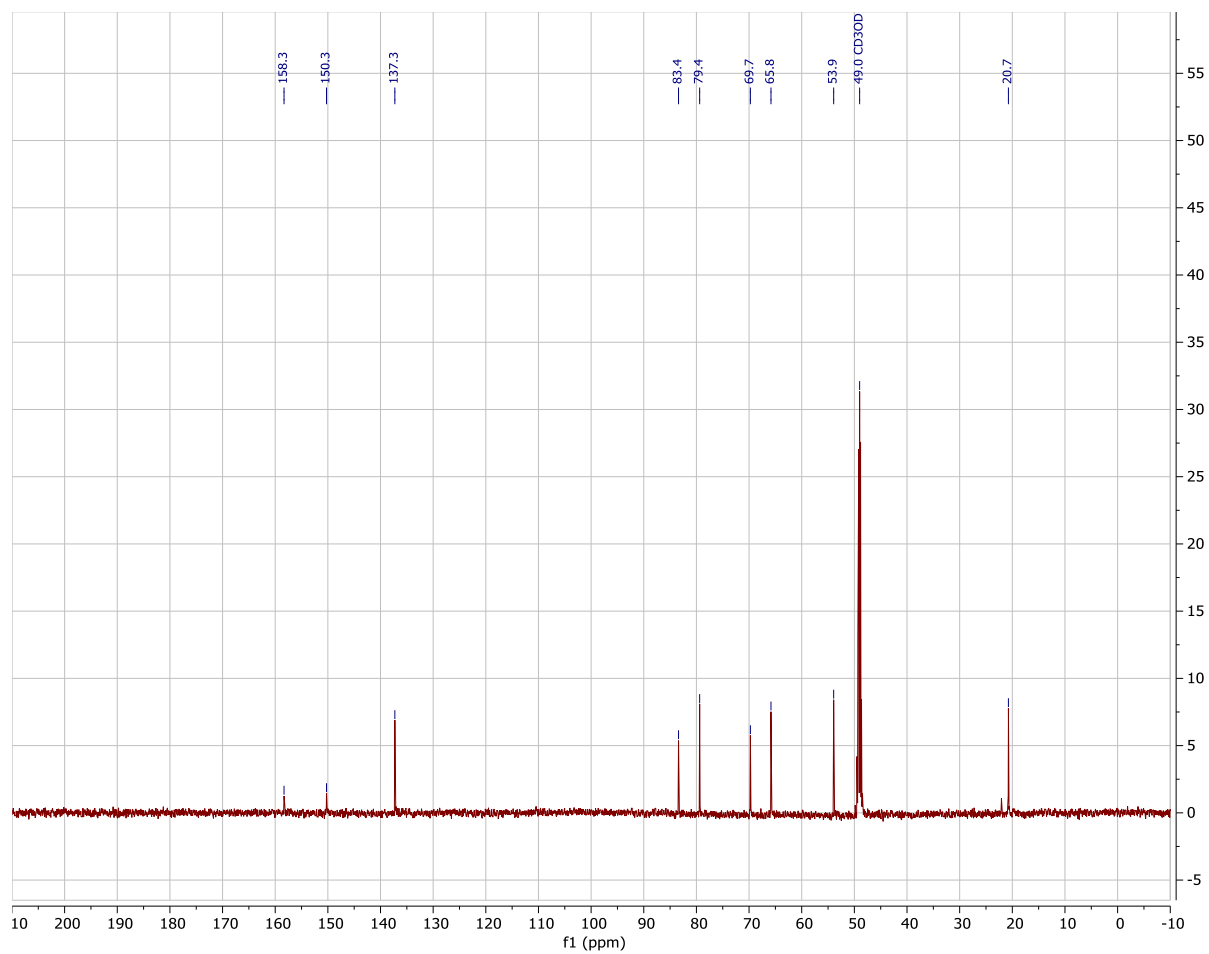


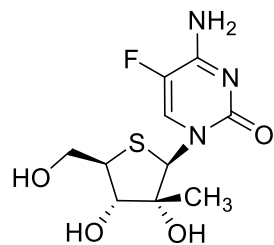
**2.11c**



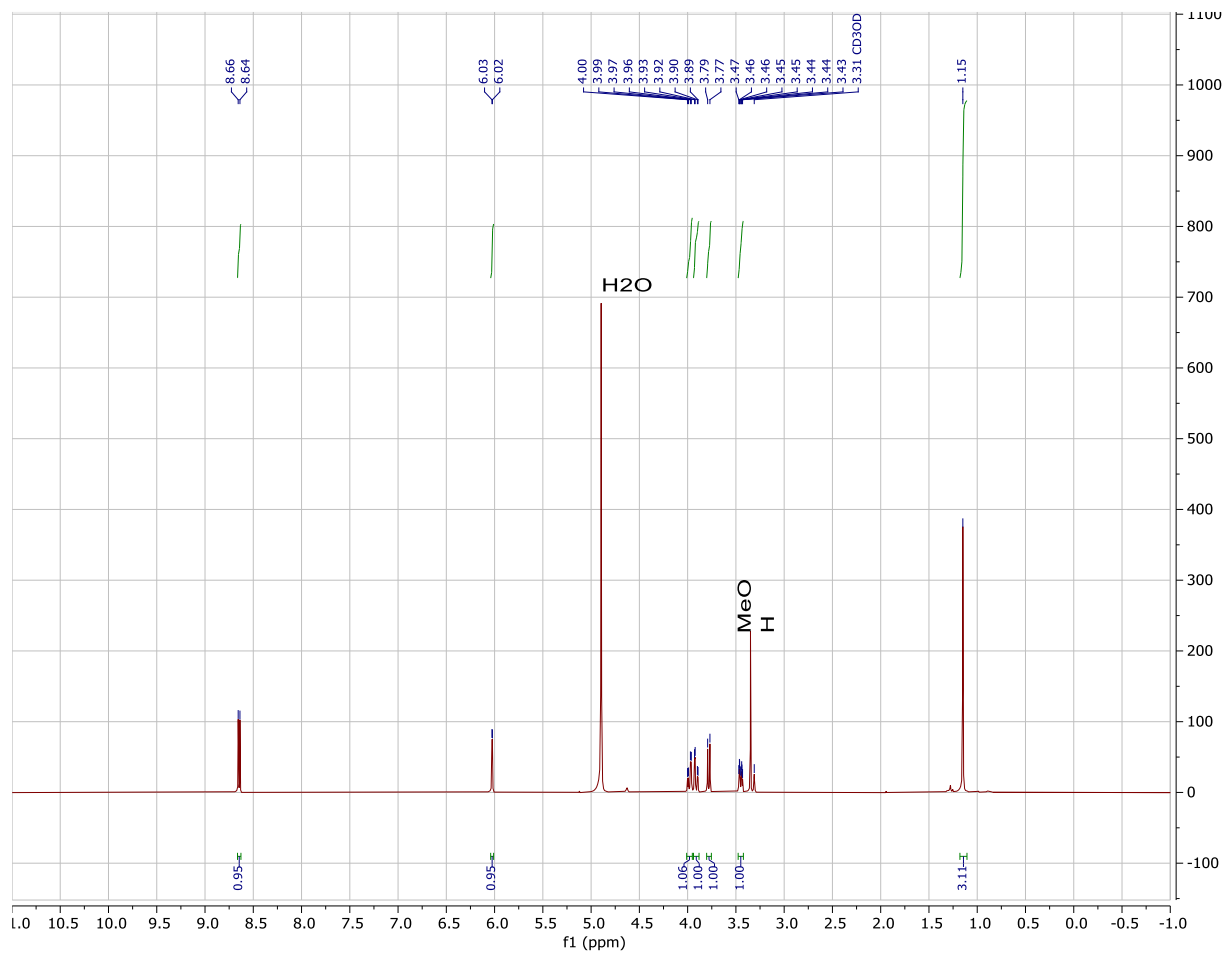
2.11d

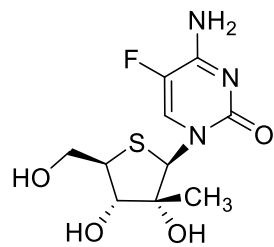


**2.11d**

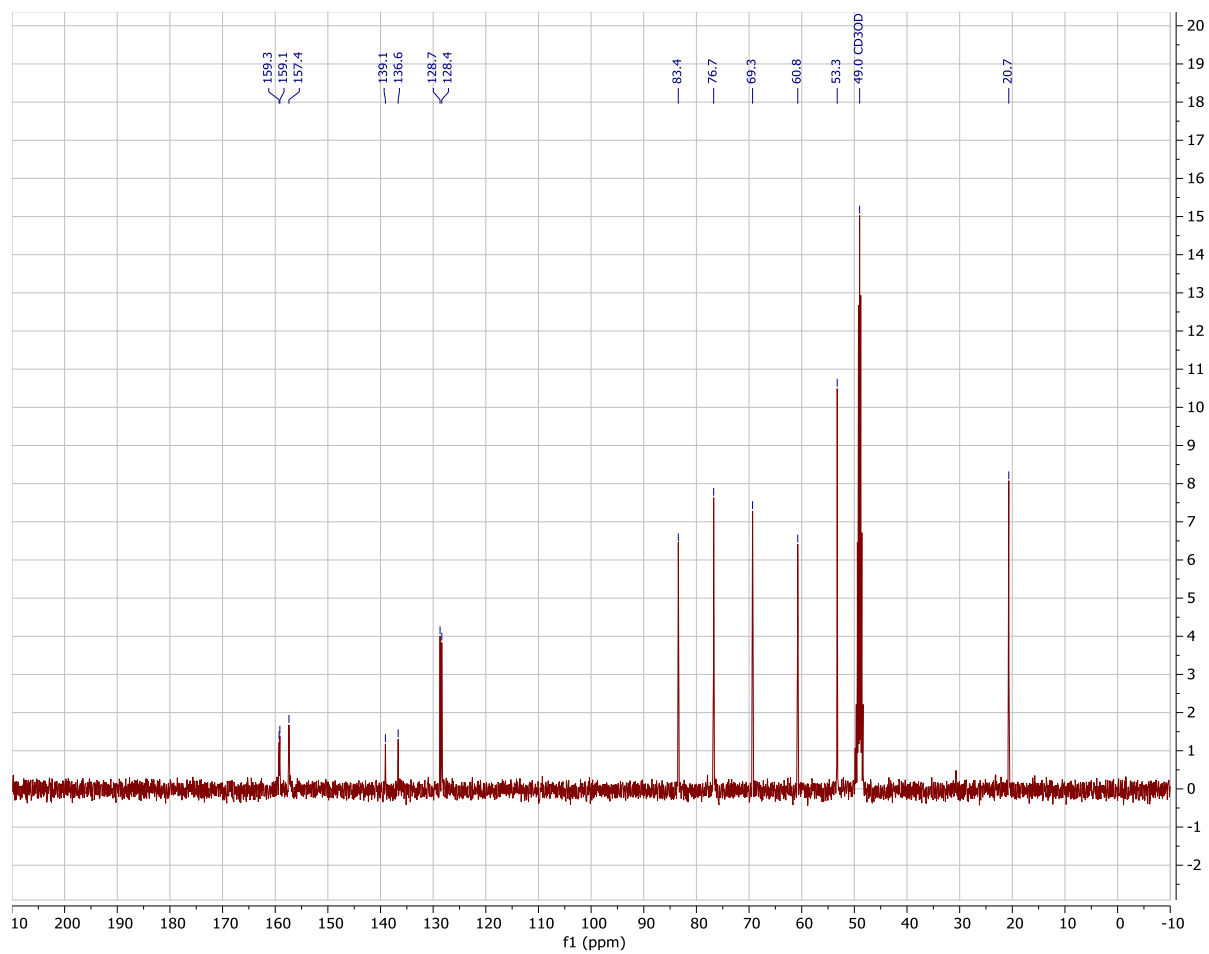


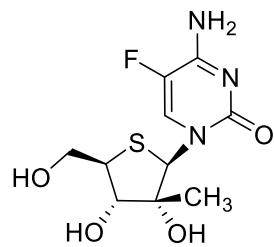
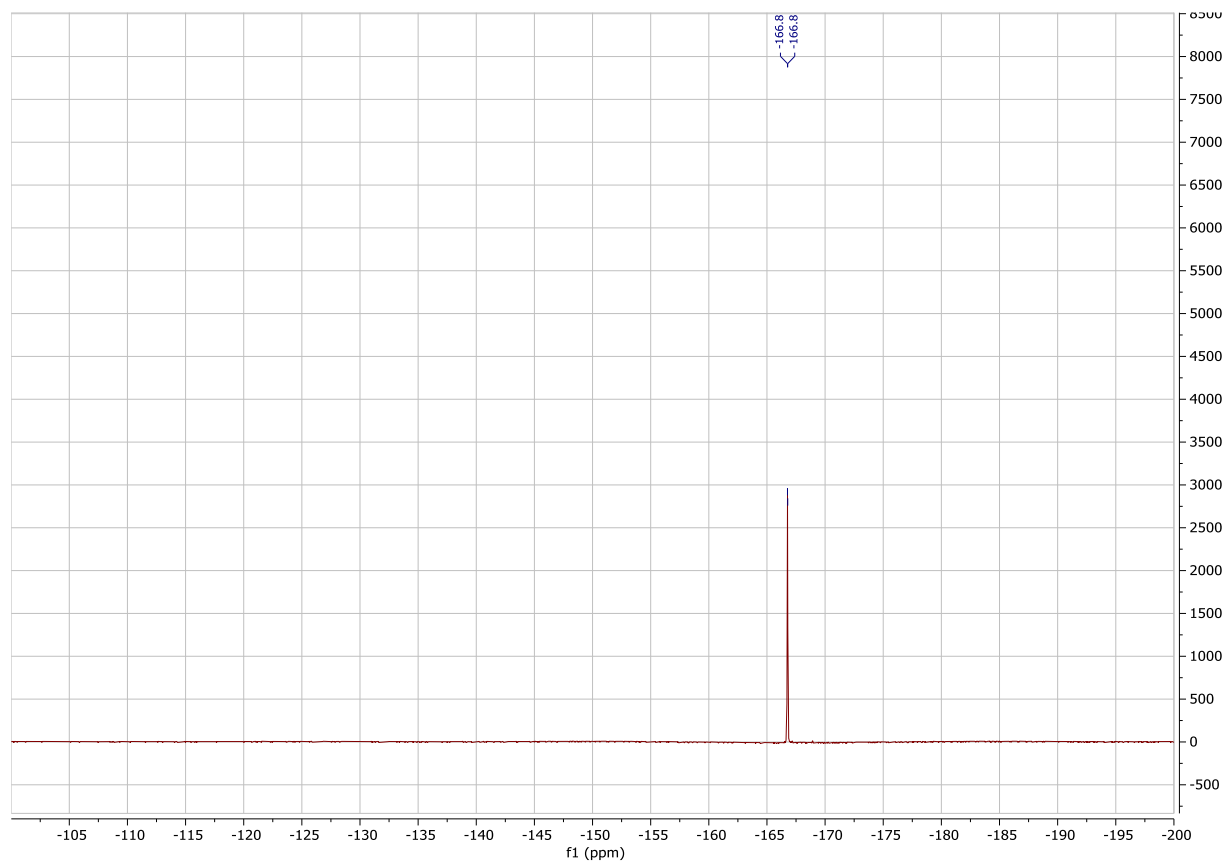
2.11e

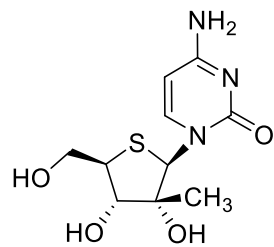




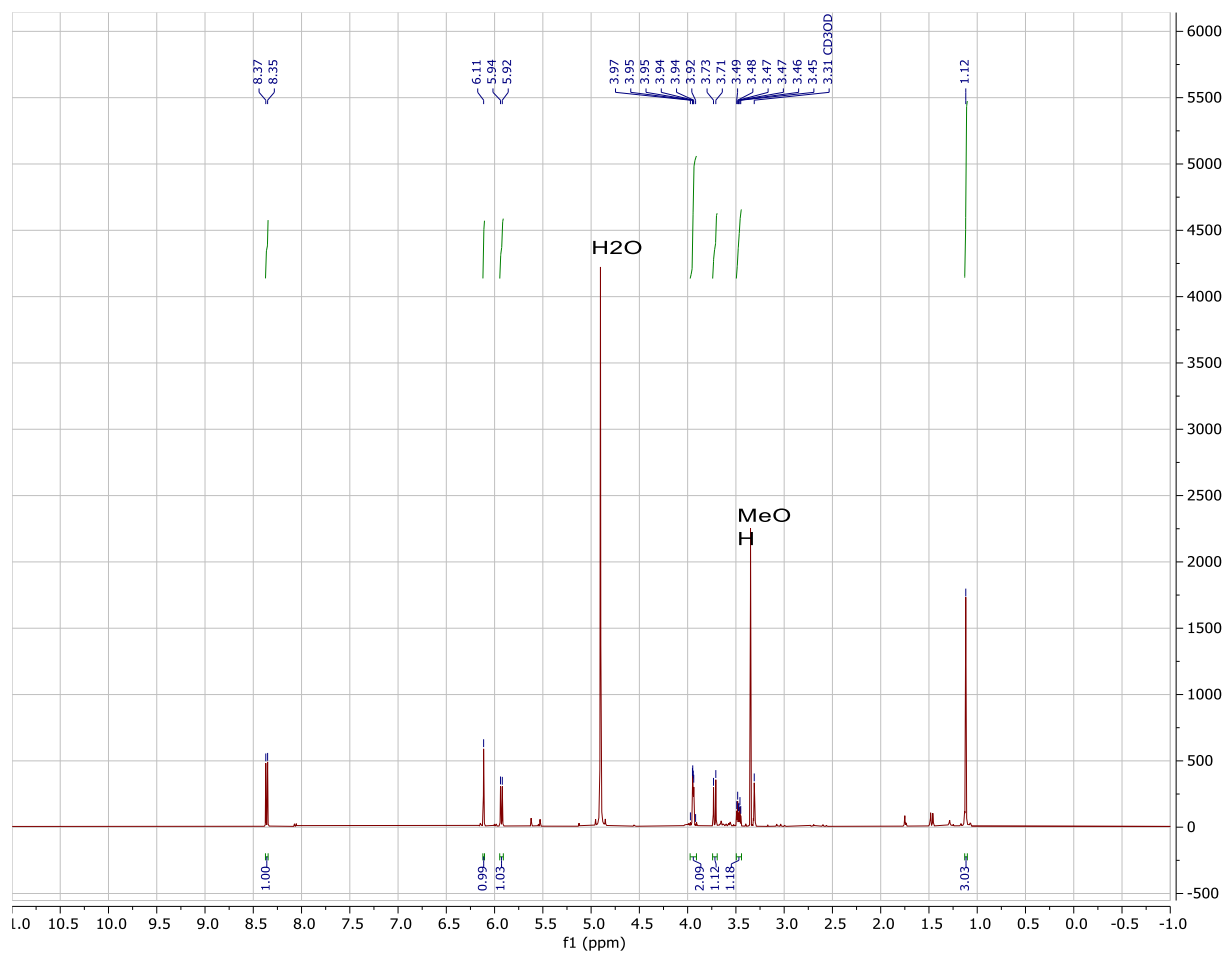
2.11e

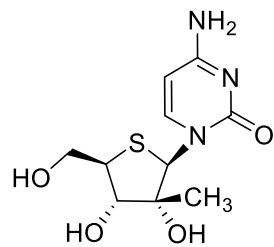


**2.11e**

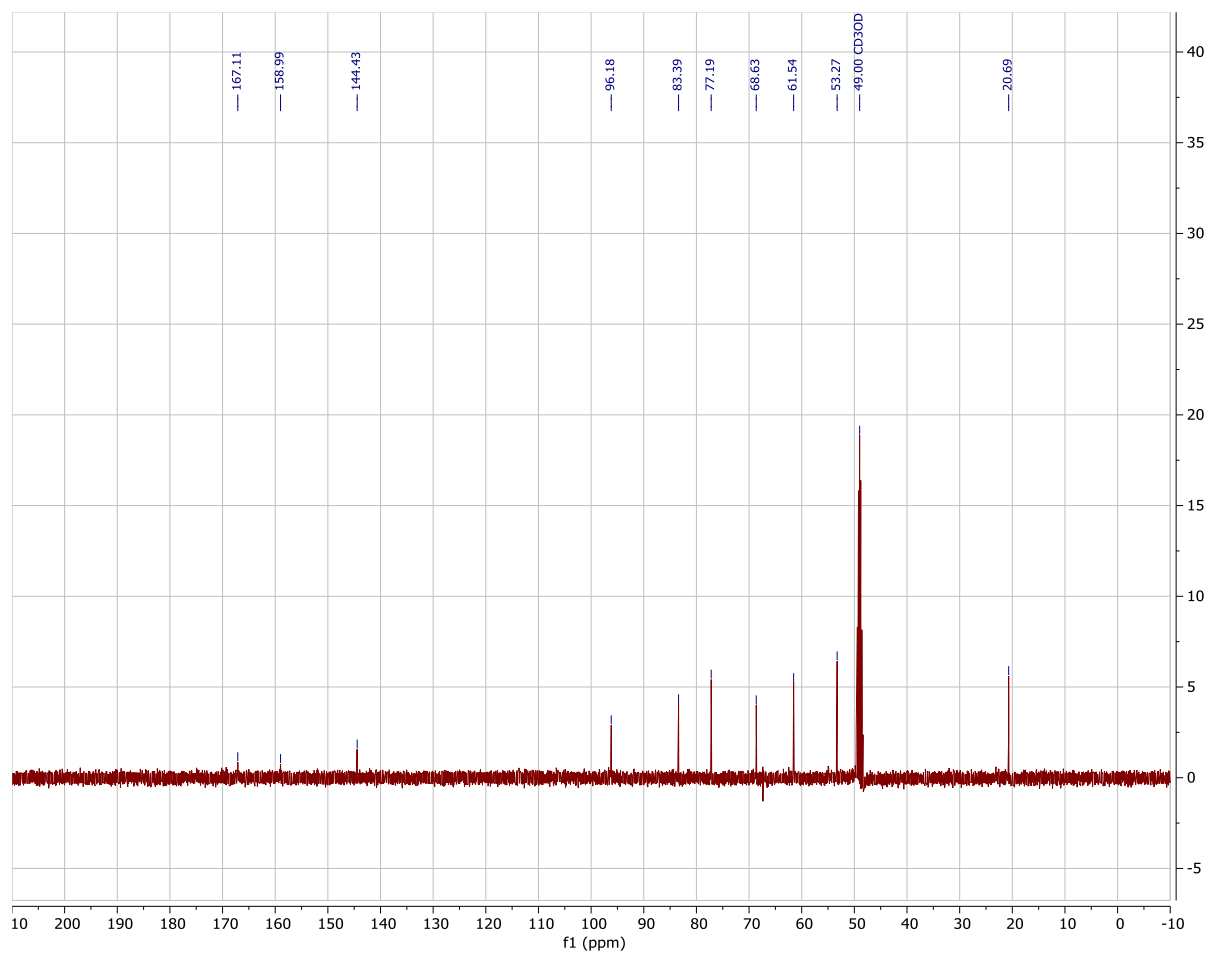


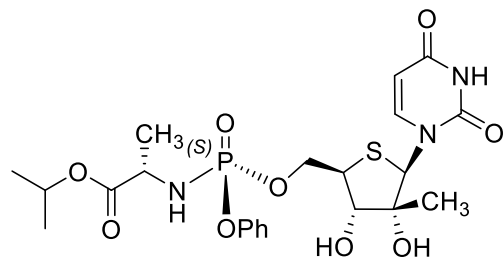
2.11f



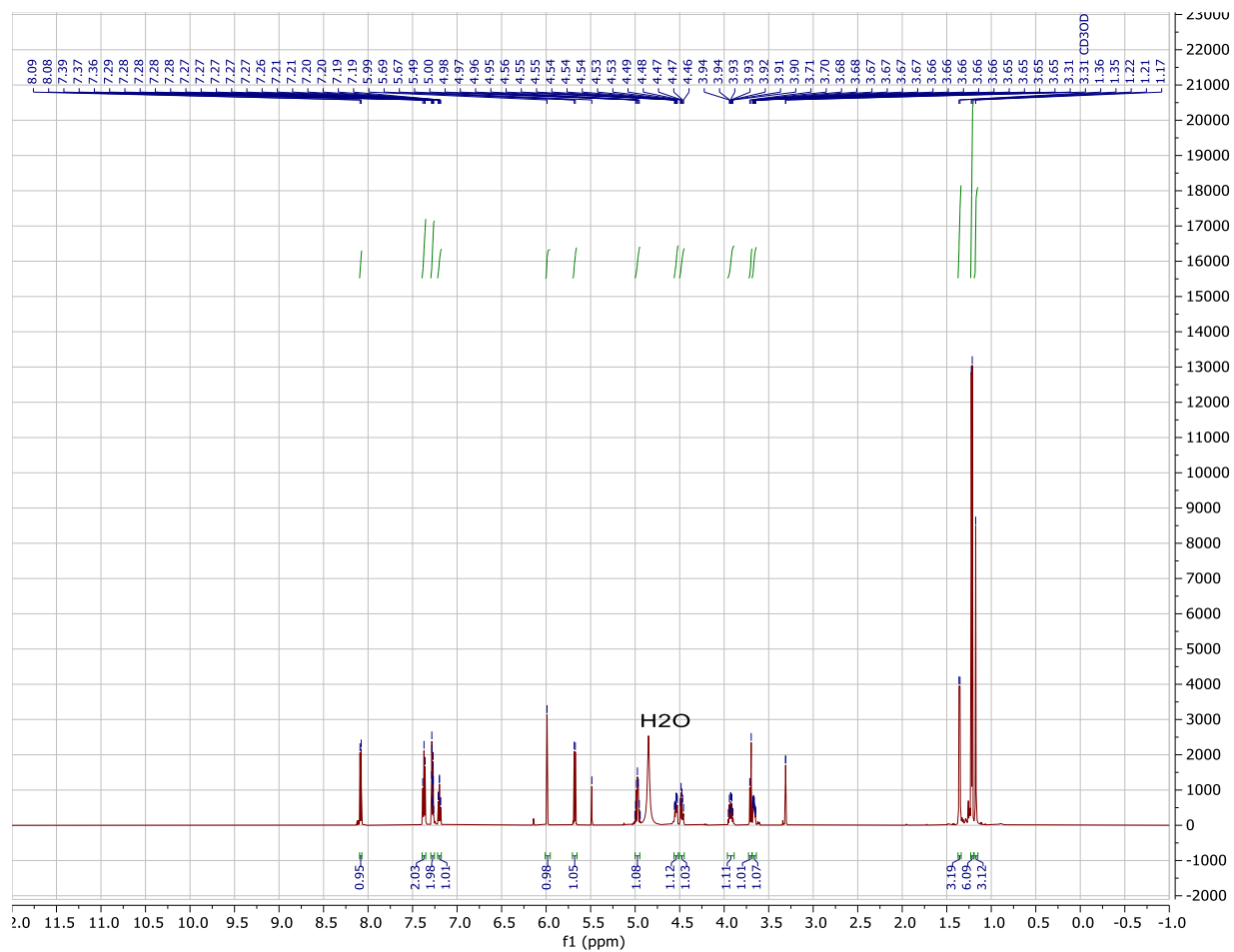


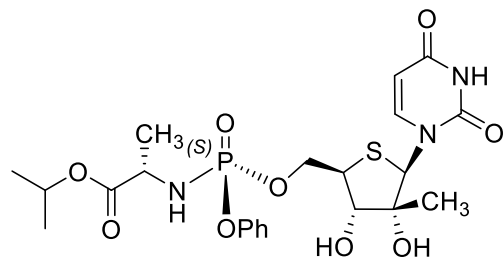
2.11f



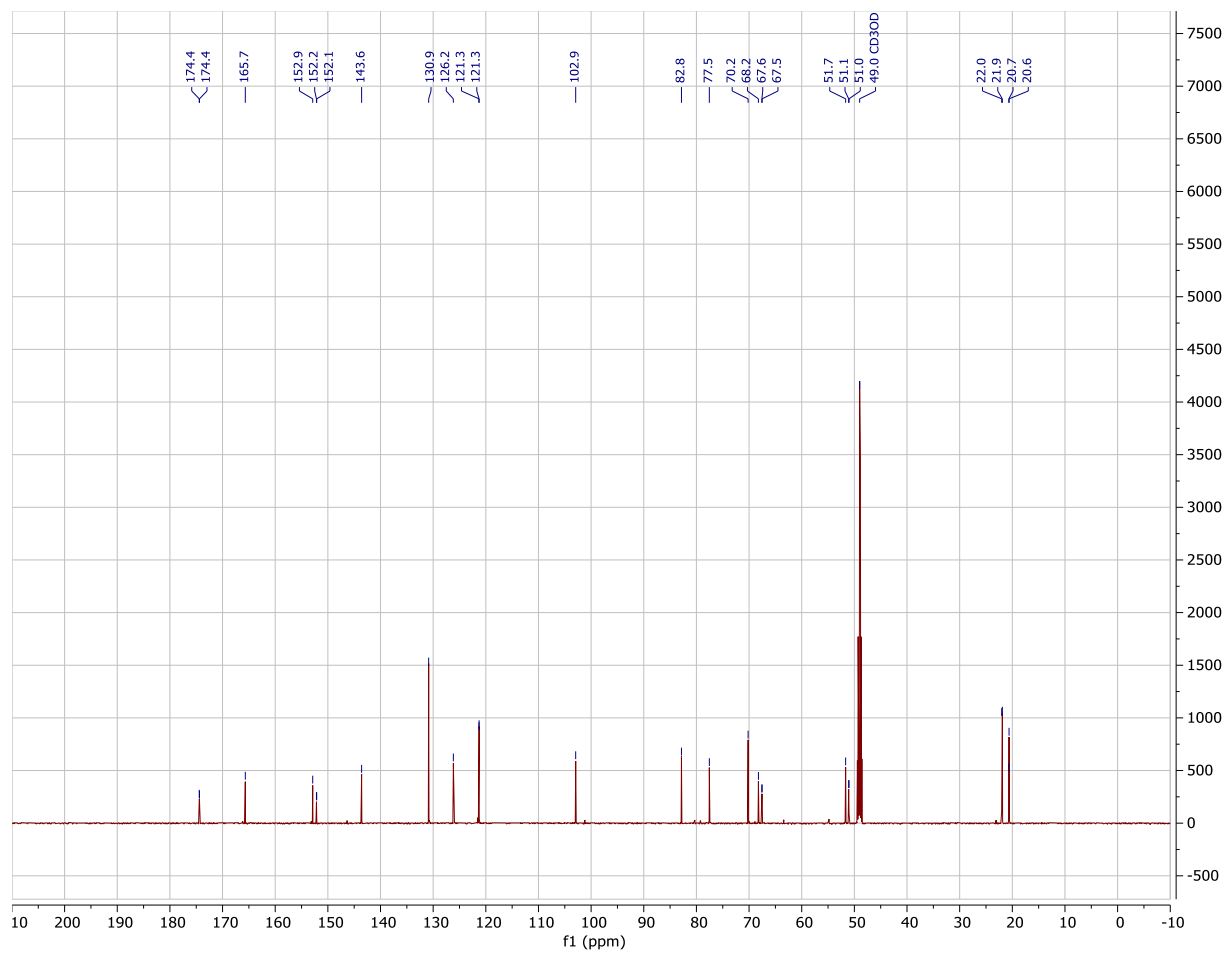


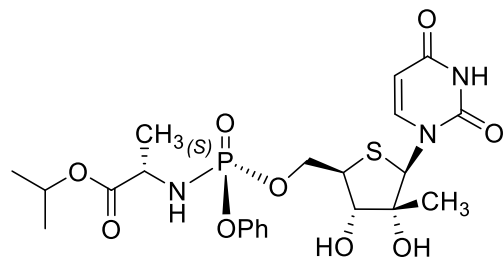
2.13a



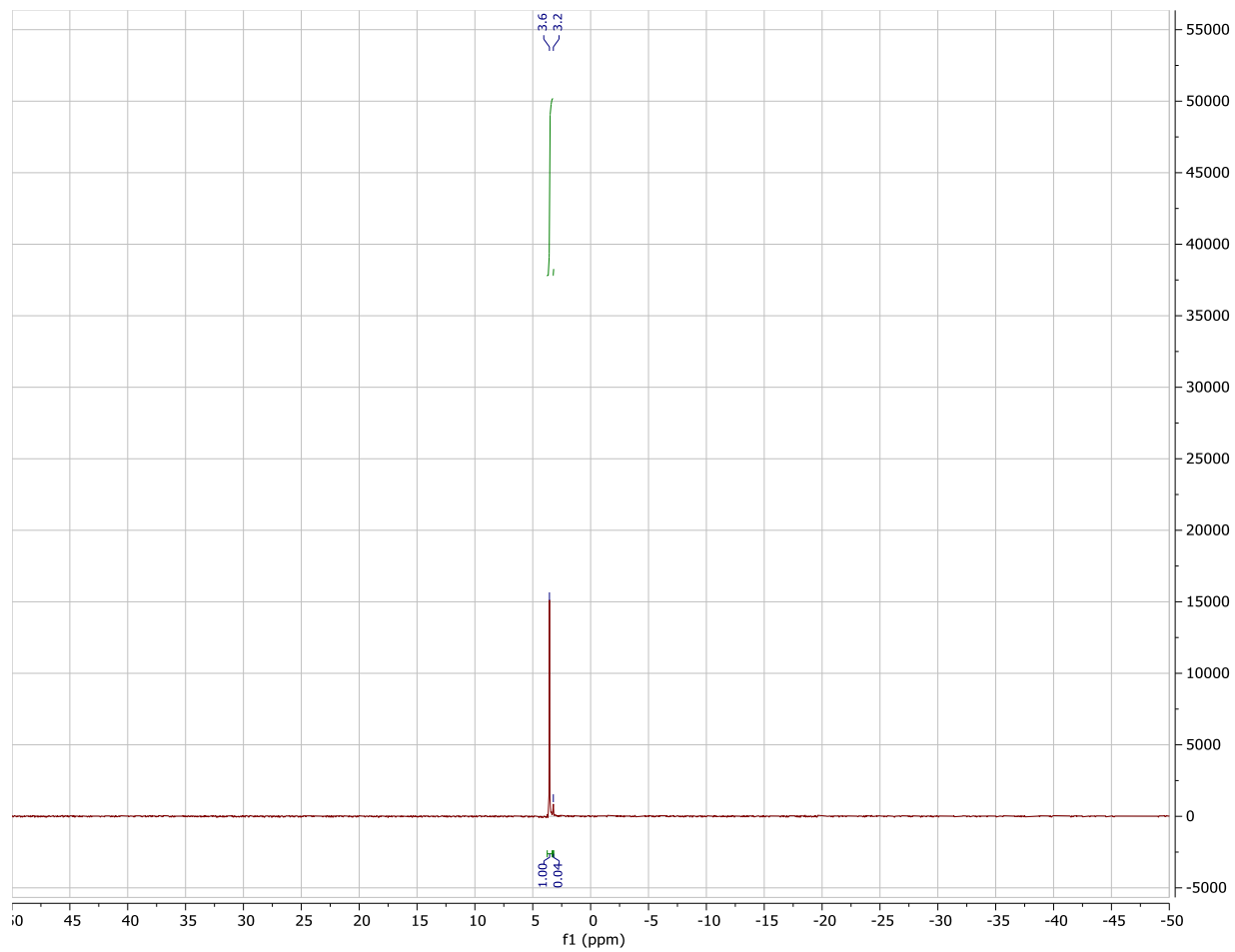


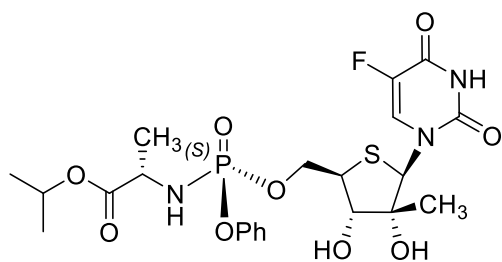
2.13a



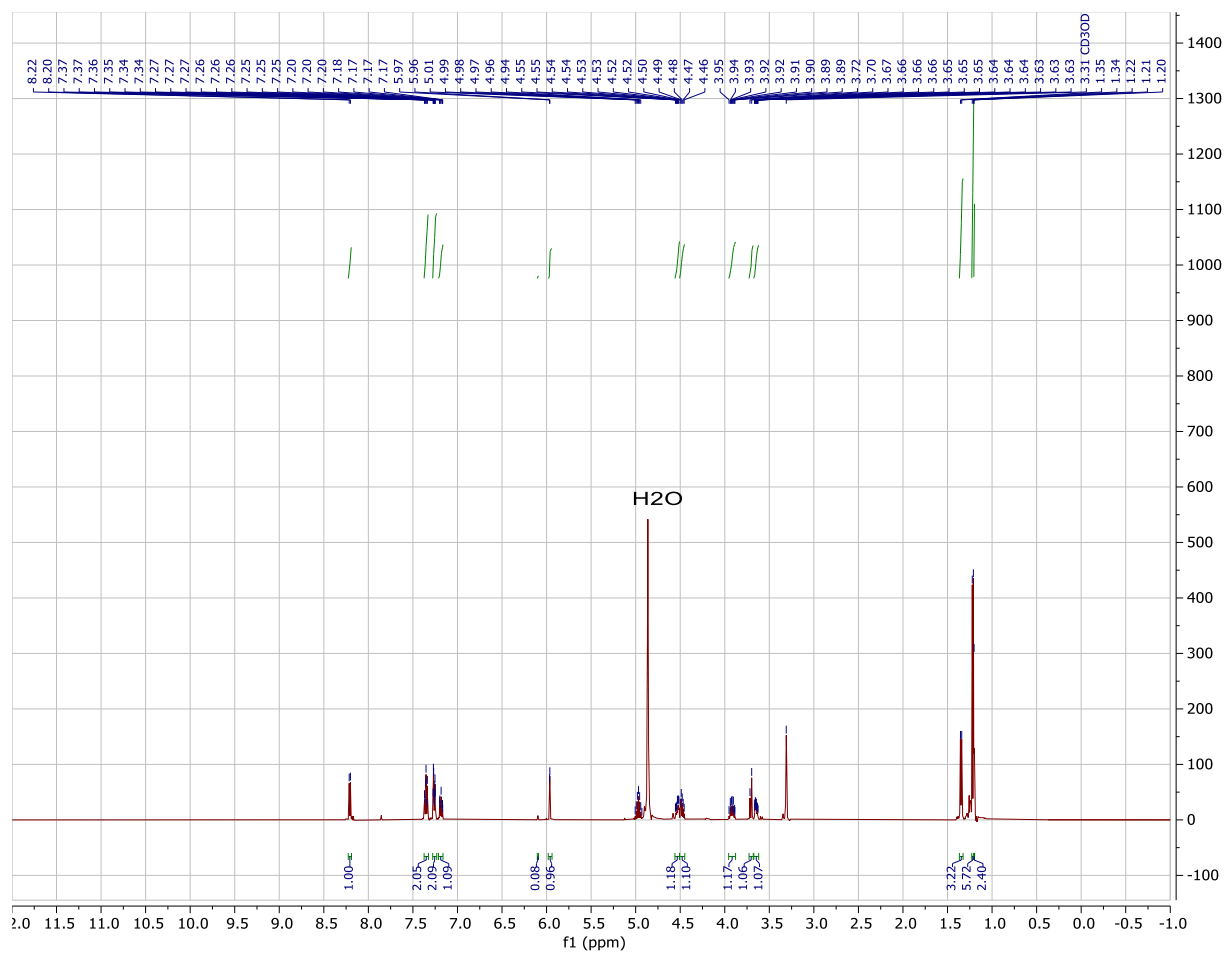


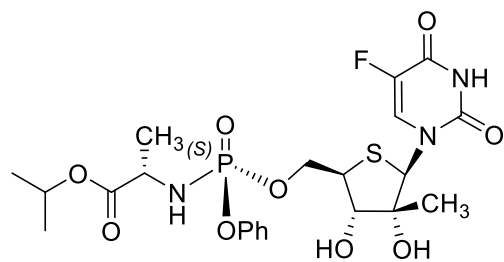
2.13a



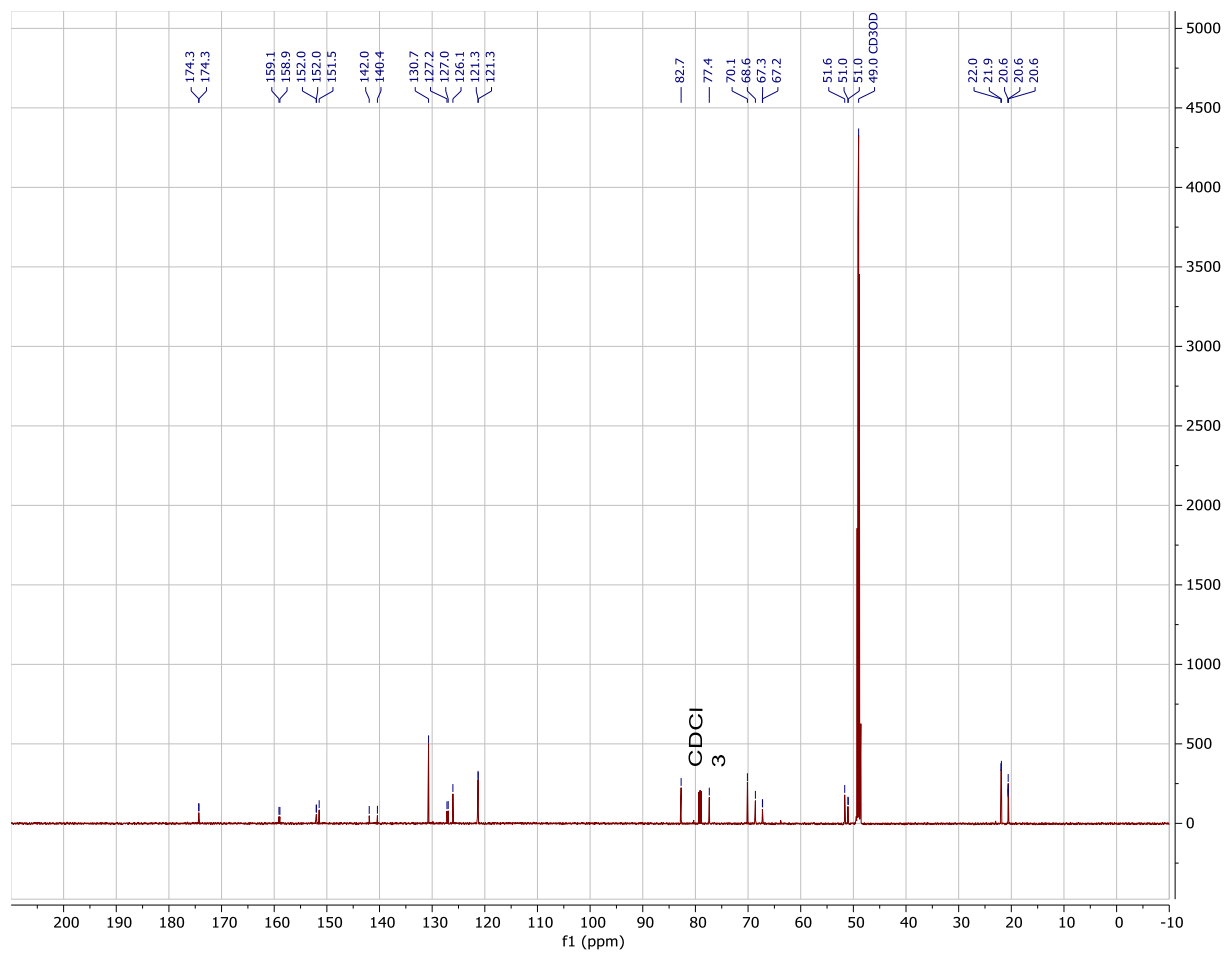


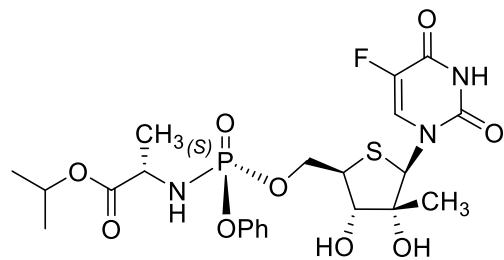
2.13b



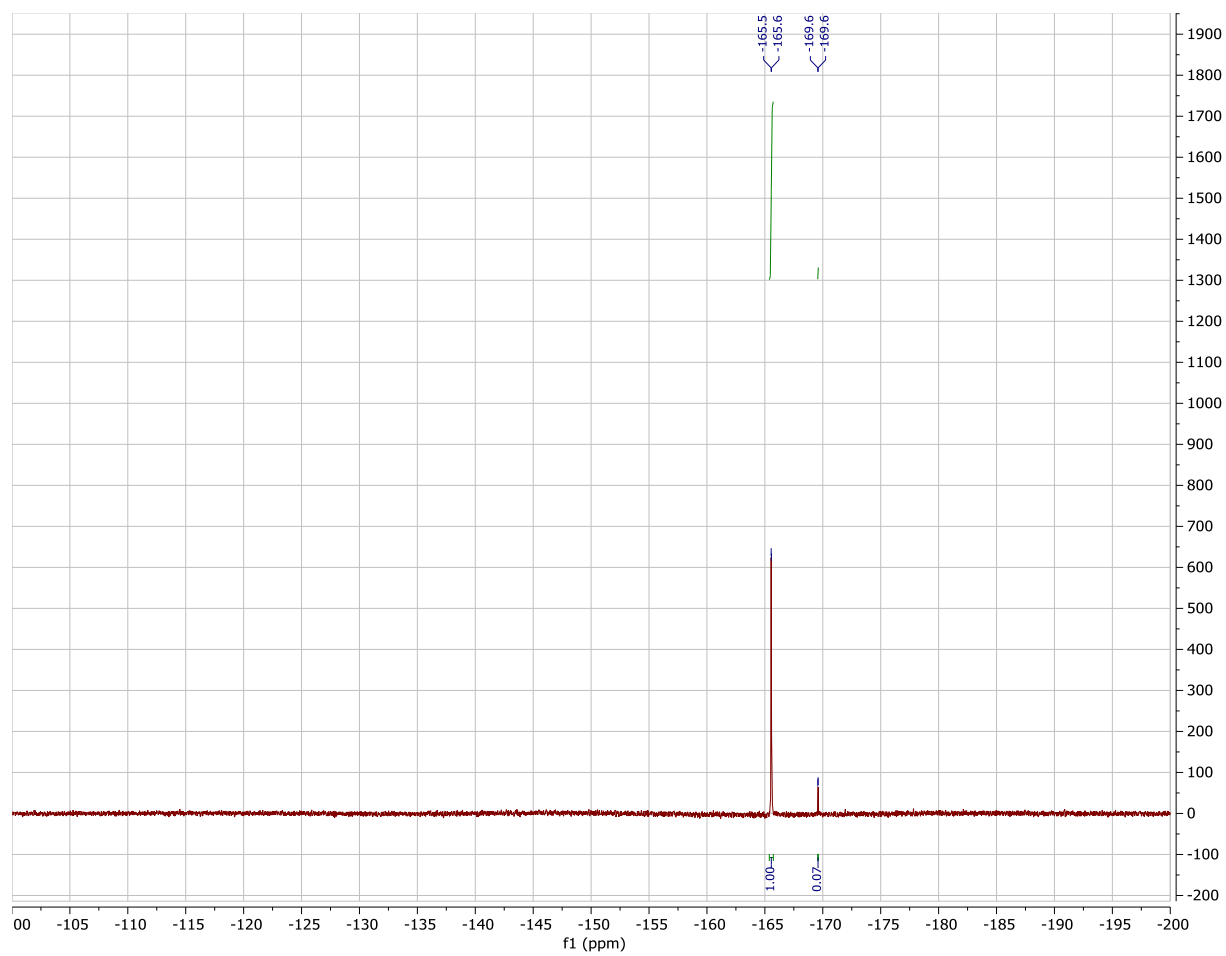


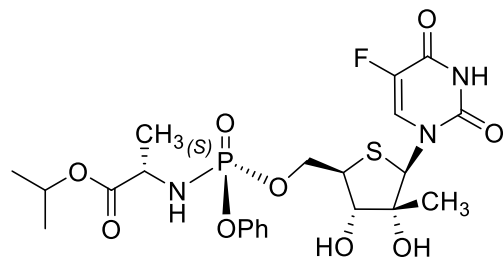
2.13b



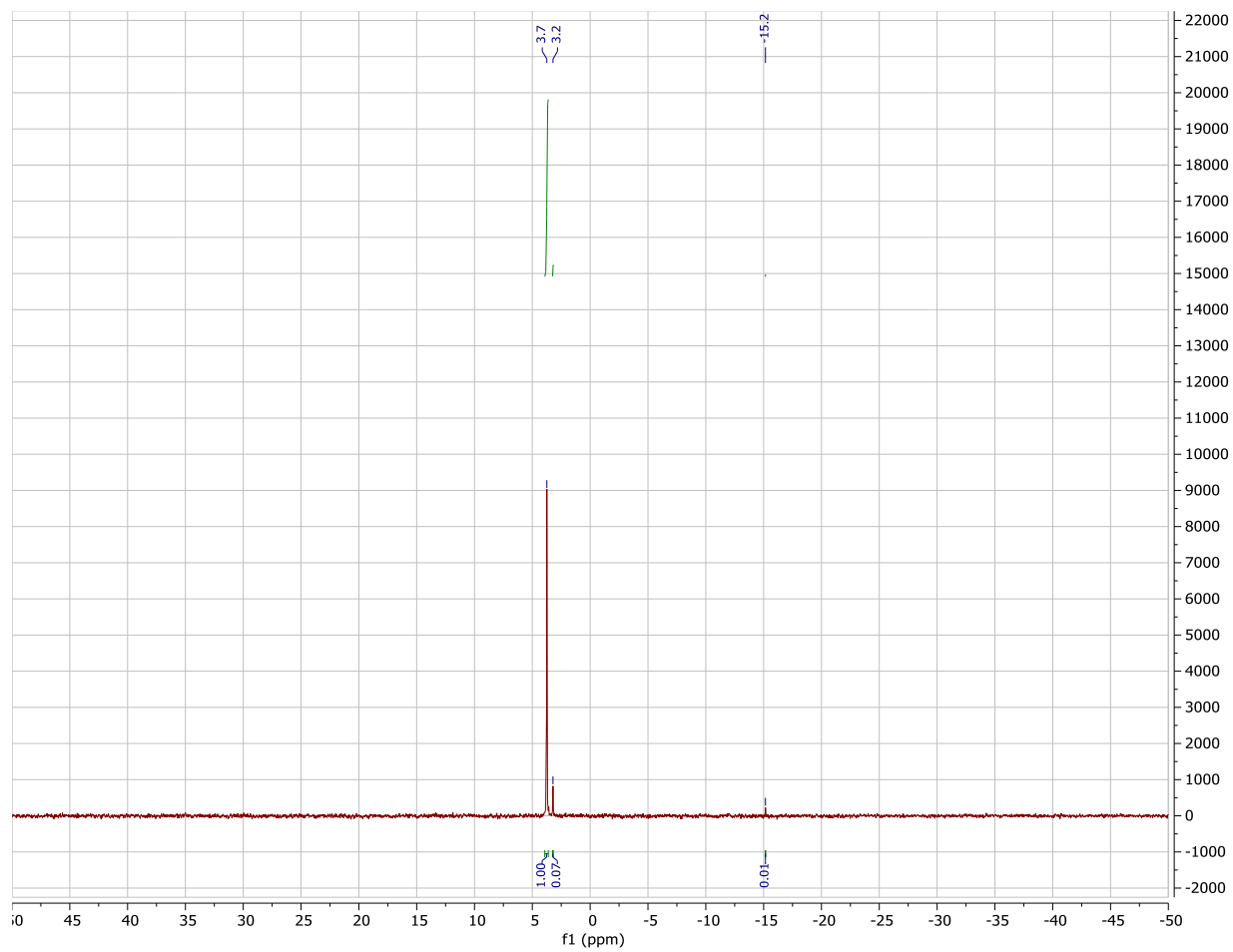


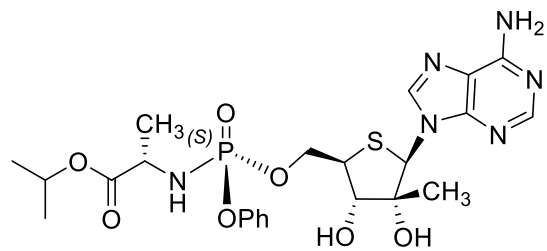
2.13b



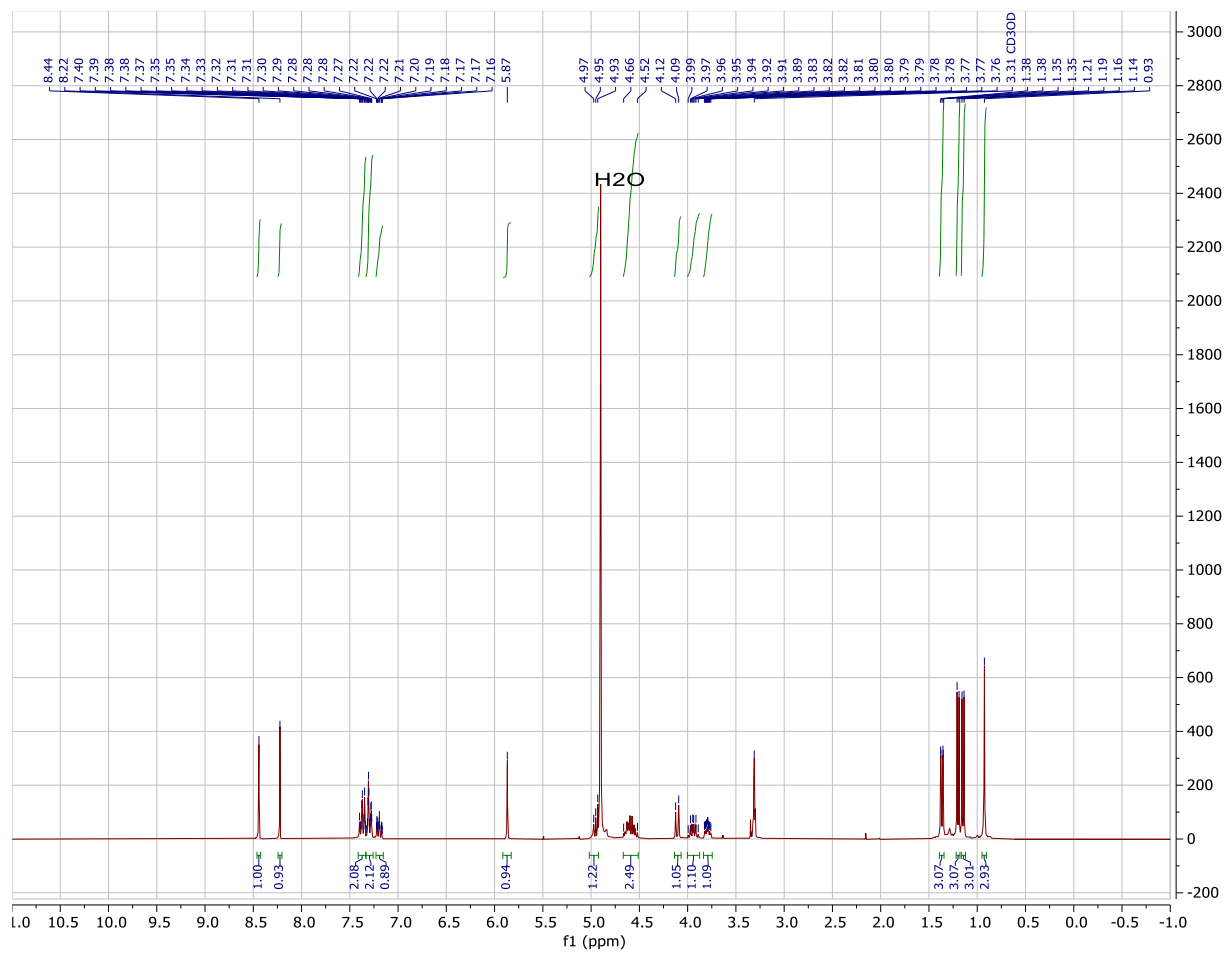


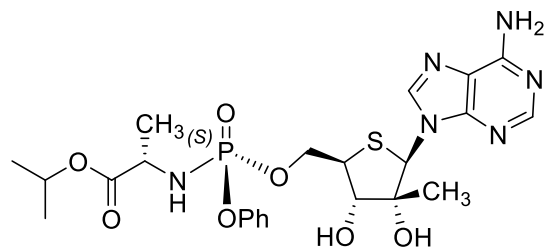
2.13b



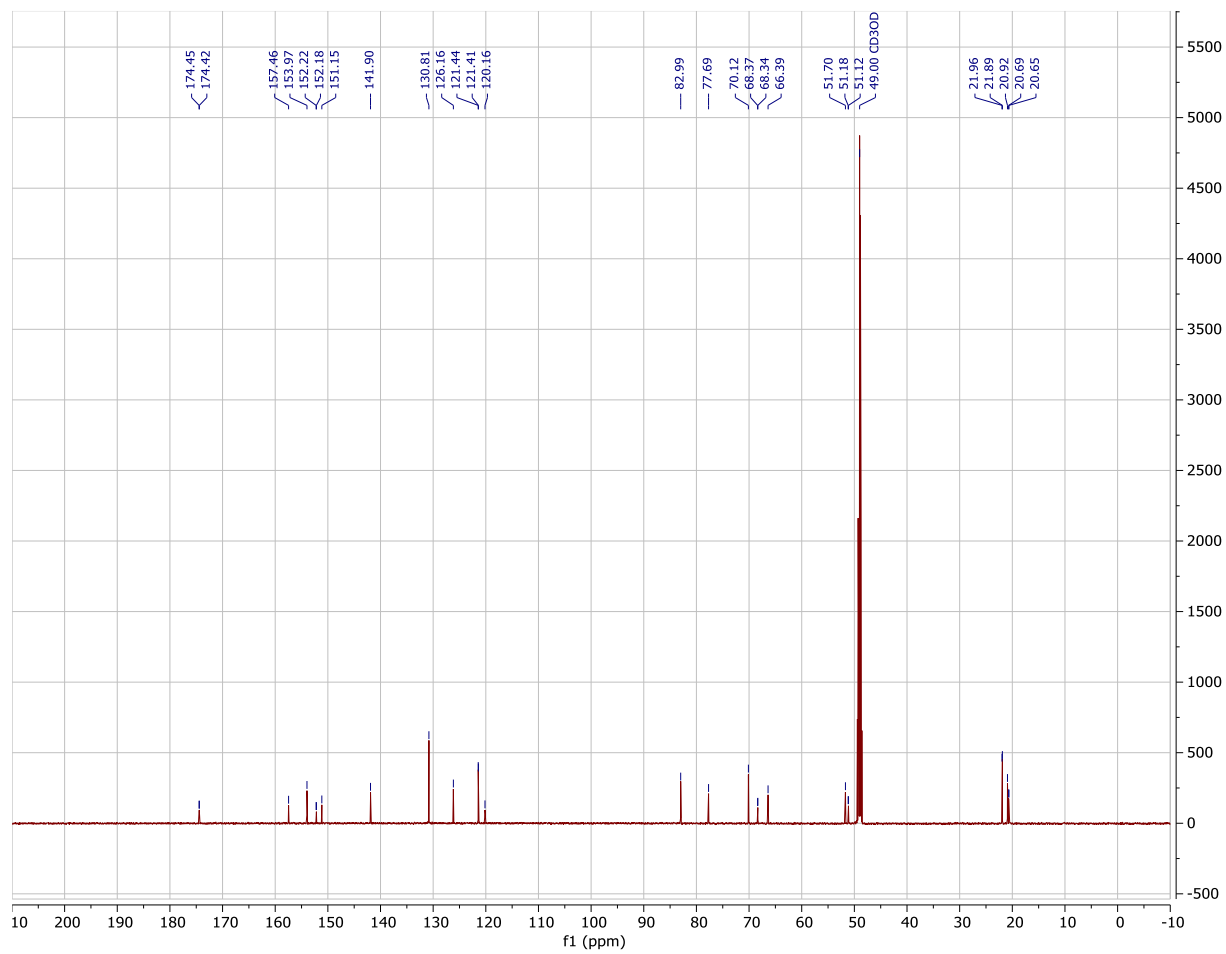


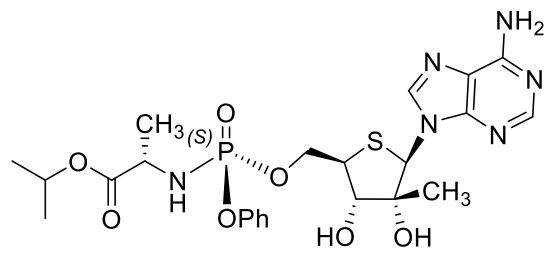
2.13c



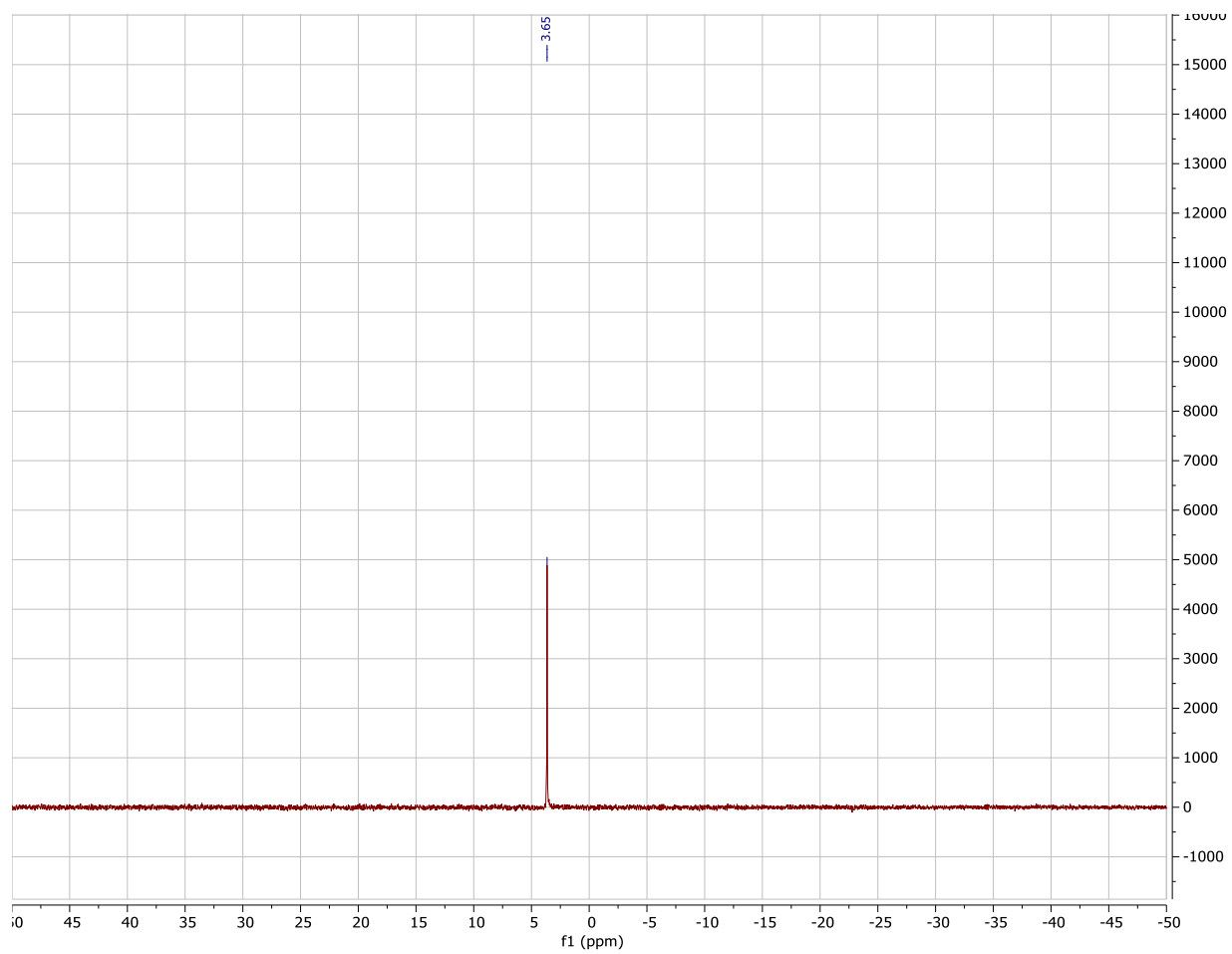


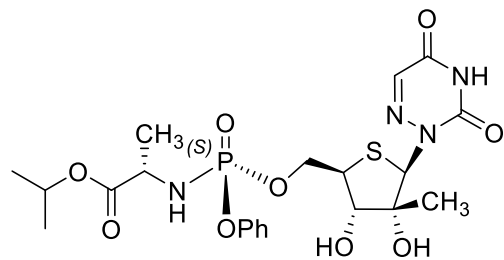
2.13c



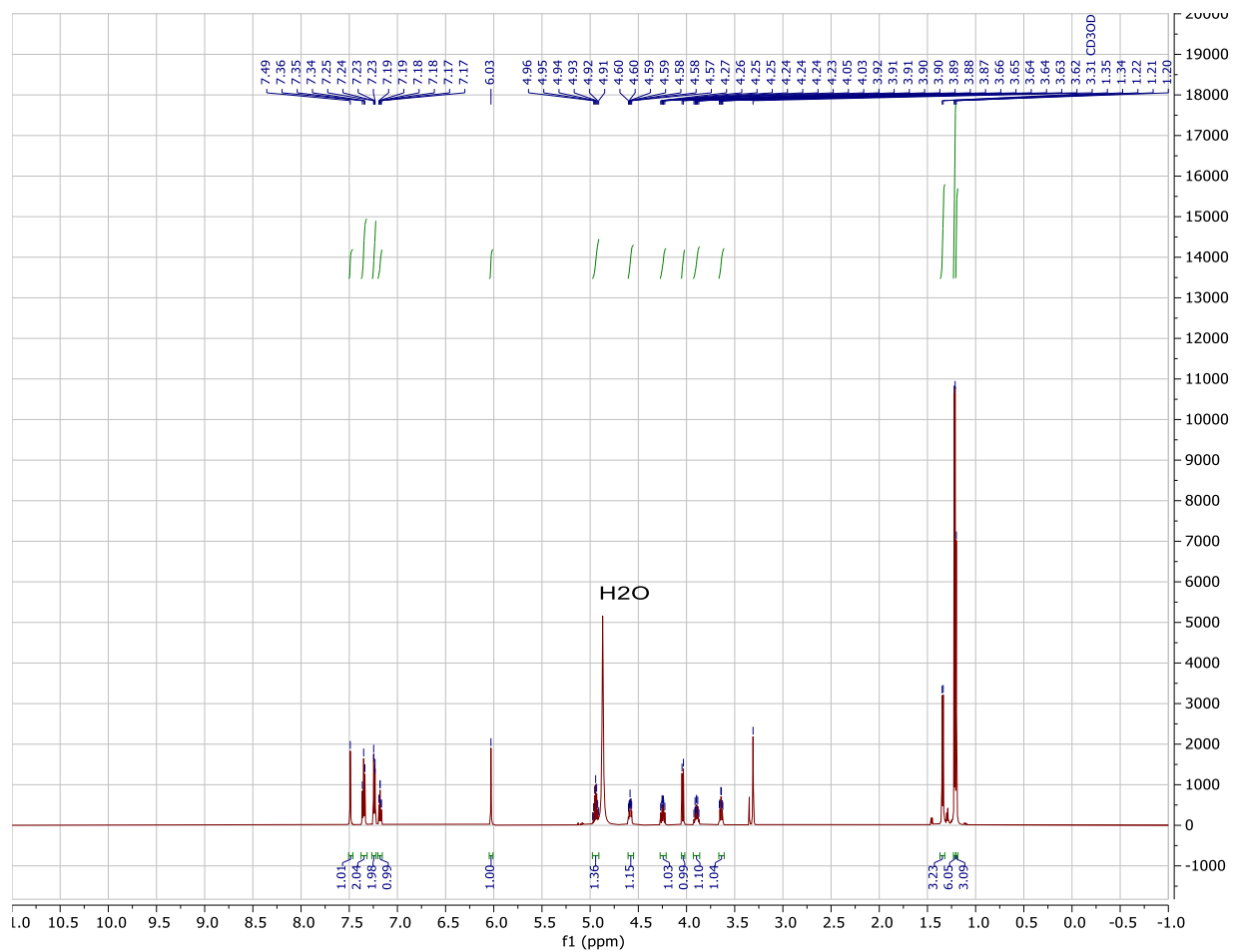


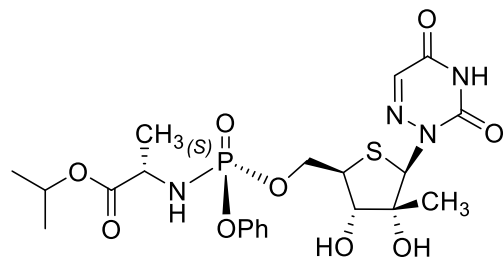
2.13c



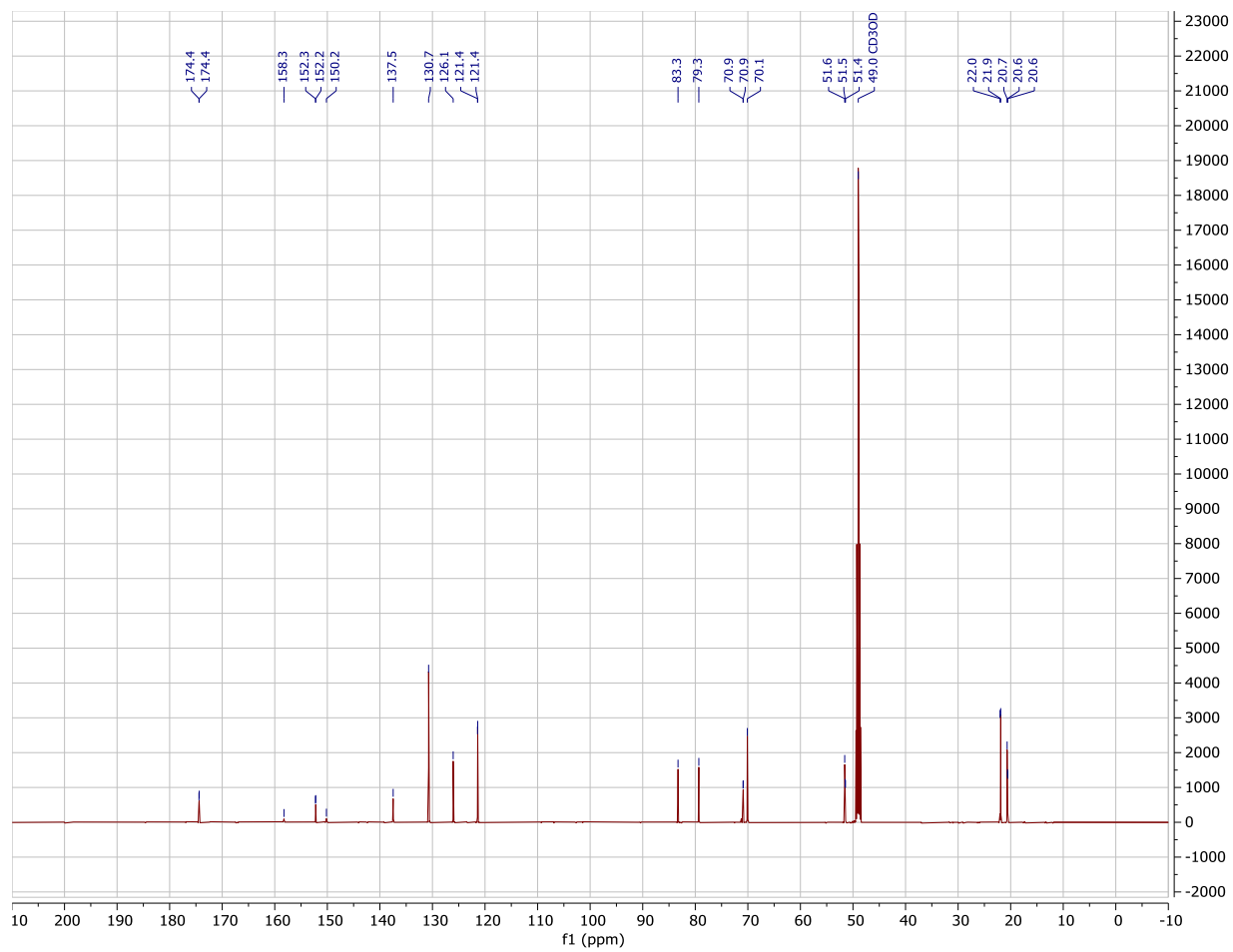


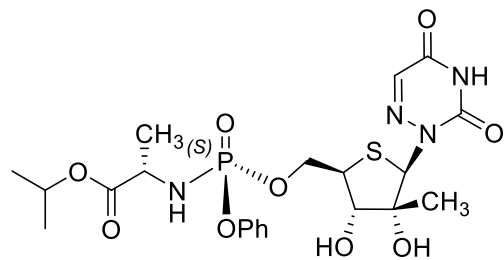
2.13d



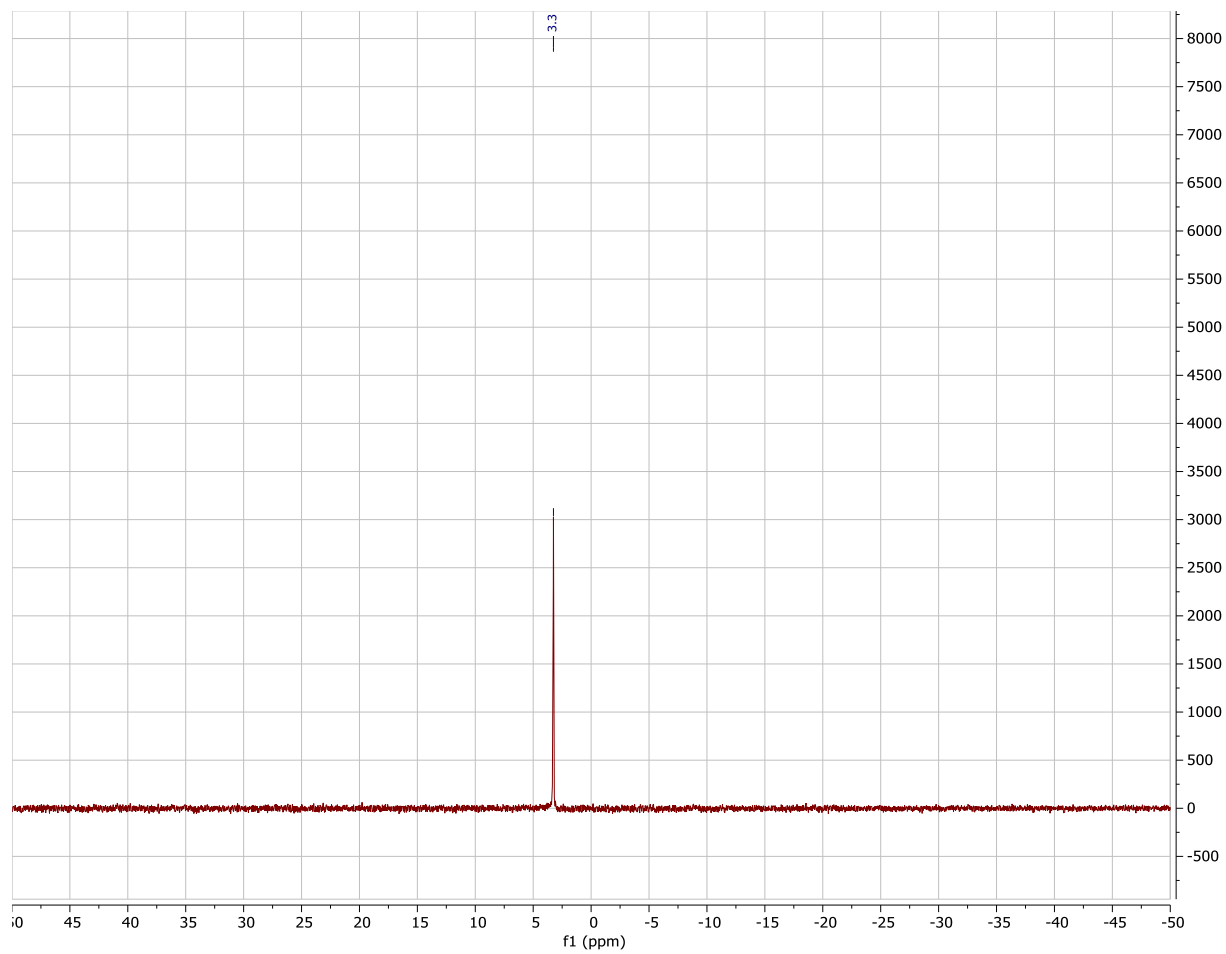


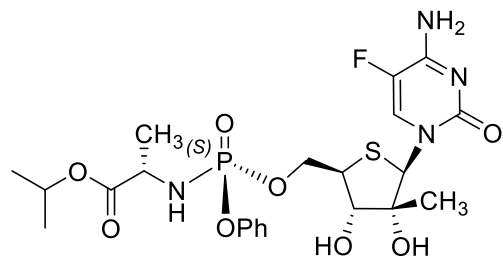
2.13d



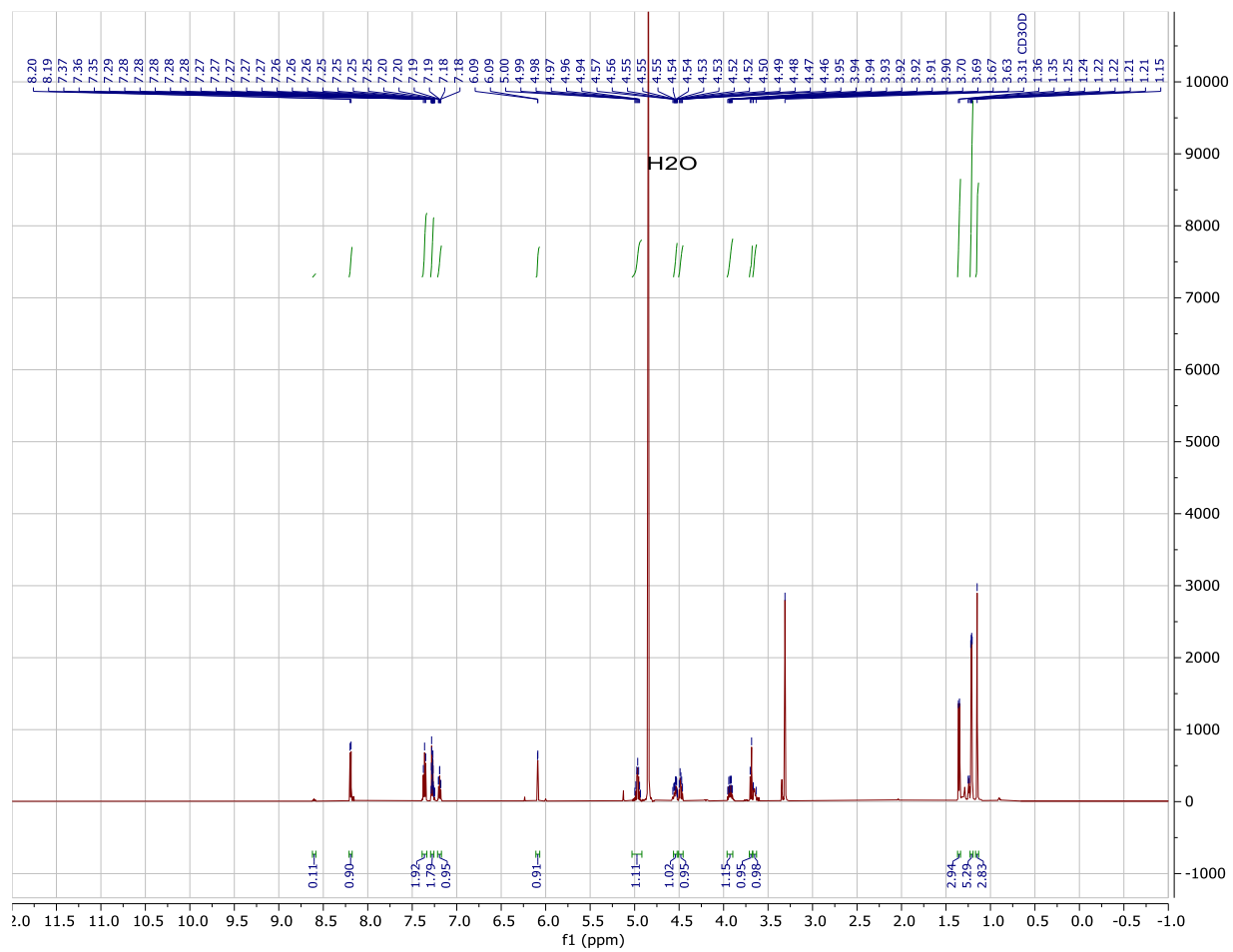


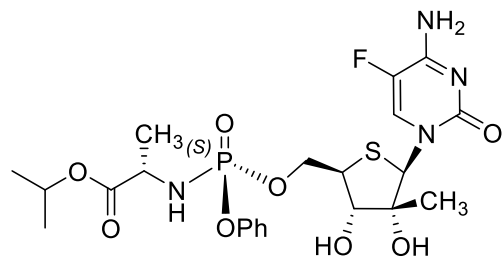
2.13d



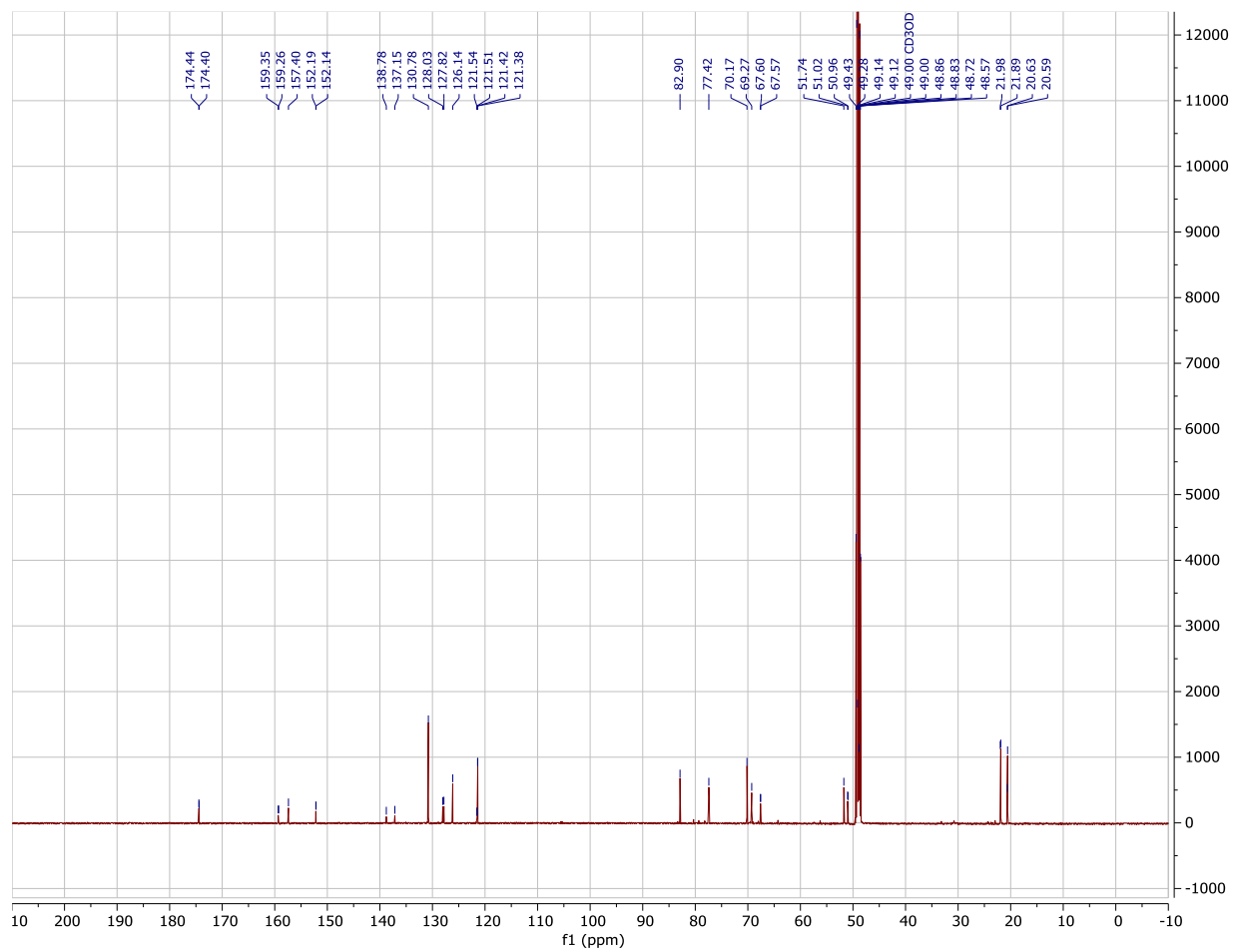


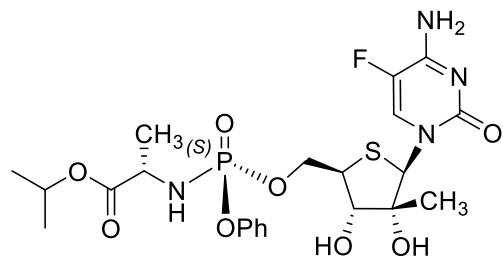
2.13e



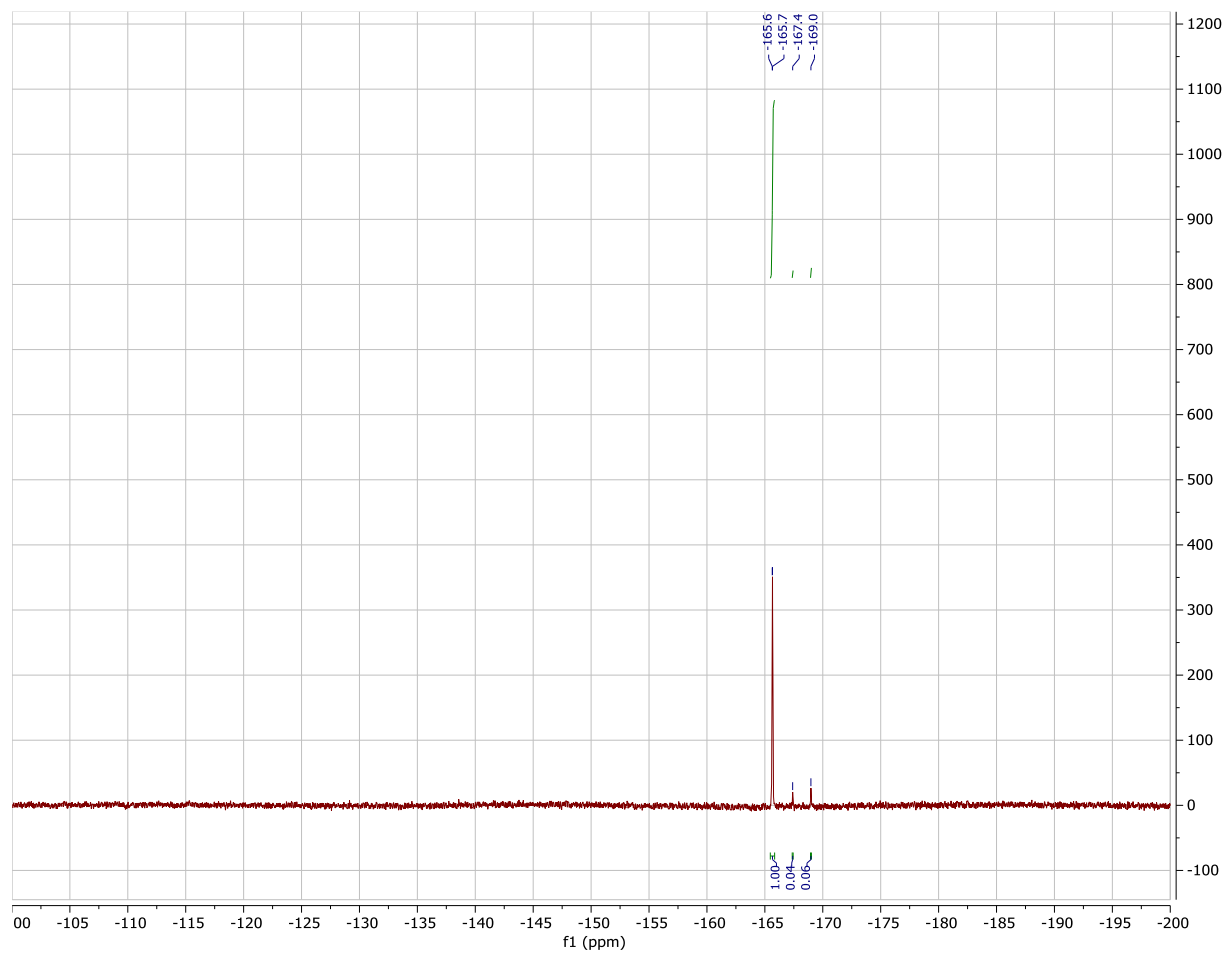


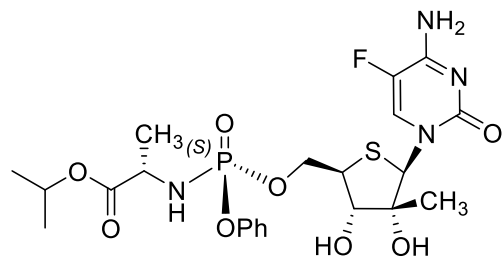
2.13e



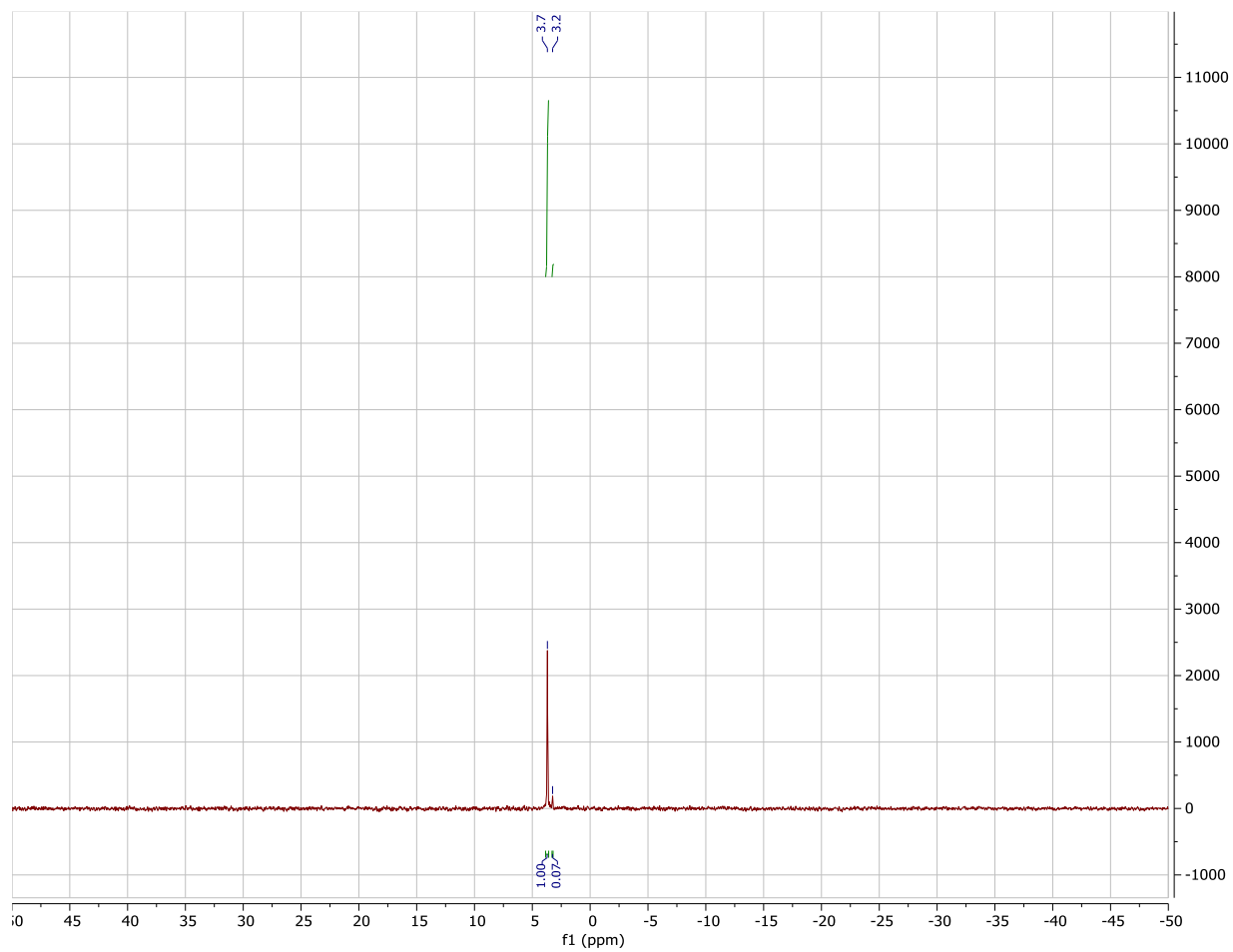


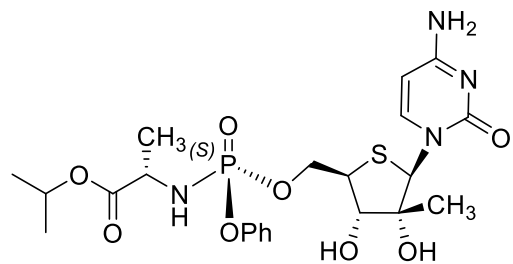
2.13e



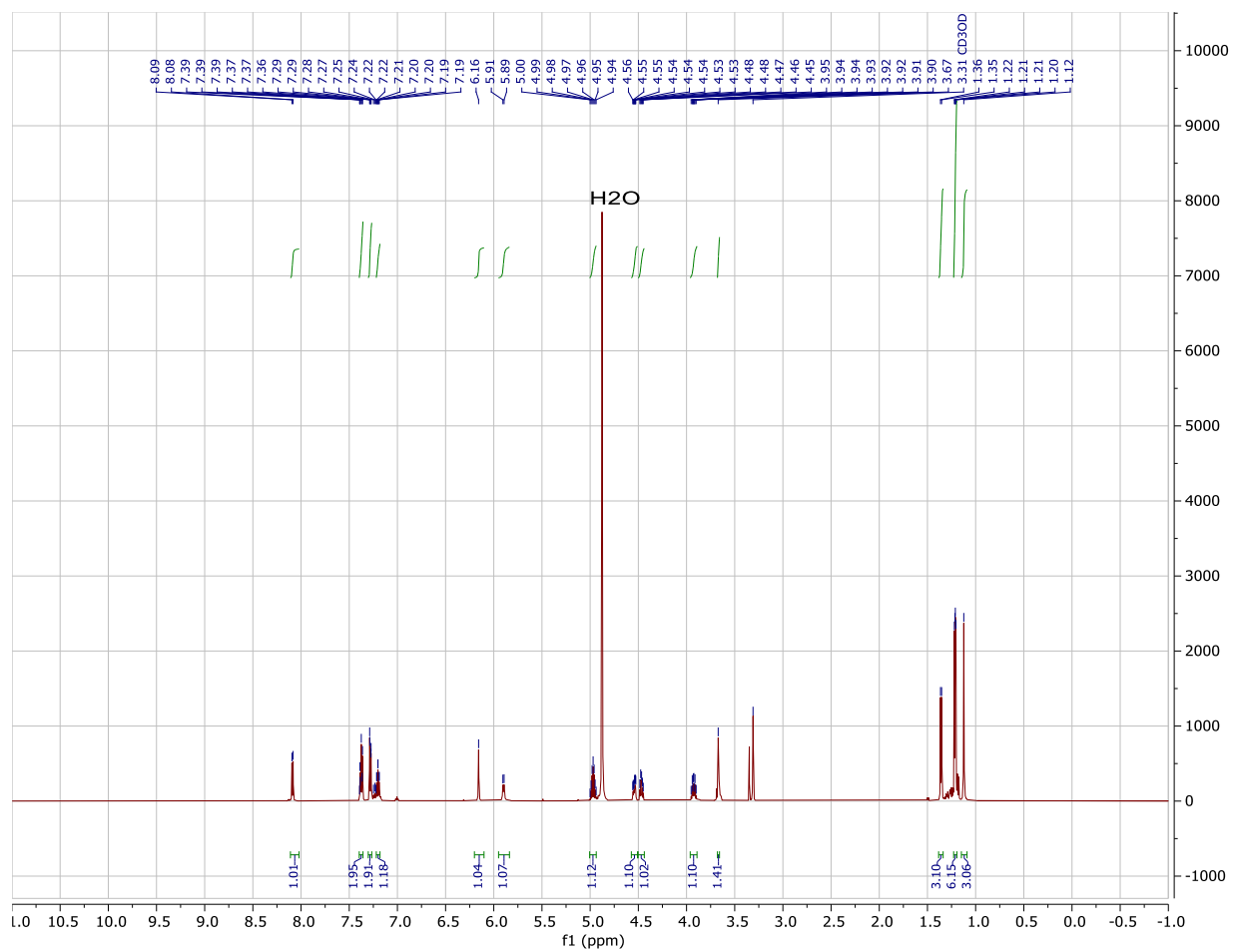


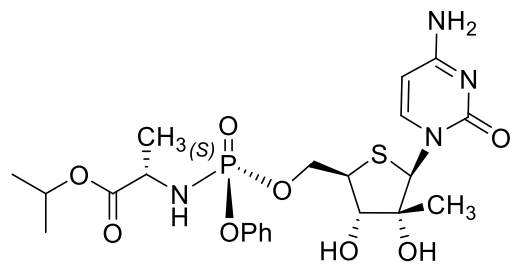
2.13e



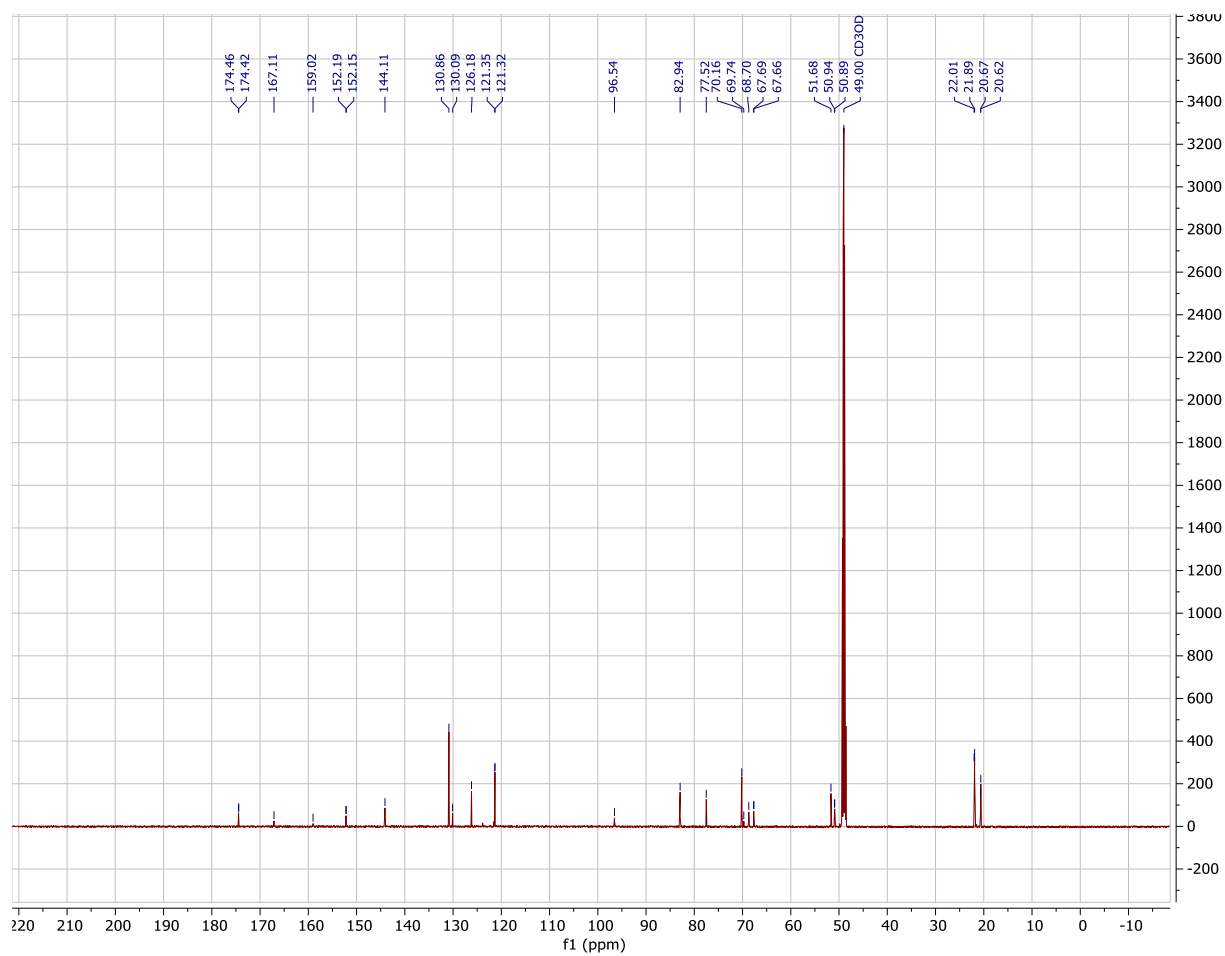


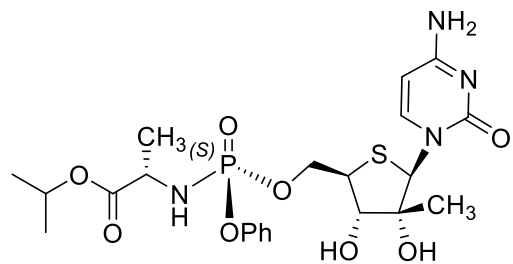
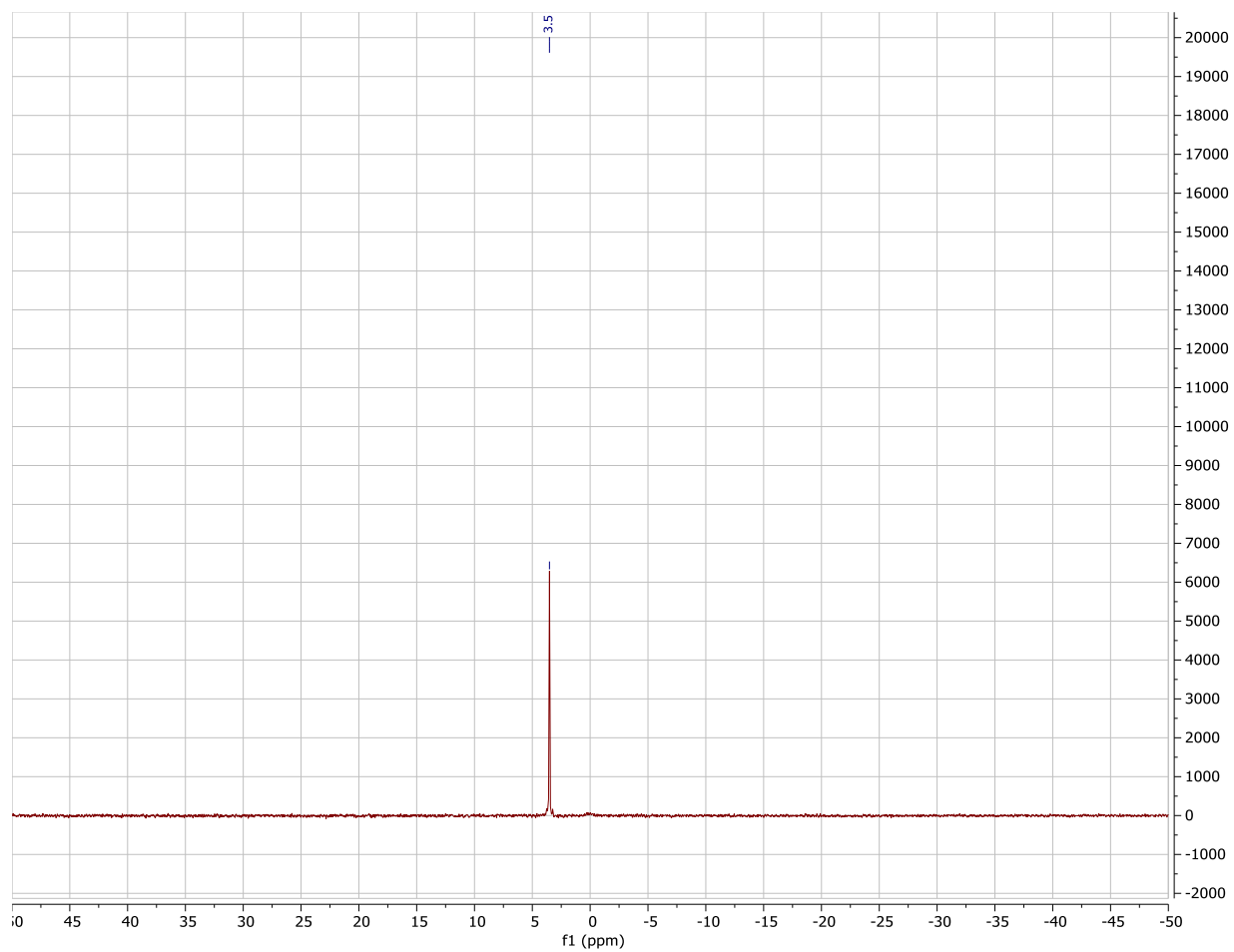
2.13f



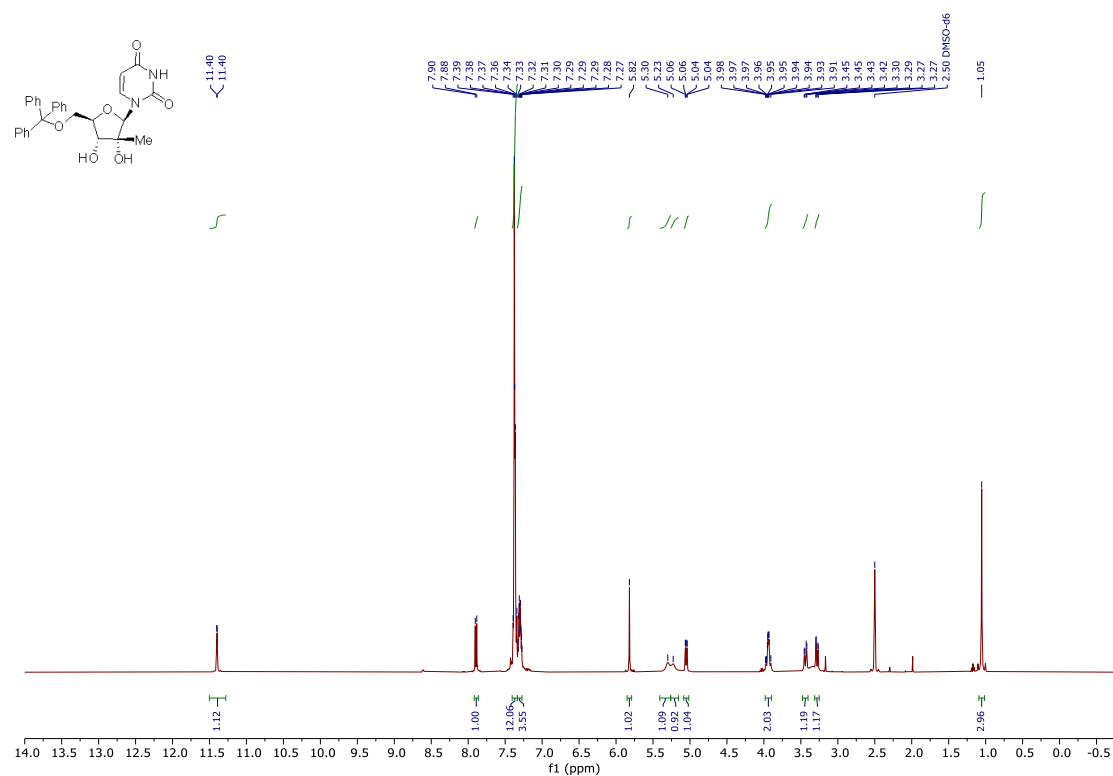
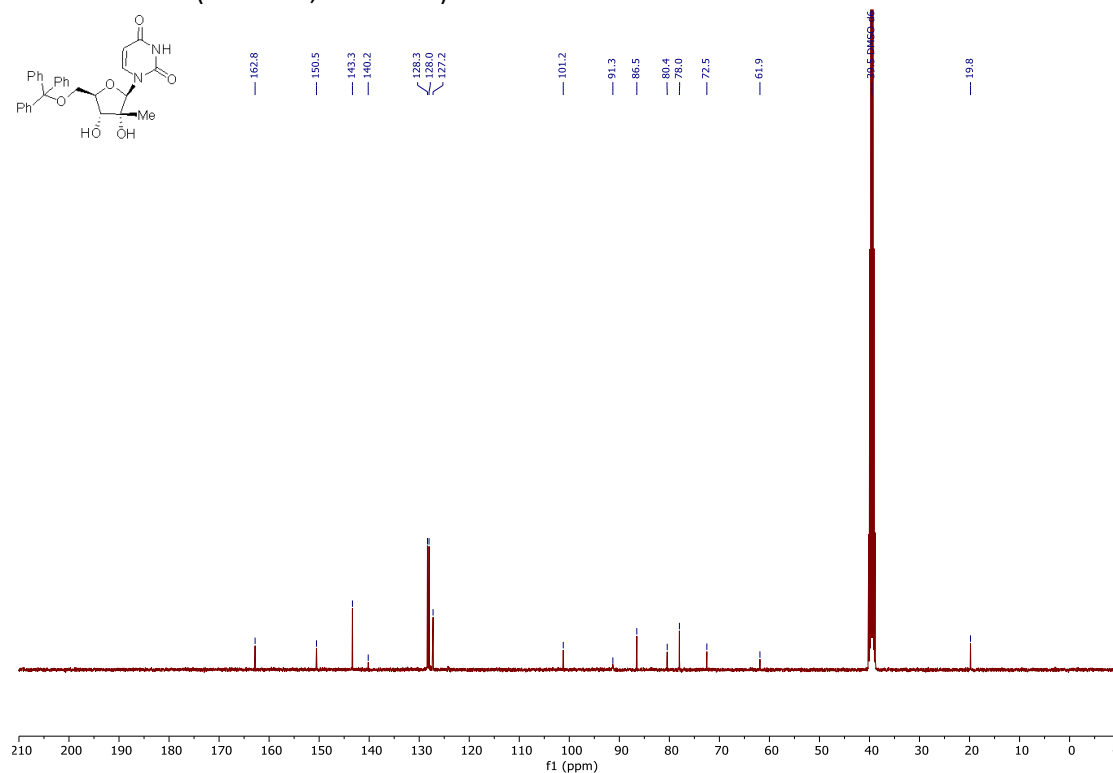


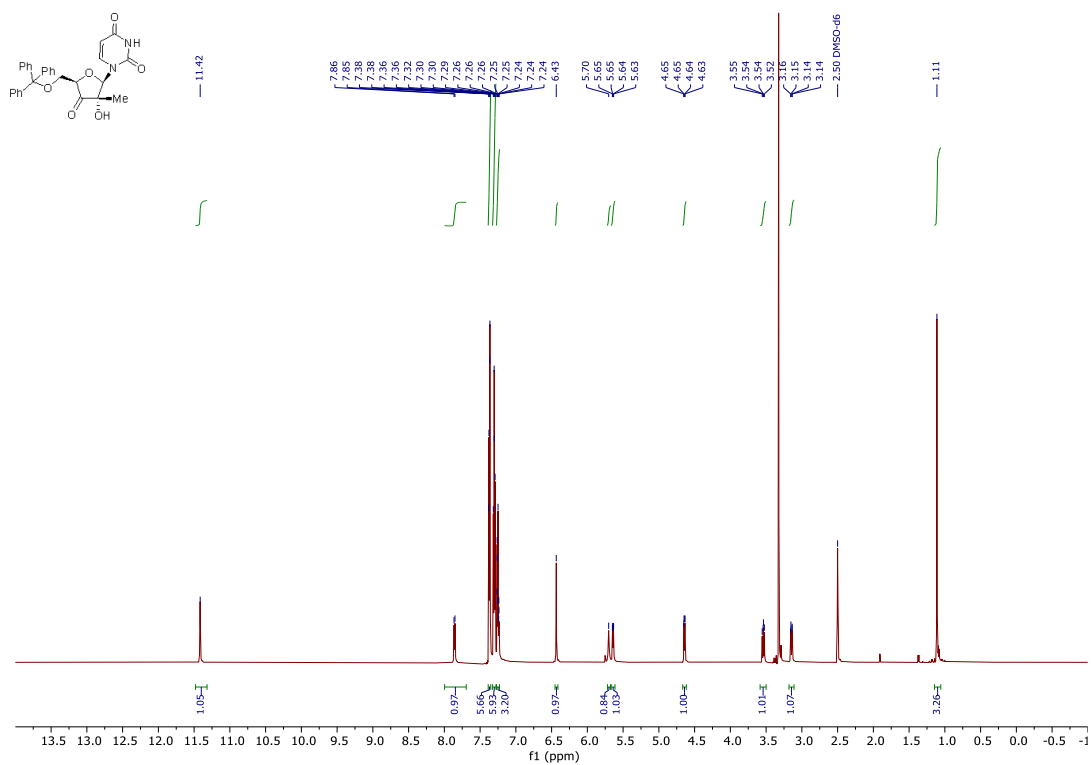
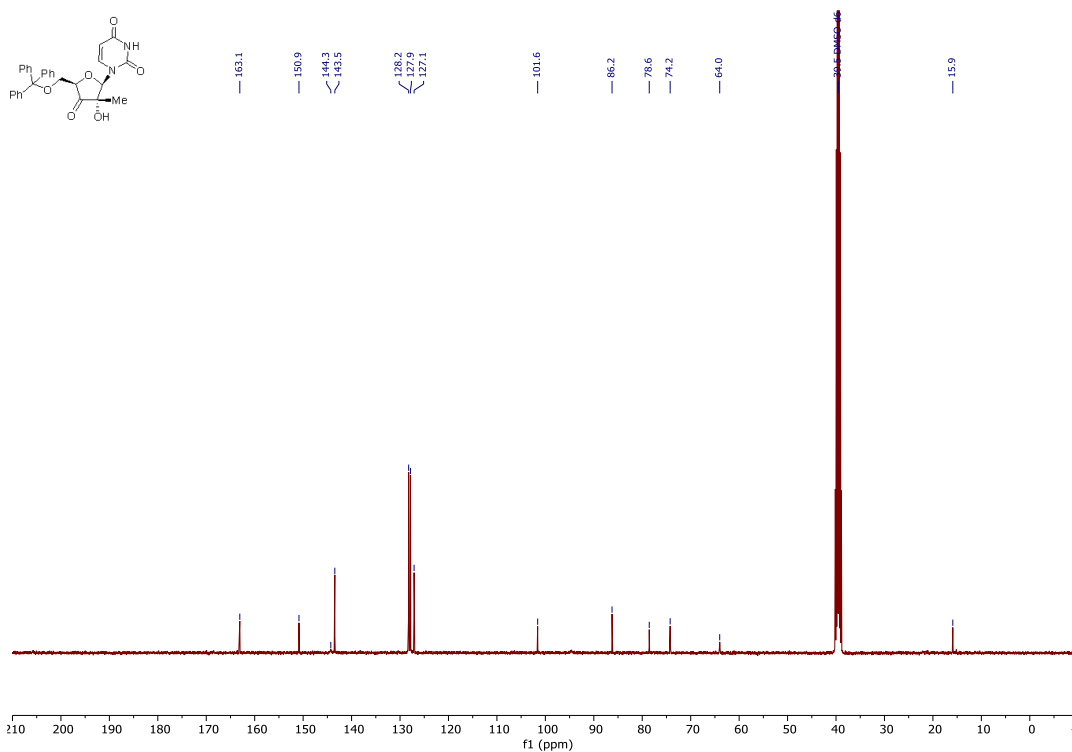
2.13f

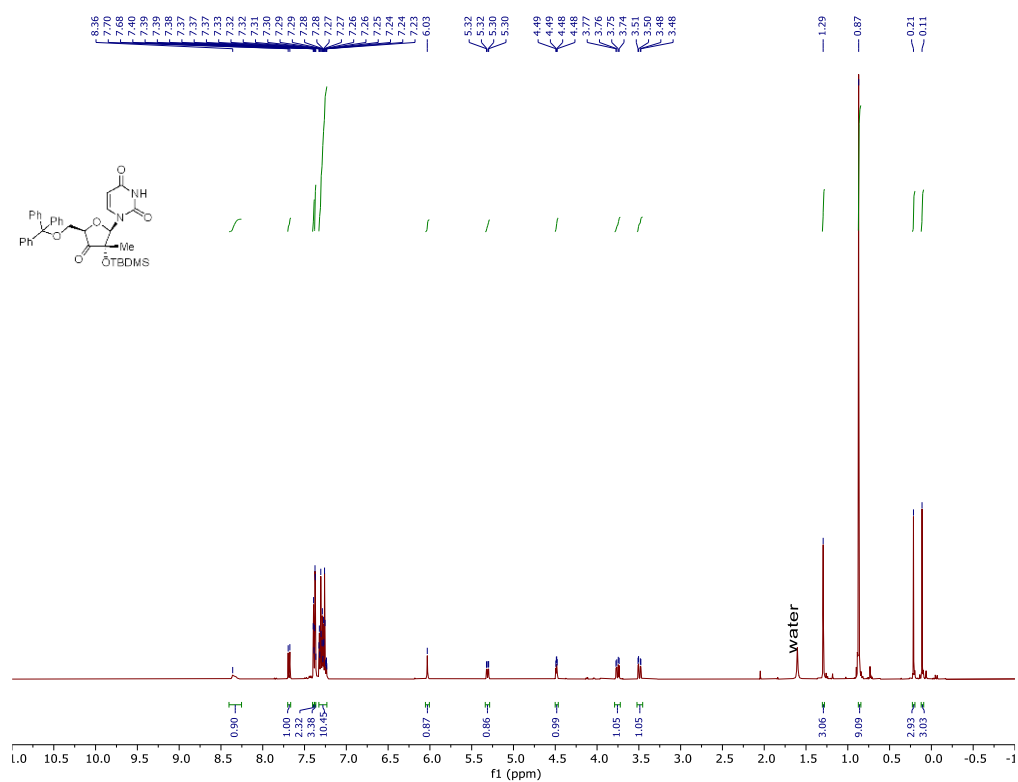
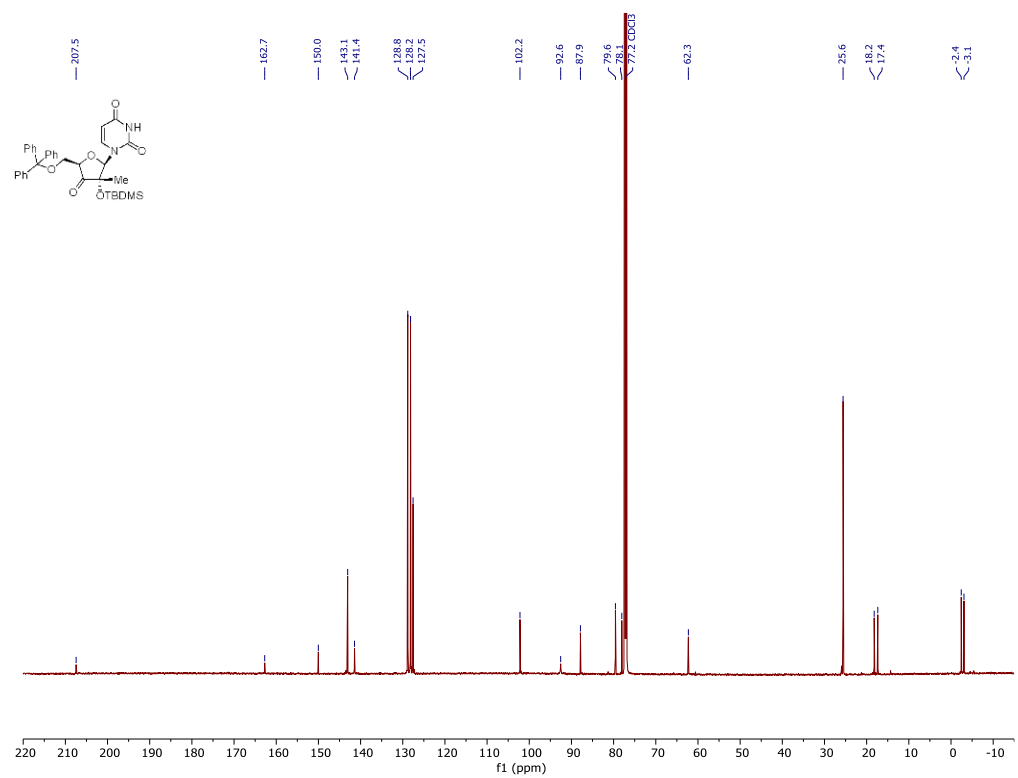


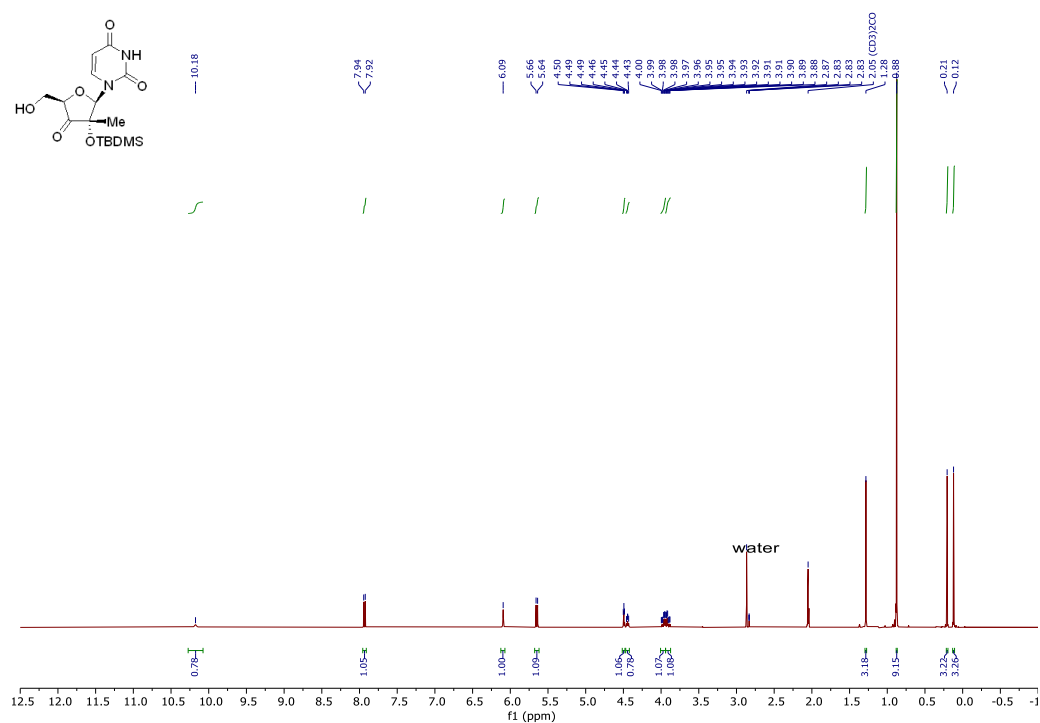
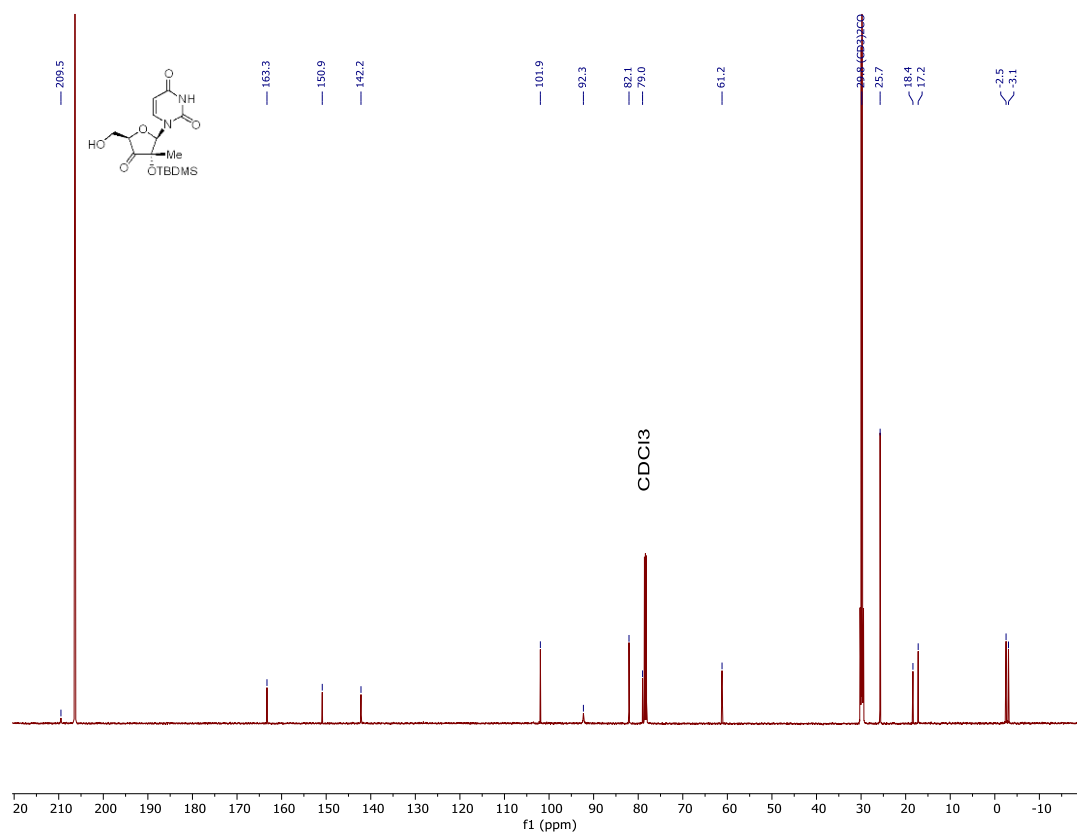
**2.13f**

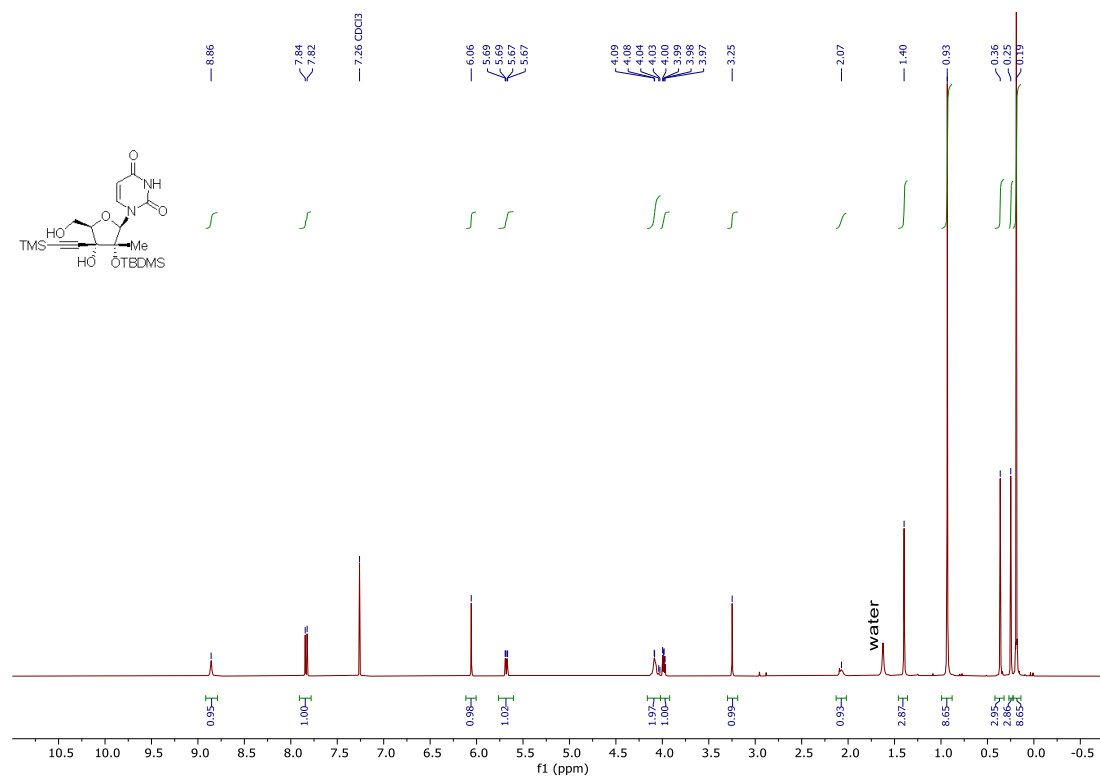
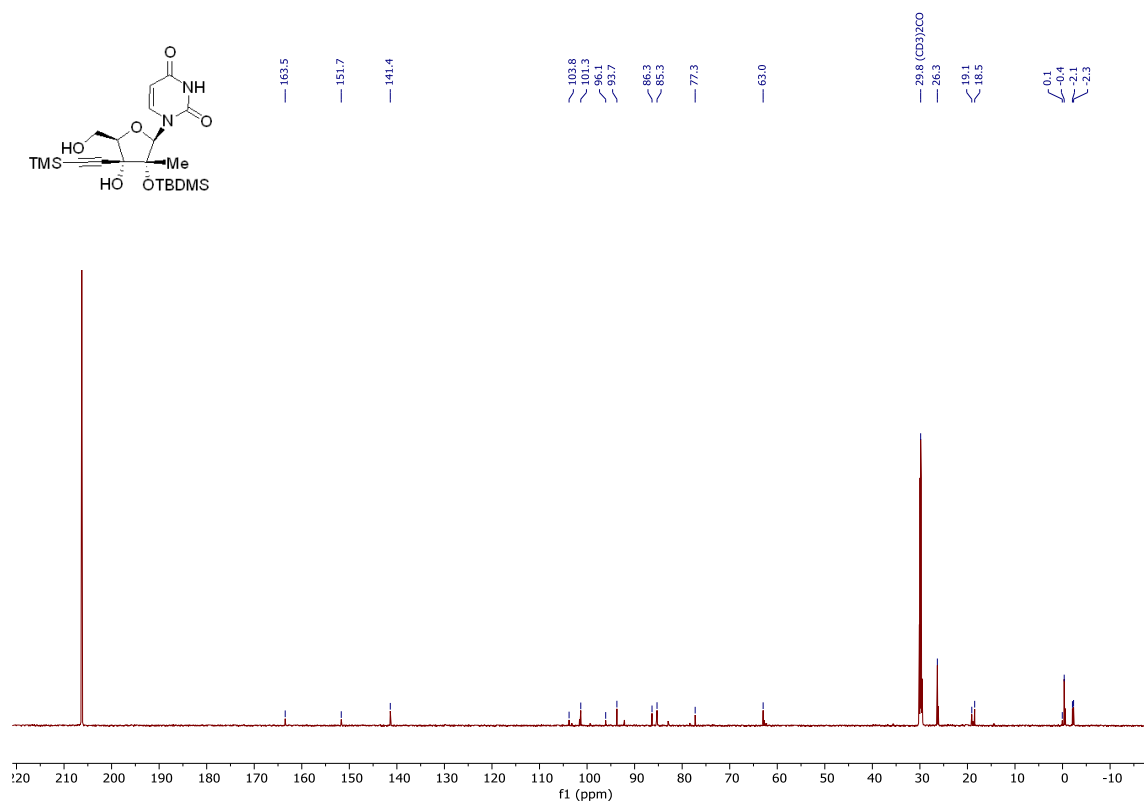
## SA.2 NMR Spectra of Compounds in Chapter 3 (3.3 – 3.11)

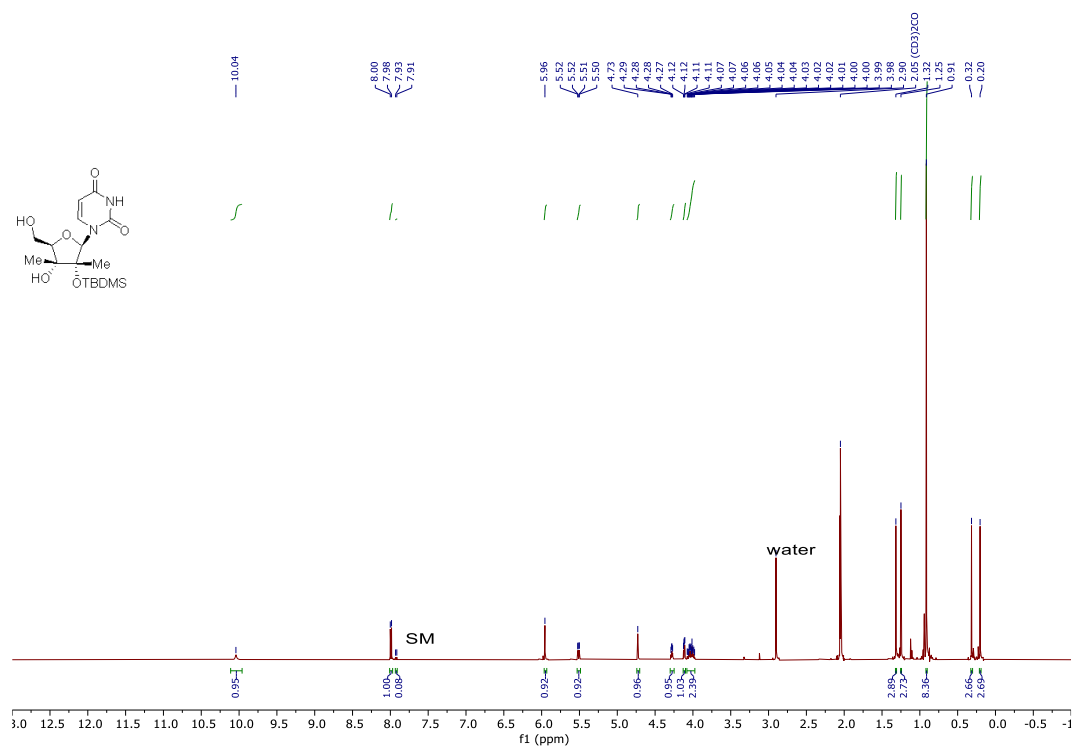
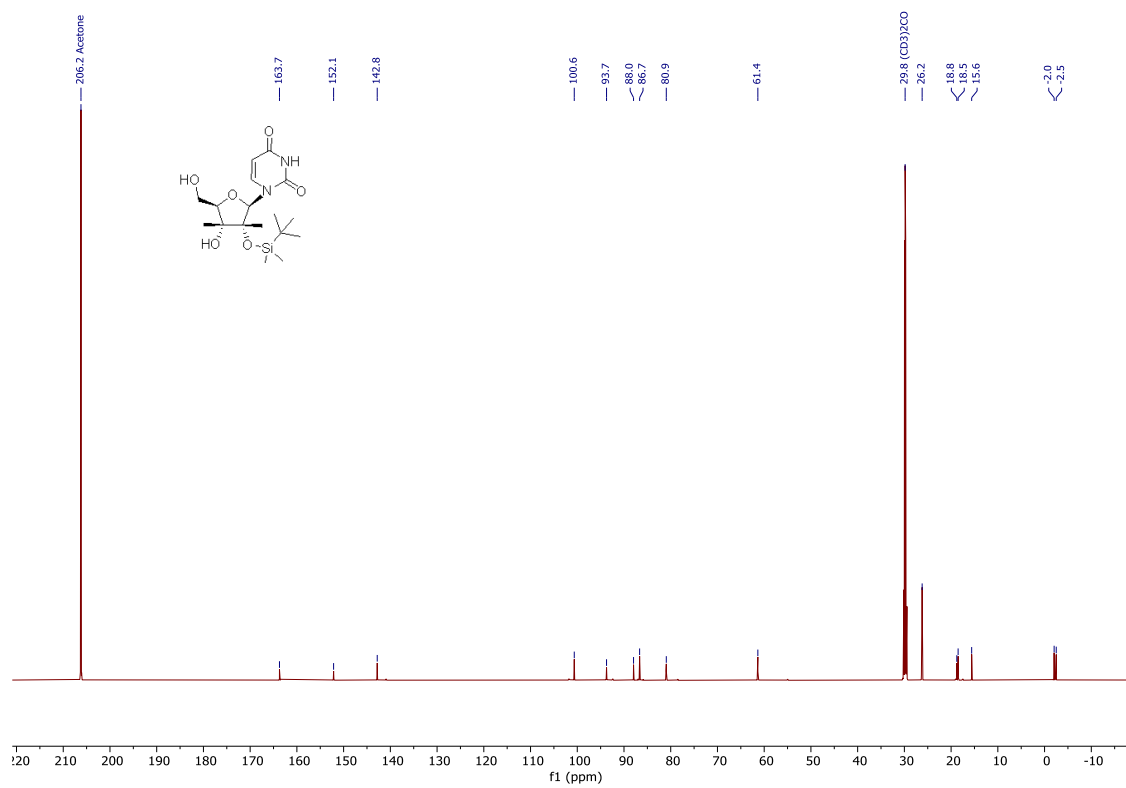
 $^1\text{H}$  NMR of **3.3** (400 MHz, d6-DMSO) $^{13}\text{C}$  NMR of **3.3** (101 MHz, d6-DMSO)

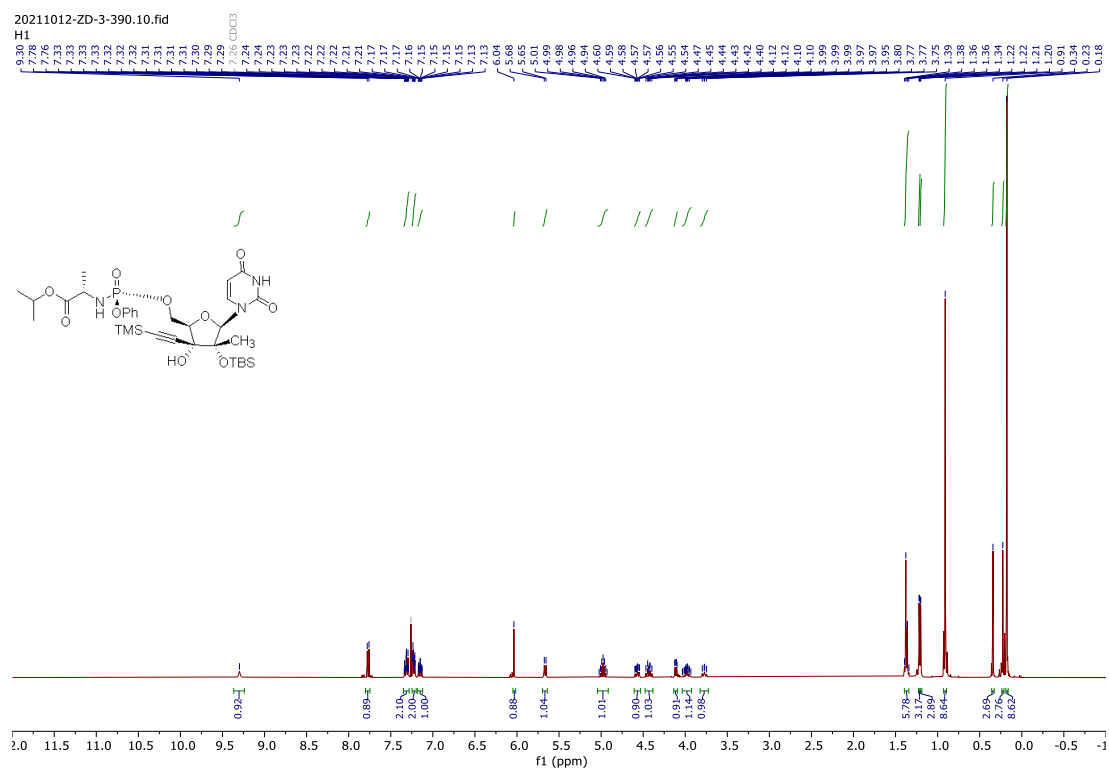
<sup>1</sup>H NMR of **3.4** (600 MHz, d<sub>6</sub>-DMSO)<sup>13</sup>C NMR of **3.4** (151 MHz, d<sub>6</sub>-DMSO)

$^1\text{H}$  NMR of **3.5** (400 MHz,  $\text{CDCl}_3$ ) $^{13}\text{C}$  NMR of **3.5** (151 MHz,  $\text{CDCl}_3$ )

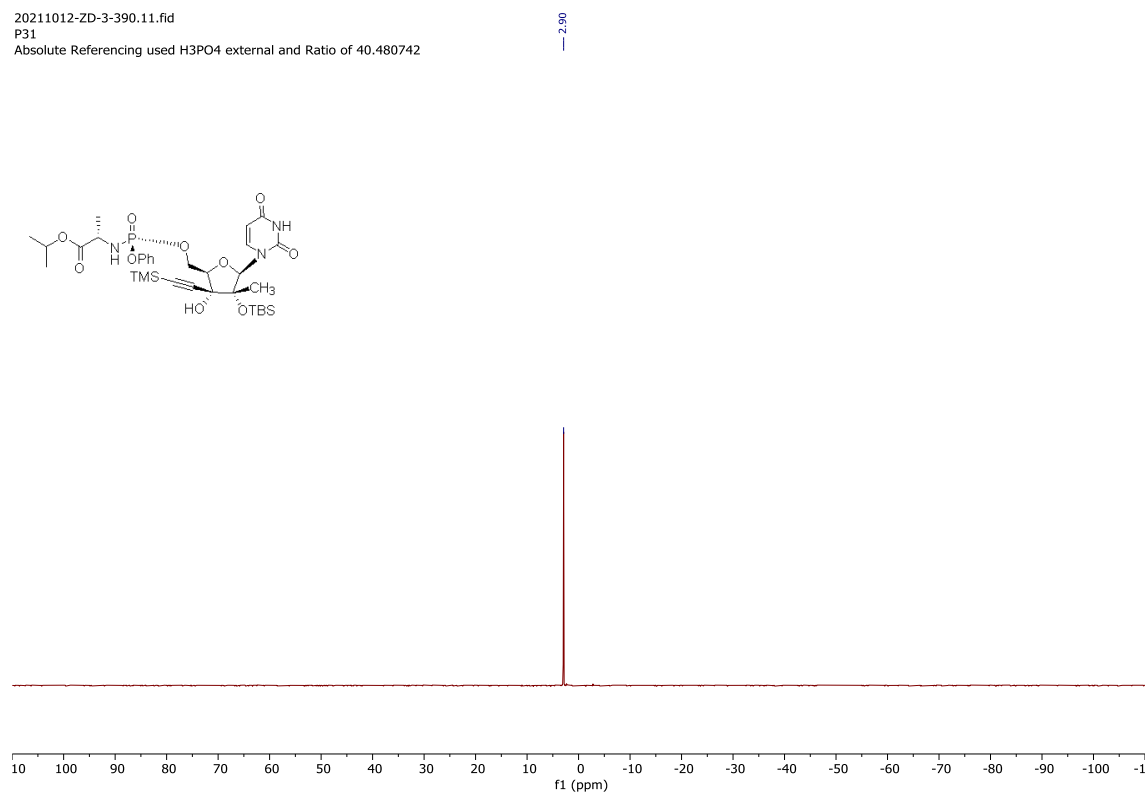
<sup>1</sup>H NMR of **3.6** (400 MHz, d<sub>6</sub>-acetone)<sup>13</sup>C NMR of **3.6** (151 MHz, d<sub>6</sub>-acetone)

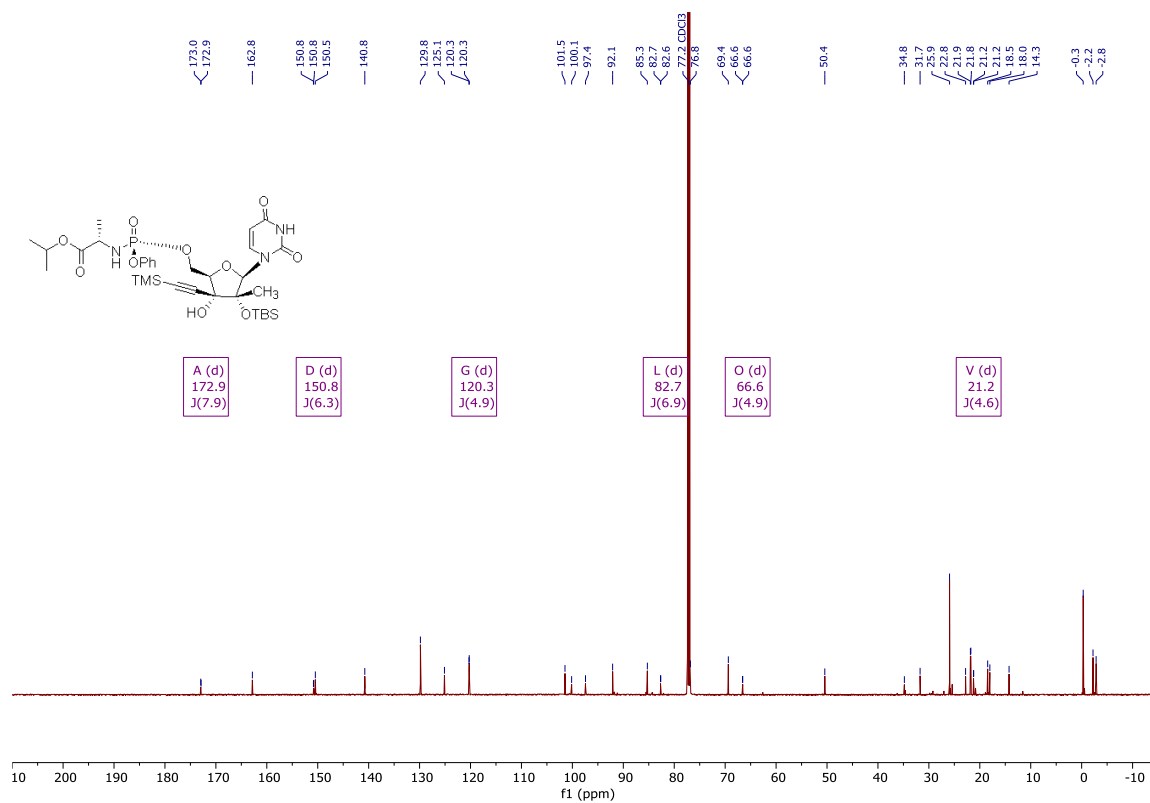
$^1\text{H}$  NMR of **3.7a** (400 MHz,  $\text{CDCl}_3$ ) $^{13}\text{C}$  NMR of **3.7a** (151 MHz,  $\text{d}_6$ -acetone)

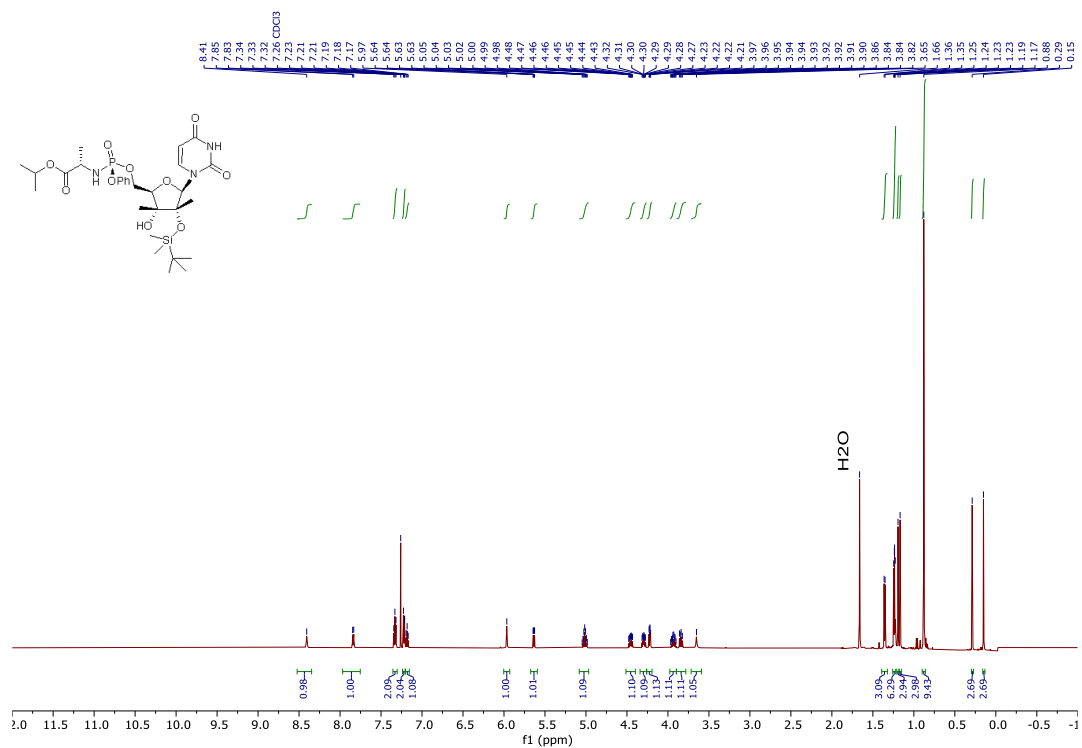
$^1\text{H}$  NMR of **3.7b**, containing 7.0% SM (500 MHz,  $\text{d}_6$ -acetone) $^{13}\text{C}$  NMR of **3.7b** (151 MHz,  $\text{d}_6$ -acetone)

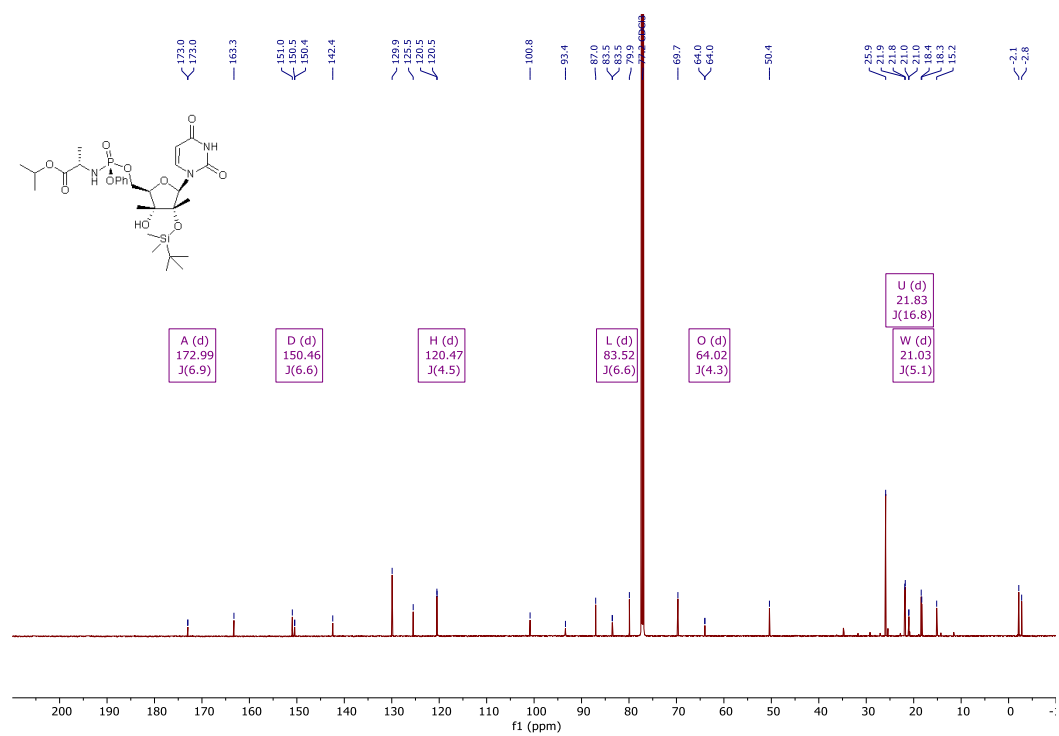
<sup>1</sup>H NMR of **3.8a** (400 MHz, CDCl<sub>3</sub>)<sup>31</sup>P NMR of **3.8a** (162 MHz, CDCl<sub>3</sub>)

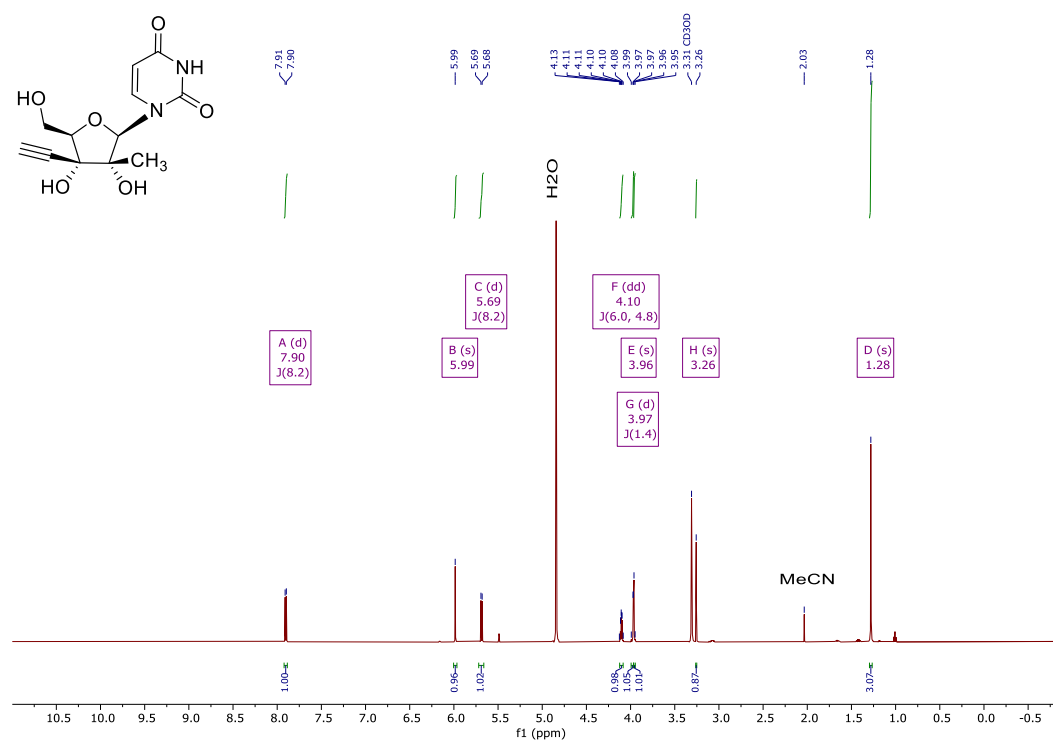
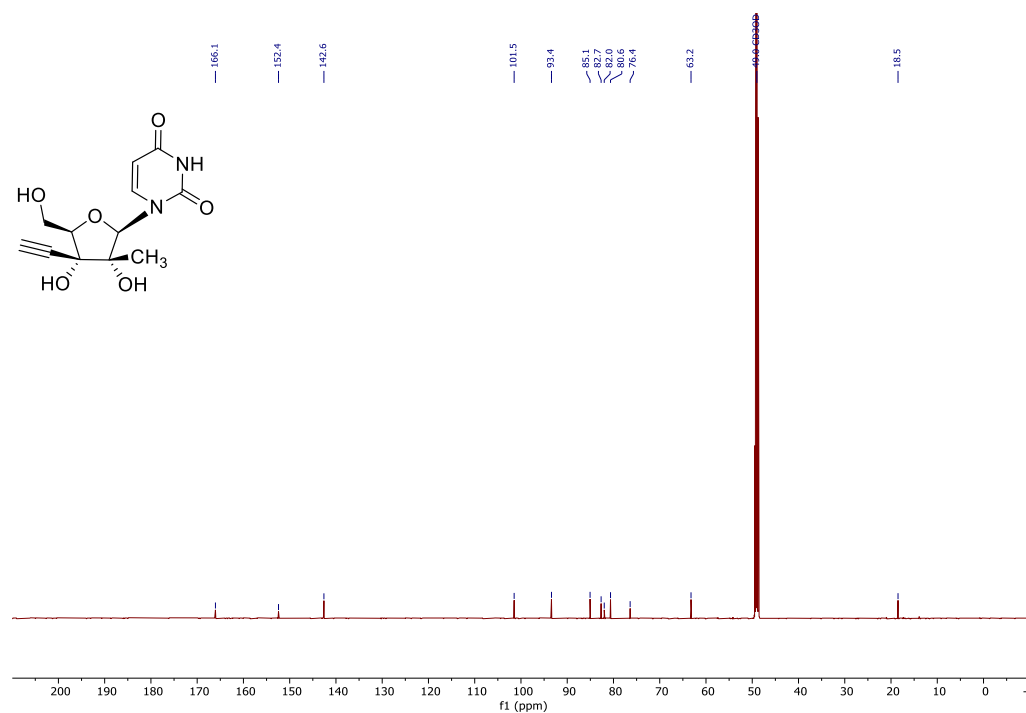
20211012-ZD-3-390.11.fid  
P31  
Absolute Referencing used H<sub>3</sub>PO<sub>4</sub> external and Ratio of 40.480742

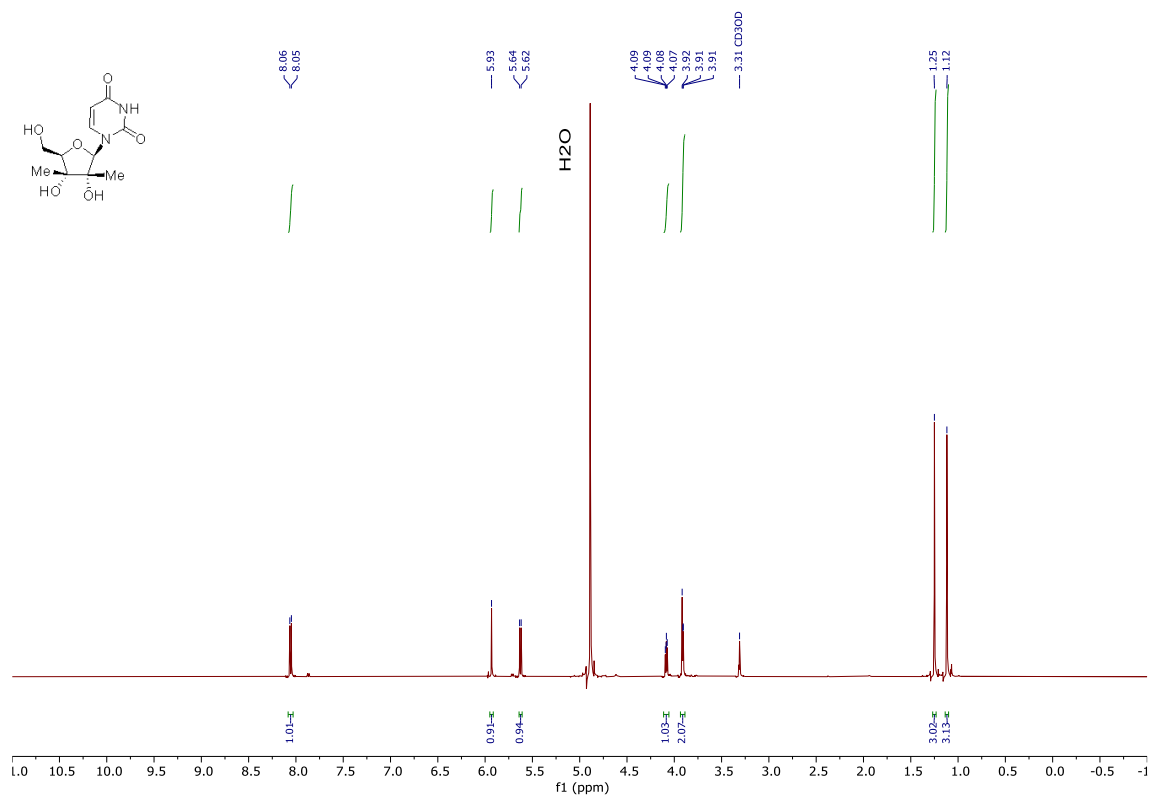
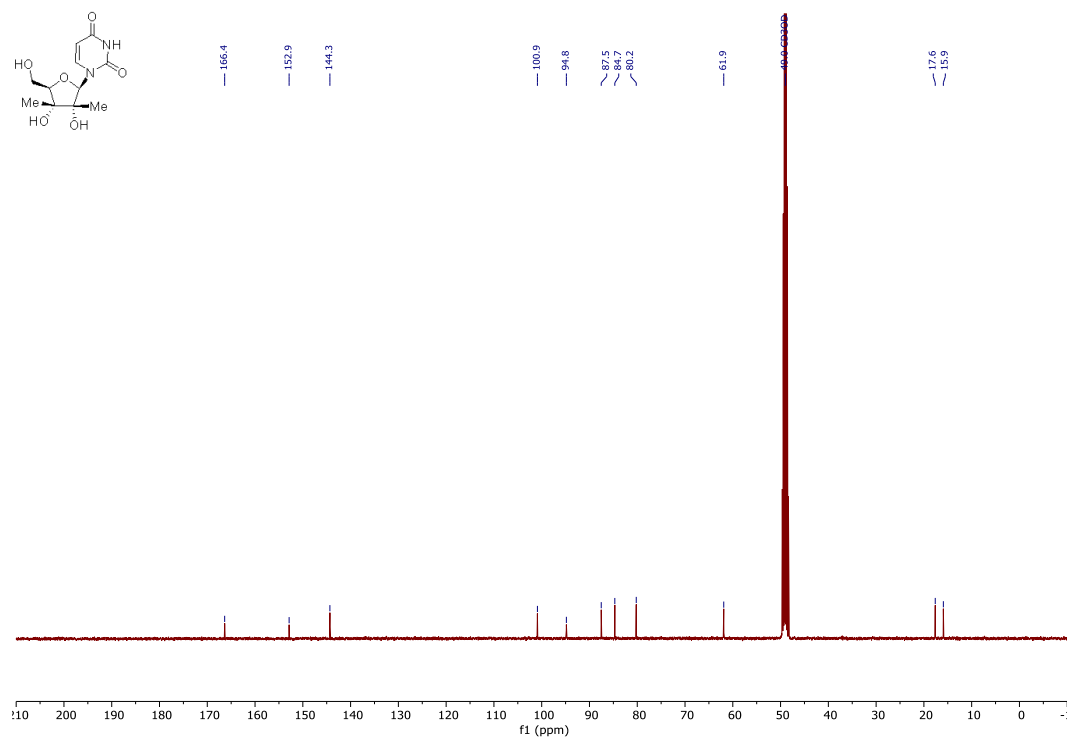


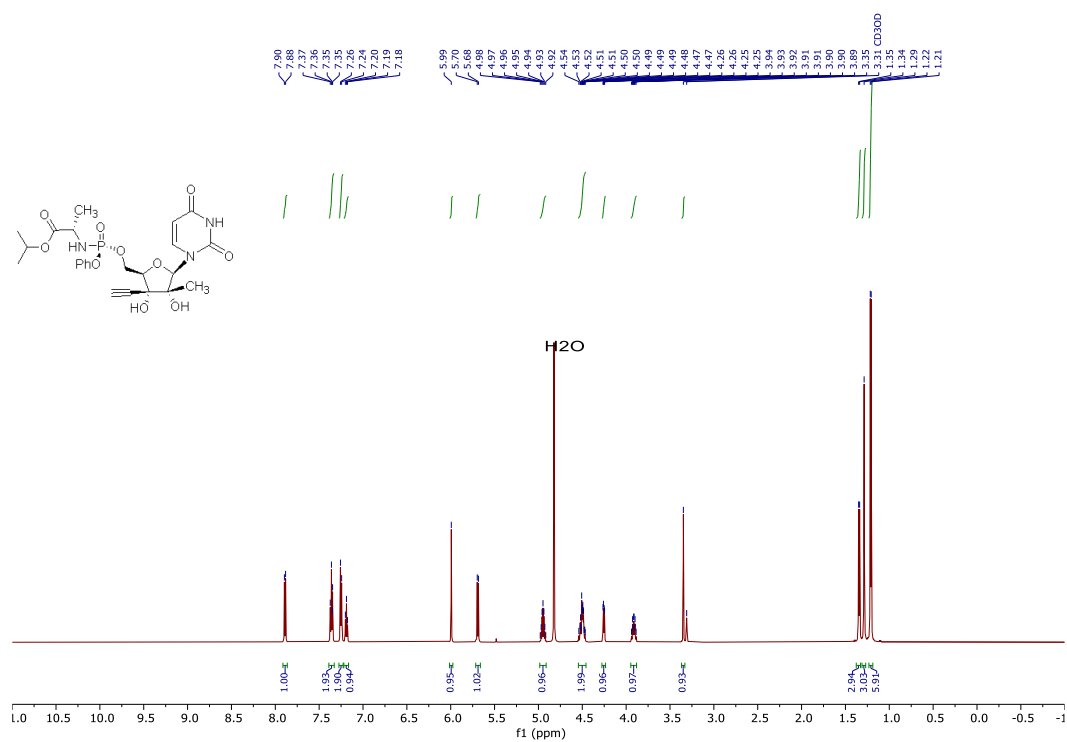
$^{13}\text{C}$  NMR of **3.8a** (151 MHz,  $\text{CDCl}_3$ )

<sup>1</sup>H NMR of **3.8b** (600 MHz, CDCl<sub>3</sub>)

$^{13}\text{C}$  NMR of **3.8b** (151 MHz,  $\text{CDCl}_3$ )

<sup>1</sup>H NMR of **3.9a** (600 MHz, CD<sub>3</sub>OD)<sup>13</sup>C NMR of **3.9a** (151 MHz, CD<sub>3</sub>OD)

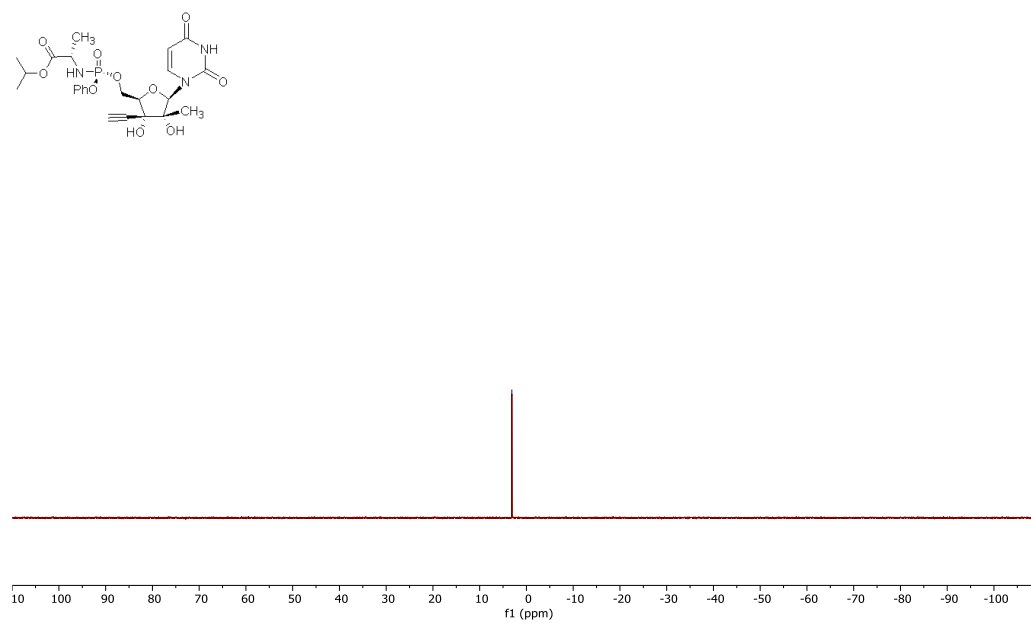
<sup>1</sup>H NMR of **3.9b** (500 MHz, CD<sub>3</sub>OD)<sup>13</sup>C NMR of **3.9b** (101 MHz, CD<sub>3</sub>OD)

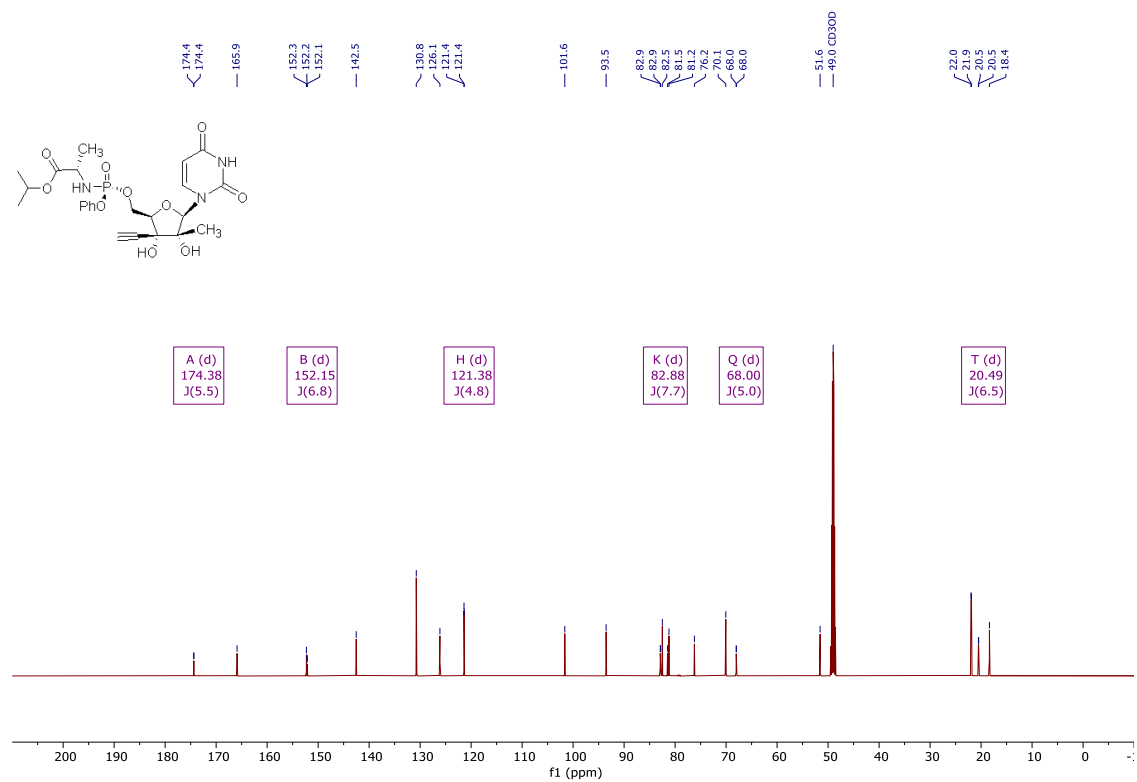
<sup>1</sup>H NMR of **3.11a** (600 MHz, CD<sub>3</sub>OD)<sup>31</sup>P NMR of **3.11a** (162 MHz, CD<sub>3</sub>OD)

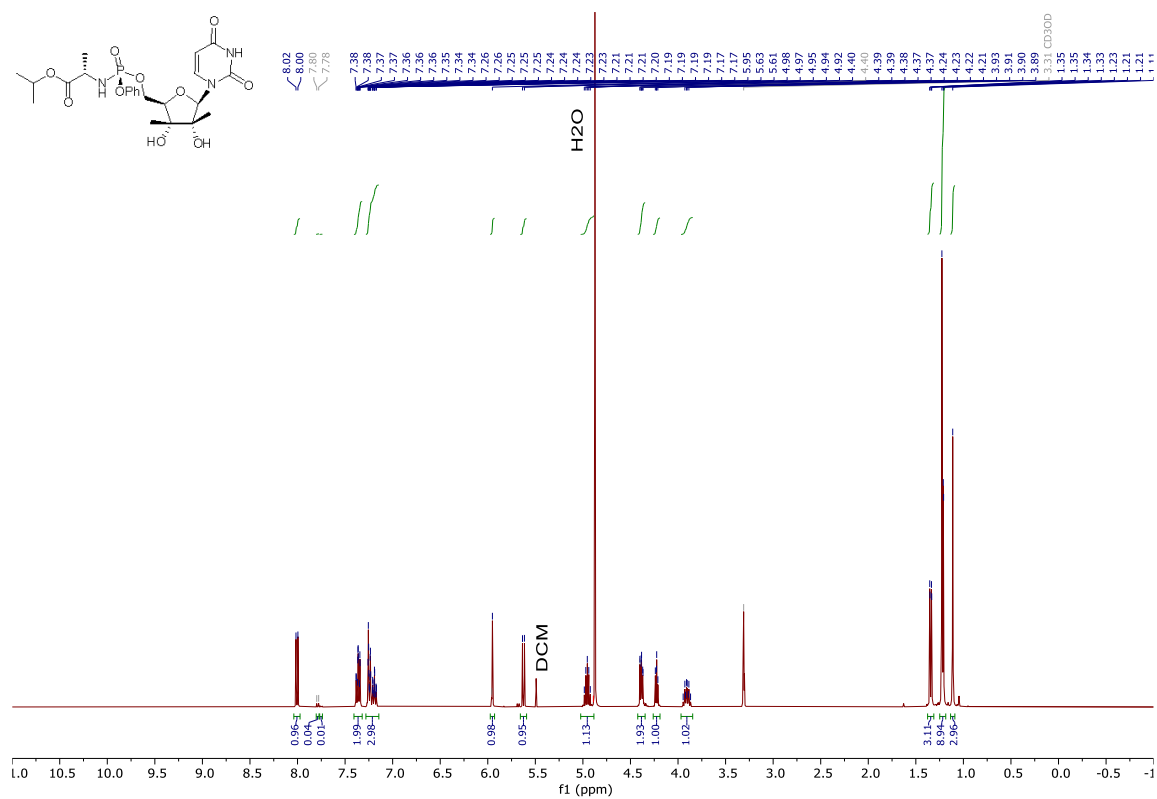
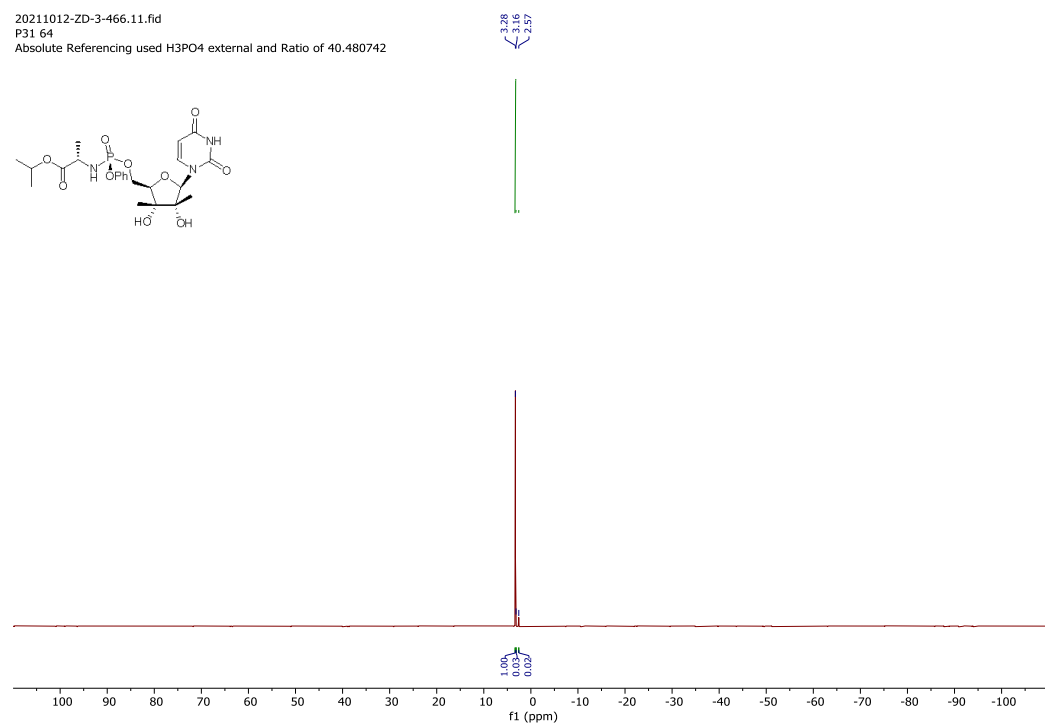
20210112-ZD-3-391.11.fid

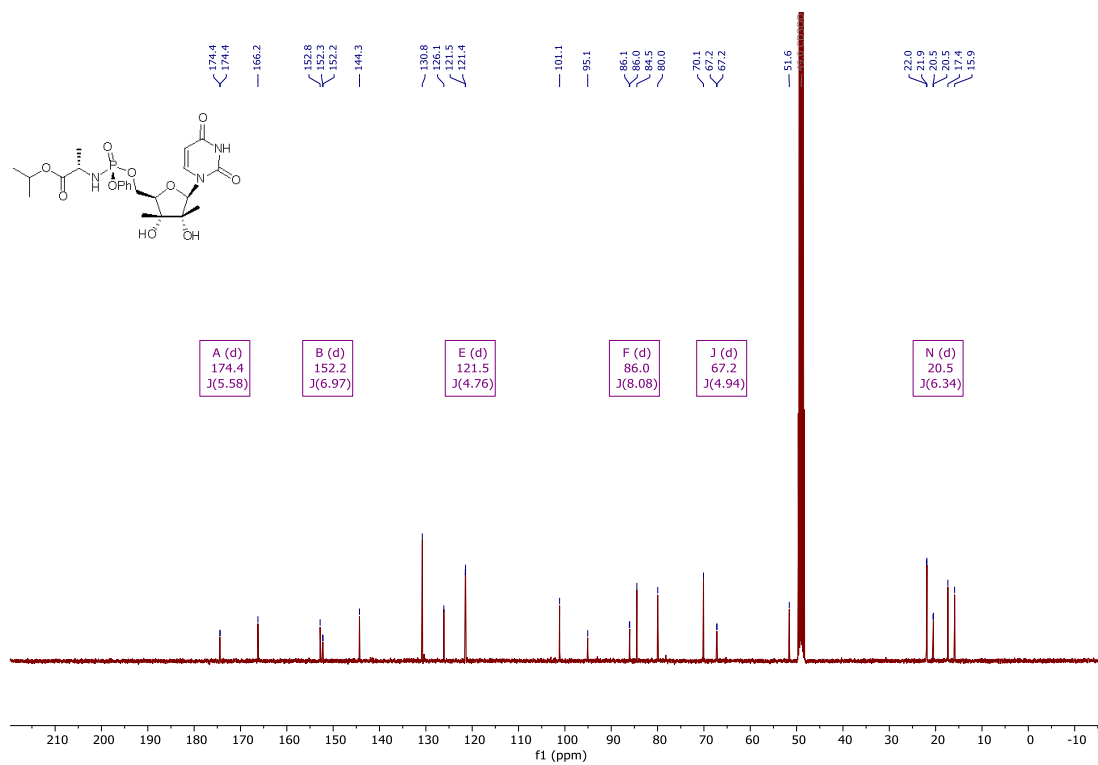
P31

Absolute Referencing used H3PO4 external and Ratio of 40.480742



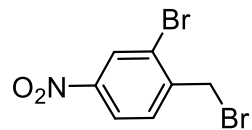
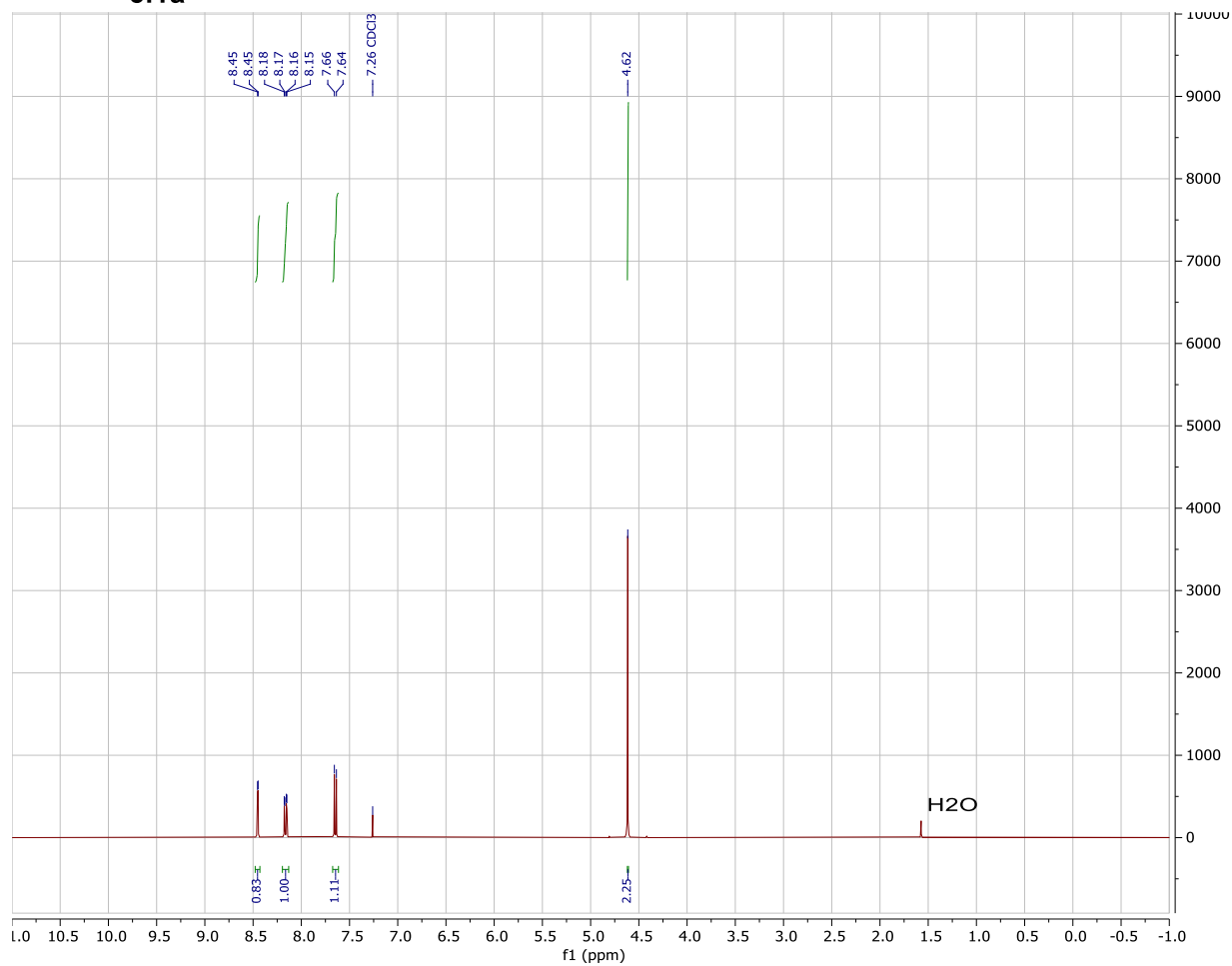
$^{13}\text{C}$  NMR of **3.11a** (151 MHz,  $\text{CD}_3\text{OD}$ )

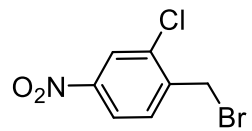
<sup>1</sup>H NMR of **3.11b** (400 MHz, CD<sub>3</sub>OD) with ca. 4.95% inseparable impurities<sup>31</sup>P NMR of **3.11b** (162 MHz, CD<sub>3</sub>OD) with ca. 4.8% inseparable impurities

$^{13}\text{C}$  NMR of **3.11b** (101 MHz,  $\text{CD}_3\text{OD}$ )

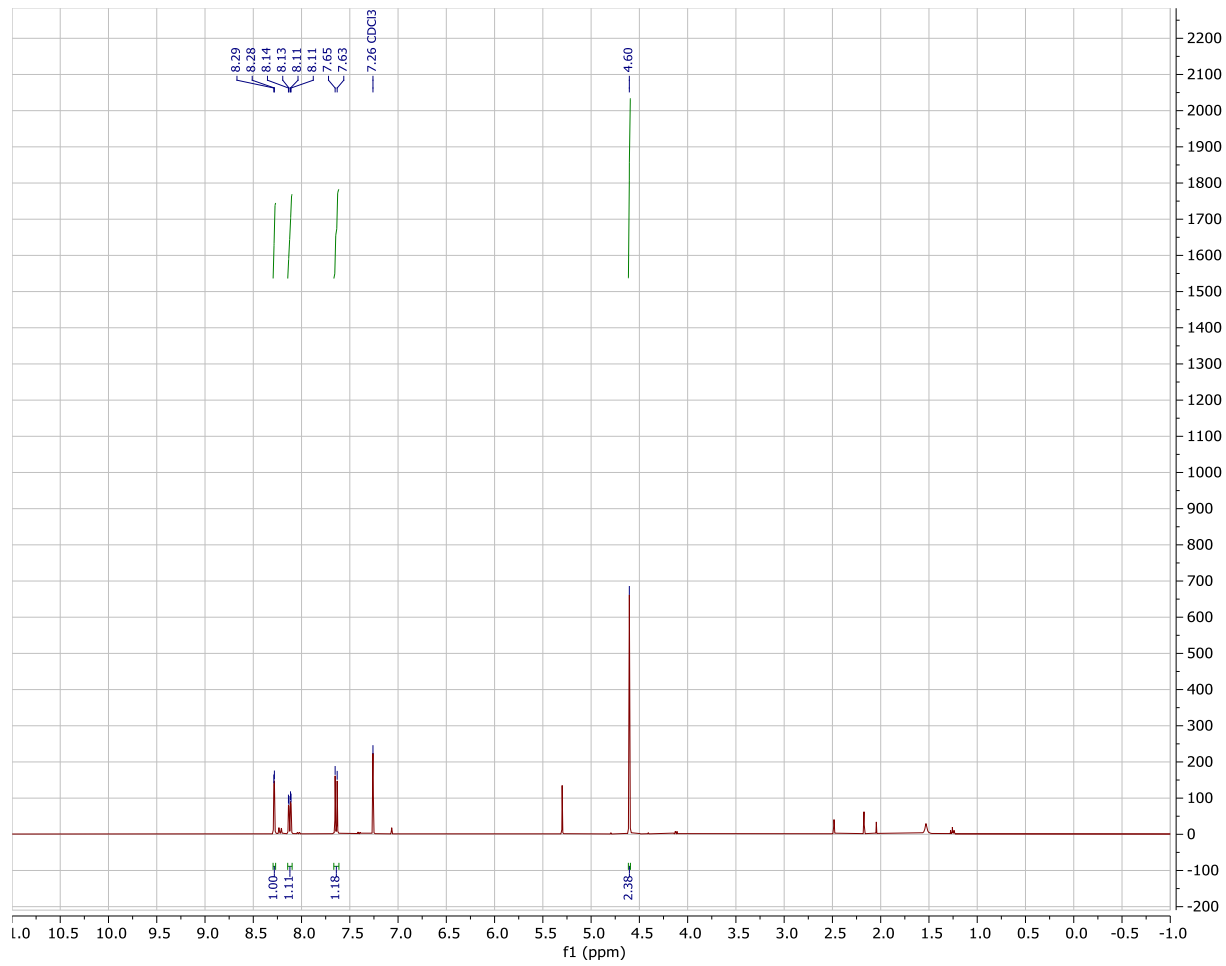
## SA.3 NMR Spectra of Compounds in Chapter 5

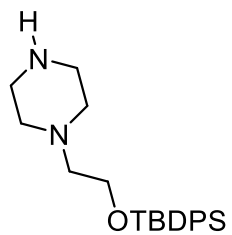
### SA.3.1 Single-NBN Compounds (5.1 – 5.9c)

**5.1a**

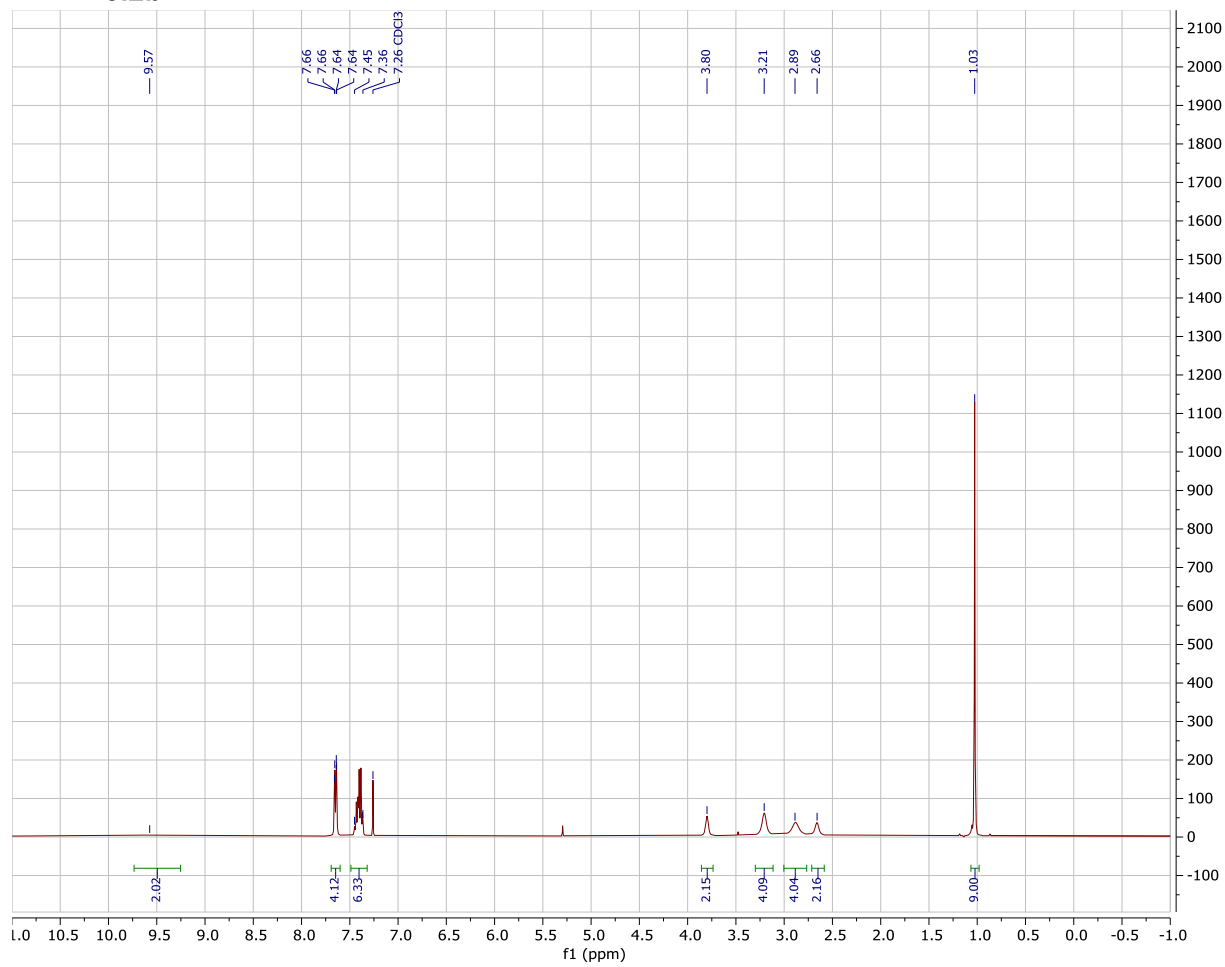


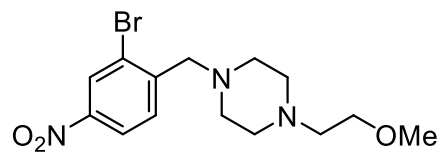
5.1b



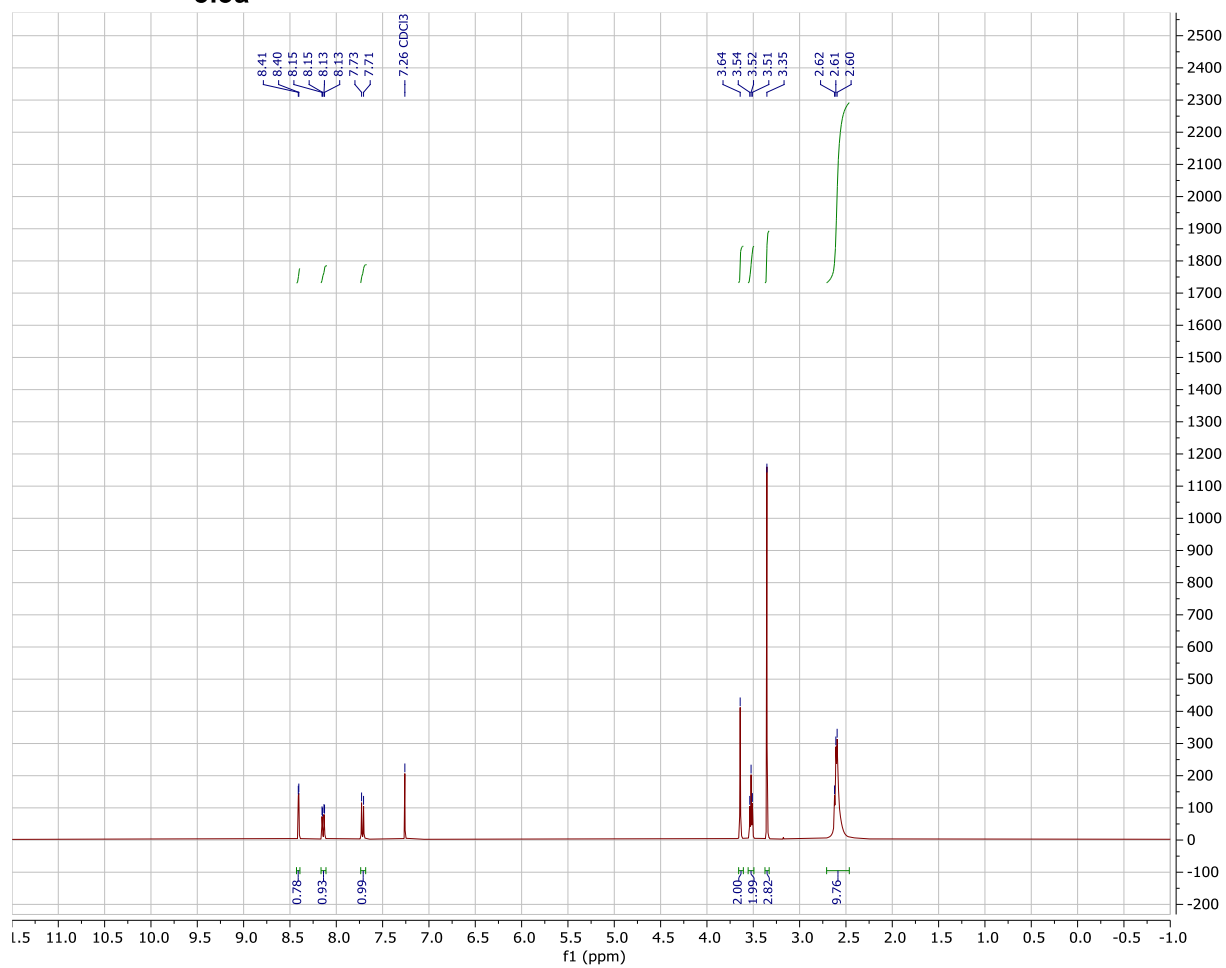


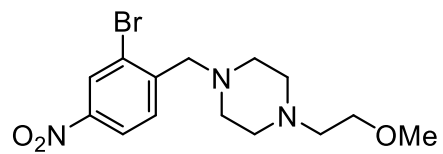
5.2b



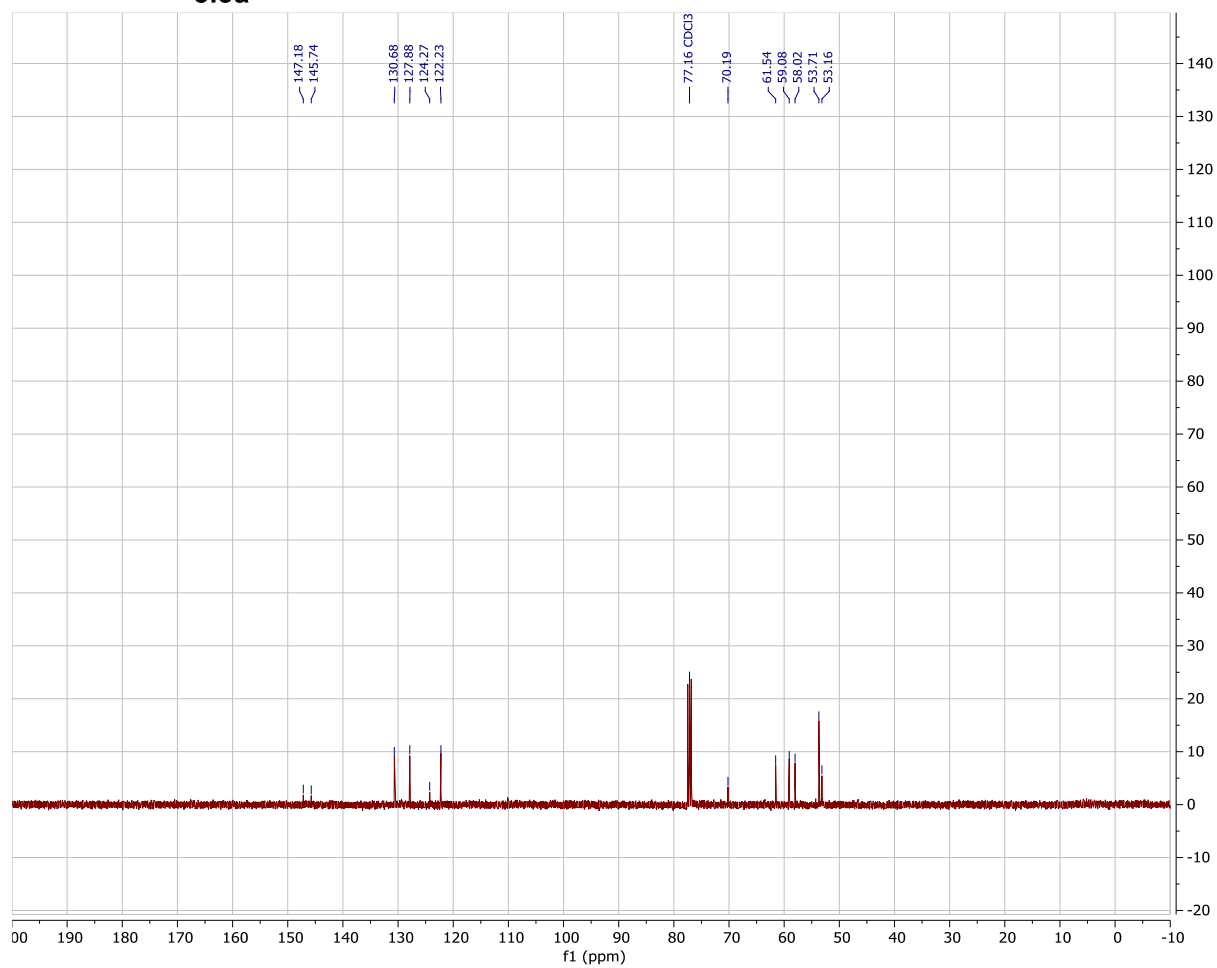


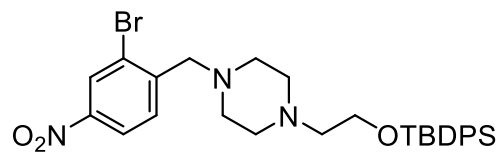
5.3a



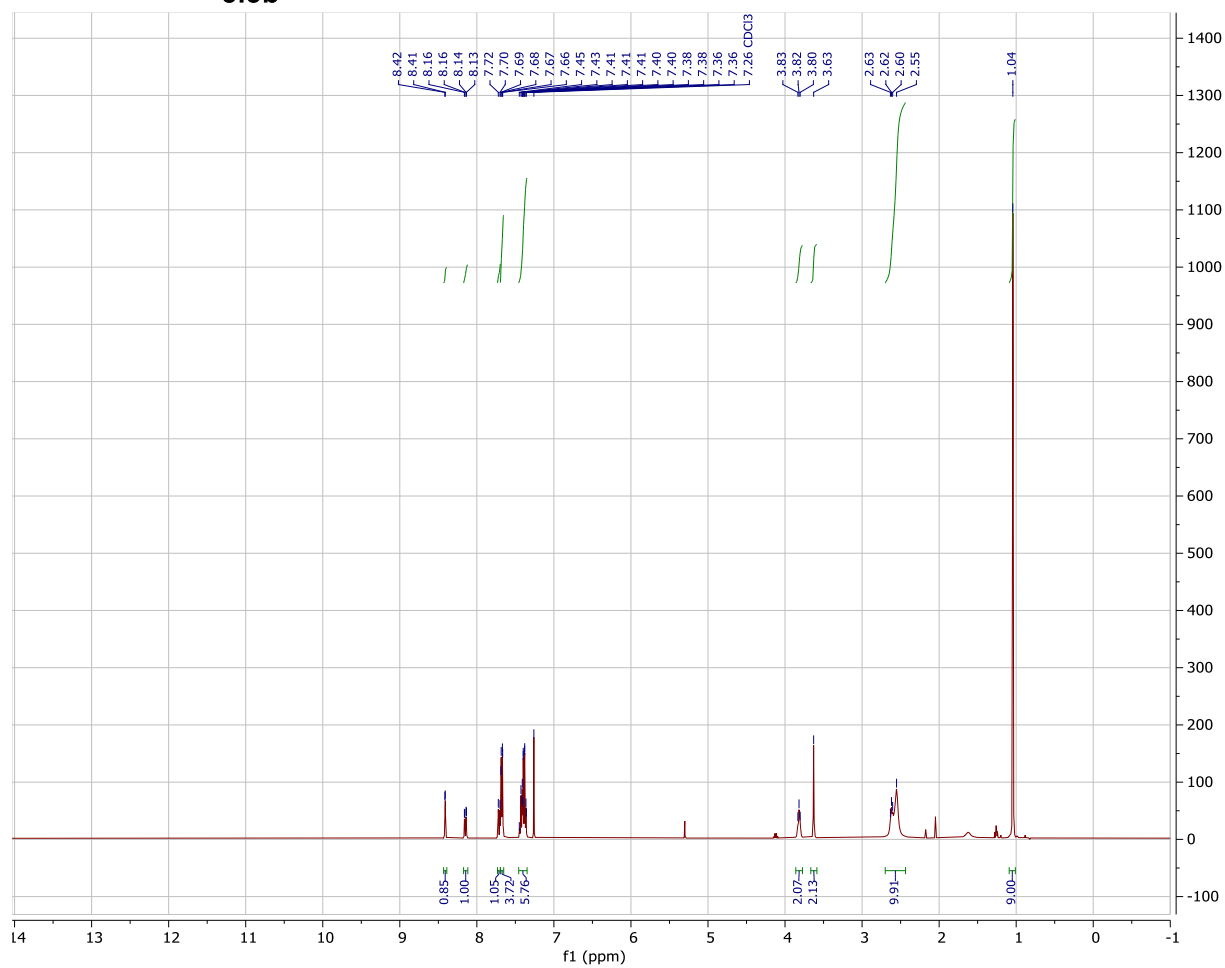


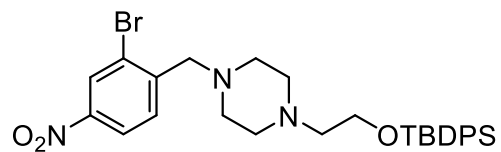
5.3a



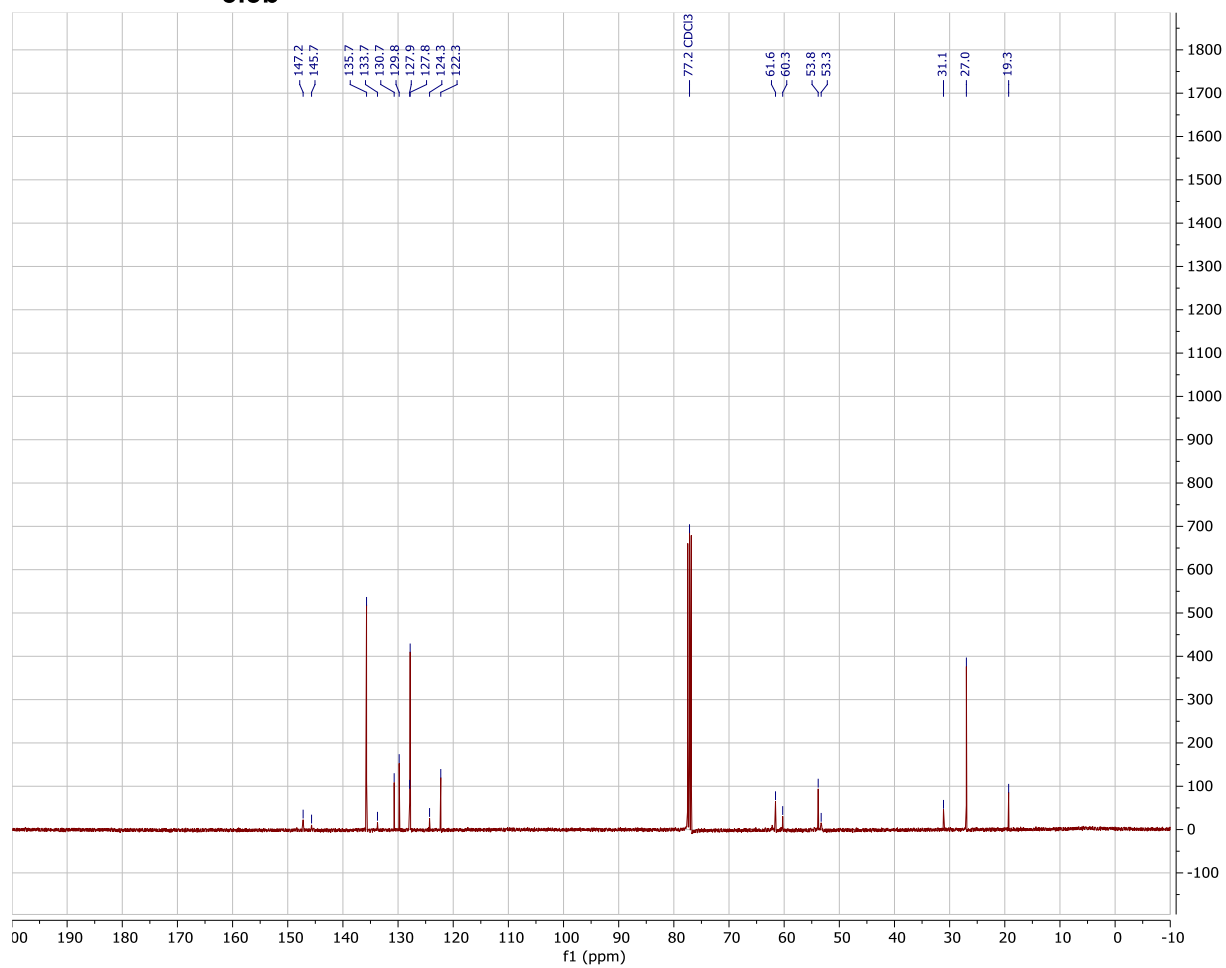


5.3b

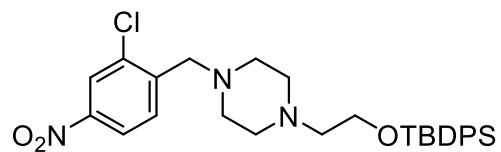




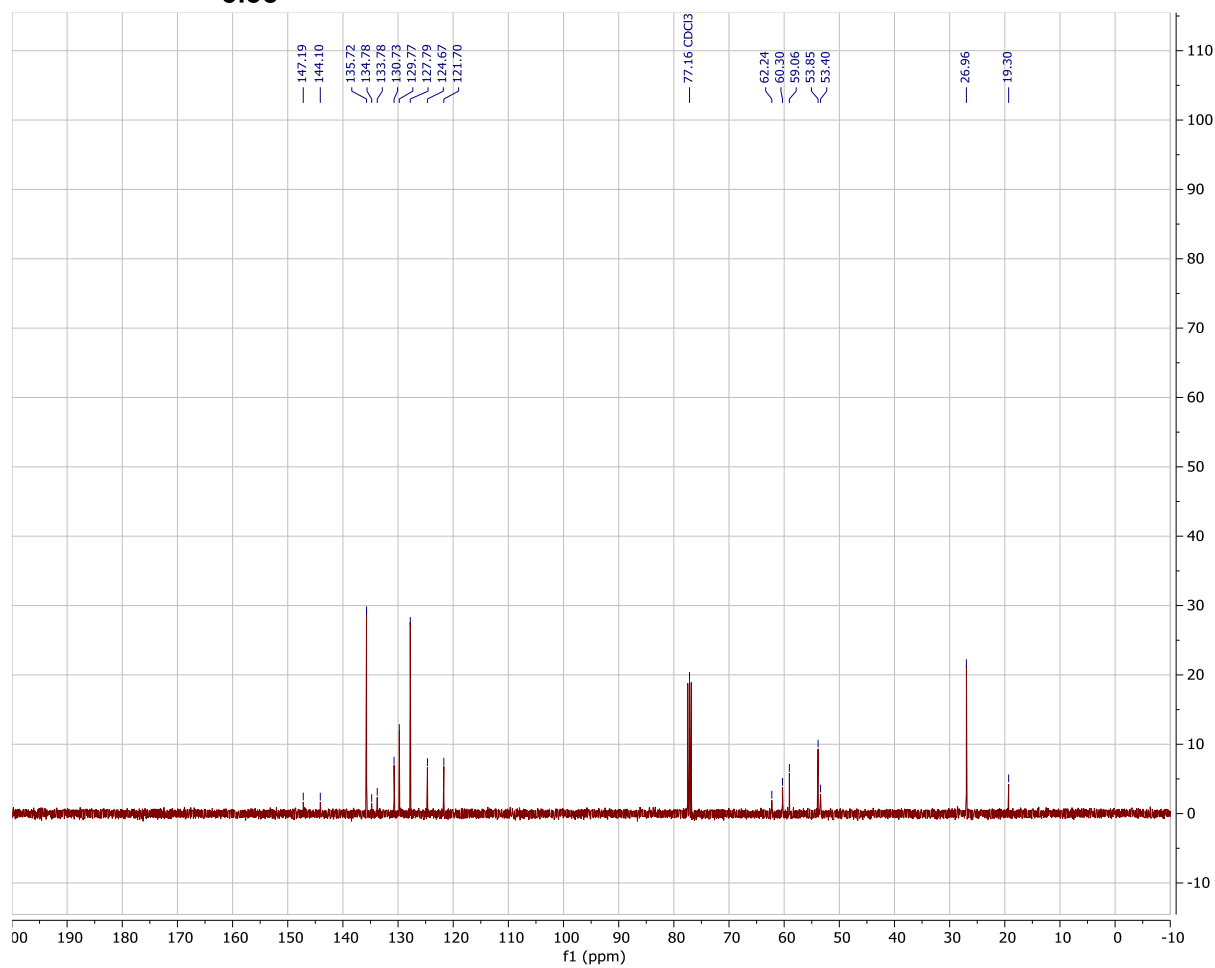
5.3b

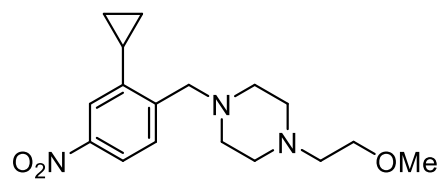
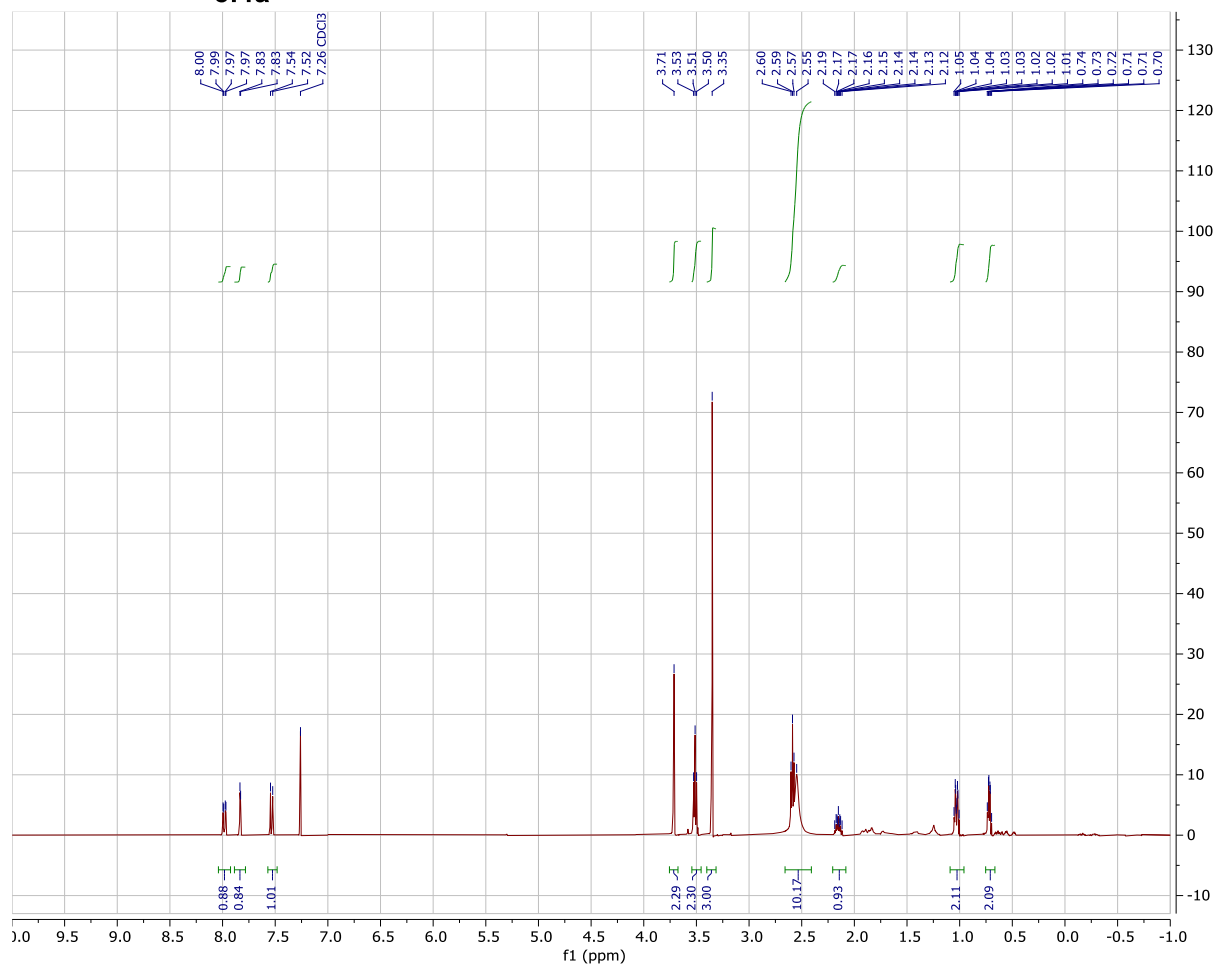


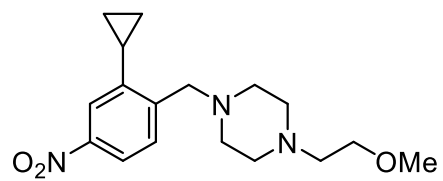
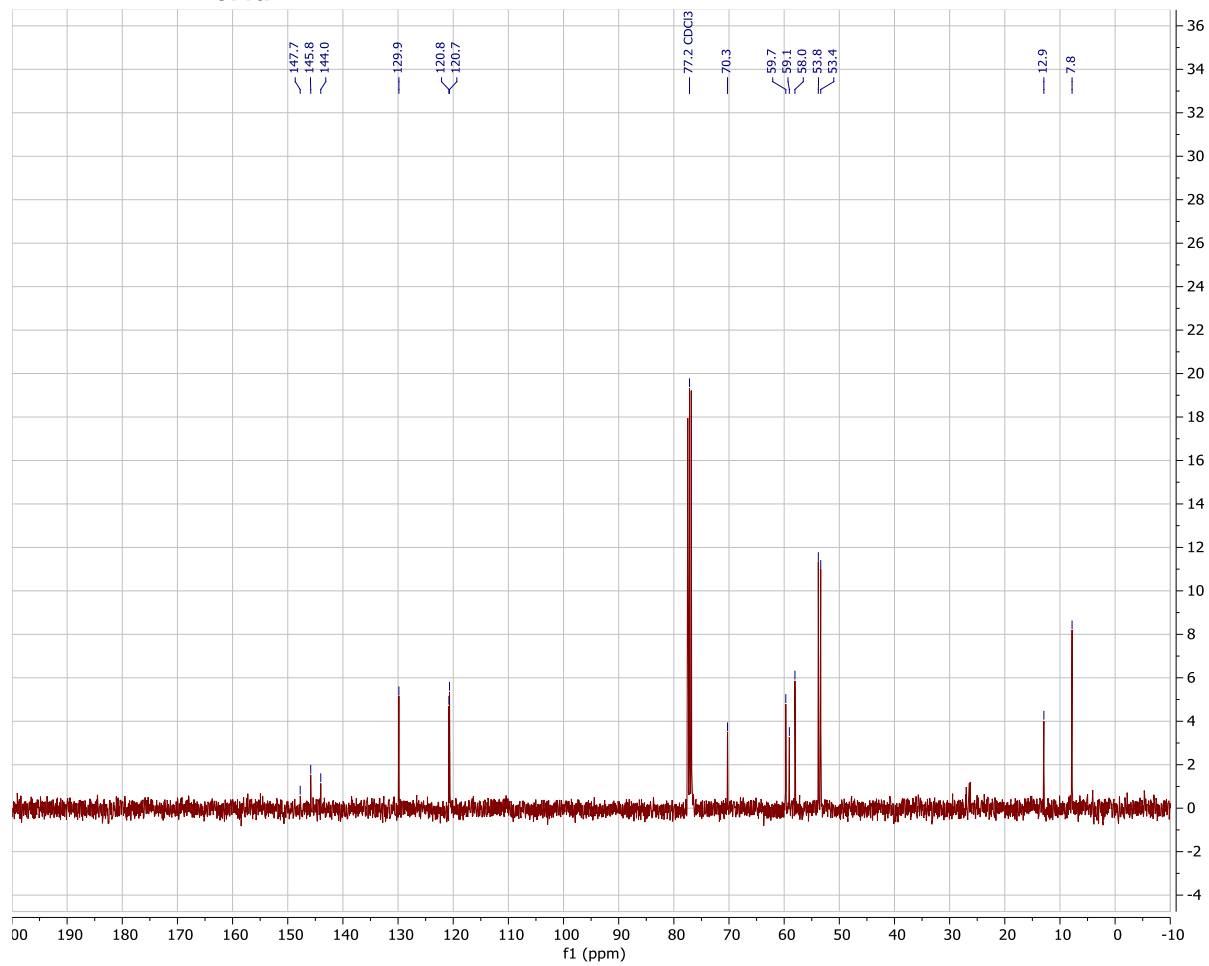


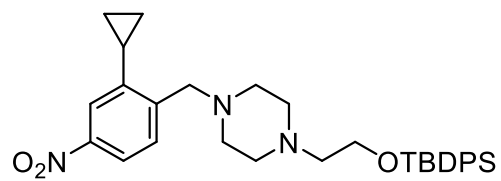


5.3c

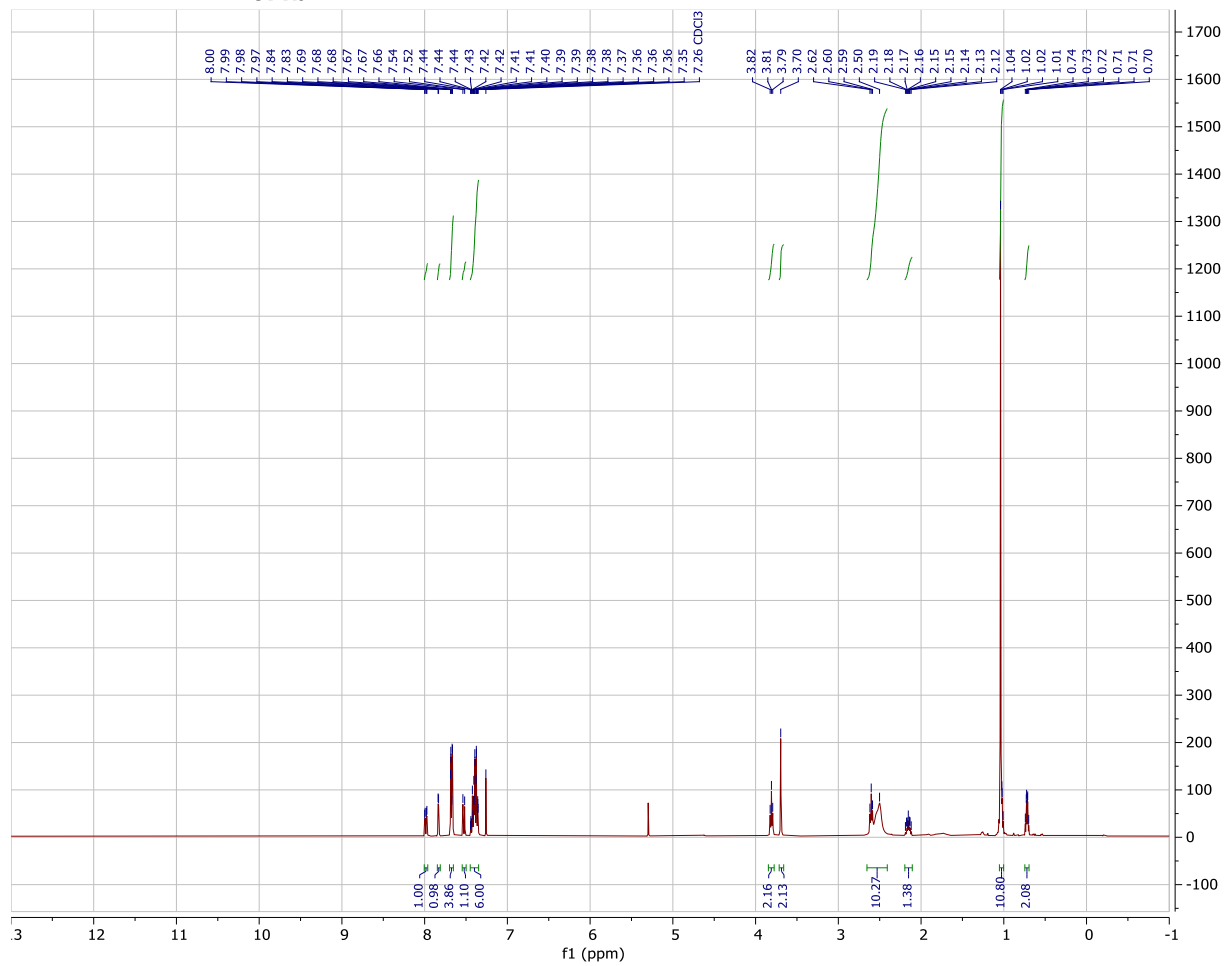


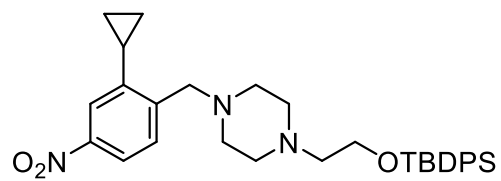
**5.4a**

**5.4a**

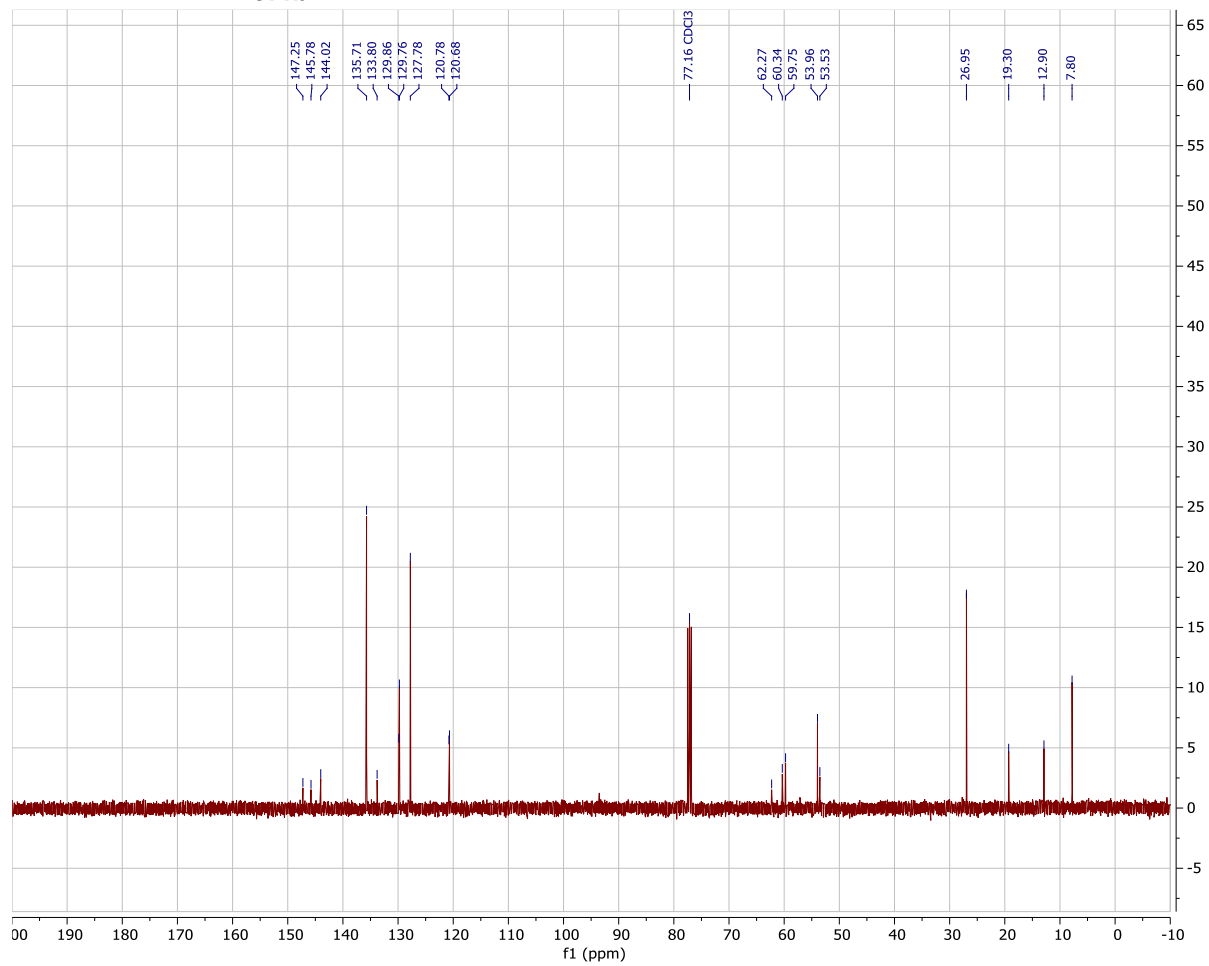


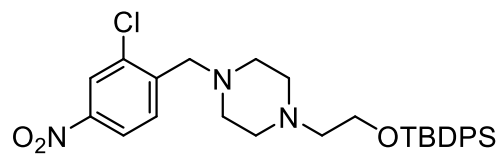
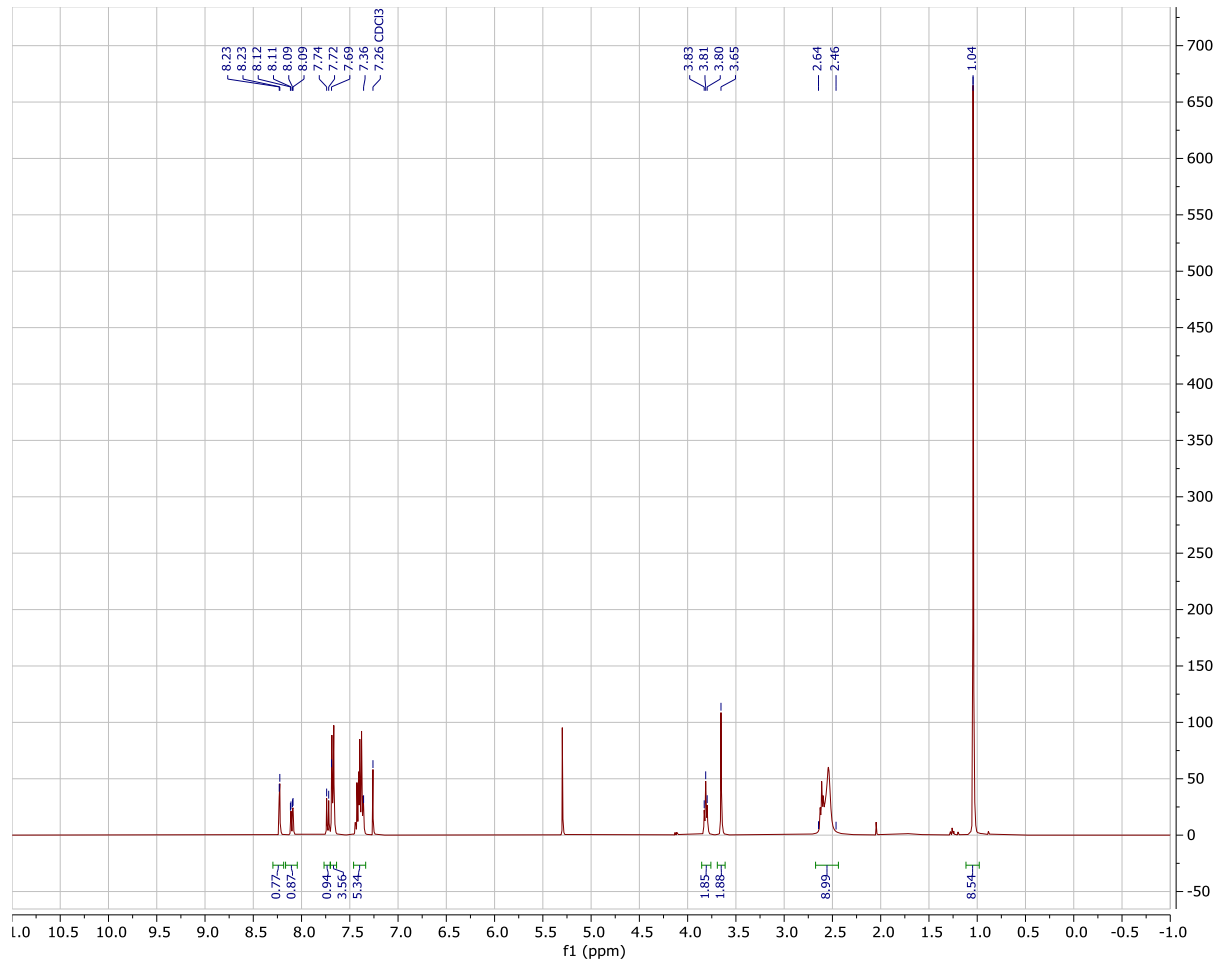
5.4b

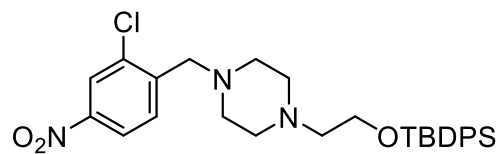




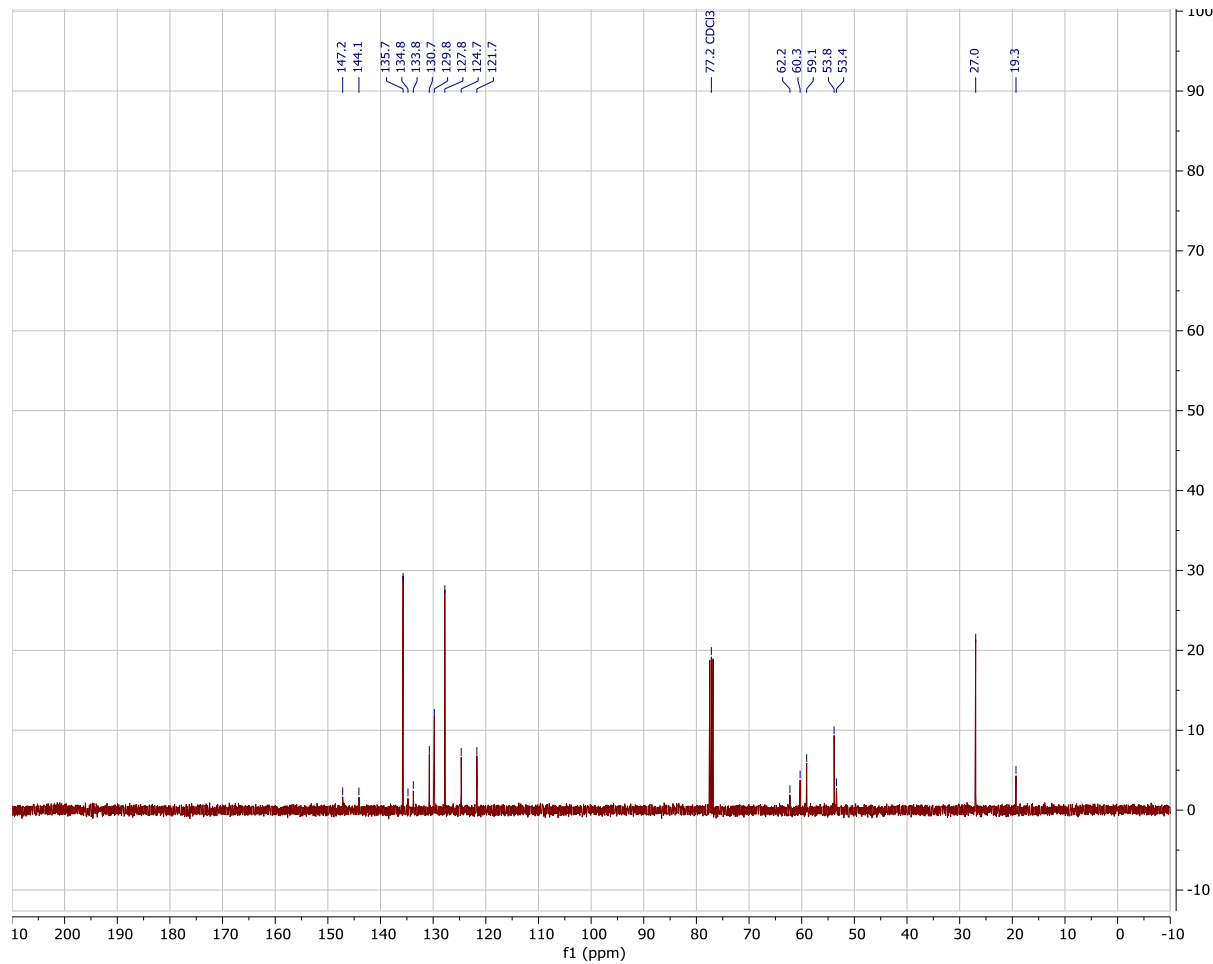
5.4b

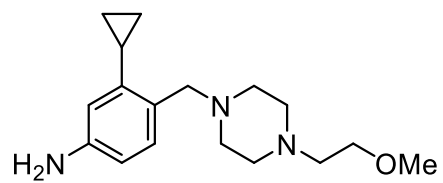


**5.4c**

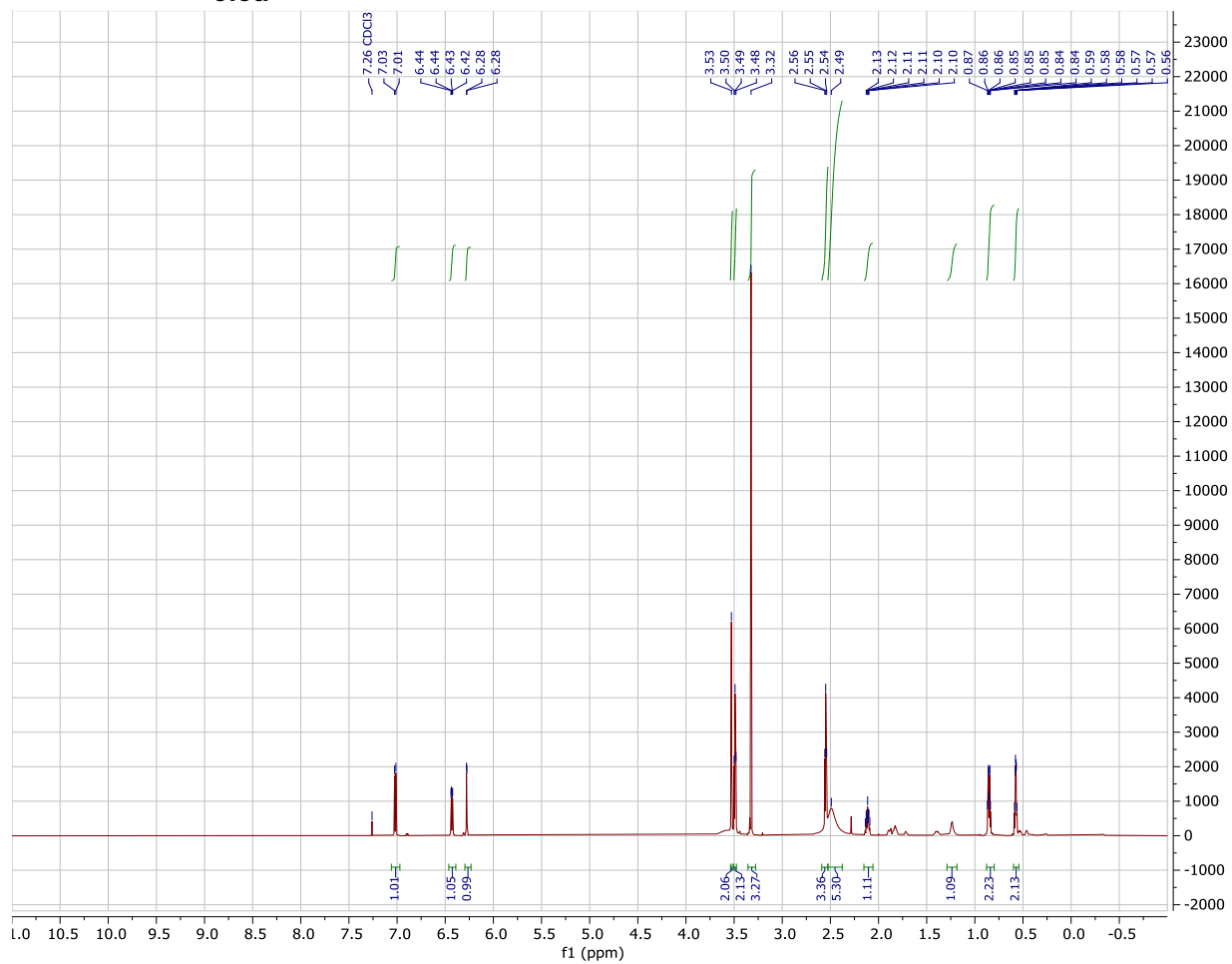


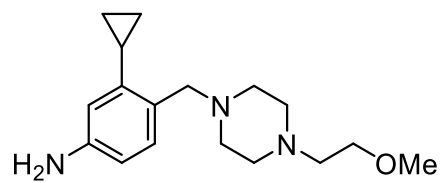
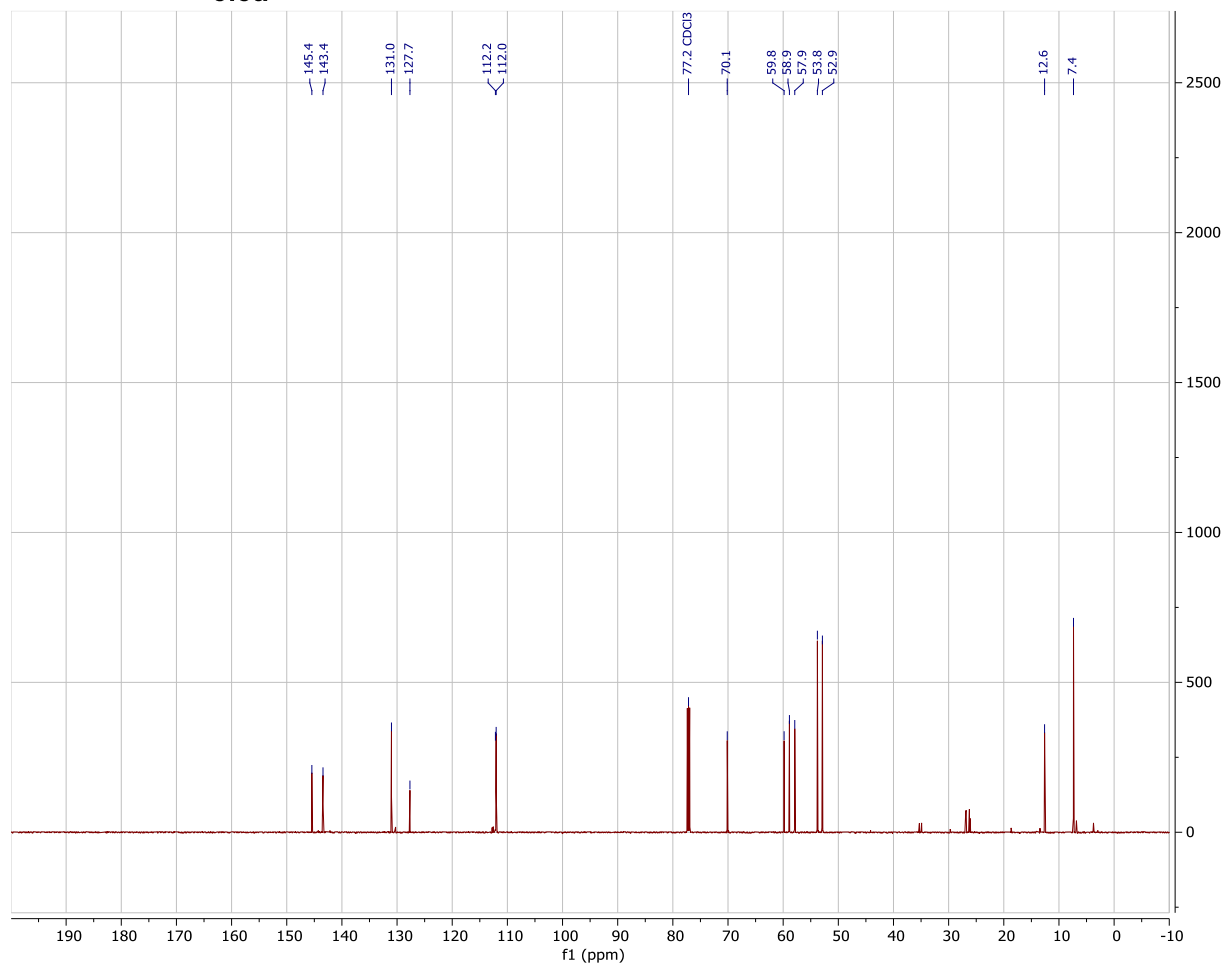
5.4c

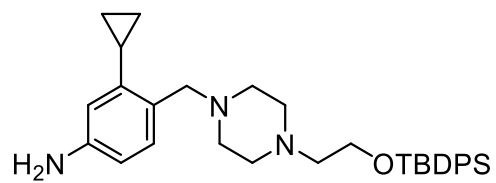
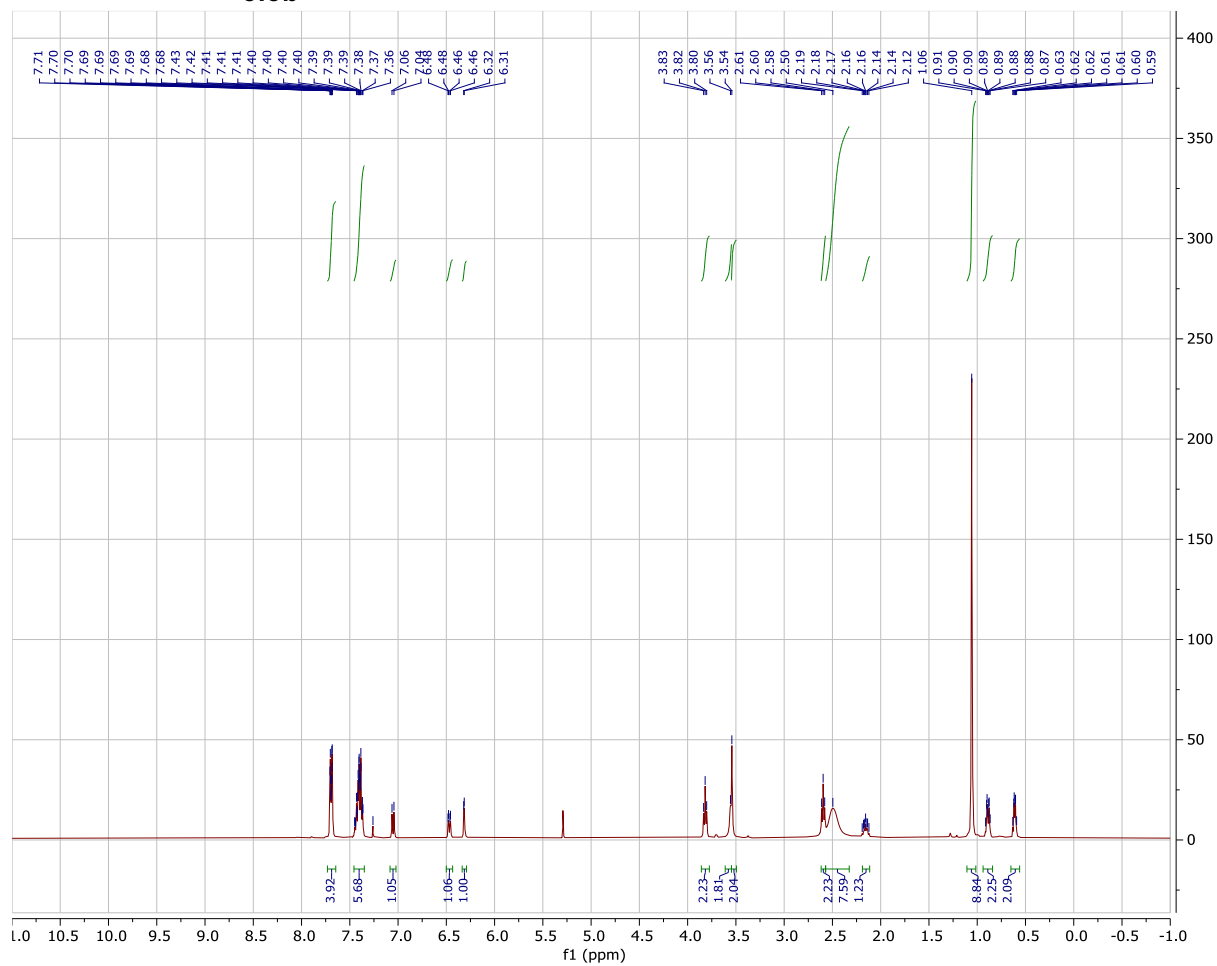


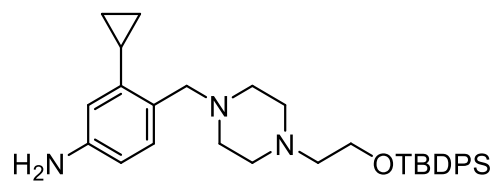
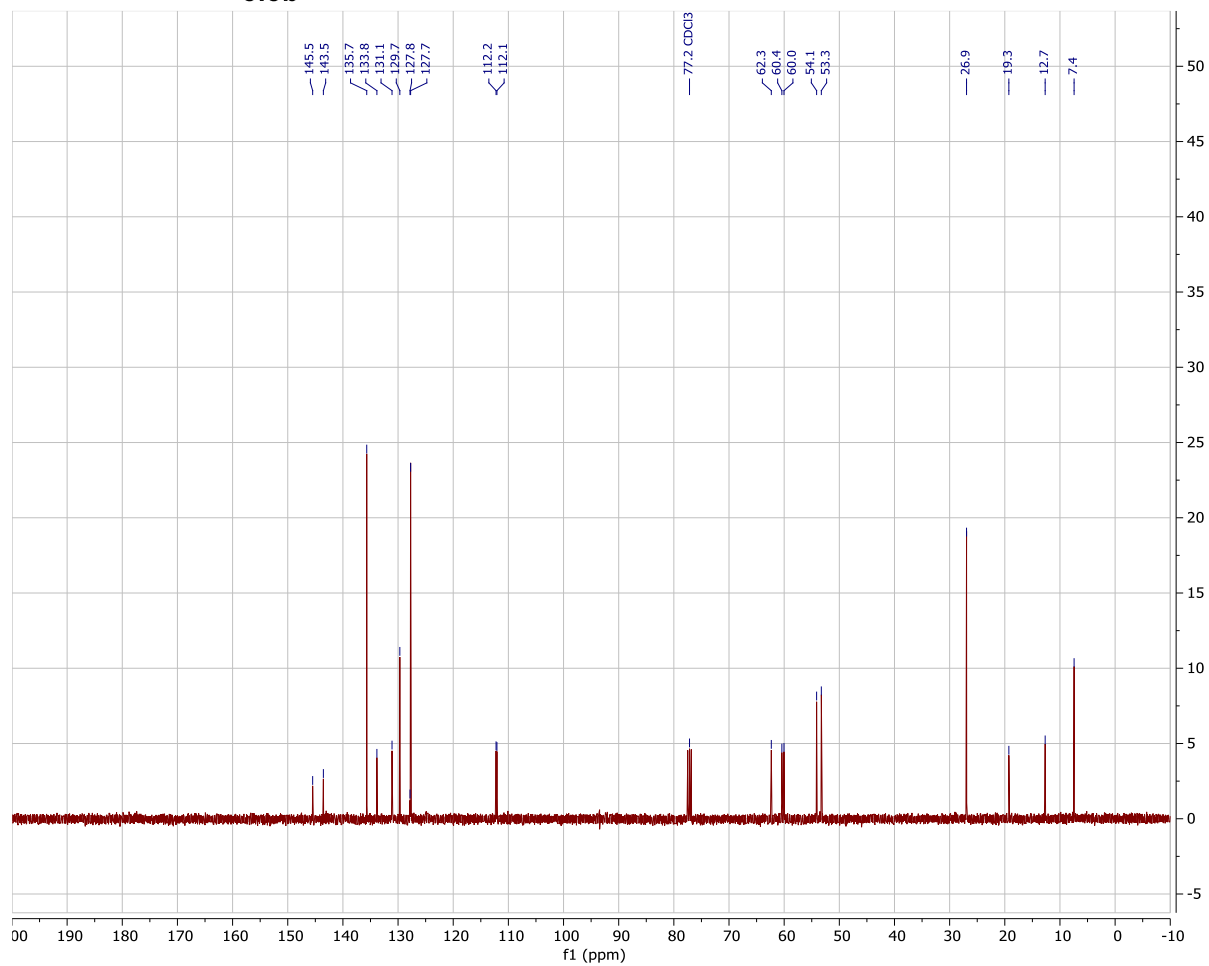


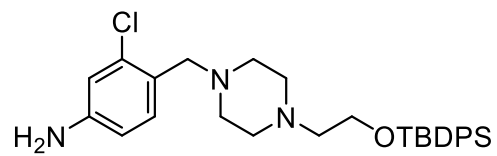
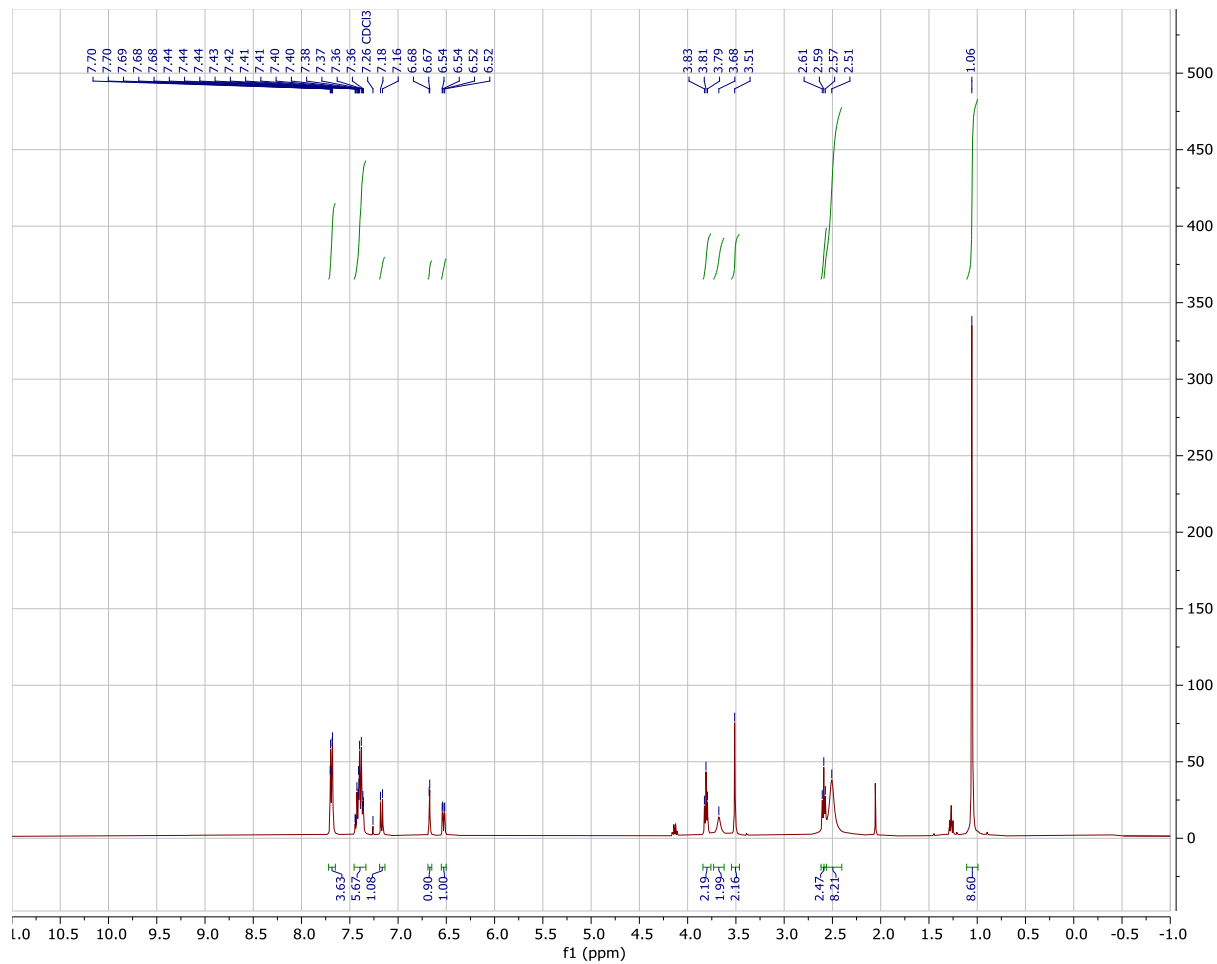
5.5a

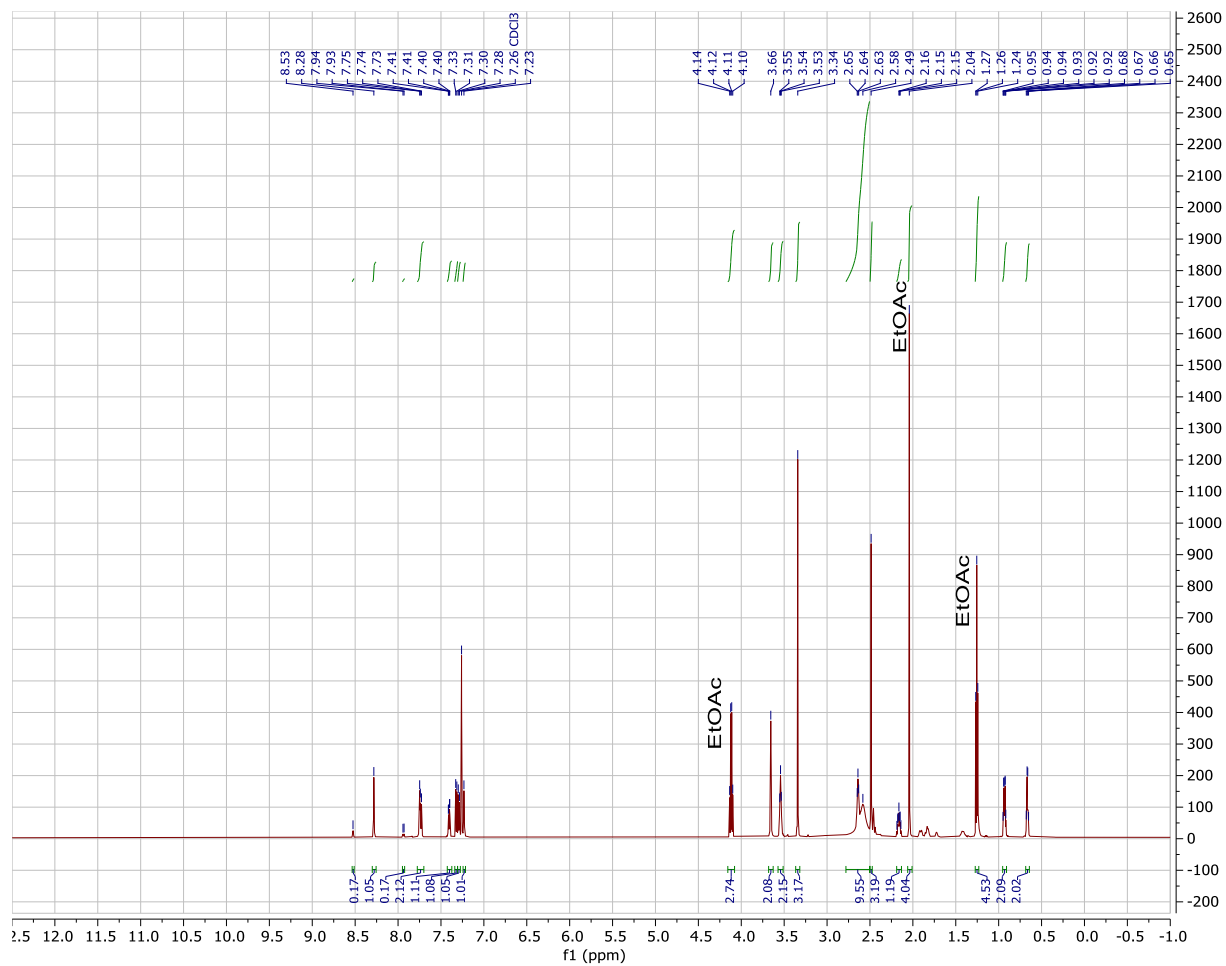
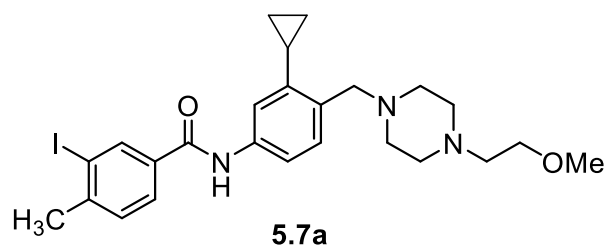


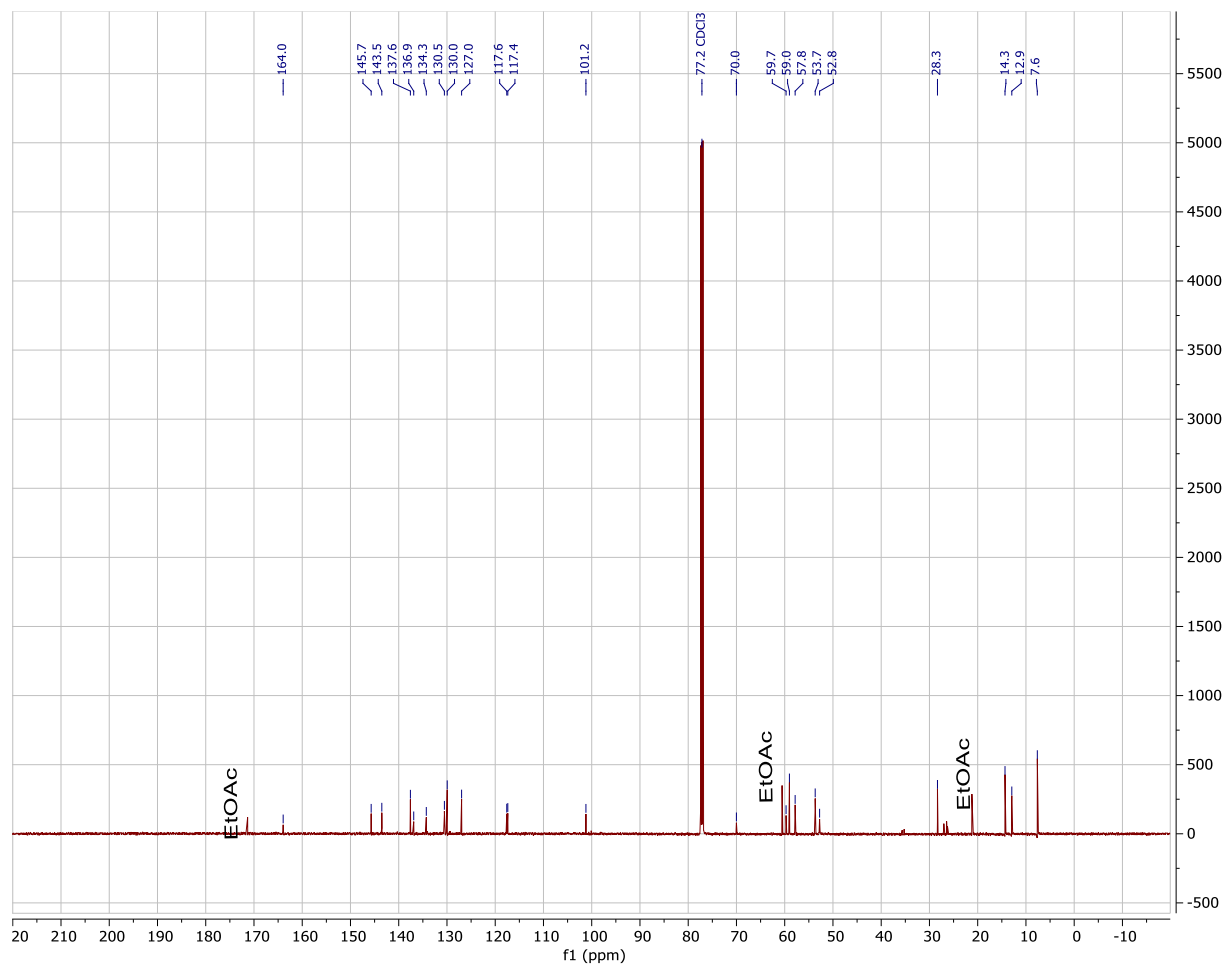
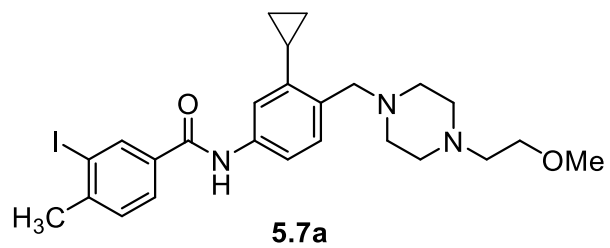
**5.5a**

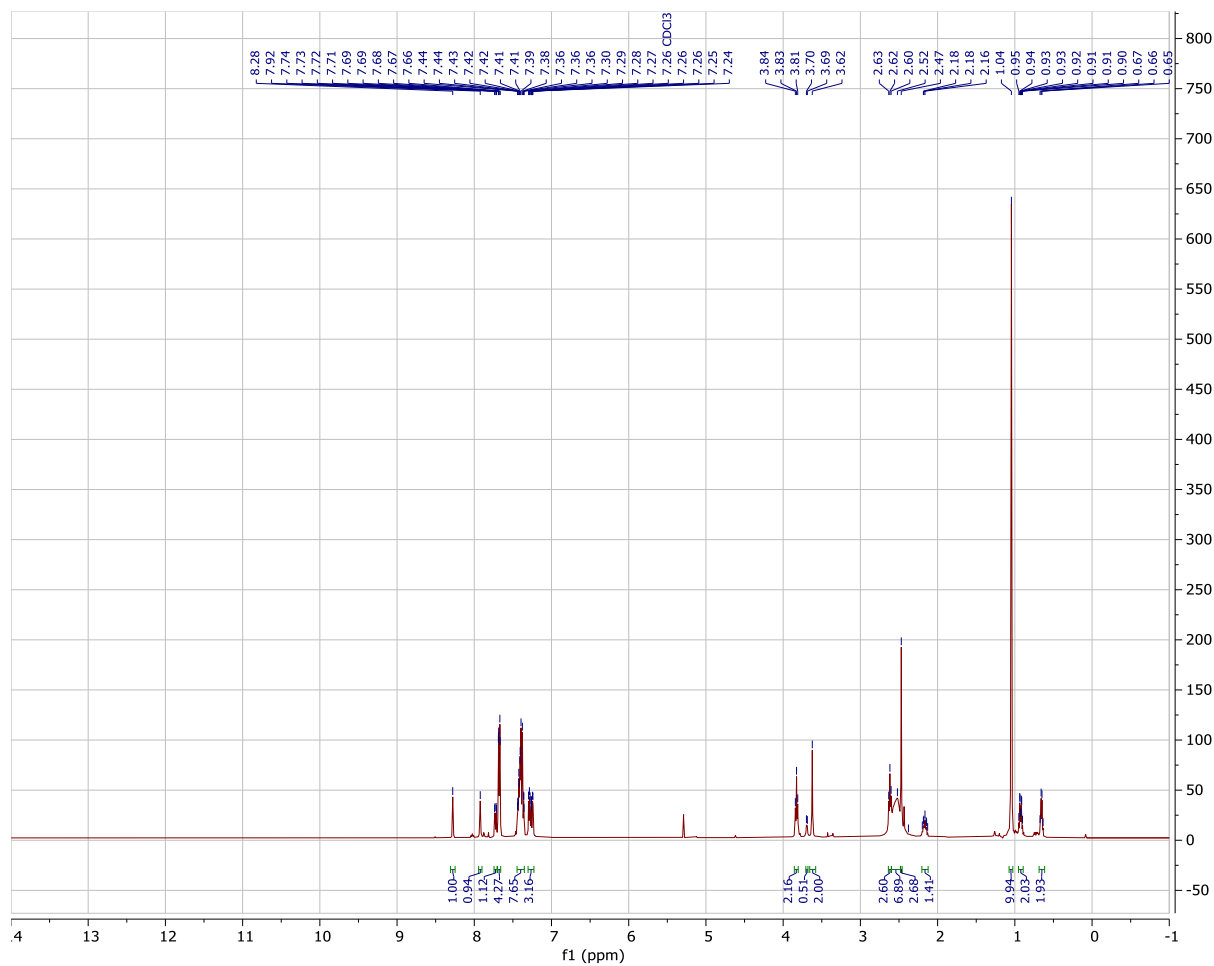
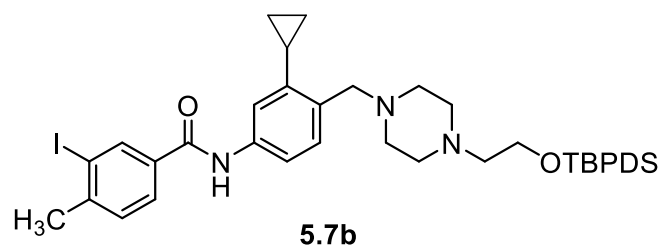
**5.5b**

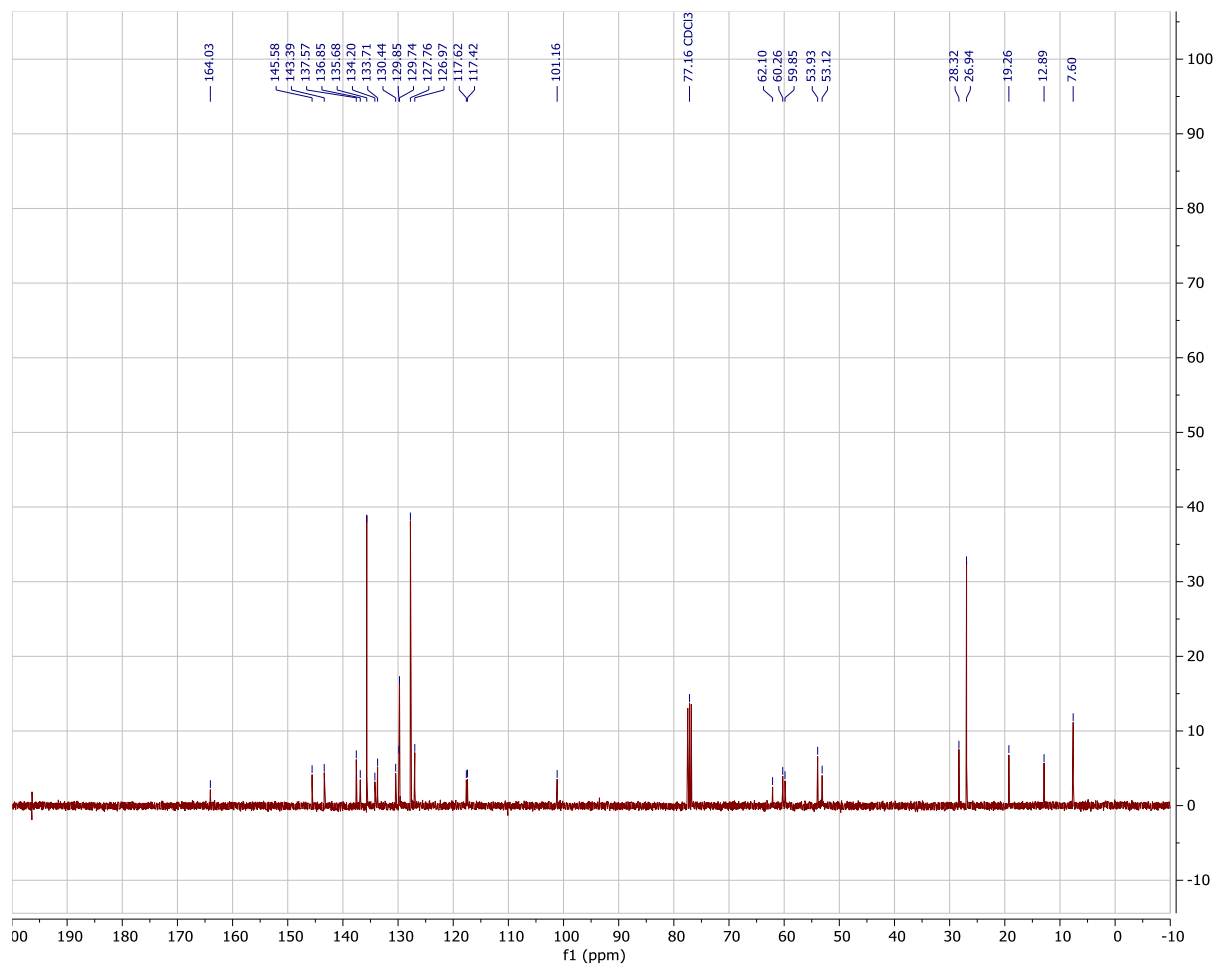
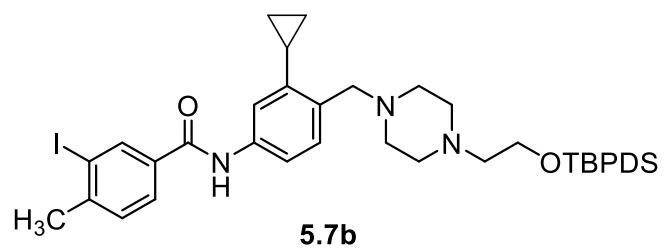
**5.5b**

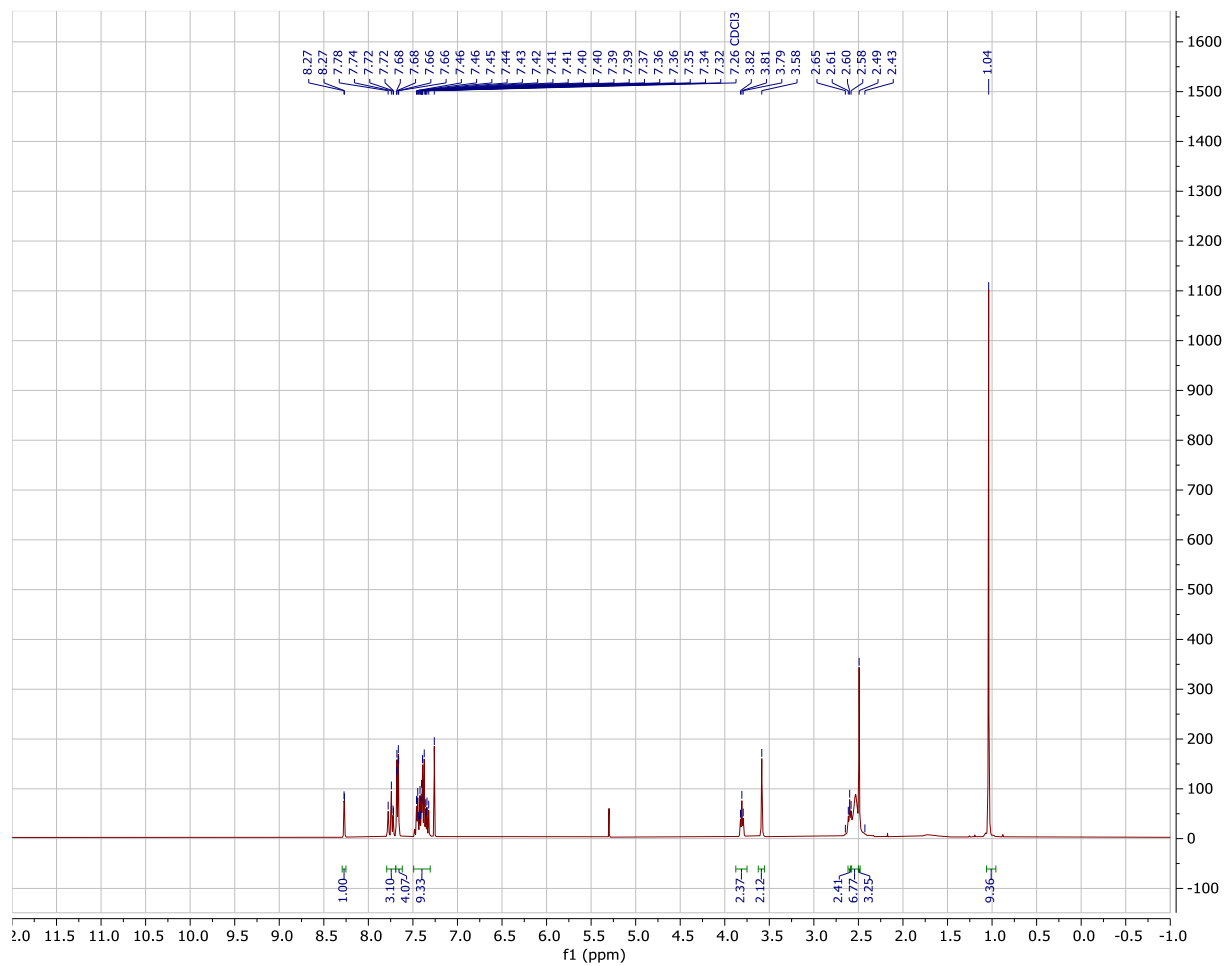
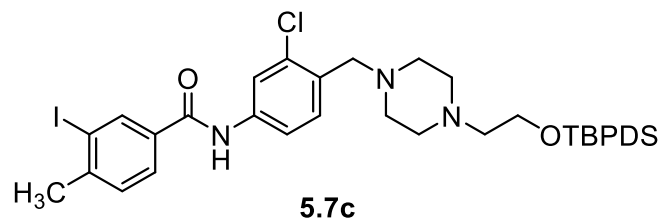
**5.5c**

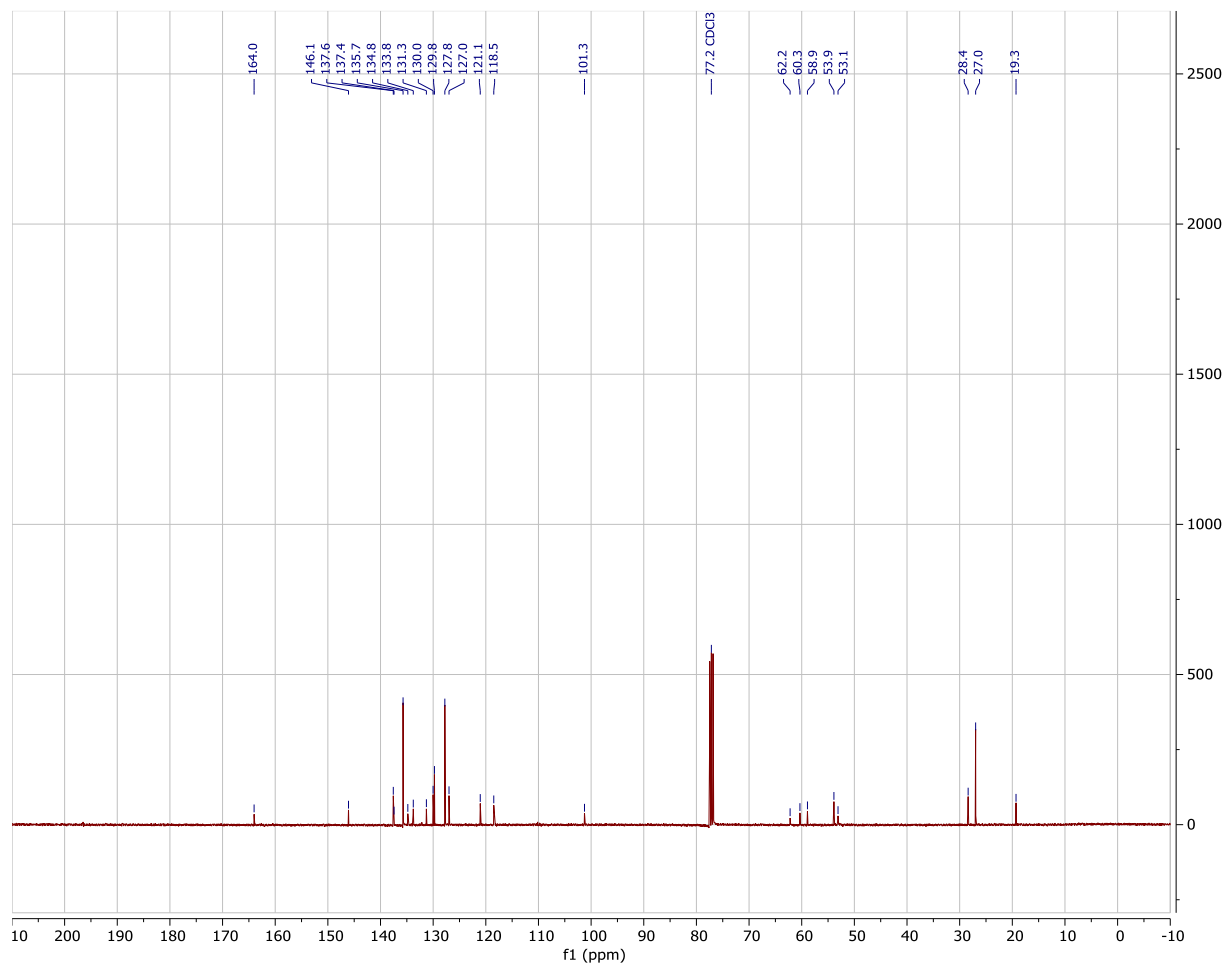
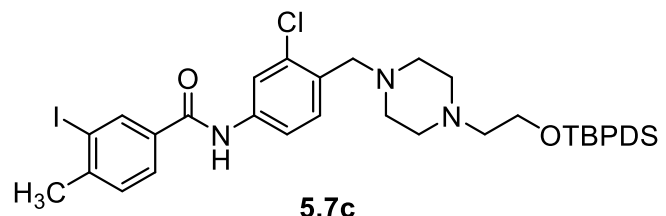


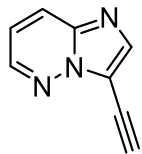




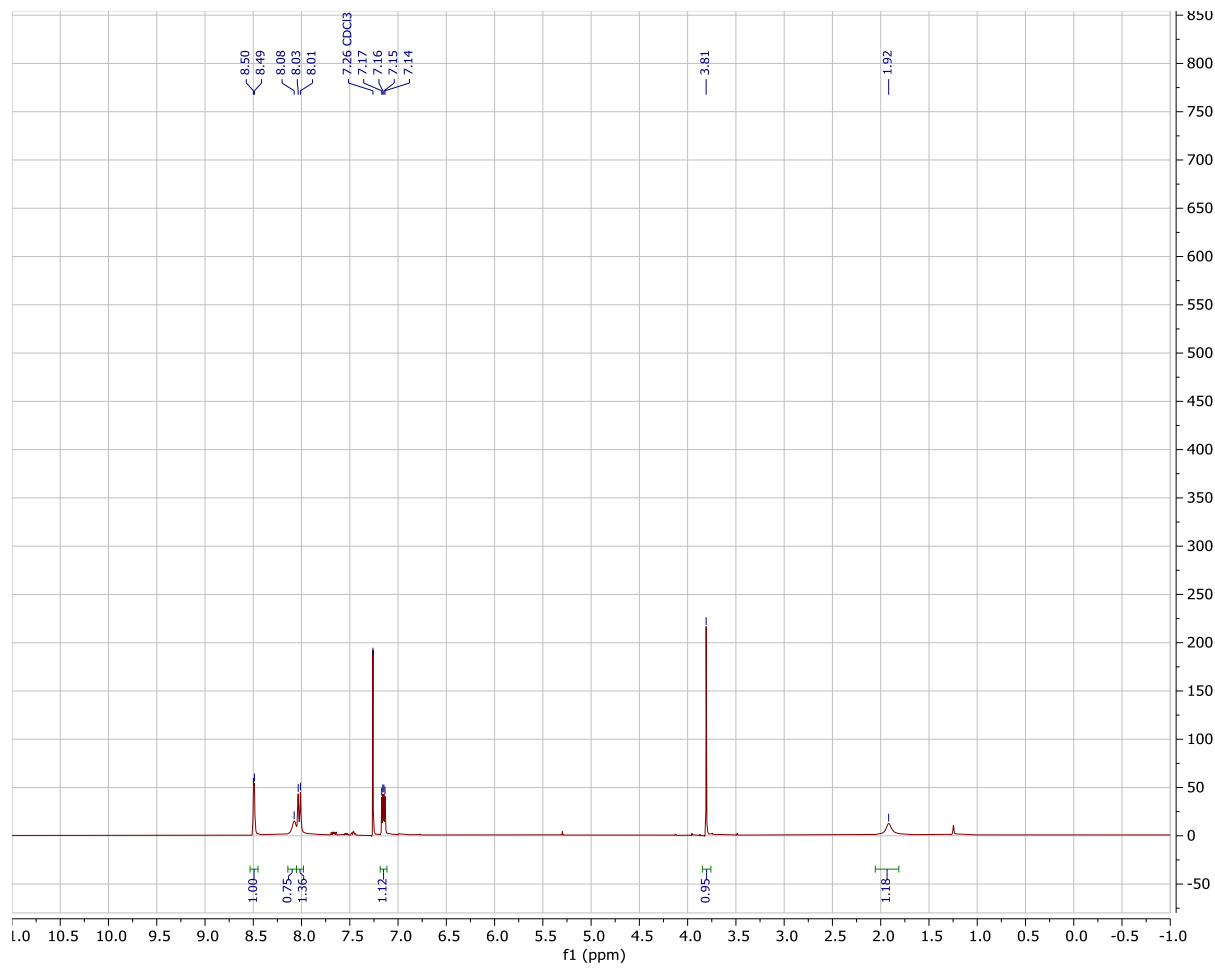


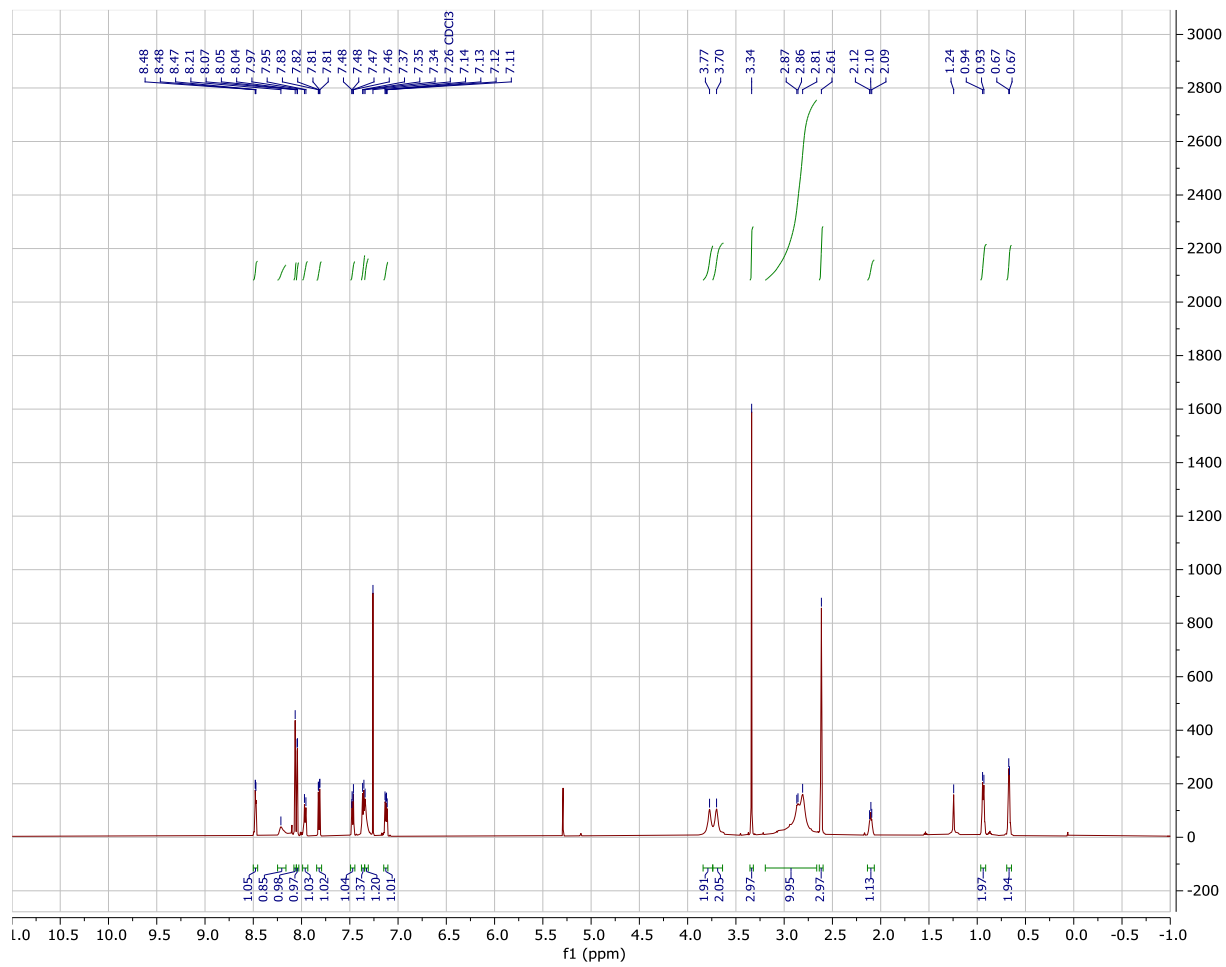
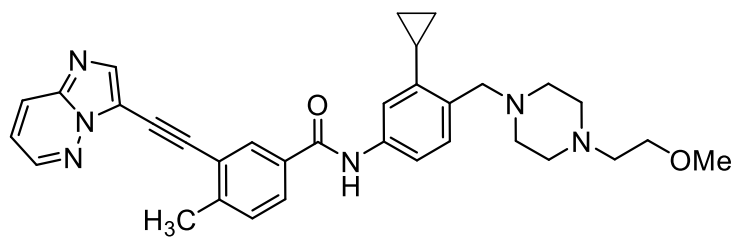


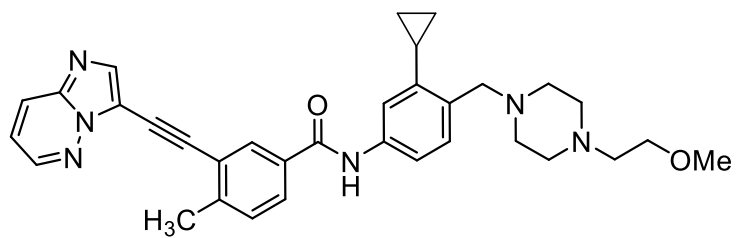
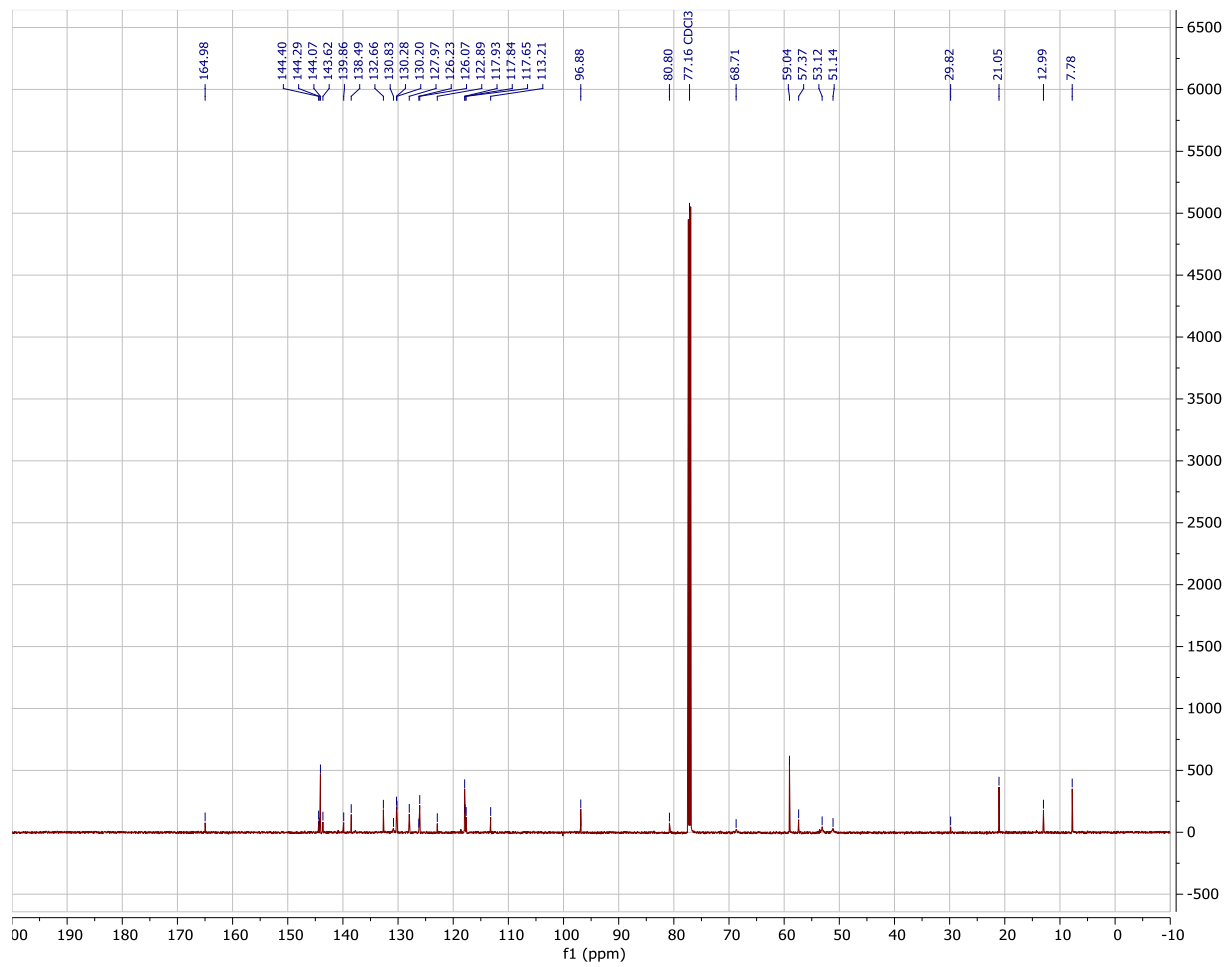


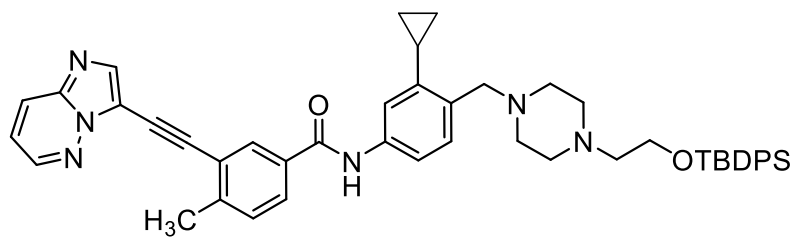


5.8

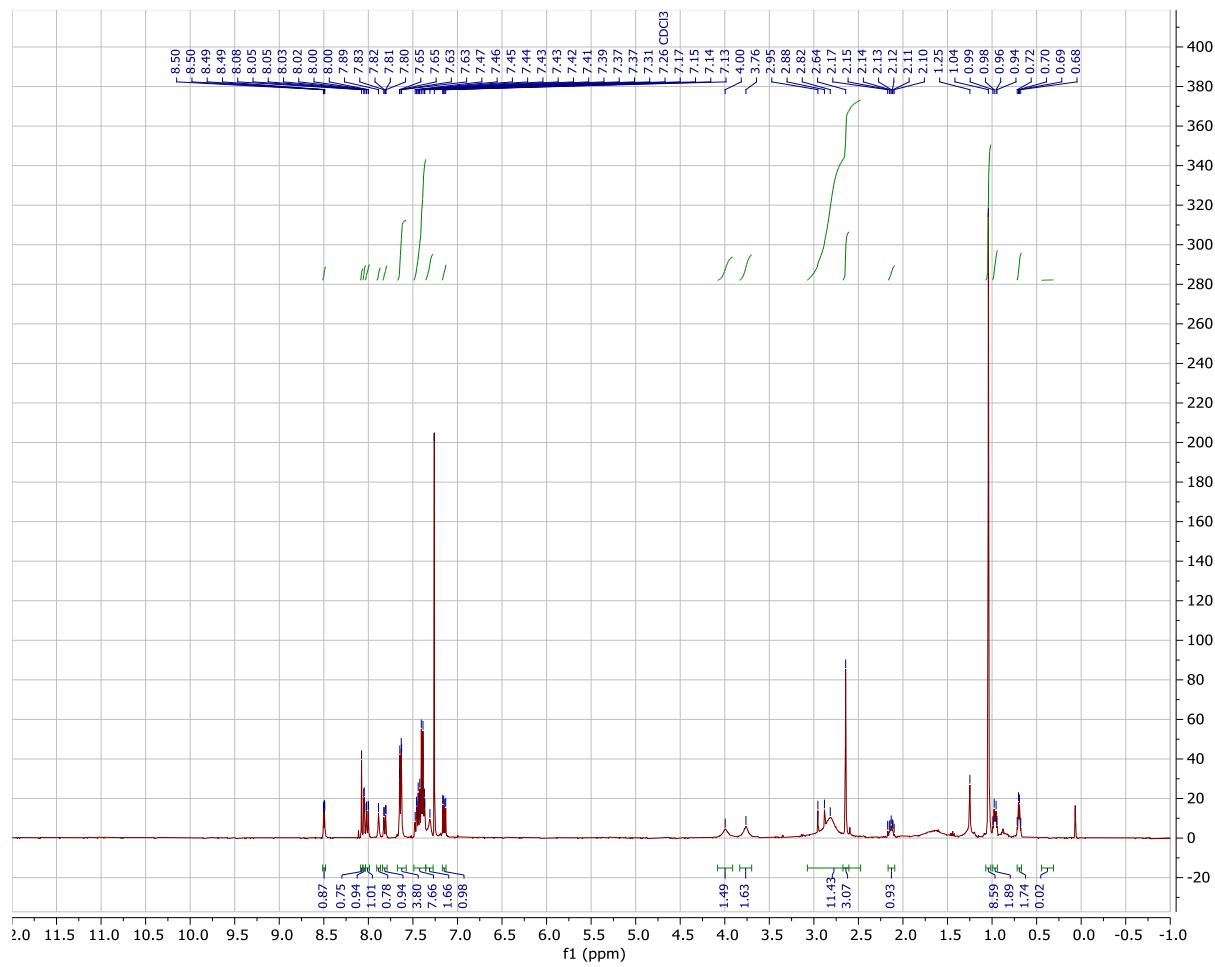


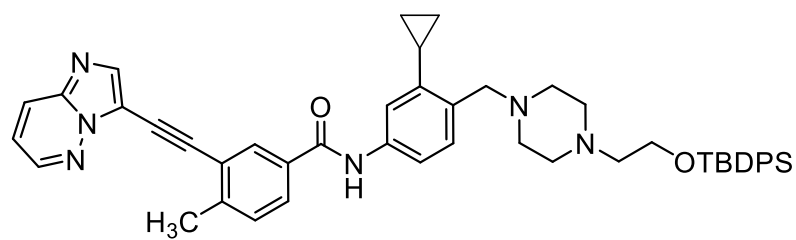
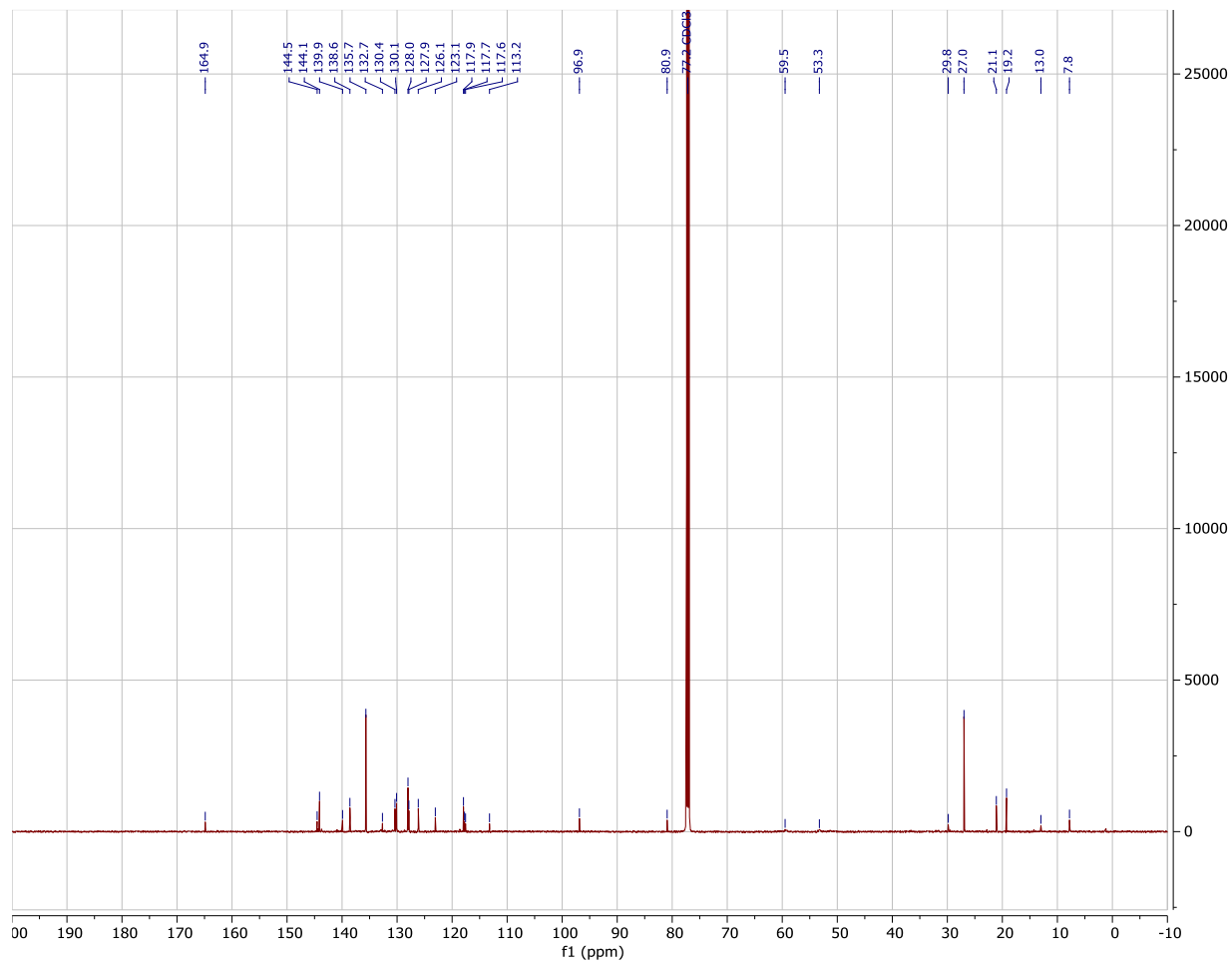


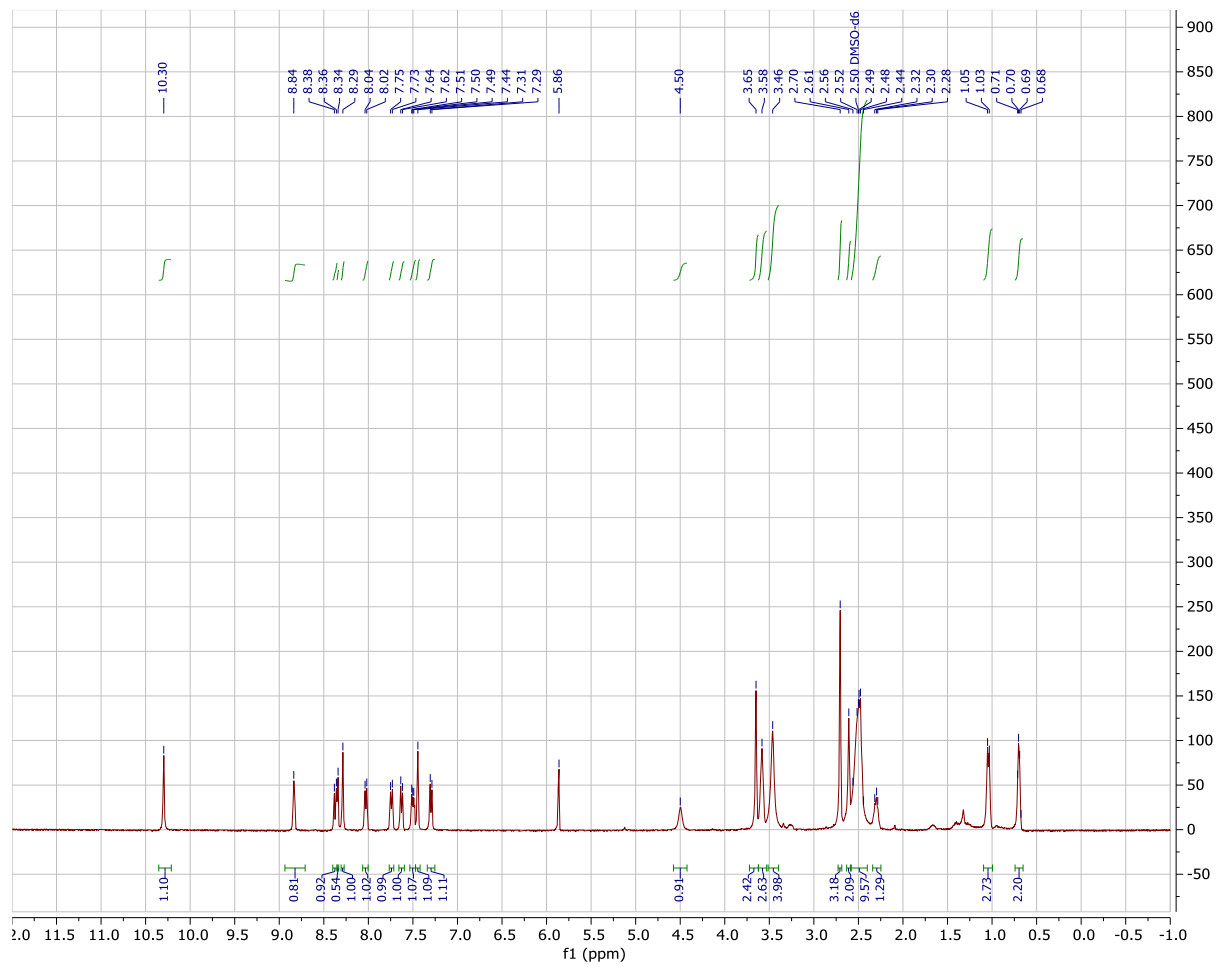
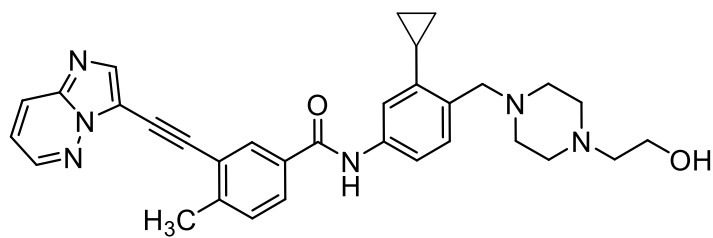
**5.9a**

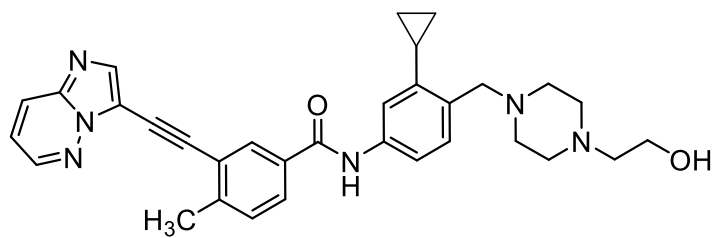


5.S1b

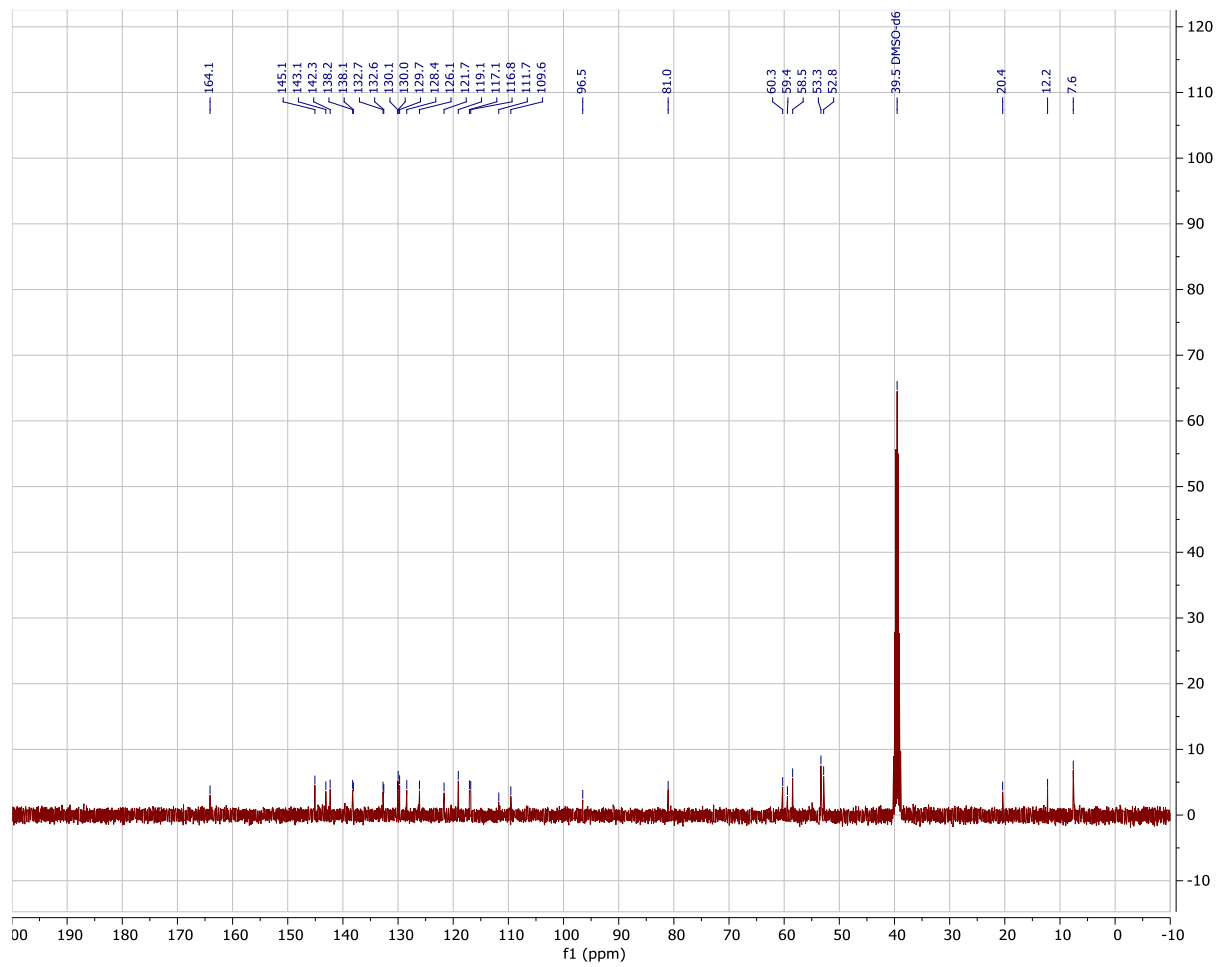


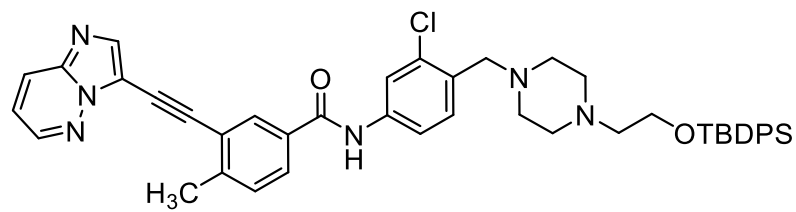
**5.S1b**



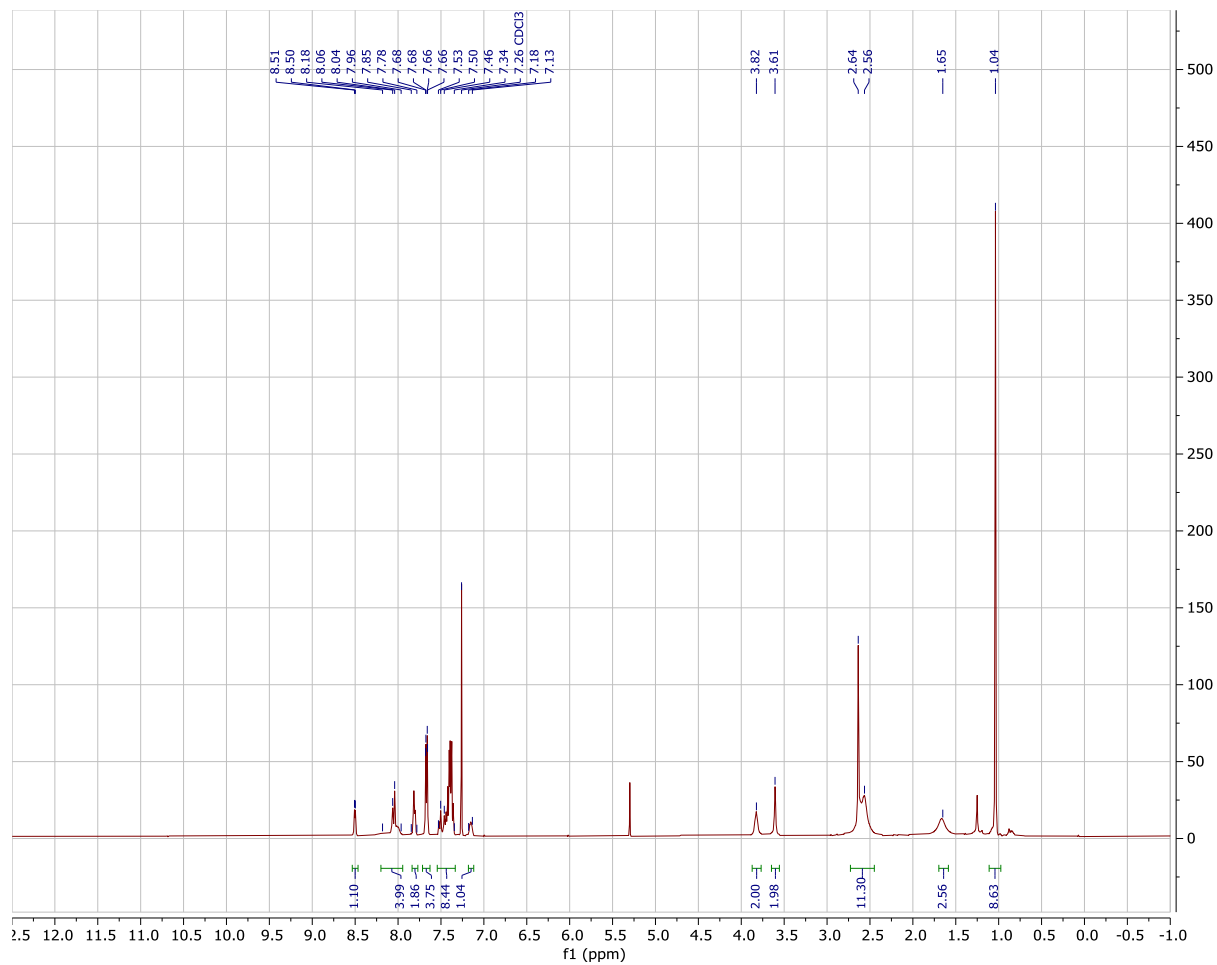


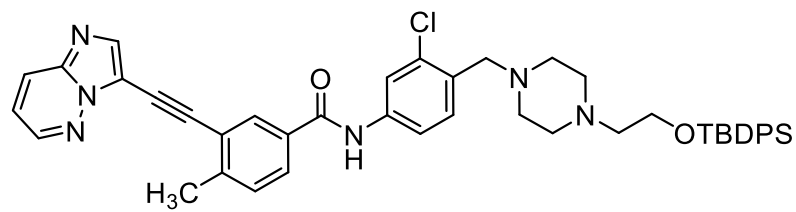
5.9b



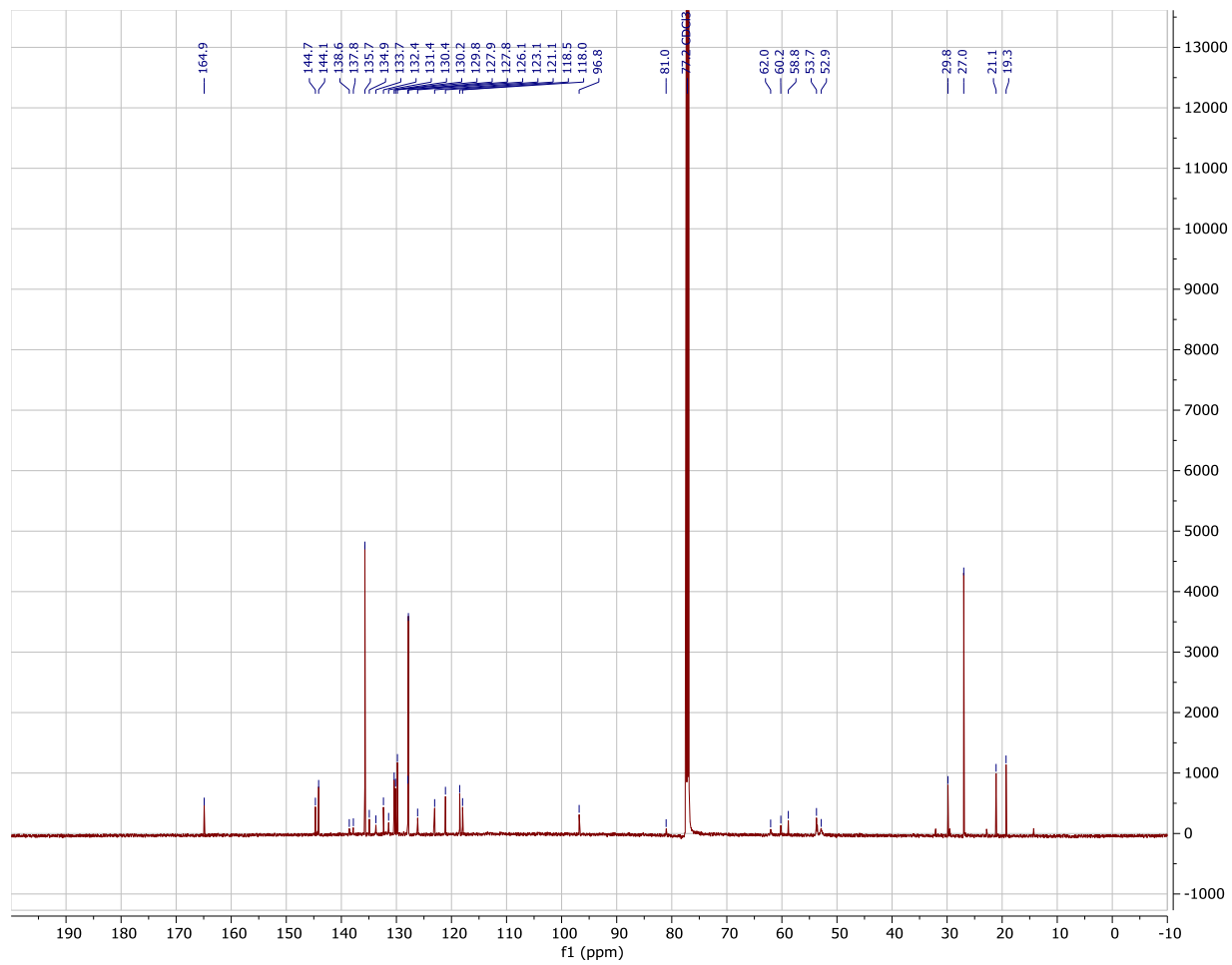


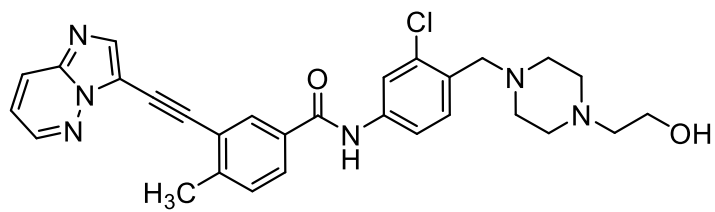
5.S1c



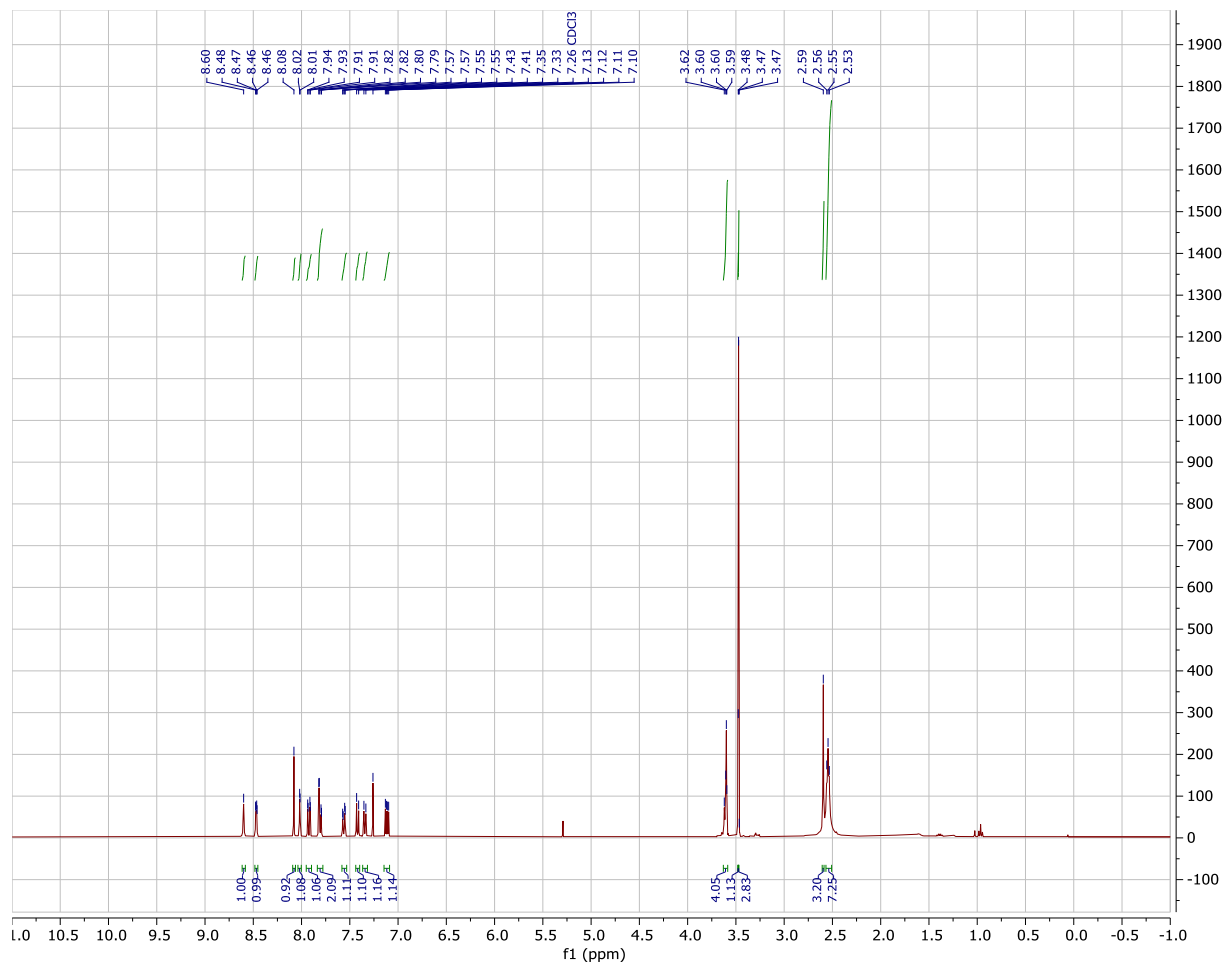


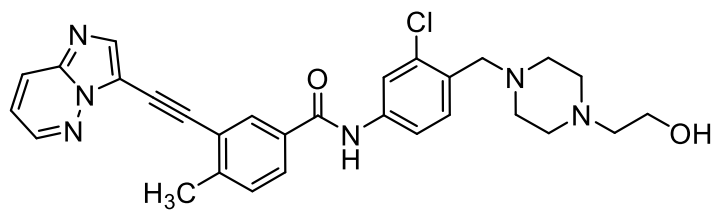
5.S1c



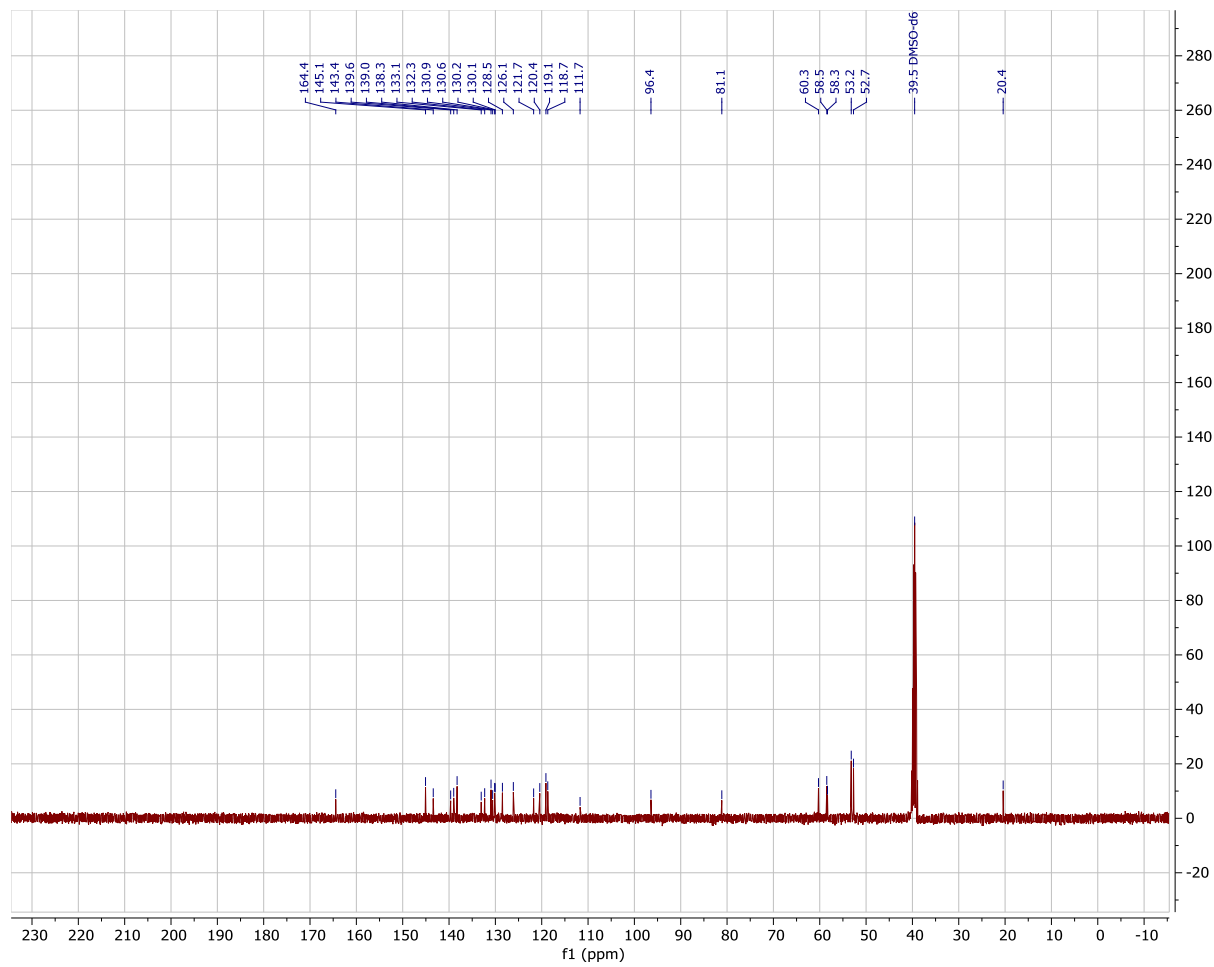


5.9c

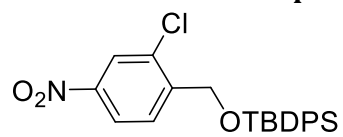




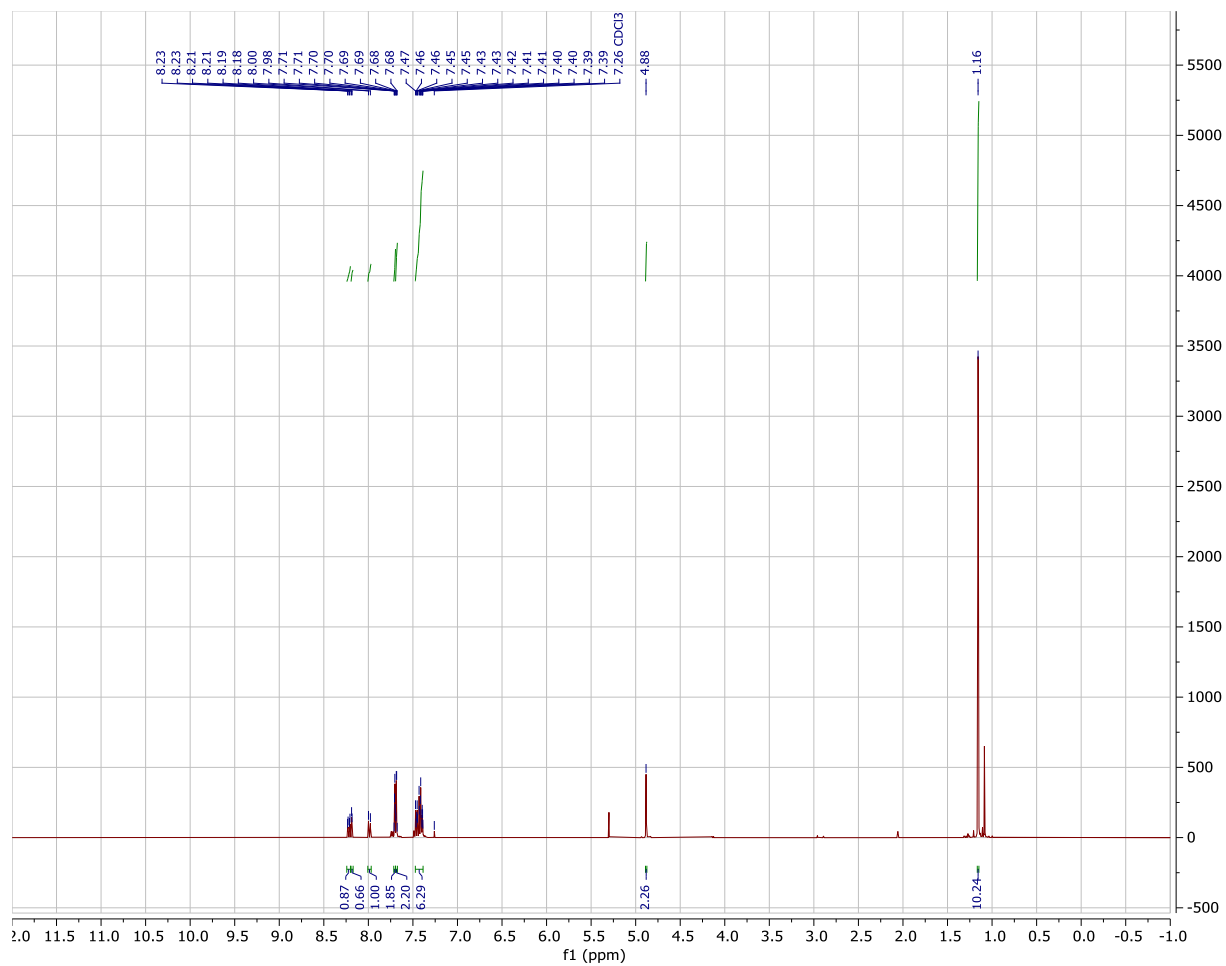
5.9c

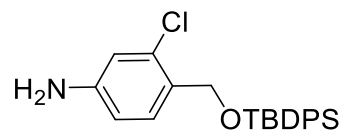


## SA.3.2 Dual-NBN Compounds (5.10 – 5.17c)

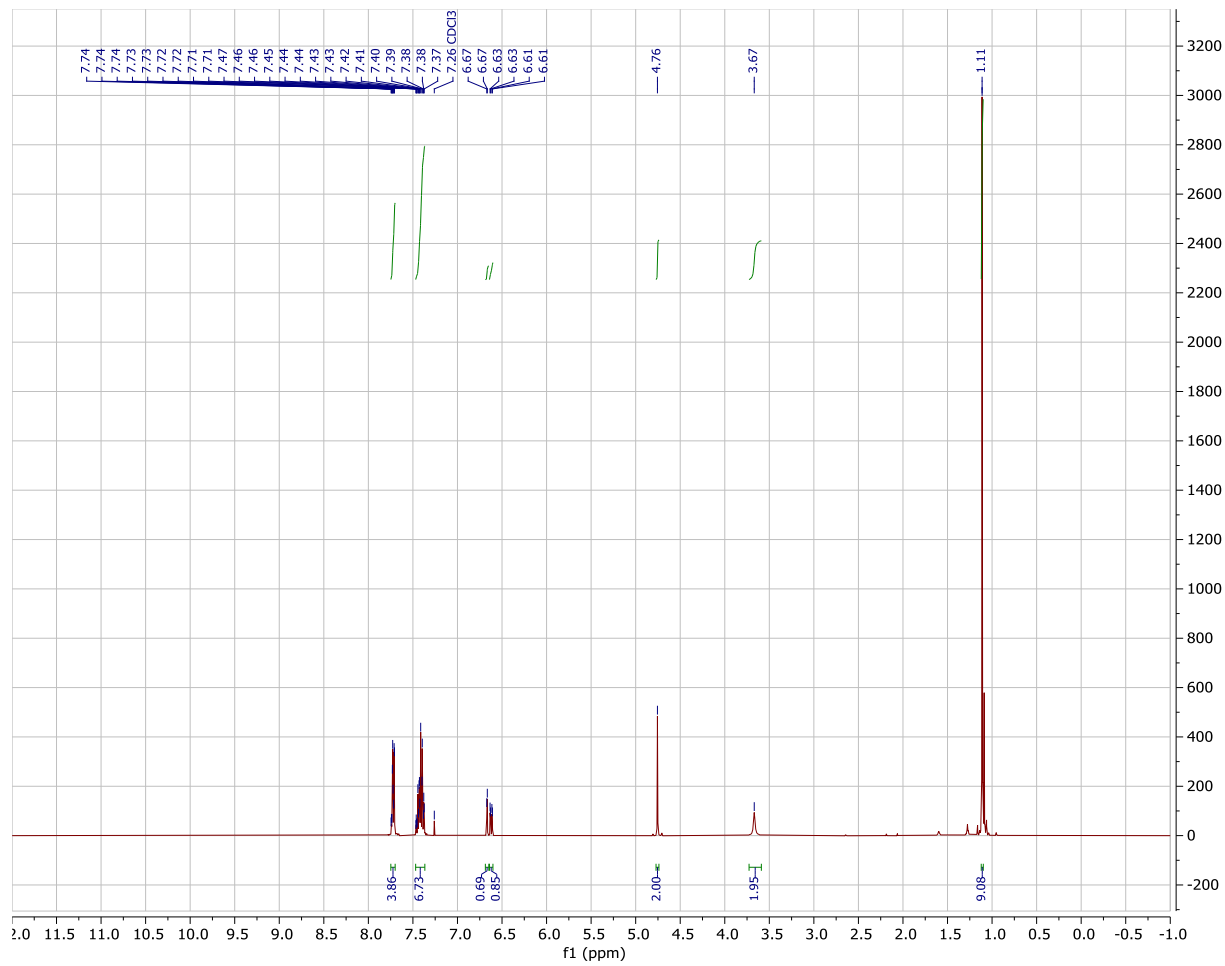


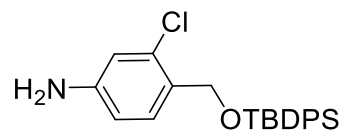
5.10



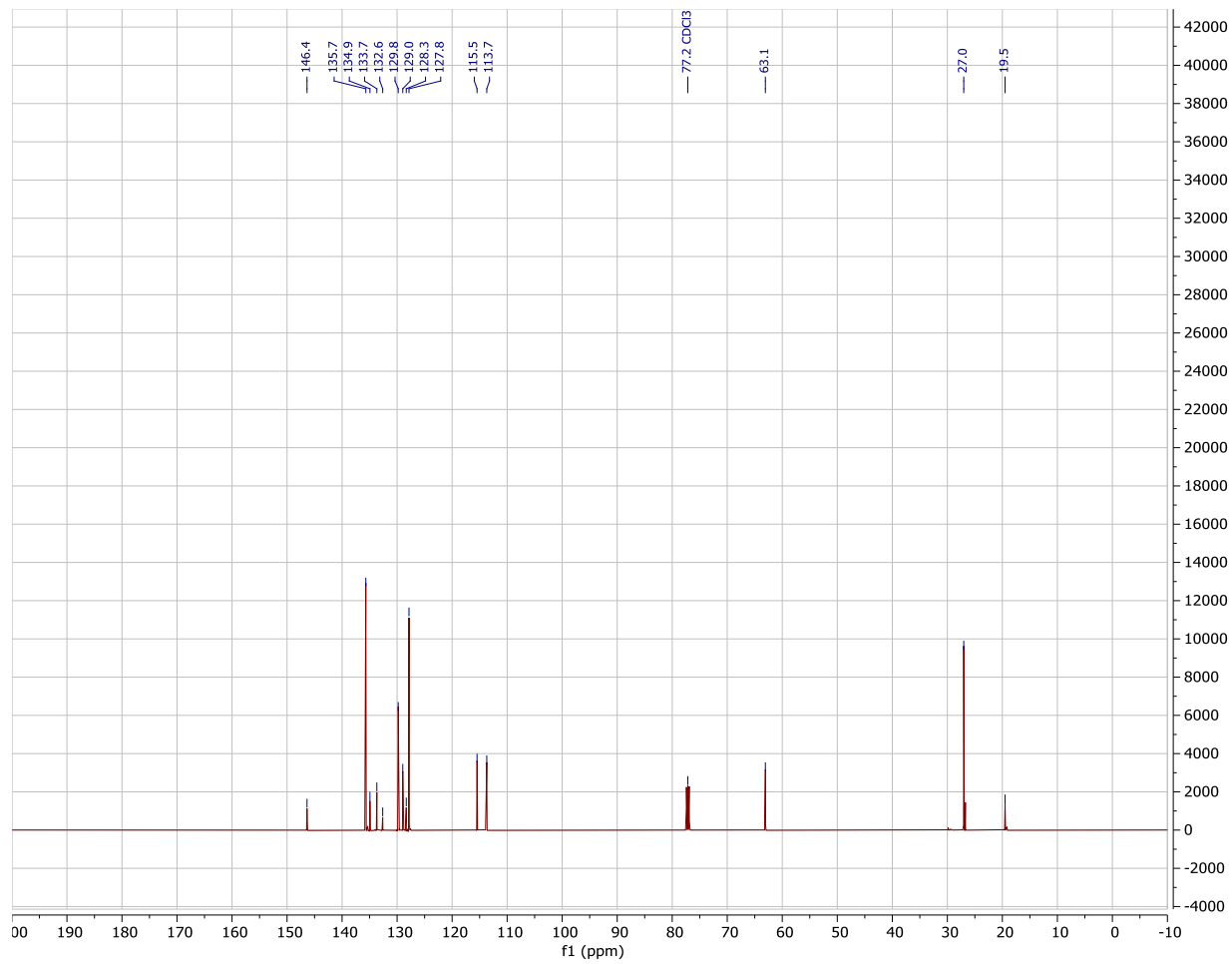


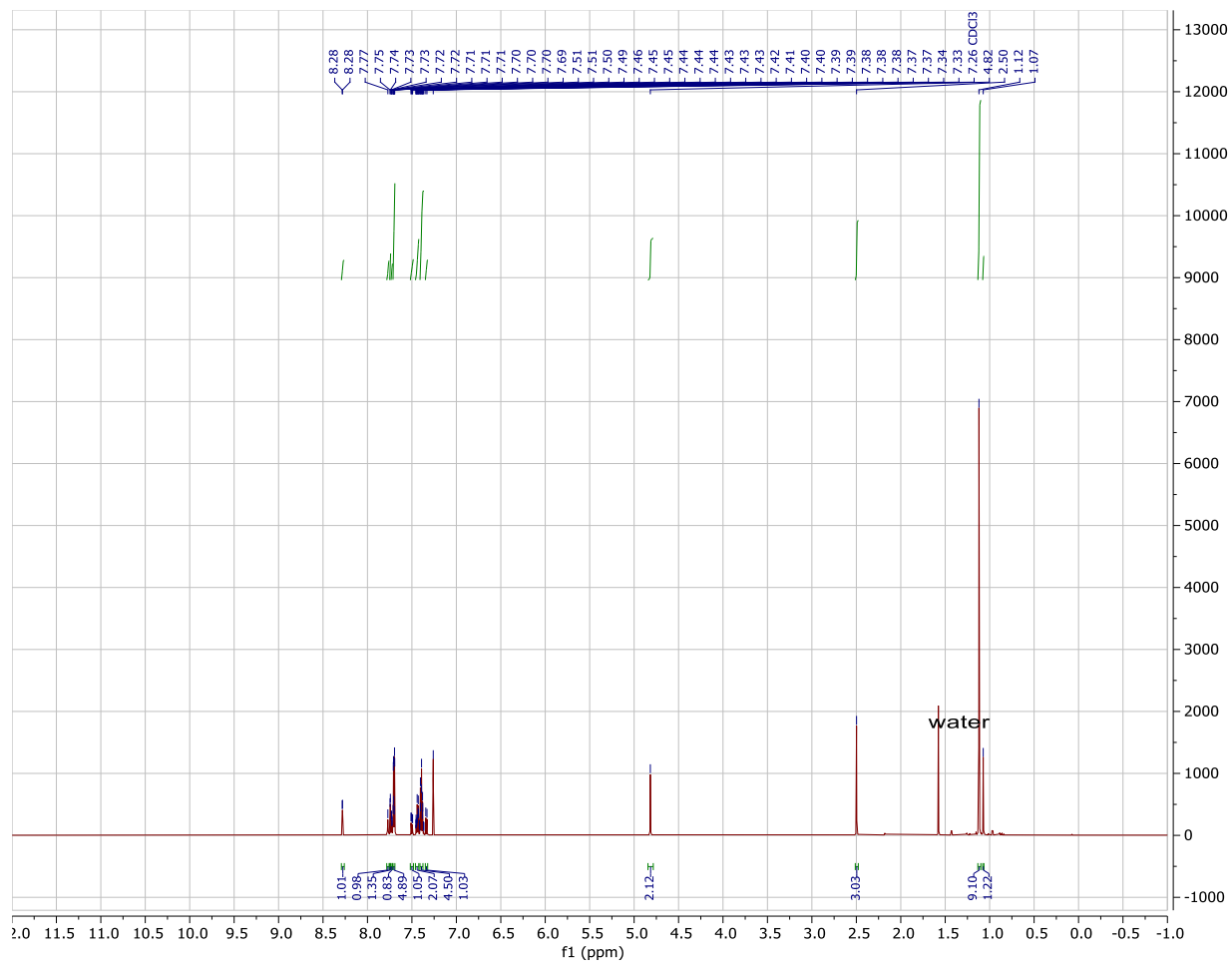
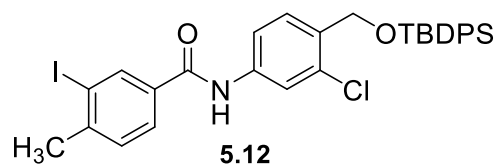
5.11

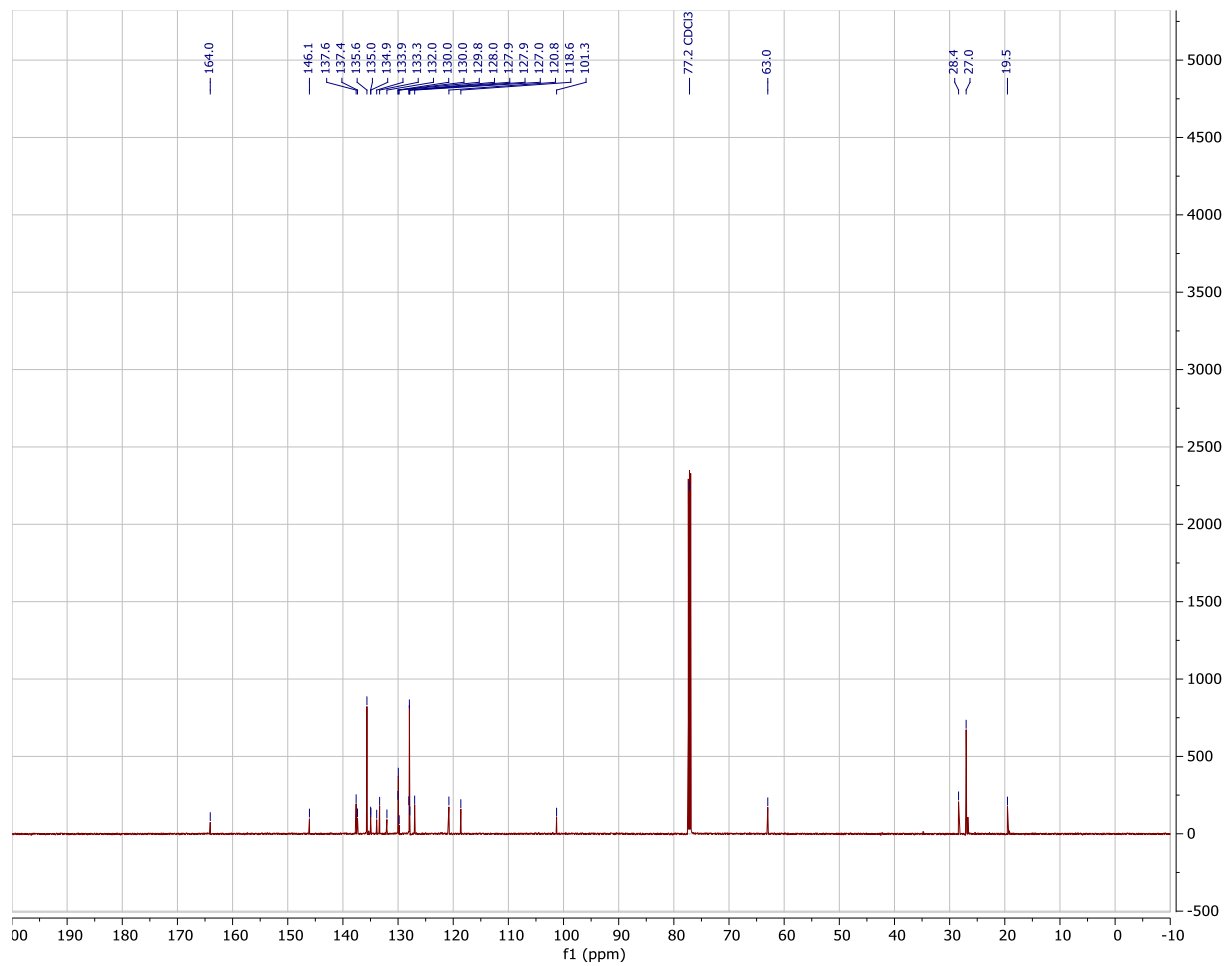
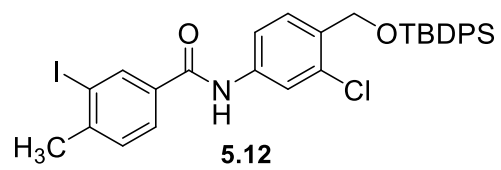


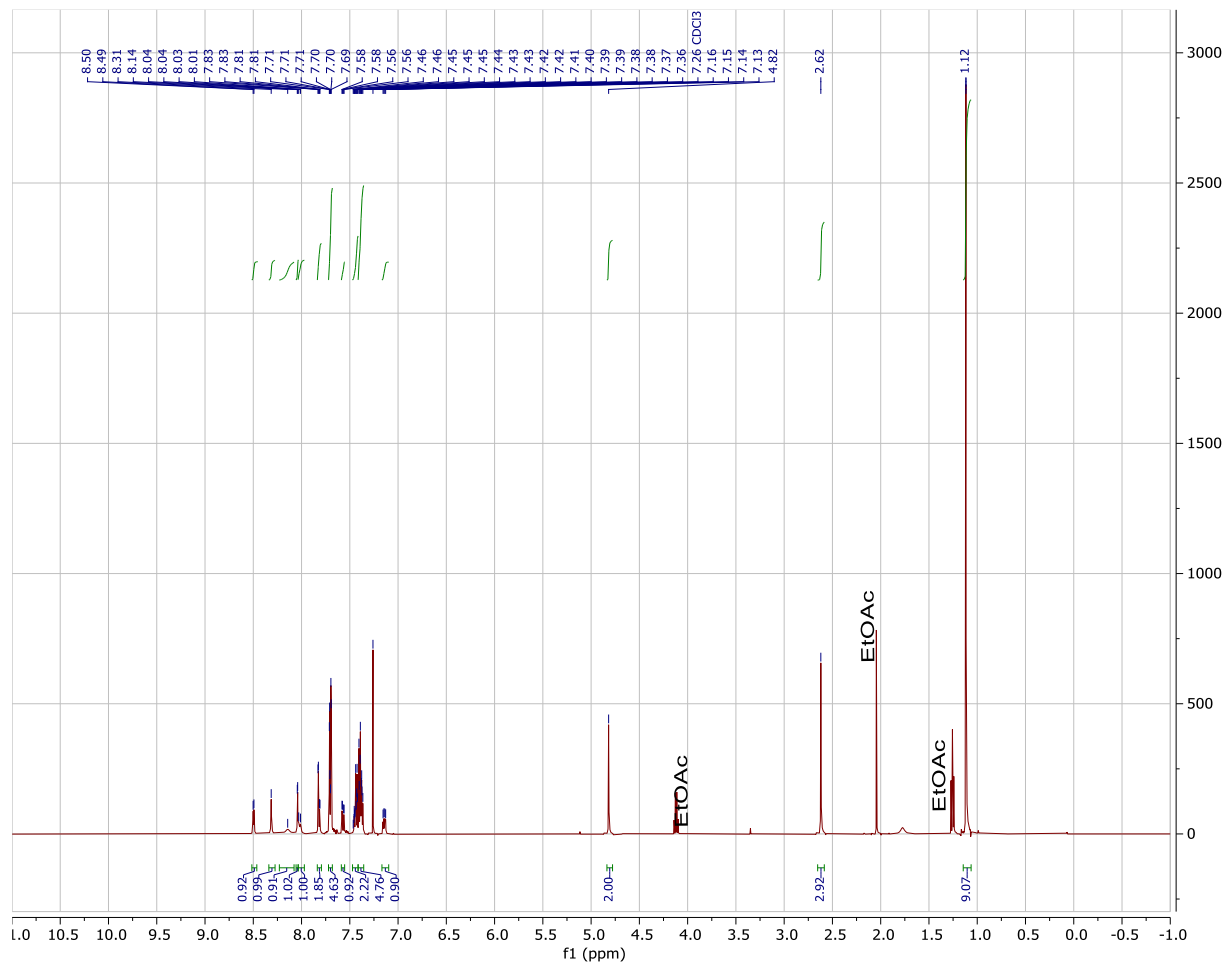
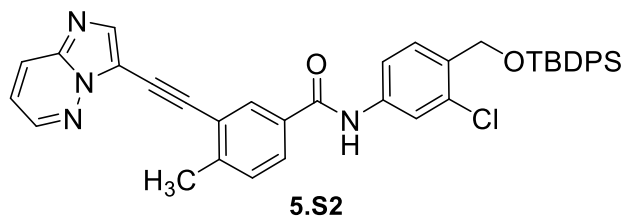


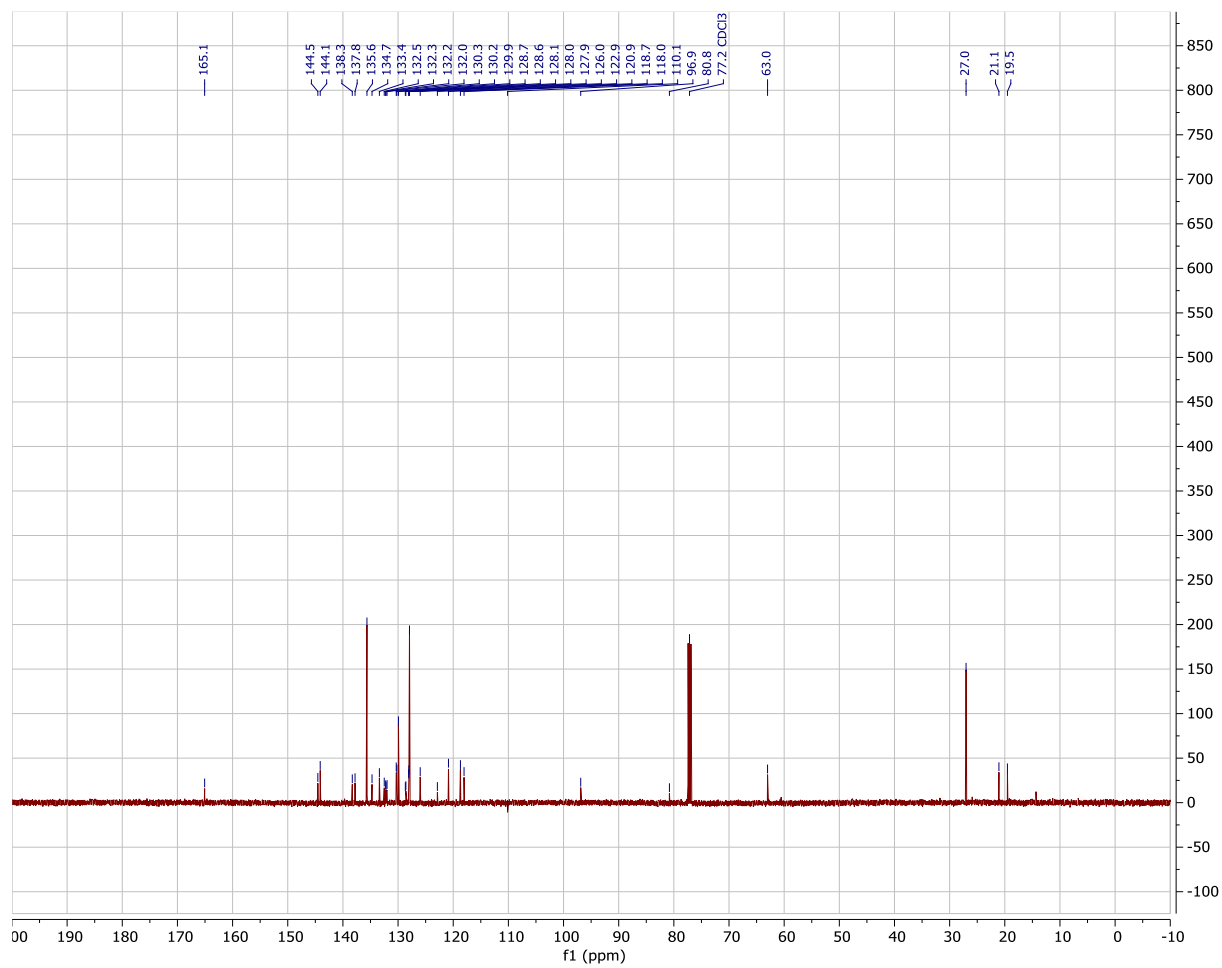
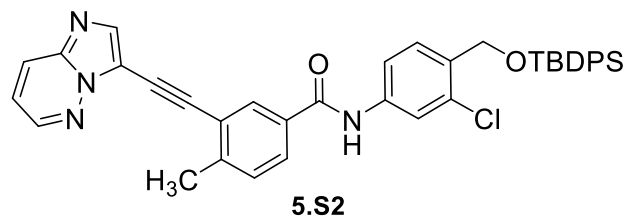
5.11

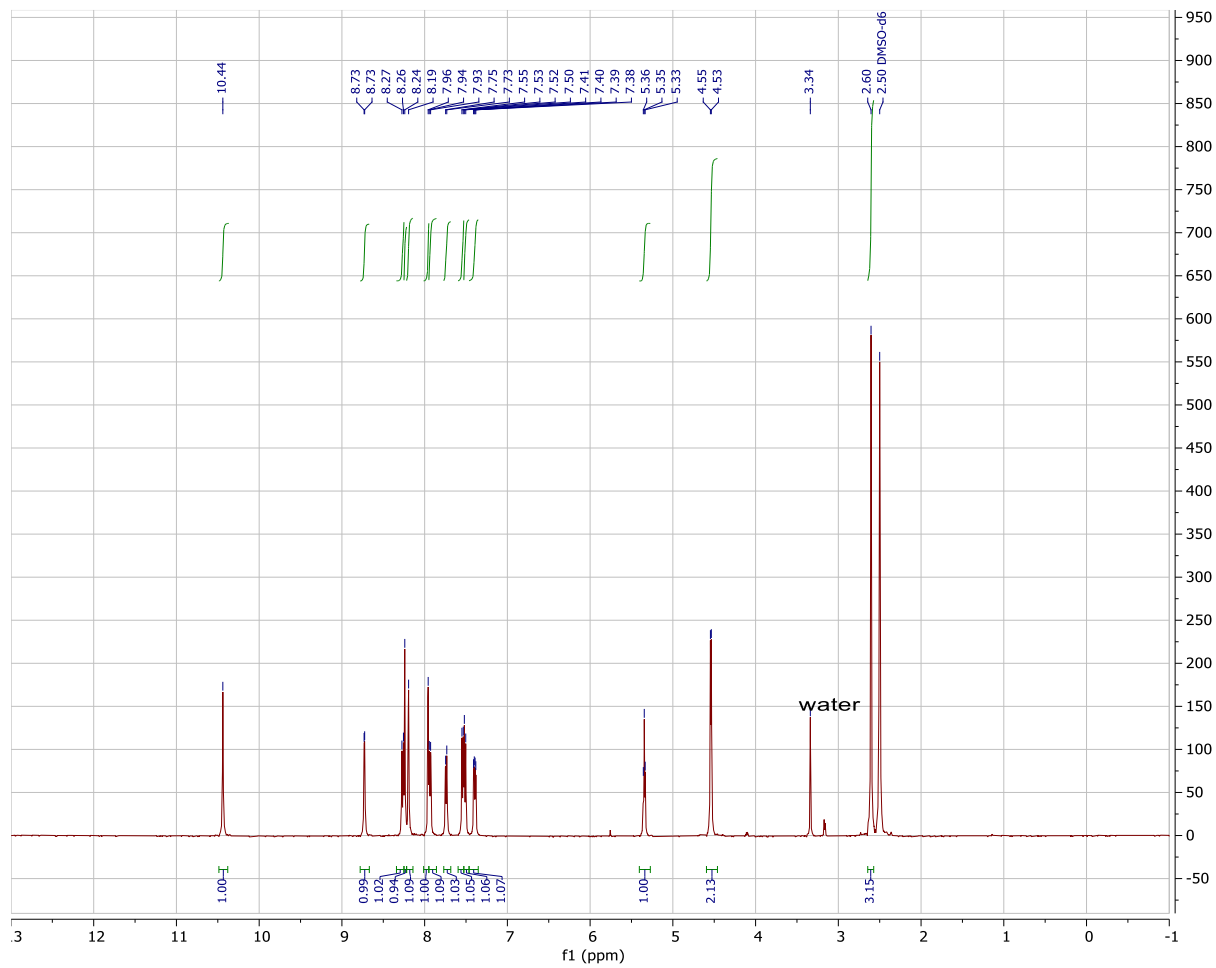
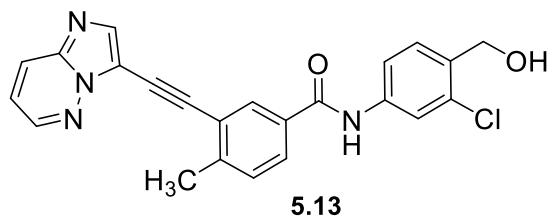


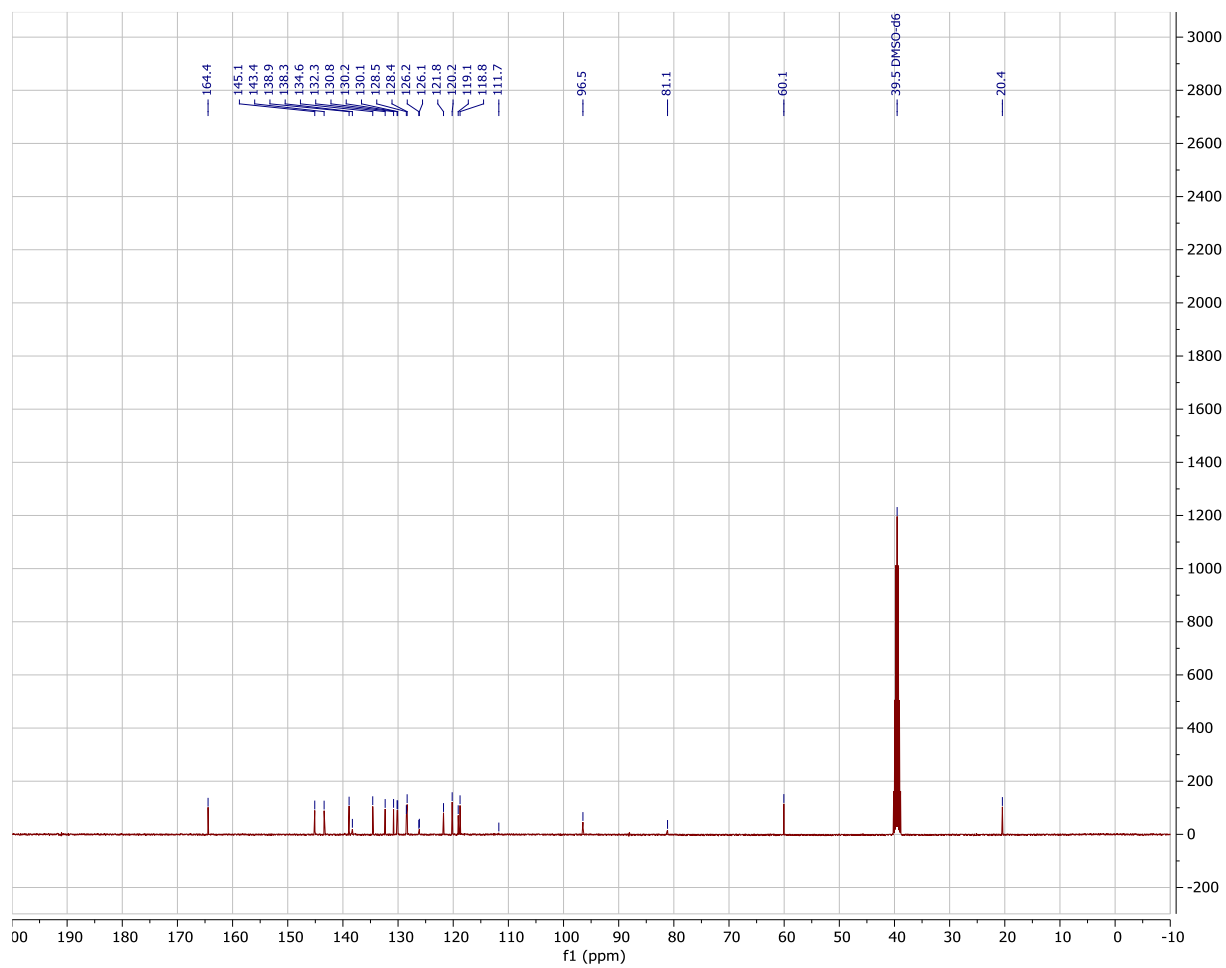
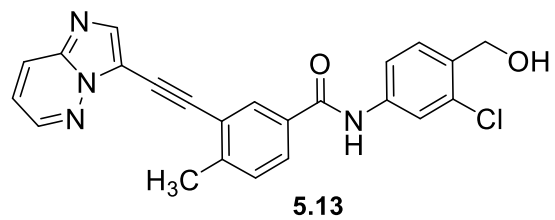


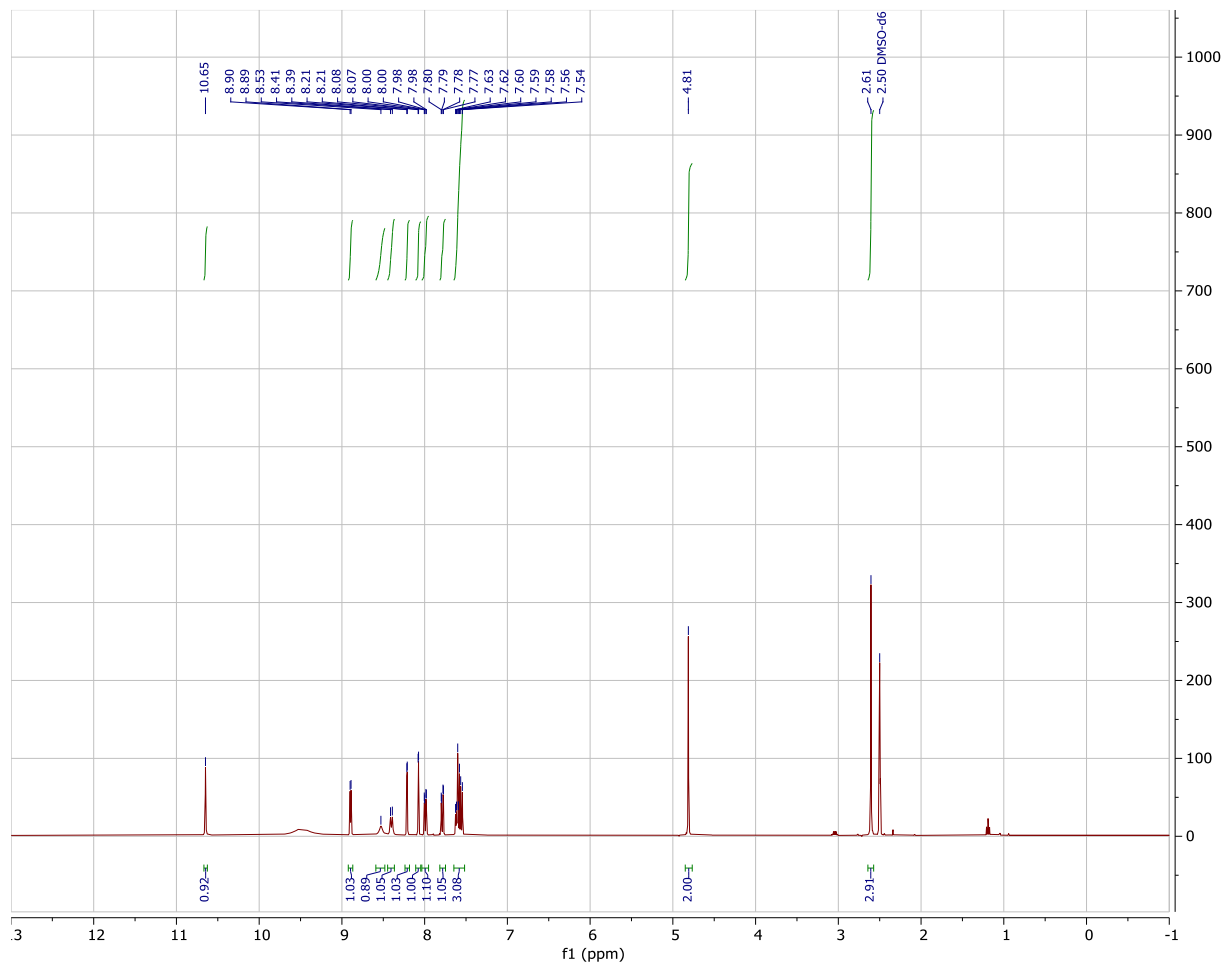
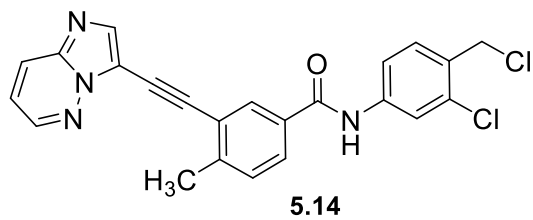


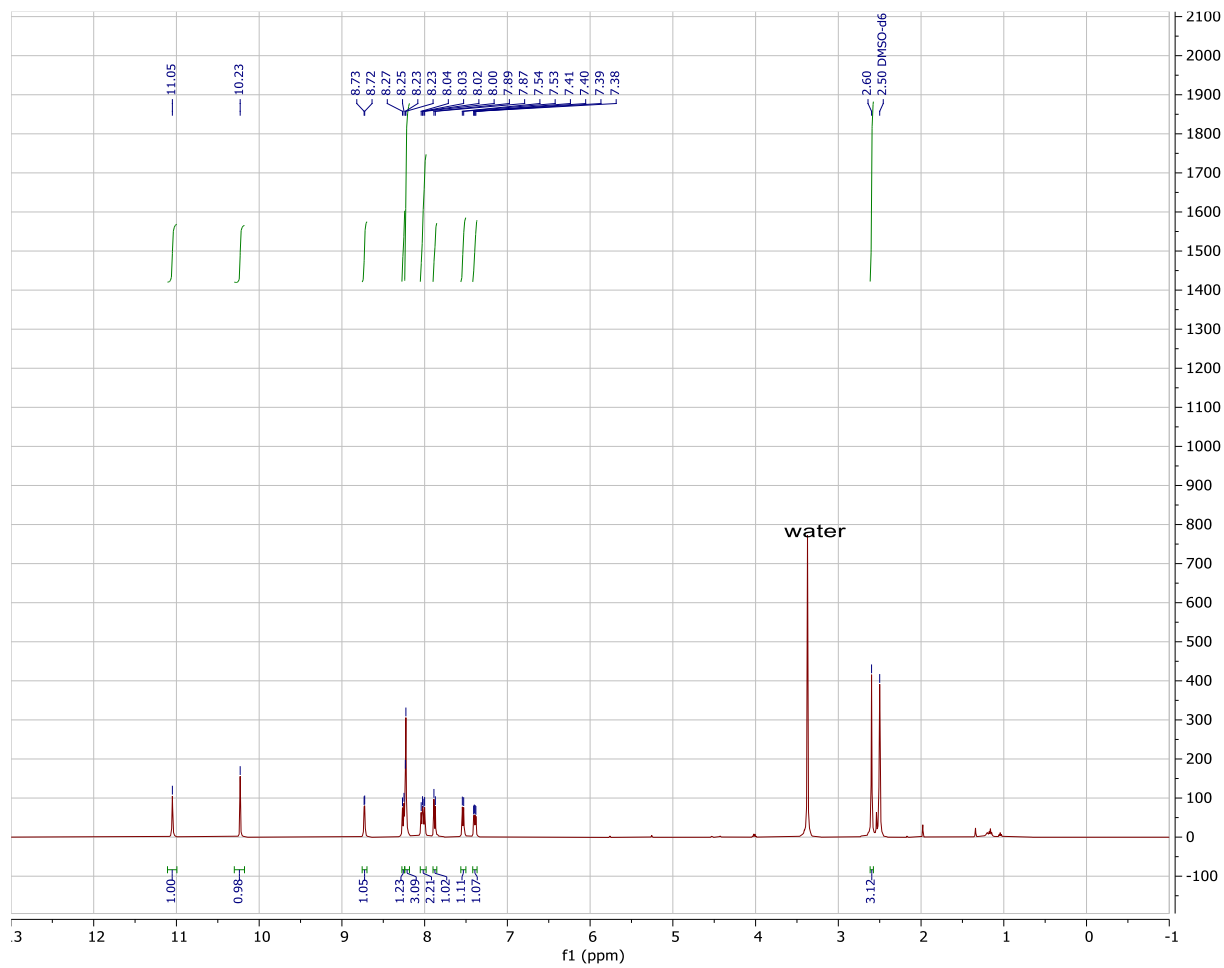
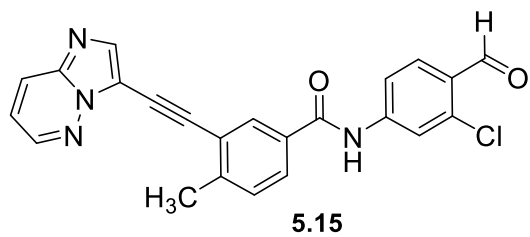


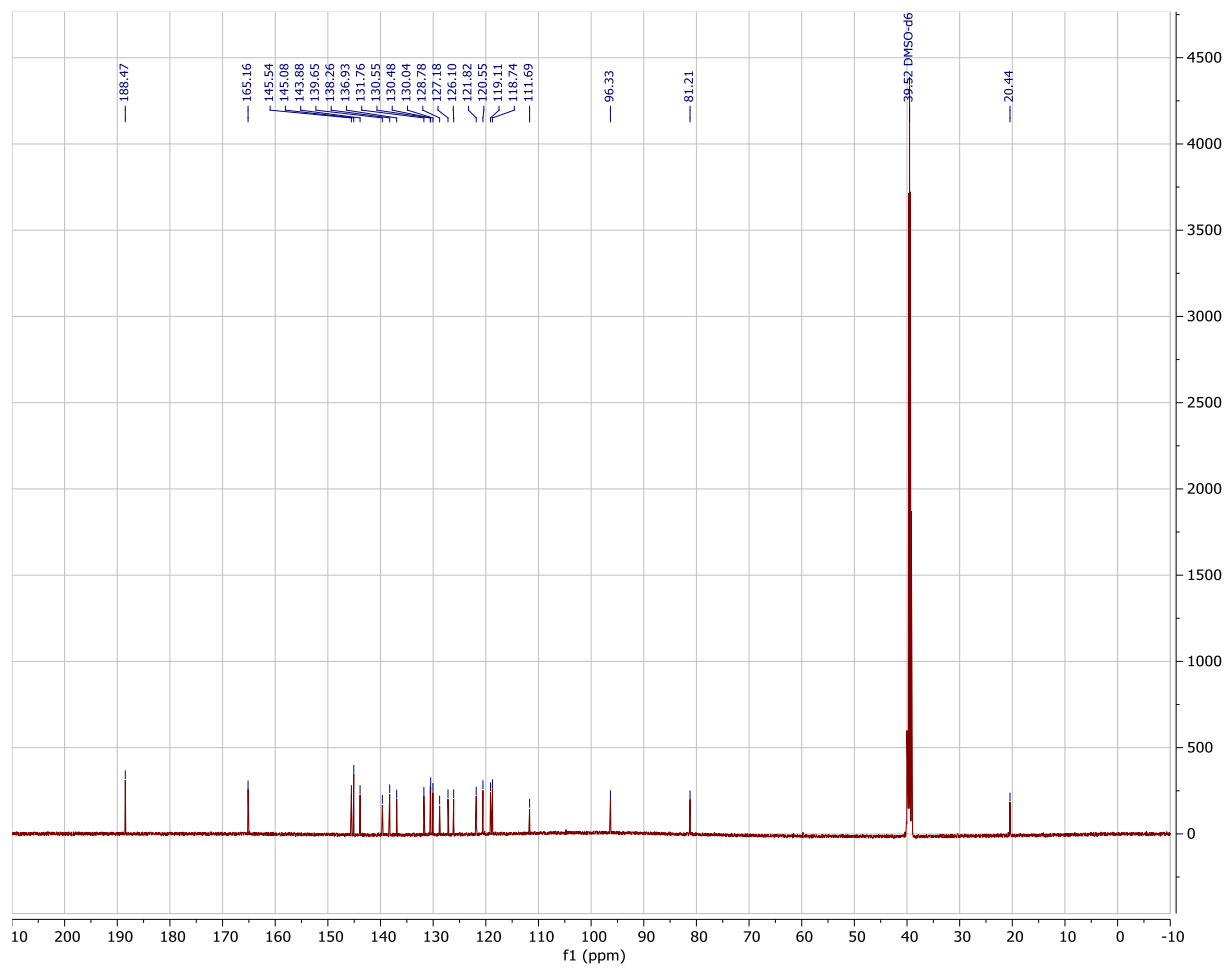
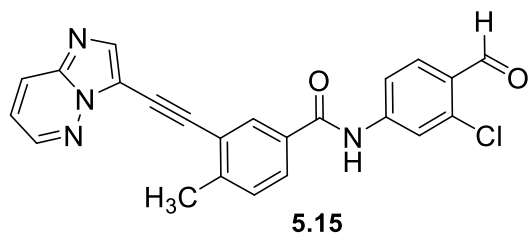


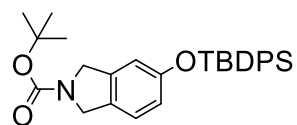




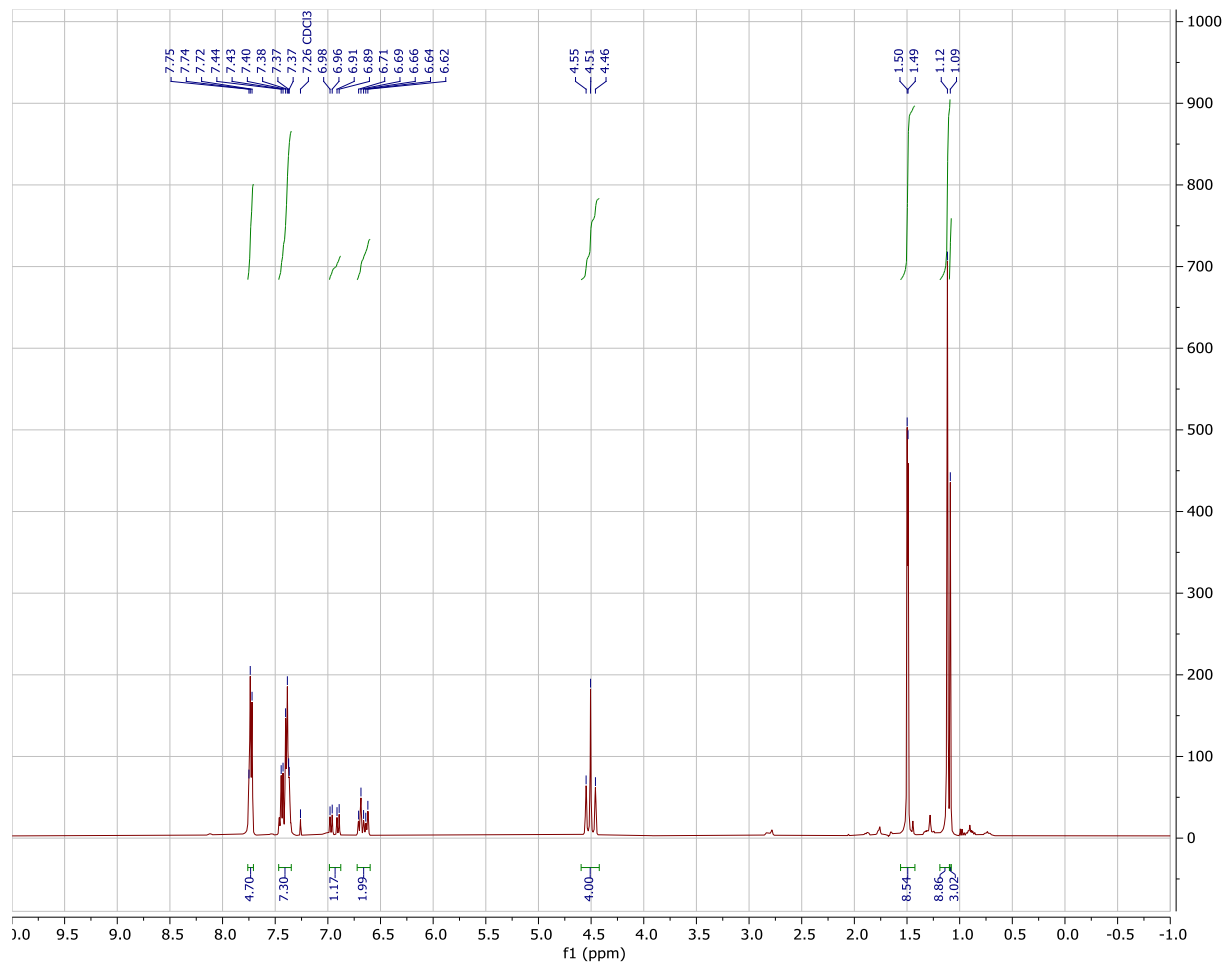


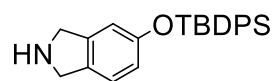




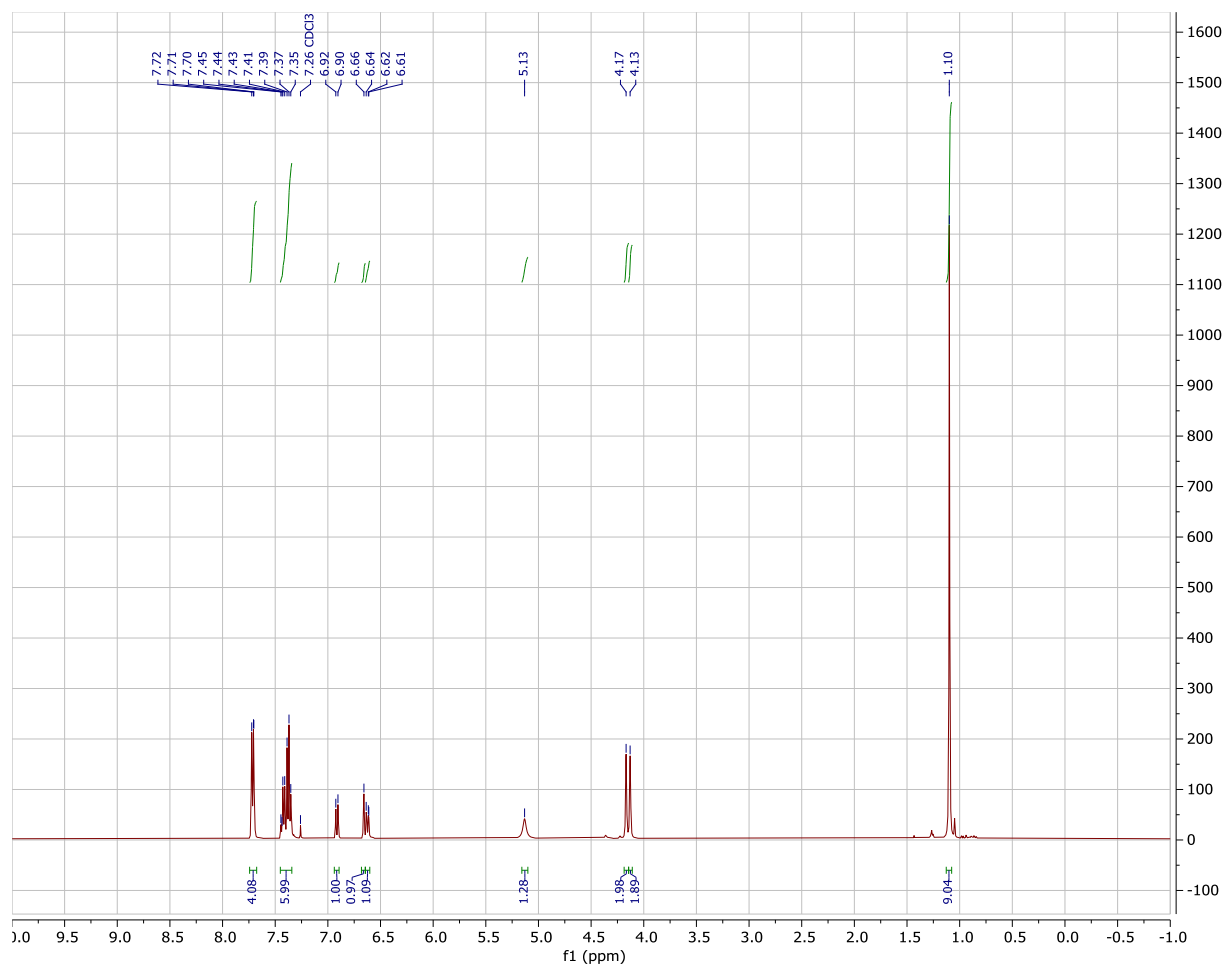


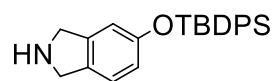
5.53





5.16d





5.16d

